Alternative splicing of *Lymnaea* Ca_V3 and NALCN ion channel genes serves to alter biophysical properties, membrane expression, and ion selectivity

by

Adriano Senatore

A thesis
presented to the University of Waterloo
in fulfillment of the
thesis requirement for the degree of
Doctor of Philosophy
in
Biology

Waterloo, Ontario, Canada, 2012

AUTHOR'S DECLARATION

I hereby declare that I am the sole author of this thesis. This is a true copy of the thesis, including any required final revisions, as accepted by my examiners.

I understand that my thesis may be made electronically available to the public.

Abstract

Evidence is presented that *Lymnaea* contains homologues for mammalian Ca_v3 and NALCN 4-domain ion channels, which retain key amino acid sequence motifs that differentiate these channels from other 4-domain types. Molecular cloning and heterologous expression of the first invertebrate Ca_v3 channel cDNA from *Lymnaea* confirms that it indeed is a true homologue to mammalian Ca_v3 channels, retaining some hallmark biophysical and pharmacological features[1]. Interestingly, the *Lymnaea* Ca_v3 channel gene also exhibits alternative splicing that is conserved with mammalian $Ca_v3.1$ and $Ca_v3.2$ channels, with homologous exons 8b in the I-II linker ($Ca_v3.1$) and 25c in the III-IV linker ($Ca_v3.1$ and $Ca_v3.2$), that can selectively be included or omitted from the full length channel (summary figure A). We show that the developmental and spatial expression patterns of these splice variants are remarkably conserved, and that these splice variants produce analogous changes in membrane localization and biophysical properties when channels are expressed in HEK-293T cells.

The *Lymnaea* Ca_v3 channel gene also undergoes alternative splicing in the domain II P-loop, with mutually exclusive exons 12A and 12B that code for a large portion of the P-loop just upstream of the selectivity filter (summary figure A). Such splicing is a novel discovery that is not conserved with vertebrates or any other deuterostome animal, all of which only contain 12A homologues of exon 12. However, protostome animals including *Lymnaea stagnalis*, *Drosophila melanogaster*, and *C. elegans* all have mutually exclusive 12A and 12B exons in their Ca_v3 channel genes. Evidence is presented that exon 12A is likely the ancestral exon for the domain II P-loop, and that alternate exon 12B evolved later. Furthermore, although the two *Lymnaea* variants possess the same selectivity filter motifs characteristic for Ca_v3 channels (i.e. EEDD), they exhibit dramatic differences in calcium vs. sodium selectivity, without significant differences in biophysical properties. This is the first account of alternative splicing used to modulate ion selectivity in a Ca_v3 channel homologue, and given that calcium is such an important electrogenic signaling molecule, these alterations are expected to have profound physiological implications.

Amazingly, *Lymnaea* NALCN was also found to undergo alternative splicing in the domain II P-loop, but in this case, the entire P-loop is replaced by mutually exclusive exons 15a and 15b such that the selectivity filter is converted from the proposed non-selective sodium-permeable configuration (15b/EKEE; EEKE in mammals, nematodes and insects), to a calcium channel-like pore (15a/EEEE; summary figure B). Thorough phylogenetic analysis reveals that NALCN is extremely

unconventional, in that alternative splicing has frequently and independently evolved to alter the selectivity filter in domains II or III, in multiple animal clades. Furthermore, the ancestral NALCN channel most likely contained an EEEE pore. This work brings into question NALCN's proposed role as a major leak sodium conductance that depolarizes neurons to help set the resting membrane potential, since some species possess only an EEEE variant, and based on homology to other 4-domain ion channels, this should render the channel calcium-selective. Unfortunately, heterologous expression and electrophysiological characterization of the two *Lymnaea* NALCN isoforms was unsuccessful, corroborating with others the inability to record NALCN ionic currents in heterologous systems.

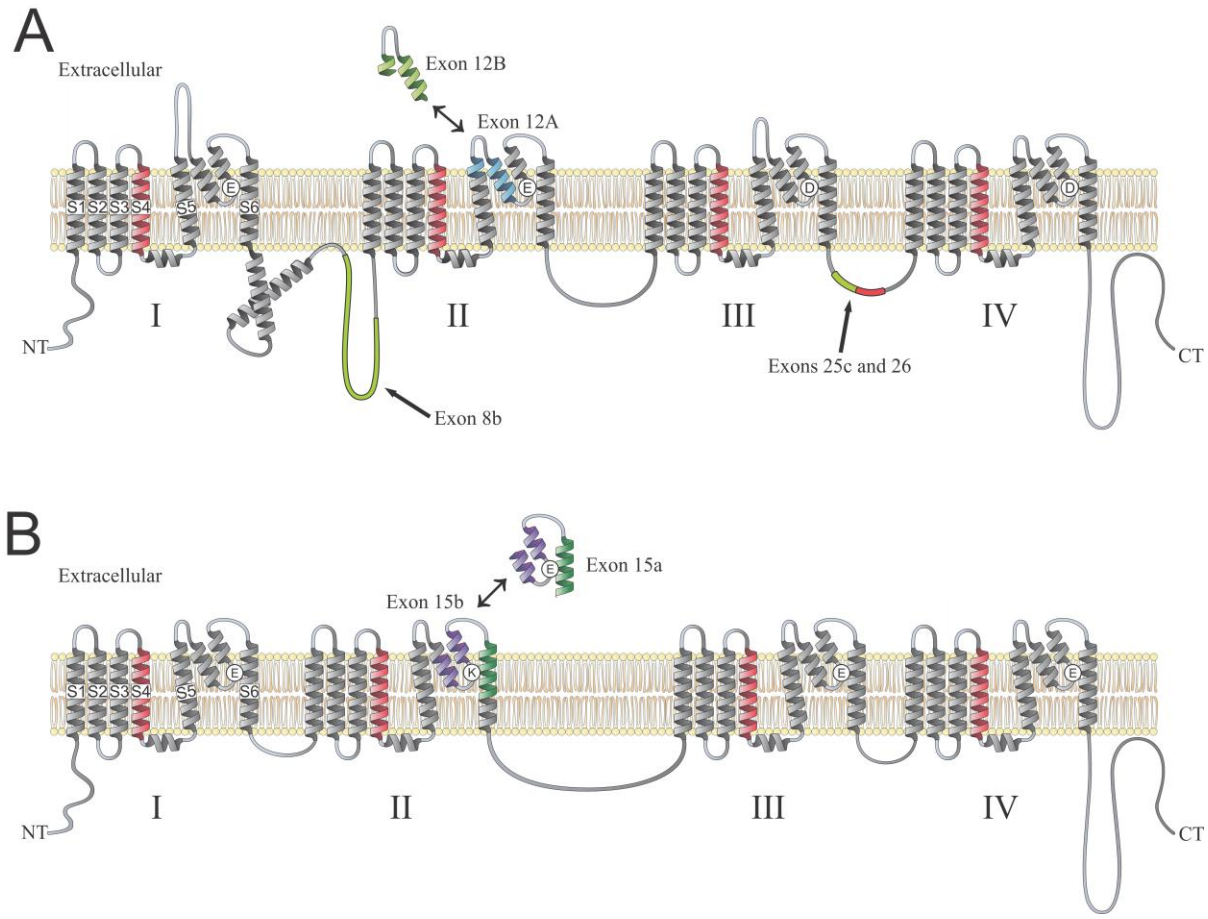

Summary Figure. Conserved and divergent splicing of *Lymnaea* Ca_v3 and NALCN channel homologues. A) Schematic illustration depicting the protein structures influenced by conserved and divergent alternative splicing in Ca_v3 channel homologues. *Lymnaea* Ca_v3 possesses an optional exon in the I-II cytoplasmic linker that is analogous to exon 8b in rodent $Ca_v3.1$. In both cases, the optional exon is removed by utilization of alternate 5' donor splices site within exon 8, resulting in omission of a large protein sequence in the I-II linker, just downstream of the gating brake helix-loop-helix structure. LCa_v3 and mammalian $Ca_v3.1$ and $Ca_v3.2$ genes also undergo alternative splicing in the III-IV linker, with optional exon 25c that can also be removed by an alternate 5' donor site within exon 25. Mammals also possess cassette exon 26, producing three possible configurations of +25c, +25c/+26, or -25c/-26 (i.e. ΔΔ). Mammalian $Ca_v3.3$ lacks optional exons in the III-IV linker, and thus always resembles ΔΔ variants. LCa_v3 also has divergent splicing from mammalian homologues, such as an alternate exon coding for a portion of the P-loop in domain II, just upstream of the selectivity filter. Remarkably, the ancestral version of this exon (12A) creates LCa_v3 channels with high permeability to monovalent cations such as sodium, while the 12B variant is much more selective for calcium. Phylogenetic analysis reveals that exon 12B evolved in a subset of invertebrates making up the protostome superphylum. **B)** *Lymnaea* NALCN also undergoes alternative splicing in the domain II pore, with alternate exon 15a inserting a glutamate (E) into the selectivity filter to produce an EEEE calcium channel-like selectivity filter. Exon 15b codes for a lysine (K) in the equivalent position, producing an EKEE selectivity filter which corresponds to the EEKE of humans and other model organisms such as *Drosophila melanogaster* and *C. elegans*. NALCN is a highly non-conventional 4-domain ion channel, in that it has frequently and independently evolved alternatively-spliced selectivity filters in domains II and III in various animal species.

Acknowledgements

Cloning LCa_v3 and its splice isoforms was surprisingly challenging (not so for LNALCN), and at times success seemed distant and unlikely. Within the first few weeks after arriving in the lab I had completed the full length sequencing of LCa_v3 and LNALCN shortly thereafter, but it took more than two years to clone the LCa_v3 cDNA for expression in mammalian cells. The bacteria, although an extremely useful tool, resisted me every step of the way. I would start by thanking my beautiful wife Victoria, and my two amazing children, Audrey and Matteo, for being there for me through the tough times and for bringing a smile to my face despite the challenges. Victoria was very patient, and gave me lots of good advice. I would also like to thank my mother Elizabeth, my sister Ana and her husband Marshall, and their two sweet daughters Myah and Chiara, who have been so nice to have close by over these past years. I would also like to thank my extended family, on Victoria's side, who shared their experiences in academia with me and always provided words of wisdom.

I would like to thank my supervisor, Dr. David Spafford, for investing in me, and for granting me the opportunity to plan and execute my own research, all the while maintaining a keen interest. David provided me with some valuable advice, and taught me a lot about the packaging of scientific information, where clarity and efficiently are important. His drive to complete and publish projects is also exemplary. I would also like to thank my committee members, Drs. Bruce McKay, Bernie Duncker, and Neil Magoski, as well my external examiner Dr. Edward Perez-Reyes, for taking the time to assess my progress and read my thesis, and my committee for providing such excellent and diverse insights. Also, I am very grateful to Dr. Arnaud Monteil and his colleagues Drs. Phillipe Lory, Jean Chemin, Emmanuel Bourinet, and Alexandre Mezghrani for hosting me for a semester at the CNRS in France, and for allowing me to observe some of their very interesting and high quality research. Finally, I would like to thank Dr. John S. Greenwood, my M.Sc. supervisor, for his constant enthusiasm and support. Truly, I am fortunate to have been exposed to such knowledgeable and talented scientists throughout both my M.Sc. and Ph.D. Their advice, mentorship, and example have had an enormous influence on me.

Over the years, I have also worked with some very talented colleagues, and it was always a pleasure to work alongside them. In particular, I would like to thank Xuan Huang, John Pham, Taylor Dawson, Stanley Lam, Humberto Vigil, Ardalan Bhozogzgrad, Adrienne Boone, Samer Khoury-Hanna, and Mickael Deage.

I would also like to thank the funding agencies, NSERC (CGS-D) and the Ministry of Training, Colleges and Universities (OGS and OGSST), for providing me with funding throughout my PhD. This financial assistance made it possible for me to focus on my research, as well as to travel to France to conduct research under a Michael Smith Foreign Study Supplement Award (NSERC).

Importantly, I would like to thank the wonderful secretaries in the Department of Biology, not only for making things run smoothly for everyone, but also for being so nice to interact with. I would especially like to thank Linda Zepf, Mila Kaufman, Jennifer Collins, and Jeannie Redpath-Erb.

Finally, I would like to thank the model organism *Lymnaea stagnalis*, for providing so many opportunities and surprises. Through working with and reading about the snail, I have come to appreciate, first hand, how beneficial it is to use invertebrates as neuroscience research subjects.

Dedication

To my wife Victoria, my children Audrey and Matteo (and any later additions). I hope that, throughout the years to come, you are all happy and successful in whatever you do.

Table of Contents

List of Figures

All figures in the introduction and materials and methods, as well as most illustrations presented in the results, are original works created by Adriano Senatore. Several figures presented in the results were prepared by Dr. J. David Spafford.

Chapter 1: Introduction

Results Chapter 2.1

Results Chapter 2.2

Results Chapter 2.3

Results Chapter 2.4

Chapter 5: Materials and Methods

List of Tables

Appendix D

List of Abbreviations

AID	alpha interaction domain
AMP	adenosine monophosphate
ATP	adenosine triphosphate
BLAST	basic local alignment search tool
BSA	bovine serum albumin
cDNA	complementary DNA
CICR	calcium-induced calcium release
CNS	central nervous system
CT	carboxy terminus (protein); cycle threshold (qPCR)
dATP	deoxyadenosine triphosphate
dCTP	deoxycytidine triphosphate
DEPC	diethylpyrocarbonate
dGTP	deoxyguanosine triphosphate
DIG	digoxigenin
DMEM	Dulbecco's modified Eagle's medium
DMSO	dimethyl sulfoxide
DNA	deoxyribonucleic acid
DNase	deoxyribonuclease
dNTP	deoxynucleotide triphosphate
DTT	dithiothreitol
dTTP	deoxythymidine triphosphate
dUTP	deoxyuridine triphosphate
EDTA	ethylenediaminetetraacetic acid
EGFP/eGFP	enhanced green fluorescent protein
EGTA	ethylene glycol tetraacetic acid
ER	endoplasmic reticulum
ERAD	endoplasmic reticulum-associated protein degradation
FBS	fetal bovine serum
GFP	green fluorescent protein
GMP	guanosine monophosphate

GTP	guanosine triphosphate
HA tag	hemagglutinin tag
HEK-293T	human embryonic kidney 293T
HEPES	4-(2-hydroxyethyl)-1-piperazineethanesulfonic acid
hnRNP	heterogeneous nuclear ribonucleoprotein
HPRT1	hypoxanthine phosphoribosyltransferase 1
HRP	horseradish peroxidase
HVA	high voltage-activated
IgG	immunoglobulin
IPTG	isopropyl β-D-1-thiogalactopyranoside
IRES	internal ribosome entry site
KO	gene knockout
LB	Luria Bertani
LTS	low threshold spike
LVA	low voltage-activated
mRFP	monomeric red fluorescent protein
mRNA	messenger RNA
NMDG	N-methyl-D-glucamine
NT	amino terminus
PBS	phosphate-buffered saline
PBST	TWEEN phosphate-buffered saline
PCR	polymerase chain reaction
PDF	pigment dispersing factor
qPCR	quantitative (real-time) RT-PCR
RACE	rapid amplification of cDNA ends
REM	rapid eye movement
RFP	red fluorescent protein
RNA	ribonucleic acid
RNase	ribonuclease
RT	reverse transcription
RTase	reverse transcriptase
RT-PCR	reverse transcription-polymerase chain reaction

SB	superbroth
SDHA	subunit A of the succinate dehydrogenase complex
SDS	sodium dodecyl sulfate
SDS-PAGE	SDS-polyacrylamide gel electrophoresis
snRNP	small nuclear ribonucleoprotein
SR proteins	serine/arginine proteins
SRC	sarcoma tyrosine kinase
TBS	tris-buffered saline
TdT	terminal deoxynucleotidyl transferase
TEA	tetraethylammonium
TTBS	TWEEN tris-buffered saline
UTR	untranslated region
UV	ultraviolet
VD4	visceral dorsal 4
VGCC	voltage-gated calcium channel
4x6TM	4x6 transmembrane helices

Chapter 1
Introduction

1.1 The basis of metazoan electrical communication

1.1.1 Animal multicellularity and the evolution of the nervous system

The evolution towards multicellularity must have depended on the adaptation of cellular mechanisms already in place, whose initial purpose was to allow single-celled organisms to sense and interact with their environment and other organisms. Indeed, many of the molecules known today to form the lexicon of multicellular communication likely formed before, or at the very early stages of multicellularity[2,3]. Metazoans in particular, which move through and interact with their environments on a relatively rapid timescale, have undergone an arms race to evolve extremely fast and sophisticated cell-to-cell signaling, manifest as the electro-chemical coupling between nerves and muscle. The resulting communication systems rely on the rapid transfer of information across the relatively impermeable hydrophobic cell membrane, a challenge facilitated by proteinaceous structures that traverse the membrane and bridge the aqueous intracellular environment with the aqueous exterior, or with the cytoplasm of another cell. Some of these proteins transport specific molecules for metabolic purposes, to set up ionic gradients or for use as signaling molecules[4]. Others act as receptors that transmit a signal into the cell upon detection of a compatible ligand[5]. Some proteins allow cells to adhere to each other (and the extracellular matrix), allowing for direct interaction and communication between cells[6,7]. Yet others, and perhaps the most rapid transmitters of information, evolved to exploit ionic gradients, where they can selectively or non-selectively conduct ionized atoms along concentration and charge gradients at extremely high rates[8]. The latter group, known collectively as ion channels and ion channel receptors, are indispensable for the rapid transmission of electrical information between and along nerves; in some cases connecting microscopic cells or cell groups within one morphological location of an animal to others located meters away.

1.1.2 Ions and excitability

There are two fundamental processes that allow for electrical communication. The first is setting up ionic concentration and electric potential gradients across the cell membrane, whereby the inside is more negatively charged than the outside, and where sodium and calcium ions are more abundant outside while potassium and inorganic anions are more abundant inside[9]. A large amount of energy is

invested by cells to maintain homeostatic ionic gradients and electric potential across the membrane, and this is primarily achieved by ATP-hydrolyzing ion pumps in combination with ion exchangers.

The second process involves the controlled release of this stored electrical and chemical energy by ion-permeable channels and receptors, which become activated under specific conditions. Seminal work by Hodgkin, Huxley, and others revealed that the action potential, an electrical impulse that moves rapidly along axons, involves first an influx of sodium through voltage-gated sodium channels which depolarizes the axon, followed by an efflux of potassium through voltage-gated potassium channels that in turn restores the negative potential inside[10,11]. This dynamic system relies on the orchestrated activation of voltage-gated sodium and potassium channels. Sodium channels activate after slight depolarization from the resting membrane potential, where they open very quickly. Incoming sodium ions create an additional depolarization that traverses to adjacent regions and activates yet other sodium channels, propagating the signal. Sodium channels also quickly shut off or inactivate, and the slower to respond potassium channels take over allowing for potassium to leave the cell, restoring the net negative charge on the inside surface of the cell membrane. Importantly, although the bulk of electrical excitability in neurons and other excitable cells most often depends on sodium and potassium, other ions and ion channels are important, including: chloride and other inorganic anions, large organic anions, protons, and calcium.

1.1.3 Calcium as an electrogenic biochemical effector

Calcium, and proteins that conduct or handle calcium, have received particular attention by researchers. What separates calcium from other biologically relevant ions is its ability to strongly interact with other molecules, including proteins, via oxygen-containing carbonyl and carboxyl groups[12]. This feature, combined with the fact that all living cells tend to remove or chelate calcium from the cytoplasm due to toxicity (i.e. ~20,000-fold gradient)[13,12], make cytosolic calcium influx an ideal mechanism for translating electrical information into biochemical information. Examples where such conversions take place include the synapse, where depolarization from an incoming action potential activates voltage-gated calcium channels to trigger calcium-dependent fusion of presynaptic vesicles and neurotransmitter release; muscle cells, where nerve input and depolarization trigger release of calcium from internal stores to flood the cytosol and activate contractile filaments; and excitation-transcription coupling, where voltage-gated calcium channel signaling complexes couple excitation at the cell soma to changes in transcription in the nucleus[14,15,16] (for review see Senatore and Spafford 2007[17]). The function of calcium is highly diverse, localized and contextual, where due

to strong cytosolic chelation[13,12], calcium-sensitive signaling complexes are often positioned in close proximity to the cytoplasmic surface of calcium-conducting proteins[18]. Calcium-activated signaling proteins can perpetuate signals further than is permitted for chelated calcium ions, leading to the concept that calcium-conducting channels "link locally [but] act globally"[19].

1.2 The 4-domain P-loop ion channel superfamily

1.2.1 Evolutionary origins of channel structures

Most metazoan ion channels that conduct sodium, potassium, and calcium are derived from modular structures that evolved long before multicellularity, in prokaryotes (i.e. bacteria and archaea). These modules include the ion conducting pore and the voltage sensor (discussed below; figures 1 and 2), as well as various other structures that serve to regulate the pore including the calcium sensor[20], which mediates channel opening upon exposure to calcium; and the cyclic-nucleotide binding domain[21,22], which activates channels upon interaction with cytosolic cAMP and/or cGMP. Channels containing these modules include inward-rectifying potassium channels, two-pore potassium channels, voltage-gated potassium channels, transient receptor potential channels, calcium-activated potassium channels, cyclic-nucleotide gated channels, hyperpolarization-activated cyclic-nucleotide gated channels, glutamate-gated channels, voltage-gated sodium and calcium channels, invertebrate-specific SC1 voltage-gated calcium channels, and NALCN channels[23,24,25,26,27] (figure 2).

Unlike prokaryotic and eukaryotic potassium channels, voltage-gated sodium and calcium channel pores are made up of only one polypeptide chain of four homologous repeat domains (termed domains I to IV; DI to DIV), with each domain resembling a single voltage-gated potassium channel subunit (figure 2). The 4-domain single peptide structure is thought to be a eukaryotic adaptation, involving first a tandem duplication of a single tetrameric subunit gene into two adjacent subunits, followed by a second duplication of the two tandem subunits into a four domain structure[28,29] (figure 2). In accordance with this hypothesis, tandem domains (i.e. I and II, III and IV), are more similar to their respective counterparts in the other half of the channel than they are to each other (i.e. I is more similar to III, II is more similar to IV)[28,29]. Also, plants[30,31] as well as humans[32,26] contain 2-domain channel subunits with two tandem repeat domains that dimerize to form functional channels (i.e. TPC1 in plants; TPCN1 and 2 in humans; figure 2), and human TPCN channels are more closely related to metazoan 4-domain channels than voltage-gated potassium channels[28,8]. To date, 4-domain channels have not been identified in prokaryotes or plants, however they are found in fungi (i.e.

CCH1[33]) and protists (i.e. CAV2[34,35]) (figure 2), indicating that this general structure arose before the metazoan divergence c.a. 1.6 billion years ago[36,37].

1.2.2 Ion permeation and selectivity

Perhaps the most defining ion channel module, the ion-conducting pore, first appeared in prokaryotic potassium channels[38,39,40]. These are tetrameric complexes, with pores made up of four similar or identical subunits, each with two transmembrane alpha helices separated by an extracellular loop (figure 2). Eight pore alpha helices come together in an 'inverted teepee' structure, lined with hydrophilic amino acids along the second helix of each subunit to create an aqueous ion permeation pathway, gated at the apex by the distal (i.e. C-terminal) ends of the second helices[39,40] (figure 1A). Channel opening involves conformational changes in the pore structure, culminating in the distancing between apex helices to create a transient permeation pathway[27,41,39]. The extracellular loops from each of the four subunits, termed *p*ore- or P-loops, together form the 'selectivity filter' (figure 1A), a structure that defines ion selectivity through specific interactions between particular amino acids in the P-loop, permeating ions and water[42,38,43,44,39,40] .

The most conclusive molecular details underlying ion permeation and selectivity through P-loop-containing ion channels have come from X-ray crystallographic studies of potassium channels[45,20,46,47]. Amino acid sequences of potassium channel selectivity filters are remarkably conserved; what the X-ray studies have shown is that backbone carbonyl oxygens from these conserved residues project into the pore to form a rigid structure that mimics hydration shell oxygen atoms that normally surround potassium ions in solution[39]. This arrangement makes it energetically feasible for surrogate carbonyl oxygen groups to displace hydrating water molecules as potassium ions pass through the pore; due to specificity in hydration shell properties, hydrated sodium or calcium ions cannot effectively permeate and thus selectivity for potassium is achieved. This fundamental pore structure was subsequently adapted to select for sodium and calcium[48,49,50,51,52,53,54], evolutionary events which took place in prokaryotes before multicellularity.

Until very recently, a crystal structure of any sodium or calcium channel has been unavailable, and the mechanisms of ion permeation through these channels have been mostly inferred from mutational studies[55,56,57] and structural modeling using potassium channels as reference scaffolds[43,42,44]. Phylogenetic studies suggest that 4-domain sodium channels evolved from calcium channels[58,9] before the evolution of the nervous system in very primitive animals[59]. In accordance, sodium and calcium permeabilities appear to be closely related[24,59], and only slight alterations in key P-loop

residues can shift selectivity in favor of one these two cations over the other[55,56,24,51]. Calcium channels tend to have negatively charged acidic amino acids (i.e. glutamate or aspartate) in each of the four P-loops that together form a selectivity filter 'ring', with the signature motifs of EEEE or EEDD (DI-DIV; figure 3A and C). Carboxylate oxygens from these residues are expected be somewhat flexible, and are proposed to chelate calcium ions as they pass through the pore[43]. Permeation is facilitated by repulsive forces from incoming calcium ions attracted to the extracellular surface of the pore[43], and selectivity for calcium over sodium is dependent on an optimized interplay between the balancing of negatively charged carboxyl oxygens in the pore by permeant cations, and geometrical constraints that define where these cations can reside[60,43]. In contrast to calcium channels, sodium channels tend to have a mixture of acidic, neutral, and positively charged residues in the selectivity filter ring, such as DEKA (aspartate$^-$, glutamate$^-$, lysine$^+$, and alanine, respectively) in animals with bilateral symmetry (figure 3 A and C) and DKEA/DEEA in more primitive animals[59].

A recent landmark publication documenting the first X-ray structure of a prokaryotic sodium channel, termed Na_vAb[52], has provided some insights into the molecular mechanisms underlying sodium selectivity. The Na_vAb pore is wider than potassium channel pores, and unlike permeation through potassium channels, sodium passes in a hydrated state, with water molecules forming bridges between negatively charged glutamate residues in the pore and resident cations. Sodium is selected over potassium because the larger diameter of the potassium ion decreases the stability of water-glutamate bridges[61].

1.2.3 Voltage-sensitivity

The contribution that the various ion channel modules, in particular the voltage sensor, have made towards nervous system evolution cannot be understated. Indeed, the ability of voltage-gated sodium and potassium channels to sense slight changes in membrane potential and transiently open their gates is critical for the formation and propagation of action potentials, and neurotransmission that permits electro-chemical communication between cells relies on voltage-gated calcium channels. The voltage sensor structure, tethered to the N-terminal side of the two pore helices of the primitive potassium channel, is comprised of 4 transmembrane alpha helices, producing a 6-helix structure with helices named segments 1 to 6 (i.e. S1 to S6; figures 1 and 3). The fourth helix is key for voltage sensitivity of channel gating, as it contains repeating, positively-charged arginine or lysine residues; upon membrane depolarization, these charges impose an outward displacement of S4 helices and conformational changes in the voltage sensor module that transfer to the pore helices and the

activation gate via a S4-S5 linker[27,41,52] (figures 1A and 3A). It is well established that 'On' gating currents can be observed just prior to channel activation, presumably due to an outward displacement of positive S4 charges across the plane of the membrane[27]. 'Off' gating currents also occur after membrane *re*polarization, due to an inward movement of the same charges. The trajectory of positively charged S4 helices upon membrane depolarization is still quite controversial. Based largely on these gating currents, two competing models emerged suggesting that S4 charges either completely translocate from one surface of the plasma membrane to the other (i.e. the membrane translocation model), or the voltage sensor merely undergoes conformational changes that exposes them to either side of the membrane (i.e. the local field model)[27]. The two models have been somewhat consolidated into the sliding-helix model, which is gaining favor as the most likely mechanism for voltage-sensor activation. Here, upon membrane depolarization, positively charged S4 helices rotate or corkscrew outwards while retaining their transmembrane localization; a process made energetically feasible through sequential ionic-pairing between cationic S4 residues and negatively charged counterparts present within S1-S3 helices of the voltage-sensor module (particularly two negative charges found in S2)[62]

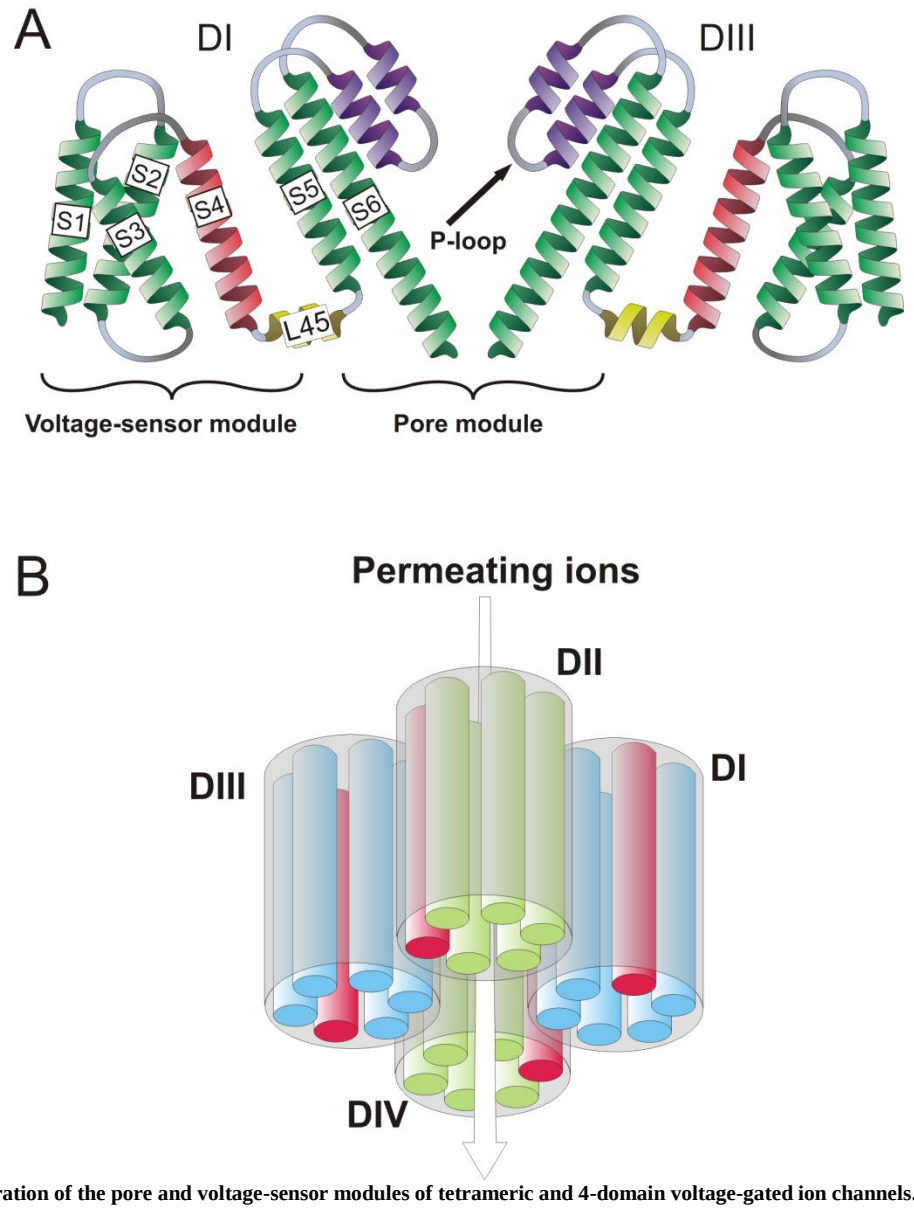

Figure 1. Illustration of the pore and voltage-sensor modules of tetrameric and 4-domain voltage-gated ion channels. A) The channel pore is made up of four subunits or domains, each contributing two transmembrane alpha helices (labeled as helices/segments S5 and S6) and a pore-loop (P-loop; shown in purple) structure that defines ion selectivity. Descending helices of the P-loop are followed by a loop that forms the narrowest part of the pore filter, and contains key amino acids that help define selectivity (known collectively as the selectivity filter). Sodium channels (and likely calcium channels), have a second ascending helix following the selectivity filter[52]. The gate is formed at the apex of the four S6 helices, which form an inverted teepee structure that projects into the cytoplasm and restricts ion permeation in the closed state. Only two of four subunits/domains are illustrated for clarity (i.e. DI and DIII). For voltage-gated channels, each subunit/domain also contains a voltage sensor module, made up of four alpha helices, with the fourth helix containing positively charged arginine and lysine residues critical for voltage sensitivity (shown in red). Conformational changes in the voltage-sensor are thought to transfer to the pore module via an S4-S5 linker (L45), allowing the apical S6 helices to transiently create an ion permeation pathway. **B)** Rough illustration of the coming together of four subunits/domains (DI-DIV) to form a tetrameric ion conducting pore in voltage-gated channels (S4 helices in red). Permeation can occur in both directions depending on voltage and ionic gradients, however, mechanisms that establish preferential inward or outward currents are common, producing inward- or outward- rectifying channels, respectively.

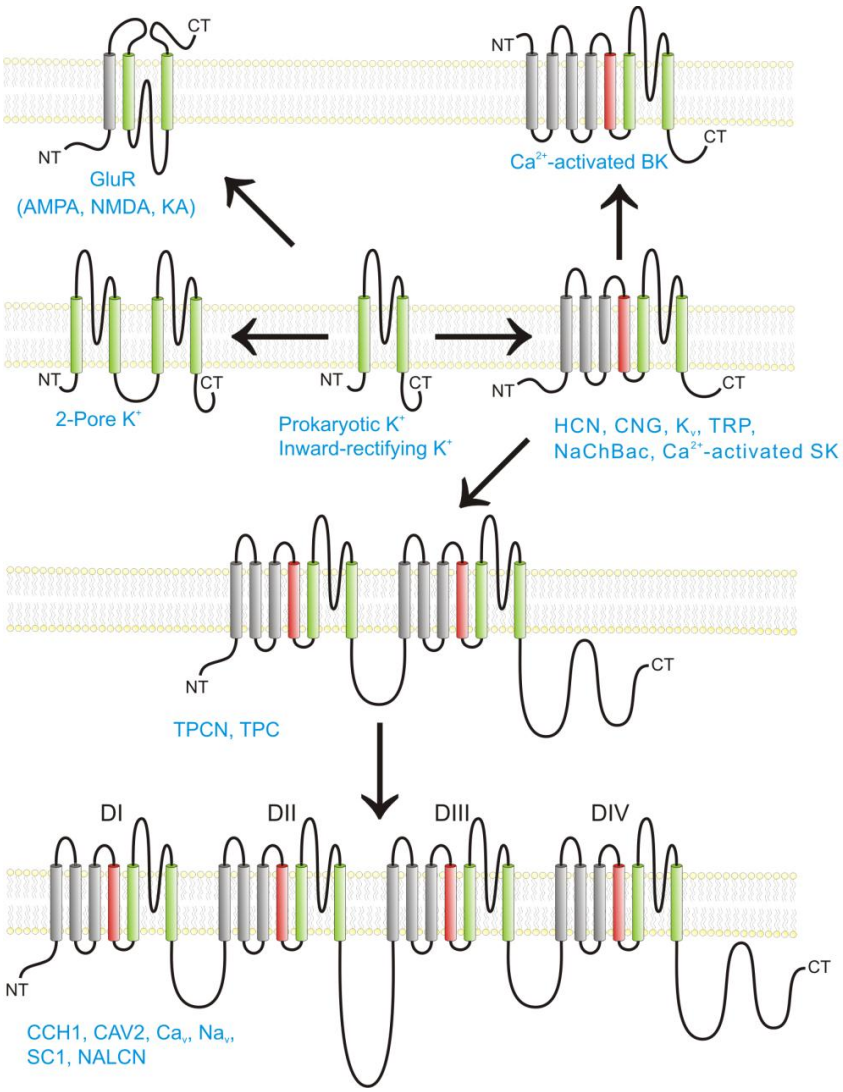

Figure 2. Proposed evolutionary lineages of various ion channel types from ancestral prokaryotic homotetrameric potassium channels. The basic prokaryotic potassium channel consists of four subunits, each with two transmembrane pore-forming helices. This ancestral pore module is highly conserved in vertebrate inward-rectifying potassium channels, as well as many other eukaryotic and prokaryotic channels that conduct potassium, sodium, and/or calcium. Evolutionary alterations in the pore region allowed for selectivity for other cations such as sodium and calcium. The voltage sensor module, made up of four alpha helices, is also of prokaryotic origins, and is coupled to the N-terminus of the pore module in prokaryotic and eukaryotic voltage-gated channels (although some channels have lost their voltage-sensitivity, such as the *t*ransient *r*eceptor *p*otential or TRP channels[63]). The fourth helix (red) of each voltage sensor contains positively charged amino acids critical for coupling voltage changes to channel gating. Additional modules, not shown here, couple the detection of ligands such as calcium (e.g. small conductance/SK and big conductance/BK potassium channels), cyclic nucleotides (e.g. HCN and CNG channels), or neurotransmitters (e.g. glutamate-gated channels GluR) to gating of the pore. Tandem duplication of the two-helix pore module produced the dimeric two-pore potassium leak channels, and inversion plus addition of an additional helix gave rise to postsynaptic glutamate-gated channels. Duplication of the voltage-gated channel subunit, exclusively in eukaryotes, gave rise to *t*wo-*p*ore *c*hannels in animals (TPCN) and plants (TPC), and a subsequent duplication of a similar two-pore ancestor gave rise to the four-domain voltage-gated sodium and calcium channels as well as NALCN. Only fungi (i.e. CCH1 calcium channel), protist choanoflagellates (i.e. CAV2 calcium channels), and metazoans (voltage-gated sodium and calcium channels, and NALCN cation channel) have been found to contain 4-domain ion channels.

1.3 Ca_v3 (T-type) voltage-gated calcium channels

The following section highlights some key and defining features of Ca_v3 channels pertinent to this thesis. For a more detailed review, please see Senatore *et al*., 2012[64].

1.3.1 Classification of voltage-gated calcium channels

Since Hodgkin and Huxley's initial description of the ionic basis of the action potential, much progress has been made to define the molecular elements underlying this and other bio-electrical phenomena, namely gene-encoded proteins such as ion channels, ion channel receptors, ion pumps, et cetera. Biochemical and molecular studies have been instrumental to this end, where researchers have been able to identify, clone and express specific cDNAs in semi-isolated conditions for characterization (e.g. mammalian Ca_v3 channels[65,66,67]). Additionally, the recent explosion of available genomic sequences is providing unprecedented insights into the relatedness and evolution of relevant genes and their products across the tree of life. With respect to voltage-gated calcium channels (VGCCs), mammals have ten genes, and these are grouped into 3 families (Ca_v1, Ca_v2, and Ca_v3) based on amino acid sequence similarity[68] (figure 4A). Voltage-sensitivity provides another distinction, where channels that activate in response to only slight depolarizing inputs (i.e. low voltage-activated or LVA) comprise the Ca_v3 family, and channels that require stronger depolarizations (i.e. high voltage-activated or HVA) make up the Ca_v1 and Ca_v2 families (figure 4B). These divergent properties allow LVA and HVA channels to provide distinct contributions in cells (see figure 4B). Mammals have three Ca_v3 channel genes ($Ca_v3.1$, $Ca_v3.2$, and $Ca_v3.3$), whose products are otherwise known as 'T-type' channels since they conduct *t*ransient barium currents with *t*iny unitary conductances, four Ca_v1 or 'L-type' channels that have *l*ong lasting currents with *l*arge unitary barium conductances ($Ca_v1.1$-1.4), and three Ca_v2 or 'non-L-type' channels further classified as 'N-type' for *n*euronal and of i*n*termediate conductance (i.e. $Ca_v2.2$), 'P/Q-type' for cerebellar *P*urkinje and granular neurons (i.e. $Ca_v2.1$), and 'R-type' which are mostly *r*esitant to Ca_v2 blockers and considered to conduct *r*esidual non-L-type currents (i.e. $Ca_v2.3$)[69] (figure 4A). Invertebrates such as *Lymnaea stagnalis* possess only single copies from each of the three VGCC gene families[64] (figure 4A), including primitive extant animals lacking muscles and nerves (*Trichoplax adhaerens*)[2], and animals with rudimentary nervous systems (*Nematostella vectensis*)[70]; multiple gene duplication events led to an enrichment of calcium and sodium channel genes in vertebrates[71,72], presumably allowing for the specialization of gene functions inherent with more sophisticated nervous systems.

1.3.2 Distinguishing features of T-type channels

Domain swapping experiments indicate that domains I, III, and IV, but not domain II (figure 3A), define low voltages of activation for the different Ca_v3 channels[73], and account for differences in voltage sensitivity between LVA and HVA calcium channels[74]. Further fundamental distinctions can be found between Ca_v3 and HVA channels. The pore-forming subunits of HVA calcium channels (a.k.a. α_1 subunits) physically interact with accessory β and $\alpha_2\delta$ accessory subunits[75,76,77], which are required for proper membrane localization of the α_1 pore subunit[77], as well as for protection from proteolytic degradation[78]. The β subunit binds α_1 via the alpha-interaction domain (AID) in the cytoplasmic I-II linker, and can alter how channels respond to voltage changes and the speed in which they open (i.e. activation kinetics) or transition to closed refractory states (i.e. inactivation kinetics). Interestingly, Ca_v3 channels have not been shown to require such associations, although a handful of publications suggest that these same accessory subunits might slightly, and perhaps indirectly, alter Ca_v3 channel functionality[79,80,81]. Instead, Ca_v3 channels lack an AID and possess a highly conserved helix-loop-helix structural motif in this analogous region (figure 3A and D), which is critical for preventing channel opening at even lower voltages than normal[82]. This 'gating brake' structure, when disrupted, creates recombinant channels with much faster gating kinetics[83], bringing them even closer in this regard to voltage-gated sodium channels, which interestingly lack a gating brake structure.

Interestingly, Ca_v3 channels are also more permeable to sodium and other monovalent cations than HVA channels, and are less selective for calcium over other divalent cations such as strontium and barium[57,84,85,86]. The selectivity filters of Ca_v3 channels are distinct from HVA channels in that they contain aspartates rather than glutamates in the P-loops of domains III and IV (i.e. EE**DD** vs. EE**EE**; figure 3A and C). Mutating the EEDD motif of $Ca_v3.1$ to EEEE does not fully account for differences in permeation between LVA and HVA channels, indicating that although this particular locus is important, permeation properties are defined by additional aspects of the pore architecture. Unexpectedly, these same studies also reveal another distinction between LVA and HVA channels: $Ca_v3.1$ EEEE mutants exhibit altered biophysical properties[87,88] (i.e. voltage-sensitivity and kinetics), indicating that gating of Ca_v3 channels is partly dependent upon the selectivity filter, in addition to the gate located at the apex of the 'inverted teepee' S6 helices (figure 1A).

1.3.3 Physiological roles of T-type channels

Members of the three VGCC families are often found to have distinct localization in neurons, as well as expression patterns in different cell types, that are in line with generalizations about their

physiological roles[89,90]. Neuronal Ca_v1 channels tend to be concentrated at the soma and proximal dendrites[90] (figure 5), where they help regulate synaptic efficacy and cell survival[91], and famously activate calcium-sensitive signaling pathways to couple excitation to changes in gene transcription[91,14,15,16,77]. Ca_v1 channels also have more general functions including roles in calcium homeostasis, and non-neuronal functions including contributions to hormone secretion and excitation-contraction coupling[91,77]. Ca_v2 channels are mostly neuronal and secretory, where they localize to pre-synaptic terminals (figure 5) and closely associate with calcium-sensitive vesicle release machinery to mediate exocytosis[77].

Such generalized physiological roles have been more difficult to ascribe to Ca_v3 channels, partly because selective blockers have, until very recently[92,93], been unavailable to help tease apart their contributions, and also because single and even double gene knockout studies have presented only mild phenotypes, indicating that Ca_v3 channels are not individually essential for any overt physiological process[64] (although redundancy and compensation might account for this). Their most definitive contribution invokes their low voltages of activation to help regulate the excitability of various cell types, including neurons, muscle, and secretory cells[64,94]. In neurons, Ca_v3 channels often project distally from the soma into the dendritic arbor[89] (figure 5), positioning them to effectively propagate and/or amplify incoming sub-threshold post-synaptic signals towards the soma to facilitate action potential initiation[64]. In thalamic (and other) neurons, Ca_v3 channels are critical for the formation of rhythmic firing patterns called low threshold spikes (LTSs), that gate sensory information from the cortex during non-REM sleep[64,94]. Here, Ca_v3 channels help cyclically depolarize the membrane potential above action potential threshold[94], which triggers discreet bursts of sodium action potentials that propagate to the cortex. Disruption of thalamic Ca_v3 channel activity is associated with sleep disturbances in mice[95,96,97], and augmented activity is associated with abnormal formation of LTSs during consciousness[98] and idiopathic generalized epilepsies[99,100,101]. Importantly, gene knockout and overexpression studies have validated these causalities[95,102,96,97,103]. Ca_v3 channels are also important in regulating the excitability of peripheral neurons, such as dorsal root ganglion neurons that transmit nociceptive (pain) signals to the spinal cord towards the brain. Here, $Ca_v3.2$ channels enhance somatic excitability, increasing the likelihood that nociceptive signals are transmitted[104,105,106].

In addition to regulating excitability, Ca_v3 channels contribute to other processes including cell division, exocytotic secretion, smooth muscle tone, and excitation-contraction coupling in cardiac and

smooth muscle cells[94,64]; however the significance and degree of their involvement is debated. Mammalian embryonic cardiac myocytes have underdeveloped transverse tubules (T-tubules), structures that in adults functionally couple membrane-localized L-type VGCCs ($Ca_v1.2$) to endoplasmic reticulum (ER)-localized calcium-induced calcium release (CICR) machinery, an association critical for excitation-contraction coupling during heart contraction. Development of T-tubules coincides with a dramatic reduction of Ca_v3 channel expression in cardiac myocytes from embryo to adult, and Ca_v3 channels are proposed to contribute to early forms of contractile activity, before T-tubule development[107,108]. Cardiac Ca_v3 channels persist somewhat in adults of smaller mammalian species[109], where they are relegated to pace-making roles in the sinoatrial node[107,108]. Invertebrates might rely more heavily on Ca_v3 channels for contraction of both striated and smooth muscle cells. Significant LVA calcium currents have been recorded in jellyfish muscle[110] and mature snail ventricular myocytes[111], and the *Caenorhabditis elegans* T-type channel CCA-1 significantly contributes to excitation-contraction coupling and the shape of muscle cell action potentials[112,113].

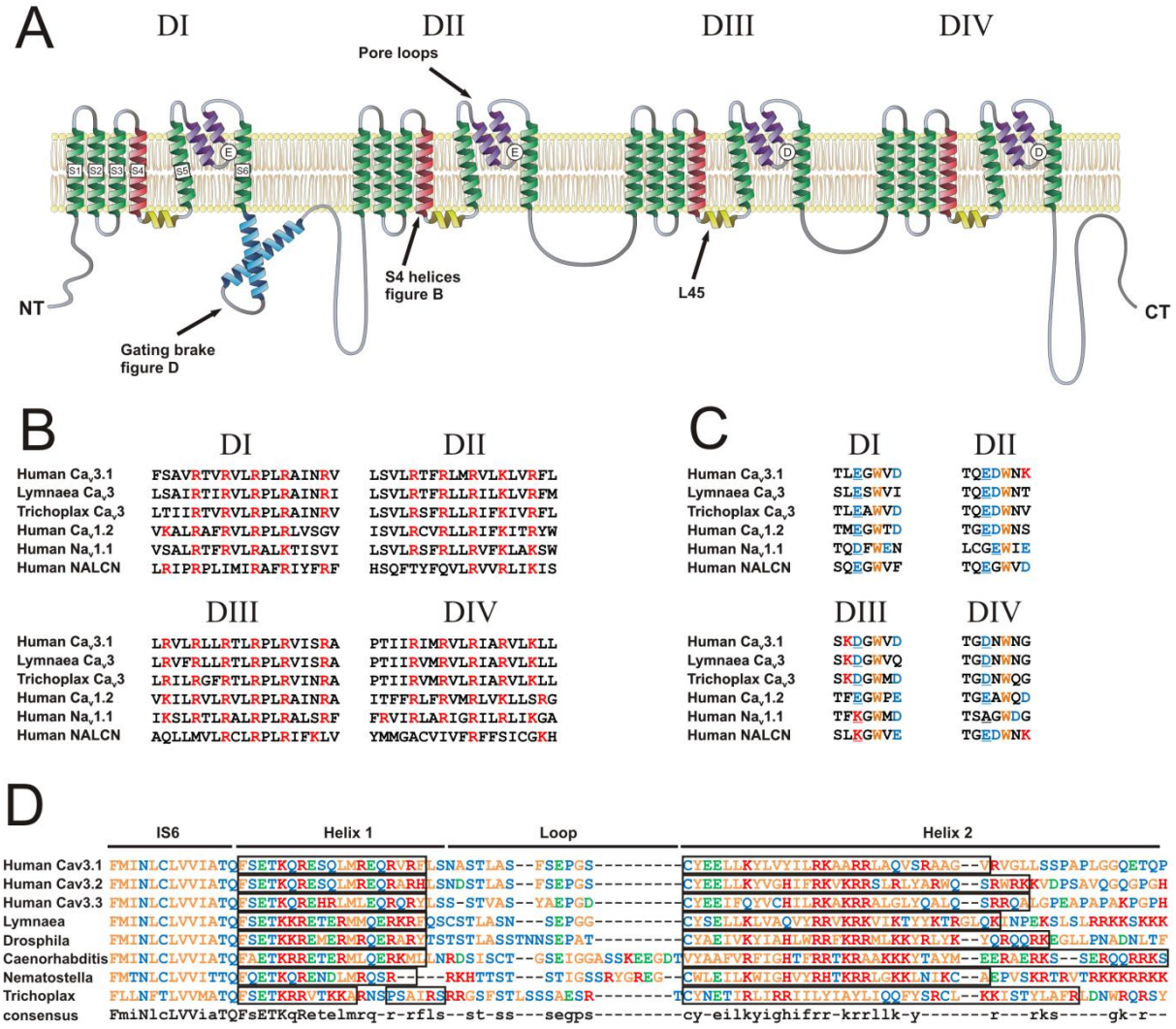

Figure 3. Key features of Ca_v3 voltage-gated calcium channels. A) Schematic illustration of the expected membrane topology and general secondary structure of Ca_v3 4-domain calcium channels. Four repeat domains (DI-DIV) each contain six transmembrane helices (S1-S6). S1-S4 make up the voltage sensor of each domain, with the S4 helix (red) bearing repeating positively charged arginine and lysine residues critical for voltage sensitivity, **(B)** conserved with Ca_v3 channels from other species (e.g. snail *Lymnaea stagnalis* and placozoan *Trichoplax adhaerens* Ca_v3 homologues) and other voltage-gated ion channels such as high voltage-activated calcium channels (e.g. human $Ca_v1.2$), voltage-gated sodium channels (e.g. human $Na_v1.1$), and cation leak channel NALCN. **C)** The pore loops from each domain together form the selectivity filter, a region that forms the narrowest part of the permeation pathway and defines ion selectivity. The Ca_v3 channel filter consists of an EEDD motif (underlined; also depicted in A); high voltage-activated channels have EEEE; while metazoan sodium channels have DEKA (e.g. Nav1.1) or DKEA (not shown). The NALCN cation leak channel has an EEKE motif in vertebrates and other invertebrates, in what is believed to be a hybrid between calcium (EEEE) and sodium (DEKA) filters. **D)** The gating brake, a predicted helix-loop-helix motif critical to restrict channel gating at very negative potentials[82] (also depicted in A), is highly conserved amongst Ca_v3 channels from across the animal Kingdom (e.g. human, snail, fruit fly, nematode, cniderian, and placozoan). The boxes depict predicted alpha helices, separated by a loop to make the proposed helix-loop-helix motif (using PSIPRED: http://bioinf.cs.ucl.ac.uk/psipred/). Positively charged amino acids are shown in red, negatively charged in green, hydrophobic in orange, and hydrophilic/other in blue. This figure has been reproduced, with permission, from Senatore *et al*., 2012[64]. Copyright Wiley-VCH Verlag GmbH & Co. KGaA.

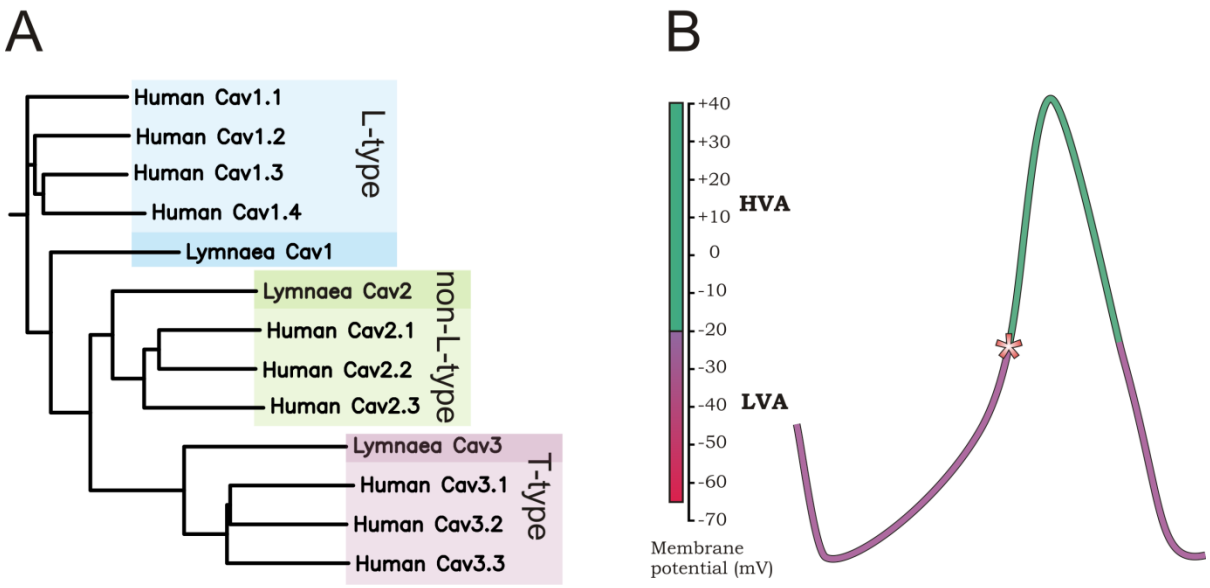

Figure 4. Classification of voltage-gated calcium channels. A) Based on amino acid sequence similarity, three families of metazoan voltage-gated calcium channels have been designated as L-type or Ca_v1, non-L-type or Ca_v2, and T-type or Ca_v3[68]. Pond snail *Lymnaea stagnalis*, like most invertebrates, contains only a single representative for each of the three calcium channel families[64]. Gene/genomic duplications in vertebrates/mammals produced ten calcium channel genes (four L-type, 3 non-L-type, and three T-type), each adopting specialized functions. **B)** Another major classification scheme for voltage-gated channels is their voltages of activation. L-type and non-L-type channels are mostly high voltage-activated (HVA), and require strong depolarizations from rest to become activated, while T-type/Ca_v3 channels require only slight depolarizations and are thus referred to as low voltage-activated (LVA) channels. These properties endow the channels with distinct contributions to cellular excitability. Ca_v3 channels, due to their low voltages of activation, tend to enhance depolarization from rest towards action potential threshold (red star), are thus often associated with regulating excitability. HVA channels on the other hand play a prominent role after action potential initiation, where they conduct calcium to couple excitation to various processes such as secretion and contraction, as well as influence the shape of action potentials by contributing a more long lasting depolarization that serves to prolong depolarization and widen action potentials[114,113]. Conversely, LVA and HVA channels can activate calcium-sensitive potassium channels such as BK and SK[114,64,113], which can lead to quick repolarization and constriction of action potential width.

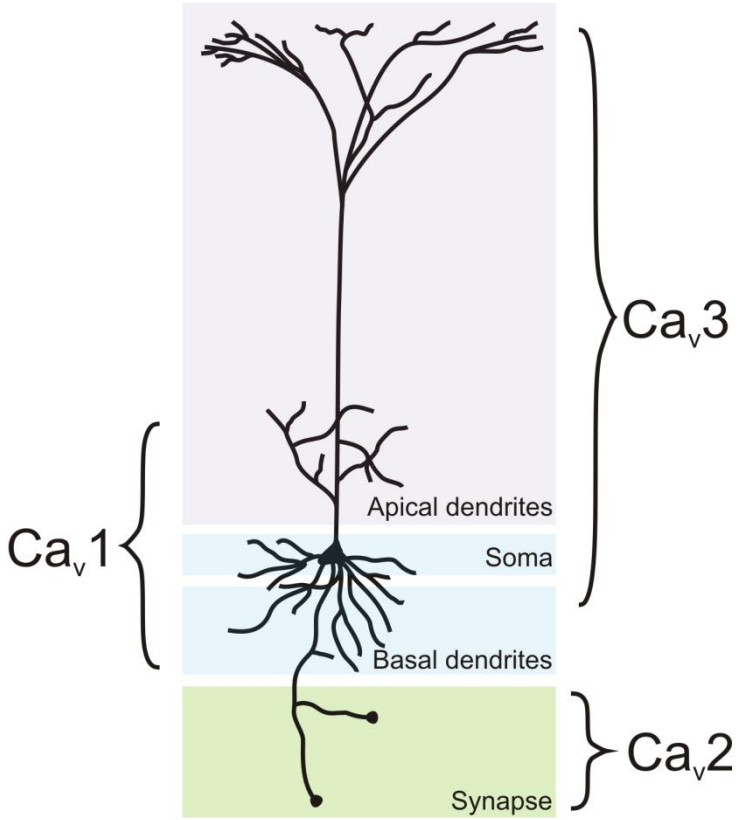

Figure 5. Generalities in the localization and function of neuronal Ca$_v$ channels. Ca$_v$2 channels (i.e. Ca$_v$2.1 and Ca$_v$2.2), are classically associated with presynaptic excitation-secretion coupling of neurotransmitters, via close association with calcium-sensitive exocytotic machinery[77]. Ca$_v$1 channels are often found in the soma and proximal dendrites, where they contribute to excitability and are important for excitation-transcription coupling that allows for adaptive changes in neurons[16,14,15]. Ca$_v$3 channels have prominent localization in the soma and dendrites, and in many neurons they are found far into the distal dendritic arbor[89], where they are poised to regulate somatic excitability and amplify distal incoming synaptic excitatory signals to initiate action potentials[64].

1.4 NALCN channels

1.4.1 Discovery and initial characterization of the NALCN channel complex

The first evidence for the existence of NALCN channels was provided by *Drosophila* geneticist Hermann Muller during his classical X-ray mutagenesis studies in the 1930s[115]. 70 years later, researchers identified the genetic locus for Muller's '*narrow abdomen*' allele[116], and found that the lesion deleted 9 nucleotides within the domain I S2 coding sequence of a unique homologue of 4-domain P-loop channels, representing a distinct family designated as NALCN in the mammalian nomenclature[117,118,119,120]. Besides the narrow abdomen phenotype, the *narrow abdomen* allele also produced disrupted and uncoordinated movement, as well as abnormalities in locomotory responses to changing light conditions[116]. The latter was associated with accumulation of circadian clock effector neuropeptide *p*igment-*d*ispersing *f*actor (PDF) in circadian pacemaker neurons, which bear otherwise undisrupted molecular clocks, consistent with failed exocytosis of PDF[121]. Two other mutant alleles, previously associated with increased sensitivity to the immobilizing action of volatile anesthetics (i.e. *har38* and *har85*; for altered *ha*lothane *r*esistance)[122], also mapped to the *Drosophila* NALCN channel gene[116]. Interestingly, both the *har* and the *narrow abdomen* alleles in *Drosophila* produce phenotypes akin to those in *C. elegans* bearing the mutant alleles *unc-79* and *unc-80*, with analogous locomotory defects (hence *unc*oordinated or unc mutants) and increased sensitivity to volatile anesthetics[123,124,125]. Subsequent characterization of the *unc-79* and *unc-80* alleles revealed that the underlying lesions altered two previously unidentified genes, conserved in other invertebrate and vertebrate animals, termed respectively Unc-79[126] and Unc-80[127,128].

Notably, although genetic screens in *Drosophila* and *Caenorhabditis* identified multiple genes that alter sensitivity to anesthetics, mutations in NALCN (i.e. *Drosohphila*'s *narrow abdomen* allele) and Unc-79/ Unc-80 in *Caenorhabditis*, distinguished themselves in that they produced little to no sensitivity to anesthetics with poor lipid solubility (e.g. enflurane), but considerable sensitivity to those with high lipid solubility (e.g. halothane)[129,123]. This phenotypic link, in addition to the similar defects in locomotion, prompted researchers to assess the possible epistatic relationships between NALCN, Unc-79, and Unc-80[130,131,132,127,128,126]. These studies have conclusively shown that 1) the three genes and their protein products are epistatic, and the proteins interact to form a functional unit[133,130,132,134,127,128,126], 2) NALCN, UNC-79 and UNC-80 post-transcriptionally regulate each other's expression levels and subcellular localization (primarily non-synaptic along axons; punctate patterns suggestive of internal vesicular localization or clusters at the membrane)[127,128,126], and 3)

UNC-80 serves as a scaffold for the recruitment of *sarc*oma tyrosine kinases (SRCs) to the channel complex, which directly interact with and phosphorylate NALCN to regulate its function[131,118,132].

1.4.2 Unique features of NALCN channels revealed by sequencing and cloning

PCR-screening of mammalian cDNA libraries, using degenerate primers designed against an *in silico* predicted and yet undefined 4-domain ion channel protein from the *Caenorhabditis elegans* genome (i.e. predicted protein C27f2), was used to successfully identify and clone the first NALCN channel cDNA from rat brain[135]. C27f2, another *Caenorhabditis in silico*-predicted protein C11D2, and the cloned rat homologue grouped into a novel 4-domain ion channel family (i.e. NALCN; figures 6A and 8), that was distinct but related to voltage-gated calcium and sodium channels[135] (*Caenorhabditis elegans* is extremely rare in that it has two NALCN genes, Nca-1/C11D2 and Nca-2/C27f2, whereas most vertebrates and invertebrates have only one gene). In spite of this relatively early molecular identification, the NALCN family has proven extremely difficult to characterize in terms of its ion channel properties (i.e. voltage-dependence, kinetics, and ion selectivity)[65,136,127,121], and it was not until 20 years later that researchers presented successful heterologous expression and characterization of NALCN as a voltage-independent, non-specific cation leak channel[137].

Structurally, NALCN can be distinguished from related voltage-gated sodium and calcium channels by several means, most strikingly by differences in the P-loop selectivity filter residues that define ion selectivity (see below; figures 6A and 7), and by a significant reduction in the number of positively-charged residues in the voltage-sensor S4 helices, especially those from domains III and IV[65,137] (figure 6A and B). In the closed state, cationic S4 charges (i.e. arginine and lysine) of voltage-gated channels are proposed to interact with negatively charged glutamate and aspartate residues present in other helices of the voltage-sensor module (i.e. S1-S3; figures 6 and 7), stabilizing S4 helices in the membrane as long as the cell interior is more negatively charged than the exterior[62]. Upon depolarization, electrostatic forces keeping the S4 helices in the membrane are relieved, and S4 is proposed to 'corkscrew' in an outward direction, such that S4 cationic charges are sequentially counter-balanced by the negatively charged S1-S3 residues[62]. The force of this movement is expected to transfer to the S5 and S6 pore helices that gate the pore, leading to channel opening via kinking of the S6 helix[62]. Bearing this in mind, the characterization of NALCN as a completely voltage-independent channel[120] is slightly unexpected, given that although there is a reduction in positive S4 charges, there still remain a significant number of these, as well as conserved negatively charged counter-ion residues in S1-S3[135] (figure 7). The absent S4 charges in NALCN tend to occur in the

most extracellular positions along S4 helices (figure 6B), which when neutralized in voltage-gated sodium, calcium, and potassium channels, disrupt (but do not abrogate) voltage-sensitivity, and in addition create channels that conduct pathological proton[138] and/or cation leak currents directly through the voltage sensors (termed gating pores)[139,140,141,62]. Such mutations in skeletal muscle $Ca_v1.1$ and $Na_v1.4$ are associated with small but constitutive monovalent cation leak currents at rest (i.e. negative membrane potentials)[142] that are associated with the disease hypokalaemic periodic paralysis[139,62]. Whether cation or proton gating pore currents occur in NALCN channels remains to be shown. Indeed, the complete voltage-insensitivity reported for NALCN might result from additional structural features that have yet to be defined.

The first molecular characterization of NALCN also revealed that the selectivity filter is distinct from 4-domain calcium (EEEE and EEDD) and sodium (DEKA and DEEA) channels, bearing what has been proposed to be a hybrid between these two pore configurations[143,135,120] (i.e. EEKE; figures 6A and 7). Mutation of a HVA calcium channel EEEE pore to EEKE changes the selectivity from calcium to monovalent sodium and potassium[144]. Importantly, evolutionarily- and structurally-related sodium and calcium channel selectivities[59,24] are determined not only by the nature of charged residues present within the filter and surrounding regions, but also by spatial constraints that define how ions are able to 'fit' within the pore as they pass through[43,60]. The complexity of permeation is well exemplified by the prokaryotic tetrameric voltage-gated sodium channel NaChBac[48], which, despite having four glutamate residues in the selectivity filter, conducts a sodium-selective current[25]. In addition, mutation of calcium-selective $Ca_v3.1$ from EEDD to EEDE/EEED unexpectedly renders the channel highly permeable to monovalent cations[57]. Given these exceptions, it is difficult to assess or predict permeability based purely on pore sequences, and functional characterization has been essential to define NALCN as a non-specific cation leak channel[143,120].

Another interesting feature, that is difficult to speculate on but worth mentioning, is an apparent lack of glycine and/or proline residues in S6 helices from domains I and II of NALCN, which are conserved in most 4-domain voltage-gated sodium and calcium channels (figure 7), as well as tetrameric potassium and sodium channels[40,25]. Instead, NALCN homologues contain several glycine residues in domain III S6 (figure 7). X-ray crystallographic studies suggest that these amino acid motifs provide inflection points that allow S6 helices to bend upon channel activation, opening the ion permeation pathway[40,25]. Mutating these residues to alter S6 flexibility significantly impacts

channel gating[145,146,147], however, the existence of channels that lack such motifs[147] indicates that they are not an absolute requirement.

1.4.3 Physiological roles of NALCN, Unc-79, and Unc-80 in invertebrates

NALCN is abundantly expressed in the nervous systems of both mammals and invertebrates[148,135,118,120,127,128,121,116], and moderately expressed in mammalian heart and some secretory glands/organs (e.g. pituitary gland and pancreas)[135,118]. Unfortunately, although knockouts of NALCN/Unc-79/Unc-80 produce strong and characteristic phenotypes, the molecular details underlying these physiological changes remain somewhat enigmatic. In invertebrates, NALCN mutants display uncoordinated movement, difficulty in transitioning to high frequency movements such as escape and swimming, abnormal circadian behaviors, and increased sensitivity to volatile anesthetics. It is notable that all of these phenotypes can be, directly or indirectly, correlated to decreased presynaptic activity and exocytosis (see below).

At the *C. elegans* neuromuscular junction, disruption of NALCN and Unc-80 reduces presynaptic excitability and exocytosis of neurotransmitter, resulting in attenuated postsynaptic responses (i.e. reduced spontaneous mini post-synaptic currents at rest and evoked postsynaptic currents during nerve stimulation)[148,127,128]. Mutation of another unc gene, unc-26/synaptojanin (a lipid phosphatase that degrades phosphatidylinositol 4,5 bisphosphate; required for synaptic vesicle recycling), results in presynaptic structural abnormalities, severe uncoordination, and a marked depletion of presynaptic vesicles presumably due to failed recycling[149,128]. Notably, the locomotory defects and loss of vesicles can be suppressed by concurrent knockout of NALCN, Unc-79, or Unc-80[128], without alleviating structural abnormalities. Accordingly, knockout of just NALCN or its subunits increases presynaptic vesicles and reduces neuromuscular transmission in an otherwise wildtype background[128]. Taken together, these observations indicate that in the wildtype condition, NALCN activity enhances neurotransmission by promoting exocytosis, and in mutants, the absence of NALCN function causes reduced exocytosis and vesicle accumulation. Indeed, the role of NALCN in circadian control of locomotory behavior in *Drosophila*, attributed to presynaptic accumulation of circadian clock effector peptide PDF[121], could be due to reduced exocytosis of PDF in NALCN knockouts. However, whether NALCN's contribution is indirect (e.g. by conducting depolarizing leak currents to facilitate activation of presynaptic VGCCs that are coupled to the exocytotic machinery), or more direct (e.g. by regulating vesicle recycling/homeostasis or the exocytotic machinery), is not clear.

In *C. elegans*, double knockout of NALCN subunits with various other genes intimately involved in exocytosis (i.e. VGCC Ca_v2/unc-2, syntaxin/unc-64, and synaptotagmin) does not consistently suppress nor enhance exocytotic defects[128], suggesting that NALCN is not a central component of the secretory apparatus. However, overexpression of a gain-of-function NALCN, containing an arginine to glutamine mutation just downstream of domain I S6, causes overexcitability and developmental defects in presynaptic active zones[150,148,127] (sites of vesicle docking and neurotransmitter release[151]). Interestingly, a similar phenotype can be created by knocking out unc-7, an invertebrate gap junction gene homologous to vertebrate pannexins, and concurrent knockout of NALCN alleviates the active zone abnormalities and overexcitability[148]. Here, NALCN seems to be more intimately associated with presynaptic exocytosis, where excessive NALCN activity leads to active zone defects and excessive neurotransmission. In the wildtype condition, gap junction protein Unc-7 likely opposes NALCN's positive influence on secretion, and loss of unc-7, or expression of a gain-of-function NALCN, tips the balance in favor of NALCN leading to presynaptic abnormalities and overexcitability. Clearly, more research is needed to delineate NALCN's presynaptic contributions to excitability and secretion; however, the data convincingly implicates the channel in these processes. It is interesting that one of the main actions proposed for volatile anesthetics, for which mutants of NALCN, Unc-80, and Unc-79 show increased susceptibility, is to attenuate presynaptic neurotransmitter release[152,153,154,155,156]. Researchers interested in the relationship between NALCN's and halothane's presynaptic effects on exocytosis failed to show a link[156], however, all of their electrophysiological recordings were carried out in low extracellular calcium (0.5 mM), a condition shown by others to mask NALCN's contribution to synaptic transmission[128].

1.4.4 Physiological roles of NALCN, Unc-79, and Unc-80 in mammals

Knockout of NALCN in mice does not produce drastic developmental defects in the embryo; however, mice die within 24 hours after birth and have severely disrupted respiratory rhythms, attributed to reduced electrical activity in spinal nerves that innervate the diaphragm[120]. Since multiple gene knockouts in mammals are far more difficult, there is no confirmatory evidence yet that the epistatic relationships, identified in invertebrates for NALCN, are evolutionarily conserved (e.g. Unc-79, Unc-80, synaptojanin, Unc-7, etc.[152,148,133,124,125,127,128,126]). However, ablation of just Unc-79 is also perinatal lethal[157,130], and interestingly, heterozygous knockout mice are more susceptible to alcohol[130], a phenomenon also observed in *C. elegans* knockouts of Unc-79, Unc-80, and NALCN[158,130]. In addition, Unc-79 heterozygous knockout mice are smaller, have less body fat, and

consume more food than wildtype littermates, consistent with increased metabolic rates and energy usage. It is tantalizing to speculate that Unc-79 and the NALCN complex might have some link to mitochondrial function. Interestingly, mitochondria represent another key target for volatile anesthetics[159,152], and in *C. elegans*, halothane is reported to accumulate more readily in the mitochondria of Unc-79 knockout animals than wildtype[152].

Cultured rodent and snail neurons, possessing either a knockout of NALCN (i.e. mouse hippocampal neurons) or RNA-mediated gene knockdown (*Lymnaea stagnalis* RPeD1), have significantly hyperpolarized resting membrane potentials, suggesting that the channel has a role in depolarizing cells[160,120]. Also, the increased sensitivity of *C. elegans* NALCN mutants to anesthetics can be partially suppressed by depolarizing neurons with light-activatable channel rhodopsins[161], so increased susceptibility is in part due to membrane hyperpolarization in NALCN knockouts. All of these data are consistent with assertions that wildtype NALCN conducts tonically depolarizing sodium leak currents into cells to help set the resting membrane potential of most neurons[143,120]. The most compelling evidence for this comes from the heterologous expression of rodent NALCN in cultured HEK-293T cells, where in the absence of accessory proteins Unc-79 and Unc-80, NALCN is reported to conduct constitutive leak currents[120,143]. However, an important caveat should be considered: even though NALCN-mediated constitutive leaks are proposed to be minute, in the long term they would be energetically costly, undermining the efforts of the ATP-dependent Na^+/K^+-ATPase. In fact, excessive sodium influx is often associated with disease[162,139], and as such leak conductances should be tightly regulated *in vivo* to prevent adverse effects. In accordance, the NALCN complex seems to be tightly regulated via G protein-coupled receptors (e.g. Takykinin/neurotensin receptor 1[132] and muscarinic acetylcholine receptor M3[118]), which, upon ligand binding, activate the channel in non-canonical, G-protein independent pathways that recruit SRC kinases to phosphorylate NALCN and Unc-80[118,132,134]. Conversely, calcium-sensitive G protein-coupled receptors have been reported to tonically inhibit NALCN, in this case, directly via activated G-proteins[134].

Of note, even though the experimental evidence strongly supports a role for NALCN in directly mediating depolarizing leak currents, there are alternate explanations for the data that are worthy of examination. For example, it has yet to be assessed whether NALCN-mediated depolarization might be attributable to *indirect* consequences of NALCN function, such as alterations to mitochondria and ATP production, and/or altered activity of the Na^+/K^+-ATPase, or alterations in the activity of other

ionic conductances that influence resting membrane potential, such as potassium channels (e.g. see Lear *et al*., 2005[121]) or cationic hemichannels (e.g. see Bouhours *et al*., 2011[148]). In addition, some have argued that NALCN does not mediate constitutive leak currents into cells *per se*, but rather, mediates highly controlled and transient depolarizing currents when activated by G-protein coupled receptors[118]. In accordance, the completely voltage-independent and non-specific cation leak currents reported in HEK-293T cells expressing rat NALCN (evidenced by a linear current-voltage relationship, with a reversal of inward-to-outward current occurring at 0 mV)[120], are inconsistent with the inward-rectifying, SRC-activated cation currents subsequently attributed to NALCN in cultured neurons[132], and the SRC-activated and more sodium-selective currents observed in pancreatic β-cell lines[118]. Clearly, NALCN's conductance and physiological contributions remain controversial, and further study is required to definitively characterize these and other properties of the channel.

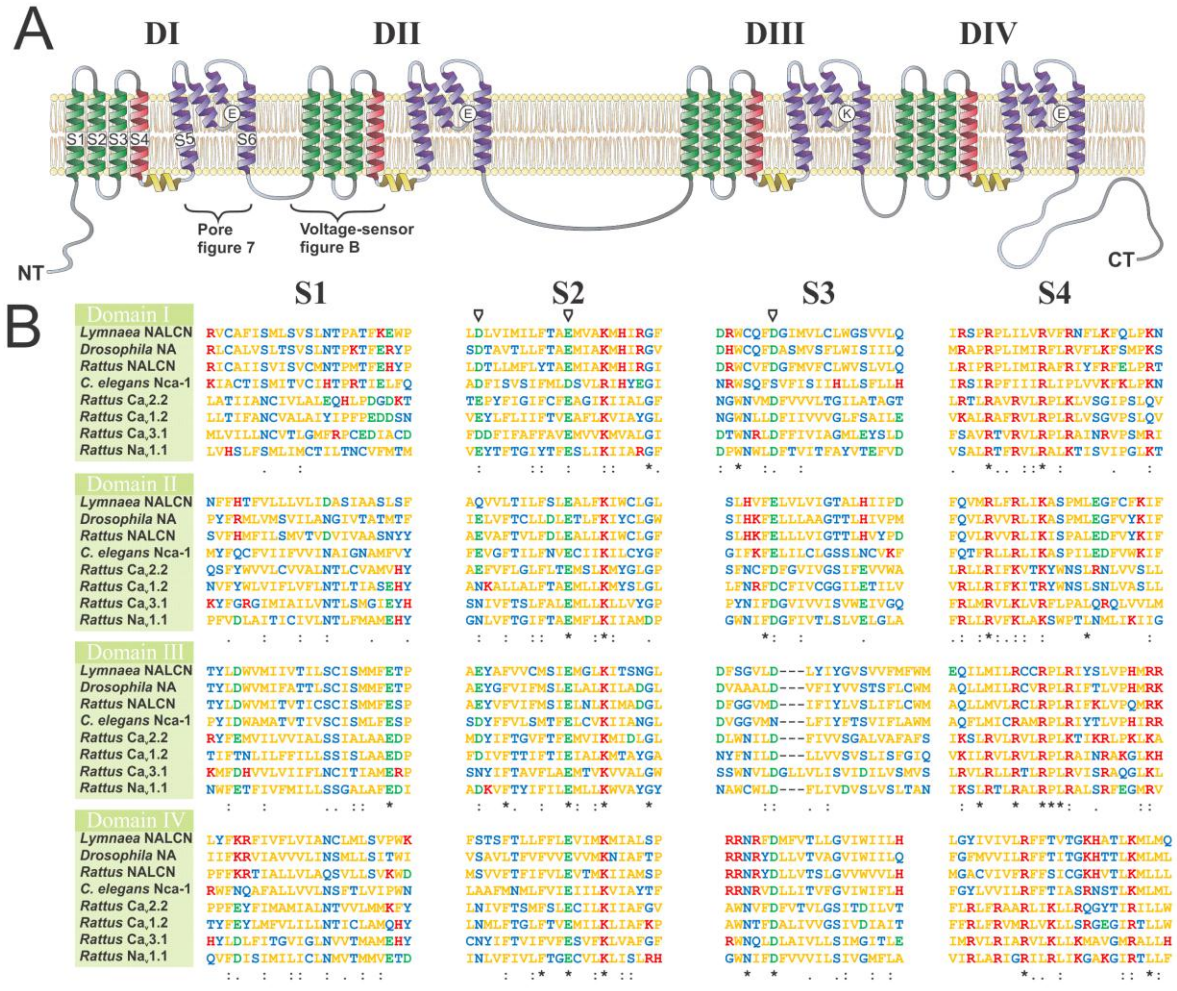

Figure 6. General features of the NALCN channel protein sequence. A) Schematic illustrating the expected membrane topology and some distinguishing features of NALCN homologues. NALCN channels belong to the 4-domain ion channel family, with each domain containing a voltage sensor module and a pore module. The selectivity filter of NALCN in mammals is EEKE, which is conserved with *Drosophila* and *C. elegans* (see figure 7). **B)** Amino acid sequences for the voltage sensor helices from various 4-domain ion channels including NALCN (i.e. snail, fruit fly, rat, and nematode; for accession numbers see figure 8), voltage-gated calcium channels $Ca_v2.2/Ca_v1.2/Ca_v3.1$ (from rat), and voltage-gated sodium channel $Na_v1.1$. Note the highly conserved negatively charged amino acids in the S2 and S3 segments (glutamate E and aspartate D; arrows), proposed to form consecutive counter-ion pairs with positively charged lysine (K) and arginine (R) residues in the S4 helices while they corkscrew out of the membrane during voltage sensor activation. NALCN channels have lost some of the positively charged S4 residues, particularly in domains III and IV, which is expected to alter voltage sensitivity but not necessarily abolish it (see text). Amino acid key: red = positively charged; green = negatively charged; yellow = hydrophobic; blue = hydrophilic/other. Symbols below the aligned amino acids depict the degree of conservation: * identical, : highly similar, . similar.

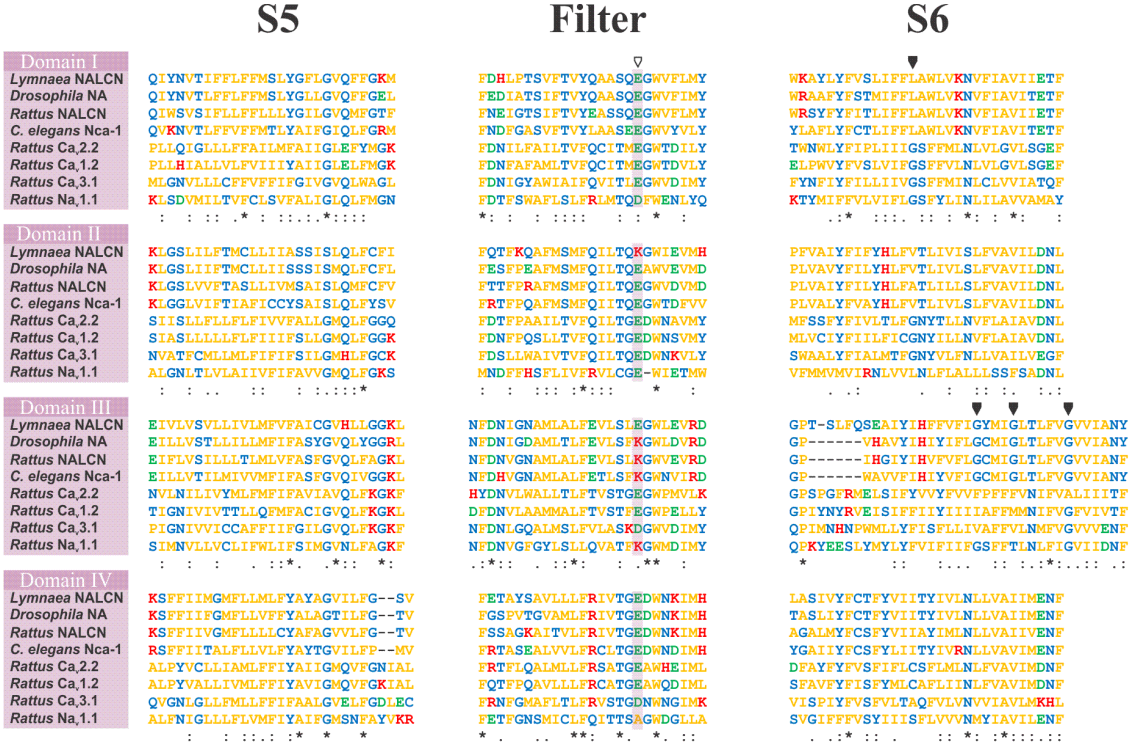

Figure 7. Amino acid sequences for the pore helices and selectivity filters of various 4-domain ion channels. NALCN channels contain an EEKE filter (shaded residues with white arrow, see figure 6A), proposed to be a hybrid selectivity filter between calcium-selective channels (e.g. $Ca_v2.2$, $Ca_v1.2$, and $Ca_v3.1$; EEEE or EEDD), and sodium selective channels (e.g. $Na_v1.1$; DEKA). Interestingly, snail NALCN has an inversion between domains II and III, with an EKEE filter. Note the general absence of glycine residues in S6 helices from domains I and II, but instead the presence of glycines in domain III (black arrows). Glycine and proline residues are proposed to be important for gating, by providing an inflection point in S6 to open the permeation pathway[40,25] (see text). Amino acid key: red = positively charged; green = negatively charged; yellow = hydrophobic; blue = hydrophilic/other.

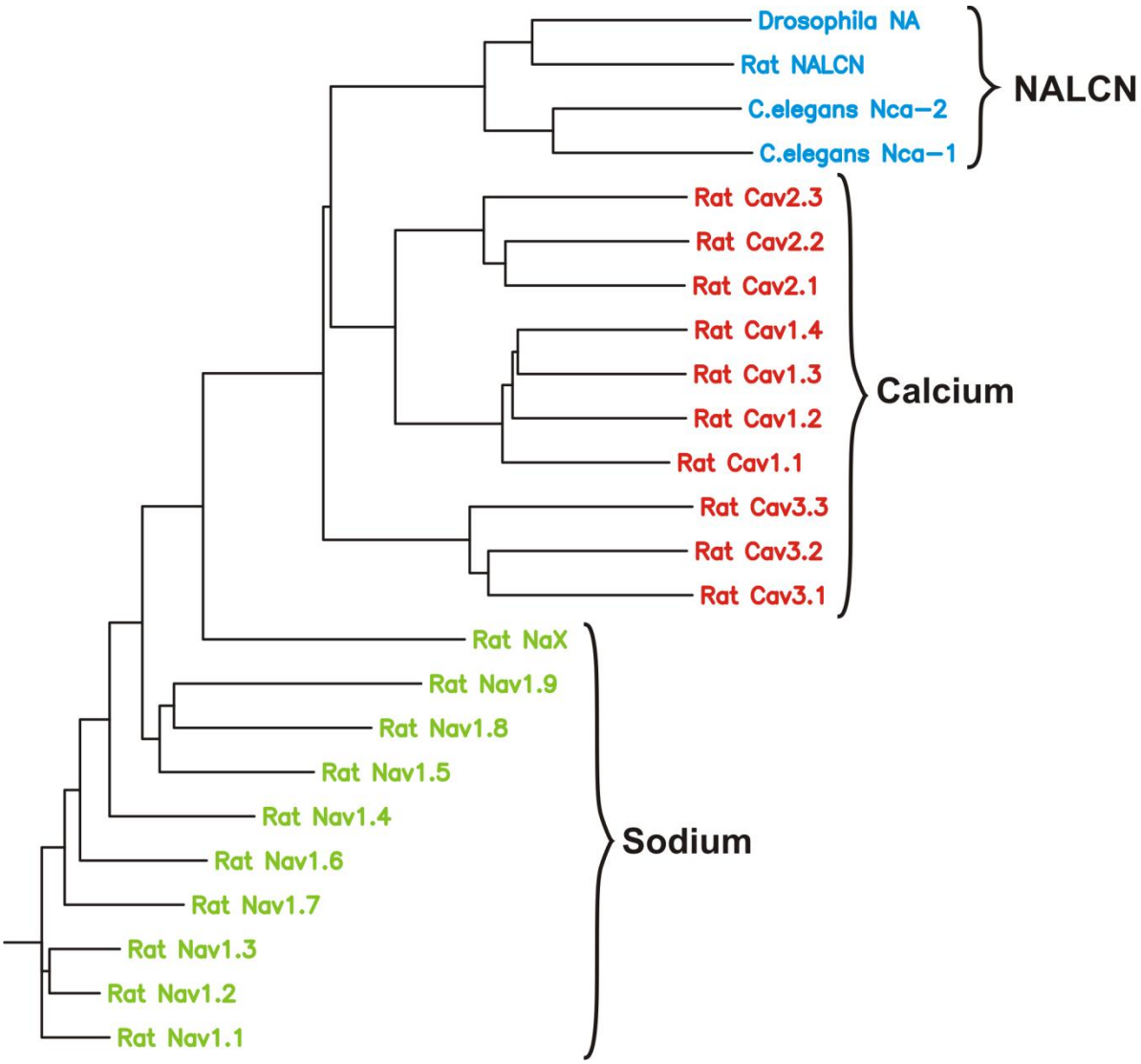

Figure 8. Phylogenetic tree depicting the three main types of metazoan 4-domain ion channels. NALCN, fist discovered in rats and *C. elegans*[135], forms a distinct family of channels conserved across the animal Kingdom. Note the abundance of sodium and calcium channels in mammals (e.g. rat; 10 genes of each channel type), compared to the single copy nature of NALCN. *C. elegans* is extremely rare in that it has two NALCN channel genes, *Nca-1* and *Nca-2*. The narrow abdomen *Drosophila* mutant, produced by Hermann Muller in the 1930s, had an X-ray-induced genetic lesion that was eventually mapped to the NALCN gene (named NA for narrow abdomen)[116]. GenBank ID numbers: 194294538 ($Ca_v1.1$); 158186633 ($Ca_v1.2$); 8393030 ($Ca_v1.3$); 16758518 ($Ca_v1.4$); 158138501 ($Ca_v2.1$); 145553966 ($Ca_v2.2$); 304555571 ($Ca_v2.3$); 24429576 ($Ca_v3.1$); 84028181 ($Ca_v3.2$); 113195659 ($Ca_v3.3$); 116447 ($Na_v1.1$); 6981506 ($Na_v1.2$); 6981510 ($Na_v1.3$); 6981512 ($Na_v1.4$); 6981514 ($Na_v1.5$); 81886863 ($Na_v1.6$); 55976160 ($Na_v1.7$); 56748617 ($Na_v1.8$); 56748616 ($Na_v1.9$); 25742828 (Na_X); 24025650 (rat NALCN); 25144895 (*C. elegans* Nca-1); 373254060 (*C. elegans* Nca-2); and 158031818 (*Drosophila* NA). The multiple sequence alignment used to create the phylogenetic tree was generated with a CLUSTALW algorithm available at SDSC Workbench (http://workbench.sdsc.edu/).

1.5 Modulation of ion channels by alternative splicing

1.5.1 Increasing the information content of genes

Genome sequencing has elucidated an unexpectedly small number of genes for animals (e.g. 20,000 to 25,000 in humans[163]), and no clear correlation between morphological complexity and gene number[164,165], undermining our pre-genomic notion that increased complexity requires more genes. However, homologous genes from different species can encode differing amounts of information[164,163], and complexity arises not only from gene number, but also from the amount of information that individual genes carry (i.e. diversity in how a gene product is expressed, its functionality, or its complexity of integration into protein-protein networks, etc.)[164,165]. There are many ways to diversify information content, at the levels of transcription (e.g. variability in chromatin structure and promoter expression, multiple promoters for one gene), RNA processing (variability in alternative splicing, polyadenylation, RNA editing, mRNA stability and localization), translation (variability in the rate or localization of translation), and post-translation (protein folding, trafficking, cleavage, degradation, phosphorylation/covalent modification, protein-protein interactions, and other molecular interactions). Human proteins tend to have greater functional capabilities (e.g. enzymes with multiple enzymatic activities) than homologues in *Drosophila melanogaster* and *Caenorhabditis elegans*[164,163]. Human genes also undergo more extensive alternative splicing than those in invertebrates (e.g. 90% in humans, 60% in *Drosophila*, 25% in *Caenorhabditis*[166,167,168,169,170]). Plant genes, although generally more numerous[171], undergo considerably less alternative splicing than in animals[172,173]; and prokaryotes have very little alternative splicing[172,173].

Alternative splicing provides the capacity to generate large (or small) alterations in protein structure, within specific tissues, and/or during specific developmental stages. Splicing-induced alterations can have intrinsic effects on a protein, influencing how it behaves (e.g. alterations in ion selectivity, gating, or voltage-sensitivity of ion channels), or can alter motifs used for modulation by other factors (e.g. phosphorylation, calcium-binding, or protein-protein interaction motifs that influence trafficking and/or complex formation, etc.)[174,175,176,177,178,179]. Alternative splicing can also introduce premature translation termination codons into the mRNA, resulting in downregulation of gene expression via nonsense-mediated decay[180], or it can take place outside of the coding sequence, in 5' or 3' untranslated regions (UTRs), influencing mRNA stability and localization[181,182]. Importantly, challenges arise not only from documenting alternative splicing and other forms of gene diversification, but also in determining the physiological significance of these alterations. Often,

alternative splicing seems to have no clear functional purpose, and represents a form of stochastic noise (that can nonetheless serve as a substrate for the evolution of emergent features)[183,180]. In other instances alternative splicing is tightly regulated[180,170], and coincides with changes in physiological states of an animal, such as development, or with distinctions between separate tissues or organs[180]. Also, developmental changes in alternative splicing are often conserved between species (e.g. mammalian vs. avian)[184,185]. Here, pertinent genes are being specifically tailored for different roles in different contexts, and evolutionary conservation of these splicing strategies underscores their physiological importance.

1.5.2 General features of alternative splicing

The spliceosome, a large ribonucleoprotein complex containing 5 highly conserved *s*mall *n*uclear *r*ibo*n*ucleo*p*roteins (snRNPs)[186], is responsible for excising introns and ligating exons together, by recognizing four key *cis* elements on transcribed pre-mRNA: 1) the 5' splice site (a.k.a donor splice site), typically a GU intronic sequence flanking the upstream exon, 2) the 3' splice site (a.k.a. acceptor splice site), typically AG, flanking the downstream exon, 3) the branch site, an adenine nucleotide located ~40 base pairs upstream from the downstream exon, and 4) the polypyrimidine tract, located between the branch site and the 3' acceptor splice site (figure 9A). Other auxiliary *cis* elements along the pre-mRNA are recognized by splicing factors that facilitate or inhibit formation the spliceosome complex to determine specific spatial and/or temporal splicing patterns. There are ~50 of these RNA-binding regulatory proteins in mammals, including serine/arginine (SR) proteins, *h*eterogeneous *n*uclear *r*ibo*n*ucleo*p*roteins (hnRNPs), polypyrimidine tract-binding proteins, and NOVA proteins[187,188,183,185]; alterations in their expression and functionality is responsible for large-scale changes in the transcriptome[187,185]. Indeed, differences in alternative splicing tend to occur on a large scale, involving many different genes, and these differences often reflect physiological transitions or distinctions between various cell types, tissues, or organs[185]. The role of any particular alternatively-spliced gene isoform is therefore highly intertwined with the entire system of alternative splicing and the corresponding protein populations.

There are five main modes in which alternative splicing can take place: 1) exon skipping, where an optional cassette exon is either omitted or included, 2) alternative 5' splice sites, where a second tandem donor splice site is present within the upstream exon, 3) alternative 3' splice sites, where an alternate 3' acceptor splice site is present within the downstream exon, 4) mutually exclusive exons, where either of two or more exons are included in the transcript, and 5) intron retention, where an

intron is retained[183] (figure 9B). Interestingly, alternative splicing in lower metazoans, fungi, and protozoa tends to occur through intron retention, while exon skipping becomes more prominent in increasingly complex animals, suggesting that exon skipping contributes more greatly to phenotypic complexity[172].

1.5.3 Alternative splicing of Ca_v3 channel genes

The human $Ca_v3.1$ channel gene is transcribed from two separate promoters that drive differential expression during neuronal differentiation[189], producing pre-mRNAs with alternative 5' UTRs. Interestingly, the 3' UTR also contains two distinct polyadenylation sites[190,191]. Human $Ca_v3.1$ mRNAs are processed from 38 exons (39 annotated on Evidence Viewer, NCBI), and alternative splicing has been documented in multiple loci along the pre-mRNA sequence[192,190,191,193]. These include optional cassette exons subject to exon skipping, and alternative donor or acceptor splice sites that selectively omit 3' or 5' portions of exons, respectively (figure 9). Rat and mouse $Ca_v3.1$ channel genes are also extensively alternatively spliced, and some loci are conserved with humans, while others appear to be specific for rodents[194,190,191,195]. One particularly interesting locus, alternatively spliced in rodents but not human, corresponds to the cytoplasmic I-II linker of the $Ca_v3.1$ channel protein. Exon 8, in rodents, contains alternative 5' donor splice sites (figure 9B) that can be used to omit 134 amino acids from the I-II linker[194,195] (summary figure A). Exon 8b, the optional portion of exon 8, has a minimal impact on the biophysical properties of $Ca_v3.1$, however, when included it causes a marked reduction in membrane localization[195]. Analysis of the human and chicken $Ca_v3.1$ exon 8 sequences (GenBank accessions NM_001256324 and XM_001232653.2), reveals that the upstream 5' donor splice site, present within rodent exon 8, is absent, likely accounting for the lack of variability for humans in this region[192,190,191,193]. However, an imposed deletion within the I-II linker of human $Ca_v3.1$, mimicking omission of exon 8b, causes an analogous increase in membrane expression[196], so the mechanisms that influence membrane trafficking via the I-II linker are likely conserved for $Ca_v3.1$ homologues. Whether some vertebrates have lost the ability to splice out exon 8b, or this is an emergent feature within select vertebrate lineages, has yet to be addressed. Conversely, analogous deletions in the other two human Ca_v3 channel isotypes, $Ca_v3.2$ and $Ca_v3.3$, cause a dramatic increase and a moderate decrease in membrane expression, respectively[196,197], indicating that although the I-II linker of all three Ca_v3 channel subtypes is used to regulate membrane expression, the mechanisms are different. Human $Ca_v3.3$ also has an optional exon in the I-II linker (cassette exon 9)[198], however unlike 8b in $Ca_v3.1$, it has a strong impact on biophysical

properties and its role in membrane expression has not been assesed[199]. Notably, the I-II linker is also used to regulate trafficking and protein stability of HVA calcium channels, through interaction with accessory β subunits that bind the I-II linker (in a similar position to the gating brake of Ca_v3 channels) to facilitate membrane localization and protection from proteosomal degradation[78]. For a recent review detailing membrane trafficking of Ca_v3 channels, see Senatore *et al*., 2012[64].

Both human $Ca_v3.2$ and $Ca_v3.3$ genes are reported to consist of 36 exons[198,200] (35 and 37 reported on Evidence Viewer, NCBI, respectively), and similar to $Ca_v3.1$, both are subject to extensive alternative splicing[201,202,203,198,200,204]. Many of these splice isoforms have been shown to influence channel properties[203,200], however, a particularly interesting locus for alternative splicing is found in the short III-IV cytoplasmic linker of $Ca_v3.2$ (and $Ca_v3.1$), but not in $Ca_v3.3$. Exon 25, in $Ca_v3.1$ and $Ca_v3.2$, contains alternative 5' donor splice sites that can selectively omit 7 amino acids from the middle of this linker (termed exon 25c). These two genes also each possess an optional cassette exon downstream of exon 25, exon 26, which can be inserted in lieu of exon 25c (+26), with 25c (+25c/+26), or neither can be included (Δ 25c/Δ26, or ΔΔ)[192,190,193,200] (summary figure A). Insertions in this region imposed by alternative splicing have dramatic influences on voltage sensitivity, such that channels activate and inactivate at more negative potentials[192,190,193,200]. In addition, exons 25c and/or 26 impose accelerated activation and inactivation kinetics, but slower deactivation kinetics[192,190,193,200]. Interestingly, ΔΔ variants of $Ca_v3.1$ and $Ca_v3.2$ are enriched in the embryo[200,190], and resemble the embryonically-abundant $Ca_v3.3$ channel[204], which lacks alternative exons in the III-IV linker (hence always ΔΔ-like) and has depolarized sensitivities for activation and inactivation, and slower kinetics[205,206,65,207].

1.5.4 Alternative splicing of NALCN channel genes

The human NALCN gene consists of ~46 exons (Evidence Viewer, NCBI). Functional documentation of alternative splicing is not available in the literature, however, according to The Protein Knowledgebase (http://www.uniprot.org/), the human NALCN gene expresses three mRNA variants (UniProtKB database IDs Q8IZF0, Q8IZF0.2, and Q8IZF0.3), two of which code for truncated proteins (Q8IZF0.2 and Q8IZF0.3). The larger of the two truncated isoforms (ID Q8IZF0.2), comprises half of the channel protein, from the N-terminus up until the beginning of the II-III linker. Interestingly, heterozygous mutations in humans that similarly truncate P/Q-type calcium channel $Ca_v2.1$, induce a dominant-negative effect over the wildtype allele by targeting its otherwise functional protein product for proteosomal degradation, leading to a pathological depletion of $Ca_v2.1$

in the cerebellum and motor dysfunction associated with episodic ataxia type-2[208]. This degradation process can be mimicked for human $Ca_v3.2$[208], and the truncated NALCN splice isoform might mediate an endogenous downregulation of full length NALCN by exploiting this same mechanism.

1.5.5 Challenges in understanding the physiological roles for alternative splicing in Ca_v3 and NALCN channel genes

Developmental and tissue-specific differences in alternative splicing are often reflected by ratiometric differences rather than a complete switching between particular mRNA isoforms[180]. As such, two different physiological states, whether they are separated spatially or by some developmental timeline, can have a considerable amount of overlap in terms of alternative splicing (e.g. 6:4 isoform A/isoform B in state 1, vs. 2:8 isoform A/isoform B in state 2), which due to lack of contrast in expression, complicates our ability assess the roles for alternative splicing within these different states. In addition, genetic redundancy, which is high in vertebrates (e.g. multiple voltage-gated sodium and calcium channel genes; see above), establishes the presence of multiple proteins with overlapping functions that can mask the effects of alternative splicing in redundant genes. Even for alternative splicing with highly contrasting expression patterns, the functional consequences can be subtle and depend on other cellular factors. Alternative splicing tends to occurs at a systems level, and temporal or spatial alterations in the splicing program are expected to influence many genes[184,185,180]. Hence, the purpose for altering alternative splicing of a particular gene might be difficult to pinpoint, since its functionality might depend on coordinated alterations in other gene products. Finally, morphological complexity in vertebrates is exceedingly elaborate, especially within the nervous system, and correlating differences in alternative splicing of one gene to a functional output within such a complex background can be difficult. To illustrate this problem, despite the thorough characterization of developmentally-regulated splicing in the III-IV linkers of $Ca_v3.1$ and $Ca_v3.2$ channel genes (see above), which are ratiometrically enriched in adults (and conversely $\Delta\Delta$ is preferred in embryos)[192,190,193,200], little is known about the physiological purpose for these developmental changes in splicing. Even less is known about the physiological role for alternative splicing in NALCN. Arguably, model systems with less genetic complexity and simpler nervous systems might help to understand how permutations in alternative splicing fit into the context of real physiological processes, such as nervous system function, development, disease, etc.

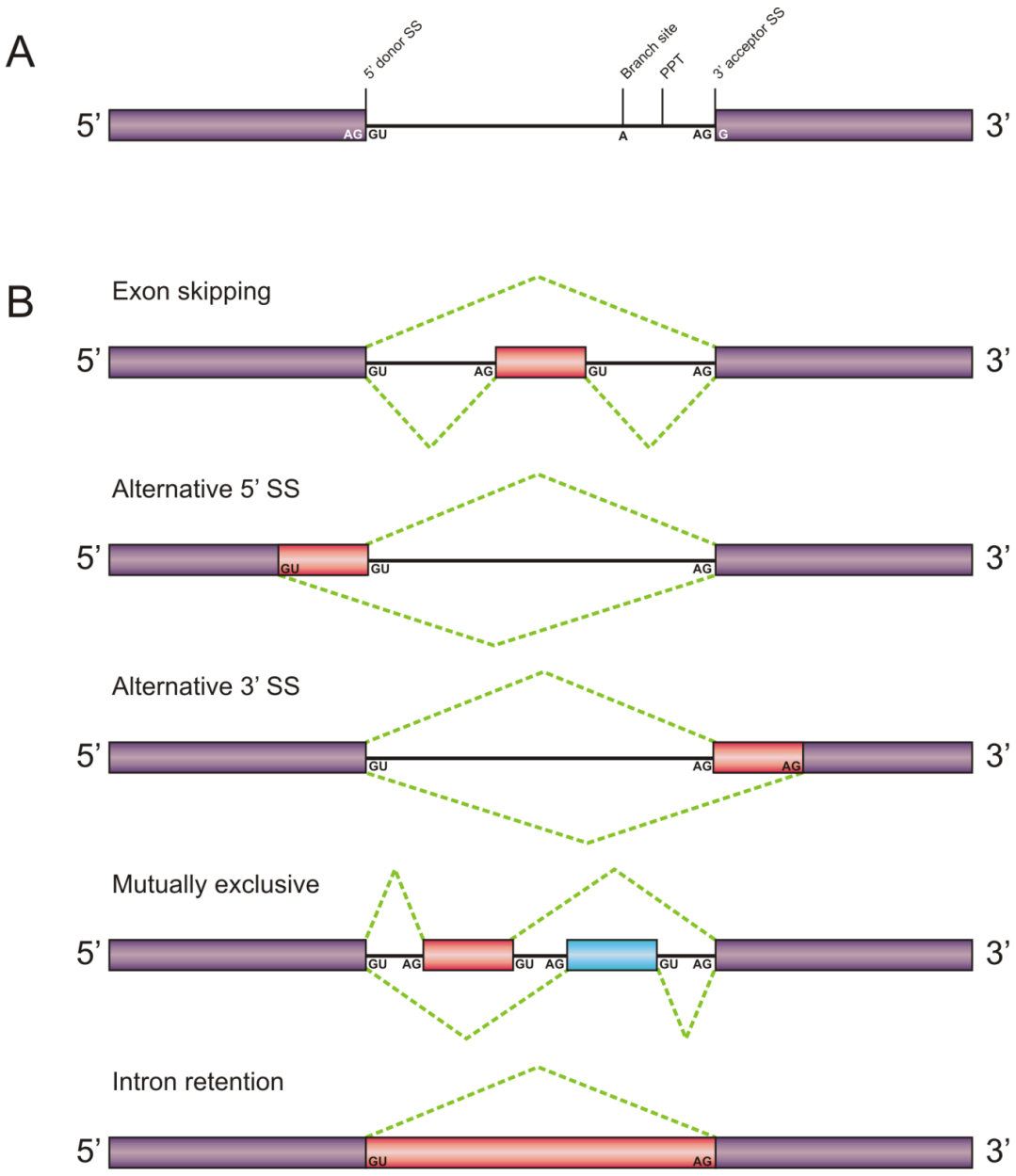

Figure 9. Alternative splicing of pre-mRNA. A) The spliceosome, a massive RNA-protein complex containing highly conserved snRNPs (U1, U2, U4, U5, and U6), recognizes four key *cis* elements along the pre-mRNA for intron excision and exon-exon ligation. The polypyrimidine tract (PPT) facilitates formation of the spliceosome complex by recruiting splicing factors to the intron. 5' and 3' donor and acceptor splice sites (SS) flank the 5' and 3' exons (purple boxes), with consensus sequences of AG-**GU** and **AG**-G recognition sequences, respectively. The GU and AG sequences, located within the intron (black line), are highly conserved. The branch site, located ~40 base pairs upstream of the 3' exon, contains an adenine (A) nucleotide that is ligated to the hydrolyzed 5' donor splice site by the spliceosome complex into an intermediate lariat structure; subsequently, cleavage of the 3' splice site and exon-exon ligation takes place. **B)** Five basic modes of alternative splicing. Optional exons are shown in red and blue. Green lines depict ligation of exons by the spliceosome. Exon skipping involves the omission of an optional exon along with flanking 5' and 3' intron sequences. Alternative 5' donor splice sites can be used to omit a portion of the 5' exon, and alternate 3' acceptor sites can be used to omit a portion of a 3' exon. Mutually exclusive exons are included in lieu of each other, and intron retention involves the optional inclusion/omission of an intron into the final mRNA.

1.6 *Lymnaea stagnalis* as a model to study ion channels

The mammalian brain is made up of trillions of neurons and glia, organized into very complex networks, each expressing a different ensemble of genes, most subject to various modes of functional diversification (see above). To circumvent issues with complexity, some researchers have resorted to invertebrate model organisms, which often possess simpler and more tractable nervous systems. The freshwater pond snail *Lymnaea stagnalis* (a.k.a. the Great Pond Snail) is one such invertebrate model, with a proven utility for neuroscience applications[209]. However, before describing the advantages, it is worthwhile discussing some of the disadvantages. *Lymnaea* belongs to the phylum Mollusca, which includes other extant species commonly used for neuroscience research including marine snail *Aplysia californica* and terrestrial snail *Heliosoma trivolvis*. Unfortunately, the molecular tools available for *Lymnaea* and other molluscs are quite limited. Until only recently, very few snail cDNA or expressed sequence tag (EST) sequences were available[210,211]. Furthermore, the *Lymnaea* genome is not sequenced; however, the *Aplysia californica* genome (The Broad Institute Aplysia Genome Project) as well as other snail genomes are being sequenced and annotated (i.e. *Lottia gigantea*: JGI Genome Project; and *Biomphalaria glabrata*: The *Biomphalaria glabrata* Genome Initiative). Also, no vectors have been developed for heterologous expression of cDNAs in *Lymnaea* cells (pNEX vector has been developed for *Aplysia*, but its expression efficiency in *Lymnaea* has not been formally tested[212]). Finally, transgenic and gene knockout/knockin technologies have not been developed for *Lymnaea* or other molluscs.

Despite these significant disadvantages, *Lymnaea* does provide some very useful advantages. Remarkably, despite the millions of years of evolution separating vertebrates and molluscs (figure 10), multiple genetic and morphological similarities persist. For example, a considerable number of genes associated with neuronal function are conserved between snails and vertebrates[210,211], including genes for voltage-gated calcium channels[59,64]. Unlike in vertebrates, these genes are often retained at single copies[71,72] (see figure 4), diminishing genetic redundancy. Moreover, these channels often play similar roles in their respective organisms. The *Lymnaea* Ca_v2 channel homologue LCa_v2, for example, has similar biophysical properties to mammalian Ca_v2 channels, and like them, mediates presynaptic neurotransmitter release[213]. The L-type homologue, LCa_v1, also has similar properties and functions as its mammalian counterparts[214,215]. Ca_v3 (and NALCN) channels from *Lymnaea* or other invertebrates, prior to this thesis, had not been successfully cloned and expressed in heterologous systems for electrophysiological characterization.

Morphologically, snails have anatomical structures with vertebrate counterparts that can be exploited for research purposes, and in some cases, these organs/tissues provide elegant preparations for experimentation. The relatively simple *Lymnaea stagnalis* central nervous system, for example, contains roughly 20,000 neurons, the somas of which are arranged into large clusters of defined ganglia[210]. Within these ganglia, neurons can be uniquely identified, extracted, and cultured with relative ease, and these can be made to reconstruct functional, synaptically-connected neuronal circuits *in vitro*[209,216]. Circuits can also be studied in semi-intact preparations, with access to specific central neurons still connected to peripheral neurons and muscle cells[217,218]. These reductionist approaches have provided powerful insights into the mechanisms that regulate oscillating circuits that drive simple rhythmic behaviors such as respiration and feeding[209], and have allowed for a dissection of how external world information is encoded into these very neurons, at the molecular level, during learning and memory formation[219,217,218]. Additionally, *Lymnaea* possesses a compartmentalized heart with an atrium and a ventricle (albeit with two chambers rather than four as in most vertebrates)[209]. Key voltage-gated channels, important for heart function in vertebrates (e.g. HVA and LVA calcium channels, A-type and delayed rectifier voltage-gated potassium channels[220]) are expressed in *Lymnaea* heart cells[111,221]. In addition, studying the *Lymnaea* heart provides insights into the evolution of heart function at the molecular level, where the contribution of specific ion channels to excitability and contraction can be compared. *Lymnaea* also contains a well-studied neuroendocrine system[209], which can be similarly compared with the vertebrate neuroendocrine system.

Lymnaea stagnalis also provides some practical advantages. In contrast to *Aplysia californica*, that must be isolated from the wild, *Lymnaea* can be easily raised in a laboratory. Furthermore, since *Lymnaea* are poikilotherms (i.e. do not regulate their body temperature), electrophysiological studies of *Lymnaea* neurons or *Lymnaea* cDNAs expressed in heterologous systems are more representative of their true physiological environment, since most recordings are carried out at ambient room temperature. Actually, significant differences in mammalian calcium channel properties have been reported when experiments were carried out at 37^{o}C rather than room temperature[222,223,224,225,226,227,228,229].

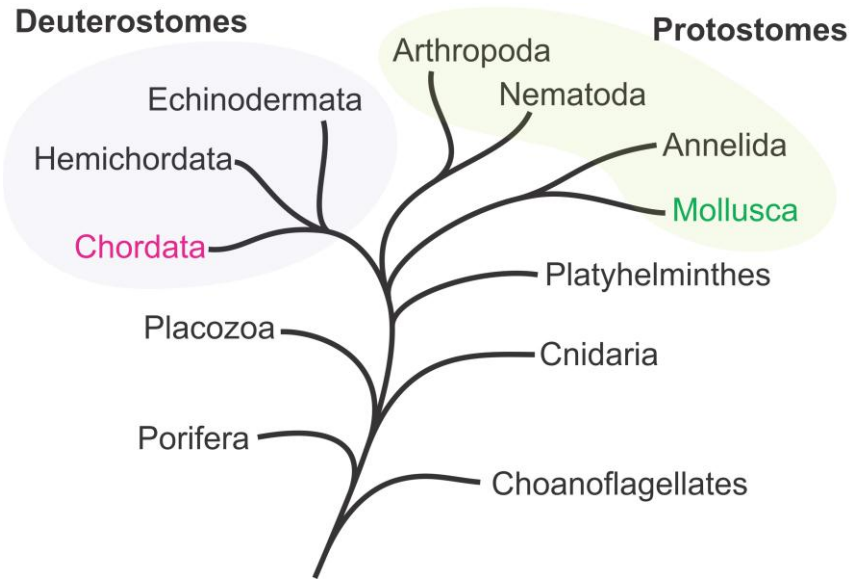

Figure 10. Illustration of some key evolutionary branch points in animal phyla. Metazoans comprise a kingdom of multicellular eukaryotic organisms (a.k.a. Animalia) that diverged from single-celled eukaryotes such as protists (e.g. Choanoflagellates) c.a. 1.6 billion years ago[36,37]. Molecular clock studies indicate that the lineages that eventually led to humans and molluscs diverged from each other more than 1 billion years ago[230]. Porifera (i.e. sponge) represent some of the most primitive extant animals, followed by Placozoa (e.g. *Trichoplax adhaerens*) which lack muscles and nerves and Cnideria (e.g. *Nematostella vectensis*) that have a rudimentary nervous system and radial body symmetry. Further along the tree, animals with bilateral symmetry emerged (e.g. flatworms/Platyhelminthes) and subsequently subdivided into two groups based on distinctions in embryonic development, with protostome animal making up one group (e.g. nematodes such as *C. elegans*, arthropods such as *Drosophila melanogaster*, molluscs such as *Lymnaea stagnalis*, and annelids) and deuterostome animas making up the other (e.g. chordates including the subphylum Vertebrata, hemichordates such as acorn worms, and echinoderms such as starfish). The tree illustrated here was derived from phylogenetic relationships depicted on The Tree of Life Web Project (http://tolweb.org/tree/), and is not intended to be metric in terms of evolutionary relationships between Phyla.

1.7 Hypotheses

The series of hypotheses addressed in this thesis are that:

1) *Lymnaea* Ca_v3 and NALCN channel homologues possess features at the amino acid level (i.e. primary sequence, predicted secondary structures, predicted functional motifs) that are conserved or divergent from mammalian channels, and these structural features are reflected by respective similarities and differences in their properties when expressed in isolation and biophysically characterized by electrophysiology.

2) The expression patterns of LCa_v3 and LNALCN mRNAs, in various organs/tissues and throughout development, resemble those of mammals. LCa_v3 transcripts are expected to be abundant in the central nervous system, heart, and in secretory cells, and are hypothesized to be similarly downregulated throughout development[64], especially in the heart[231]. LNALCN is also expected to be abundant in the central nervous system, heart, and secretory cells, similar to mammals[118].

3) The LCa_v3 and LNALCN channel genes are subject to alternative splicing, some of which is conserved with mammalian channels, and some of which is unique to snails and closely related species. Conserved splicing imposes analogous changes in channel properties, while divergent splicing manifests as unique functional attributes.

4) The alternative splice isoforms of LCa_v3 that are conserved with mammals are hypothesized to undergo similar changes in expression throughout development as reported for mammals, and to exhibit similar expression profiles in various organs/tissues such as the central nervous system, heart, and secretory cells.

5) Expression patterns of conserved and divergent alternatively spliced LCa_v3 and NALCN mRNAs allude to their function, particularly if differences in splicing between two tissues or developmental stages are significant.

1.8 Objectives

The initial objective was to clone and characterize two homologues of mammalian 4-domain ion channels from the freshwater snail *Lymnaea stagnalis*: a Ca_v3 (T-type) voltage-gated calcium channel, and a NALCN non-specific cation leak channel. Prior to this, invertebrate homologues of these channels had not been successfully cloned and expressed in heterologous systems for electrophysiological characterization. Determining the properties of these channels in such a way would provide insights into their adaptation in different species. Given the significant evolutionary distance separating molluscan invertebrates from mammals, the channels were expected to have undergone some degree of structural divergence, which would lead to differences in their ion-conducting properties and in turn their physiological contributions. On the other hand, conserved features would point to functional constraints on these channels, alluding to key structural and functional elements that define them across the animal kingdom. Inherent to this work was to establish a foundation for studying these specific ion channel types within the simplified *Lymnaea* model, which has a tractable, well characterized, and relatively simple nervous system, and importantly, has only single-copy genes representing the major 4-domain ion channel subtypes such as Ca_v1, Ca_v2, Ca_v3, and NALCN (vertebrates possess multiple copies giving rise to redundancy issues; NALCN is single-copy is most animal species).

To this end, the first step was to determine the full length consensus sequences of *Lymnaea* Ca_v3 and NALCN channel mRNAs (results chapters 2.1 and 2.4). The confirmed cDNA sequences were then used to construct mammalian expression vectors for heterologous expression in cultured mammalian cells, for the purpose of characterizing the ion conducting properties of these channels by electrophysiological recording. The latter was successfully done for the *Lymnaea* Ca_v3 homologue (results chapters 2.1 to 2.3), but not so for *Lymnaea* NALCN, corroborating with others the inability to electrophysiologically record NALCN cDNAs (mammalian or invertebrate) in heterologous expression systems[135,118,127].

During consensus sequencing of the *Lymnaea* Ca_v3 and NALCN channel cDNAs, several alternative splice isoforms were identified. For LCa_v3, optional exons 8b in the I-II linker and 25c in the III-IV linker were found (summary figure A) and thought to be evolutionarily conserved with analogous exons found in mammalian Ca_v3 channels, while mutually exclusive exons 12A and 12B, in the domain II P-loop, were found to be unique to invertebrates. *Lymnaea* NALCN was also found to undergo alternative splicing in the domain II P-loop, with exons 15a and 15b that alter the

selectivity filter from a purported non-specific cation leak configuration[137] (EKEE), to a calcium channel-like configuration (EEEE; summary figure B). The secondary objective of this thesis was thus to determine the evolutionary history of these splicing events by phylogenetic analyses (results chapters 2.2 to 2.4), to determine the expression profiles of these splice variants in *Lymnaea* tissues throughout development, and when possible, to determine the functional impacts of these splicing events in channels expressed in mammalian cells. The various splice isoforms were thus cloned into mammalian expression vectors for electrophysiological recording, a strategy that was successful for *Lymnaea* Ca_v3 splice variants (results chapters 2.2 and 2.3). Due to the inability to record *Lymnaea* NALCN currents in mammalian cells, the domain II splice isoforms of exons 15a and 15b could not be functionally characterized.

Chapter 2
Results

2.1 Cloning and characterization of a *Lymnaea* Ca_v3 channel homologue

The research presented in the following section is published in The Journal of Biological Chemistry: Adriano Senatore and J. David Spafford. **Transient and big are key features of an invertebrate T-type channel (LCa_v3) from the central nervous system of *Lymnaea stagnalis*.** *J Biol Chem*. 2010; 285: 7447-58. © the American Society for Biochemistry and Molecular Biology.

This manuscript, containing research conducted by Adriano Senatore while in the laboratory of Dr. J. David Spafford, as well as *in silico* analyses conducted by Dr. Spafford, presents the first successful cloning, heterologous expression, and electrophysiological recording of an invertebrate Ca_v3 channel homologue. The major conclusion that can be drawn from this work is that the snail channel, despite millions of years of divergent evolution with mammalian homologues, retains some key defining features attributed to Ca_v3 or T-type channels. These include 1) characteristic protein sequences and predicted structural regions (e.g. the gating brake in the I-II linker, the EEDD selectivity filter, the voltage-sensors), 2) no obligatory association with high voltage-activated β and $\alpha_2\delta$ accessory subunits for high-level expression in mammalian cells, 3) conducts calcium currents with low-voltages of activation, 4) contains a putative window current for minute but constitutive calcium influx near resting membrane potential, 5) rapid channel activation and inactivation upon depolarization, 6) slow deactivation or closing upon membrane hyperpolarization, and 7) similar sensitivity to non-selective T-type channel blockers nickel and mibefradil.

The materials and methods for this manuscript can be found in Appendix A.

2.1.1 Abstract

Here we describe features of the first non-mammalian T-type calcium channel (LCa_v3) expressed *in vitro*. This molluscan channel possesses combined biophysical properties that are reminiscent of all mammalian T-type channels. It exhibits T-type features such as 'transient' kinetics, but the 'tiny' label, usually associated with Ba^{2+} conductance, is hard to reconcile with the 'bigness' of this channel in many respects. LCa_v3 is 25% larger than any voltage-gated ion channel expressed to date. It codes for a massive, 322-kDa protein that conducts large macroscopic currents *in vitro*. LCa_v3 is also the most abundant Ca^{2+} channel transcript in the snail nervous system. A window current at typical resting potentials appears to be at least as large as that reported for mammalian channels. This distant gene provides a unique perspective to analyze the structural, functional, drug binding, and evolutionary aspects of T-type channels.

2.1.2 Introduction

T-type calcium channels open in response to slight depolarizations in the low voltage range. Paradoxically, they are also recruited after membrane hyperpolarization as occurs during rebound burst firing[232]. A window current of T-type channels is a feature that permits Ca^{2+} entry at rest[233] and contributes to differentiation and growth promoting functions in both excitable and non-excitable cells[234]. T-type channels are also a leading pharmaceutical drug target and are implicated in a wide range of conditions such as epilepsy, pain, hypertension, cancer, and mental disorders[235].

T-type Ca^{2+} currents were first measured in starfish eggs using a two-electrode voltage clamp[236]. Currents conducted by 'Channel I' were evoked by small depolarizations (low voltage-activated), visible as a hump in a current amplitude *versus* test potential plot beside the Channel II currents elicited by larger depolarizations (high voltage-activated). Ca^{2+} channel types would be discriminated further by Tsien and co-workers[237] on the basis of properties where Ba^{2+} is the charge carrier. High voltage-activated L-type channels have a large unitary Ba^{2+} conductance with long-lasting openings, N-type (or non-L-type) channels are typically associated with neurons of intermediate unitary conductance, and the low voltage-activated, T-type channels produce transient currents that are of tiny unitary conductance in Ba^{2+} and close slowly upon membrane repolarization, producing a slowly deactivating tail current[237].

T-type channels remain as the least understood among the Ca^{2+} channel families. Although most of the 10 mammalian Ca^{2+} channel genes were characterized in the late 1980s, an additional decade was

required for a description of the three T-type genes, $Ca_v3.1$ (α1G), $Ca_v3.2$ (α1H), and $Ca_v3.3$ (α1I)[94]. Progress in understanding T-type channel functions continues to be hampered by the lack of highly selective blockers that discriminate between Ca_v3 channel types or separate Ca_v3 channels from related L-type (Ca_v1) and non-L-type (Ca_v2) Ca^{2+} channels, which usually produce more robust Ca^{2+} entry into the same cells[94].

Here we describe the *in vitro* expression characteristics of the first non-mammalian T-type channel, LCa_v3, cloned from the pond snail, *Lymnaea stagnalis*. This structurally distant channel has quintessential features of T-types such as transient kinetics. LCa_v3 is big in many respects, such as its protein size; it expresses large macroscopic currents in human cells, it is the most abundant Ca^{2+} channel transcript in the snail nervous system, and it generates window currents that appear to be at least as large as those reported for mammalian channels. LCa_v3 provides a unique perspective to analyze the structure, function, and drug binding of T-type channels and serves as a useful surrogate in residue swapping experiments. Searches for the fundamental mechanisms that regulate this singleton invertebrate T-type channel will be facilitated by the simple molluscan preparation, where accessible and identified neurons underlying well described behaviors can be studied in isolated *Lymnaea* neurons, cultured synapses, or within intact, identified networks *in situ*. Also, LCa_v3 provides nourishment for evolutionary speculation. Although the first gastropods (500 million years ago) are likely quite distant from this ancestral branch point, the extant snail homolog, *LCa_v3*, is reminiscent of the gene that predates the speciation that led to the emergence of the three distinct, mammalian T-type channel genes.

2.1.3 Results

Identity of an Invertebrate T-type Channel (LCa_v3)

A novel invertebrate T-type channel transcript (9031 bp) was assembled from cDNA derived from the central nervous system of the freshwater pond snail, *L. stagnalis*, with a coding region that starts as an almost perfect match to an Expressed Sequence Tag data base entry from the marine snail *Aplysia californica* (accession no. EB302921). The *LCa_v3* open reading frame predicts a 2886-amino acid protein, with an estimated ~322-kDa molecular mass. The start and end of the LCa_v3 amino acid sequence also resembles those of the human $Ca_v3.1$ channel (Fig. 1*A*). Consistent with other related cation channels of this type, LCa_v3 has four repeat domains (DI to DIV) with each domain containing six membrane-spanning segments similar to the voltage-gated K channels (Fig. 3*A*). LCa_v3 is the largest voltage-gated ion channel expressed to date, being 25% larger than the mammalian T-types,

50% larger than a T-type homologue from *Caenorhabditis elegans* (cca-1b), and significantly larger than other Ca^{2+} channels (Ca_v1, Ca_v2), sodium channels (Na_v), and NALCN (Fig. 1*B*). The extra size is mostly due to long cytoplasmic N and C termini and the cytoplasmic I-II and II-III linkers (Fig. 1*C*).

Snails, like most invertebrates, appear to have branched before the genomic duplication events that led to the expansion of gene isoforms and as such bear only single representatives for each of the three Ca^{2+} channel gene families (Ca_v1, Ca_v2, and Ca_v3) compared with the 10 different Ca^{2+} channel genes in mammals (Fig. 2*A*). The snail T-type gene diverges dramatically in amino acid sequence from the mammalian genes (mean identity/similarity = 37.6/46.1), whereas the mammalian homologues are clustered closer together (mean identity/similarity = 50.7/57.9) (Fig. 2*C*). The single copy nature of the *LCa_v3* gene in the genome is evidenced by Southern blotting, producing a single banding hybridization pattern, except for a gel lane where the restriction enzyme (*EcoR*V) cuts the genomic DNA within the probe sequence, leading to two bands of weaker intensity (*lane a*, Fig. 2*B*). The *LCa_v3* transcript is more abundant than other Ca^{2+} channels (*LCa_v1* and *LCa_v2*) or *LNALCN* in central nervous system tissue as measured by semiquantitative RT-PCR (Fig. 2*D*). The higher expression of *LCa_v3* compared with these others was also found by single cell, quantitative real-time PCR of individual VD4 neurons in a previous study using different primer sets (see Spafford *et al.*[238] and Fig. 2).

Fig. 3*A* illustrates a running window of similarity between aligned LCa_v3 and human $Ca_v3.3$ channel protein sequences. The strongest homology is observed in the six-transmembrane segments and pore (P)-loops of each domain (Fig. 3*A*). Side chains of conserved negative residues lining the four P-loops contribute to a DDEE selectivity filter in T-type channels[94], including LCa_v3 (Fig. 3*B*). The pores of LCa_v3 and all voltage-gated Ca^{2+} channels also include a highly conserved aspartate adjacent to the selectivity-filter glutamate in Domain II (Fig. 3*B*), which may serve to attract incoming Ca^{2+} ions to the ion selective pore[43]. One noticeably conserved region outside of the membrane-spanning domains is the gating brake present in the proximal I-II cytoplasmic linker (Fig. 3*C*). Comparison of LCa_v3 with $Ca_v3.3$ residues suggests conserved elements in the gating brake, including a putative helix-loop-helix hydrophobic core, a putative salt bridge, and potential protein-protein interaction sites facing away from the hydrophobic core (Fig. 3*C*)[82].

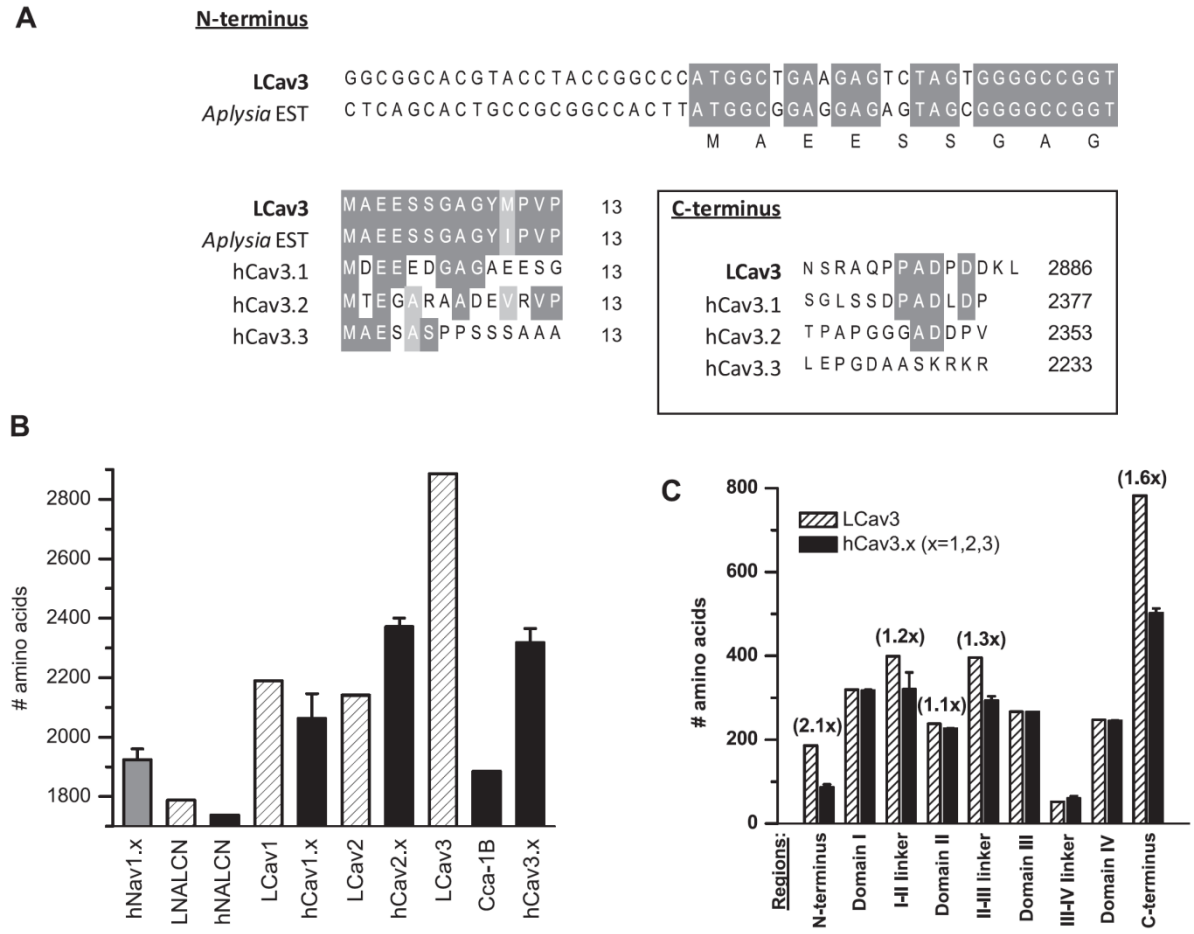

FIGURE 1. Full-length snail LCa$_v$3 is the largest identified voltage-gated ion channel expressed to date. It is coded by a 9031-bp cDNA transcript that forms a 2886-amino acid protein with a molecular mass of 322 kDa. *A*, the N terminus closely matches with a putative start site derived from marine snail *A. californica* EST (EB302921) and slightly resembles the N and C termini of human Ca$_v$3.1–3.3. *B*, LCa$_v$3 is 1.25× larger than human Ca$_v$3 channels and 1.5× larger than nematode T-type, cca-1B, and all other four repeat ion channels. *C*, LCa$_v$3 is larger than human Ca$_v$3 channels in the N and C terminus and also the I-II and II-III cytoplasmic linkers.

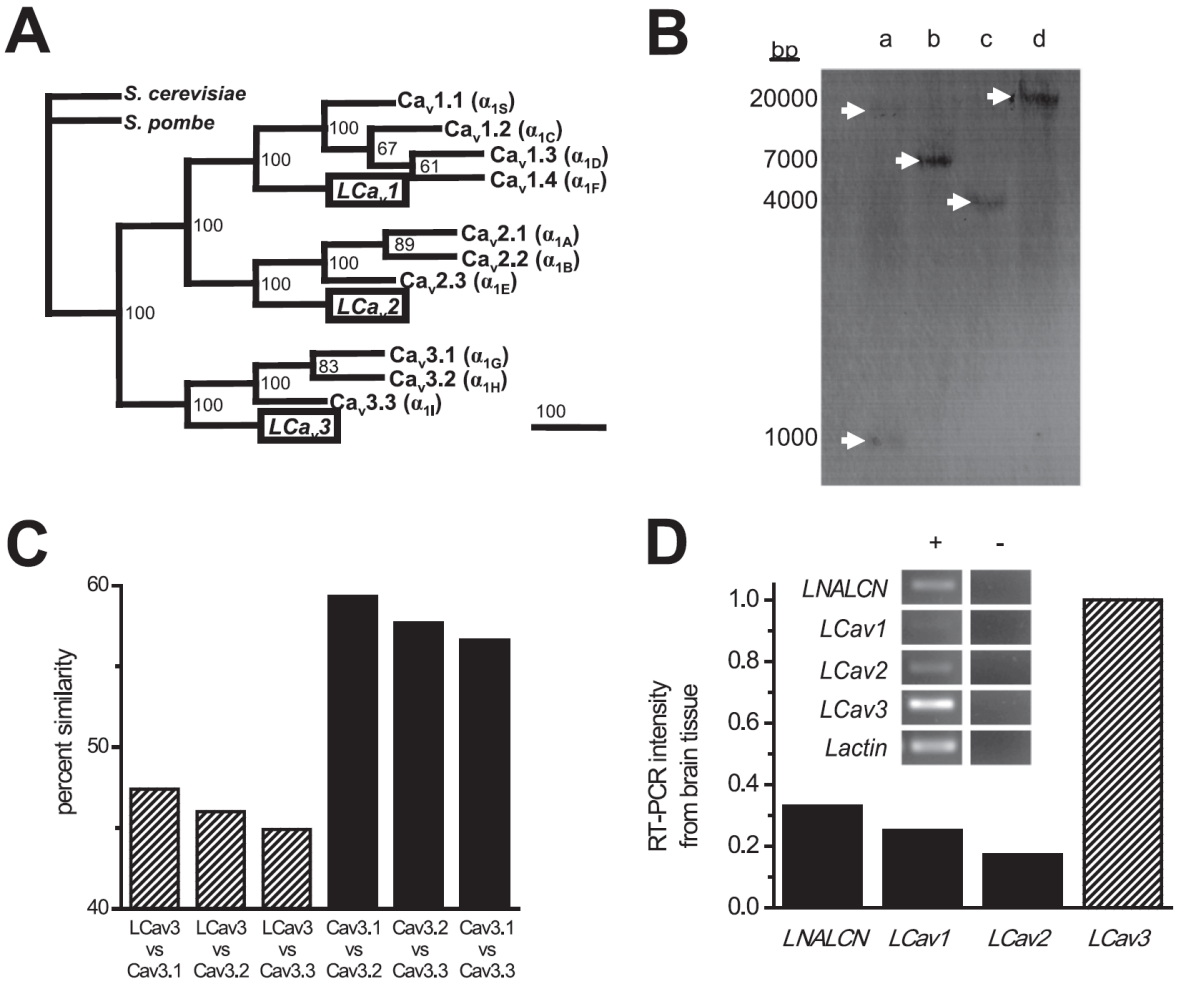

FIGURE 2. Singleton, snail T-type Ca^{2+} channel gene is distantly related to vertebrate homologs and is the most abundant Ca^{2+} channel transcript in the snail brain. *A*, shown is the most parsimonious gene tree generated using multiple aligned sequences, analyzed in PAUP4.0 (D. L. Swofford) and illustrated with TreeView (R. D. M. Page). Sequences include official human sequences (IUPHAR database); *LCa_v3* (GenBank™ accession no. AF484084) and yeast gene *Cch1* from *Schizosaccharomyces pombe* (GenBank™ accession no. CAB11726) and *Saccharomyces cerevisiae* (GenBank™ accession no. CAA97244). *Numbers* at branch points represent bootstrap values based on 100 replicates in heuristic search. Phylogram branches are scaled by their length and rooted with *Cch1* Ca^{2+} channel homologs from fungi species. *C*, percent amino acid similarity scores were generated from EMBOSS NEEDLE (EMBL). *B*, Southern blot indicates a single copy gene in the *Lymnaea* genome. A T-type probe hybridized to create a banding pattern (*white arrows*) on the blot was created from membrane transfer of genomic DNA digested with either *Eco*RV (*a*), *Hind*III (*b*), *Eco*RI (*c*), or *Xho*I (*d*). The probe contained an *Eco*RV restriction site, so the probe hybridized to two genomic DNA fragments digested with *Eco*RV. *D*, densitometric intensity of RT-PCR bands (illustrated in the *inset*) was generated from *Lymnaea* brain tissue.

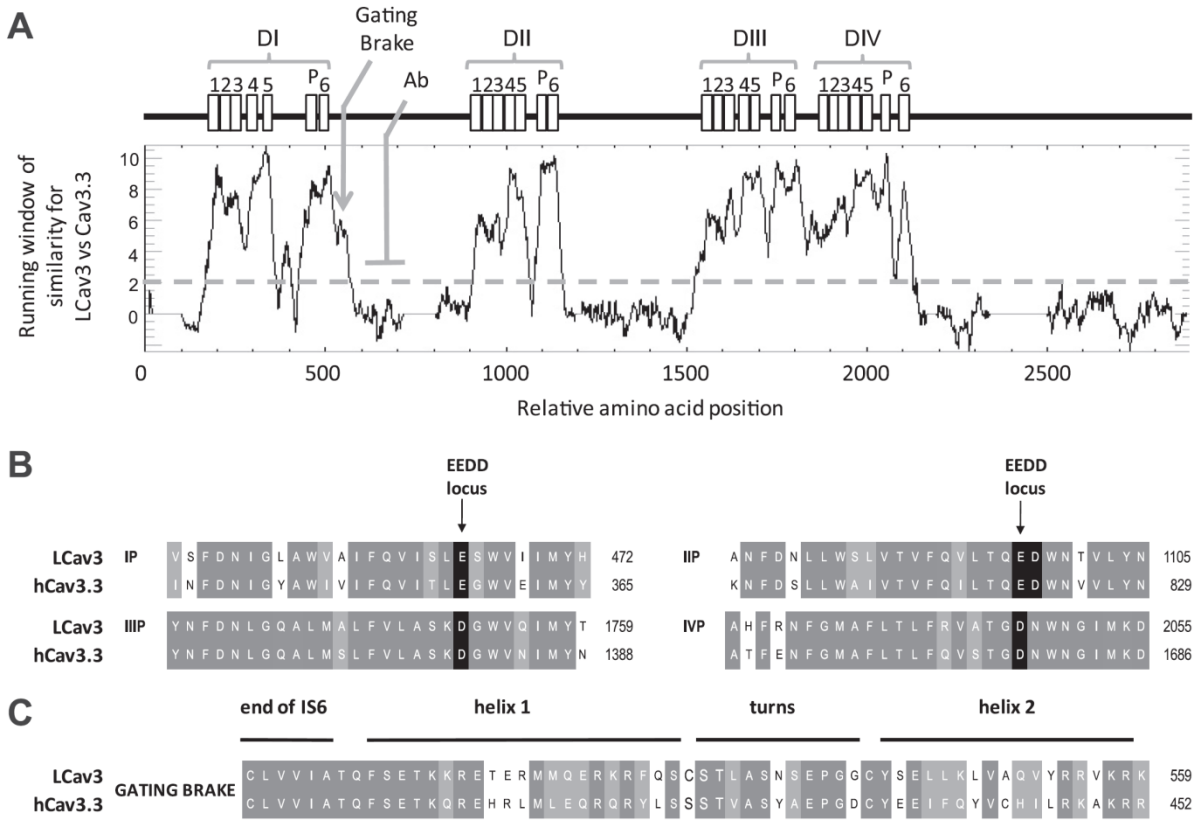

FIGURE 3. Running window of similarity (*A*) and alignments (*B* and *C*) between amino acid sequences of distant T-type channel homologs (snail *LCa$_v$3* and human Ca$_v$3.3) reveal that the invariant structures for T-type channels are harbored in six membrane-spanning segments in all four domains (I, II, III, and IV), including an ion conducting pore (S5-P-loop-S6) and voltage sensor (S1-S4). Illustrated is the position in the I-II linker where *LCa$_v$3* polyclonal antibody (*Ab*) was generated in rabbits against a 200-amino acid peptide. *B*, shown is amino acid sequence alignment of the re-entrant P-loop located between S5 and S6 of each of the four domains illustrating the signature sequence (EEDD locus) that influences Ca^{2+} ion permeation and selectivity. The conserved aspartate residue (1097 in *LCa$_v$3*) in a position downstream of the selectivity filter glutamate residue is positioned to attract incoming Ca^{2+} ions to the pore[43]. *LCa$_v$3* contains a neutral isoleucine in the outer pore at position 468 where mammalian T-type channels have a negatively charged residue (Glu or Asp) that influence pore blocking drugs. *C*, alignment of the cytoplasmic gating brake in proximal I-II linker is shown. The gating brake is thought to prevent T-type channel gating at more hyperpolarized potentials.

Expression Characteristics of LCa_v3 in HEK-293T Cells

Transient transfection of *LCa_v3* cDNA contained in pIRES2-EGFP vector reveals membrane-delimited staining of HEK-293T cells (*box*, Fig. 4*A*) with a rabbit polyclonal antibody generated against the I-II cytoplasmic linker of LCa_v3 (see Fig. 3*A* for the relative location of the epitope). Antibody staining was not apparent in *LCa_v1*-transfected cells[214] or when preimmune serum was used to detect LCa_v3 (Fig. 4*A*). Channel expression levels generally correspond to the EGFP intensity in HEK-293T cells, as would be expected with the *LCa_v3* cDNA expressed on the same mRNA as EGFP using the bicistronic expression vector, pIRES2-EGFP. The optimal level of HEK-293T expression for electrophysiological recording (200 pA to 1.5 nA) corresponds to 3 days after transfection, whereas larger currents of up to 10 nA were possible by allowing protein expression to continue for up to 6 days (Fig. 4*B*). Typical transient kinetics of T-type currents are revealed in whole cell recordings of LCa_v3. Small voltage steps above threshold (−70 to −65 mV) are slow to activate and inactivate (requiring 10s of ms). Larger voltage steps elicit currents with progressively faster activation and inactivation kinetics that cross over each other with each successive step toward a maximal current for a voltage step of −35 mV (Fig. 4*C*). τ of inactivation kinetics follows the change in the time to peak and τ of activation kinetics with increasing voltage steps (Fig. 4*E*) (see Table 1 for a detailed comparison of biophysical parameters between Ca_v3 channels).

The pairing of activation and inactivation with LCa_v3 is typical of T-type currents and has led some to suggest that T-type channel inactivation is voltage-independent[57]. The voltage sensitivity of LCa_v3 approximates a typical low threshold T-type current that peaks at −35 mV (Fig. 4*d*), although technically LCa_v3 is slightly lower threshold than mammalian T-types (peak between −30 and −25 mV). Channel availability at steady state was assessed after a 1-s prepulse protocol (Fig. 5*A*) and a 5-s prepulse protocol (data not shown), revealing a surprisingly steep and positively shifted availability curve compared with mammalian T-type channels (Fig. 5*B*). The combination of the very low threshold of channel activation and the large fraction of possible available channels creates a potentially large and persistent window current near the resting membrane potential of typical neurons[233] (Fig. 5*C*). An estimated window current was gathered by the product of available channels under steady-state conditions and the relative peak conductance. As many as 1.8% of total T-type channels may contribute to this current at −65 mV (Fig. 5*C*), a value at least as high as that calculated for recombinant mammalian channels gathered under similar conditions. A measure of the persistent, steady-state current amplitude was assessed after 1 s of sustained potentials held from a range of −70

to −50 mV in 5-mV increments. The largest, persistent current corresponded to the estimated maximal window current size at resting membrane potentials of −65 mV (Fig. 5*c*, *inset*).

One of the characteristic features of T-type channels is a slow rate of deactivation[94]. Deactivation is measured as the rate of current decay from a tail current generated by the rapid return to lower, more hyperpolarized potentials with maximally opened channels (held at −35 mV) (Fig. 6). Deactivation rates of LCa_v3 are fastest at hyperpolarized potentials (−110 mV) and quickly slow with depolarization steps to resting potentials (−60 mV) (Fig. 6). LCa_v3 fits within the faster end of the range of deactivation kinetics for mammalian T-type channels but is still manyfold slower than Ca_v1 and Ca_v2 channels. The slowness of deactivation kinetics suggests that native LCa_v3 currents may pass a deactivating tail current upon membrane repolarization.

Macroscopic, native Ca^{2+} currents are typically equal or larger than Ba^{2+} currents at equimolar concentrations, although the unitary conductance is reported to be equal in high Ca^{2+} or Ba^{2+}[239]. Macroscopic Ca^{2+} currents range from smaller, equal, or larger than Ba^{2+} currents for recombinant $Ca_v3.2$, $Ca_v3.3$, or $Ca_v3.1$ channels, respectively[204]. Reasons for the relative differences in Ca^{2+} and Ba^{2+} permeability of different channel types are not clearly understood. LCa_v3 resembles $Ca_v3.2$ and other high voltage-activated snail Ca^{2+} channels, conducting larger amplitude whole cell Ba^{2+} currents than Ca^{2+} currents (Fig. 7*A*)[94]. Ba^{2+} as a charge carrier results in a slight hyperpolarizing shift in the current-voltage relationships compared with Ca^{2+} (Fig. 7*B*), but there is still a ∼50% increase in whole cell Ba^{2+} conductance compared with Ca^{2+} in the absence of driving force changes (Fig. 7*C*). Kinetics are also faster when Ba^{2+} is the charge carrier, with faster time to peak (Fig. 7*D*) associated with more rapid inactivation kinetics (Fig. 7*E*). Ca^{2+}-dependent inactivation typically associated with Ca_v1 channels is not a property of LCa_v3 or other T-type channels[204].

Ni^{2+} traditionally has been considered to be a blocker that distinguishes T-types from other channels, but only one of the three cloned mammalian T-channels, $Ca_v3.2$, is strongly inhibited by Ni^{2+}[240]. LCa_v3 is approximately equally sensitive to Ni^{2+} as $Ca_v3.1$ and $Ca_v3.3$, with an IC_{50} of 300 ± 29.24 μm (Fig. 8*A*), but all of these T-type channels are ∼20–60-fold less sensitive than $Ca_v3.2$[240]. Lee and co-workers[241] identified that the unusual Ni^{2+} sensitivity of $Ca_v3.2$ critically involves His-191, imbedded in a helix-turn-helix motif known as the S3b-S4 voltage sensor paddle in Domain I[242] (Fig. 8*C*). Interestingly, LCa_v3 does not have a corresponding His-191 residue of $Ca_v3.2$, but neither does the sequence of the S3b-S4 voltage sensor paddle of LCa_v3 compare well with any of the Ca_v3 channels (Fig. 8*C*). LCa_v3 has an eight-amino acid insert in this short linker region and extra positive

and negative charges compared with the mammalian Ca_v3 channels (Fig. 8*C*). The Ni^{2+} dose-response curve does not perfectly fit the data (Fig. 8*B*), but a biphasic dose-response curve does, having a high affinity IC_{50} of 27.25 ± 2.74 μm (38%) and a lower affinity IC_{50} of 1064.54 ± 79.11 μm (62%) (Fig. 8*B, inset*).

Mibefradil was marketed by Roche Applied Science as a drug for treatment of hypertension and angina[243] before it was withdrawn in 1998 for its potential side effects. It is a non-selective antagonist but typically has a ~10-fold greater selectivity for T-type channels over L-type Ca^{2+} channels. LCa_v3 is in the range of sensitivity to mibefradil (680 ± 0.03 nm) as mammalian T-type channels (Fig. 8*D*). Caution must be heeded when directly comparing results from different studies as mibefradil is highly sensitive to the charge carrier, charge carrier concentration, and holding potential[244].

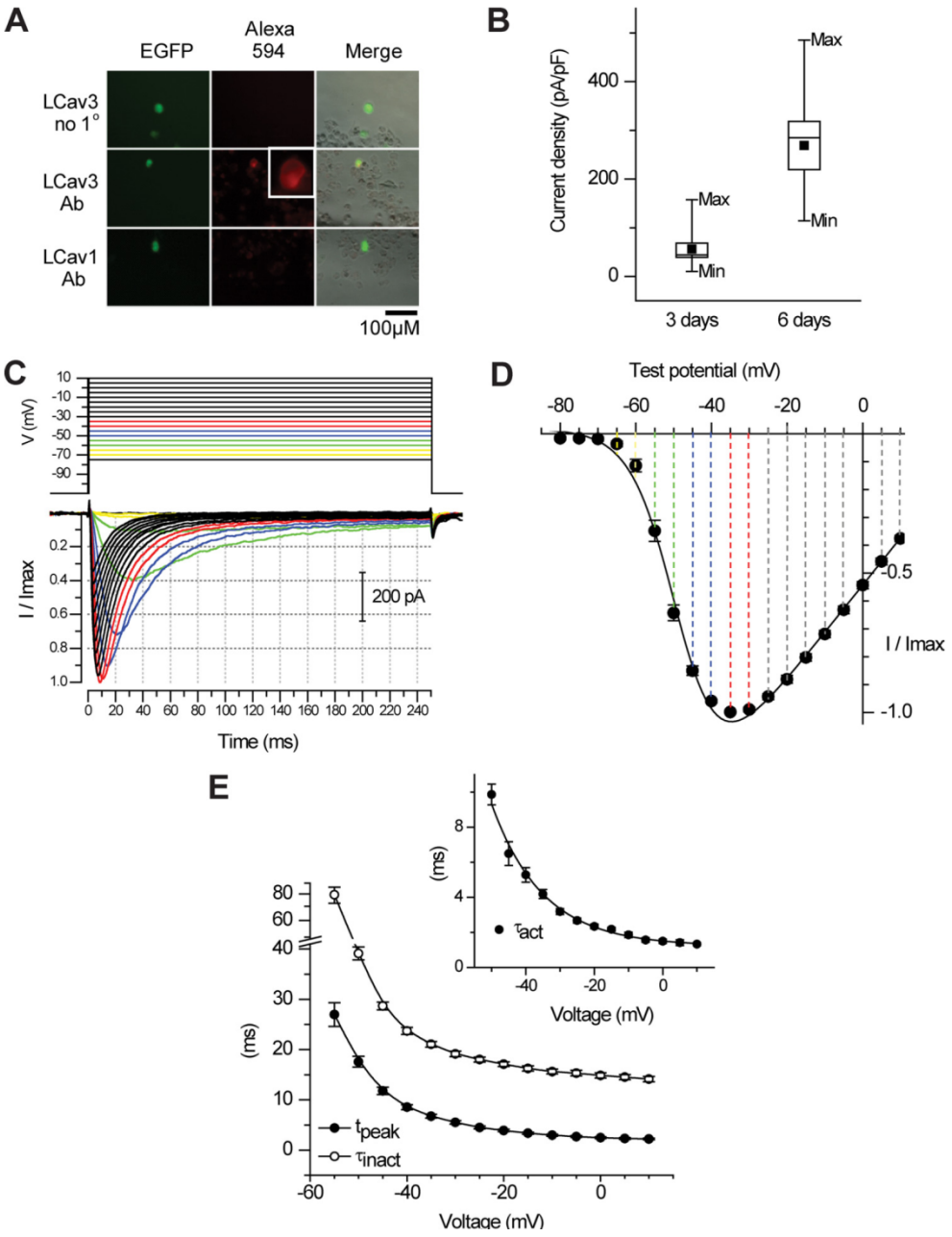

FIGURE 4. Transient transfection of HEK-293T cells harboring the pIRES2-EGFP plasmid containing invertebrate T-type channel cDNA reveal highly abundant channels and characteristic T-type channel properties. *A*, membrane delimited staining of LCa_v3 (inset) is evident in EGFP-positive cells but only with LCa_v3-specific antibody and not with preimmune serum or with *LCa_v1*-transfected cells. *B*, the box chart indicates the current density (pA/pF (picofarads)) of LCa_v3 expression on 3 or 6 days after transfection. The *box chart* also illustrates mean, median ± 1 S.D., min/max current densities. *C*, sample LCa_v3 currents are shown in response to 5-ms voltage steps from a −110 mV holding potential. Illustrated is an ensemble of rapidly activating and inactivating Ca^{2+} currents where each trace 'crosses over' the previous one from rest to peak, and the resulting normalized peak currents are plotted as a function of voltage step, indicating low threshold of activation (−65 mV) and maximal currents generated at a step to −35 mV (*D*). Current-voltage relationships were curve-fitted with an Ohmic-Boltzmann function. *E*, the increase in inactivation kinetics (τ_{inact}) closely follows the increasing speed at which the current approaches peak (t_{peak}), also reflected in the faster rate of activation, curve-fitted and represented by τ_{act}.

TABLE 1 Comparison of biophysical parameters for recombinant LCa$_v$3 and mammalian T-type channels expressed in human cell lines. NA, not available.

Electrophysiology	*LCav3*	*n*	Ca$_v$3.1	Reference	Ca$_v$3.2	Reference	Ca$_v$3.3	Reference
Activation								
$V_{½}$	−48.42 ± 0.34	5	−44.6 ± 0.7[a] −42.1 ± 1.1[b]	196, 195	−42.7 ± 0.7[b] −43.8 ± 0.8[b]	247, 197	−40.2 ± 0.8[b]	196
K	5.81 ± 0.30	5	5.8 ± 0.2 5.3 ± 0.2	196, 195	6.0 ± 0.1 6.3 ± 0.1	247, 197	5.8 ± .2	196
Peak of IV (mV)	−35	5	−30, −30	196, 195	−30	247	−25	196
Inactivation								
$V_{½}$	−65.40 ± 0.15	7	−77.7 ± 0.7[b] −74.1 ± 1.6[b]	196, 195	−77.7 ± 0.8[b] −78.1 ± 1.2[b]	247, 197	−68.6 ± 0.7[b]	196
K	2.76 ± 0.13	7	−5.0 ± 0.2[b] −5.3 ± 0.2[b]	196	−5.7 ± 0.2[b] −5.7 ± 0.1[b]	247, 197	−5.5 ± 0.5[b]	196
Kinetics at −20 mV								
τ_{act}	2.34 ± 0.12	5	1.6 ± 0.2[a]	195	2.9 ± 0.1[a]	197	NA	
τ_{inact}	17.11 ± 0.46	5	13.9 ± 1.1[a]	195	17.4 ± 0.9	197	NA	
Kinetics at −30 mV								
τ_{act}	3.19 ± 0.17	5	2.9 ± 0.4	205	3.8 ± 0.1[a]	205	14 ± 1.0[b]	205
τ_{inact}	19.16 ± 0.57	5	17 ± 6	205	16 ± 1	205	80 ± 5[b]	205
Deactivation								
−100 mV	1.03 ± 0.15	10	2.6 ± 0.2[b,c]	267	3.6 ± 0.4[b,c]	267	1.12 ± 0.1[c]	267
−70 mV	2.91 ± 0.64	10	6.2 ± 0.4[b,c]	267	8.5 ± 1.1[b,c]	267	2.1 ± 0.1[a,c]	267
Pharmacology								
Nickel (IC$_{50}$ μM)	300.00 ± 29.24	4	250 ± 22[d]	242, 243	4.9 ± 2.0[b,d] 12 ± 2[b,d]	242, 243	216 ± 9[a,d]	242
Mibefradil (IC$_{50}$ μM)	0.68 ± 0.03	4	1.2 ± 0.2[d]	246	1.1 ± 0.2[d]	246	1.5 ± 0.1[b,d]	246

[a] $p < 0.05$ (one-way analysis of variance).
[b] $p < 0.005$ (one-way analysis of variance).
[c] 2 mM instead of 5 mM Ca^{2+} in extracellular solution.
[d] 10 mM Ba^{2+} in extracellular solution.

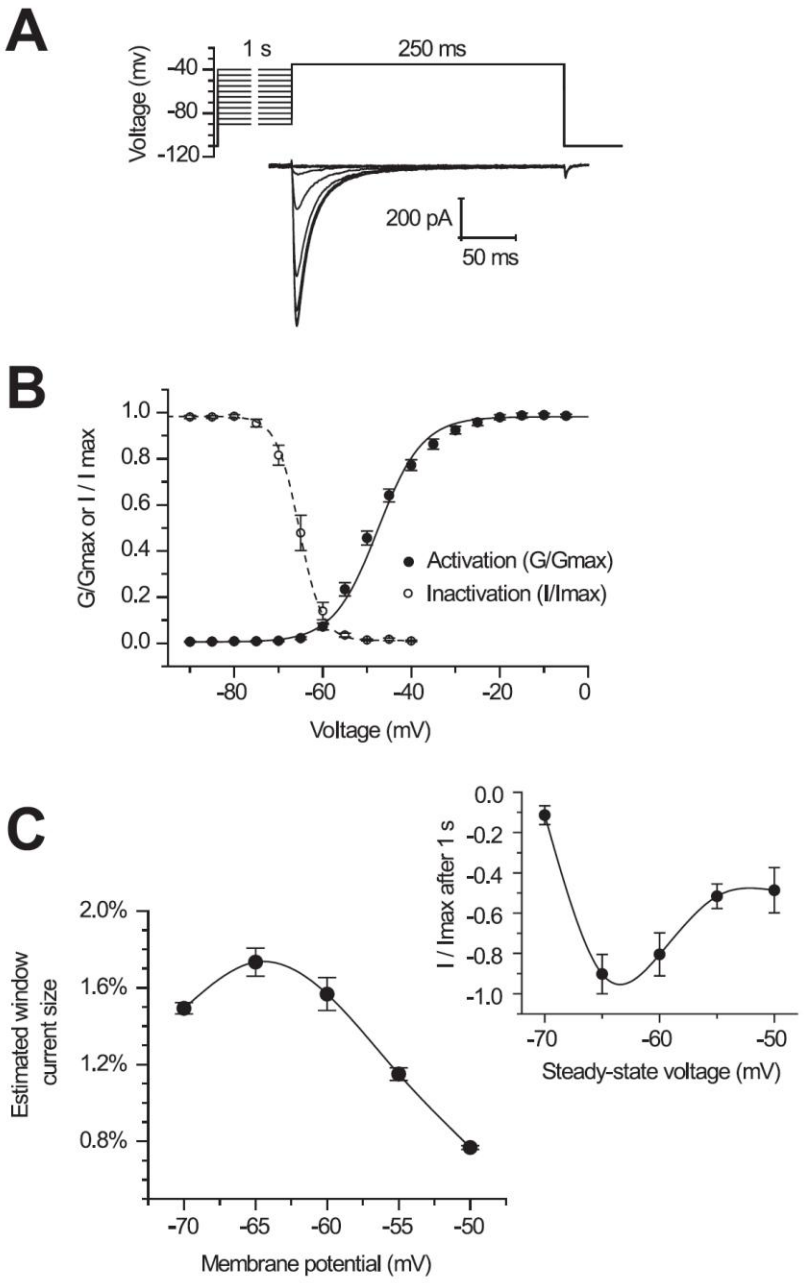

FIGURE 5. Invertebrate LCa$_v$3 has a large, persistent window current up to 1.8% of the total current near the resting membrane potential. *A*, sample current traces of maximal Ca$_v$3 currents (step to −35 mV) in response to a 1-s inactivating prepulse. *B*, a Boltzmann-fitted inactivation curve was generated by plotting the fraction of maximal current as a function of prepulse voltage. The fraction of maximal conductance at each voltage was plotted as an activation curve, curve-fitted with a Boltzmann function. The activation curve was derived from the current-voltage relationship minus the ohm-changes due to the driving force (illustrated in Fig 4*D*). *C*, calculation of the window currents were based on the product of the fraction of the whole cell conductance and fraction of available, non-inactivated channels at each voltage. *Inset*, a window current was measured at the end of a long, 1-s voltage-step. At 1 s, the majority of open channels will have been inactivated, leaving only open channels that persist under steady-state conditions, with a maximum at the resting membrane potential (−65 mV).

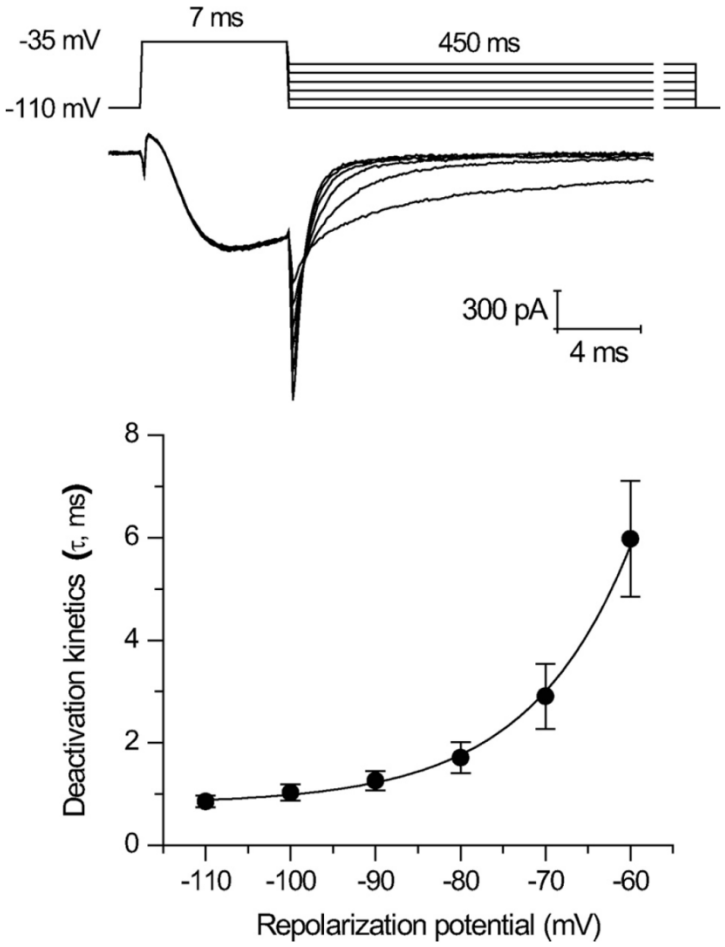

FIGURE 6. Invertebrate LCa,3 slowly deactivates similar to mammalian T-type channels. Sample tail currents and curve fitting of decay rate of tail currents (τ, ms) were generated by hyperpolarizing steps between −110 and −60 mV for 450 ms from a 7-ms depolarizing step to −35 mV.

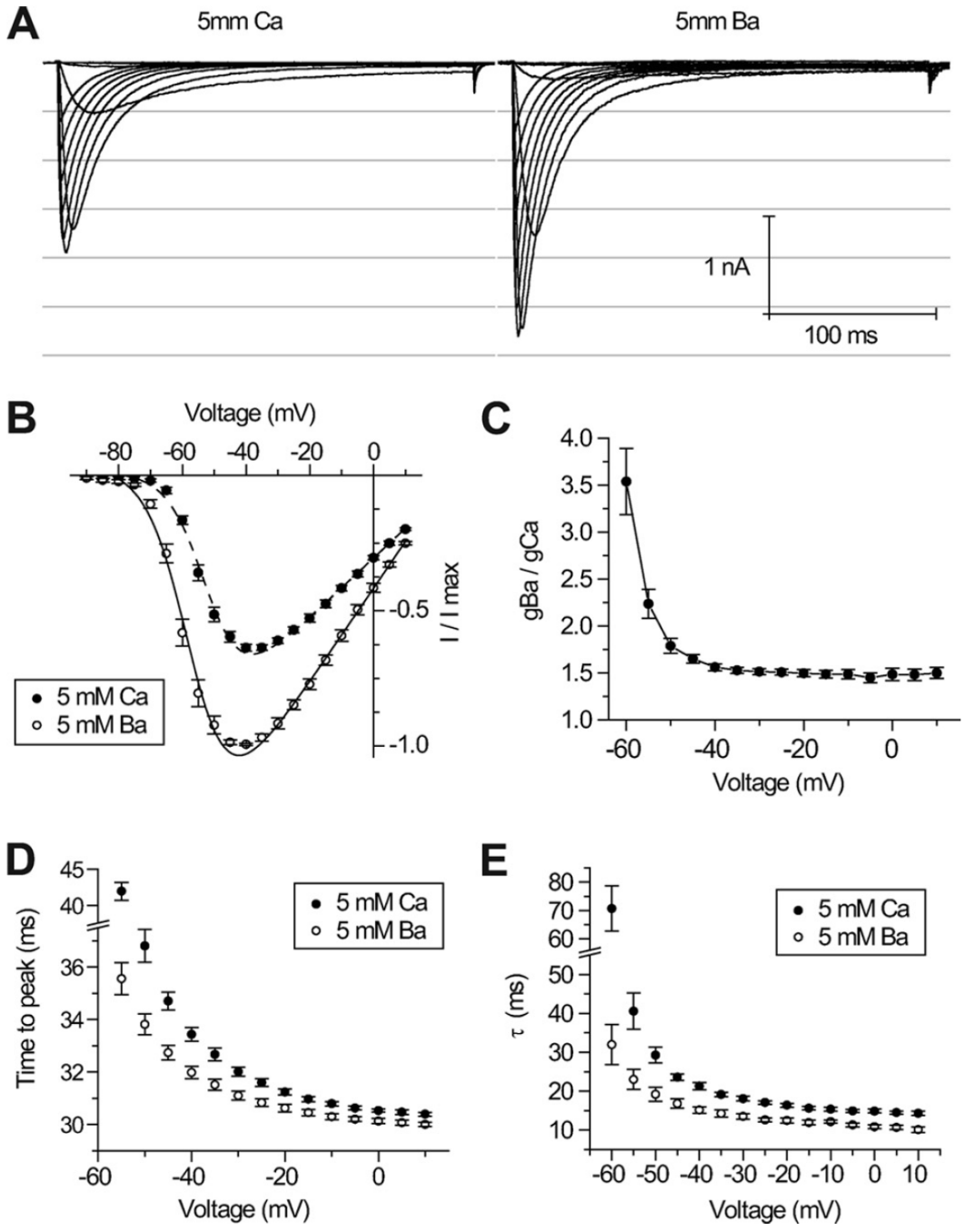

FIGURE 7. LCa$_v$3 currents are larger and faster when Ba^{2+} is the charge carrier. Sample traces (*A*) and current-voltage relationships (*B*) of LCa$_v$3 currents were generated from depolarizing voltage steps from a holding potential of −110 mV while microperfusing extracellular solution containing either 5 mm Ba^{2+} or 5 mm Ca^{2+}. Whole cell Ba^{2+} conductance was estimated to be ~50% greater than Ca^{2+} conductance at all voltages (*C*). Kinetics of activation (time to peak current, ms) (*D*) and inactivation decay (tau curve fit, ms) (*E*) are faster when barium instead of calcium is the charge carrier.

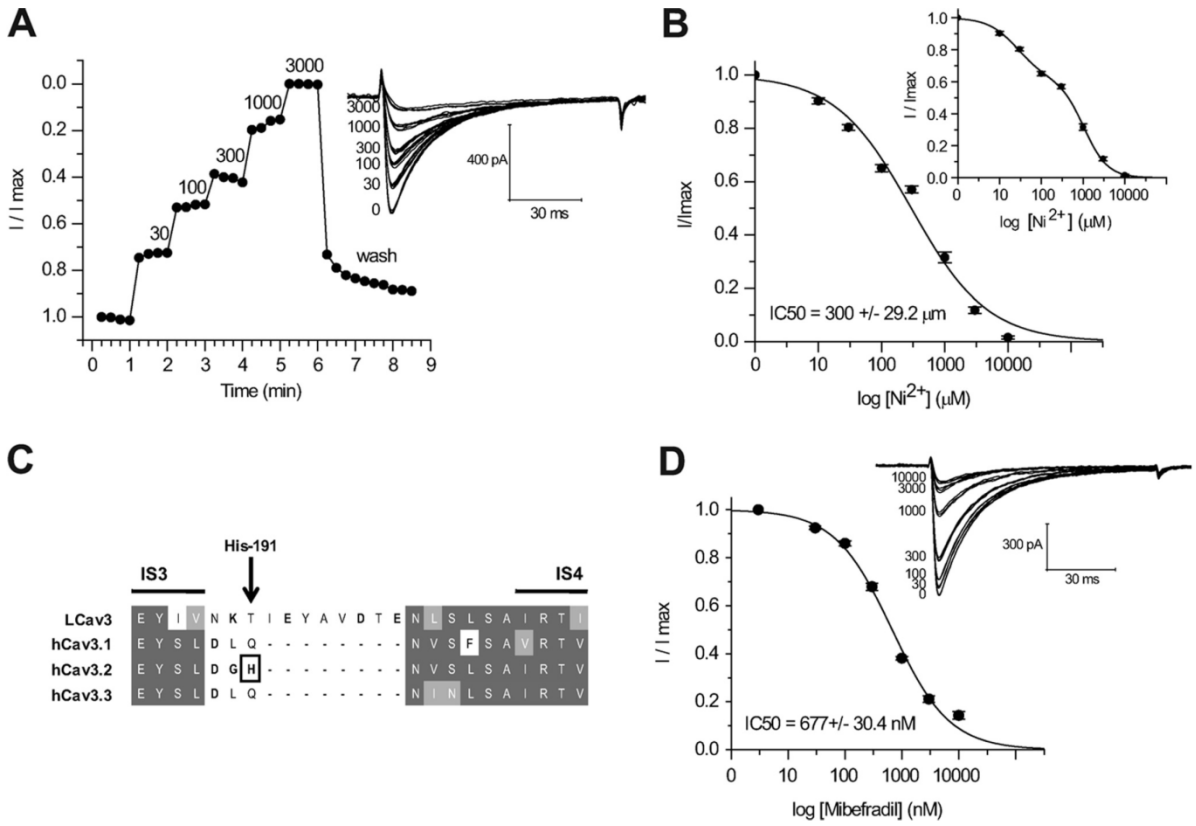

FIGURE 8. Invertebrate T-type channels have similar Ni^{2+} and mibefradil sensitivity as mammalian T-types. *A*, shown is the time course of Ni^{2+} inhibition of normalized LCa_v3 peak currents (*inset*, representative traces). *B*, cumulative dose-response is illustrated, with an IC_{50} (300 ± 29.2 µm) value that overlaps with IC_{50} of $Ca_v3.1$ (304.8 ± 6.2 µm; Kang *et al.*[241]). *Inset*, a better fit illustrated with a biphasic dose-response curve is shown. *C*, T-type channel alignments in the region of the S3b-S4 paddle of Domain I illustrate the His-191 required for high Ni^{2+} sensitivity of $Ca_v3.2$ channels. LCa_v3 has an eight-amino acid insert with additional charged residues in the relative position of the His-191 residue in $Ca_v3.2$. *D*, shown is a cumulative dose-response curve of mibefradil block of LCa_v3 (*inset*, representative traces), indicating an IC_{50} (300 ± 29.2 µm) value that is reminiscent of the IC_{50} for mammalian Ca_v3 channels.

2.1.4 Discussion

Introduction to LCa$_v$3

Here we describe the first *in vitro* expression characteristics of a snail homolog of mammalian T-type channels and, also remarkable, is that *LCa$_v$3* is only one of two full-length cDNA sequences determined for non-mammalian T-types to date. cDNAs are assembled from predicted exons from a number of invertebrate sequenced genomes (*e.g. Drosophila melanogaster* Ca-α1T-RB, accession no. NM_132068), but low homology outside of the conserved transmembrane domains indicates that the predicted transcript assemblies are likely erroneous when analyzed with multiple sequence alignments of cDNAs derived from mRNA (*LCa$_v$3* and *C. elegans cca-1B*, human *Ca$_v$3.1* to *Ca$_v$3.3*). *LCa$_v$3* codes for a 322-kDa protein of 2886 amino acids, which is the largest protein of any reported four-repeat ion channel expressed to date, including 1.25 times larger than mammalian T-type channels and 1.5 times larger than cca-1B from *C. elegans*, the only other reported invertebrate cDNA coding for a T-type channel. Whether T-type channels in other phylogenetic groups are this large or possibly even larger is not known.

Permeation and the DDEE Selectivity Filter

The transmembrane regions are not responsible for most of the extra mass of LCa$_v$3 and include the highly conserved, voltage-sensor domain (S1 to S4) the outer helix (S5), the P-loop, and inner helix (S6) in all four repeat domains[94]. A unique DDEE selectivity filter[88] and a gating brake[245] are two trademarks of T-types that distinguish them from the Ca$_v$1 and Ca$_v$2 Ca^{2+} channel families. Flexible side chains of each domain harboring key glutamate residues (EEEE) contribute to the selectivity filter by extending into the permeation pathway, where they are expected to bridge Ca^{2+} ions as they pass through the pore of high voltage-activated Ca$_v$1 and Ca$_v$2 channels[43]. A highly conserved aspartate residue upstream in the selectivity filter and adjacent to the glutamate residue in Domain II may serve to attract incoming Ca^{2+} ions to the ion-selective pore of all Ca^{2+} channels, according to modeling studies by B. Zhorov[43]. T-type channels are reported to have a lower Ca^{2+} selectivity over monovalent cations as the estimated reversal potential is less positive than high voltage-activated Ca$_v$1 and Ca$_v$2 channels (+40 *versus* +60 mV)[246]. Shortened carbon side chains in Domains I and II of T-types (DDEE instead of EEEE) may bridge Ca^{2+} ions less stringently, resulting in lower pore selectivity for Ca^{2+} ions in favor of faster kinetics that is typical for T-type Ca^{2+} channels. Interestingly, inactivation kinetic changes mirror changes in activation kinetics in T-types[57], and a modified EEDD locus alters gating properties[88].

No obvious conclusion can be drawn from differences in permeability for Ba^{2+} and Ca^{2+} ions among T-type channels. Only LCa_v3 and mammalian $Ca_v3.2$ channels have larger macroscopic Ba^{2+} than Ca^{2+} currents. Interestingly, greater macroscopic currents in Ba^{2+} over Ca^{2+} are a consistent feature with snail Ca^{2+} channels expressed in HEK-293T cells including LCa_v1[214] and LCa_v2[213].

Gating Brake

A gating brake shared among T-type channels is considered to prevent channel opening at hyperpolarized potentials, as nucleotide polymorphisms in patients with childhood absence epilepsy or strategically placed deletions in this region produce channels that open at even more negative potentials than typical T-type channels[197]. The proximal I-II loop of LCa_v3 is predicted to contain the helix-loop-helix gating brake structure[245], and more distally the I-II loop has been ascribed to regulating the surface expression of T-types[196]. It may be more than coincidence that the gating brake is in the equivalent position where β subunits associate with and alter the biophysical properties of high voltage-activated Ca_v1 and Ca_v2 channels as well as regulate/modulate their expression (*e.g.* protein folding, turnover, and membrane trafficking)[247]. Indeed, invertebrate LCa_v3 does not require accessory β or $\alpha_2\delta$ subunits and robustly expresses in human HEK-293T cells at an efficiency that rivals the mammalian T-type channels. Continued transfection in the presence of G418 antibiotic selection has generated a number of stable HEK-293T cell lines for LCa_v3. A high constitutive expression of LCa_v3 under the strong mammalian cytomegalovirus promoter argues in favor of greater transcriptional controls for T-type channel expression in native cells compared with perhaps more post-translational checkpoints regulating the expression of Ca_v1 and Ca_v2 channels that are known to form complex, multimeric assemblies along the secretory pathway.

Overall Shared Features of T-type Channels

Scoring of the overall amino acid conservation between invertebrate and mammalian genes can lead to overestimates of the degree of structural divergence, as a sequence not under selection will drift substantially over the hundreds of millions of years separating their evolution. Comparing the *in vitro* expression characteristics between LCa_v3 and mammalian T-types suggests a structural equivalency in core regions despite the overall sequence divergence of different channels, revealing a set of quintessential properties shared by all T-types. Voltage properties are tightly regulated with fast and transient kinetics, slow deactivation, window currents produced by overlapping activation, and availability curves and channel activity limited to a narrow window of subthreshold voltages where channels are available and conducting. Also, similar drug sensitivities of LCa_v3 for Ni^{2+} ions and

mibefradil suggest conserved residues in the outer pore and the aqueous permeation pathway between the selectivity filter and the aqueous, pore-lined, inner S6 helices (inverted tepee-shape) as predicted from the three-dimensional structure of crystallized K channels[45]. Probing the affinity of a number of different T-type channel drugs will assist in interpreting the structural variants in the snail channel pore *versus* the mammalian ones.

Primitive Features in Invertebrate Channels

Invertebrate Ca^{2+} channels of the high voltage variety are also highly conserved in their biophysical properties. Rat $Ca_v1.2$ and snail LCa_v1 channels, for example, are so alike that there are no reliable biophysical features outside of drug sensitivity that separate the two channels transfected in HEK-293T cells[215]. Differences outside of biophysical features appear to reflect the primitiveness of the invertebrate homologue, reminiscent of a state preceding the evolution of specializations in electromechanical coupling, such as the tetrad organization in skeletal muscle where mammalian $Ca_v1.1$ channels are directly coupled to ryanodine receptors of the sarcoplasmic reticulum[248]. Invertebrate muscles lack tetrads or an equivalent $Ca_v1.1$ channel that mediates muscle contraction[248]. More indirect coupling, with Ca^{2+} serving as a short range transmitter, is also a feature of invertebrate neurotransmission. Invertebrate Ca_v2 channels that are responsible for transmitter release lack a II-III loop structure containing the synaptic protein binding site of $Ca_v2.1$ and $Ca_v2.2$ channels[238] and also exhibit a synaptic organization lacking key structural proteins present in mammalian synapses (such as Bassoon and CAST) and a synaptic substructure, such as a *Drosophila* T-bar, which is unlike the mammalian presynaptic density[249].

T-type Channel Diversity

T-type channels are modulated through intracellular signaling cascades and are coupled to other ion channels[250], but there is little to indicate that T-types serve as instruments for electromechanical coupling in cell-type specific, multisubunit complexes in the manner of Ca_v1 and Ca_v2 channels[251]. Structural diversity in the three mammalian T-type channels arose out of genomic duplication, perhaps creating some overlapping redundancy in function. Yet the presence of unique biophysical properties, tissue specificity, modulation, and putative protein-protein interactions sites suggests otherwise, indicating that the different genes may provide specialized functions in mammals. Examples that illustrate this functional divergence include the contribution to rebound burst firing in thalamocortical neurons by $Ca_v3.1$, the involvement of $Ca_v3.2$ in pain sensitivity, relaxation of coronary arteries and secretion of aldosterone, and the involvement of $Ca_v3.3$ in long-lasting bursts in

the inferior olive and habenula served by its slower kinetics and a larger window current range compared with other T-type channels[94]. Distinct, regional antibody staining within individual central neurons suggests that each gene may serve particular roles within somatic, dendritic, and perinuclear compartments[89,252]. Whether the diversity of mechanisms in mammals is contained within a single invertebrate Ca_v3 gene and its alternative splicing has not been explored.

Wide Range of Functions Expected for Abundant T-type Channel Transcript

Here we show that *LCa_v3* is the most abundant Ca^{2+} channel transcript in the *Lymnaea* nervous system, and our previous analysis indicates that this reflects a transcript profile in an individual snail neuron[238]. Quantitative RT-PCR of single identified respiratory VD4 neurons, measured in replicates of six neurons, indicated that *LCa_v3* is manyfold more abundant than either *LCa_v1* or *LCa_v2* channel expression[238]. Their abundance in invertebrates may reflect a wide range of functions associated with T-type channels such as (*a*) shaping nerve action potentials and pacemaking, (*b*) a non-electrogenic role for T-types in providing Ca^{2+} through window currents[233], and (*c*) roles in differentiating and proliferating cells (3) and (*d*) secretion[253]. Some invertebrates also appear to have additional roles that are not served by mammalian T-type channels, such as excitation contraction coupling in jellyfish muscle cells[110] or facilitating the contraction of pharyngeal muscles in nematodes[254]. Interestingly, T-type spikes can provide qualitatively different information than sodium spikes in the same invertebrate axons. Weak depolarizations initiate slow swimming via T-type spikes, whereas stronger pacemaking inputs initiate a fast escape swimming response mediated by overshooting sodium spikes in the same axons, presumably operating in the availability range outside of T-type channels[255].

Drug Binding; Nickel

LCa_v3 has equal (~300 μm IC_{50}) Ni^{2+} sensitivity as $Ca_v3.1$ and $Ca_v3.3$ channels. We report that the Ni^{2+} dose-response curve for LCa_v3 is biphasic, indicative of two components of drug block. A similar biphasic Ni^{2+} block is apparent in the dose-response data for mammalian recombinant channels (Fig. 3*D* in Ref. [241], Fig. 2*B* in Ref. [240], and Fig. 7*B* in Ref. [256]) and in native currents (Fig. 3*A* in Ref. [257], Fig. 6*B* in Ref. [258], and Fig. 7*B* in Ref. [258]). A biphasic response might result from two Ni^{2+} binding sites. Jones and co-workers suggest that $Ca_v3.1$ indeed has two binding sites, one in the outer pore and another deeper site within the pore pathway that is strongly affected by the permeant ion[259].

Unusually sensitive Ni^{2+} block (5–10 μm IC_{50}) is a property of $Ca_v3.2$ channels and critically involves a His-191 residue[241] in what has been described as the S3b-S4 voltage sensor paddle for sodium channels based on the x-ray structure of potassium channels[260]. More than His-191 may be critical in the S3b-S4 voltage sensor paddle as a similar high affinity cation block of $Ca_v3.2$ channels by extracellular Zn^{2+} involves the His-191 residue and two residues directly upstream of His-191, in particular, Asp-189 and Gly-190[261].

The S3b-S4 is considered to carry most of the gating charge and likely drives the conformational changes required for pore opening and closing. It seems probable that Ni^{2+} associates with the S3b-S4 paddle motif of $Ca_v3.2$ in a manner similar to how tarantula and scorpion toxins immobilize the voltage sensor of sodium channels[242]. $Ca_v3.2$ is inhibited by Ni^{2+} independently of voltage and is similarly blocked with Ca^{2+} or Ba^{2+} as a charge carrier, which is consistent with an inhibition by a mechanism outside the permeation pathway[259]. Interestingly, LCa_v3 has an eight-amino acid insert in this short S3b-S4 region with extra positive and negative charges compared with Ca_v3 channels. The effect of the insert on Ni^{2+} block or voltage-gating, if any, is not known.

Other regions may also contribute to Ni^{2+} block. High affinity Zn^{2+} block in $Ca_v3.2$ channels also involves a neutral Ala-140 in IS2 that is negatively charged (Asp-140) in corresponding position of less sensitive $Ca_v3.1$ and $Ca_v3.3$ channels[262]. Future chimera work may be important to evaluate whether LCa_v3 with a positively charged His-140 at this position influences cation block.

Drug Binding; Mibefradil

A number of new and potent T-type channel blockers are being explored, and mibefradil serves as the first T-type channel blocker that was clinically available[243]. Interestingly, mibefradil block of snail LCa_v3 channel is in the range of potency of mammalian T-types. With doses spanning the mid-range of the IC_{50} (680 ± 0.03 nm), we observed that the mibefradil block of LCa_v3 would not readily stabilize, with accumulation of a slow but progressive block during long periods (tens of min) of continuous perfusion. We assume that this reflects a use-dependence often ascribed to mibefradil block[262]. A slow time course of mibefradil block may also be explained by a reported accumulation of a hydrolyzed metabolite and more membrane-impermeant form of mibefradil (dm-mibefradil) that has an affinity for calcium channels from the cytoplasm[263]. Further probing of different structures with mammalian and snail homologs will provide an opportunity for describing the high affinity drug binding in T-type channels.

Summary and Future Prospects

Expression characteristics of an invertebrate T-type channel have combined features that are reminiscent of all mammalian $Ca_v3.1$, $Ca_v3.2$, and $Ca_v3.3$ channels (see Table 1). LCa_v3 is 25% larger than any voltage-gated ion channel expressed to date and is the most abundantly expressed Ca^{2+} channel transcript in the snail nervous system. Window currents in invertebrate and mammalian T-type channels suggest a likely non-electrogenic role for T-types in providing Ca^{2+} for proliferating and differentiating cells and in the developing embryo. Alternative splicing of the single invertebrate gene may provide the structural diversity for shaping the window current and firing patterns catered for individual network requirements. We anticipate that the snail will provide unique perspectives for probing T-type channel physiology. Much can be learned from the simple molluscan preparation where only a single T-type channel gene is expressed in native cells and where there is relative ease in probing the physiological mechanisms in single identified cultured neurons and intact networks in the brain that underlay well described behaviors[216]. An invertebrate channel also provides an opportunity to reflect on evolutionary mechanisms. Channel I as it was first described has turned out to be the most challenging Ca^{2+} channel to analyze since it was identified by Hagiwara *et al.*[236] more than 35 years ago. There is some truth in the following summary statement by Gray and Macdonald[264], reflecting on the present status of the T-type channel field: "[The] Physiologic regulation of T-type channels is simultaneously well documented and very obscure."

2.1.5 Acknowledgements

We thank E. Perez-Reyes and B. Zhorov for helpful discussions, H. Vigil-Guitierrez for assistance in generating LCa_v3 antibodies, S. Lam for support in setting up the electrophysiological experiments, and A. N. Boone for editing the manuscript.

This work was supported by the Natural Science and Engineering Research Council (NSERC) of Canada and a NSERC Alexander Graham Bell Canada Graduate Scholarships (doctoral) (to A. Senatore).

2.1.6 Other details

The nucleotide sequence(s) reported in this paper has been submitted to the GenBank™/EBI Data Bank with accession number(s) AF484084.

2.2 Conserved alternative splicing between the invertebrate LCa$_v$3 channel gene and mammalian Ca$_v$3 homologues

This research is published in the journal PLoS ONE: Adriano Senatore and J. David Spafford (2012). **Gene Transcription and Splicing of T-Type Channels are Evolutionarily-Conserved Strategies for Regulating Channel Expression and Gating.** PLoS ONE. 7(6):e37409. © Peter Binfield, Publisher, PLoS ONE and Community Journals.

The manuscript contains research conducted by Adriano Senatore while in the laboratory of Dr. J. David Spafford, *in silico* structural comparisons of several vertebrate and invertebrate 4-domain ion channels, and a comprehensive inventory of relevant biophysical data available for mammalian Ca$_v$3 channels for comparison with *Lymnaea* Ca$_v$3 (conducted by Dr. Spafford). Here, we propose the existence of evolutionarily conserved splicing between *Lymnaea* and mammalian Ca$_v$3 channel homologues in their respective I-II and III-IV cytoplasmic linkers (i.e. optional exon 8b in the I-II linker and 25c in the III-IV linker). Remarkably, the temporal and spatial expression of these exons are highly analogous in their respective organisms, with similar expression patterns for LCa$_v$3 and mammalian Ca$_v$3.1 and Ca$_v$3.2 channel splice isoforms in the heart and CNS at different stages of development. Functionally, the alternative splicing-induced alterations in channel structure produce analogous influences on membrane expression (exon 8b) and biophysical properties (exon 25c). All of these features suggest that alternative splicing in the I-II and III-IV linkers are evolutionarily conserved, or at least arose through convergent evolution, and serve to modulate T-type channel function for different roles throughout development and in different tissues.

Materials and methods, as well as supplementary materials and methods that are part of this manuscript, can be found in Appendix B.

2.2.1 Abstract

T-type calcium channels operate within tightly regulated biophysical constraints for supporting rhythmic firing in the brain, heart and secretory organs of invertebrates and vertebrates. The snail T-type gene, *LCa$_v$3* from *Lymnaea stagnalis*, possesses alternative, tandem donor splice sites enabling a choice of a large exon 8b (201 aa) or a short exon 25c (9 aa) in cytoplasmic linkers, similar to mammalian homologs. Inclusion of optional 25c exons in the III-IV linker of T-type channels speeds up kinetics and causes hyperpolarizing shifts in both activation and steady-state inactivation of macroscopic currents. The abundant variant lacking exon 25c is the workhorse of embryonic Ca$_v$3 channels, whose high density and right-shifted activation and availability curves are expected to increase pace-making and allow the channels to contribute more significantly to cellular excitation in prenatal tissue. Presence of brain-enriched, optional exon 8b conserved with mammalian Ca$_v$3.1 and encompassing the proximal half of the I-II linker, imparts a ~50% reduction in total and surface-expressed LCa$_v$3 channel protein, which accounts for reduced whole-cell calcium currents of +8b variants in HEK cells. Evolutionarily conserved optional exons in cytoplasmic linkers of Ca$_v$3 channels regulate expression (exon 8b) and a battery of biophysical properties (exon 25c) for tuning specialized firing patterns in different tissues and throughout development.

2.2.2 Introduction

Ca$_v$3 channels are known for gating 'transient' currents at low voltages near the resting membrane potential, and often depolarize cells to threshold in a cyclical manner to promote rhythmic firing (for reviews see Senatore *et al*., 2012[64] and Perez-Reyes 2003[94]). Animals with Ca$_v$3 channels appear in relatives of extant multicellular organisms without tissues or organs (e.g. *Trichoplax*), and within Cnidarians, the simplest phlyum to harbor a nervous system (e.g. sea anemone *Nematostella*; **Fig. 1*A***). Soft-bodied invertebrates, precursors to various animal phyla including molluscs, likely first appeared in the Late Vendian Period (650 to 543 mya), prior to the divergence of the single ancestral Ca$_v$3 channel gene into three mammalian genes *CACNA1G* (Ca$_v$3.1 or α_1G), *CACNA1H* (Ca$_v$3.2 or α_1H) and *CACNA1I* (Ca$_v$3.3 or α_1I)[64]. Recently, we have cloned and expressed the first non-vertebrate Ca$_v$3 channel *in vitro*, LCa$_v$3, from the pond snail *Lymnaea stagnalis*[1]. Here, we describe two optional exons in the I-II and III-IV cytoplasmic linkers of *LCa$_v$3* that are evolutionarily conserved with vertebrate Ca$_v$3 channels and likely play critical roles in regulating membrane expression and an array of biophysical properties during development. The evolutionarily distant

LCa$_v$3 channel highlights key and fundamental features for T-type channels, providing an important perspective for understanding Ca$_v$3 channel regulation.

2.2.3 Results

Structural conservation in Ca$_v$3 channels

Comparisons between Ca$_v$3 channels reveal that mammalian genes cluster more closely in overall sequence similarity amongst themselves than to the more evolutionarily distant and solitary *Ca$_v$3* gene in snails (**Fig. 1 *A* and *B***). Much of the divergence from the snail sequence lies in the tethered, cytoplasmic loops between transmembrane domains, which also bear surprisingly conserved islands of conservation (**Fig. 1*C***). A signature helix-loop-helix in the proximal I-II cytoplasmic linker forms a 'gating brake' that is unique to all Ca$_v$3 channels, which when deleted augments characteristic features by shifting low-voltages of activation to even more hyperpolarized potentials, and increases kinetics of channel opening and closure[245,196]. Downstream of the gating brake in vertebrate Ca$_v$3.1 and invertebrate Ca$_v$3 channels is a region that contains a large cluster of histidine residues, followed by an isolated and conserved 'APRASPExxD/E' motif that is surrounded by unconserved sequences (**Fig. 1*D***).

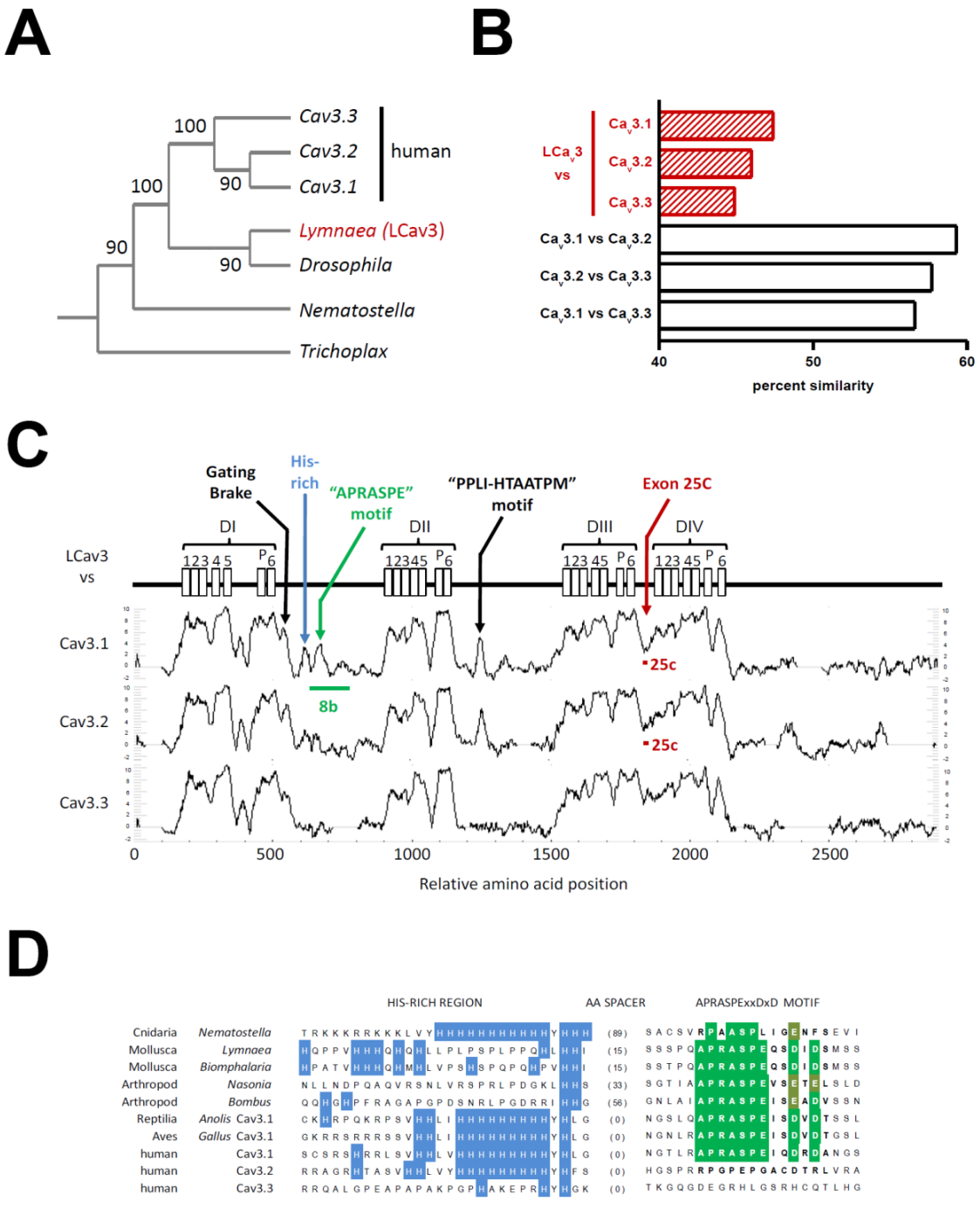

Figure 1. LCa$_v$3 channel from snail is a distant homolog to mammalian Ca$_v$3.1, Ca$_v$3.2 and Ca$_v$3.3, with conserved structural features in the cytoplasmic loops. (A) Phylogeny of T-type calcium channels using maximum parsimony with bootstrap scores indicated on branches. (B) Percent similarity of amino acid sequences of T-type channels (snail vs. human) using the Needleman-Wunsch global alignment algorithm. (C) Running average of similarity of snail versus human T-type channel amino acid sequences using a window of 25 aa (plotcon, EMBOSS http://emboss.open-bio.org/). (D) Alignment of T-type channel sequences in the I-II linker. Amino acids between the Histidine rich region and the APRASPE motif vary from 0 to 89 aa.

Conserved splicing of exons 8b and 25c

Interestingly, the 'APRASPE' motif is contained within an optional portion of exon 8 that normally spans from Domain I segment 6 across ~70% of the cytoplasmic I-II linker. The optional portion of exon 8 (termed exon 8b), is similarly spliced out in snail and mammalian[195] Ca_v3 channel genes by use of alternative, upstream, intron donor splice sites within exon 8 that truncate the I-II linker coding sequences of *LCa_v3* and *$Ca_v3.1$* by 603 and 402 bp, respectively (**Fig. S1)**. Exon 8b occurs downstream of the gating brake, and its omission shortens the I-II linker of LCa_v3 channels by 201 aa (~50%) and $Ca_v3.1$ by 134 aa (~39%; **Fig. 2*A***). A second conserved region of alternative splicing corresponds precisely with the middle of the III-IV cytoplasmic linker (**Fig. 2*B***), which is similarly short in closely related Na_v and Ca_v channels (54 +/-1 aa; **Fig. 2*C***). Splicing at alternative and more upstream, phase 1 intron donor splice sites shortens the III-IV linker by between 7 and 11 aa in different snail Ca_v3 and mammalian $Ca_v3.1$ and $Ca_v3.2$ channels (**Figs. 2*B*, S2, S3**). *$Ca_v3.1$* and *$Ca_v3.2$* genes also possess downstream, similarly short optional cassette exons, termed exon 26, that code for between 6 and 19 aa, and that may be included in lieu of exon 25c or appear in tandem with it (**Figs. 2*B* and S4**). A consensus amino acid sequence or a number of positively or negatively charged residues is not a consistent feature of 25c exons. The only consistent feature is the first residue coding serine (coded by AGT) that completes the consensus kinase phosphorylation site (KKRKS for LCa_v3), which also contributes to the consensus upstream 5' donor splice site (GTRAGT; **Figs. 2*B* and S4**).

A simple evolutionary pattern has many invertebrate and mammalian *$Ca_v3.3$* channel genes having 'ΔΔ' isoforms lacking exons 25c or 26. Snail *LCa_v3* possesses exon 25c besides ΔΔ, but analyses of over 48 independent RT-PCR products from snail embryonic and adult RNA did not uncover an optional cassette exon 26 for *LCa_v3* (**Fig. S5**). Vertebrate *$Ca_v3.1$* and *$Ca_v3.2$* possess both exons 25c and 26, and have correspondingly larger intron sizes spanning these regions than genes lacking either exon 26 (e.g. snail *Ca_v3*), or both exons 25 and exons 26 (e.g. *$Ca_v3.3$*; **Fig. 2*D***). Larger intron sizes suggest more extensive regulation of alternative splicing for these short exons.

Lymnaea (snail) LCa_v3 I-II linker (GenBank Accession: JQ313138):

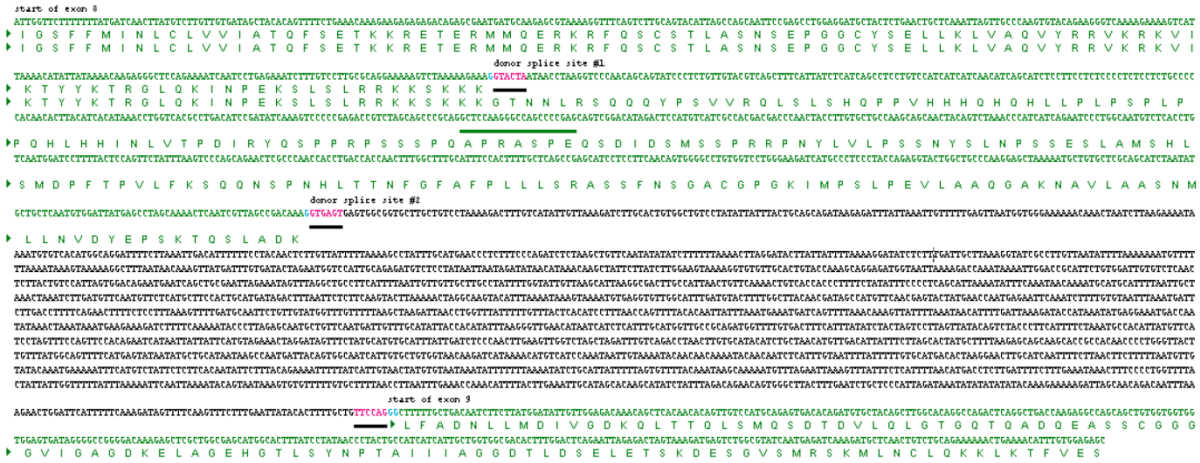

Rat $Ca_v3.1$ I-II linker (GenBank Accession: EF116283):

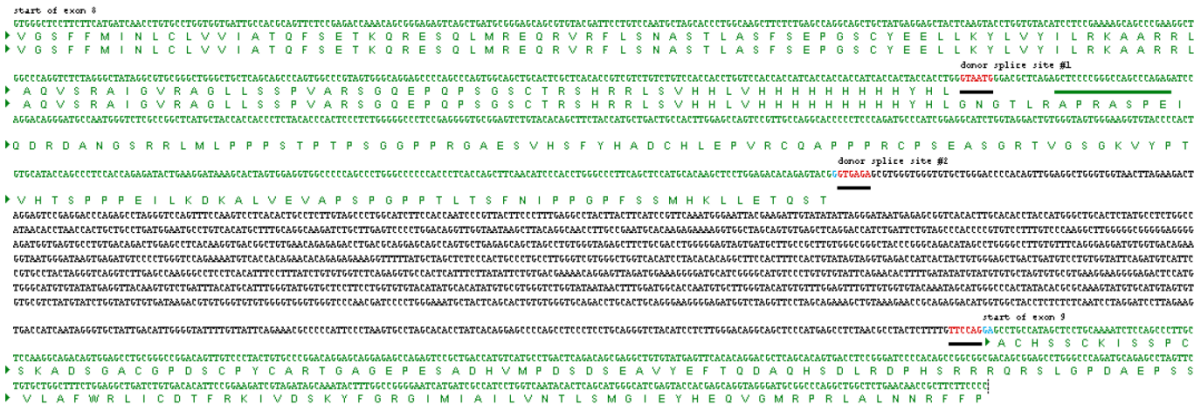

Supplementary Figure 1. Genomic region spanning region surrounding tandem 5' donor splice sites, that lead to the optional inclusion of exon 8b and a conserved APRASPE motif in the I-II linker of snail LCa_v3 and mammalian $Ca_v3.1$ T-type channels.

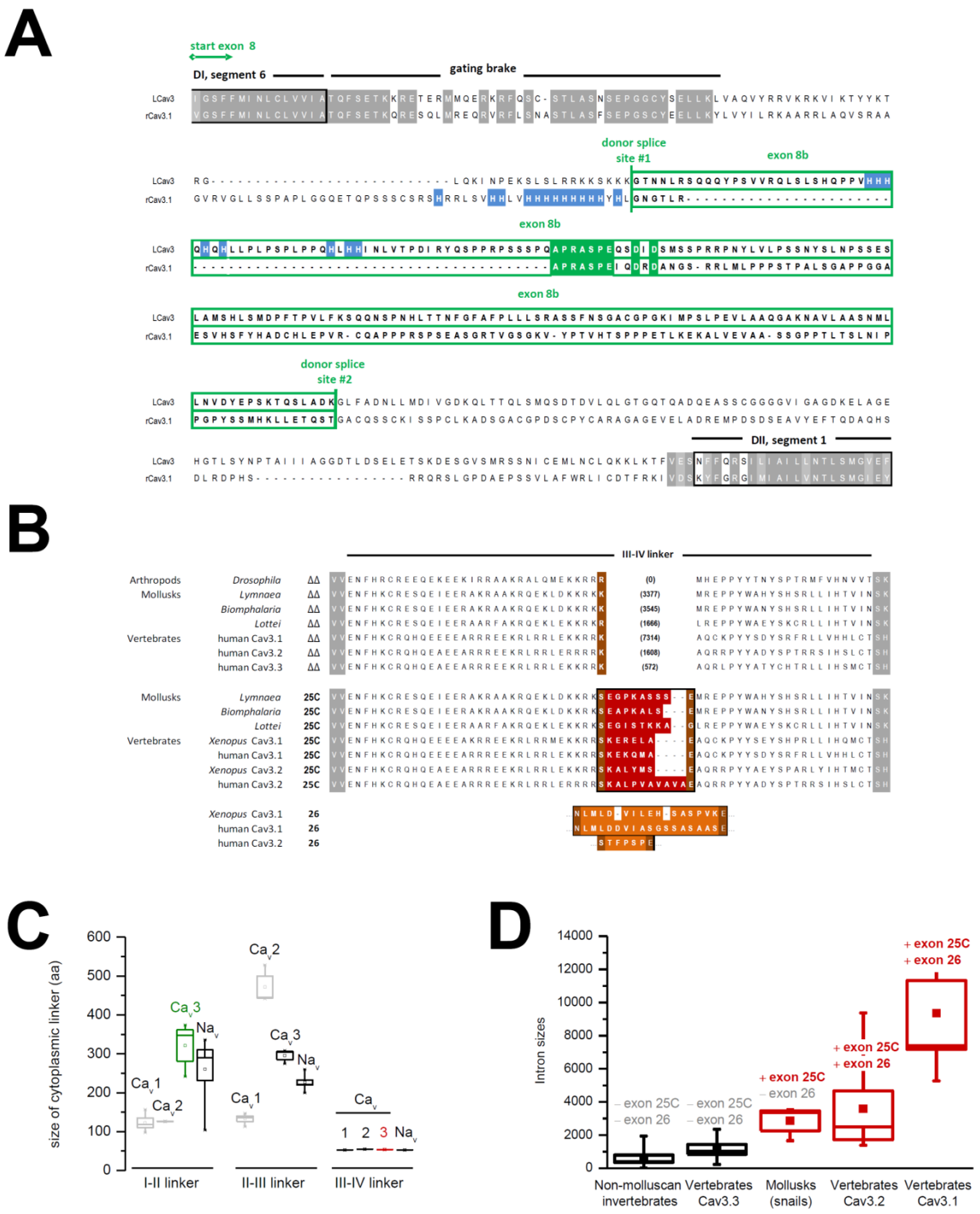

Figure 2. T-type calcium channels utilize alternative 5' donor splice sites to generate optional exon 8b (I-II linker) and exon 25c (III-IV linker) isoforms. (A) Alignment of the snail LCa$_v$3 and human Ca$_v$3.1 channel cytoplasmic I-II linkers, illustrating the conserved APRASPE motif in optional exon 8b. (B) Alignment of cytoplasmic III-IV linkers from invertebrates and vertebrates, illustrating the conservation of optional exon 25c and optional cassette exon 26. The numbers in brackets are the intron sizes at this position, ranging from 0 bp (*Drosophila*) to 7314 bp (human Ca$_v$3.1). (C) Box plots showing size range distributions of cytoplasmic linkers from human Ca$_v$1.1-1.4, Ca$_v$2.1-2.3, Ca$_v$3.1-3.3 and sodium channels Na$_v$1.1-1.9 plus Na$_v$X (mean +/- s.e.m.). (D) Box plot of intron sizes (mean +/- s.e.m.) for different T-type channels lacking or containing exon 25c and sometimes exon 26.

Lymnaea (snail) LCa_v3 III-IV linker (Genbank accession: JQ313139):

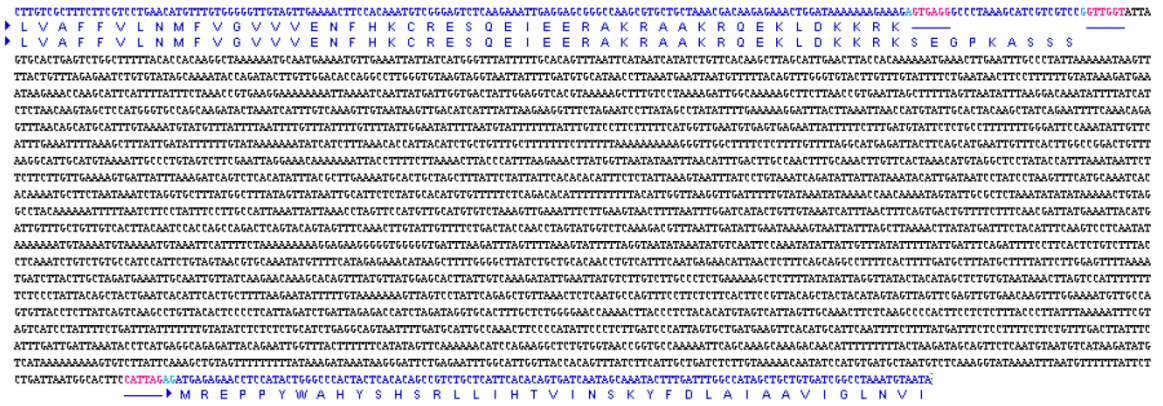

Biomphalaria (snail) $Ca_v3.1$ III-IV linker (WUGI: Contig 251):

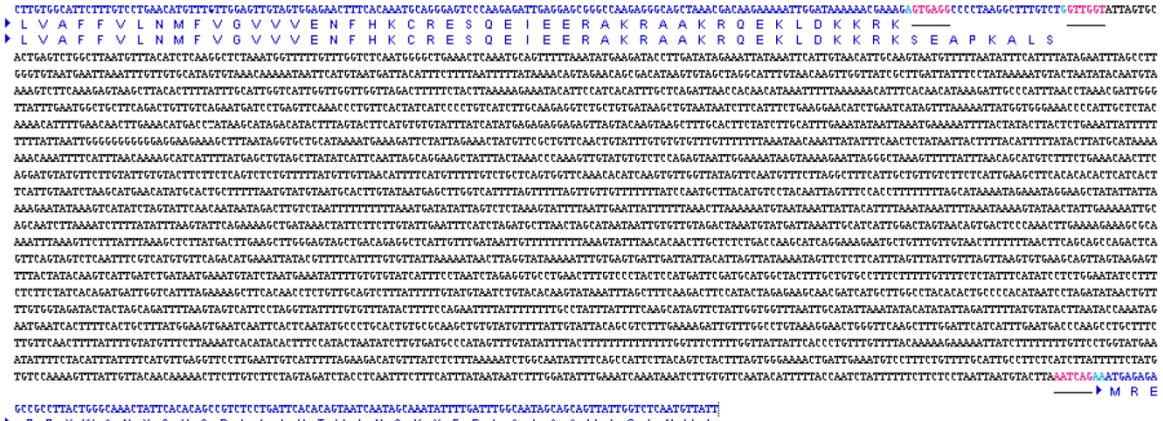

Lottia (snail) $Ca_v3.1$ III-IV linker (JGI: scaffold 59):

Supplementary Figure 2. Genomic region spanning region surrounding tandem 5' donor splice sites, that lead to the optional inclusion of exon 25c in the III-IV linker of *Lymnaea* LCa_v3 and other snail T-type channels.

Human $Ca_V3.1$ alpha1G III-IV linker (GenBank: 224589808):

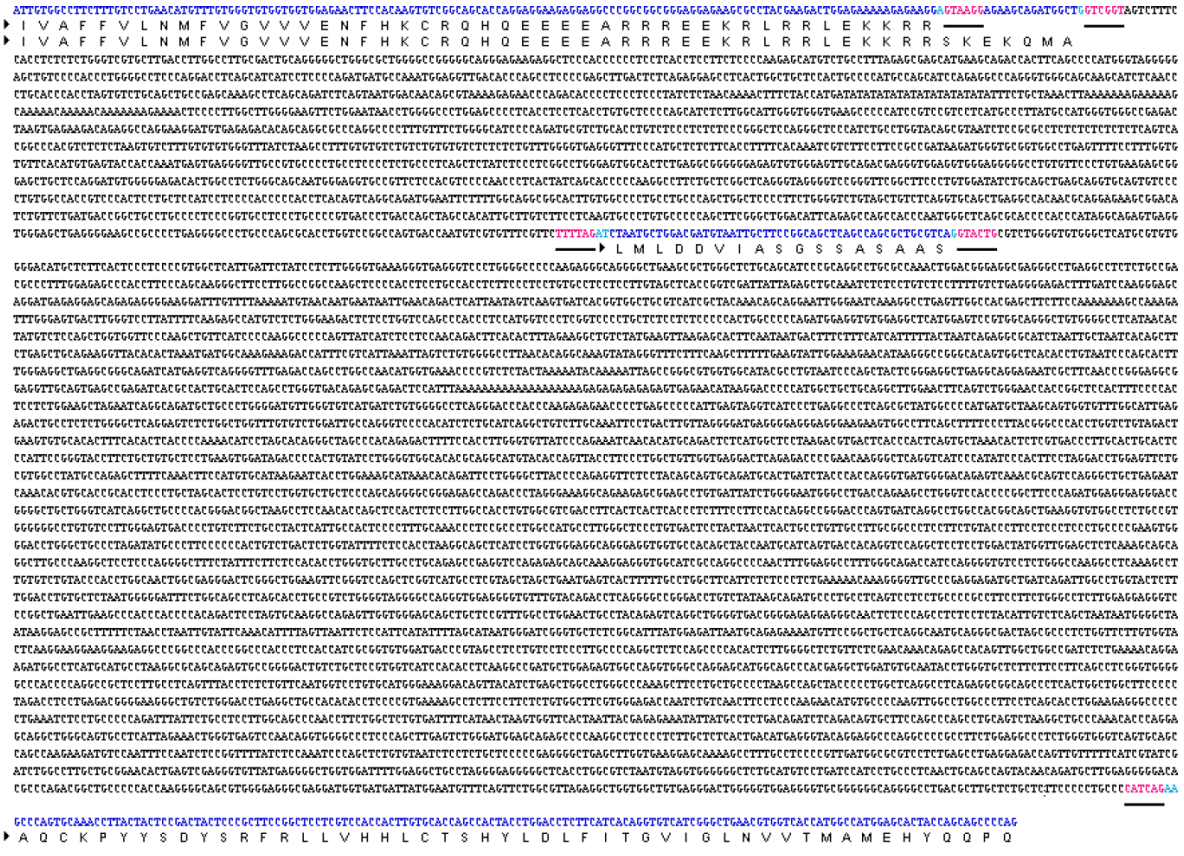

Human $Ca_V3.2$ alpha1H III-IV linker (GenBank: NG_012647):

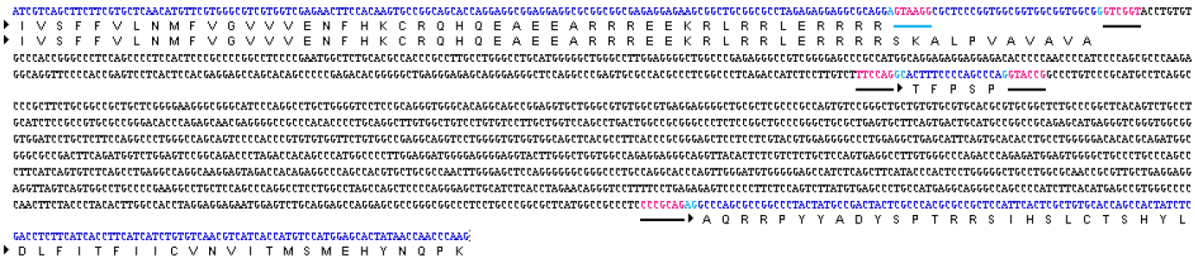

Supplementary Figure 3. Genomic region spanning region surrounding tandem 5' donor splice sites, that lead to the optional inclusion of exon 25c in the III-IV linker of human T-type channels. Also shown are the splice sites for exon 26.

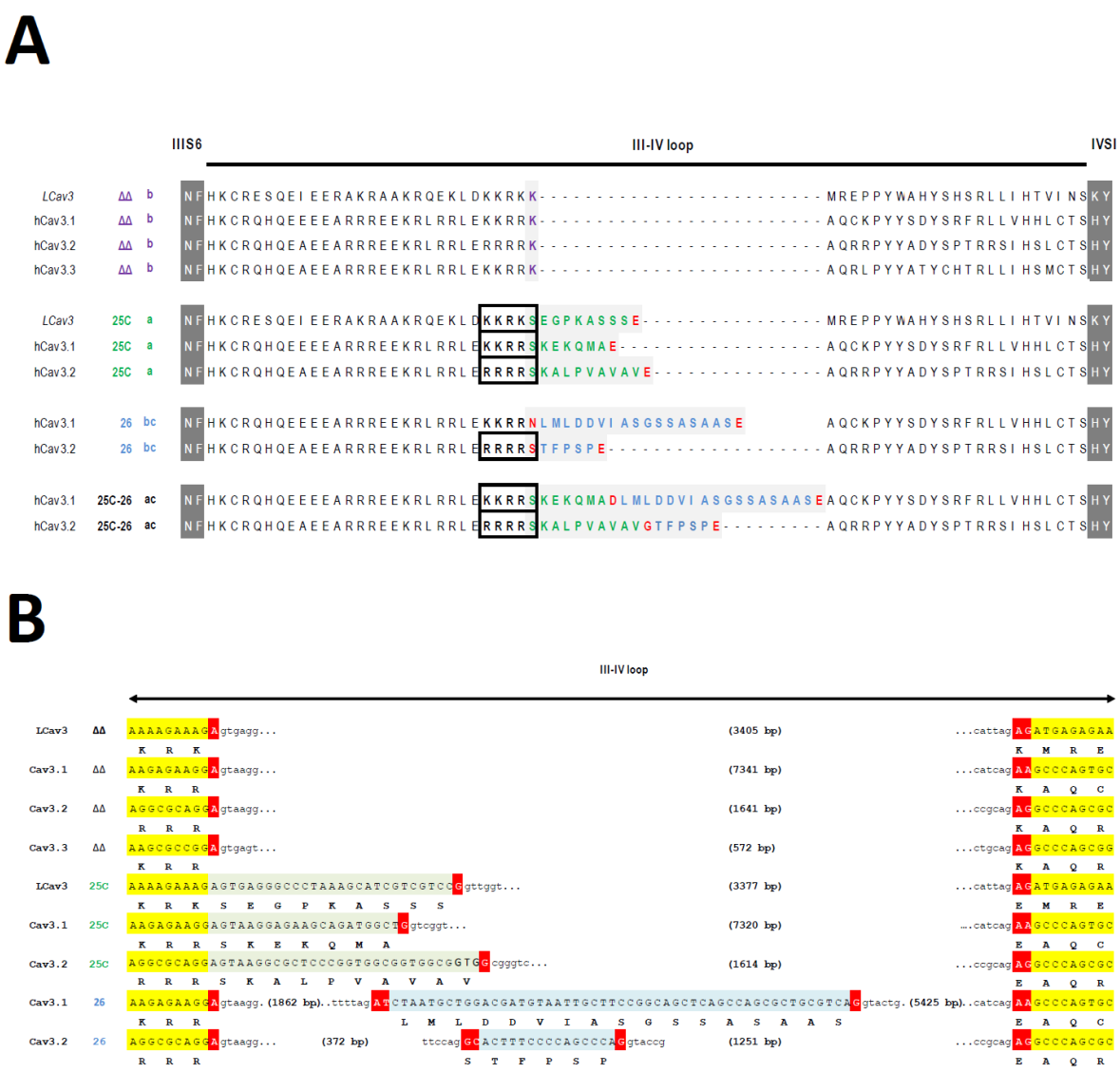

Supplementary Figure 4. (A) Alignment of amino acid sequences illustrating the conservation of ΔΔ and 25c alternative splice isoforms in the III-IV linker of snail LCa$_v$3 and vertebrate Ca$_v$3.1 and Ca$_v$3.2 channels. Presence of Exon 25c creates a consensus protein kinase A site (boxed) in LCa$_v$3, Ca$_v$3.1 and Ca$_v$3.2 channels. Optional Exon 26 is only found in Ca$_v$3.1 and Ca$_v$3.2 channels. Ca$_v$3.3 only has the ΔΔ exon isoform. (B) **Illustration of the aligned DNA sequences flanking exons ΔΔ , 25c and 26**. Intron sizes are in brackets.

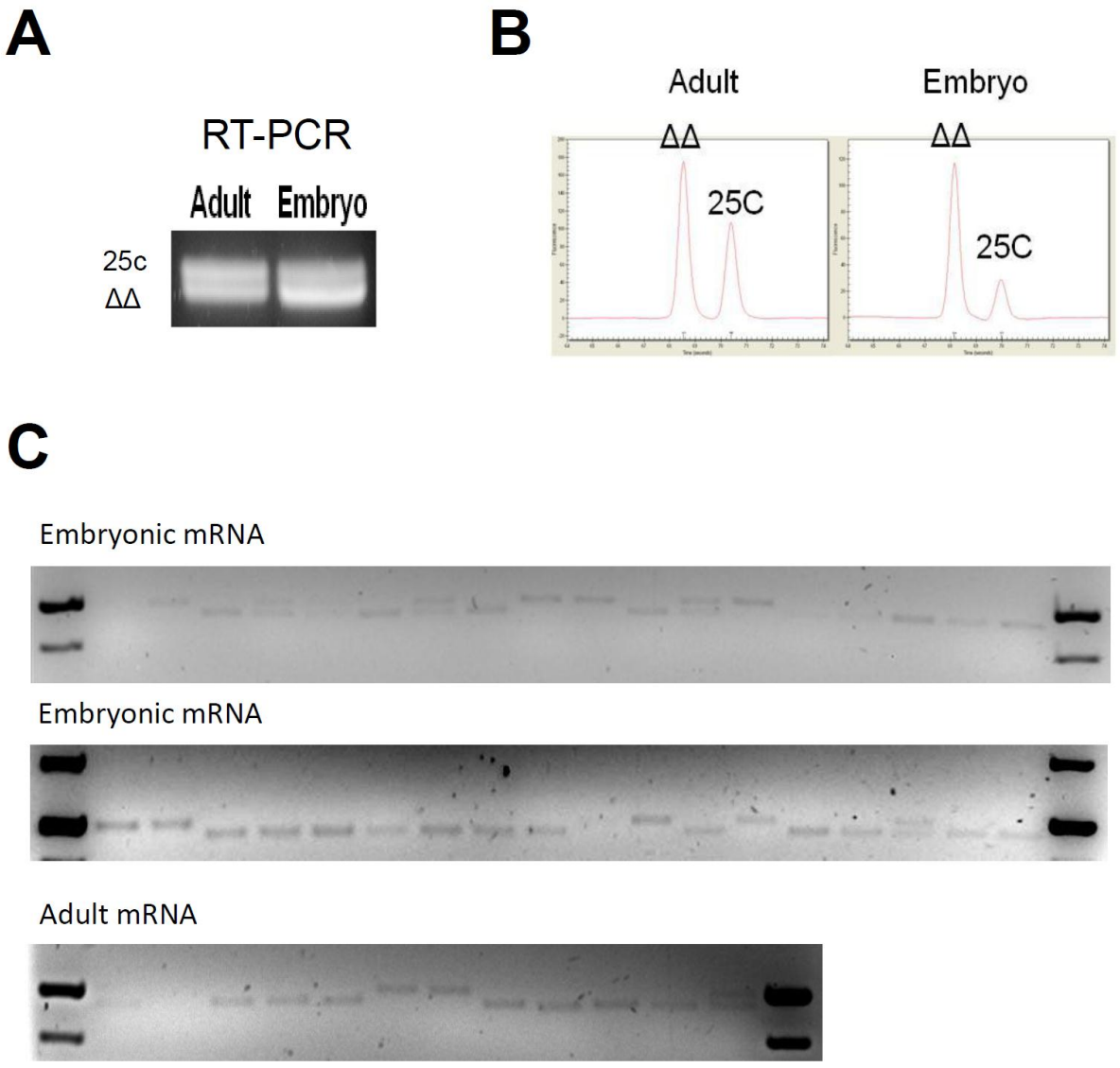

Supplementary Figure 5. PCR amplification of adult and embryonic cDNAs spanning the III-IV linker coding sequence of snail LCa,3 reveal two mRNA transcripts coding for ΔΔ and 25c alternative-splice isoforms, but not optional cassette exon 26. (A) Original PCR of III-IV linker inserts derived from adult and embryonic mRNA from snails. (B) High resolution and quantification of the two III-IV linker gel insert sizes using 1 kb DNA Lab-On-Chip technology with Experion (Bio-Rad) automated gel electrophoresis system. (C) Diagnostic gel pattern of the two different clone sizes in cloned pGEM-T Easy insert samples, assayed by *EcoR*I restriction digest and confirmed by DNA sequencing. Note the predominance of ΔΔ clones over exon 25c in samples of embryonic RT-PCR clones.

LCa$_v$3 channel expression patterns are consistent with those in mammals

mRNA transcript levels measured by quantitative RT-PCR suggest that LCa$_v$3 channels are most abundant in the brain, with intermediate expression in the heart and secretory glands (albumen and prostate), and almost non-detectable levels in buccal and foot musculature of adult snails (**Fig. 3*A***). The overall profile of expression closely matches that of *Ca$_v$3.1*, which is more abundant in the CNS, but not exclusively expressed in the adult brain (i.e. *Ca$_v$3.3*), nor is it expressed more widely outside the brain (i.e. *Ca$_v$3.2*)[204].

A general precipitous decline in mRNA transcript levels of *LCa$_v$3* occurs from mid-embryo stage (50-75% embryonic development) to near hatching (100% embryonic development) to juvenile snails (**Fig. 3 *B* and *D***), corresponding to a similar decline of mammalian *Ca$_v$3* calcium channel gene expression during development (reviewed in Senatore *et al*., 2012[64]). There is a continued, slight decline in Ca$_v$3 channel expression from juvenile to adult animals except for a spike in expression in the albumen gland, likely associated with sexual maturation, and a dramatic decline in the heart, that also parallels the precipitous fall in *LCa$_v$3* expression during mammalian heart development (**Fig. 3*C***)[108].

Conserved regulation of exon 8b and 25c splicing

LCa$_v$3 transcripts with and without 8b exons are of approximately equal abundance in the central nervous system and secretory glands (such as albumen gland; **Fig. 3*A***), which approximates the findings in rat brain where there is significant mRNA expression of *Ca$_v$3.1* with and without 8b exons[195]. We observe that the +8b isoform is less associated with the snail heart (16%) and buccal/foot musculature, compared to the higher levels in the brain and secretory glands (**Fig. 3*A***). Exon 25c has a more striking developmentally-regulated pattern, with a precipitous decline in *LCa$_v$3* transcripts lacking exon 25c from embryo to adults (**Fig. 3 *B* and *D***), especially in the heart (**Fig. 3*C***). The continued down-regulation of Ca$_v$3 channels lacking exon 25c from juveniles to adults gives the appearance of a switch with an increasing relative expression of the plus exon 25c isoform in the adult brain and secretory albumen and prostate glands (**Fig. 3*C***). Exon 25c-containing isoforms of *LCa$_v$3* predominate in the adult heart (79%; **Fig. 3*A***) and enhance in expression in most adult snail tissues (**Fig. 3*C***). The relative absence of exon 25c before and at birth and its predominance in adults is consistent between snail *LCa$_v$3* and mammalian *Ca$_v$3.1*[190,265,193] and *Ca$_v$3.2*[266,200] (**Fig. 3*E***). Correlative analysis of normalized qPCR data for plus and minus 8b and 25c variants, across all juvenile and adult tissues tested, reveals that +8b and -25c variants share similar variability in

expression between the different tissues (correlation coefficient R^2=0.885), and that -8b and +25c also share similar expression patterns (R^2=0.898), while +8b/+25c and -8b/-25c have much lower correlation coefficients (**Fig. S6**).

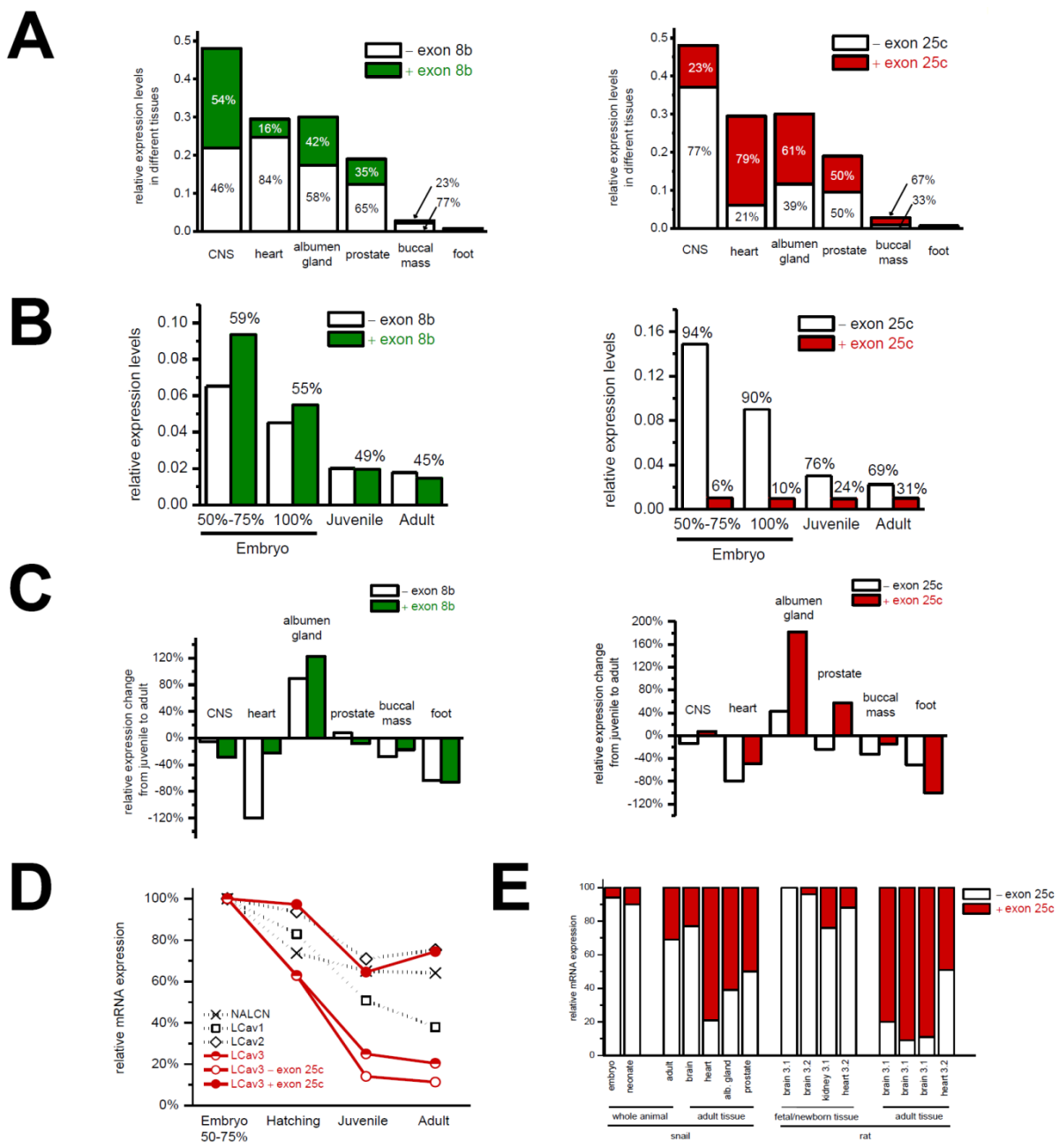

Figure 3. mRNA expression levels of LCa$_v$3 and exon 8b and exon 25c splice variants, measured using quantitative RT-PCR. All expression values for (A) to (D) are standardized to *Lymnaea* HPRT1 control gene. (A) mRNA expression levels of LCa$_v$3 (full bar values) and +/- exon 8b variants (left panel, green and white respectively) and +/- exon 25c variants (right panel, red and white respectively) in different adult snail organs. (B) mRNA expression levels of 8b (left panel) and 25c (right panel) LCa$_v$3 variants in whole animals during different developmental stages (early embryo: 50-75%, near hatching embryo: 100%, juvenile and adult snails). (C) Change in mRNA levels of 8b and 25c variants in different snail organs from juvenile to adult. (D) Percent change in mRNA expression of snail cation channel genes. (E) Percent of library clones or mRNA expression levels of snail and rat T-type channels with and without exon 25c.

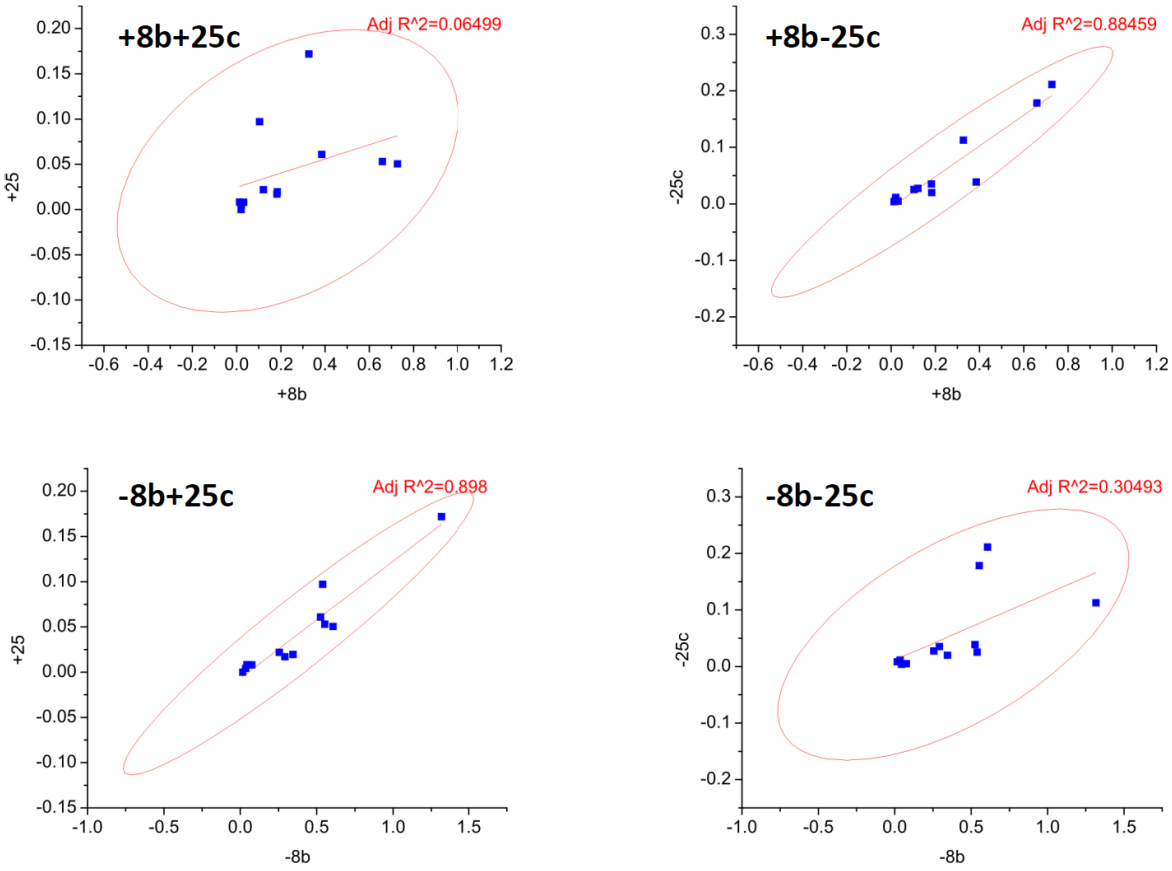

Supplementary Figure 6. Scatter matrix analysis of normalized mRNA qPCR values for the various alternative splice sites of LCa$_v$3 reveals that +8b and -25c variants tend to have similar expression patterns amongst the various adult and juvenile tissues tested (correlation coefficient R^2 of 0.885); -8b and +25c also have a high R^2 value of 0.898. Confidence regions of 95% for the correlated values are depicted by the red ellipses. Analysis was carried out using Origin 8.5 software (OriginLab).

Exon 25c selectively alters biophysical properties of LCa_v3

Using whole cell patch clamp technique we examined the biophysical consequences of the absence or presence of exons 8b and 25c in cloned LCa_v3 variants heterologously expressed in HEK-293T cells, and performed one-way analysis of variance to assess statistical significance (**Table 1**). Surprisingly, the absence or presence of the large I-II linker 8b exon has comparatively little influence on the biophysical properties of LCa_v3 (**Figs. 4 and 5**) when compared to the small 25c insert. The peaks of the rapidly-activating and inactivating calcium currents were measured in response to 5 mV steps in the presence of 2 mM extracellular calcium (**Fig. 4 *A* and *B*)**. Inclusion of exon 25c induces statistically significant -3.7 mV (+8b) and -3.8 mV (-8b) hyperpolarizing shifts in the half-maximal activation ($V_{0.5}$) of LCa_v3 calcium currents, extrapolated from the fitted Boltzmann of the plot of the fraction of maximal conductance at each voltage step (**Fig. 4*C* and Table 1**). Exon 25c also causes parallel -3.9 and -6.9 mV hyperpolarizing shifts in half-maximal inactivation for +/- exon 8b LCa_v3 variants, respectively (**Fig. 4*C* and Table 1**). Boltzmann-fitted inactivation curves were generated by measuring residual peak currents at -35 mV following a series of inactivating, pre-pulse voltage steps (**Fig. 4*C***). Similar hyperpolarizing shifts in the half maximal values for activation and inactivation curves are apparent for exon 25c inserts, regardless of the difference in their sequence or gene isoform type for snail LCa_v3, or mammalian $Ca_v3.1$[192,190] or $Ca_v3.2$ channels[266,267,200] (**Fig. 4*D* and Table 1**). The effect of exon 25c on the hyperpolarizing shift is greater than the differences in voltage-sensitivities between different T-type channels (**Fig. 4*E***). Optional exon 26 also causes shifts in the voltage-sensitivities of activation and inactivation for $Ca_v3.1$and $Ca_v3.2$ (**Fig. 4*D***), although generally the differences are much less dramatic than those imposed by exon 25c.

Exon 25c also promotes a significant speeding up of channel kinetics, most apparent in currents elicited by small voltage steps (-60 or -55 mV; **Fig. 5*A* and Table 1**). Activation kinetics are significantly faster in the presence of exon 25c, especially when exon 8b is also present, as measured as the delay to time to peak current (**Fig. 5*B***), as are inactivation kinetics, as measured by single exponential tau curve fits (**Fig. 5*C***). A role of exon 25c in promoting faster channel activation and inactivation is common to both snail and mammalian Ca_v3 channels (**Fig. 5*D***). Deactivation kinetics are slowed by exon 25c, which corresponds to a slower rate of closure of Ca_v3 channels from the open state, especially those currents elicited from voltage steps down to negative voltages such as resting membrane potential or more hyperpolarized than rest (-100 to -65 mV; **Fig. 5*E***). A slowing of deactivation kinetics in the presence of exon 25c is also a shared feature of snail and mammalian[267,192]

Ca_v3 channels (**Fig. 5*F***). Exon 25c also promotes a slowing of the recovery rate from inactivation at the earliest time points of recovery (<0.2 seconds; **Fig. 5*G* inset and Table 1**), reminiscent to the slowing of inactivation promoted by exon 25c in mammalian Ca_v3 channels[192]. It should be noted that LCa_v3 is relatively slow to recover from inactivation compared to mammalian Ca_v3 channels, even in the absence of exon 25c (**Fig. 5*G***). Exon 8b can fine tune the biophysical changes imparted by exon 25c, such as influencing kinetics at depolarized potentials (i.e. above -45 mV; **Fig. 5 *B, C*, Table 1**), or speeding up deactivation, more pronounced in the presence of exon 25c, near resting membrane potential (i.e. -60 to -70 mV; **Fig. 5*E* and Table 1**). In summary, snails and mammals possess highly variable short 25c exons that exert near identical biophysical changes to Ca_v3 channels during development.

Table 1: Summary of biophysical parameters of LCa_v3 channel variants containing exons 8b and 25c expressed in HEK-293T cells, with one-way analysis of variance to assess statistical significance.

	LCa_v3 +8b -25c (A)	LCa_v3 -8b -25c (B)	LCa_v3 +8b +25c (C)	LCa_v3 -8b +25c (D)	Significance A vs. B	A vs. C	A vs. D	B vs. C	B vs. D	C vs. D
Activation										
$V_{0.5}$ (mV)	-53.48 ±0.34 (13)	-53.36 ±1.22 (6)	-57.13 ±0.35 (18)	-57.15 ±0.54 (14)	n.s	***	***	***	**	n.s.
Slope (mv)	5.46 ±0.14 (13)	5.45 ±0.20 (6)	4.34 ±0.09 (18)	4.60 ±0.14 (14)	n.s.	***	***	***	**	n.s.
Inactivation										
$V_{0.5}$ (mV)	-70.89 ±0.49 (16)	-69.91 ±0.5 (14)	-74.80 ±0.28 (16)	-76.78 ±0.29 (15)	n.s.	***	***	***	***	***
Slope (mV)	2.93 ±0.08 (16)	3.11 ±0.10 (14)	3.12 ±0.05 (16)	3.14 ±0.04 (15)	n.s.	*	*	n.s.	n.s.	n.s.
Activation kinetics										
Rise -55 mV (ms)	12.62 ±0.70 (16)	13.87 ±0.96 (7)	10.09 ±0.44 (18)	12.25 ±0.86 (14)	n.s.	**	n.s.	***	n.s.	*
Rise -10 mV (ms)	2.35 ±0.12 (16)	2.58 ±0.23 (7)	1.75 ±0.09 (18)	2.32 ±0.26 (14)	n.s.	***	n.s.	***	n.s.	*
Inactivation kinetics										
τ -55 mV (ms)	40.07 ±2.56 (16)	39.20 ±3.46 (7)	23.64 ±0.87 (n18)	28.46 ±1.51 (14)	n.s.	***	***	***	**	**
τ -10 mV (ms)	15.67 ±0.56 (16)	16.81 ±0.74 (7)	15.10 ±0.43 (18)	18.51 ±0.79 (14)	n.s.	n.s.	**	*	n.s.	***
Deactivation kinetics										
τ -100 mV (ms)	1.37 ±0.05 (19)	1.22 ±0.04 (11)	1.60 ±0.05 (18)	1.72 ±0.06 (14)	*	***	***	***	***	n.s.
τ -60 mV (ms)	5.45 ±0.52 (19)	6.89 ±0.52 (11)	7.31 ±0.41 (18)	8.95 ±0.36 (14)	n.s.	**	***	n.s.	**	**
Inactivation Recovery										
% recovery at 50 ms	4.98 ±0.46 (14)	4.62 ±0.50 (12)	2.82 ±0.19 (16)	2.26 ±0.13 (23)	n.s.	***	***	***	***	*
% recovery at 2000 ms	81.82 ±0.93 (14)	84.69 ±1.33 (12)	88.67 ±0.63 (16)	86.87 ±0.61 (23)	n.s.	***	***	**	n.s.	*
$T_{0.5}$ (sec)	908.04 ±27.05 (14)	822.04 ±32.92 (12)	817.90 ±27.03 (16)	949.48 ±34.77 (23)	*	*	n.s.	n.s.	*	*
Current density (pA/pF)										
	135.70 ±18.22 (13)	244.49 ±22.53 (13)	123.77 ±18.98 (13)	251.56 ±33.72 (13)	***	n.s.	**	***	n.s.	**

n.s. not significant; * p<0.05; ** p<0.005; *** p<0.001

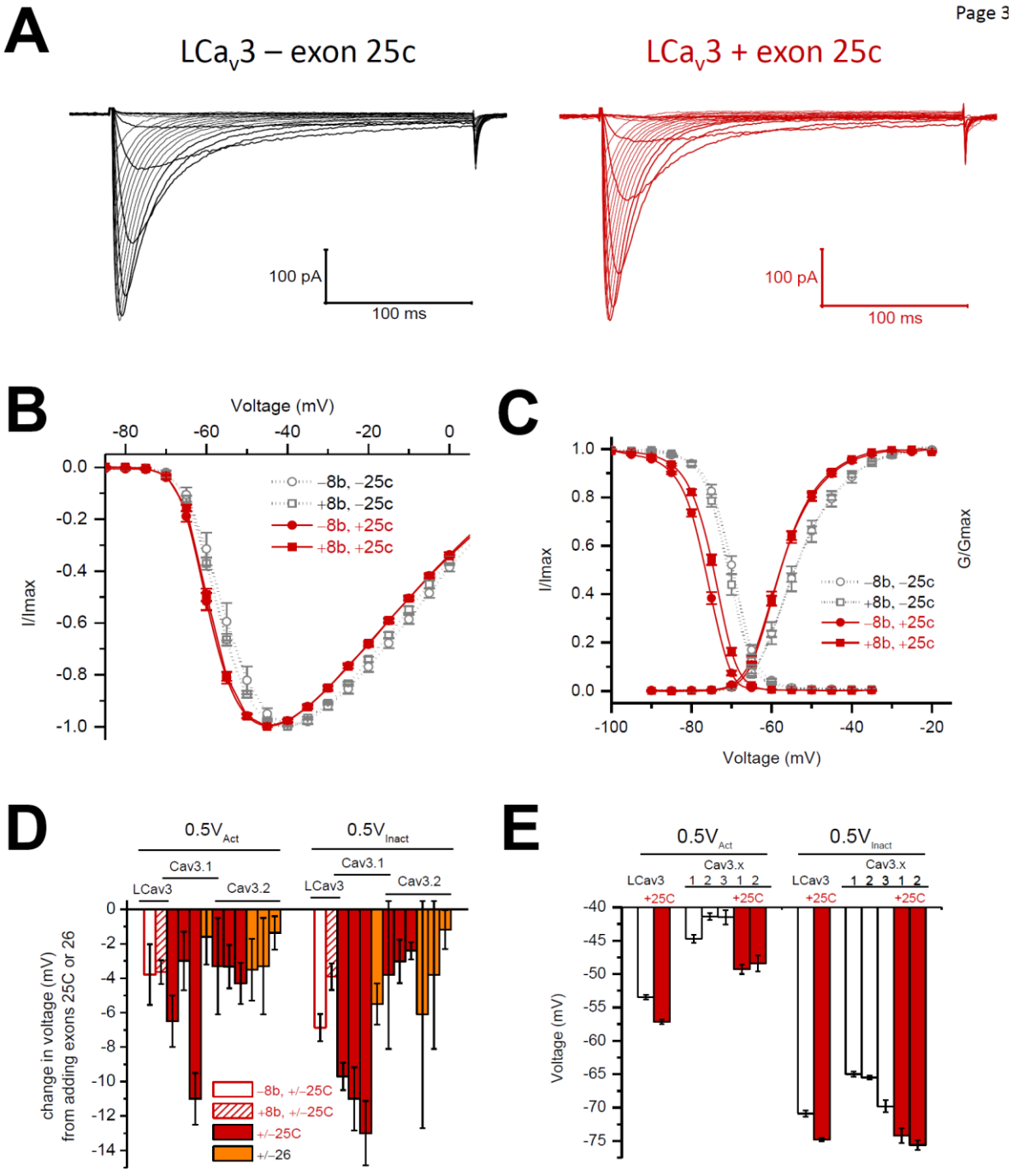

Figure 4. Changes in voltage-sensitivities of LCa$_v$3 in response to the presence or absence of optional exons 8b and 25c. (A) Ensemble LCa$_v$3 variant currents generated from a holding potential of -110 mV in 5 mV voltage steps from -90 mV to +10 mV. (B) Current-voltage curves for the four possible 8b and 25c variants (i.e. +8b -25c, -8b -25c, +8b +25c, and -8b +25c). (C) Combined activation and steady-state inactivation curves. (D) Changes in voltages of half-maximal activation (0.5VAct) and inactivation (0.5VInact) associated with inclusion of exon 25c in LCa$_v$3, compared to \ changes imposed by exons 25c and 26 in mammalian Ca$_v$3.1 and Ca$_v$3.2 reported in other manuscripts: (E) Voltages of half-activation and inactivation of LCa$_v$3 and reported mammalian T-Type channels resulting from inclusion or exclusion of exon 25c.

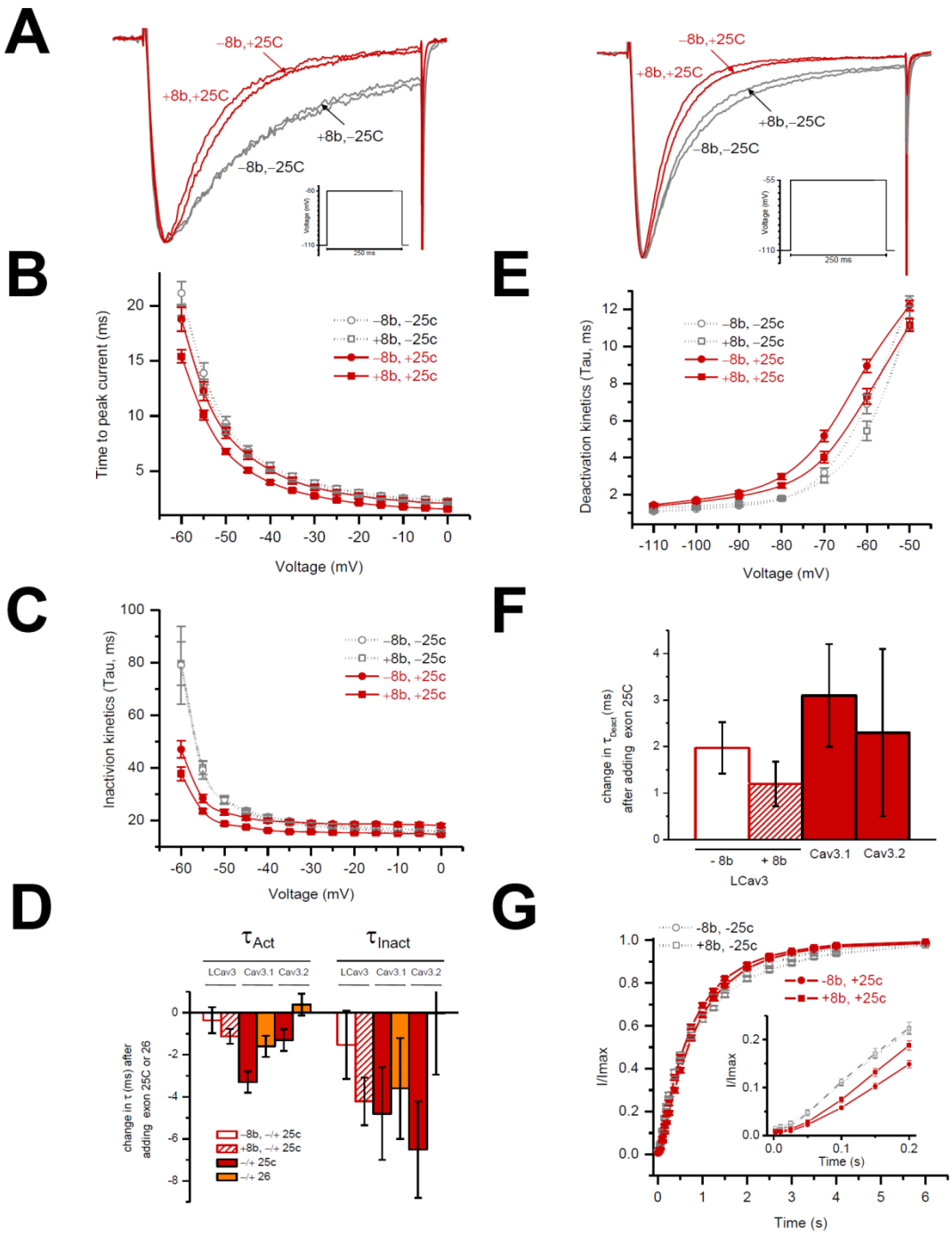

Figure 5. Changes in the kinetic properties of LCa$_v$3 in response to the presence or absence of optional exons 8b and 25c. (A) Representative calcium current traces in response to voltage steps for the different cloned LCa$_v$3 variants. (B) Activation kinetics of LCa$_v$3 variants measured by time to peak current. (C) Tau curve fits of inactivation kinetics. (D) Change in activation and inactivation kinetics of LCa$_v$3 at steps to -40 mV (tau, ms), compared to changes documented for Ca$_v$3.1 and Ca$_v$3.2. (E) Deactivation kinetics (tau, ms) (F) Change in deactivation kinetics at steps to -70 mV (tau, ms) associated with 25c exons in LCa$_v$3, Ca$_v$3.1 and Ca$_v$3.2 (G) Recovery from inactivation for LCa$_v$3 channel variants, (inset has 2.5 ms to 0.2 s timescale).

Exon 8b selectively alters LCa$_v$3 expression

The large optional exon 8b has a major role likely associated with controlling the expression of Ca$_v$3 channels, since transfection of equal molar quantities of cloned LCa$_v$3 vectors into HEK-293T cells produces approximately 2-fold increases in current density recordings when variants lack 8b (**Fig. 6*A*, Table 1**). In contrast, current density does not change in the absence or presence of exon 25c. Increased currents were also reported for mammalian Ca$_v$3.1 lacking exon 8b[195], suggesting that analogous regulatory mechanisms might act on snail and mammalian 8b exons to control membrane expression. The only obvious similarity between exon 8b amino acid sequences of LCa$_v$3 and Ca$_v$3.1 is an APRASPE motif (**Fig. 1*D***), which, when deleted, surprisingly has no effect on LCa$_v$3 channel current density (**Fig. 6*A***).

The doubling of current densities in the absence of exon 8b, attributable to an increase in the number of channels present at the membrane, could arise from increases in total protein expression or strictly increased trafficking to the membrane[195]. A possible change in membrane trafficking of LCa$_v$3 associated with exon 8b was assessed by separating and quantifying biotinylated, membrane-delimited channel variants expressed in HEK-293T cells, relative to channels present in whole cell fractions on immunoblots labeled with polyclonal LCa$_v$3 antibodies[268]. Antigen specificity of the polyclonal antibodies for these experiments was confirmed by immunolabeling of HEK cells transfected with either the T-type channel cDNA (+8b -25c), or that of snail LCa$_v$1 calcium channel (**Fig. 6*D***), and further tested on Western blots using expressed and purified LCa$_v$3 I-II linker peptides (**Fig. S7**). Biotinylation experiments revealed dramatic increases in both total and membrane-expressed fractions of transfected LCa$_v$3 variants lacking exon 8b (**Fig. 6 *B* and *C***), indicating that the doubling of current densities is likely due to an increase in protein expression, and not specifically increased membrane trafficking. We also inserted hemagglutinin (HA)-epitope tags in the extracellular Domain I P-loop of LCa$_v$3 variants, to quantify the chemiluminescent signals of labeled, membrane-delimited epitope by luminometry[195]. Surprisingly, luminometry experiments were inconclusive, since there was a doubling of signal in permeabilized transfected cells compared to non-permeabilized conditions, regardless of the treatment, including cells transfected with untagged LCa$_v$3 (i.e. +8b +25c) (**Fig. S8**). In addition, all HA-tagged channels, regardless of their insert, produced <20-fold smaller recordable currents than their wild type channel counterparts (**Fig. S9**).

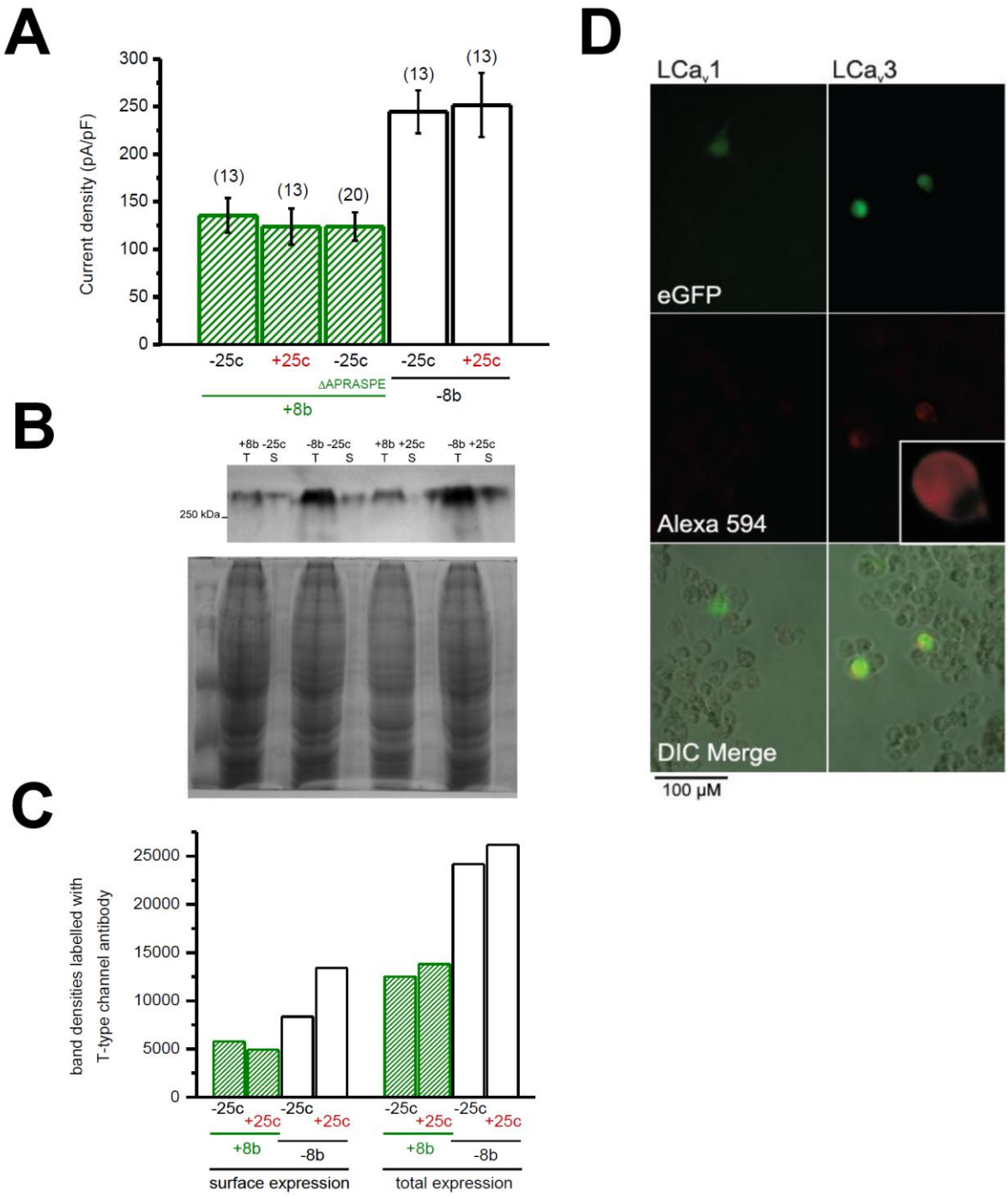

Figure 6. Changes in total and membrane expression of snail LCa_v3 T-type channel in response to the presence or absence of optional exons 8b and 25c. (A) Current density (pA/pF) of peak calcium currents in the presence of optional exons (n=13 for each variant), including a +8b -25c variant without the $APRASPE_{xx}D$ motif (n=20). (B) Top: Western blot showing biotinylation-mediated fractioning of surface-expressed proteins; membrane expression (S); total protein extracts (T) of HEK-293T cells. Bottom: Coomassie-stained replicate SDS-PAGE gel as the one used in the above blot. (C) Quantification of bands visible on the Western blot using densitometry. (D) Immunolabeling of HEK-293T cells transfected with pIRES2-EGFP expression constructs containing either LCa_v3 (+8b -25c) or LCa_v1 cDNA.

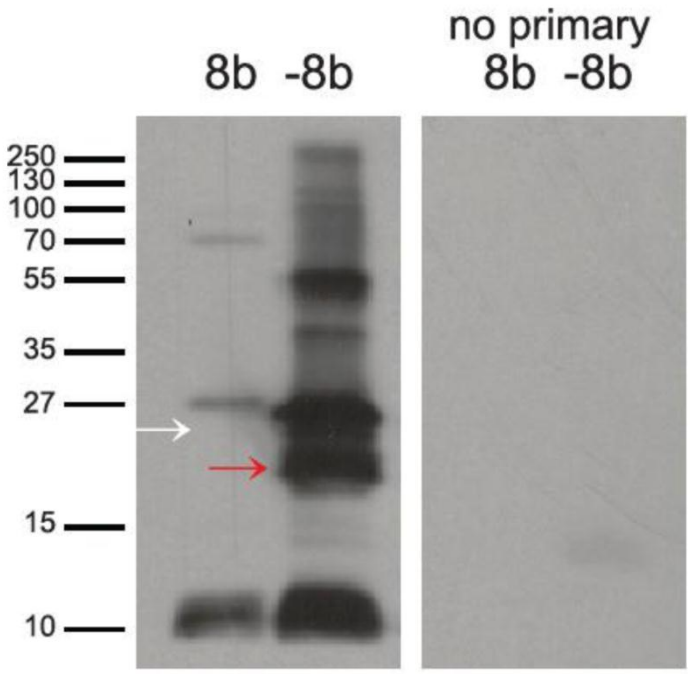

Supplementary Figure 7. Confirmation of specificity of snail LCa$_v$3 polyclonal antibodies for bacterially-expressed epitope peptide using Western blotting. Polyclonal antibodies raised against a 17.6 kDa peptide corresponding to the I-II linker of LCa$_v$3 lacking exon 8b, detect bacteria-expressed and Histidine tag-purified I-II linker protein on western blots (red arrow), and do not detect a similarly expressed 23 kDa protein corresponding to exon 8b (white arrow).

		well 1	well 2	well 3	well 4	AVG	permeabilized/ non-permeabilized
LCav3+8b-25c-HA	non-permeabilized	201957.00	186668.00	152836.00	159542.00	175250.75	
	permeabilized	435516.00	417340.00	398200.00	441675.00	423182.75	2.41
LCav3-8b-25c-HA	non-permeabilized	198571.00	180376.00	180705.00	120598.00	170062.50	
	permeabilized	417205.00	430982.00	378600.00	362166.00	397238.25	2.34
LCav3+8b+25c-HA	non-permeabilized	192132.00	200138.00	171642.00	180818.00	186182.50	
	permeabilized	477092.00	515405.00	434244.00	466337.00	473269.50	2.54
LCav3-8b+25c-HA	non-permeabilized	1446.00	343318.00	329886.00	298165.00	243203.75	
	permeabilized	960320.00	938967.00	863361.00	848336.00	902746.00	3.71
LCav3+8b+25c wt	non-permeabilized	212259.00	290838.00	163107.00	130832.00	199259.00	
	permeabilized	573987.00	552698.00	446989.00	384938.00	489653.00	2.46

Supplementary Figure 8. Membrane-expression of HA-tagged LCa$_v$3 variants could not be measured using luminometry. More than a doubling of ELISA signal was recorded when permeabilized transfected cells were compared to non-permeabilized conditions, regardless of the treatment, including cells transfected with HA-epitope tags or untagged (wt) LCa$_v$3 channels. HA epitopes were introduced into the IS5-S6 extracellular loops of the LCa$_v$3 variants, and identified in transfected homogenates of HEK-293T cells with labelled anti-rat HA monoclonal antibody. Secondary goat anti-rat HRP (horse radish peroxidase) catalyzed the chemiluminescence quantified using a FilterMax F5 Multi-Mode Microplate Reader (Molecular Devices).

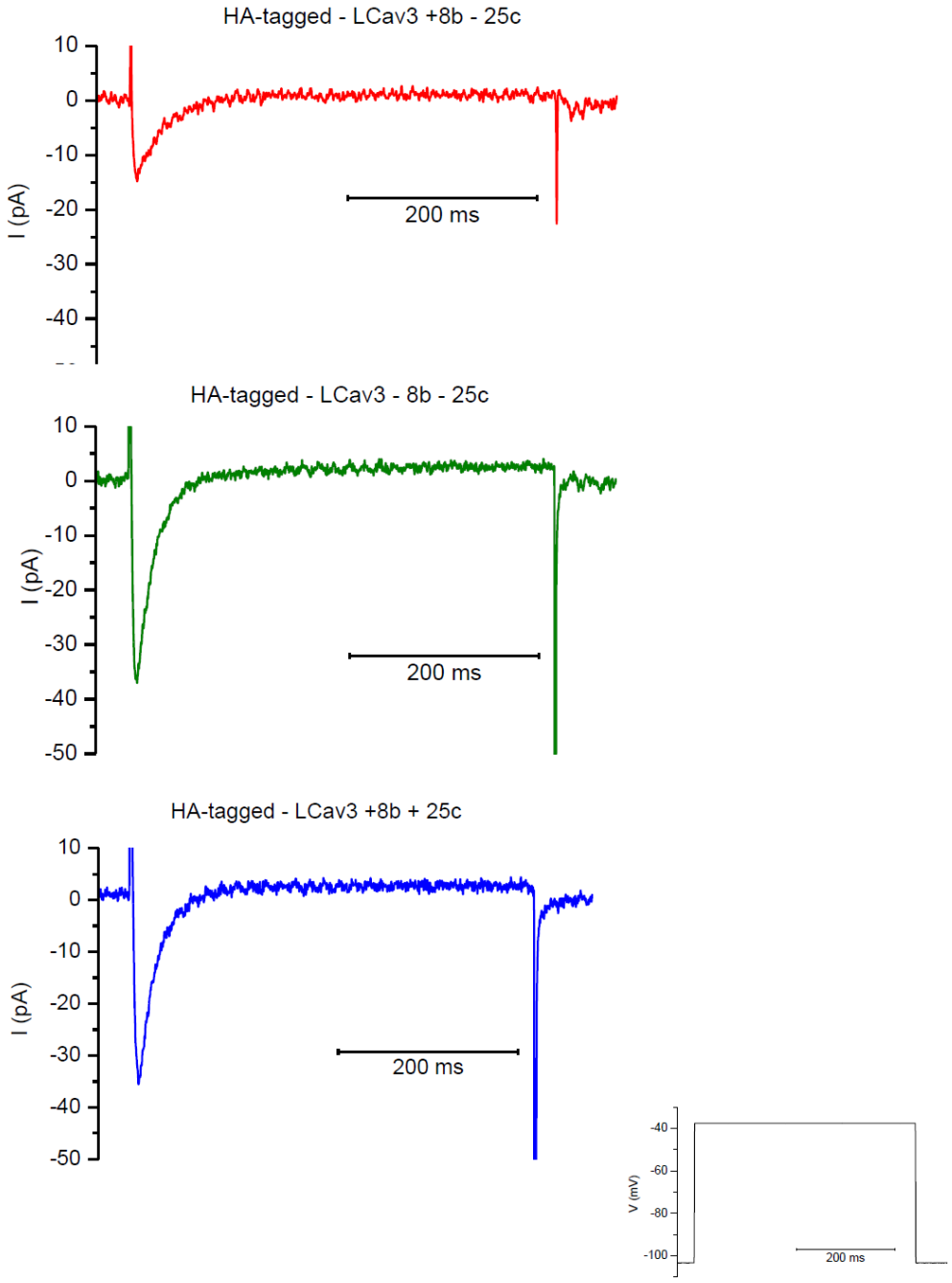

Supplementary Figure 9. HA-tagged LCa$_v$3 variants expressed >20 fold less than un-tagged LCa$_v$3 variants in HEK-293T cells. Above is the largest-sized currents of three LCa$_v$3 variants (+8b-25c, -8b-25c, and +8b+25c) transfected and recorded in HEK-239T cells by whole cell patch clamp technique and generated by voltage-steps to -40 mV from -110 mV holding potential. These currents for HA-tagged channels were carried out under optimal transfection efficiency and culturing conditions. Usually for untagged clones, peak currents were usually greater than 2000 pA, recorded three days post-transfection, and we selected for smaller currents. No recorded HA-tagged channel was as large as 100 pA.

2.2.4 Discussion

Evolution and development of Ca_v3 channels

Invertebrates possess only a single Ca_v3 channel gene which provides a reference point for evaluating fundamental features of T-type channels. We illustrate here two highly conserved and developmentally regulated optional exons in cytoplasmic linkers shared between invertebrates and mammals, that provide insights into the fundamental roles that alternative splicing has played in the early evolution of Ca_v3 channels.

Ca_v3 channels likely first appeared in early multicellular organisms, since single-celled animals, such as the choanoflagellates, have a single calcium channel homolog, an L-type (Ca_v1), but no Ca_v3 channel[64]. Likely, gene duplication of the L-type calcium channel gene generated a synaptic Ca_v2, 'N-type like' channel gene and a Ca_v3 channel gene, in a close ancestor of primitive multi-cellular organisms (i.e. *Trichoplax*) or within an animal phylum with the most primitive nervous system, the Cnidarians, which both possess a full complement of single Ca_v1, Ca_v2 and Ca_v3 channel genes[59] (**Fig. 1*A***). The snail homolog from *Lymnaea stagnalis* closely matches the mammalian $Ca_v3.1$ and $Ca_v3.2$ channels in the quintessential features of Ca_v3 channels, which appear optimized for generating rhythmic firing patterns, with a low voltage range of gating and rapid kinetics to drive membrane depolarization from resting membrane potential to threshold quickly, and a property of slow deactivation kinetics, which keeps Ca_v3 channels open to maximize their effectiveness, if they are not in a refractory, inactivated state[64]. Conserved features in invertebrates also extend to their developmental expression profile. Ca_v3 channel mRNA levels fall precipitously (80%) from embryo to juvenile snails in comparison to a more gradual decline of related channels, such as Ca_v2 and NALCN (~20%) or L-type calcium channels (60%) (**Fig. 3*D***). This decline in Ca_v3 channel transcripts continues from juvenile to adults in most tissues and is most dramatic in the heart compared to the brain. The higher density of Ca_v3 expression correlates well with the faster embryonic heart rate, and drops sharply with the slower heart rate after the rapid phase of growth (embryo/neonate to juvenile animals). Ca_v3 channel expression is also highest in animals of smaller sizes[108], which have faster heart and metabolic rates associated with allometric scaling. A prominent Ca_v3 current remains in adult snails[111], but this is diminished in the pace-making cells of increasingly large mammals, to a level that may be imperceptible in the adult human heart[108]. In the tissues we studied, only albumen and prostate glands, which grow dramatically in size from juvenile to adult

snails, exhibit increases in Ca_v3 channel expression, consistent with organ maturation and emergent properties for Ca_v3 channels in secretory roles of sexually-mature animals.

A high embryonic level of Ca_v3 channel expression is associated with expanded roles in the early proliferative states such as myoblast fusion[269], and recapitulated to high levels in disease states such as cancer[270] and ventricular hypertrophy[231]. Extracellular calcium contributes to contraction in immature muscle, which lacks the elaborate calcium delivery system in adult muscle involving transverse tubules signalling to intracellular calcium release units via coupling to membranal L-type calcium channels[248]. Adult invertebrate muscle is also primitive, lacking tetradic organization and striations[248], where Ca_v3 channels can serve as the only calcium source for muscle contraction (*Polyorchis* jellyfish muscle)[110], are a major contributor to muscle action potentials (nematode)[254], provide an alternative to sodium spikes in giant motor neurons (*Aglantha* jellyfish)[255] or are a prominent source of calcium for the adult heart[111].

Evolution of cytoplasmic linkers

The fall in mRNA expression from embryo to adult snails is almost exclusively with Ca_v3 channels that lack exon 25c in the cytoplasmic III-IV linker (**Fig. 3B**), leading to a change in mode of T-type channel activity in the transition from embryo to adult. Remarkably, III-IV linkers have been restricted to a discrete size of 54 +/- 1 aa in all human calcium and sodium channels, whereas the other cytoplasmic linkers substantially vary in size ranging from ~100 to >500 aa (**Fig. 2*C***). The shortness constrains the III-IV linker so that it is tightly coupled to the cytoplasmic end of the pore, preventing it from protruding too deeply into it. The III-IV linker is a primary agent for fast inactivation of Na_v channels, serving as a manhole cover with a hydrophobic latch (IFM) flanked by an alpha helix on either side that pivots on a flexible hinge to occlude the cytoplasmic pore[271]. The 'inactivation particle' of the III-IV linker of Na_v channels is conserved down to single-celled choanoflagellates, is absent in all Ca_v channels[59], but a parallel role is likely played by the similarly sized III-IV linkers of Ca_v3 channels. Evolution of an alternative 5' donor splice site expands the middle of the III-IV linker to retain intron sequence as a 7 to 11 aa coded exon, extending exon 25 (dubbed exon 25c) in molluscs and vertebrate $Ca_v3.1$ and $Ca_v3.2$ channels beyond the tightly-regulated size of 54 +/-1 aa. Corresponding with III-IV linker exon variants, there is an added complexity of the regulation of alternative splicing, with a dramatic increase in intron size from non-molluscan invertebrates and vertebrate $Ca_v3.3$ channel genes that lack optional exons in the III-IV linker, to the molluscan Ca_v3 channel with an exon 25c, to vertebrate $Ca_v3.1$ and $Ca_v3.2$ channels

which contain two differentially-regulated optional exons 25c and 26 **(Fig. 2*D*)**. Splicing factors in spliceosomes have varying compositions in different developmental stages and cell types, to generate unique mRNAs from heteronuclear pre-mRNA with the guidance of specific nucleotide sequences within introns and adjacent exons[272]. Larger intron sizes suggest extensive regulation of alternative splicing for these short exons in different tissues[272]. Interestingly, +8b and -25c variants have a significantly correlated expression pattern amongst the juvenile and adult tissues tested by qPCR (correlation coefficient R^2=0.885), as do -8b and +25c (R^2=0.898), while +8b/+25c and -8b/-25c have lower R^2 values (**Fig. S6**). This suggests that there is a co-ordinated splicing of LCa$_v$3 isoforms containing either +8b with -25c, or -8b with +25c in different tissues, and that these are the most physiologically relevant isoforms in juvenile and adult snails. However, alternative splicing can be somewhat stochastic[180,170], and given the presence of all four splice variants together in many different tissues (**Fig. 3**), it is probable that all four possible configurations are present in the animal, at least to some degree.

Biophysical consequences of 25c and 26

Modeling studies suggest that there are general truisms associated with Ca$_v$3 channel splicing, although Ca$_v$3 channel behavior will vary considerably with background cellular context such as other ionic conductance and the resting membrane potential, as well as with subcellular localization[273]. Exon 25c imparts a hyperpolarizing shift in the activation and inactivation curves of Ca$_v$3 channels (by a few to 10 mV), that restricts their activity because they are unavailable and inactivated at rest. If the membrane potential does not change significantly throughout development, enrichment of exon 25c in adults would serve to dampen the contribution of these channels to excitability. These variants would be more adept at driving post-inhibitory rebound excitation after strong hyperpolarizing input, which together with the faster activation and inactivation kinetics reported for plus exon 25c variants, would generate calcium spikes with a faster onset and faster attenuation after hyperpolarization, reminiscent of low threshold spikes (LTS) in thalamocortical neurons[274]. Within action potential bursts that sometimes ride over LTS, the depolarizing contribution of Ca$_v$3 calcium currents during action potential repolarization is maximized by the long delay of channel closure from the open state (slower deactivation kinetics) imparted by exon 25c[192,275]. Exon 25c, the more prominent isoform in adults, promotes inactivation to limit excitability, and also slows the recovery from complete inactivation at the earliest time point of recovery. Given that Ca$_v$3 channels play important roles in setting the rhythmicity of oscillatory firing, the above features suggest that the enrichment of exon

25c in adults, along with the developmental down-regulation of Ca_v3 channel expression, serve to slow down oscillatory firing or diminish the contribution of Ca_v3 channels to excitability in general.

Embryonic Ca_v3 channels lacking exon 25c have properties more similar to $Ca_v3.3$, with slower activation and inactivation kinetics, as well as right-shifted activation and steady-state inactivation curves[275]. ΔΔ variants conduct less calcium into the cell during a single burst, and are better suited for prolonged spiking at higher frequencies (e.g. burst firing in nRT neurons[276,272]) due to a lower propensity for cumulative inactivation during high frequency firing. Rather than dampen, $Ca_v3.3$ channel currents actually facilitate through the first few spikes in a train. Since ΔΔ variants are the predominant isoform in the embryo of both snails and mammals, the default state is likely one which favours a contribution of Ca_v3 channels to more rapid firing patterns in embryonic cells relative to adult ones. In addition, Ca_v3 channels without exon 25c are less inactivated at rest, with a more positive-shifted activation and inactivation curves, and are more readily available to open in response to depolarization, rather than relying on hyperpolarizing input. $Ca_v3.3$ channels generally have a brain-specific, somato-dendritic localization where they extend further into the dendritic arbour than $Ca_v3.1$ and $Ca_v3.2$[89]. Dendritic T-type channels are implicated in synaptic integration, where they serve to amplify post-synaptic inputs to the soma[277], and the slower activation and inactivation kinetics of $Ca_v3.3$ might facilitate this role by allowing the channels to overcome the high input resistance of dendrites. Interestingly, modelling suggests that dendritic T-type channels are subject to a hyperpolarizing shift in their activation during somatic depolarization[273], which for $Ca_v3.3$ channels would approximate their depolarized activation curves to match those of the more hyperpolarized and somatic $Ca_v3.1$ and $Ca_v3.2$.

Exon 25c sets the framework for the major biophysical differences between Ca_v3 channels. Snail LCa_v3 and mammalian $Ca_v3.1$ and $Ca_v3.2$ utilize exon 25c to differentiate themselves from $Ca_v3.3$, with shifted activation and inactivation gating to significantly more hyperpolarized potentials, not achievable by merely switching to the expression of a different mammalian channel gene (i.e. $Ca_v3.1$, $Ca_v3.2$ or $Ca_v3.3$; **Fig. 4*E***). Indeed, systematic replacement of different trans-membrane and cytoplasmic regions of $Ca_v3.1$ into $Ca_v3.3$ creates chimeric channels that resemble $Ca_v3.1$ only when an exon 25c-containing III-IV linker is inserted into $Ca_v3.3$[278]. These changes (measured in *Xenopus* oocytes) include dramatically shifted activation and inactivation curves in the hyperpolarizing direction (-9.5 mV and -8.6 mV, respectively), and increases in the kinetics of activation and inactivation[278].

Structure of exon 25c and exon 26

Sequence comparisons do not elucidate a consistent picture for the structural requirements of exon 25c, since the number of charged residues can vary even amongst closely related species (e.g. freshwater and sea snail Ca_v3 channels; *Lymnaea* SEGPKASSSE vs. *Lottia* SEGISTKKAG), size can vary considerably (e.g. between frog and human $Ca_v3.2$ channels; SKALPVAVAVAE vs. SKALYMSE respectively) and a requirement for the first position being a serine residue to complete a consensus phosphorylation site is lacking when comparing human exon 25c and 26 inserts (SKEKQMA vs. NLMLDDVIASGSSASAASE respectively; **Fig. 2*B***). An effective, threshold size of 8 aa may be required for III-IV inserts, since the slightly shorter exon 26 insert of $Ca_v3.2$ channels (STFPSPE), imparts only small biophysical changes such as a shift in the curve for steady-state inactivation (**Fig. 4*D***), an no significant changes in kinetics of activation and inactivation (**Fig. 5*D***). A role for residue charge would be consistent with Na_v channels, where clusters of charged residues in the III-IV linker differentially regulate the kinetics of fast inactivation[279].

Role of exon 25c in gating

Dynamic clamp simulations suggest that minimal changes in the biophysical properties of the Ca_v3 channel currents, especially in the voltage range corresponding to the base of the current-voltage curve, drastically alter the contribution of Ca_v3 channels to calcium spikes[274], such as the low threshold calcium spikes in the thalamus characterized in states such as physiological sleep or pathological states such as epilepsy. LTS are often crowned with sodium channel-dependent action potential spike trains, whose frequency and longevity highly depends on the shape of the underlying calcium spike and thus Ca_v3 channel activity[94]. While the suite of biophysical changes associated with inclusion of exon 25c provides $Ca_v3.1$ and $Ca_v3.2$ channels for fast post-inhibitory depolarizing responses with calcium spikes crowned by relatively fast but short lived spike trains (e.g. thalamocortical LTS), omission of exon 25c (and 26) creates variants better suited for LTS with a more delayed onset, less dependent on hyperpolarization, and crowned by longer lasting sodium channel spike trains (e.g. nRT LTS)[275]. Clearly even subtle differences may drastically influence the contribution played by Ca_v3 channels under different conditions. These include differences in the channel genes (e.g. recovery from inactivation of $Ca_v3.1$ vs. $Ca_v3.2$), other splice variants that modulate gating and trafficking (such as exons 8b and 38b for $Ca_v3.1$, exon 35a for $Ca_v3.2$, and exon 14 for $Ca_v3.1$/$Ca_v3.2$)[192,190,200], G protein modulation and phosphorylation (largely a capacity of $Ca_v3.2$ channels[280]), potentiation by glutamate receptors ($Ca_v3.1$ channels in cerebellar Purkinje

fibers)[281], association with K^+ channels[282], as well as being influenced by the shape of the trigger (e.g. synaptic input)[274].

Role of exon 8b in expression

Exon 8b has only a minor influence on biophysical properties, while its omission dramatically increases the membrane expression of snail LCa_v3 and mammalian $Ca_v3.1$ (by ~2-fold) in transfected human cells (**Fig. 6*A***). A conserved APRASPE motif is an obvious, shared feature of exon 8b in invertebrate and $Ca_v3.1$ channels, but its absence has little effect on the current densities of snail LCa_v3 in mammalian cell lines. It may indicate that the APRASPE motif is not critical for protein and/or membrane expression, or that its function depends on tissue-specific factors not present in HEK-293T cells. Exon 8b is abundant in the snail brain and secretory organs and mostly lacking in the heart. It is contained in the largest cytoplasmic linker of Ca_v3 and Na_v channels (**Fig. 2*C***), which is also the primary domain for regulating expression of all Ca_v and Na_v channels. Expression of closely related high voltage-activated (HVA) Ca_v1 and Ca_v2 channels is promoted by assembly with an accessory β subunit binding to the proximate I-II linker (in the homologous position of the gating brake of Ca_v3 channels)[78]. Increases in the expression of HVA channels have recently been shown to depend on the β subunit interaction that protects the channels from targeted degradation via the endoplasmic reticulum-associated protein degradation (ERAD) pathway[78]. It has been proposed that misfolding in the I-II linker of $Ca_v2.1$ is responsible for pathological ER retention and ERAD of mutant channels associated with episodic ataxia[208].

Subunit assembly with accessory subunits is not a likely control mechanism for Ca_v3 channel expression or protein stability, but the I-II linker of snail and mammalian Ca_v3 channels is a key region for its regulation. Large deletions in the I-II linker (downstream of the gating brake) for snail LCa_v3 and mammalian $Ca_v3.1$, $Ca_v3.2$ and $Ca_v3.3$ moderately enhances, moderately enhances, dramatically enhances, and depresses membrane expression respectively[196]. Lower current densities observed in the presence of exon 8b could be attributed to regulation of channel trafficking to the cell membrane, or the depression of total protein expression of Ca_v3 channels, or a combination of these factors. Our results indicate that inclusion of exon 8b, regardless of the presence or absence of exon 25c, causes dramatic decreases in both total protein *and* membrane expression of LCa_v3 channels (**Fig. 6 *B* and *C***).

Conclusions from snail work

Work with snails provides a unique perspective for defining the fundamental features of Ca_v3 channels. We show that the snail and mammalian channels operate within tightly regulated biophysical constraints for supporting rhythmic firing in the brain, heart and secretory organs, and that there are many remarkable parallels in expression patterns between respective Ca_v3 channels and exon 8b and 25c splice isoforms. The presence of exon 25c in the III-IV linker, a region whose length is highly invariable in sodium and calcium channels of the 4-domain superfamily, suggests that this locus was exploited during T-type channel evolution to provide splice variants with markedly different biophysical properties. We suggest that the snail channel is more akin to $Ca_v3.1$ because of the common regulation of membrane expression with exon 8b, which is enriched in the brain of both snails and mammals. If indeed $Ca_v3.1$ is more reminiscent of the ancestral channel type, then $Ca_v3.2$ deviated from $Ca_v3.1$ less in biophysical terms, but rather in its greater capacity for modulation. $Ca_v3.3$ became the most divergent of all T-type channels with a restricted tissue expression profile in the brain, and lacking an exon 25c. In the embryo, T-type channels are highly abundant and lack exon 25c, which supports accelerated rhythmic firing, and high channel density might also serve expanded roles such as the calcium delivery for contraction of immature muscle. In adults, there is an upregulation of T-type channels in secretory glands, coinciding with sexual maturation and active secretion of vesicular components into reproductive tracts. Further insights into T-type channels are facilitated in snails which have only a single Ca_v3 channel gene, and a highly tractable and accessible preparation for studying its associated functions in brain, heart and secretory organs.

2.2.5 Acknowledgements

This work was funded through a NSERC Canada Graduate Scholarship award to A.S. and a NSERC Discovery grant to J.D.S. We would like to thank Dr. A.N. Boone for her helpful suggestions and assistance in designing the qPCR experiment, A. Bozorgzad, Dr. J. Gurska and L. Sauder for their assistance, and Drs. J. Neufeld and T. Dieckmann for providing access to their equipment and facilities.

2.3 Invertebrate-specific alternative splicing in the *LCa$_v$3* gene that dramatically alters permeability to monovalent cations

The data presented in this section is unpublished, and is a draft manuscript written by Adriano Senatore in preparation for submission to a peer-reviewed journal:

Adriano Senatore and J. David Spafford (2012). Alternative splicing in the domain II P-loop of T-type calcium channels dramatically alters monovalent cation permeability without changing the selectivity filter.

The presented research and phylogenetic analyses, conducted by Adriano Senatore, describe the identification of alternative splicing in the domain II P-loop of the *Lymnaea* Ca$_v$3 channel. Two alternative domain II isoforms, generated by mutually exclusive exons 12A and 12B, create channels with identical Ca$_v$3 selectivity filters (i.e. EEDD), however, with dramatically altered cation selectivities. Phylogenetic analyses revealed that the ancestral 12A exon, contained in the most distant Ca$_v$3 channel genes (e.g. placozoan *Trichoplax adhaerens* and cnidarian *Nematostella vectensis*), is retained as the lone exon 12 in the deuterostome lineage that includes vertebrates, while protostomal invertebrates possess both 12A and 12B exons. Remarkably, although minimal influences on biophysical properties are detected, the 12A variant of *Lymnaea* Ca$_v$3 is highly permeable to monovalent cations such as sodium, while the 12B variant is considerably more selective for divalent calcium. The *Lymnaea* Ca$_v$3 channel containing exon 12B is therefore more similar to mammalian Ca$_v$3 channels, that only bear exon 12A and are significantly calcium-selective. Based on the properties of these *Lymnaea* Ca$_v$3 splice variants, as well as on the phylogeny, It is hypothesized that ancestral 12A-containing Ca$_v$3 channels were poorly selective for divalent over monovalent cations, and that in vertebrates, Ca$_v$3 channels evolved calcium-selectivity by incorporating structural changes at other loci along the channel protein; protostomes evolved two splice isoforms, a calcium-selective one (12B), and a non-selective one (12A), that have the potential to provide highly divergent contributions to cellular excitability and calcium-dependent biochemical processes.

Annotated splicing of various metazoan Ca$_v$3 channel genes, within the domain II pore region (i.e. exons 12A and 12B), are presented in Appendix C.

2.3.1 Abstract

We have identified mutually exclusive exons, termed 12A and 12B, within the domain II P-loop of the *Lymnaea* Ca_v3 channel gene, *LCa_v3*. The alternatively spliced exons, which alter a region just five amino acids upstream of the domain II selectivity filter glutamate, are abundantly expressed in snails, with almost exclusive expression of 12A in the heart and 12B in secretory glands, while both are found in the central nervous system. Phylogenetic analysis revealed that exons 12A and 12B are conserved in protostome invertebrates, including *Drosophila melanogaster* (arthropods) and *C. elegans* (nematodes). Based on highly conserved features that distinguish the two exons from each other, exon 12A is proposed to be ancestral in animals, while 12B likely evolved later by a tandem duplication of 12A. Remarkably, despite having identical selectivity filters, the two exon 12 variants of LCa_v3 possess dramatically different monovalent cation permeabilities, with the exon 12A variant being highly permeable to external sodium, even in the presence of physiological calcium levels, while the 12B variant is much more calcium-selective. In contrast, selectivity for Ba^{2+} over Ca^{2+} is unaltered, indicating that different mechanisms account for divalent (Ca^{2+}) vs. monovalent (Na^{+}) and divalent (Ba^{2+}) vs. divalent (Ca^{2+}) selectivity. The two variants of LCa_v3 are expected to play different roles in snails, with the sodium-permeable LCa_v3 channel bearing exon 12A providing prominent pace-making sodium currents in the heart, and the more calcium-selective 12B variant providing calcium influx, perhaps for calcium-dependent exocytosis, in secretory glands.

2.3.2 Introduction

The pore-loops (P-loops) of tetrameric potassium channel subunits contain highly conserved amino acids, whose backbone carbonyl oxygens project into the pore to form a rigid structure (i.e. the selectivity filter) that mimics hydration shell oxygen atoms that surround potassium ions in solution[39]. This configuration makes it energetically feasible for surrogate oxygen groups to displace hydrating water molecules as potassium ions permeate. Due to specificity in hydration shell properties, the orientation of these carbonyl oxygens is not compatible with hydrated sodium and calcium ions, and thus selectivity for potassium is achieved. This fundamental pore structure was subsequently adapted to select for sodium and calcium[48,49,50,51,52,53,54], evolutionary events which took place in prokaryotes before metazoan multicellularity.

Until very recently, the crystal structure of any sodium or calcium channel has been unavailable, and the mechanisms of ion permeation through these types of channels have been mostly inferred from mutational studies[55,56,57] and structural modeling using potassium channels as reference

scaffolds[43,42,44]. Phylogenetic studies suggest that metazoan 4-domain sodium channels evolved from calcium channels[58,9], before nervous system evolution[59]. Appropriately, sodium and calcium permeabilities appear to be closely related[24,59], and only slight differences in key pore residues can shift selectivity in favor of one these two cations over the other[56,55,24]. However, the molecular features that determine selectivity for calcium over sodium, or vice versa, are poorly understood. 4-domain calcium channels have negatively charged acidic amino acids (i.e. glutamate/E or aspartate/D) in conserved positions within the extracellular P-loops from each domain, and together these form a selectivity filter 'ring', with the signature motifs of EEEE or EEDD. Flexible and asymmetrically arranged carboxylate oxygens from these residues are proposed to bind calcium with high affinity[283,43], and permeation is facilitated by repulsive forces from incoming calcium ions attracted to the negatively charged extracellular surface of the pore[43]. Selectivity for calcium over sodium is dependent on a complex interplay between the need to counter-balance the negatively charged carboxyl oxygens, and geometrical constraints that define where permeant cations can reside[60,43]; these parameters are optimized to create a much higher binding affinity for calcium than for sodium. In contrast, 4-domain sodium channels tend to have a mixture of acidic, neutral, and positively charged residues in the selectivity filter ring, such as DEKA (aspartate$^-$, glutamate$^-$, lysine$^+$, and alanine, respectively) in animals with bilateral symmetry and DKEA/DEEA in more primitive animals[59]. Mutation of the lysine and alanine residues of DEKA to glutamates (i.e. DEEE), confers calcium selectivity on sodium channels[56], and conversely, replacing a glutamate for a lysine in domain III of an L-type calcium channel (i.e. EEEE to EEKE) confers sodium-selectivity[283,284]. Together, the data indicate that the charges of selectivity filter ring residues are critically important for defining calcium vs. sodium selectivity in 4-domain ion channels.

Like potassium channels, prokaryotic voltage-gated sodium channels are homotetrameric structures. However, their pore architecture is quite distinct from potassium channels[61,285,48]. A recent landmark publication, documenting the first X-ray structure of prokaryotic voltage-gated sodium channel Na_vAb, has revealed that the pore is considerably wider than for potassium channels[52]. Each P-loop contains two short alpha helices that project the selectivity filter residues towards the center of the pore. Unlike permeation through potassium channels, sodium passes through in a partially hydrated state[286,61], with water molecules forming bridges between the permeating sodium ions and negatively charged pore residues. Sodium is selected over potassium because the larger diameter of the potassium ion decreases the stability of water-glutamate bridges[61]. Of note, the selectivity filter ring of prokaryotic sodium channels consists of four glutamate residues (i.e. EEEE), which differs

from metazoan sodium channel filters of DEKA/DEEA. The inconsistency between the sodium-selective EEEE filter of prokaryotic sodium channels, and the calcium-selective EEEE and EEDD filters of 4-domain channels, is attributed to the asymmetrical orientation of these residues in 4-domain channels, vs. their planar symmetrical arrangement in prokaryotic homotetrameric channels[286,61,285].

Unfortunately, 4-domain calcium (and sodium) channels are large and complex structures that are presently not amenable to crystallization, and as such the molecular details underlying permeation are poorly resolved. Calcium channels can be classified based on differences in their voltages of activation (i.e. low voltage-activated/LVA vs. high voltage-activated/HVA); of note, LVA or Ca_v3 channels are more permeable to sodium and other monovalent cations than HVA channels, and are less selective for calcium over other divalent cations such as strontium and barium[57,84,85,86]. The selectivity filters of Ca_v3 channels are distinct from HVA channels in that they contain aspartates rather than glutamates in the P-loops of domains III and IV (i.e. EE**DD** vs. EE**EE**). Mutating the EEDD motif of $Ca_v3.1$ to EEDE, EEED, or EEEE does not fully account for differences in permeation between LVA and HVA channels[287,87], and counter intuitively, channels become even more permeable to sodium[87]. This anomaly indicates that although the selectivity filter is important, permeation properties are defined by additional aspects of the pore architecture. These same studies revealed another distinction between LVA and HVA channels: $Ca_v3.1$ EEEE mutants exhibit altered biophysical properties[87,287] (i.e. voltage-sensitivity and kinetics), indicating that Ca_v3 channel gating is partly dependent upon the selectivity filter, in addition to the gate located at the apex of the 'inverted teepee' S6 helices. A comprehensive analysis of heterologously expressed mammalian channels $Ca_v3.1$, $Ca_v3.2$, and $Ca_v3.3$ revealed that like HVA calcium channels, the three LVA isotypes possess high affinity binding sites for calcium within their pores (albeit with 10-fold weaker affinities for calcium), which bind Ca^{2+} at μM concentrations to block Na^+ currents[288]. Due to the weaker affinities for calcium however, Ca_v3 channels are less calcium-selective than HVA channels and are expected to carry mixed Ca^{2+}/Na^+ currents under physiological conditions, most pronounced for $Ca_v3.3$[288]. On the other hand, the pore affinity for different divalent cations (i.e. Ca^{2+} vs. Ba^{2+} vs. Sr^{2+}), is not very different, and selectivity is determined by how the ions affect open channel probability (i.e. the probability that a channel is open as a function of time and voltage)[288].

During our sequencing of a *Lymnaea* Ca_v3 channel homologue[1], we identified alternative splicing of mutually exclusive exons (termed 12A and 12B) within the domain II P-loop coding sequence.

Interestingly, the 3' splice sites of both exons are located just five codons (i.e. amino acids) upstream of the selectivity filter glutamate (i.e. E**E**DD). Given that this splicing occurs in a region critical for ion selectivity and gating, we set out to determine whether the two exon 12 variants of LCa_v3 exhibit differences when heterologously expressed in HEK-293T cells. Despite the fact that the selectivity filter region is known to influence voltage-sensitivity and kinetics for Ca_v3 channels[87,287], the two variants were nearly indistinguishable in most biophysical parameters, with some differences in the speed of deactivation and recovery from inactivation. However, the macroscopic currents conducted by the exon 12A variant of LCa_v3 exhibited a dramatic increase in amplitude (i.e. ~15.5-fold) when sodium was added to the extracellular solution, even in the presence of 2 mM Ca^{2+} (which normally blocks sodium currents through mammalian Ca_v3 channels[288]). Given that both variants contain the same EEDD selectivity filter motif, our results indicate that for Ca_v3 channels, selectivity for calcium over sodium can be heavily influenced by factors residing outside of the selectivity filter.

2.3.3 Results

Lymnaea Ca_v3 has an alternatively spliced domain II P-loop

Consensus sequencing of the *Lymnaea* Ca_v3 channel cDNA[1], revealed multiple loci for alternative splicing. Optional exons 8b and 25c, in the I-II and III-IV linker coding sequences respectively, were proposed to be evolutionarily conserved and found to be functionally analogous to corresponding optional exons in mammalian Ca_v3 channel genes[289]. Interestingly, the *LCa_v3* gene undergoes a previously undocumented form of alternative splicing, within the domain II pore-loop (P-loop) coding sequence, with mutually exclusive exons 12A and 12B corresponding to the sole exon 12 for mammalian $Ca_v3.1$ (numbered with respect to the human $Ca_v3.1$ channel gene; figure 1A and B). Structural prediction suggests that the alternatively-spliced exons code for a portion of the domain II S5 helix, the adjacent extracellular loop, and the descending helix, that is purported to project into the pore towards the selectivity filter in prokaryotic voltage-gated sodium channel Na_vAB[52] (figure 1A and C). Remarkably, the 3' splice sites for exons 12A and 12B occur only five codons/amino acids upstream of the invariable domain II selectivity filter glutamate (figure 1B and C), which together with selectivity filter residues from the other three domains (i.e. EEDD selectivity filter motif; figure 1A) is critical for defining ion selectivity[57]. The most striking differences between these exons are their lengths, with 39 amino acids for exon 12A and 50 for exon 12B, and the arrangement of four and five respective cysteine residues along the extracellular loops (figure 1B and C).

PCR amplification from a *Lymnaea* embryonic cDNA library, using nested primers flanking this region (Table 1), produced two DNA products visible on ethidium bromide-stained agarose gels, with size differences corresponding to exon 12B (484 bp) and exon 12A (451 bp; figure 2A). PCR-amplified DNA was TA-cloned into pGEM®-T Easy vector, and excision of inserts with *EcoR*I confirmed the presence of only two DNA fragments (figure 2B); sequencing confirmed that the larger inserts contained the exon 12B coding sequence, while the smaller contained 12A. In addition, both inserts were present at equal frequencies (i.e. 5/10 clones each), suggesting that both exons are expressed at appreciable levels in the embryo.

To determine the probable splicing strategy used to generate 12A and 12B variants of LCa_v3, we looked at the Ca_v3 genes from various other mollusk species, namely marine molluscs *Aplysia californica* and *Lottia gigantea*, and the freshwater snail *Biomphalaria glabrata*. For all three species, we found putative exon 12A and 12B homologues in their Ca_v3 channel genes, with exon 12A located in an upstream position from exon 12B (hence the nomenclature; figure 3). In addition, the differences in size and number of cysteines between exons 12A and 12B, as seen in *Lymnaea*, are very consistent, with the smaller exon 12A coding for 39:3 (*Aplysia*), 38:3 (*Lottia*), and 39:3 (*Biomphalaria*) amino acids:cysteines, and the larger exon 12B coding for 51:5, 51:4, and 50:6 amino acids:cysteines, respectively. Splicing consists of a phase 2 splice junction between exons 11 and 12A/12B, and a phase 0 junction between exons 12A/12B and 13 (figure 3).

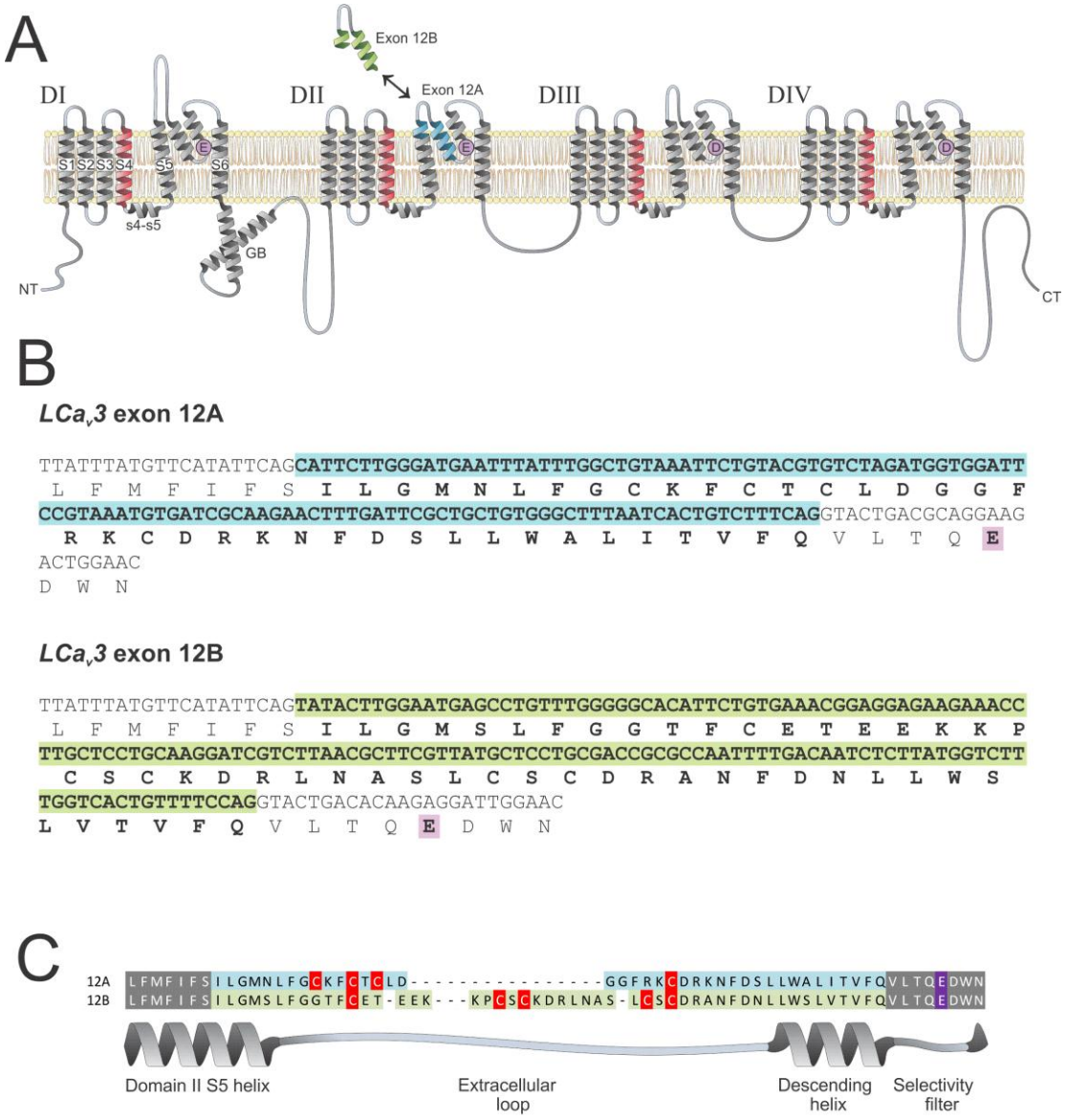

Figure 1. Mutually exclusive exons identified in the domain II P-loop of LCa$_v$3. A) Schematic illustration of the expected membrane topology and general secondary structure of LCa$_v$3. The channel contains 4 homologous repeats, termed domains I to IV. Each domain consists of 6 transmembrane helices, termed segments 1 to 6 (S1-S6), with S1-S4 forming the voltage sensor module and S5-S6 the pore module for each repeat. S5 and S6 helices are separated by an extracellular loop, called the pore-loop (P-loop), which contains two small alpha helices that project the selectivity filter residues from each domain into the center of the pore (purple). Ca$_v$3 channels are distinct from high voltage-activated (HVA) calcium channels in that the pore motif is made up of two glutamate and two aspartate residues (i.e. EEDD) vs. four glutamates in HVA channels (EEEE). Mutually exclusive exons 12A and 12B correspond to the domain II P-loop of LCa$_v$3, coding for a portion of the domain II S5 helix and the small helix that descends into the pore vestibule in prokaryotic sodium channel homologue Na$_v$Ab[52]. **B)** Confirmed nucleotide sequences for LCa$_v$3 exons 12A and 12B are highlighted in blue and green, respectively. *In silico* translation of the coding sequences confirms that the exons maintain the reading frame of the flanking LCa$_v$3 coding sequence, and interestingly, the 3' splice sites are located just five amino acids upstream of the domain two selectivity filter glutamate. **C)** Alignment of the two exon 12 variants of LCa$_v$3 reveals that 12A (highlighted blue) codes for 11 amino acids less than 12B (highlighted green). *Lymnaea* exon 12A also contains 1 less cysteine than 12B, and these are arranged quite differently along the protein sequence, which is expected to produce distinct secondary structures via disulfide bond formation. Below the alignment is a representation of the predicted secondary structures for the domain II pore region of LCa$_v$3 (using PSIPRED Protein Structure Prediction Server: http://bioinf.cs.ucl.ac.uk/psipred/). Both exons are predicted to form small alpha helices at their 3' ends that would descend into the pore to project the selectivity filter glutamate into the selectivity filter ring.

Table 1. Nested primers flanking the domain II pore sequence of the *Lymnaea* Ca_v3 channel cDNA. Expected sizes for PCR-amplified products are 451 bp for cDNA containing exon 12A, and 484 bp for exon 12B.

Application	Name	Sequence
Sequencing LCa_v3 domain II pore		
	LCa_v3 DIIP 5'1	CGACACTTTGGACTCAGAATTAGAGACTAG
	LCa_v3 DIIP 3'1	TCTCCTGAATTAAGGCAACTTTTAGCACTC
	LCa_v3 DIIP 5'2	GTTGCGCACCATGGACAATGTAGC
	LCa_v3 DIIP 3'2	AATGTTATTGTTTTCAGCCAAACGTTGC

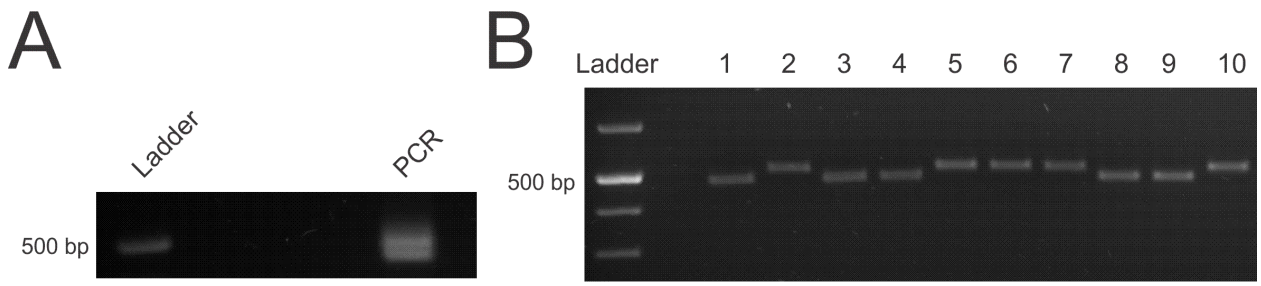

Figure 2. Confirming the expression of exons 12A and 12B in *Lymnaea stagnalis* cDNA. A) PCR amplification with nested primers flanking the mutually exclusive exons 12A and 12B (Table 1), from snail embryonic cDNA, produced two DNA fragments that could be distinguished in size on an agarose gel. B) Cloned DNA from A was excised from the pGEM-T Easy vector with *EcoR*I, and electrophoresed inserts were of only two sizes (451 bp for exon 12A, 484 bp for exon 12B; larger sizes are due to additional polylinker sequence from the pGEM vector). Sequencing of multiple inserts of each size confirmed that the smaller product contained the exon 12A coding sequence, and the larger 12B.

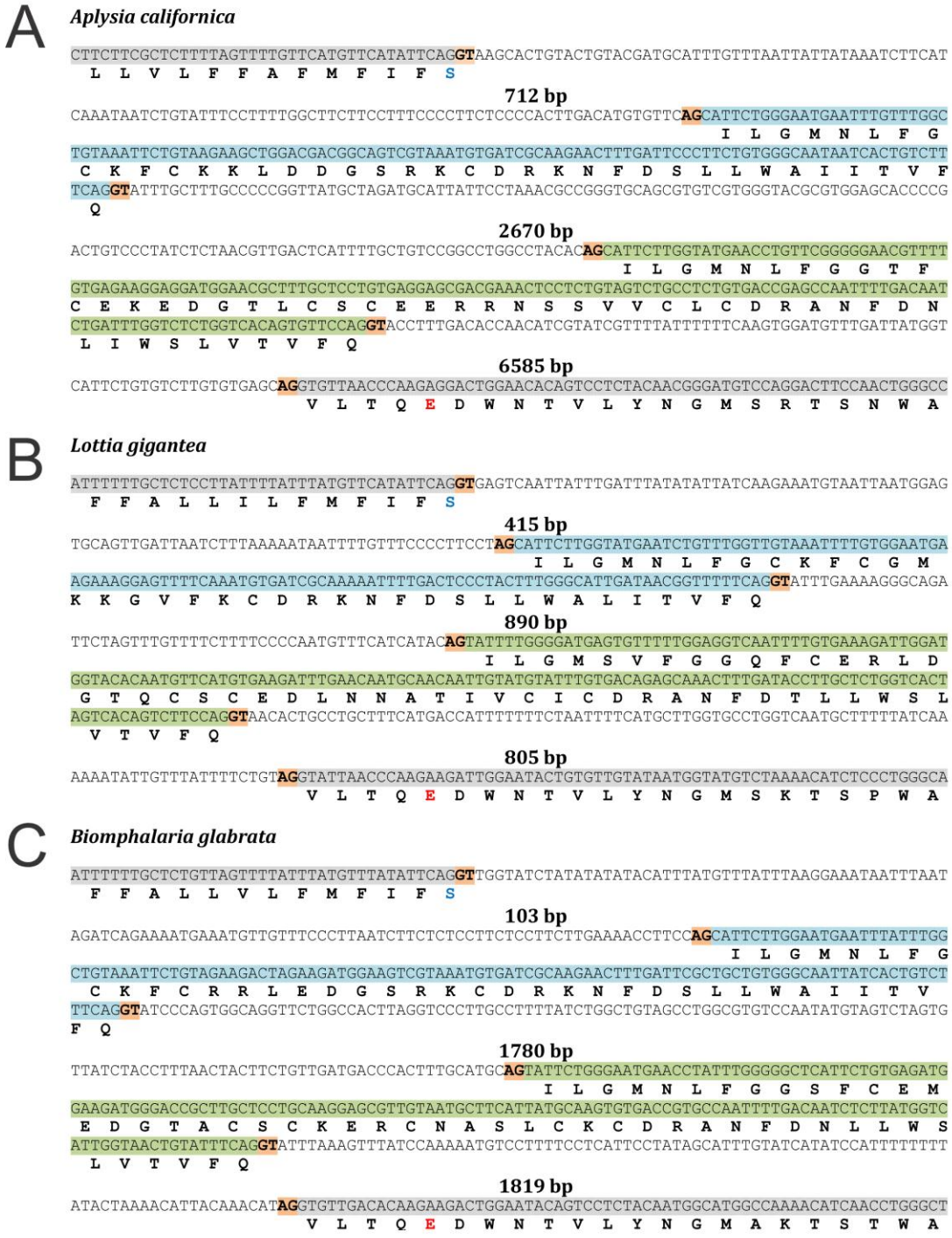

Figure 3. Splicing of mutually exclusive exon 12A and 12B homologues in the Ca_v3 genes from different molluscs. Exon 12A and 12B coding sequences, in 5' to 3' orientation, are highlighted in blue and green respectively. Exons 11 and 13 are highlighted in grey, and amino acid sequences for all exons are shown below the nucleotide sequences. Intronic donor splice sites (GT) and acceptor splice sites (AG) are highlighted in orange. For all species, exon 12A is situated upstream of 12B, with phase 2 splice sites between exons 11 and 12A/12B, and phase zero splice sites between exons 12A/12B and 13. Also, exon 12A is smaller and contains less cysteines for all three species. Marine molluscs A) *Aplysia californica* (UCSC Genome Bioinformatics aplCal1_dna range=scaffold_1525:56054-67089), and B) *Lottia gigantea* (JGI scaffold 59:70243-103522), and C) freshwater snail *Biomphalaria glabrata* (NCBI Contig188.27).

Expression of exons 12A and 12B is differentially regulated

Quantitative PCR was used to determine the expression patterns of exons 12A and 12B in various *Lymnaea* tissues, using primers designed to selectively amplify exons 12A and 12B, as well as an invariable region of the LCa_v3 transcript (Table 2). As previously shown, LCa_v3 expression is strongly developmentally downregulated in the whole embryo[289] (figure 4A), with a sharp decline from mid embryo stage (50-75% embryonic development) to near hatching (100% development, based on gross morphological changes[290,291]); a pattern largely mimicked by exons 12A and 12B. Expression of LCa_v3 continues to decline as sexually immature juvenile snails transition into adulthood (classified based on increases in shell length correlated with sexual maturation[292]). Interestingly, there appears to be an enrichment of exon 12B relative to 12A in juvenile animals, and this becomes more apparent in adults, with a 39.8% decrease in 12A and 17.5% increase in 12B from juvenile to adult (figure 4A). There is also a marked decline in heart Ca_v3 channel expression from juvenile to adult (~61%), resembling a similar decline in Ca_v3 channel expression in the developing mammalian heart[293] (figure 4B), and modest (32%) and sharp (73%) declines in the buccal mass and foot, respectively (albeit with lower expression in the latter two tissues relative to others tested). Conversely, LCa_v3 undergoes a marked increase in expression in the female reproductive albumen gland (150%; figure 4B), coinciding with sexual maturation where the gland takes up a role secreting factors that facilitate egg mass formation[294]. In contrast, only a marginal decline in Ca_v3 transcripts are detected in the central nervous system (CNS) from juvenile to adult (7.5%; figure 4B).

The expression of exons 12A and 12B within different *Lymnaea* tissues and organs is also tightly regulated. In the heart, remarkably, the channel is expressed almost exclusively with exon 12A (99%; figure 4B), while the opposite occurs in the male and female secretory reproductive glands of the hermaphroditic snail (i.e. 90-95% exon 12B in the prostate gland and 87-95% in the albumen gland). Indeed, the general downregulation of Ca_v3 transcripts bearing exon 12A in the heart, buccal mass and foot, and the upregulation of transcripts with 12B in sexual secretory glands (figure 4B) from juvenile to adult, coincides with the pattern seen for whole juvenile and adult animals where there is a relative enrichment of exon 12B (figure 4A).

Table 2. Primers used for qPCR of LCa_v3, exon 12A, and exon 12B. PCR efficiency (E), goodness of fit R^2 values, and slopes for the standard curves used to characterize qPCR primer pairs are shown in red.

Real time RT primers:		GenBank Accession	Ampl. Length	length	Tm (NN)	GC%	qPCR E	R2	Slope
Lymnaea HPRT1 5'	TGTAGAAGACATCATTGACACTGG	ES578163.1	145	24	53.86	42	90.4	0.985	-3.576
Lymnaea HPRT1 3'	GCCAATATAATCTGGTGCGTAAC			23	53.06	43			
LCa_v3 Univ 5'	CAGAGTGACACAGATGTGCTACAG	AF484084	139	24	57.34	50	104.7	0.986	-3.215
LCa_v3 Univ 3'	GGTTATAGGATAAAGTGCCATGCT			24	54.14	42			
LCa_v3 12A 5'	CGCACCATGGACAATGTAGCAAC	NA	134	23	57.05	52	92.3	0.977	-3.523
LCa_v3 12A 3'	CGATCACATTTACGGAATCCACCATC			26	57.29	46			
LCa_v3 12B 5'	CGCACCATGGACAATGTAGCAAC	AF484084	145	23	57.05	52	90.4	0.984	-3.576
LCa_v3 12B 3'	CGTTAAGACGATCCTTGCAGGAG			23	57.82	52			

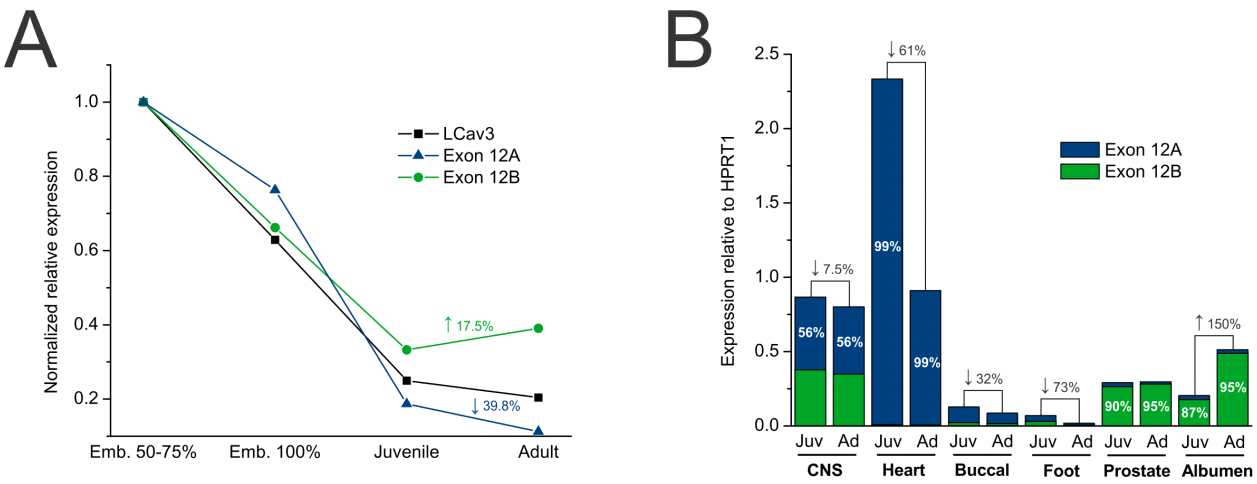

Figure 4. Quantitative PCR analysis of LCa$_v$3 transcripts and exon 12A and 12B splice variants. A)) Universal primers targeted against an invariable region of LCa$_v$3 reveal that there is a marked downregulation in the developing snail (black line), from mid embryo (50-75% development) to near hatching (100% development)[290,291], and continuing through to juvenile (shell length 1.0-1.5 cm) and sexually mature adult animals (shell length 2.0-2.5 cm)[292]. Primers that specifically amplify cDNA containing exons 12A (blue) and 12B (green), reveal that both are developmentally downregulated in conjunction with the LCa$_v$3 universal primers, however, there is relative enrichment of 12B (17.5%) and a relative decrease in 12A (39.8%) from juvenile to adult. **B)** Comparing LCa$_v$3 transcript levels between various juvenile and adult snail tissues. Both exon 12 variants of LCa$_v$3 are expressed at appreciable levels in the juvenile and adult central nervous system (CNS), with slightly more expression for LCa$_v$3-12A (i.e. 56% vs. 44%). In the heart, LCa$_v$3 transcripts possess almost exclusively exon 12A (99%), while in the albumen and prostate sexual secretory glands, 12B is predominant (87-95%). LCa$_v$3 is least abundant in the buccal mass and foot, where exon 12A is also more abundant. There is a general decline on total LCa$_v$3 expression relative to reference gene HPRT1, from juvenile to adult, in tissues that preferentially express exon 12A (blue plus green). This trend is most marked in the heart, where there is a 61% decline in Ca$_v$3 expression. In contrast, in the albumen gland that expresses almost exclusively 12B, there is a 150% increase in transcript levels for LCa$_v$3 from juvenile to adult. The downregulation of LCa$_v$3 transcripts bearing exon 12A and the concurrent increase in transcripts with exon 12B, within selected *Lymnaea* tissues, corresponds with the relative downregulation of 12A and upregulation of 12B in whole juvenile and adult animals (figure 4A).

Evolution of mutually exclusive exons 12A and 12B

Mutually exclusive exons 12A and 12B, within the domain II P-loop coding sequence of Ca_v3 channels, have not been previously reported. We thus analyzed various other genomes to determine whether a similar type of splicing occurs in non-molluscan species. The Ca_v3 genes of the most basal extant metazoans, including placozoan *Trichoplax adhaerens* and cnidarian *Nematostella vectensis*, lack alternate exons corresponding to exon 12B, and interestingly, the intron separating exons 11 and 12 (based on the human $Ca_v3.1$ gene) is absent (figure 5A and B). This intron is first apparent in the planarian *Schmidtea mediterranea* (Figure 5C), which is still basal with respect to higher invertebrates and vertebrates, but is more closely related due to its bilateral body symmetry. In fact, all higher metazoans possess Ca_v3 channel genes with an intron separating exons 11 and 12A (or 12B when exon 12A has been lost; see below). Furthermore, the amino acid sequence corresponding to the primitive 'exon 12', fused to exon 11, is short (between 34 and 40 amino acids; Table 3), which corresponds the length of exon 12A in molluscs (i.e. 38 to 39 amino acids; figure 1; figure 3; Table 3). Indeed, similarly short 12A exons are almost ubiquitous in animals, whereas the much longer exon 12B is found only in protostome invertebrates including molluscs, arthropods (i.e. *Drosophila*), and nematodes (i.e. *C. elegans*) (figure 6; Table 3), with exon 12A always situated upstream of exon 12B (Appendix C). Annelids are peculiar in that some species bear only exon 12A (e.g. *Lumbricus rubellus* and *Helobdella robusta*), while others only 12B (e.g. *Capitella telata*; Table 3; Appendix C). However, given the prevalence of both exons in protostomes, it is likely that the common ancestor of the annelid phylum had exons 12A and 12B, and that these were differentially lost in extant species. Conversely, chordate subphyla such as Vertebrata (e.g. *Homo sapiens* and *Xenopus laevis*), Tunicata (e.g. *Ciona intestinalis*), Cephalochordata (e.g. *Branchiostoma floridae*), as well as hemichordates (e.g. *Saccoglossus kowalevskii*) and echinoderms (e.g. *Strongylocentrotus purpuratus*), all of which group into the deuterostome superphylum based on embryonic development, only possess the short exon 12A (figure 6; Table 3; Appendix C).

Comparison of the amino acid sequences encoded by exons 12A and 12B, from protostome species that possess both exons, is consistent with the observation in molluscs that exon 12A encodes a considerably smaller peptide than 12B (i.e. 39.5 ±0.16 amino acids vs. 52.0 ±0.18 amino acids; figure 7A). In addition, exon 12A encodes less cysteine residues (i.e. 3.1 ±0.03 vs. 5.1 ±0.05; figure 7B); exon 12A from primitive animals, and deuterostomes that only possess exon 12A, closely resemble the protostomal exon 12A (i.e. 38.5 ±0.11 amino acids in length and 1.5 ±0.09 cysteines;

figure 7A and B). A likely scenario is that the ancestral Ca_v3 channel gene contained exclusively 'exon 12A' fused to exon 11, and that in higher metazoans, a rare intron insertion event[295] led to the formation of exon 12A. The Ca_v3 gene in protostomes was further elaborated by addition of downstream exon 12B, perhaps by duplication of exon 12A (figure 7C). In agreement, full length protein sequences of primitive Ca_v3 channels, from extant basal metazoans *Nematostella vectensis* and *Trichoplax adhaerens*, cluster together at the base of a phylogenetic tree derived from a multiple protein alignment (figure 8). Intron insertion to produce 12A likely occurred before the deuterostome-protostome split, and deuterostome Ca_v3 channels remained with only exon 12A in the domain II pore loop (figure 8). With the exception of some annelid species, protostome channels possess both exons 12A and 12B, suggesting that the evolution of mutually exclusive exons at this position along the Ca_v3 gene occurred only once.

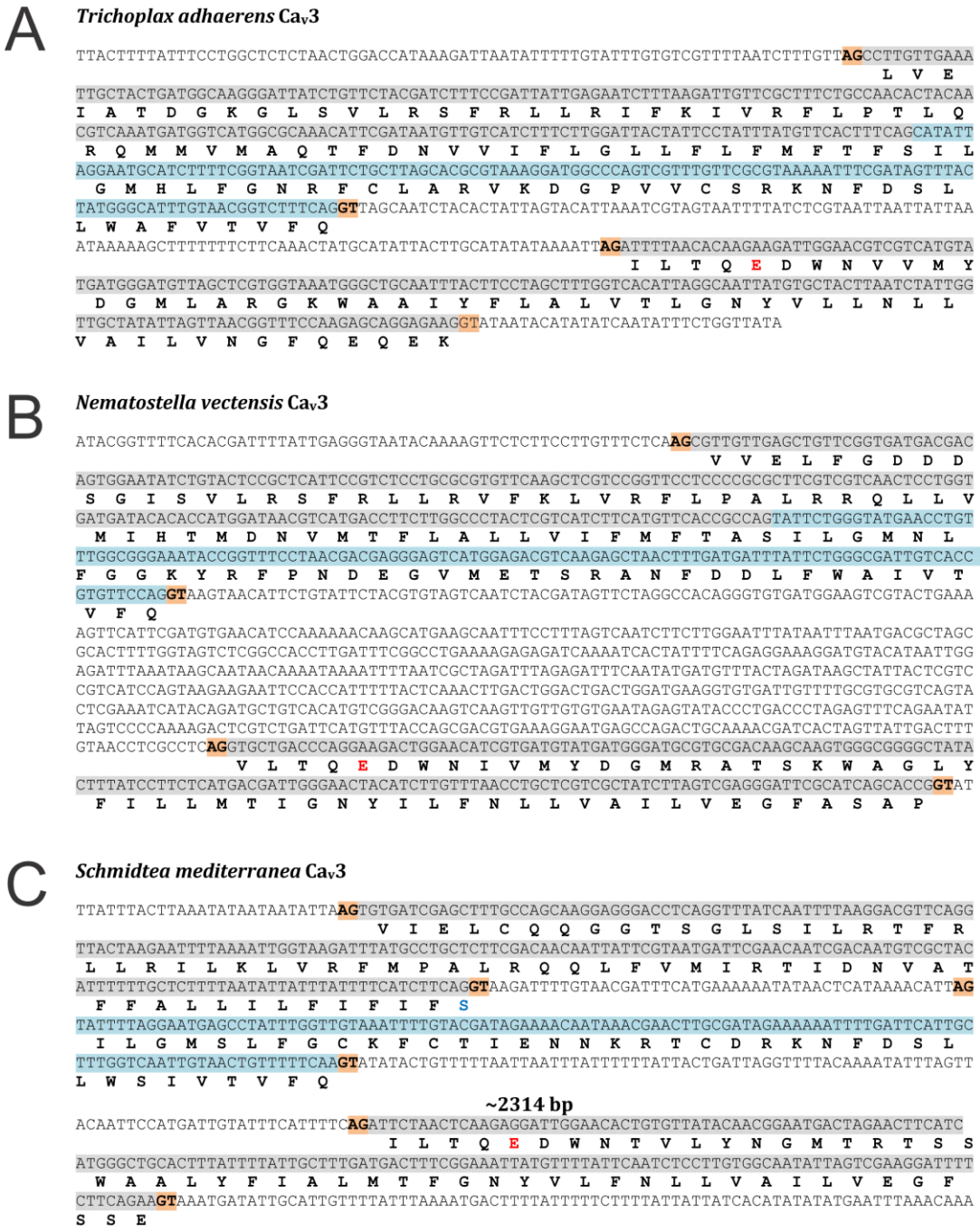

Figure 5. Genetic structure flanking the domain II P-loop coding sequence of Ca_v3 channel genes from primitive animals. A) *Trichoplax adhaerens*, which lacks muscles and nerves nor any apparent body symmetry, contains a Ca_v3 channel gene with exons 11 and 12 fused together. The amino acid sequence corresponding to exon 12, highlighted in blue, matches exon 12A from animals that possess both exons in terms of amino acid length (40) and a low number of cysteine residues (2) (JGI scaffold 2:6781672-6793175). **B)** Cniderian *Nematostella vectensis*, an animal with radial body symmetry and a very simple nervous system, also has an exon 12A-like coding sequence fused to exon 11 (JGI scaffold 154:248090-279585). In fact, all extant basal metazoans observed contained 12A-like exons, with no intron between the exon 11 and 12A coding sequences, suggesting that this was the state of the ancestral Ca_v3 gene, before the advent of bilateral body symmetry. **C)** The planarian *Schmidtea mediterranea*, a primitive extant bilaterian, does have an intron separating exons 11 and 12A (The Genome Center contig 13897), and this configuration is conserved in all animals with bilateral symmetry.

Table 3. Genomic features of homologous DII P-loop exons from representative species across the animal Kingdom.

Phylum	Class	Species	Common Name	Exon 12A	Exon 12B	11/12A Intron	Size 12A	Size 12B	Cys 12A	Cys 12B
Basal metazoans										
Cnideria	Anthozoa	*Nematostella vectensis*	Starlet sea anemone	✓	X	X	39	NA	0	NA
Cnideria	Anthozoa	*Acropora digitifera*	Table coral	✓	X	X	39	NA	0	NA
Cnideria	Hydrozoa	*Hydra magnipapillata*	Hydra	✓	X	X	34	NA	0	NA
Placozoa	Tricoplacia	*Trichoplax adhaerens*	NA	✓	X	X	40	NA	2	NA
Platyhelminthes	Turbellaria	*Schmidtea mediterranea*	Planarian	✓	X	✓	38	NA	3	NA
Deutersostomes										
Chordata	Ascidiacea	*Ciona intestinalis*	Sea vase	✓	X	✓	38	NA	3	NA
Chordata	Leptocardii	*Branchiostoma floridae*	Lancelet	✓	X	✓	41	NA	2	NA
Echinodermata	Echinoidea	*Strongylocentrotus purpuratus*	Purple sea urchin	✓	X	✓	38	NA	4	NA
Chrodata	Amphibia	*Xenopus tropicalis* $Ca_v3.1$	Western clawed frog	✓	X	✓	38	NA	1	NA
Chrodata	Amphibia	*Xenopus tropicalis* $Ca_v3.2$	Western clawed frog	✓	X	✓	38	NA	1	NA
Chrodata	Amphibia	*Xenopus tropicalis* $Ca_v3.3$	Western clawed frog	✓	X	✓	39	NA	1	NA
Chrodata	Mammalia	*Homo sapiens* $Ca_v3.1$	Human	✓	X	✓	38	NA	1	NA
Chrodata	Mammalia	*Homo sapiens* $Ca_v3.2$	Human	✓	X	✓	39	NA	1	NA
Chrodata	Mammalia	*Homo sapiens* $Ca_v3.3$	Human	✓	X	✓	39	NA	1	NA
Hemichordata	Enteropneusta	*Saccoglossus kowalevskii*	Acorn worm	✓	X	✓	39	NA	3	NA
Protostomes										
Arthropoda	Insecta	*Drosophila melanogaster*	Fruit fly	✓	✓	✓	38	55	3	5
Arthropoda	Insecta	*Drosophila mojavensis*	Fruit fly	✓	✓	✓	38	55	3	5
Arthropoda	Insecta	*Apis mellifera*	Western honey bee	✓	✓	✓	40	52	3	5
Arthropoda	Insecta	*Anopheles gambiae*	African malaria mosquito	✓	✓	✓	40	55	3	5
Arthropoda	Arachnida	*Ixodes scapularis*	Blacklegged tick	✓	✓	✓	39	52	3	6
Arthropoda	Chilopoda	*Strigamia maritima*	Coastal centipede	✓	✓	✓	38	52	3	5
Mollusca	Gastropoda	*Lymnaea stagnalis*	Great pond snail	✓	✓	✓	39	50	4	5
Mollusca	Gasropoda	*Aplysia californica*	California sea hare	✓	✓	✓	39	51	3	5
Mollusca	Gastropoda	*Lottia gigantea*	Giant owl limpet	✓	✓	✓	38	51	3	4
Mollusca	Gastropoda	*Biomphalaria glabrata*	Bloodfluke	✓	✓	✓	39	50	3	6
Nematoda	Secernentea	*Caenorhabditis elegans*	Roundworm	✓	✓	✓	43	51	3	5
Nematoda	Secernentea	*Caenorhabditis briggsae*	Roundworm	✓	✓	✓	43	50	3	5
Annelida	Polychaeta	*Capitella teleta*	Polychaete worm	X	✓	✓	NA	50	NA	5
Annelida	Clitellata	*Lumbricus rubellus*	Earthworm	✓	X	✓	40	NA	3	NA
Annelida	Clitellata	*Helobdella robusta*	Leech	✓	X	✓	41	NA	3	NA

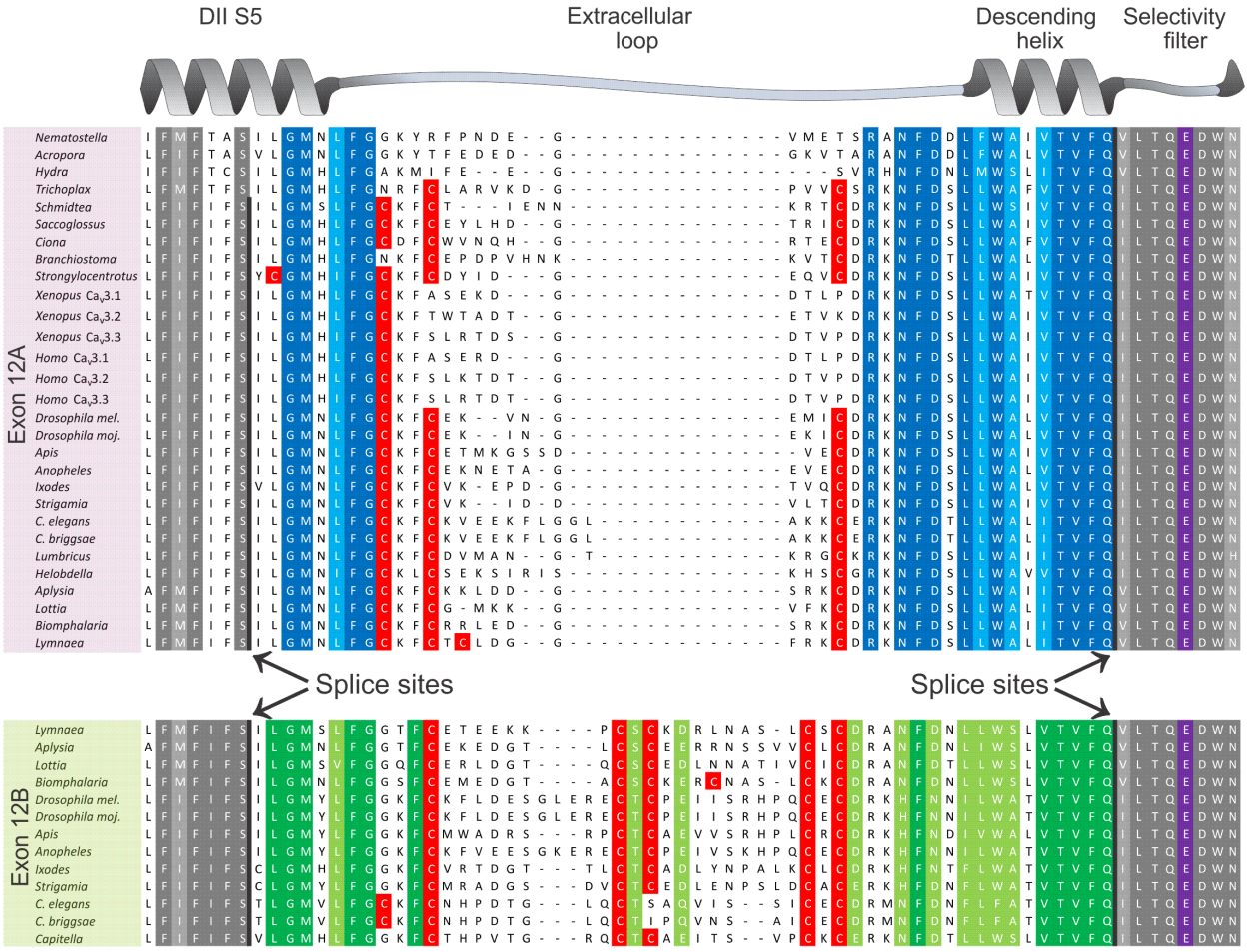

Figure 6. Multiple alignment of P-loop amino acid sequences from various metazoan Ca_v3 channel homologues. Highly conserved amino acids are highlighted in dark tones, and moderately conserved in lighter tones. Exon 12A is ubiquitous in animals with the exception of annelid *Capitella telata*, which likely lost the exon, while exon 12B is unique to protostome invertebrates. In primitive species either with radial body symmetry or lacking body symmetry altogether, exon 12A is fused to upstream exon 11; intron insertion in a primitive ancestor of bilaterians (exemplified by basal bilaterian *Schmidtea mediterranea*) created a true exon 12A (black lines). Note the larger size and number of cysteines (red) for exon 12B relative to 12A. There is also conserved pattern in the arrangement of cysteines between the loops separating the domain I S5 helix from the descending pore helix, with some exceptions (top schematic; based on structural prediction of using PSIPRED). Exons 12A in *Lymnaea* and echinoderm *Strongylocentrotus purpuratus* Ca_v3 genes are unique in that they encode an additional cysteine residue, located in the S5 helix for *Strongylocentrotus* and the extracellular loop for *Lymnaea*. Note also the complete absence of cysteines in Cnidierians, and the presence of only two in *Trichoplax adhaerens*. Alignment was generated using the CLUSTALW algorithm[296] available on San Diego Supercomputer Biology Workbench (http://workbench.sdsc.edu/).

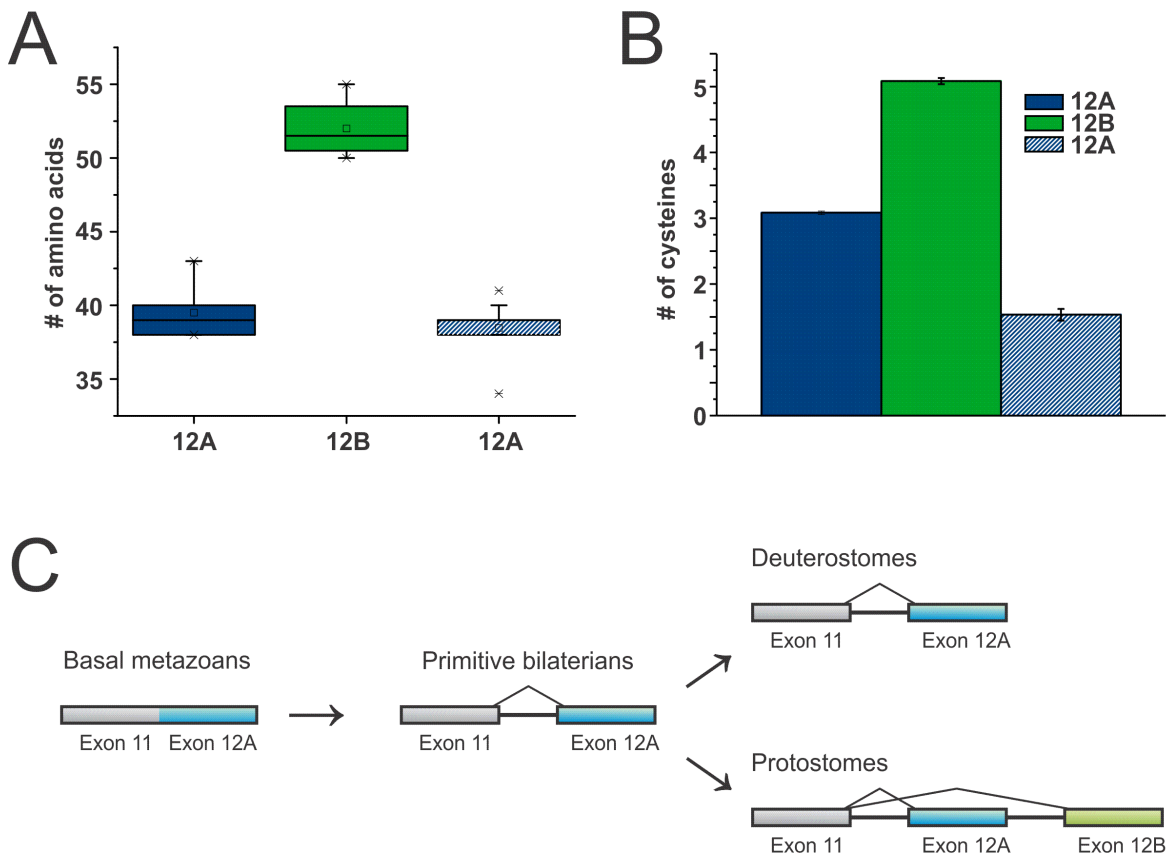

Figure 7. Conserved features distinguishing exons 12A and 12B suggest exon 12A is ancestral. A) A box plot comparing amino acid lengths of exons 12A and 12B (blue and green boxes respectively), only from protostomes that possess both exons (Table 3), reveals that 12A is considerably smaller than 12B (i.e. 39.5 ±0.16 amino acids vs. 52.0 ±0.18 amino acids). The 'exon 12' amino acid sequences from primitive animals, that lack an intron between the exon 11 and 12 coding sequences, and deuterostomes that only possess one exon 12, are short similar to protostome 12A (i.e. 38.5 ±0.11 amino acids; blue box with white lines). **B)** Protostome 12A exons also contain less cysteine residues than 12B (i.e. 3.1 ±0.03 vs. 5.1 ±0.05), and this is also true for exon 12 from primitive and deuterostome animals (1.5 ±0.09). **C)** Proposed evolutionary history for exons 12A and 12B in metazoan Ca_v3 channel genes. In basal metazoans, that diverged before the advent of bilateral symmetry (i.e. either lacking body symmetry or having radial body symmetry), a 12A-like exon coding sequence was fused to exon 11 (blue and grey boxes, respectively). Intron formation, likely via insertion of non-coding DNA between the exon 11 and 12 coding sequences[295], produced a true exon 12A in an ancestor to bilaterian animals (introns depicted by straight lines, spliceosome-mediated ligation of exons by chevrons). Deuterostomes retained this configuration, while protostome invertebrates duplicated exon 12A to produce exon 12B (green box).

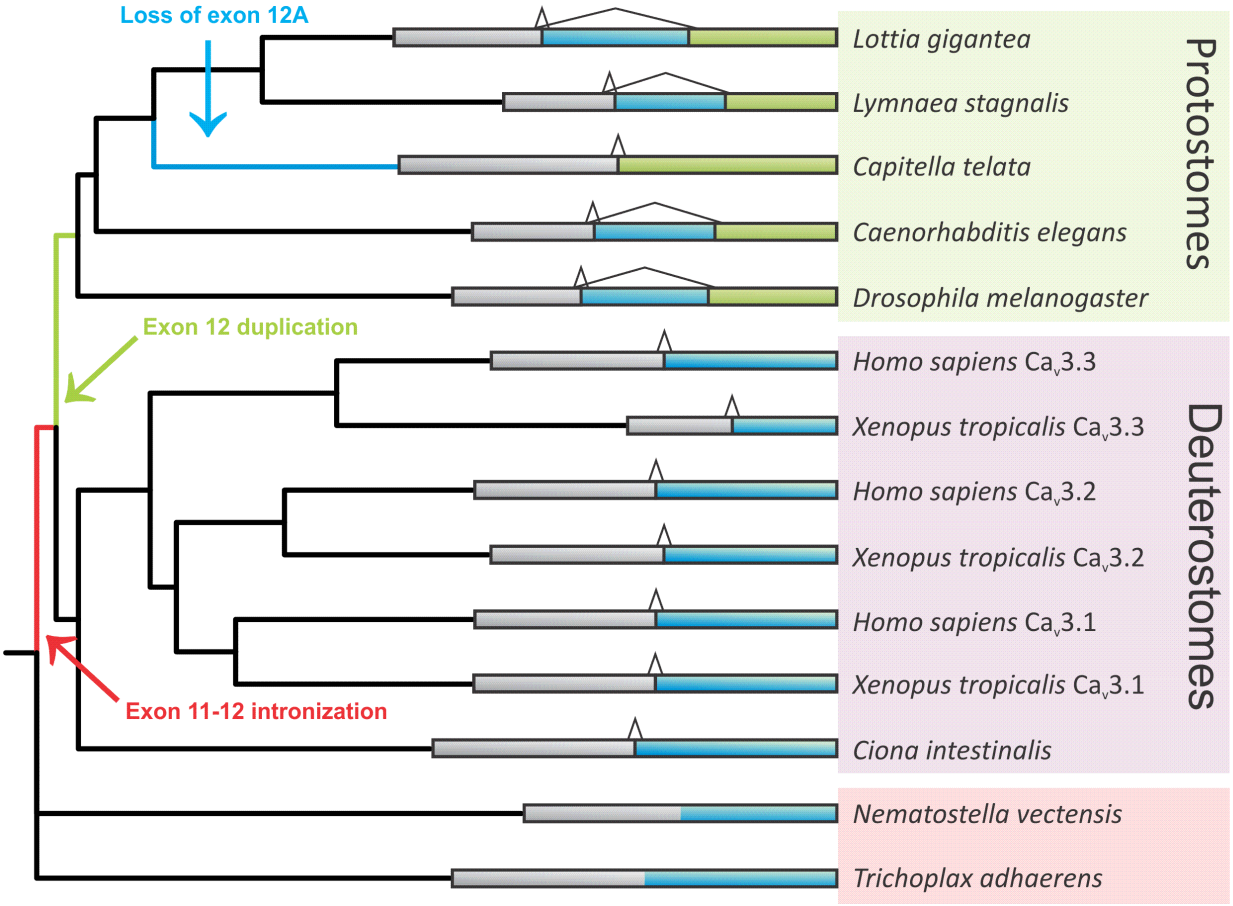

Figure 8. The arrangement of taxa in a phylogenetic tree of full length protein sequences from various metazoan Ca_v3 channel homologues corroborates the proposed evolutionary history for 12A and 12B exons. Ca_v3 channels from basal metazoans *Nematostella vectensis* and *Trichoplax adhaerens*, which possess exon 12A fused to exon 11, cluster together at the base of the tree. Intron insertion between exons 11 and 12 is retained in all animals with bilateral symmetry (depicted in red). After the split between deuterostomes and protostomes, exon 12A was duplicated in protostomes (green) while deuterostomes retained only 12A. For some reason, annelid species have lost either exon 12A or 12A (i.e. *Capitella telata*; depicted in blue). Protein accession numbers: *Lottia gigantea* Ca_v3 (12A) JGI Protein ID 220094; *Capitella telata* Ca_v3 (12B) JGI Protein ID 89566; *Caenorhabditis elegans* Ca_v3 (12A) GenBank accession number CCD68020; *Drosophila melanogaster* Ca_v3 (12A) GenBank accession number NP_572296.2; *Homo sapiens* $Ca_v3.3$ (12A) Ensembl Protein ID ENSP00000385019; *Xenopus tropicalis* $Ca_v3.3$ (12A) JGI protein ID 323418; *Homo sapiens* $Ca_v3.2$ (12A) Ensembl Protein ID ENSP00000334198; *Xenopus tropicalis* $Ca_v3.2$ (12A) JGI protein ID 311573; *Homo sapiens* $Ca_v3.1$ (12A) Ensembl Protein ID ENSP00000339302; *Xenopus tropicalis* $Ca_v3.1$ (12A) JGI protein ID 380951; *Ciona intestinalis* Ca_v3 (12A) JGI Protein ID 269719; *Nematostella vectensis* Ca_v3 (12A) JGI protein ID 170705; *Trichoplax adhaerens* Ca_v3 (12A) JGI Protein ID 21513.

Exons 12A and 12B impose minimal influences on voltage sensitivity

In order to determine the biophysical consequences of exons 12A and 12B on the *Lymnaea* Ca_v3 channel, the cDNA of both variants were cloned into mammalian expression vector pIRES2-EGFP, which allows for identification of positively transfected cells via bicistronic expression of eGFP[297,289,1]. Voltage steps from -110 mV to various depolarized potentials (-90 to +40 mV) elicited typical low voltage-activated calcium currents when LCa_v3-transfected HEK-293T cells were recorded by whole-cell patch clamp in 2 mM calcium (figure 9A). The current-voltage relationships of the two exon 12 variants, plotted as the peak currents for given depolarizing voltages, are almost indistinguishable at potentials ranging from -90 to 0 mV (figure 9B). At more positive potentials, the 12A variant of LCa_v3 produced large outward currents, presumably carried by monovalent cesium ions present in the internal solution, while the 12B variant showed strong rectification and little outward current at +40 mV (figure 9A and B). Despite the marked difference in outward current at positive potentials, the voltage sensitivities of channel activation and steady-state inactivation of the exon 12 variants are statistically indistinguishable (figure 9C; Table 4). Boltzman transformation of the current-voltage relationships (figure 9C) reveals a ½ maximal activation ($V_{0.5}$) of -53.63 ±0.35 mV for LCa_v3-12A and -53.48 ±0.34 mV for LCa_v3-12B (Table 4). Furthermore, plotting of peak residual current after various 1 second inactivating voltage pulses (ranging from -100 to -45 mV; figure 9C), produces ½ maximal steady-state inactivation values ($V_{0.5}$) of -70.21 ±0.38 mV for LCa_v3-12A and -70.89 ±0.49 mV for LCa_v3-12B (Table 4). The slopes of the activation curves for LCa_v3-12A and LCa_v3-12B variants are also indistinguishable (i.e. 5.60 ±0.09 mV vs. 5.46 ±0.14 mV, respectively) and there is only a slight difference in the inactivation curve slopes (2.72 ±0.04 mV for LCa_v3-12A vs. 2.93 ±0.08 mV for LCa_v3-12B; Table 4).

Minimal influences on activation and inactivation kinetics

The kinetic properties of macroscopic calcium currents produced by the exon 12 variants are also largely indistinguishable. The exon 12B variant exhibits marginally faster activation kinetics than LCa_v3-12A (measured as time to peak for inward calcium current at various depolarizing potentials; figure 10A), with a statistically significant difference at -55 mV (i.e. 14.68 ±0.63 ms vs. 12.62 ±0.70 ms for 12A and 12B respectively) waning at more depolarized potential such as 10 mV (i.e. 3.19 ±0.39 ms vs. 2.35 ±0.12 ms for 12A and 12B respectively; Table 4). Inactivation kinetics, measured as tau values for mono-exponential curve fits over the inactivating phase of the inward calcium currents, are also marginally faster for LCa_v3-12B, with a small statistical significance at -10 mV (i.e.

17.20 ±0.48 ms vs. 15.67 ±0.56 ms for 12A and 12B, respectively), and no significance at -55 mV (i.e. 38.40 ±1.67 ms vs. 40.07 ±2.56 ms for 12A and 12B respectively; Table 4).

Deactivation kinetics and recovery from inactivation are faster for LCa_v3 variants with exon 12B

Deactivation, where channels transition directly from an open state to a closed non-inactivated state (i.e. voltage step from -110 to -35 mV for 7 ms, then hyperpolarize the membrane to between -110 to -50 mV; figure 10C), is one property where the two LCa_v3 channel variants significantly diverge. At voltages below the typical resting membrane potential of most neurons (i.e. -110 to -70 mV), tau values for mono-exponential curve fits over deactivating tail currents are smaller for LCa_v3-12B than for LCa_v3-12A (figure 10D). The more rapid kinetics of the exon 12B variant are strongly significant at -100 mV (i.e. 1.97 ±0.06 ms vs. 1.37 ±0.05 for 12A and 12B respectively), however at -60 mV and above, the significance is lost (i.e. 6.05 ±0.30 vs. 5.45 ±0.52 for 12A and 12B at 60 mV, respectively; Table 4).

Finally, recovery from inactivation is also different between the two exon 12 two variants. Currents elicited from fully inactivated channels, after hyperpolarization to -110 mV for increasing periods of time (figure 11A), recovered faster for LCa_v3-12A within the first second (figure 11B). 33.14 ±0.96% of maximal current recovered for LCa_v3-12A after 0.25 seconds of hyperpolarization, while only 26.19 ±0.86% recovered for LCa_v3-12B (Table 4). The time for 50% recovery of maximal currents was also faster for LCa_v3-12A (Table 4), however after 4 seconds of hyperpolarization, maximal currents for both variants had recovered to ~93% (figure 10F; Table 4).

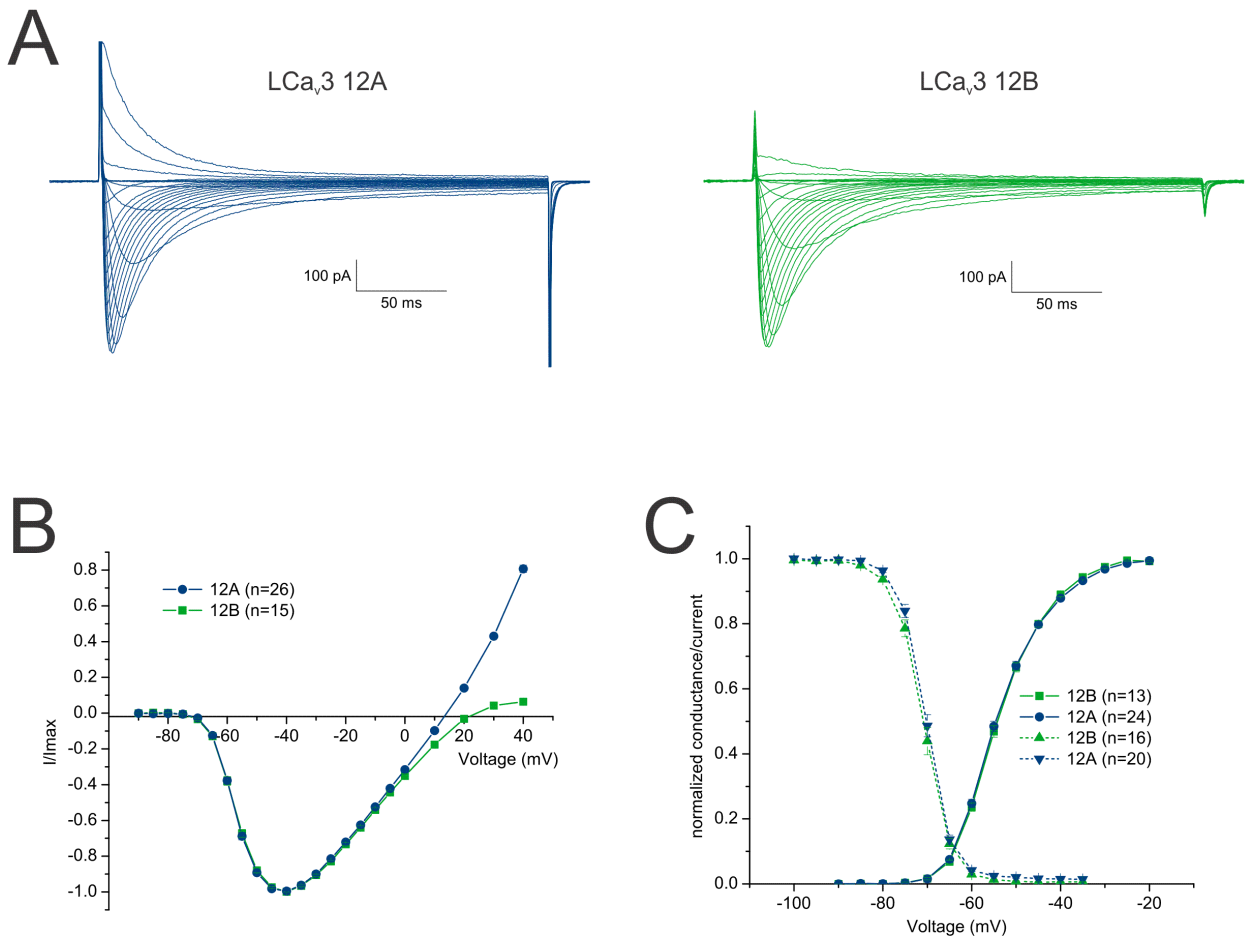

Figure 9. Voltage properties of calcium currents through LCa_v3-12A and LCa_v3-12B channel isoforms heterologously expressed in HEK-293T cells. A) Calcium currents elicited by depolarizing voltage-clamped cells from -110 mV to various depolarizing potentials (-90 to +40 mV) were almost indistinguishable for the two exon 12 variants at voltages below 0 mV, after which LCa_v3-12A conducted large outward currents likely carried be Cs^+ present in the internal solution of the patch pipette. **B)** Plotting the peak absolute currents resulting from depolarizing voltage steps, as a function of step voltage, produces two completely overlapping current-voltage relationship plots for the two LCa_v3 variants below 0 mV. However, at voltages above 0 mV the two isoforms diverge where LCa_v3-12A conducts large outward currents while LCa_v3-12B currents show inward rectification indicative of poor permeability to internal cations. **C)** Boltzman transformation of the current-voltage plots from B produces completely overlapping activation curves, with full channel activation near -25 mV, and ½ maximal activation occurring near -53 mV (see Table 4). Steady state inactivation, determined by measuring maximal inward current after 1 second inactivating pulses at various depolarized potentials, reveals that both variants begin to inactivate near -75 mV, with full inactivation occurring near -55 mV, and ½ maximal inactivation near -70 mV. Of note, there is a marginal difference in the slope of the inactivation curves (see Table 4). Both variants are expected to conduct depolarizing window currents at rest, carried by a small fraction of channels that are available (not inactivated) at the foot of the activation curve.

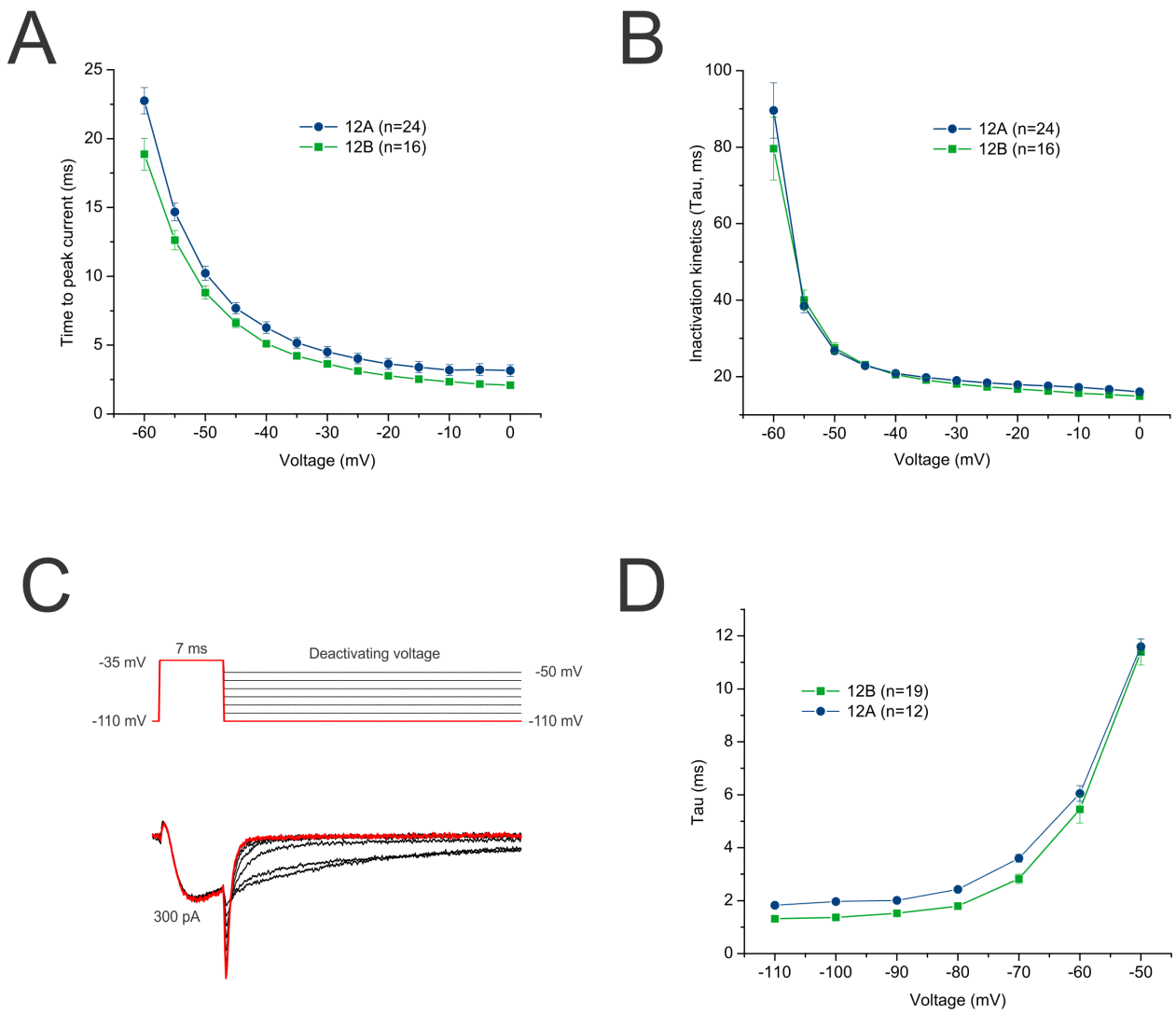

Figure 10. Subtle differences in kinetics between the two exon 12 variants of LCa$_v$3. A) Activation kinetics, measured as the time required for macroscopic currents to reach peak after the onset of depolarization, get progressively faster with depolarization and are marginally faster for LCa$_v$3-12B relative to LCa$_v$3-12A, with a mild statistical difference occurring below -55 mV (Table 4). **B)** Inactivation, measured as tau values for mono-exponential curve fits over the inactivating phase of macroscopic currents elicited at various depolarized potentials, are indistinguishable at low voltages and show a minimal statistical difference at -10 mV (Table 4). **C)** Illustration of voltage clamp protocol used to measure deactivation kinetics (top panel), and an example current trace recording obtained using this protocol (bottom panel). 7 ms depolarizing voltage pulses to -35 mV were used to open channels, and then the voltage was dropped to elicit deactivating tail currents (i.e. -110 to -50 mV). **D)** Tau values for mono-exponential curve fits over deactivating tail currents reveal that LCa$_v$3-12B has considerably faster deactivation than LCa$_v$3-12A at voltages below -60 mV (see Table 4).

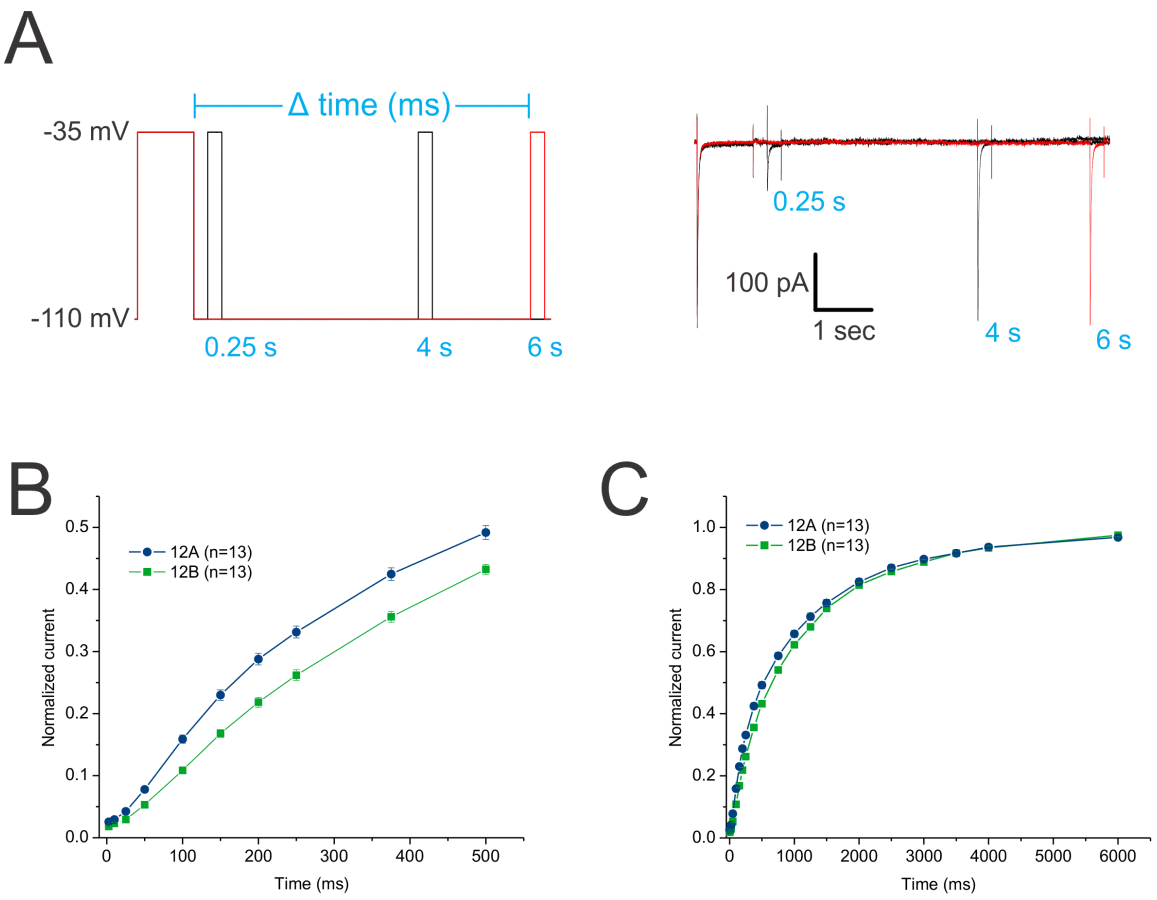

Figure 11. Differences in recovery from inactivation for LCa$_v$3 exon 12 variants. A) Illustration of the voltage clamp protocol used to measure recovery from inactivation. One second long inactivating voltage pulses at -35 mV were followed by hyperpolarization to -110 mV for various time intervals to allow channel to recover; subsequently, a depolarizing step again to -35 mV was to measure recovery of inactivated current (left panel). The right panel shows an example current trace recording with recovered inward calcium current increasing in amplitude as a function of duration of hyperpolarization (i.e. 0.25, 4, and 6 seconds). **B)** Recovery of peak inward current in the time scale between 10 and 500 ms is significantly faster for LCa$_v$3-12A vs. LCa$_v$3-12B, with respectively ~33% and ~26% of channels recovering after 250 ms of hyperpolarization (Table 4). **C)** In the longer time frame of 10 to 6000 ms, the two variants are largely indistinguishable in recovery.

Table 4. Comparison of the biophysical parameters for currents recorded from exon 12 variants of LCa_v3 in HEK-293T cells.

	LCa_v3 12A	LCa_v3 12B	Significance
Activation			
$V_{0.5}$ (mV)	-53.63 ±0.35 (n24)	-53.48 ±0.34 (n13)	n.s.
Slope (mv)	5.60 ±0.09 (n29)	5.46 ±0.14 (n13)	n.s.
Activation NMDG			
$V_{0.5}$ (mV)	-63.50 ±0.60 (n4)	-67.40 ±0.78 (n5)	**
Slope (mv)	6.00 ±0.01 (n4)	5.57 ±0.43 (n5)	n.s.
Inactivation			
$V_{0.5}$ (mV)	-70.21 ±0.38 (n20)	-70.89 ±0.49 (n16)	n.s.
Slope (mV)	2.73 ±0.04 (n20)	2.93 ±0.08 (n16)	*
Activation kinetics			
TTP -55 mV (ms)	14.68 ±0.63 (n24)	12.62 ±0.70 (n16)	*
TTP -10 mV (ms)	3.19 ±0.39 (n24)	2.35 ±0.12 (n16)	n.s.
Inactivation kinetics			
τ -55 mV (ms)	38.40 ±1.67 (n24)	40.07 ±2.56 (n16)	n.s.
τ -10 mV (ms)	17.20 ±0.48 (n24)	15.67 ±0.56 (n16)	*
Deactivation kinetics			
τ -100 mV (ms)	1.97 ±0.06 (n12)	1.37 ±0.05 (n19)	***
τ -60 mV (ms)	6.05 ±0.30 (n12)	5.45 ±0.52 (n19)	n.s.
Inactivation Recovery			
% recovery at 0.25 s	33.14 ±0.96 (n13)	26.19 ±0.86 (n13)	***
% recovery at 4 s	93.69 ±0.69 (n13)	93.42 ±0.58 (n13)	n.s.
$T_{0.5}$ (ms)	921.49 ±22.45 (n13)	767.76 ±26.09 (n13)	***

Values are expressed as mean +/- S.E.M. and n is the numbers of cells used. Statistical comparisons were done using a one-way ANOVA combined with a Student-Newman-Keuls post hoc test with * P≤0.05, ** P≤0.01 and *** P≤ 0.001; n.s., not significant.

No difference in Ni^{2+} sensitivity and Ca^{2+} vs. Ba^{2+} permeability

Non-specific Ca_v3 channel blocker nickel blocks mammalian $Ca_v3.2$ with high affinity via a critical histidine residue located in the domain I S3-S4 extracellular loop of the channel[241]; this residue is absent from the other less sensitive mammalian isotypes ($Ca_v3.1$ and $Ca_v3.3$) as well as *Lymnaea* Ca_v3[1]. However, other binding sites are expected to contribute to nickel block, as well as block by other divalent metal cations such as zinc and copper[261,259]. We therefore tested whether the two exon 12 variants of LCa_v3, with divergent domain II P-loop structures, were differentially blocked by Ni^{2+}. Previously, we showed that the solubilized ion blocks peak currents through heterologously expressed LCa_v3-12B with a similar affinity as mammalian $Ca_v3.1$ (i.e. IC_{50} ~ 300 μM)[241,1]. Perfusion 300 μM Ni^{2+} over patch-clamped cells revealed that both domain II pore variants of LCa_v3 were equally susceptible at this concentration (figure 12A), with a 37.28 ±1.54% block for LCa_v3-12A, and 39.10 ±1.84% block for LCa_v3-12B (not statistically different).

The three mammalian isotypes can also be distinguished by their relative permeabilities to barium with respect to calcium, with rodent $Ca_v3.1$, $Ca_v3.2$ and $Ca_v3.3$ being less, more, and equally permeable to Ba^{2+}, respectively[204]. Like $Ca_v3.2$, LCa_v3-12B was also found to be more permeable to barium over calcium[1], however, differences in the pore structure imposed by exon 12A could potentially alter this property. Perfusion of 2 mM solutions of Ca^{2+} and Ba^{2+} over patch-clamped cells revealed that LCa_v3-12A and LCa_v3-12B are both equally more permeable to barium (figure 12B), with relative increases in peak current at -40 mV (i.e. $I_{peak}\ Ba^{2+}/I_{peak}\ Ca^{2+}$) of 1.34 ±0.04 for LCa_v3-12A vs. 1.35 ±0.06 for LCa_v3-12B (not statistically different).

Exons 12A and 12B impart dramatic differences in monovalent cation permeability

The large outward currents carried by LCa_v3-12A at positive potentials (figure 9A and B), suggested that this variant is more permeable to monovalent cesium, which was the major cationic constituent in the internal solution used for whole-cell patch clamp recording. To confirm this, an internal solution was prepared where Cs^+ was replaced with impermeant monovalent cation $NMDG^+$. Indeed, the large outward current of LCa_v3-12A was greatly reduced with this internal solution (figure 13A), with a drop in the ratio of peak outward current at +40 mV to maximum peak inward current (i.e. $I_{peak\ outward\ at\ +40\ mV}/I_{max\ inward}$) from 80.65 ±2.04% to 19.61 ±2.20% (75.7% drop; figure 13B). Interestingly, the presence of NMDG in the internal solution also caused a marked hyperpolarizing shift in the activation of both LCa_v3 variants, with maximal peak inward currents occurring at -50 mV for LCa_v3-12A and -55mV for LCa_v3-12B (figure 13C; compare with -40 mV in figure 9B). Boltzman

transformed current-voltage relationships for the LCa_v3 12A and 12B variants, recorded with the NMDG internal solution, revealed hyperpolarizing shifts of ~10 mV for LCa_v3-12A (-63.50 ±0.60) and ~14 mV for LCa_v3-12B (-67.40 ±0.78), with minimal changes in slope (figure 13D; Table 4).

The increased cesium permeability of exon 12A LCa_v3 variants prompted us to test whether sodium, the most abundant extracellular monovalent cation, is also more permeable. Switching from 2mM Ca^{2+} external solution to one containing 2 mM Ca^{2+} and 135 mM Na^{+} produced a dramatic fold-increase in peak current at -40 mV for LCa_v3-12A (i.e. 15.48 ±1.70), and only a slight increase for LCa_v3-12B (2.74 ±0.24) (figure 14). Together, our data indicates that the ancestral exon 12A, located in the P-loop adjacent to the selectivity filter glutamate of domain II, causes a dramatic increase in permeability to both internal and external monovalent cations. Conversely, protostome-specific exon 12B renders LCa_v3 more calcium-selective. Remarkably, in spite of this physiologically drastic alteration in functionality, exon 12 variants of LCa_v3 remain largely indistinguishable in their biophysical properties, Ni^{2+}-sensitivity, and Ca^{2+} vs. Ba^{2+} divalent cation permeability.

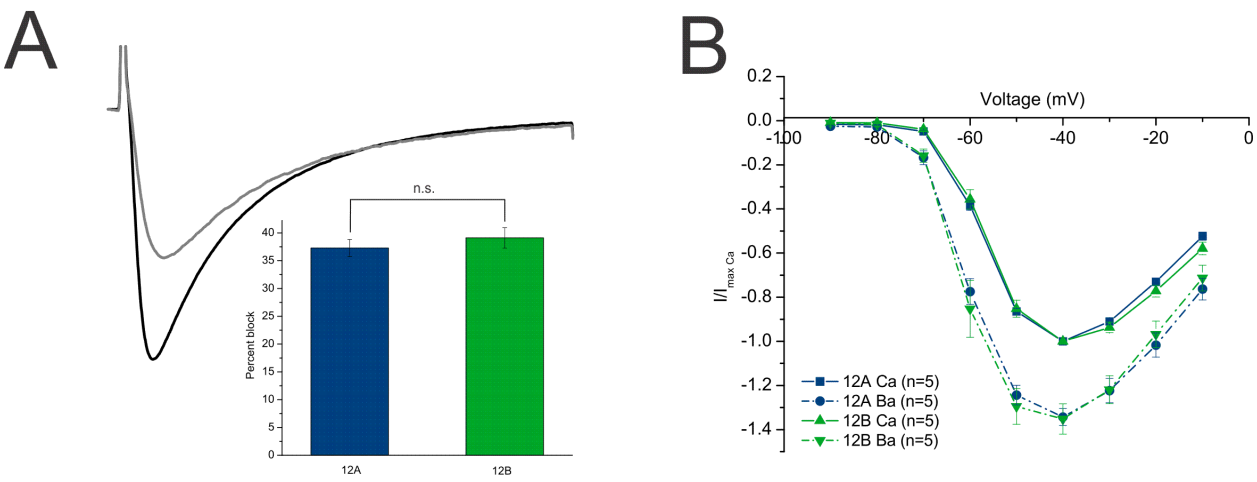

Figure 12. Ni^{2+}-block and Ba^{2+} vs. Ca^{2+} selectivity are unaltered between exon 12 variants of LCa_v3. A) LCa_v3 calcium currents underwent 37% and 39% reduction in peak values upon perfusion of 300 µM Ni^{2+} over patch clamped cells (n.s. not statistically different; n=4 for 12A and n=3 for 12B). Above the bar graph are example current traces elicited by depolarization from -100 to -35 mV, in the absence and presence of Ni^{2+} (black and grey respectively). **B)** Current-voltage plot of currents recorded while perfusing 2 mM Ca^{2+} then 2 mM Ba^{2+} over the same patched cells reveals a ~1.3-fold increase in peak current at -40 mV for both LCa_v3-12A and LCa_v3-12B, with no shift in the maximal peak inward current of -40 mV. Peak current values from each cell were normalized against the corresponding maximal inward current in 2 mM Ca^{2+}.

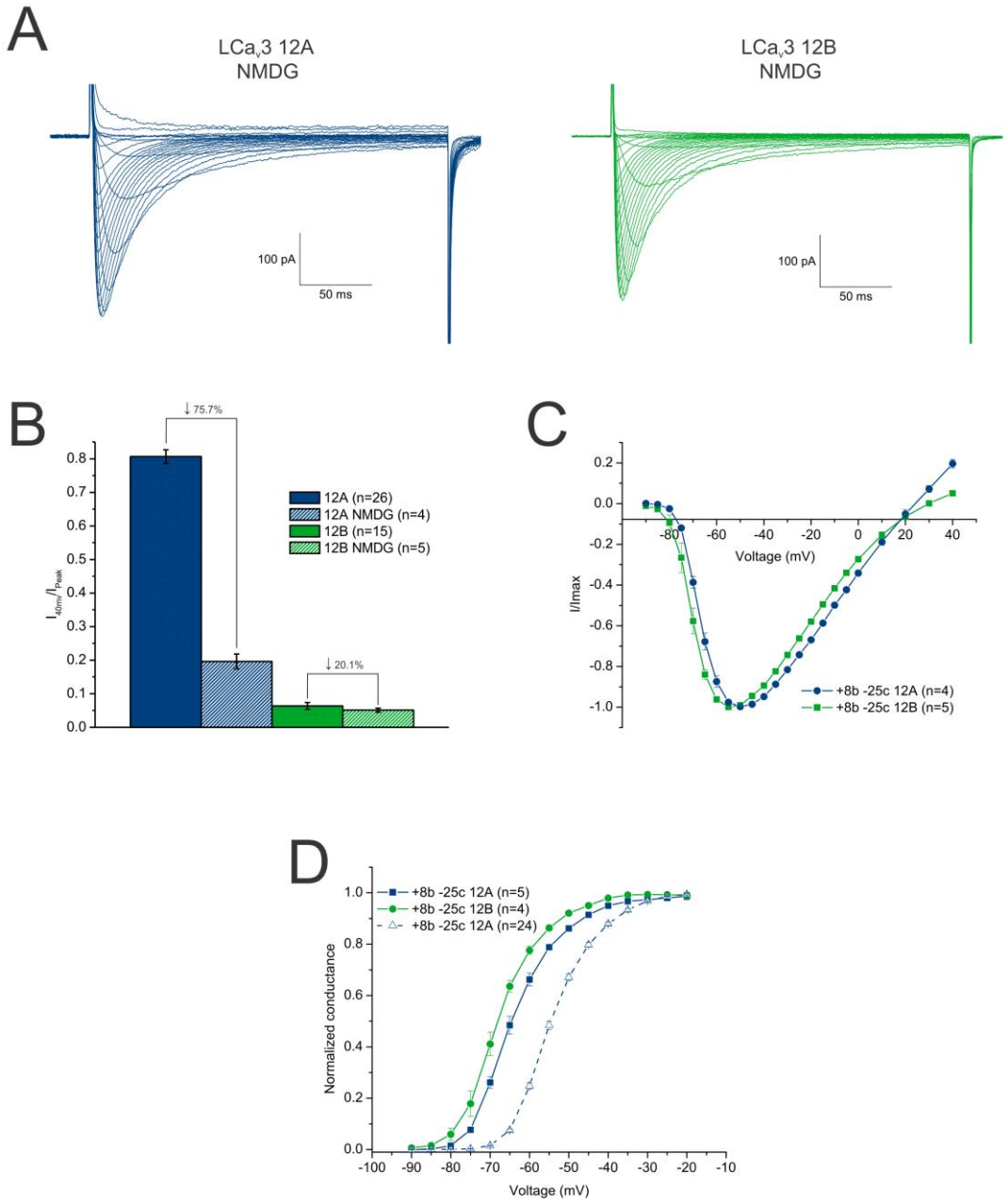

Figure 13. Block of outward current through LCa$_v$3-12A by replacement of internal Cs^+ with impermeant $NMDG^+$. A) Sample current traces recorded from LCa$_v$3-12A and LCa$_v$3-12B at various depolarizing potentials, with 110 mM Cs^+ replaced in the internal recording solution with equimolar N-methyl-D-glucamine ($NMDG^+$), show a marked attenuation of outward currents through the 12A variant. **B)** The ratios of maximal peak outward current at +40 mV divided by the corresponding maximal peak inward current for each recorded cell decrease dramatically for LCav3-12A in the presence of internal NMDG+ (i.e. 75.7%). LCa$_v$3-12B, which conducts only small outward currents at +40 mV in the presence of Cs^+, also showed a modest reduction in the outward to inward current ratio (i.e. 20.1%). This indicates that most of the outward current observed for LCa$_v$3-12A (figure 9A) is attributable to monovalent cesium. **C)** Current-voltage plots of the two variants of LCa$_v$3 show a dramatic hyperpolarization in maximal peak inward current in the presence of internal $NMDG^+$, shifting from -40 mV to -55 mV for 12B and -50 mV for 12A (compare with figure 9B). **D)** Boltzman transformation of the current-voltage data reveals large hyperpolarizing shifts in half maximal activation for the two exon 12 variants in the presence of $NMDG^+$, with a more pronounced shift for LCa$_v$3-12B vs. LCa$_v$3-12A (i.e. $V_{0.5}$ of -67.40 ±0.78 mV for LCa$_v$3-12B vs. -63.50 ±0.60 mV for LCa$_v$3-12A; Table 4).

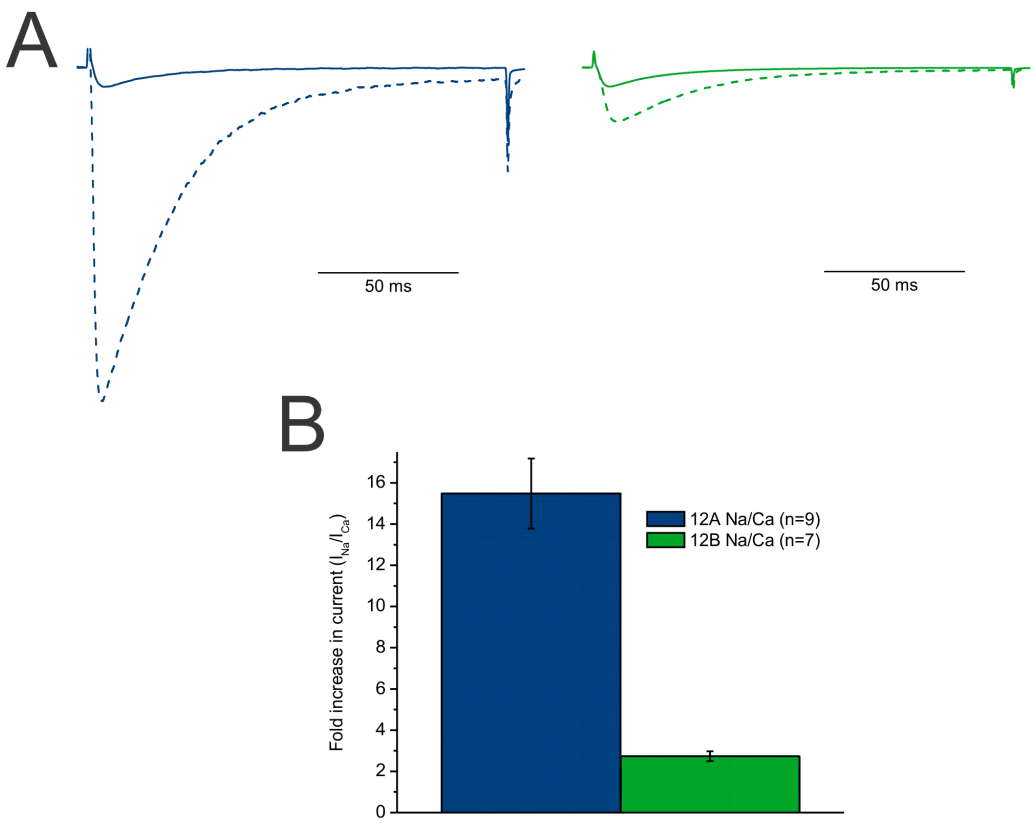

Figure 14. LCa$_v$3-12A currents undergo a stunning increase in amplitude in the presence of 135 mM external sodium. A) Sample current traces for LCa$_v$3-12A (blue, left) and LCa$_v$3-12B (green, right) perfused with either 2 mM Ca^{2+} external (solid lines) or 2 mM Ca^{2+} plus 135 mM Na^+ external (dotted lines). Currents were normalized to the peak inward current in 2 mM Ca^{2+}. **B**) Bar graph depicting the average increase in peak inward current in the presence of external Na^+, with a 15.48 ±1.70-fold increase for LCa$_v$3-12A (~1450%) and a 2.74 ±0.24-fold increase for LCa$_v$3-12B, indicating that the 12A variant is highly permeable to monovalent sodium, even in the presence of 2 mM Ca^{2+} external.

2.3.4 Discussion

Alternative splicing in the domain II P-loop of LCa_v3

Sequencing of the *Lymnaea* Ca_v3 channel cDNA revealed multiple sites for alternative splicing, including putatively evolutionarily conserved optional exons 8b and 25c in the respective I-II and III-IV linker coding sequences[289]. Exon 8b, also found in mouse and rat $Ca_v3.1$[194,195] but not the human orthologue[190,191], codes for 201 amino acids in snails and 134 in rodents. Interestingly, inclusion of this large exon has little influence on biophysical properties of the channels; however, its absence leads to a marked increase in membrane-localization when channels are expressed in mammalian cells[289,195], suggesting the exons contains some evolutionarily-conserved information that serves to regulate membrane trafficking and/or protein expression. Exon 25c in the III-IV linker of LCa_v3, which is conserved with mammalian $Ca_v3.1$ and $Ca_v3.2$ channels, is developmentally upregulated in both snails and mammals, and in contrast to the large 8b exon, imposes significant alterations in biophysical properties without affecting membrane expression[289].

Here, we have identified splicing of mutually exclusive exons, termed 12A and 12B, in the *LCa_v3* gene that alter the region between the S5 helix and the selectivity filter glutamate of domain II (figure 1). The 3' portions of these exons are predicted to encode short alpha helices (figure 1B), which based on the X-ray structure of the prokaryotic sodium channel Na_vAb[52], descend into the transmembrane vestibule of the channel to project the selectivity filter residue towards the center of the pore. Notably, the 3' splice sites of these exons are just five amino acids upstream of the domain II glutamate of the E**E**DD selectivity filter motif (figure 1B and C), critical for defining ion permeability as well as gating properties in Ca_v3 channels (see below). Analysis of Ca_v3 genes from other molluscs (i.e. *Aplysia californica*, *Lottia gigantea*, and *Biomphalaria glabrata*) revealed that exon 12A is situated in an upstream position along the gene relative to 12B (figure 3). The two most striking similarities between 12A and 12B exon pair coding sequences in molluscs are their size differences, and the number of cysteine residues that they contain, with the downstream exon 12B being 11 to 13 amino acids longer, and containing more cysteines than 12A (Table 3).

Mutually exclusive exons 12A and 12B are evolutionarily conserved

We were able to identify exon 12 homologues, with mutually exclusive exon 12A positioned upstream of exon 12B, in the Ca_v3 genes of many other animal species including arthropods (i.e. *Drosophila melanogaster*) and nematodes (e.g. *C. elegans*; Table 3; Appendix C). These phyla, as well as molluscs, are grouped into a division of animals with bilateral symmetry called the

protostomes, which distinguish themselves from the other bilaterian group, the deuterostomes, by whether the first opening in the developing embryo becomes the mouth (i.e. protostomes) or the anus (i.e. deuterostomes)[298]. Annelids, which are also protostomes, are atypical in that some species were found to possess only exon 12A (e.g. *Lumbricus rubellus* and *Helobdella robusta*), whereas others only 12B (e.g. *Capitella telata*; Table 3). With the limited number of annelid genomes available, we were unable to identify a species that possessed both exons. However, the Ca_v3 genes of all other protostomes observed contained exons 12A and 12B (Table 3), so it is likely that that the common ancestor to annelids also had both. For some reason, in annelids, there was no pressure to retain both exons and these were differentially lost in the sampled species.

Comparing the amino acids sequences for exons 12A and 12B, only from protostome Ca_v3 channels that possess both, confirms a strong conservation in size difference, where exon 12B is 7 to 17 amino acids longer that 12A (average difference of 12.5 amino acids; figure 7A; Table 3). Also, in all observed protostome species, exon 12B contains more cysteines (figure 7B). Using these criteria to differentiate the exons, only 12A was found in deuterostome phyla such as chordates (i.e. vertebrates/mammals), echinoderms, and hemichordates, and in primitive extant animals such as placozoan *Trichoplax adhaerens*, that lacks muscle and nerves, and cniderian *Nematostella vectensis*, which has radial body symmetry (Figure 5A and B; Table 3; Appendix C). Interestingly, in these extant basal metazoans that diverged before the advent of bilateral symmetry, the coding sequence corresponding to exon 12A is fused to that of exon 11 (figure 5A and B; figure 6; Table 3). This suggests that the ancestral Ca_v3 channel gene most likely lacked an intron separating these exons, and that a rare intron insertion occurred in a primitive bilaterian ancestor, exemplified by extant planarian *Schmidtea mediterranea* (figure 5C). The proposed evolutionary history for exons 12A and 12B therefore is that exon 12A is ancestral, and that intron insertion created a true exon 12 in animals with bilateral symmetry. After the subsequent split between protostomes and deuterostomes, a tandem duplication of exon 12A occurred in protostomes to create mutually exclusive exons. Such tandem exon duplications are actually quite common, where 10.7%, 7.1%, and 7.5% of human, *Drosophila*, and *C. elegans* genes contain duplicated exons, respectively[299]. Deuterostomes, on the other hand, retained a single exon 12A in the domain II P-loop of the channel coding sequence (figure 7C). In accordance, the proposed evolutionary history of exons 12A and 12B can be superimposed over a phylogenetic tree derived from alignment of full length Ca_v3 channel protein sequences from various animals (figure 8). Ca_v3 channels from the most primitive metazoans, that lack an intron between exons 11 and 12A, cluster together at the base of the tree. Ca_v3 channels from animals with bilateral

symmetry, which all possess exon 11-12A/12B introns, form distinct taxa corresponding to the deuterostome and protostome superphyla. Annelid Ca_v3 channel from *Capitella telata*, which likely lost exon 12A, appropriately segregates with other protostome Ca_v3 channels in the phylogenetic tree (figure 8).

Alternate exons 12A and 12B impart minimal changes on biophysical properties

Whole cell patch clamp recording of HEK-293T cells, transfected with LCa_v3-12A and LCa_v3-12B cDNAs in mammalian bicistronic expression vector pIRES2-EGFP, produced large macroscopic currents in 2 mM external Ca^{2+} (figure 9A). Analysis of the peak currents elicited at various depolarizing potentials revealed that the two LCa_v3 variants both produced maximal inward currents at -40 mV, with the two current-voltage relationships nearly indistinguishable at potentials below 0 mV (figure 9B). The only difference could be seen at potentials above 0 mV, where LCa_v3-12A conducted large outward currents, likely due to increased permeability of monovalent cesium (see below), while LCa_v3-12B showed strong inward rectification. Boltzman transformation of the current-voltage relationships to asses channel activation, and analysis of the steady state inactivation (figure 9C), revealed almost no differences in these biophysical parameters between the two channel variants (Table 4). Also, the speeds by which macroscopic currents reached peak and subsequently inactivated were largely indistinguishable (figure 10A and B; Table 4). With the alternate exons being spliced just five codons upstream of the domain II glutamate from the E**E**DD selectivity filter motif (figure 1), we were surprised that there were only minimal changes in all of these biophysical properties, which have been shown to be strongly influenced by alterations in the selectivity filter of mammalian $Ca_v3.1$[287,300,87].

In contrast, the kinetics for deactivation and the time required from recovery from inactivation, which are also influenced by changes in the selectivity filter for $Ca_v3.1$[87], were significantly different between LCa_v3-12A and LCa_v3-12B. Deactivation was faster for LCa_v3-12B at voltages below -70 mV (figure 10D; Table 4). As such, the slowly deactivating 12A variant can be expected to conduct prolonged depolarizing currents during the repolarization phase of the action potential, producing wider action potentials which at the synapse translates to increased neurotransmission[114]. Conversely, LCa_v3-12B is more suited to neurons that undergo higher-frequency firing, where rapid repolarization is a requirement. Recovery from inactivation is also different, with LCa_v3-12A recovering faster in the 10-1000 millisecond timeframe (figure 11B), where after 250 milliseconds of hyperpolarization, ~33% of LCa_v3-12A channels have recovered from inactivation while only ~26% of LCa_v3-12B have

recovered (Table 4). Currents through LCa$_v$3-12A would therefore be more resistant to accumulated inactivation during prolonged excitability (i.e. trains of action potentials), while currents through LCav3-12B would attenuate more quickly due to more pronounced accumulation of inactivated channels.

Altered monovalent vs. divalent permeability through exon 12 variants of LCa$_v$3

Carboxyl oxygens from selectivity filter glutamates of HVA calcium channels (i.e. EEEE) are proposed to project into the pore to form a high affinity binding site for Ca^{2+}. Occupancy of this site at just nanomolar concentrations of extracellular Ca^{2+} leads to repulsion of Na^+, and a 1000-fold difference in calcium vs. sodium permeability[301]. Instead, Ca$_v$3 channels possess EEDD selectivity filter motifs, where shortened aspartate side chains are expected to lower the binding affinity for Ca^{2+} (i.e. 10 times weaker than HVA channels), leading to reduced repulsion and increased permeability of monovalent cations[86,85,288]. Under physiological conditions, mammalian Ca$_v$3 channels are thus thought to carry mixed Ca^{2+}/Na^+ currents, with Ca$_v$3.1 being the least sodium permeable and Ca$_v$3.3 the most[288]. Counter intuitively, mutation of Ca$_v$3.1 EEDD to more resemble HVA channels (i.e. EEDE or EEED) actually increases monovalent cation permeability rather than render the channel more calcium-selective[87]. Furthermore, prokaryotic homotetrameric sodium channels, possessing HVA calcium channel-like EEEE selectivity filters, are sodium-selective indicating that the amino acid sequence of the selectivity filter motif is not necessarily deterministic for ion selectivity. Rather, selectivity is likely multifactorial, and although selectivity filter amino acids play a critical role, additional factors such as their orientation and/or mobility within the pore are significant.

Interestingly, we found that the *Lymnaea* Ca$_v$3 channel variant possessing exon 12A conducted large outward currents above +20 mV (figure 9A and B), indicative of increased permeability to intracellular ions. Since monovalent cesium was the main cation present in the internal solution, we replaced it with an equimolar amount of impermeant cation $NMDG^+$, resulting in a major attenuation of outward current (~76%; figure 13 A and B). Of note, some residual outward current persisted for LCa$_v$3-12A in the presence of $NMDG^+$ (figure 13B); however, this might be accounted for by low amounts of monovalent lithium present in the internal solution (0.6 mM), monovalent impurities from other reagents, or slight permeability to $NMDG^+$. Replacement of monovalent cesium with impermeant $NMDG^+$ also caused a marked hyperpolarizing shift in the current-voltage relationships, with maximal peak inward currents changing from -40 to -50 mV for LCa$_v$3-12A (i.e. a -10 mV shift), and -40 to -55 mV for LCa$_v$3-12B (i.e. -15 mV; figure 13C). The activation curves obtained by

Boltzman transformation of the current-voltage data (figure 13D) show half maximal activation voltages of -63.50 ±0.60 and -67.40 ±0.78. This indicates that the absence of monovalent Cs^+ (or presence of $NMDG^+$) somehow allows the channels to activate at significantly lower potentials. The mechanisms accounting for this are unclear; however, one possibility is that $NMDG^+$ and Cs^+ exert differential charge-screening effects on the membrane. The lower mobility expected for the large $NMDG^+$ might lead to increased cationic charge accumulation at intracellular surface (or conversely, decreased anionic charges such as Cl^-), effectively reducing the local membrane potential such that activation can take place at seemingly lower voltages. However, LCa_v3-12B, which has the same activation properties as LCa_v3-12A when recorded with intracellular Cs^+ (Table 4), is less affected by Cs^+ substitution (~4 mV smaller shift in activation; figure 13D; Table 4). Therefore, charge screening cannot fully account for the hyperpolarized activation since the effects are not consistent between the two LCa_v3 isoforms. Another possibility is that small mobile cations such as Cs^+ can directly interact with the intracellular surface of the channel to counter voltage-dependent activation mechanisms; in the absence of monovalent cesium, channels can activate at lower voltages. The 12A variant of LCa_v3, which is more permeable to internal Cs^+, is more susceptible to this effect, so exons 12A and 12B would have to impose slight differences to the intracellular surface of the channel to allow for this inconsistency. Of note, the helix-loop-helix gating brake structure, unique to Ca_v3 channels, is critical for preventing channel gating at hyperpolarized potentials[245,82]. It is tantalizing to speculate that either small monovalent internal cations, or $NMDG^+$ itself, can directly interact with the gating brake to influence its functionality.

To determine whether the 12A variant also conducts large *inward* monovalent currents, we replaced 135 mM of impermeant TEA^+ from the external solution with 135 mM Na^+, while maintaining calcium at 2 mM. Remarkably, currents through the 12A variant underwent a ~15.5-fold increase in amplitude (i.e. 1450%) in the presence of external sodium (figure 14 A and B). Such an effect is drastically different from what is seen for even the most sodium-permeable LVA channel from mammals, $Ca_v3.3$, whose current merely doubles in amplitude when 120 mM of external $NMDG^+$ is replaced with 120 mM Na^+ (in the presence of 0.2 mM calcium)[288]. In fact, currents through the 12B variant of LCa_v3 only underwent a ~2.7-fold increase in amplitude, indicating that this splice variant more closely resembles the conventional calcium-selective Ca_v3 channels from mammals. LCa_v3-12A, on the other hand, is much more permeable to sodium, and under physiological conditions, this channel would act more like a sodium channel than a calcium channel.

Since the selectivity filters between LCa_v3-12A and LCa_v3-12B are identical, the differences in sodium permeability might be attributed to alterations in the placement of selectivity filter residues within the pore, reducing the binding affinity for calcium to such a degree that divalent selectivity is largely disrupted (or conversely, divalent affinity is unaltered but the affinity for monovalent cations is increased). Indeed, the *Lymnaea* 12A and 12B exons encode peptides of quite different sizes, with amino acids lengths of 39 and 51, respectively. Also, cysteine residues, that can form sulfhydryl bridges with each other or with cysteine residues from other channel regions, are differentially numbered and localized along the exon coding sequence. Together, these differences are poised to significantly impact the structure of the loop that separates the domain II S5 helix from the short helical structure that projects the selectivity filter glutamate into the pore (figure 1A), and hence it is likely that the structure of the pore is significantly affected by the exons. Clearly, although important, the selectivity filter is not the sole determinant for ion selectivity in Ca_v3 channels, but rather, the way in which charges are positioned within the pore produces geometrical constraints that can be optimized for one ion vs. another.

Ba^{2+} vs. Ca^{2+} permeability is unaltered

The permeability for Ba^{2+} over Ca^{2+} is unaffected by exons 12A and 12B, indicating that the factors that define divalent vs. monovalent permeability are different from those that define divalent vs. divalent selectivity. Unlike Ca^{2+} vs. Na^{+}, the affinity for Ca^{2+}, Ba^{2+}, and Sr^{2+} within the mammalian Ca_v3 channel pore is roughly the same[288]. Differences observed for macroscopic currents in the presence of equimolar concentrations of each ion are attributed to their influence on open channel probability (i.e. the likelihood of finding a channel in the open state as a function of time and voltage). For example, $Ca_v3.1$ conducts larger macroscopic Ca^{2+} currents than Ba^{2+}, while $Ca_v3.2$ conducts larger Ba^{2+} currents[204,288]. Analysis of how these extracellular ions influence the open probability of the two channels reveals that $Ca_v3.1$ has a higher open probability in the presence of calcium, while $Ca_v3.2$ has a higher open probability in the presence of barium[288]. The Ca_v3 channel from the snail is similar to $Ca_v3.2$ in that it conducts larger macroscopic Ba^{2+} currents[1], regardless of which exon 12 is present, and it is possible that alterations in the pore structure imposed by exon 12A cause a parallel reduction in the binding affinity for both Ca^{2+} and Ba^{2+} equally, and therefore, with respect to each other, their permeabilities seem unaltered. However, it is also possible that exon 12 has no bearing on affinity for divalent cations in the pore, but rather, its effects are strictly towards the

affinity for monovalent cations, in which case the permeation pathways for monovalent cations might be distinct from that for divalent cations.

No changes in Ni^{2+} sensitivity

Early reports of highly nickel-sensitive LVA calcium currents in native mammalian tissues were confounded by others that claimed low sensitivity[94]. Molecular cloning of the three mammalian LVA calcium channel isotypes revealed that only $Ca_v3.2$ was significantly sensitive to nickel[240], subsequently attributed to a unique histidine residue located in the domain I S3-S4 extracellular loop of the channel[241]. Low affinity block of $Ca_v3.1$ has been attributed to nickel ions directly binding to and occluding the pore[259], which prompted us to test whether the two domain II pore variants of LCa_v3 were differentially sensitive to nickel. Application of 300 μM Ni^{2+} blocked the two variants almost equally by ~40% (figure 12A), indicating that its binding affinity is not noticeably influenced by exons 12A and 12B. Indeed, the apparent binding affinity for Ba^{2+} vs. Ca^{2+} is also unaffected by these exons, and Ni^{2+} might occupy the same binding site as Ba^{2+} and Ca^{2+}, possibly the selectivity filter as proposed for mammalian $Ca_v3.1$[259,288].

The ancestral Ca_v3 channel: sodium or calcium selective?

Our analyses suggest that exon 12A in Ca_v3 channel genes is ancestral with respect to its mutually exclusive counter-part, exon 12B. In *Lymnaea*, exon 12A produces Ca_v3 channels with pronounced monovalent cation permeability, while in mammalian Ca_v3 channels, which only possess exon 12A, the exon forms part of a more calcium-selective pore. Exon 12B, on the other hand, produces a more calcium-selective LCa_v3, which when compared to the mammalian homologues, resembles the least calcium-selective isotype, $Ca_v3.3$. A possible explanation for the conflicting role for exon 12A, where in *Lymnaea* it imparts sodium permeability while in mammalian channels it allows for high calcium selectivity, is that the ancestral 12A-containing Ca_v3 channel was less calcium-selective, and evolutionary adaptations in other regions of the Ca_v3 channel (e.g. the other three P-loops), increased calcium selectivity in a primitive ancestor to mammals. Indeed, phylogenetic analyses suggest that sodium channels evolved from Ca_v3 channels very early on during animal evolution[9,59], and the ancestral Ca_v3 precursor could have carried intermediate features between sodium and calcium channels. In accordance, Ca_v3 and Na_v channels are similar in that they lack association with β subunits in the cytosolic I-II linker as occurs with HVA calcium channels, and both tend to have low voltages of activation to mediate depolarization. By continuation, protostome animals evolved a different means to improve calcium selectivity, via duplication of exon 12A to produce a larger 12B

variant with more cysteine residues. Importantly, whether the different properties imposed on the *Lymnaea* Ca_v3 channel by exons 12A and 12B are conserved with other protostome invertebrates remains to be evaluated. However, given the strong conservation in size difference and cysteine content between these two exons, it is expected that permeation properties will be variable to some degree.

Expression patterns of exons 12A and 12B suggest different physiological roles

There is a continuous downregulation of Ca_v3 transcript expression from embryo to adult in *Lymnaea* (figure 4A), analogous to declines documented for mammals during development[234,64]. The reason for this decline in expression is not fully understood, and the contributions of Ca_v3 channel to development are unclear. Ca_v3 channels are implicated in cell division and in regulating growth and morphology of neurons and myocytes[234,293,64,107]. However, inconsistencies in the literature make it difficult to unequivocally correlate Ca_v3 channels to development, and knockout of Ca_v3 channels only imparts mild phenotypes[64]. However, cardiac Ca_v3 channels are highly expressed in embryonic mammals, where they are proposed to mediate excitation-contraction coupling before the establishment of transverse tubules and calcium release from internal stores[293,107]. Conversely, adult mammals have very little Ca_v3 channel expression, which follows a pattern of allometric scaling where smaller animals that tend to have faster heart rhythms express more Ca_v3 channels[109]. In *Lymnaea*, prominent LVA Ca_v3 channel currents have been documented in adult ventricular myocytes[111], and LCa_v3 transcripts are abundant in adult hearts despite a marked decline from juvenile to adult (figure 4B). It may be that invertebrates rely more heavily on Ca_v3 channels for regulating heart rhythm. The downregulation of Ca_v3 channels in *Lymnaea* heart might therefore coincide with allometric scaling during development, where more prominent LCa_v3 currents in small embryos could coincide with faster heart rhythms. On the other hand, LCa_v3 might be involved in cellular growth and modeling during heart development, similar to what has been proposed in mammals[293,109,64,107].

The sharp contrast in expression between exons 12A and 12B, with LCa_v3-12A expressed exclusively in the heart vs. LCa_v3-12B in secretory glands (figure 4B), suggests that alternative splicing is being used to tailor the Ca_v3 channel for different functions in different cell types. In the heart, exon 12A imparts high sodium permeability, along with slower deactivation and faster recovery from inactivation (figure 10D; figure 11B; figure 14). Cardiac Ca_v3 channels in *Lymnaea* can thus be expected to provide prominent depolarizing sodium currents for pace-making, with slow deactivation

serving to prolong the repolarization phase of the action potential, and faster recovery from inactivation preventing rundown of Ca_v3 channel currents due to accumulated inactivation. Fast sodium channels are absent from the *Lymnaea* heart[302,111], so the sodium permeable LCa_v3-12A isoform provides sodium-dependent depolarization to activate HVA calcium channels for excitation-contraction coupling[302,111]. Conversely in secretory glands, the predominant LCa_v3-12B isoform is expected to provide more calcium-selective currents, where the channel might contribute not only to regulating oscillatory excitability, but also to calcium influx for excitation-secretion coupling, as occurs with mammalian Ca_v3 channels in select circumstances[64].

Conclusions

Extracellular sodium and calcium exert very different influences on cells, where sodium serves as a major depolarizing current for the rising phase of the action potential, while calcium also depolarizes cells but in addition converts electrical information into different biochemical processes, exemplified by excitation-secretion coupling in neurons and secretory cells, excitation-contraction coupling in muscle, and excitation-transcription coupling in various cell types. Clearly, the complement of ion channels that a particular cell type uses reflects the basic functionality of that cell, and given that calcium is toxic to cells[12], its influx must be tightly regulated. LVA Ca_v3 channels, which in mammals provide prominent pace-making currents in multiple cell types and serve to regulate excitability of neurons, are different from HVA calcium channels in their increased permeability to sodium[288]. Appropriately, the highly calcium-selective HVA channels are classically associated with the coupling of excitation to calcium-dependent biochemical processes, while Ca_v3 channels seem peripheral in this regard[64]. Conversely, the low voltages of activation of Ca_v3 channels position them to regulate excitability, by contributing depolarizing currents in cells towards action potential threshold. Here, calcium is less important as a charge carrier, perhaps justifying the increased sodium permeability of Ca_v3 channels. Nevertheless, calcium influx through Ca_v3 channels is important in certain circumstances, for example in regulating calcium-activated potassium channels and mediating low threshold exocytosis in neurons[64].

Interestingly *Lymnaea*, and perhaps all protostome invertebrates, have evolved a means to modulate the selectivity of their Ca_v3 channels by alternative splicing. Such functional modulation is unprecedented, since the identity of ions that permeate a channel pore are intrinsically related to the functionality of that channel, and variability in permeation is associated with distinct evolutionary lineages and divergent genes[26]. As such, it is not surprising to see such contrasting expression patterns

between exons 12A and 12B in the heart and secretory glands, where they are expected to provide highly divergent contributions to excitability and calcium-dependent processes. In the central nervous system, both variants are expressed at similar levels, and their function in *Lymnaea* neurons remains to be characterized. However, the existence of a sodium-permeable Ca_v3 channel could be very useful, for example to reduce the calcium load in neurons that undergo high frequency firing. In addition, the characteristic window currents which occur through a small subset of open Ca_v3 channels at rest[94,64] (figure 9C), can depolarize cells without flooding the cytosol with calcium.

Although the recent X-ray structure of a prokaryotic sodium channel has provided much insight into permeability through calcium/sodium-type pores, the mechanisms by which metazoan 4-domain ion channels discriminate between monovalent sodium and divalent calcium are poorly understood. Prokaryotic sodium channels such as Na_vAb are tetrameric structures with calcium channel-like selectivity filters of EEEE; the reason attributed to their sodium selectivity is the arrangement of these four glutamates, symmetrically positioned along a two dimensional plane[25,61,52], vs. an asymmetrical arrangement in 4-domain calcium channels[43]. Here, we have shown that the *Lymnaea* Ca_v3 channel can dramatically alter its monovalent cation permeability without changing its selectivity filter motif residues of EEDD. Instead, discrimination for calcium over sodium is influenced by factors outside of this locus, perhaps by alterations imposed on the placement or mobility of these residues within the pore, or perhaps by altering a secondary permeation route specific for monovalent cations. Clearly, much more research is needed to understand selectivity for these two very important cations, whose conductance into cells is mediated by channels with intertwined and often blurred evolutionary histories. Indeed, 4-domain sodium channels might have evolved from Ca_v3 channels in animals[9], and 4-domain channels themselves might have evolved from prokaryotic, tetrameric sodium channels, bearing calcium channel-like selectivity filters[52,48].

2.3.5 Acknowledgements

Part of the funding for this research came from an NSERC Alexander Graham Bell Canada Graduate Scholarship (doctoral) and an Ontario Graduate Scholarship to A.S. We would like to thank Martin Rioux for his contribution towards generating the LCa_v3-12A clone in pIRES2-EGFP.

2.4 Cloning and characterization of a *Lymnaea* NALCN homologue with an alternatively-spliced selectivity filter

The manuscript presented in this section is submitted to PLoS ONE:

Adriano Senatore, Arnaud Monteil, Jan van Minnen, Agust Smitt and J. David Spafford. NALCN leak conductance channels have alternatively-spliced selectivity filters that resemble calcium or sodium channels.

The manuscript contains research done by Adriano Senatore in the laboratory of Dr. J. David Spafford, pertaining to the full length consensus sequencing of a *Lymnaea* NALCN channel homologue, and remarkably, the identification of alternatively spliced P-loops in domain II of the channel, that alter the selectivity filter motif from a proposed non-specific sodium-permeable configuration (i.e. EEKE) to a calcium channel-like configuration (EEEE). qPCR analysis revealed that both variants are abundantly expressed in various snail tissues including the CNS, heart, and secretory glands. An extensive phylogenetic analysis carried out by Dr. David Spafford reveals that the ancestral NALCN channel was probably calcium channel-like (EEEE), and that alternative splicing evolved several times independently within distinct animal clades to alter the selectivity filter at domains II and III, making NALCN an extremely rare 4-domain channel. The cDNAs of the two pore variants of *Lymnaea* NALCN were cloned for expression in mammalian cells by Adriano Senatore, and despite successful expression of the channel proteins (tested by Dr. Arnaud Monteil), extensive attempts at electrophysiological recording were unsuccessful, similar to what many other laboratories have found when trying to express NALCN homologues from various species. Additional contributions by Drs. Jan van Minnen and Guus Smit, show that *Lymnaea* NALCN is expressed along axons, similar to what has been documented for other invertebrates. This work thus brings into question NALCN's proposed role as a major conductor of leak currents that serve to depolarize the membrane potential in animal cells including neurons, since many species only harbor the ancestral version with an EEEE selectivity filter, that should have, based on patterns seen for all 4-domain ion channels, reduced monovalent selectivity (i.e. Na^+ and K^+), and enhanced divalent selectivity (i.e. Ca^{2+}).

The materials and methods, as well as additional materials that are part of this manuscript, can be found in Appendix D of this thesis. However, supplementary appendices A and B of the manuscript were not included due to their large size.

2.4.1 Abstract

NALCN is a member of the family of ion channels with four homologous, repeat domains that include voltage-gated calcium (Ca_v) and sodium (Na_v) channels. NALCN is a highly conserved gene from simple, extant multicellular organisms without nervous systems such as sponge and *Trichoplax,* and mostly remains a single gene compared to the Ca_v and Na_v channels which diversified into 20 genes in humans. The single NALCN gene has alternatively-spliced exons at exons 15 or exon 31 that splice in novel selectivity filter residues that resemble Ca_v channels (EEEE) or Na_v channels (EKEE or EEKE). NALCN channels with alternative calcium- (EEEE) and sodium- (EKEE or EEKE) selective pores are conserved from simple animals like flatworms to non-chordate animals. Expression patterns of EKEE-NALCN in pond snail *Lymnaea stagnalis* suggest roles for NALCN in secretion, with abundant expression in brain, and up-regulation in secretory organs of sexually-mature adults such as albumen and prostate glands. EEEE-NALCN is as abundant as EKEE-NALCN overall, but is less expressed in the brain compared to EKEE-NALCN, and more abundantly expressed in heart and other muscle tissue than EKEE-NALCN. NALCN (EEEE and EKEE) isoforms from *Lymnaea* express heterologously in the membranes of mammalian cells (HEK-293T), and show preferential expression in cells also expressing key NALCN auxiliary subunit, UNC-80. The single NALCN gene is limited as a sodium channel with a lysine (K)-containing pore in vertebrates, but originally, NALCN was calcium channel-like, and evolved to operate as both a calcium and sodium channel via alternative splicing in many invertebrate clades.

2.4.2 Introduction

Sodium non-selective leak conductance channel NALCN ($Na_Vi2.1$) is a family member of ion channels with four repeat domains of six transmembrane segments (4x6TM), which also includes voltage-gated Ca_v and Na_v channels[135]. NALCN is a single-copy gene crucial for survival in mammals, where gene knockdown is lethal in mice within 24 hours after birth due to severely disrupted respiratory rhythms[137]. Hippocampal neurons have resting membrane potentials ~10 mV more hyperpolarized in NALCN-/- mice[137], and the channel is considered to provide a resting Na^+ conductance in wild type neurons which drives membrane excitability associated with rhythmic neural activity, not just in mammals[137,143] but also in nematodes (*C. elegans*)[148,161,127], fruit fly (*Drosophila*)[121,116] and snail (*Lymnaea*)[160]. Perhaps there is also a link between NALCN and ionic balance, since heterozygous NALCN knockout mice have significantly elevated serum sodium levels[303].

A key feature of NALCN is its role as a channel gating Na^+ ions, providing a resting leak conductance to drive membrane excitability[137,143,160]. Ion selectivity of the 4x6TM calcium channels has been defined by signature residues of the selectivity filter, contributed by a single residue from each of the four repeat domains (I-IV), forming a ring of negatively-charged glutamate residues (EEEE) in Ca_v1 (L-type) and Ca_v2 calcium channels[56,304,44], or EEDD in Ca_v3 channels (T-type)[57]. Traditional sodium (Na_v1) channels bear a DEKA pore in the equivalent position, and mutagenesis studies indicate that the lysine (K) residue in Domain III is both necessary and sufficient to generate ion channels with high Na^+ selectivity over Ca^{2+} ions[56,304,57,44]. Equivalent sodium-selective channels in motile jellyfish have a DKEA pore configuration where the lysine (K) residue has migrated to Domain II from Domain III[305]. Jellyfish Na_v channels with DKEA pores are Na^+-selective, but mutagenesis studies suggest that they are slightly less selective for Na^+ ions than are DEKA Na_v channels[306]. Mammalian NALCN channels have the hallmark lysine (K) residue in Domain III, characteristic of Na_v channels with an EEKE pore[135]. As expected from its EEKE structure, expression studies indicate that mammalian NALCN is most permeable Na^+ ions[137].

Our analyses indicate that NALCN may have expanded roles outside of serving as a Na^+ leak conductance channel. The ancestral NALCN has a selectivity filter that more resembles Ca^{2+} channels, and most invertebrates have two alternatively-spliced isoforms of NALCN, one with a standard selectivity filter that resembles Na_v channels (EEKE or EKEE), and a second isoform that resembles Ca_v channels (EEEE). Both the Ca^{2+} channel and Na^+ channel isoforms of NALCN are abundantly expressed in snails, with unique expression profiles in different tissues.

2.4.3 Results

NALCN is an unusually conserved and short, four repeat ion channel

NALCN is slightly closer in sequence to a yeast calcium channel[307] than to voltage-gated sodium (Na_v) and calcium (Ca_v) channels within the 4x6TM ion channel family (Fig. 1 A), and has remained mostly a single gene, compared to the evolution of 20 different Ca_v and Na_v channel genes in vertebrates. The exceptions for a single NALCN gene in an animal is sponge: *Amphimedon*, anthozoan cnidarian *Nematostella* and nematode *Caenorhabditis*, which have two genes. Snails, like most invertebrates, have three Ca_v channel genes, two Na_v genes and only one NALCN channel gene (Fig. 1 A). Comparing protein sizes between snails and humans, NALCN is almost invariant in size and smaller than most Na_v and Ca_v channels, with especially short amino termini and I-II linkers, and with invariant III-IV linkers that are 53 or 54 amino acids, common to all of these 4x6TM channels

(Fig. 1B). Comparisons between snail and human sequences illustrate a highly conserved NALCN structure across the whole protein (69% similarity), from the N-terminus to the C-terminus. The similarity between NALCN homologues is remarkable, given that similar comparisons between snail and human Na_v and Ca_v channels reveal more marked divergence (i.e. 48.4% and 58.2% respectively) (Fig. 1C).

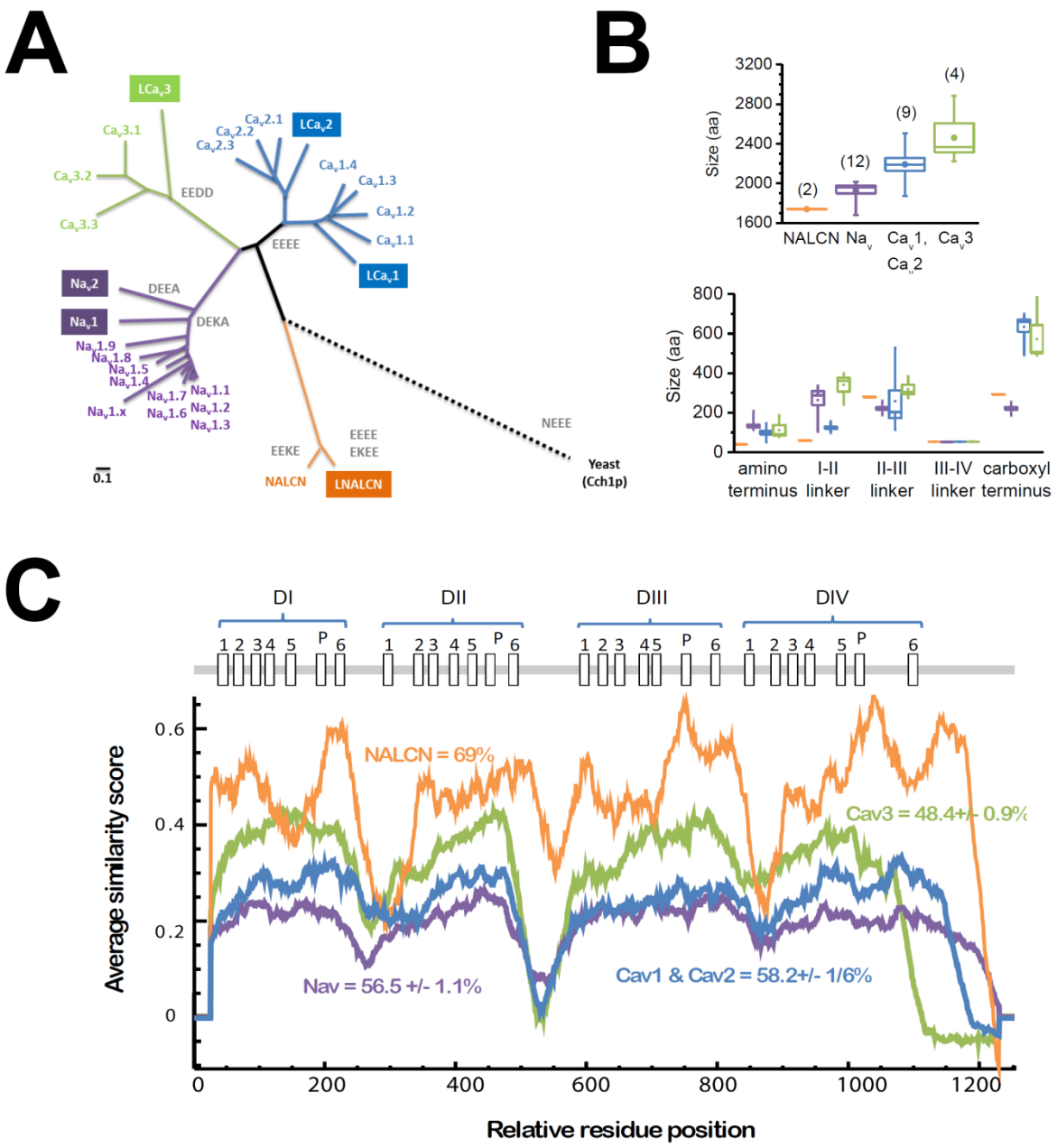

Fig. 1 NALCN is unique amongst related four domain repeat, voltage-gated cation channels in it being a singleton gene in reported genomes (except *C. elegans*), and a coding region of small size and high conservation. Comparisons in panels A, B, and C are made between LNALCN, LCa_V1, LCa_V2, LCa_V3, Na_V1, Na_V2 and the 21 human homologs. (A) Gene tree of aligned sequences suggest a distant relationship to voltage gated Ca and Na channels, and closer to the singleton yeast calcium channel. Grey letters indicate selectivity filter residues. (B) NALCN is a shorter than other cation channels in total size (top panel) largely because of its short amino terminus and I-II linker (bottom panel). Snail and human NALCN are within +/- 3 aa of each other in sizes of individual domains and cytoplasmic linkers. (C) Running averages of similarity indicate that snail and human NALCN is much more conserved than other cation channels, with a high level of conservation even in the generally hypervariable cytoplasmic linkers and amino-termini of voltage-gated cation channels.

NALCN genes can have alternatively-spliced pores

In light of the relative invariance of NALCN sequences, it is remarkable that we identified alternative splicing within a pore domain when cloning the full length homolog from the pond snail *Lymnaea stagnalis* (see Suppl. Materials and Methods). Alternative exons 15a and 15b span the re-entrant pore helices and selectivity filter residues to the proximate end of segment 6 in Domain II (Fig. 2A). The obvious difference between exons 15a and 15b is the key selectivity filter residue for ion permeation, located at the most constrictive point of the 'hourglass' pore of the three-dimensional, prokaryotic sodium channel[52]. The other three domains in homologous positions have mostly a glutamate (E) residue in Domains I, III and IV contributing to the EEEE pore (with exon 15a) and EKEE pore (with exon 15b) (Fig. 2A). Searching though other invertebrate genomes revealed homologous alternative exons 15a and 15b, with a 5' exon 15a with glutamate (E) in the selectivity filter, and a 3' exon 15b coding for lysine (K) in the selectivity filter (Fig. 2A). Dual EEEE/EKEE pores are present in the genomes of species of platyhelminths (flatworms), and lophotrochozoan protostomes (mollusks and annelids), and non-chordate deuterostomes (echinoderms and hemichordates). Similarly, exon 31 is alternatively-spliced in what is likely a completely separate evolutionary event, coding for the pore in Domain III instead of Domain II, that similarly generates a 5' exon 31a with glutamate (E) in the selectivity filter, and the 3' exon 31b coding for lysine (K) in the selectivity filter within the arthropods, including species of Myriapod (e.g. centipedes) and Chelicerates (mites and ticks; Fig. 2B). The only animal groups that don't appear to contain species with alternative (EEEE) and (EKEE or EEKE) NALCN pore, coincidentally, include the species most often used as animal models, including nematodes (i.e. *C. elegans*), insects (*Drosophila*) and chordates (rat and mouse).

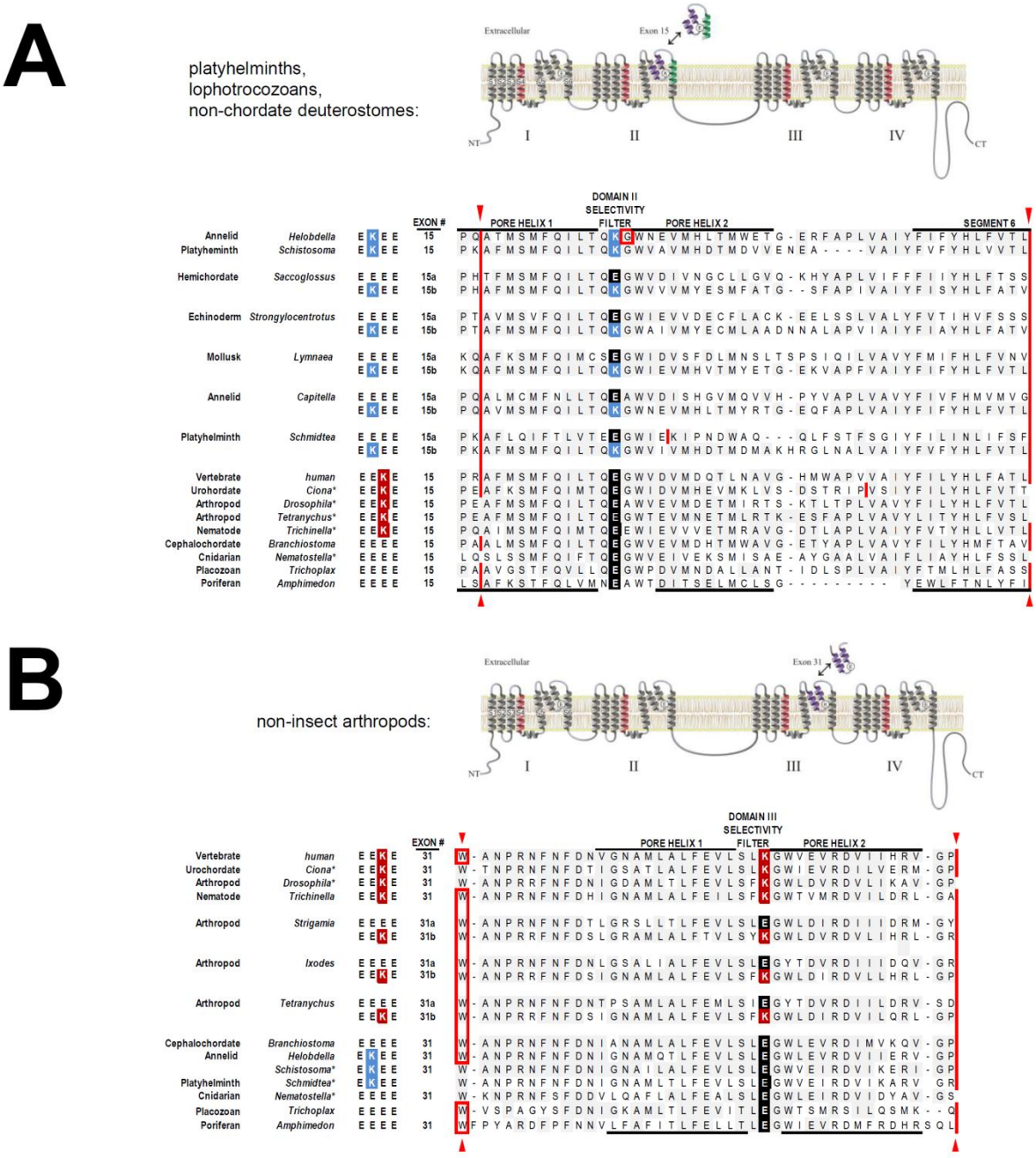

Fig.2 Representative NALCN sequences of alternative calcium- and sodium-selective pores generated by alternative exons (A) exon15 (EEEE/EKEE) and (B) exon 31 (EEEE/EEKE). Exons 15 and exon 31 (delimited by splice junctions shown in red), span the re-entrant, P-loop (pore helices surrounding the selectivity filter) in Domains II and III, respectively. Exon 15 also includes the proximate region of segment 6, while exon 31 includes the distal portion of the extracellular turret. Splice junctions for exons 15 and exon 31 are conserved in the earliest metazoans (sponge, placozoans), which are duplicated in most invertebrate phyla to produce tandem mutually-exclusive exons where the 5' exon codes for exon 'a' with E in the selectivity filter (15a, 31a) and the 3' exon codes for exon 'b' with K in the selectivity filter (15b, 31b). Either the donor or acceptor site of exon 15 or 31 are lost in most species outside chordates (indicated by *) that don't have alternative-splice junctions to generate both calcium and sodium selective pores. Exons 15a/15b has variable sequence between the pore and segment 6 for generating a gene tree (see fig. 4).

Patterns of evolution of NALCN's alternatively-spliced pores

The simplest multicellular organisms (sponge, *Trichoplax* and cnidarians) lack a Na^{+}-like selectivity filter with a lysine (K) residue (EKEE or EEKE) (Fig. 2, 3), and thus it is likely that the ancestral NALCN was Ca^{2+} channel-like with an EEEE (or EDEE) pore. We can also assume that the EKEE pore evolved from an exon duplication of a NALCN Ca^{2+} channel (EEEE pore) in a common ancestor to all species with an EKEE pore, including platyhelminths (flatworm), mollusks, annelids, echinoderms and hemichordates (acorn worm). Alternative exon 15 has variable sequences between pore helix 2 and segment 6 that enable an analysis of a proposed evolution of exons 15a and 15b (Fig. 2A). All 15b exons cluster together, appearing monophyletic in a gene tree of exon 15a and exon 15b sequences (Fig. 4). Alternative exons 31a and 31b are delimited to the highly conserved pore helices, and are highly similar to one another except for the pore selective 'E' or 'K' residue, which prevents assessment of their evolutionary history (Fig. 2B). Interestingly, alternative exons 31a and 31b are organized in genomes in a similar pattern as are exons 15a/15b, where exon 'a' with pore residue 'E' precedes the exon 'b' with pore residue 'K'. Animals with alternative EEEE and EEKE pores likely arose once, in a common ancestor because animals with these dual pores are clustered within a lineage of Arthropods (Fig. 3). Insects and crustaceans, and more distantly related Phyla, such as nematodes, urochordates and vertebrates only have a NALCN with an EEKE pore, which could each have arisen independently from an ancestral EEEE isoform.

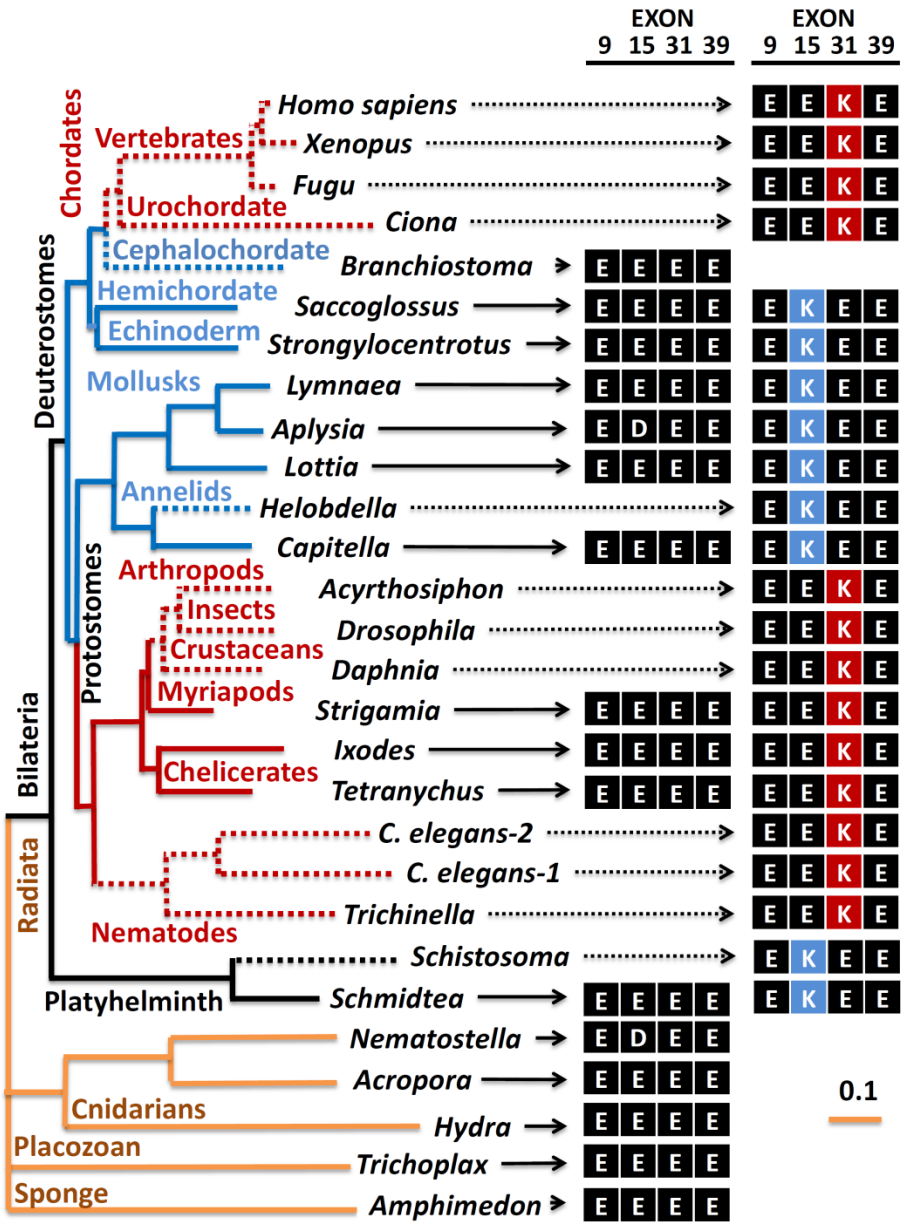

Fig.3 Gene tree illustrates that the NALCN gene is conserved in reported metazoan genomes with alternative, selectivity filters that generate a choice of calcium-selective and sodium-selective pores in invertebrates. NALCN first appears with a selectivity filter resembling a calcium-selective pore (EDEE or EEEE) in the earliest metazoans (sponges and placozoans) with a simple body plan**.** A duplication of Exon 15 coding for the selectivity filter residue in Domain II creates alternative calcium-selective (EEEE) and sodium-selective (EKEE) pores in the early nervous systems of Bilateria, including platyhelminthes, the planarian (*Schmidtea*) and protostomes of the lophotrochozoan lineage (mollusks and annelids), and non-chordate deuterostomes (echinoderms and hemichordates). A duplication event in Exon 31 of the Ecdysozoan lineage creates different alternative calcium-selective (EEEE) and sodium-selective (EEKE) pores that is retained in myriapods (includes centipedes, millipedes) and chelicerates (includes Arachnids like mites and ticks). The cephalochordate genome (*Branchiostomia*, amphioxus) only has a calcium-selective pore (EEEE), and chordates (urochordates, vertebrates) is the only lineage to lack a calcium-selective pore and bears only a sodium-selective pore (EEKE). Dashed lines indicate a likely loss of an alternative exon 15 or 31.

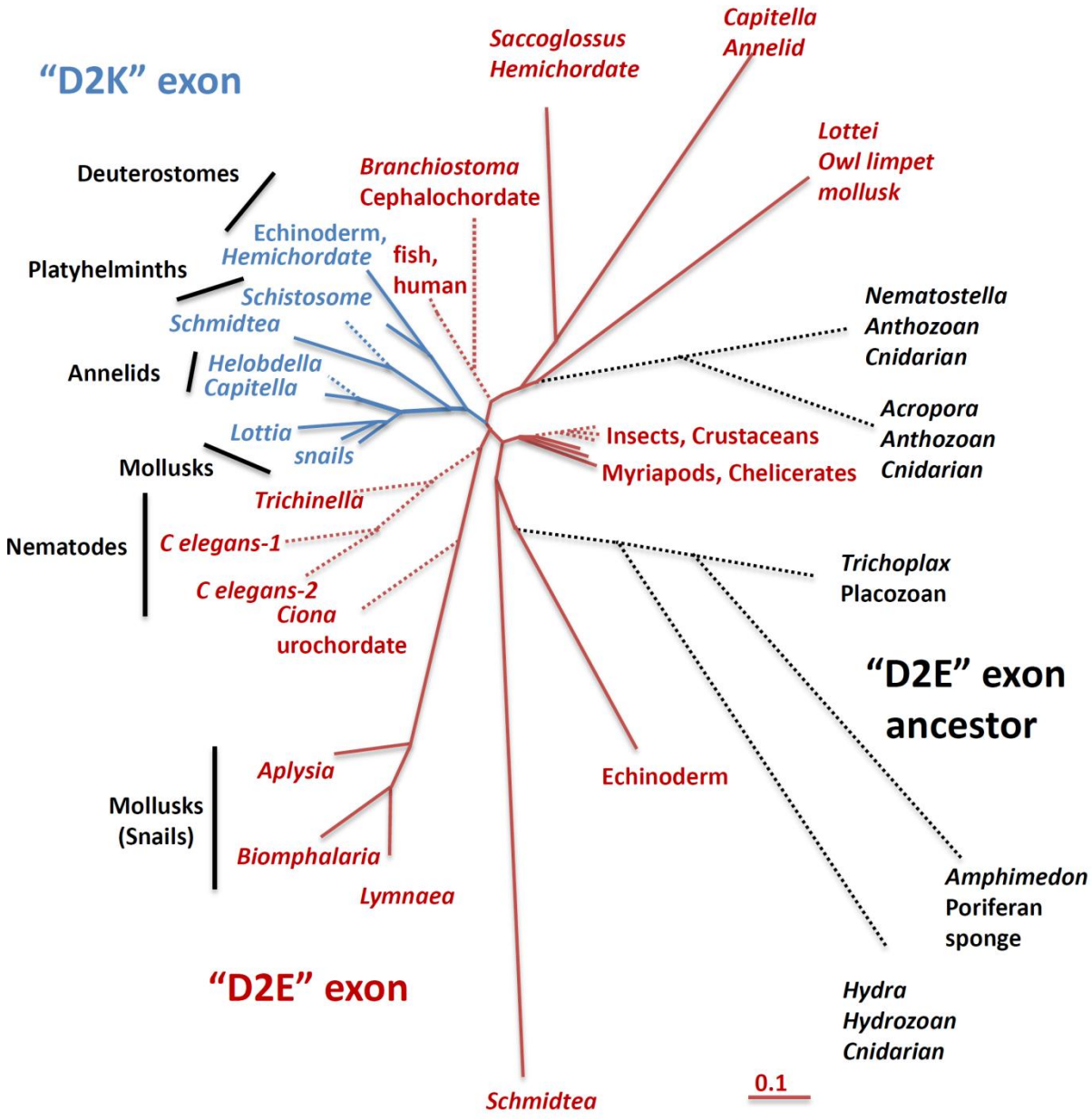

Fig. 4 Gene tree of exons 15a/15b indicates that tandem exon 15b coding for Lys (K) in the selectivity filter is monophyletic. Exon 15b duplicated from exon 15a coding for Glu (E) in the selectivity filter from an ancestor in early metazoans with a single exon 15a (sponge, *Trichoplax*, cnidarian), creating an exon 15b with Lys (K). The common root of exon 15b suggest that the dual, mutually-exclusive, exon 15a (E) and exon 15b (K) originated in early metazoans (represented in planarian *Schmidtea*, a Platyhelminth), evolving once and retained in lophotrochozoans (annelids, mollusks) and hemichordates, before being lost in chordates. There was a secondary loss of exon 15a in some invertebrates such as platyhelminth (*Schistosoma*) and annelid (*Helobdella*). No NALCN gene codes for EKKA, so exon 31b (with a K) likely evolved from exon 31a in an arthropod ancestor with EEEE selectivity filter common to myriapods and chelicerates, with exon 31a being secondarily lost in insects and crustaceans. Exon 31 is shorter and more highly conserved than exon 15, only spanning some of the extracellular turret and the downstream selectivity filter. Exon 31a and 31b barely differ outside of the single E and K residue in the selectivity filter suggesting that exon 31b could have had a separate evolution from an EEEE ancestor in nematodes and chordates.

Expression patterns of alternatively-spliced pore isoforms

Polyclonal antibody raised against snail NALCN sequence, identify a NALCN-sized protein in Western blots (Fig. 5A), and label in a dense-staining pattern along a particular subset of snail neurons identified in brain sections (Fig. 5B) that is consistent with NALCN staining patterns in the *C. elegans* nervous system[127]. Additionally, we find that blots spotted with cDNA coding for 760 bp of the NALCN gene in the C-terminus, but not related snail Ca_v channels genes, hybridize with a probe consisting of cDNA generated from mRNA of isolated snail axons (Fig. 5C), suggesting localization of NALCN mRNA within axons. The dense immune-staining of the brain is consistent with the general expression pattern of snail NALCN measured by quantitative RT-PCR, which is highest in the brain, followed by secretory glands (albumen and prostate), then heart, followed by muscle (buccal mass and foot) (Fig. 5D). Isoform-specific primers indicate that the expression of EKEE-NALCN is 2x greater than EEEE-NALCN in the brain, and only EKEE-NALCN upregulates from juvenile to adult snails in the brain and in albumen and prostate glands that mature into secretory organs (Fig. 5E1 and E2). EEEE-NALCN is 2x less abundant than EKEE-NALCN in the brain, while EEEE-NALCN expresses more in the heart (40 to 50% more) and also muscle, such as buccal mass (40 to 70% more) compared to EKEE-NALCN (Fig. 5F1 and F2). The differences between the tissue expression profiles of EEEE-NALCN and EKEE-NALCN suggest that they are associated with different functions in different cell types, which likely depend solely on their different selectivity filters, since the remainder of the channel protein is lacking in alternative splicing (see suppl. materials and methods).

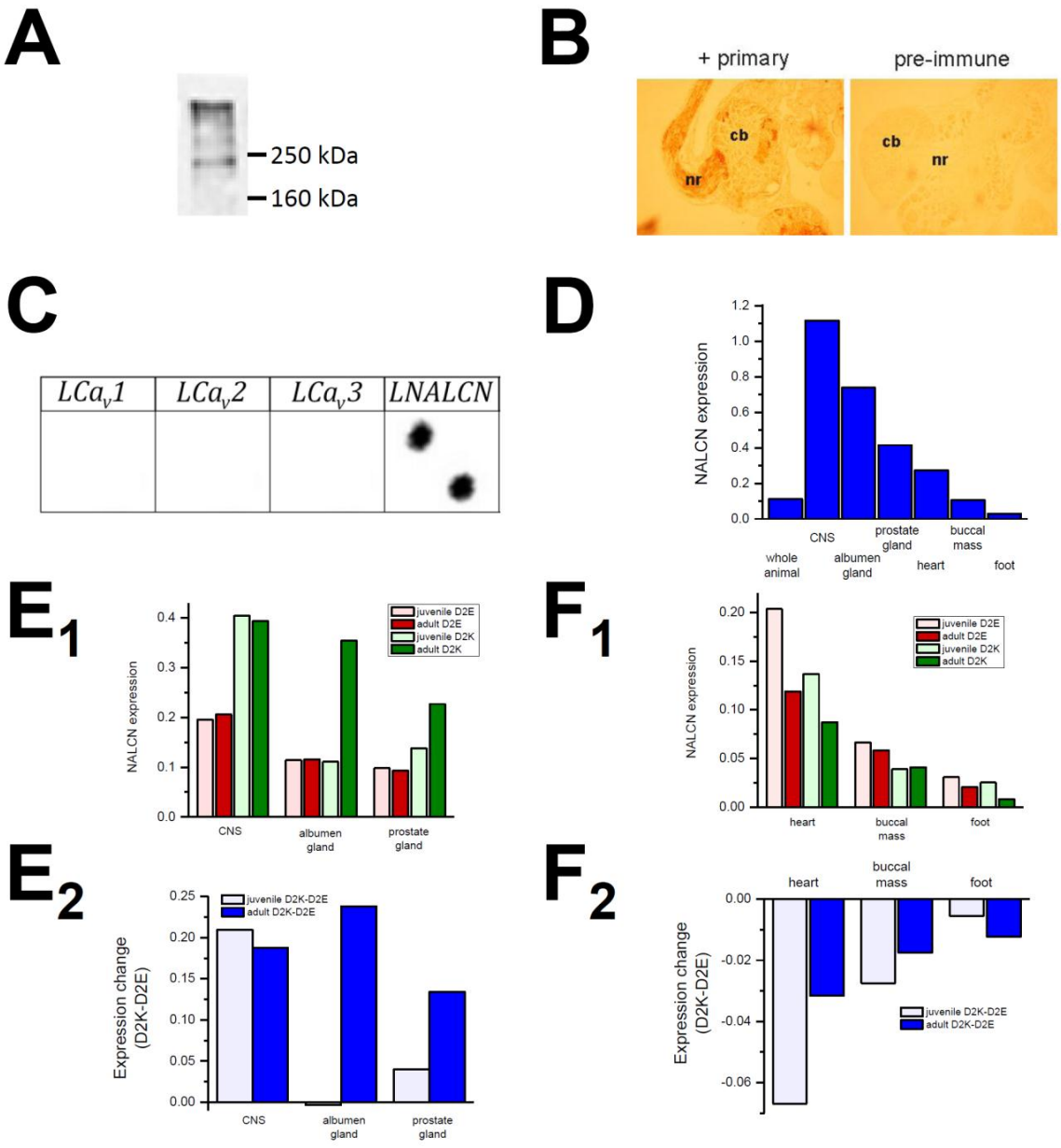

Fig. 5 NALCN mRNA expression in *Lymnaea* pond snail measured by quantitative PCR reveals unique expression profiles of sodium selective pore (EKEE) and calcium selective pore (EEEE) variants. (A) *Lymnaea* NALCN antibody identifies appropriately-sized ~200 kDa NALCN protein in *Lymnaea* brain homogenate of a Western blot. (B) Antibody staining of *Lymnaea* brain using polyclonal antibodies reveals that NALCN protein is enriched in neurites (nr) protruding from cell bodies (cb). (C) Reverse-northern blotting reveals that the LNALCN mRNAs specifically accumulate in neurites. (D) NALCN is more abundantly expresed in secretory organs (brain, albumen gland and prostate) than muscle (heart, buccal mass and foot). (E_1) NALCN expression of EKEE-NALCN is twice as abundant in the brain than EEEE-NALCN, and EKEE specifically rises in reproductive organs (albumin gland and prostate) during sexual maturation of juveniles to adult animals. (E_2) The substantially higher expression of EKEE-NALCN versus EEEE-NALCN in the brain and reproductive organs of sexual mature snails, suggest that EKEE-NALCN isoform is associated with secretion. (F_1) NALCN expression falls in heart, buccal mass and foot from juvenile to adult snails. (F_2) There are greater expression levels of EEEE-NALCN in heart, buccal mass and foot compared to EKEE-NALCN, which suggest that EEEE-NALCN has greater functions associated with muscle (heart, buccal mass, foot).

In vitro expression of snail and human NALCN genes

We would have liked to have confirmed the selectivity differences between snail EEEE- and EKEE-NALCN using patch clamp electrophysiology, but we corroborate others who have reported difficulties in measuring the expression of transfected NALCN genes in mammalian cells[135,127], and without receptor activation[118]. EGFP-tagged snail NALCN EEEE and EKEE isoforms are identifiable as expressed proteins on Western blots of transfected HEK-293T cells at the appropriate size (EGFP =27 kDa, snail NALCN = ~200 kDa) using a GFP antibody (Fig. 6A1). Transfected, GFP-tagged snail NALCN isoforms are mostly delimited to the membranous compartments of HEK-293T cells (Fig. 6A2), compared to the relatively generalized cell staining of co-expressed mRFP (dsRED2). We also co-expressed UNC-80 which serves as a key accessory subunit for NALCN expression and function in invertebrates[128,127] and mammals[132,134]. Positively-transfected cells expressing snail NALCN-EEEE and snail NALCN-EKEE isoforms were identified by mRFP/DsRed2 expression, using NALCN transfected in bicistronic vector pIRES2-mRFP (Fig. 6B). mRFP positive, snail NALCN-expressing cells corresponded to the same cells that were EGFP-positive, co-transfected with human UNC-80 in bicistronic vector pIRES2-EGFP (Fig. 6B). mRFP expressing cells did not correspond to EGFP-positive, UNC-80 expressing cells, when pIRES2-mRFP was transfected without snail NALCN in the bicistronic vector (Fig. 6B). While UNC-80 associates in the same transfected cells as snail NALCN, UNC-80 is not required for snail NALCN expression and possibly membrane trafficking in HEK-293T cells (Fig. 6 A1, 6A2). We can measure leak conductance currents in HEK-293T cells when snail EEEE-NALCN and EKEE NALCN isoforms are co-expressed with auxiliary subunits of NALCN (UNC-80 and a constitutively active SRC kinase) that are expected to enhance NALCN expression *in vitro*[132,134] (Fig. 7). However, we also record the same Na^+ leak currents in our HEK-293T cells, impermeant to NMDG ions, even without transfecting NALCN cDNAs in HEK-293T cells (Fig. 7). As such, the alternative splicing of *Lymnaea* NALCN, that alters the selectivity filter residues and is thus expected to dramatically influence permeability and selectivity, will be evaluated in future studies, but outside of mammalian cell lines such as HEK-293T which possess native sodium leak currents that are indistinguishable from those reported from NALCN-transfected cells[137].

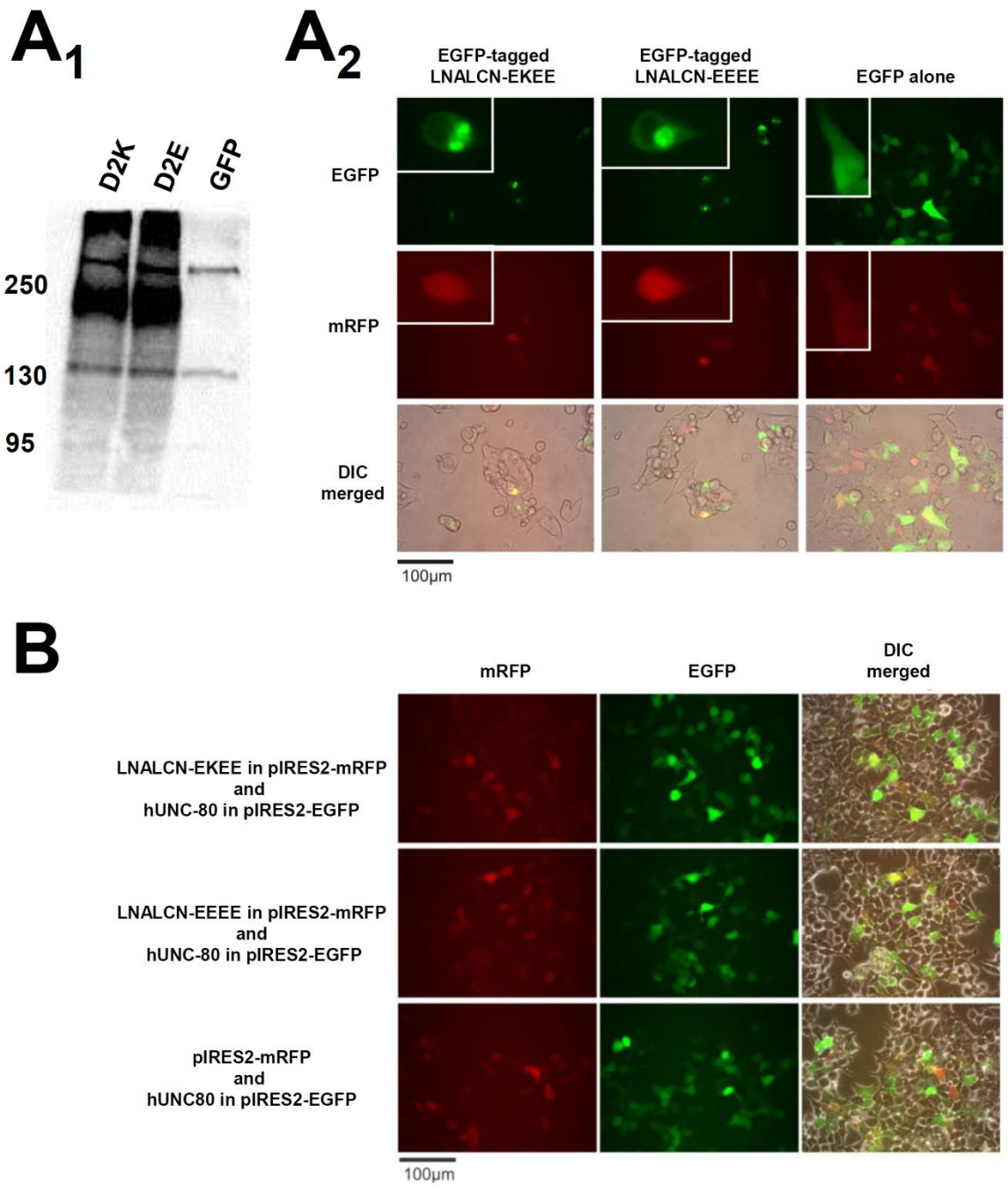

Fig. 6 Snail LNALCN-EKEE and LNALCN-EEEE isoforms express in the membrane of HEK-293T cells, co-localized with key auxiliary subunit hUNC-80. (A1) EGFP-coupled snail LNALCN cDNAs express in HEK-293T cells as appropriately-sized proteins (EGFP = 27 kDa, LNALCNs = 200 kDa) on Western blots detected by GFP antibody (Amsbio, Lake Forest, CA, USA). Western blot banding pattern of transfected EGFP alone or shown for comparison. (A2) EGFP-coupled snail LNALCN isoforms appear as membrane-delimited staining (inset) compared to more generalized staining resulting from co-transfected mRFP. (B) LNALCN and UNC-80 co-transfected in bicistronic pIRES2 vectors indicate that the abundance of LNALCN isoform expression (mRFP label) correlates with abundance of expressed hUNC-80 (EGFP label). Human UNC-80 expression does not co-relate with mRFP expression lacking snail NALCN cDNAs on the pIRES2 vector.

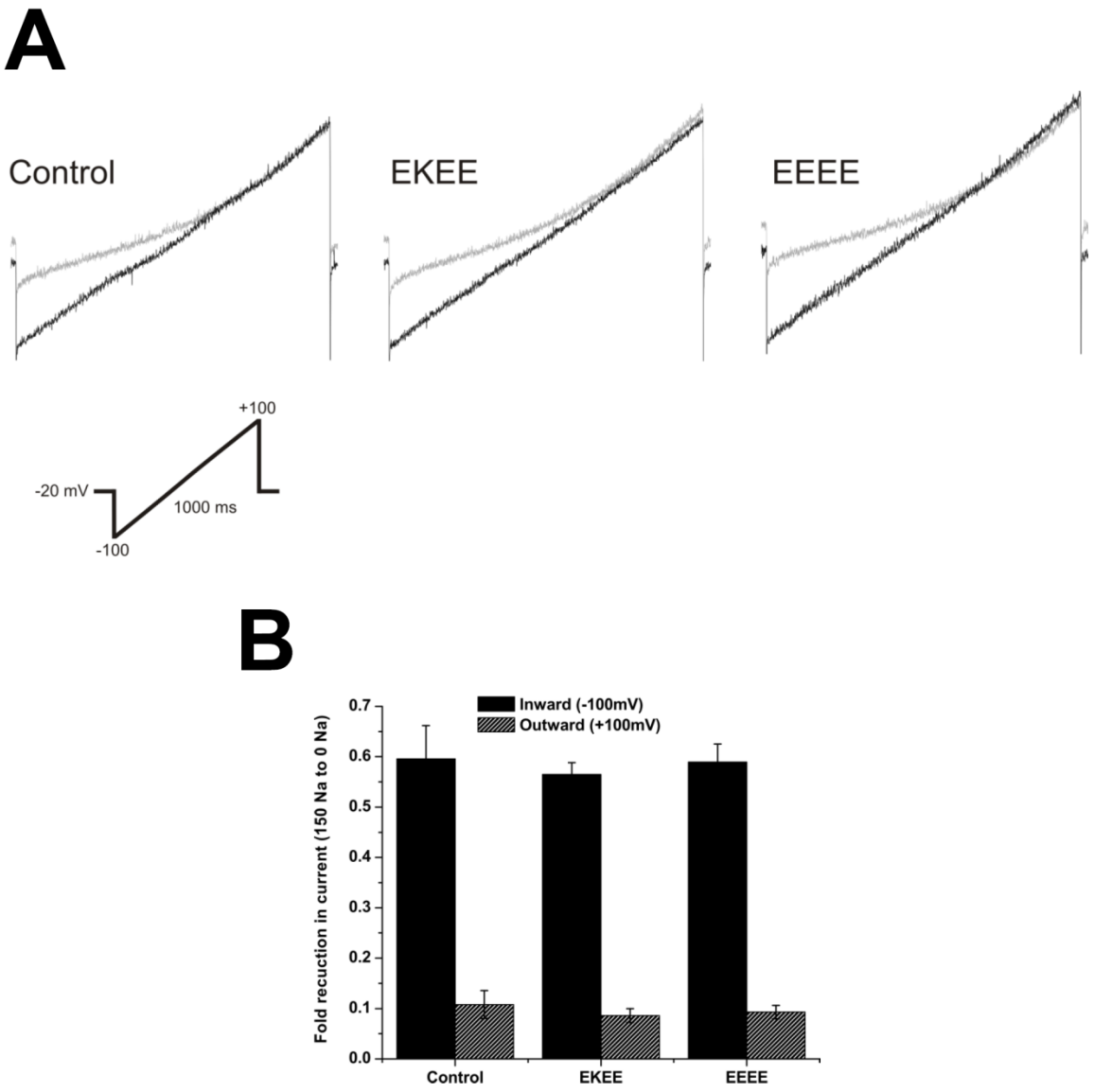

Fig. 7 Leak currents from snail LNALCN-expressing HEK-293T cells were indistinguishable from those in control cells. (A) Sample traces showing the block of inward current when replacing 150 mM external sodium (black) with NMDG (grey). HEK-293T cells were co-transfected with either 1 μg of *Lymnaea* NALCN pore variants (EKEE and EEEE) in bicistronic pIRES2-mRFP (monomeric red fluorescent protein) vectors or pIRES2-DsRed2 (control), plus 1 μg of human UNC80 in pIRES2-eGFP (enhanced green fluorescent protein), and 1 μg of vector expressing a constitutively active SRC (Y529F). Leak currents, recorded under whole-cell voltage clamp using a ramp protocol (inset), were observed under all conditions. (B) A similar reduction in both inward and outward currents (i.e. at -100 mV and +100 mV respectively) was observed when 150 mM external sodium was replaced with impermeant cation NMDG via perfusion (control n=5; EKEE n=7; EEEE n=4).

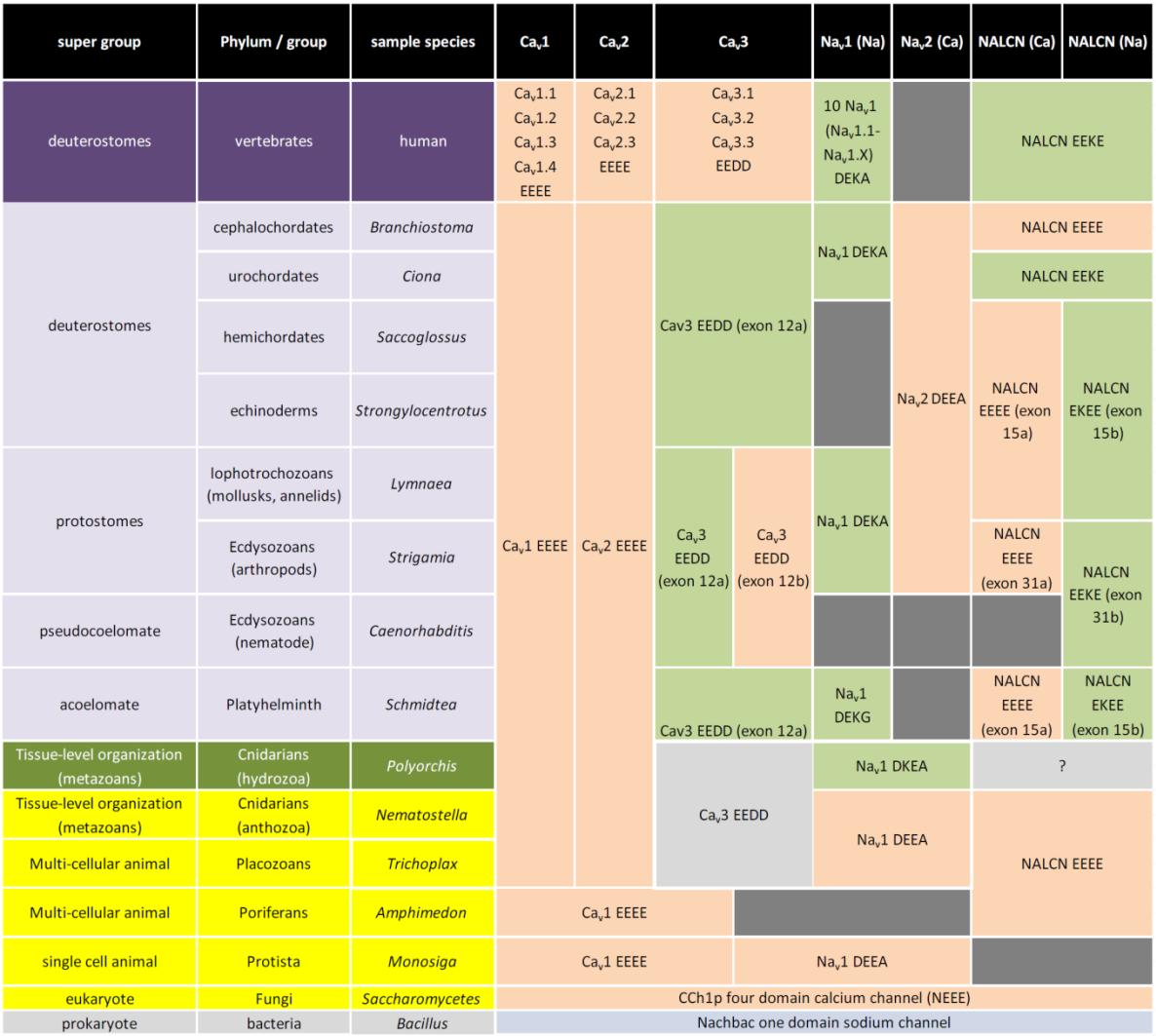

Fig.8 Conservation pattern suggest a greater flexibility in calcium and sodium selectivity in four repeat cation channels, before the evolution of vertebrates. All four repeat cation channels evolved with calcium-selective pores Ca_v (EEEE), Na_v (DEEA) and NALCN (EEEE). The first sodium selective pores (DKEA) arose in the extant relatives of the simplest animals with a pelagic lifestyle and a nervous system that required sodium-dependent action potentials (hydrozoan jellyfish). Dual sodium and calcium selectivity evolved in all four repeat channels outside of Ca_v1 and Ca_v2 channels, by different means. Na_v channels have a traditional isoform of the 10 vertebrate Na_v genes with mostly a DEKA pore (Na_v1), but also created a closely-related Na_v2 calcium-selective gene in the sodium channel class with a DEEA pore. Dual sodium and calcium selectivity were created for NALCN by alternative splicing of selectivity filter residues contained in exon 15 or exon 31. T-type calcium channels have alternatively-spliced 'turret' residues in exon 12 which enable invertebrate channels to be sodium-permeant T-type channels in addition to conducting calcium ions. Vertebrate genes become more exclusively sodium-selective, with loss of a calcium-selective Na_v2 gene, and loss of a NALCN splice isoform with the calcium selectivity filter (EEEE). Vertebrate T-type calcium channels lose the capacity for permeation of sodium as well as calcium without alternative 'turret' residues found in invertebrate T-type channels.

2.4.4 Discussion

NALCN has been described as a Na^+ leak conductance channel which contributes to membrane excitability and rhythmic behaviors[121,137,160,116,143]. Here we report that the snail NALCN homolog has alternatively-spliced isoforms that generate a selectivity filter that resembles a Ca^{2+}-selective channel as well as a Na^+-selective channel. The selectivity filter is exquisitely structured to define the selectivity of ions that interact with and permeate though the pore, and as such, alterations by alternative splicing are expected to alter the relative affinity for the two major inward-permeating ions, Ca^{2+} and Na^+. Both NALCN isoforms are abundantly expressed in snail tissues, and the alternative Ca^{2+} channel-like and Na^+ channel-like pores of NALCN channels, evolved at least twice within completely different lineages of invertebrates, via alterations in domains II and III. We looked at 4x6TM channels across the animal kingdom to gain insights into the origin and function of NALCN channels with putative Ca^{2+} and Na^+ selective pores.

Evolution of 4x6TM channels

Four domain (4x6TM) ion channels likely evolved from single domain (1x6TM) ancestors such as those in prokaryotes, through duplication of domains and divergence of these domains. All 4xTM channels in animals have an invariant III-IV linker size that is 53 or 54 amino acids, a region in Na_v channels serving in a fast inactivation gating mechanism[289]. Na_v and Ca_v channels have more in common with each other than NALCN, and a shared genomic heritage with locations of shared intron splice sites, including rare U12-splice sites[58].

Structure of 4x6TM channel pores

A defining feature of each 4x6TM channels is its pore selectivity, largely governed by the P-loop which ascends to a most constrictive point of the 'hourglass' pore where side chains of a critical residue contributed by each domain face into the pore (which is either E, D, K or A) between two highly conserved, pore helices (ten aa in length), demonstrated in the three-dimensional structure of the single domain, prokaryotic Na_v channel[52]. The symmetrical pore of this prokaryotic homomultimeric one domain channel has a glutamate (E) in this critical position, forming a Na^+-selective channel. Mutagenesis of 4x6TM channels reveals that each re-entrant pore is not equal in its contribution as in homomultimeric channels, but instead, each side chain of the signature residues lies asymmetrically with respect to the plane of the conducting pore. The three lineages of 4x6TM channels (Ca_v, Na_v and NALCN) appear to follow universal rules, almost without exception, in eight

established pore configurations, including Ca^{2+}-selective channels with negatively-charged glutamates and aspartates (EEEE, EDEE, EEDD, DEEA) and Na^{+}-selective channels with a positively-charged lysine (K) in either the 2nd or 3rd domain (EKEE, EEKE, DKEA, DEKA) (Fig. 6).

Evolution of 4x6TM channel pores

The lineage of Ca_v channels have an EEEE pore for highest calcium selectivity, but Ds can replace Es; NALCN and Na_v channels have DxxA and ExxE pores, respectively, where xx = EE or EK or KE. Simplest organisms (choanoflagellates, sponges, placozoans and anthozoan cnidarians such as coral, sea anemone) lack Na^{+}-dependent action potentials and have pore configurations lacking an internal K residue (e.g. DEEA, EEEE) when cation channel genes are present in these organisms (Fig. 8). The first appearance of animals with a nervous system and a pelagic adult lifestyle are the hydrozoan[305] and scyphozoan[308] jellyfish which are also the simplest organisms to have a lysine residue (K) in their Na_v channel (DKEA) (Fig. 8). Within invertebrate groups, Na_v (DEEA/DKEA/DEKA) and NALCN (EEEE/EDEE/EKEE/EEKE) channels adopt multiple pore configurations with alternative selectivity for Ca^{2+} and Na^{+} ions, when K can appear in lieu of an internal E in Domains II or III. The dual Ca^{2+} or Na^{+} selectivity filters are lost in vertebrate NALCN and Na_v channels, and are restricted to EEKE and DEKA configurations, respectively which has the lysine residue in Domain III, positioned where it is expected to have the highest selectivity for Na ions, compared to the less selective EKEE and DKEA pores where the lysine residue is in Domain II instead, found in some invertebrates (Fig. 8). The overall pattern of evolution suggest a primordial world of four domain channels gating Ca^{2+} ions, an experimentation and diversity of mixed Ca^{2+} and Na^{+} signaling in invertebrates, to a lack of Ca^{2+} signaling in vertebrate Na_v channels and NALCN (Fig. 8).

Parallel evolution of NALCN and Na_v channel pores

The co-appearance of NALCN and Na_v channels with a lysine residue in the pore is consistent with the evolution of Na^{+} ions to generate membrane excitability in nervous systems, circumventing the toxicity that intracellular Ca^{2+} ions have as agents for membrane depolarization[9]. There may also be a link between NALCN and Na_v channels to Na^{+} homeostasis, since many vertebrates with the lysine residue-containing pore are terrestrial vertebrates where Na^{+} retention and Na^{+} transport is especially critical. The presence of Ca^{2+}-selective pores of NALCN and Na_v channels in invertebrates may relate to a more flexible signaling using Ca^{2+} and/or Na^{+} ions, and perhaps related to ion homeostasis, serving as an adaptation for invertebrates for the more variable Ca^{2+} levels in the aquatic environment

and to service the high Ca^{2+} required in the exoskeletons of many invertebrates. It is interesting to note that the EEEE isoform of NALCN, as well as Na_v channels, are present in flatworms such as the free-living planarian *S. mediterranea*, but these are lost in closely-related trematodes, *S. mansoni* and *C. sinensis*. These endoparasites cycle between living in the regulated environment within snails and vertebrates, where there is less need for ion homeostasis and less requirement for a nervous system with rapid action potentials carried by Na^+ ions.

NALCN resembles intracellular channels

Plasma membrane-associated ion channels are noted for an almost universal explosion in the duplication of genes, which for 4x6TM channels increase in number from five channel genes (three Ca_v, two Na_v, and one NALCN) in invertebrates to 21 vertebrate channel genes (ten Ca_v, ten Na_v, and one NALCN). Increasing gene numbers in Ca_v and Na_v channels endows novel adaptations in different tissue environments such as brain, heart, or skeletal muscle[309]. Other membrane-associated ion channels also have large numbers of genes such as Trp channels (27 genes)[310] or two pore, KCNK K^+ leak channels (18 genes)[311]. NALCN is unusual in remaining a single gene, expressing a relatively short and highly conserved protein end to end, outside of the variability in the pore. NALCN more resembles intracellular channels which often have resisted increasing gene numbers from single-cell choanoflagellates and multicellular organisms like sponges which lack highly-specialized cells, to humans, associated with complex tissue evolution, such as the brain, where NALCN is most abundant[312].

All selectivity filter sequences of 4xTM channels fall into either Na^+ or Ca^{2+}-selective categories

The configuration of selectivity filter residues of every NALCN gene in more than a dozen animal phyla, abide by a set of rules that can be categorically identified as calcium-selective channels, with calcium-like EEEE/EDEE pores, resembling the invariant EEEE calcium-selective filter of Ca_v channels and the DEEA configuration of calcium-permeable, invertebrate Na_v2 channels. Or, categorically, the NALCN pore is consistent with sodium-selective pores with an EKEE/EEKE configuration, resembling the DEKA/DKEA pores of Na_v1 channels. NALCN pores also parallel the pores of Na_v channels in evolution, with NALCN and Na_v2 channels bearing primordial calcium channel-like pores that become more sodium selective in invertebrates. While the phylogenetic data is highly consistent with NALCN pores with calcium (EEEE/EDEE) or sodium (EKEE/EEKE) selectivity, we were unable to confirm this by *in vitro* expression.

NALCN as a calcium and/or sodium sensor

A perceived interchangeability of Ca^{2+} and Na^{+} selectivity in NALCN channels of this otherwise exceptionally conserved gene, is hard to reconcile given the very different roles that these ions play in excitability, where the relatively inert Na^{+} is much more abundant than Ca^{2+} and serves mostly in an electrogenic role, while Ca^{2+} is maintained at very low levels in cells due to cytotoxicity, and serves as an exquisitely-sensitive signaling molecule[9]. One would also expect a more generalized distribution and function for such a highly invariant, mostly brain-related gene, yet NALCN is relegated to only a subset of snail neurons (Fig. 5b), and perturbations in NALCN knockouts suggest a highly specialized role in a subset of pacemaking neurons in *C. elegans*[133] and *Drosophila*[121]. It is conceivable that NALCN is a specialized receptor for calcium or sodium ions, but not always permeable as a typical membrane-associated channel, such as the $Ca_v1.1$ channel that has specialized in vertebrates as a calcium-sensor for muscle contraction[313], or Na_X, the sodium channel that serves as a salt level sensor in the subfornical organ[314]. The NALCN gene is necessary for generating rhythmic neural activity associated with breathing[137,160], and its absence leads to hyperpolarized membrane potentials. The ion selectivity of NALCN is clearly important for its function since the wild-type EEKE NALCN but not a mutated calcium-like EEEE isoform rescues the NALCN mutant phenotype in *Drosophila*[121]. How NALCN, with its EKEE pore, plays a role in rescuing the fly mutant phenotype doesn't appear simply as a replacement of a missing sodium leak conductance though. The fly NALCN mutant is associated with an increased outward potassium current, without altering an inward cation current[121]. There was significant evolutionary pressure to retain the ancestral state with a Ca^{2+} channel-like, EEEE-NALCN pore in many invertebrates, which could serve as a potential calcium leak conductance current reported in invertebrates[315], and least one chordate (amphioxus) appears to possess a NALCN channel with only an EEEE pore, which may not generate Na^{+} leak currents at all, according to current physiological models.

2.4.5 Acknowledgements

This work was funded through an NSERC Discovery grant to J.D.S., as well as an NSERC Canada Graduate Scholarship and an NSERC Michael Smith Foreign Study Supplement Award to A.S.

Chapter 3
Discussion

3.1 Characterizing an invertebrate Ca_v3 channel homologue

3.1.1 Defining features for Ca_v3 channels retained by the Lymnaea homologue LCa_v3

Successful sequencing and cloning of an invertebrate Ca_v3 channel from *Lymnaea stagnalis* has revealed that despite significant accumulation of divergent amino acids between mammalian Ca_v3 channels and the *Lymnaea* homologue, LCa_v3 retains some key features that distinguish Ca_v3 channels from other 4-domain types. At the pore, the snail channel contains an EEDD selectivity filter motif characteristic to Ca_v3 channels (Chapter 2.1 figure 3B), which is distinct from the more calcium-selective EEEE selectivity filter of Ca_v1 and Ca_v2 channels. In the I-II linker, LCa_v3 and Ca_v3 channel homologues from even the most primitive animals, retain a predicted helix-loop-helix structure[64] that serves to regulate channel gating at hyperpolarized potentials[82] (Chapter 1 figure 3A and D; Chapter 2.1 figure 3C). An equivalent structure is not found in Na_v channels, NALCN, nor HVA calcium channels, however the latter possess binding sites for accessory β subunits in the corresponding site (i.e. the alpha interaction domain/AID), which interestingly also serves to regulate channel gating[75,76,77]. Disruption of the gating brake structure creates Ca_v3 channels that activate at even lower voltages than normal, and have faster kinetics for activation and inactivation[245,196,83,82,197]. LCa_v3 is atypical, in that it is much larger than other Ca_v3 channel cDNAs for which the full length sequence is known, however most of the divergence in size, and indeed in amino acid sequence, occurs in the cytoplasmic N- and C-termini as well as the linkers joining domains I to IV (Chapter 2.1 figure 1B and C; figure 3A). The conservation of these core distinguishing features prompted us to hypothesize that the *Lymnaea* Ca_v3 homologue would conduct calcium currents similar to those documented for mammalian channels when heterologously expressed in HEK-293T cells.

3.1.2 Heterologously expressed LCa_v3 conducts calcium currents with biophysical characteristics similar to mammalian homologues

Remarkably, despite c.a. one billion years separating mollusks and mammals[230], transfection of a cloned LCa_v3 channel cDNA produces robust calcium currents in HEK-293T cells with biophysical characteristics highly analogous to those of the mammalian isotypes (Chapter 2.1 Table 1). Specifically, currents begin to activate after only slight depolarization, typical for LVA Ca_v3

channels, with macroscopic currents bearing rapid kinetics of activation and inactivation, and slow deactivating tail currents. In addition, LCa_v3 is expected to conduct a constitutively depolarizing window current at voltages near resting membrane potential (Chapter 2.1 figure 5C), another characteristic feature of Ca_v3 channels whose physiological purpose is not fully understood. Finally, the sensitivity of LCa_v3 to non-specific Ca_v3 channel blockers Ni^{2+} and mibefradil was found to be quite similar to that of mammalian channels (Chapter 2.1 figure 8), indicating that the structures that these drugs bind to might be conserved. Clearly, despite the significant divergence at the amino acid level, LCa_v3 has retained key structures that endow it with the functionality of Ca_v3 channels, where it conducts characteristic calcium currents at voltages near resting membrane potential in neurons and other cells types. Based on sequence, the conservation of these features likely extend beyond LCa_v3 into Ca_v3 channels from other distant phyla, and it may be that Ca_v3 channels have a universal function in cells to mediate rapid sub-threshold currents to regulate excitability, and conduct minute but prolonged depolarizing window currents at rest. In addition, calcium influx through Ca_v3 channels might serve other conserved functions, such as regulating calcium-dependent channels, signaling pathways or biochemical processes including myocyte contraction and secretion of vesicles[94,64].

3.1.3 Conserved splicing in the I-II linker modulates protein abundance and membrane expression

During our sequencing of LCa_v3, we identified multiple sites for splice variability along the transcript. The presence of optional exons in the I-II and III-IV linker coding sequences of LCa_v3 intrigued us because mammalian channels also possess alternative splicing in these locations. More detailed analysis revealed that the large optional exon in the I-II linker of LCa_v3 is very similar to an optional exon termed 8b in rodent $Ca_v3.1$[194,195], with alternate 5' donor splice sites that can be used to remove 201 and 134 amino acids from the LCa_v3 and $Ca_v3.1$ I-II linkers respectively (Chapter 2.2 figure 2A; supplementary figure 1). In the central nervous system of both animals, exon 8b is present in roughly half of all Ca_v3 channel transcripts[195] (Chapter 2.2 figure 3A), indicating that both isoforms are expressed at physiologically relevant levels. Interestingly, exon 8b splicing has not been documented for humans, so its occurrence in *Lymnaea* and rodents suggests that either it was lost in humans and perhaps other species, or conversely, exon 8b splicing resulted from convergent evolution between rodents and snails. Nevertheless, exon 8b of LCa_v3 contains an APRASPExxD/E

amino acid motif found only in mammalian $Ca_v3.1$ and other invertebrate Ca_v3 channels, but not $Ca_v3.2$ or $Ca_v3.3$ (Chapter 2.2 figure 1D).

We found that omission of exon 8b in LCa_v3 (i.e. 201 aa) produced only minimal changes in biophysical properties in HEK-293T cells (Chapter 2.2 Table 1), but caused a two-fold increase in maximal inward currents (normalized against membrane surface area by capacitance) suggestive of more abundantly expressed channels at the membrane (Chapter 2.2 figure 6A). This mirrors what was documented for rodent $Ca_v3.1$, where omission of exon 8b produced a 1.8-fold increase in inward current amplitudes[195]. Of note, HVA calcium channel expression and membrane localization is also controlled at the I-II linker, via association with the β subunit[75,76,77] which mediates trafficking and provides protection from proteosomal degradation[78]. The mechanisms that regulate protein and surface expression of Ca_v3 channels are poorly understood[64], and given that analogous deletions in the I-II linkers of $Ca_v3.1$, $Ca_v3.2$ and $Ca_v3.3$ cause a moderate increase, a robust increase, and moderate decrease in membrane expression respectively, it is likely that different mechanisms govern the expression and trafficking of the three mammalian isotypes. Deletion of the APRASPExxD/E motif, conserved within 8b exons of LCa_v3 and rodent $Ca_v3.1$, had no impact on LCa_v3 current amplitudes, indicating that other regions of the optional I-II linker sequence, not overtly apparent on protein alignments, are influencing membrane expression. Indeed, the I-II linkers of LCa_v3 and $Ca_v3.1$ both contain multiple lysine (K) residues (Chapter 2.2 figure 2A) that can be targets for ubiquitination for the purposes of proteosomal degradation[316] or intracellular/membrane trafficking[317]. Importantly, whereas for $Ca_v3.1$ the increase in surface expression was attributed to increased membrane trafficking without a concurrent increase in total channel expression[195], we found that LCa_v3 lacking 8b underwent a doubling of both surface-expressed channels *and* total channel protein levels (Chapter 2.2 figure 6B and C). The inconsistency between our observations and those for $Ca_v3.1$ might be attributable to differences in underlying mechanisms, which would not be surprising given the divergent sequences in the I-II linker outside of the APRASPExxD/E motif. However, another possibility is that insertion of a hemagglutinin (HA) epitope tag into an extracellular loop of a channel, as was done for $Ca_v3.1$ for measuring membrane expression vs. total expression[195], can cause unforeseen artifacts. In our studies on LCa_v3, insertion of an HA tag into the equivalent position as $Ca_v3.1$ (i.e. the domain I S5-S6 loop) caused a dramatic reduction in current amplitudes (Chapter 2.2 supplementary figure 9).

In a preliminary study, we cloned the entire I-II linkers of LCa_v3 with and without exon 8b, fused to C-terminal HA tags, into a mammalian expression vector. Interestingly, only the -8b isoform could be detected on western blots of cell lysates with anti-HA antibody (not shown), and it is possible that the same mechanisms that determine full length LCa_v3 channel protein expression are preventing/attenuating expression of the +8b I-II linker. If so, these constructs will serve as useful tools to probe the cellular mechanisms responsible for the difference in expression at the levels of mRNA (i.e. stability/turnover[318]), protein translation (i.e. inhibition of translation such as by PERK kinase activation[318]), or post-translation degradation (i.e. lysosomal or proteosomal degradation[208]).

3.1.4 Conserved splicing in the III-IV linker modulates channel gating

In the III-IV linker of LCa_v3, we identified a small optional exon (coding for 7 amino acids) very similar to exon 25c in mammalian $Ca_v3.1$ and $Ca_v3.2$ homologues[192,190,193,200]. Like 8b, exon 25c is excluded from mRNA via an upstream tandem donor splice site (Chapter 2.2 figure 2B; supplementary figure 2); mammals also possess an optional cassette exon downstream of 25c, termed exon 26, producing possible configurations in the III-IV linker of: +25c/+26; +25c/Δ26; Δ25c/+26; and Δ25c/Δ26. $Ca_v3.3$ lacks exons 25c and 26 and is thus always ΔΔ-like, and interestingly, all 4-domain channels including Na_v, HVA Ca_v, NALCN, and ΔΔ Ca_v3 have III-IV linkers with very confined lengths of 54 ±1 amino acid (Chapter 2.2 figure 2C; Chapter 2.4 figure 1B). Not surprisingly, small insertions in the III-IV linkers of LCa_v3, $Ca_v3.1$ and $Ca_v3.2$ imposed by exon 25c (and 26 in mammals) cause a battery of strong and highly analogous alterations in channel gating properties, including hyperpolarizing shifts in activation and steady state inactivation (Chapter 2.2 figure 4C to E), faster activation and inactivation kinetics (Chapter 2.2 figure 5B to D), slower deactivation kinetics (Chapter 2.2 figure 5E and F), and slower recovery from inactivation (Chapter 2.2 figure 5G). Conversely, lack of exons in the III-IV linker produces Ca_v3 channels with features more akin to $Ca_v3.3$[205,206,65,207], with depolarized activation and inactivation voltage dependencies, slower activation and inactivation kinetics, and faster deactivation.

Remarkably, not only were the functional consequences of exon 25c found to be conserved between snails and mammals, but qPCR analysis revealed that there is also a parallel downregulation of Δ25c variants in developing snails and mammals, leading to a relative enrichment of +25c isoforms in adults (Chapter 2.2 figure 3D and E). This pattern of expression is also evident in the heart, where $LCa_v3/Ca_v3.2$ transcripts bearing exon 25c are enriched in adults[266] (Chapter 2.2 figure 3C). Furthermore, there is a continuous and significant downregulation of Ca_v3 channel expression in

both snails (Chapter 2.2 figure 3D) and mammals[234] throughout development, suggesting that the respective channels play similar and more pronounced roles during early stages of animal development. It may be more than coincidence that $Ca_v3.3$[204], as well as ΔΔ variants of $Ca_v3.1$ and $Ca_v3.2$ are enriched in the embryo (Chapter 2.2 figure 3D), where channels with depolarized voltage dependencies for inactivation would be less inactivated at rest and thus contribute more to excitability. In adults, the +25c and/or +26 variants are better suited for rebound burst firing, requiring hyperpolarization following an action potential to relieve inactivation, with channels bearing rapid activation kinetics to quickly depolarize cells towards threshold.

We found an interesting parallel between the diminishing levels of both LCa_v3 transcripts *and* Δ25c isoforms throughout development (Chapter 2.2 figure 3D). It is tempting to speculate that there is a coupling between the control of LCa_v3 expression at the promoter, and the control of splicing via *cis* elements located in the intron just downstream of exon 25c. Indeed, pre-mRNA splicing is known to be closely associated with RNA polymerase activity and vice versa, and some proteins can act as regulators for both transcription and splicing[319]. Furthermore, the conserved pattern of exon 25c enrichment throughout development, observed for both snails and mammals, suggests that the mechanisms responsible are conserved to some degree. If so, one would expect that the *cis*- and *trans*-acting factors that regulate these processes share some degree of conservation.

3.1.5 Unique splicing in the domain II P-loop that alters ion selectivity

We also identified splicing, not previously reported for mammalian Ca_v3 channels, of mutually exclusive exons 12A and 12B within the domain II P-loop coding sequence (Chapter 2.3 figure 1). Notably, the 3' splice sites for these exons were found to be located just 5 codons upstream of the glutamate of the E**E**DD selectivity filter motif (Chapter 2.3 figure 1B), critical for ion selectivity. Phylogenetic analysis revealed that such splicing occurs not only in mollusks, but in a superphylum of invertebrate animals called protostomia that includes model organisms *Drosophila melanogaster* and *Caenorhabditis elegans* (Chapter 2.3 Table 3; Appendix C).

To our amazement, exon 12 variants of LCa_v3 had dramatically different permeabilities to monovalent cations, and only minimal alterations in biophysical properties, when electrophysiologically recorded in HEK-293T cells. LCa_v3-12A, which had comparatively slower deactivation and faster recovery from inactivation (Chapter 2.3 figure 10D; figure 11 respectively), produced striking outward Cs^+ currents at potentials above 0 mV (Chapter 2.3 figure 9A and B), and upon application of 135 mM external Na^+, maximal peak inward current increased ~15.5-fold or

1450% (Chapter 2.3 figure 14). Conversely, LCa$_v$3-12B showed only marginal outward Cs^+ currents and only a 2-fold increase in inward current upon addition of external sodium (Chapter 2.3 figure 9A and B; figure 14 respectively), more reminiscent of mammalian Ca$_v$3 channel isotypes[288]. Importantly, the external solutions used in these experiments contained 2 mM Ca^{2+} (i.e. 2 mM Ca^{2+} ±135 mM Na^+), a physiologically relevant concentration shown to effectively block Na^+ current through mammalian Ca$_v$3 channels (although Ca$_v$3.3, the least Ca^{2+}-selective isotype, is less sensitive to Ca^{2+}-block and conducts somewhat of a mixed Ca^{2+}/Na^+ current under physiological conditions)[288]. Consequently, LCa$_v$3-12A is expected to conduct pronounced LVA *sodium* currents into *Lymnaea* cells under physiological conditions, while LCa$_v$3-12B conducts a more conventional calcium current.

Due to time constraints, the relative permeabilities of physiologically relevant cations through pore variants of LCa$_v$3 were not quantified (i.e. pCa^{2+} vs. pNa^+ vs. pK^+); neither were the properties of native currents, for example in the *Lymnaea* heart and secretory glands which almost exclusively express LCa$_v$3-12A and LCa$_v$3-12B respectively (Chapter 2.3 figure 4B). In addition, no assessment was made as to whether ions in the internal and external solutions influence biophysical properties, which is important for understanding how the channels behave under physiological conditions. Finally, it remains to be determined whether 12A-bearing Ca$_v$3 channel homologues from other protostome invertebrates also have reduced Ca^{2+}-selectivity. Such characterization will be crucial for understanding why such splicing takes place in protostome invertebrates.

Unexpectedly, studying a *Lymnaea* Ca$_v$3 channel homologue has provided novel insights into ion permeation through Ca$_v$3 channels (and indeed all four domain channels), where alterations outside of the selectivity filter can dramatically influence ion selectivity. Ca$_v$3 channels in mammals resemble the ancestral Ca$_v$3 channel, with short exon 12A-like domain II P-loops, and it will be interesting to see if Ca$_v$3 channels from extant primitive animals such as *Trichoplax adhaerens* and *Nematostella vectensis* are less Ca^{2+}-selective similar to LCa$_v$3-12A, or more calcium selective similar to mammalian Ca$_v$3 channels. If the former is true, then it is likely that the ancestral Ca$_v$3 channel was actually more of a LVA cation channel for conducting sodium currents at negative voltages. By extension, somewhere along the deuterostome lineage that led to mammals, a 12A-bearing Ca$_v$3 channel acquired structural changes in other regions to produce a much more Ca^{2+}-selective permeation pathway.

3.2 Characterizing an invertebrate NALCN channel homologue

3.2.1 A highly conserved voltage-gated channel structure

NALCN channels represent a third major branch of 4-domain ion channels, with conserved features that distinguish them from the voltage-gated sodium and calcium channel families[119] (Chapter 2.4 figure 1A). Comparing the amino acid sequences between *Lymnaea* and human homologues for NALCN, Na_v and Ca_v channels reveals that NALCN is particularly short when compared to sodium and calcium channels, and much more conserved (i.e. 69% vs. 48 to 58% similarity), with strong conservation extending beyond the transmembrane helices into the usually more divergent N- and C-termini and II-III linker (Chapter 2.4 figure 1C). Notably, the four repeat domains of LNALCN, as well as mammalian, insect, and nematode homologues, all retain mostly intact voltage sensors (i.e. S1-S4 helices), with conserved negatively charged residues in the S1-S3 helices, as well as positively-charged lysine/arginine residues in S4 critical for voltage-sensor function[62] (albeit with a reduced number in S4; Introduction figure 6). The characterization of NALCN as completely voltage-independent[120] is therefore somewhat surprising, given the significant conservation of these charged amino acids. For voltage-gated channels, loss of S4 charges is associated with alterations in voltage sensitivity, but not a complete abrogation of the voltage response[62]. Indeed, there might be other regions in NALCN, not yet defined, that disrupt voltage-sensitivity. However, this begs the question as to why the 'non-functional' voltage sensors, and in particular, the charged S1-S4 residues, are so conserved despite billions of years of divergent evolution[230].

3.2.2 An unusually divergent selectivity filter

During our sequencing of the *Lymnaea* NALCN cDNA, we were surprised to find that the sole selectivity filter lysine, instead of being located in domain III as reported for other species, was in domain II (i.e. E**K**EE instead of EE**K**E; Introduction figure 7). In mammals (e.g. *Rattus norvegicus*), arthropods (e.g. *Drosophila melanogaster*) and nematodes (e.g. *C. elegans*), which have NALCN channels with EE**K**E selectivity filters (Introduction figure 7), the lysine in domain III is thought to produce a non-selective cationic pore[137], representing a hybrid structure between HVA calcium (i.e. **EE**E**E**) and sodium (DE**K**A) channel selectivity filters. Instead, *Lymnaea* NALCN more resembles a hybrid between HVA calcium channels (**E**E**EE**) and primitive jellyfish sodium channels (i.e. D**K**EA)[59], where placement of the lysine residue in domain II instead of III renders jellyfish sodium channels less sodium-selective and more non-selective for cations than DEKA channels[306,304].

Therefore, it can be postulated that if EEKE NALCN channels conduct non-selective cationic currents[137,118], the *Lymnaea* homologue, with an EKEE pore, should also conduct non-selective currents.

Intriguingly, similar to LCa_v3, we identified mutually exclusive alternative splicing in the domain II P-loop of *Lymnaea* NALCN. Unlike LCa_v3 however, mutually exclusive exons 15a and 15b were found to alter the selectivity filter motif from a proposed non-selective configuration of E**K**EE (i.e. exon 15b) to a calcium channel-like configuration of E**E**EE (exon 15a; Chapter 2.4 figure 2A). To our knowledge, the use of alternative splicing to alter the selectivity filter in such a way has never been documented for 4-domain channels, and changes at the selectivity filter are normally attributed to distinct evolutionary lineages of ion channel genes. We therefore conducted a comprehensive search for alternative splicing in other animal species, using genome sequences available online. Interestingly, mutually exclusive splicing in domain II of NALCN, to produce EKEE and EEEE pores, was found to be conserved in mollusks and other animals with bilateral symmetry including annelids (e.g. *Capitella telata*), echinoderms (e.g. *Strongylocentrotus purpuratus*) and hemichordates (e.g. *Saccoglossus kowalevskii*; Chapter 2.4 figure 2A; figure 3). Vertebrates (e.g. *Homo sapiens*) and urochordates (e.g. *Ciona intestinalis*), which form part of the chordate phylum, are closely related to echinoderms and hemichordates yet lack mutually exclusive splicing in domain II, possessing only EEKE selectivity filters. A likely scenario is that an ancestor to chordates lost exon 15b in domain II, retaining only the glutamate-bearing 15a and thus an EEEE selectivity filter, and subsequently a lysine in position III (i.e. EE**K**E) arose via nucleotide substitution (Chapter 2.4 figure 3). In accordance, extant chordate ancestor *Branchiostoma floridae* (i.e. phylum Cephalochordata) has an intermediary EEEE selectivity filter for NALCN (Chapter 2.4 figure 3).

To our surprise, analysis of NALCN channel genes from certain subphyla within protostomal arthropod invertebrates (i.e. Myriapoda and Chelicerata) revealed a similar splicing pattern of mutually exclusive exons altering the selectivity filter, but rather in domain III. Here, mutually exclusive exons similarly introduce either a glutamate (i.e. exon 31a) or a lysine (i.e. exon 31b) into the selectivity filter of NALCN to produce EE**E**E and EE**K**E pores respectively; Chapter 2.4 figure 3). Coincidentally, two of the most commonly used protostome animals for molecular neuroscience research, *Drosophila melanogaster* and *C.elegans*, lack alternative splicing in the pore and only possess vertebrate-like EEKE selectivity filters (Chapter 2.4 figure 3), giving the impression that EEKE is the consensus for NALCN[121,120,127]. Instead, our analyses reveal that despite an unusually

high conservation in amino acid sequence at the whole channel level, the NALCN pore has been subject to unprecedented levels of variability throughout evolution, and that some animals can selectively alter the pore via alternative splicing from a proposed non-selective configuration of EEKE/EKEE, to a putatively calcium-selective configuration of EEEE/EDEE (Chapter 2.4 figure 3).

Even more remarkable is that extant primitive metazoans such as cniderians (i.e. *Nematostella vectensis*, *Acropora digitifera*, and *Hydra magnipapilatta*), placozoans (i.e. *Trichoplax adhaerens*), and sponge (i.e. *Amphimedon queenslandica*), which also lack alternative splicing in the pore, have exclusively calcium channel-like selectivity filters of EEEE, and indeed this configuration is likely ancestral for NALCN (Chapter 2.4 figure 3). Hence in bilateral animals with alternative splicing in the pore, exon duplication of ancestral glutamate-containing exons 15a or 31a likely gave rise to lysine-containing mutually exclusive exons 15b and 31b, respectively. Notably, since we were unable to identify a NALCN channel gene containing two lysines (i.e. EKKE), there is likely a constraint in the pore to have either a calcium channel-like selectivity filter (EEEE/EDEE), or a hybrid calcium-sodium channel-like filter (EEKE/EKEE). By extension, the limited configurations allowable for the NALCN pore imply that the selectivity filter residues play an important role in the function of the channel protein.

3.2.3 Difficulties in characterizing LNALCN's ion conduction properties

Unfortunately, we were unable to record currents through cloned LNALCN pore variants expressed in HEK-293T cells (Chapter 2.4 supplementary figure 2), corroborating with others the difficulty in electrophysiological recording of NALCN in heterologous systems[135,118,127]. In fact, since NALCN's early molecular characterization in the late 90s[135], it was only recently that the channel was characterized as voltage-independent and non-selective[120]. Such currents however are very difficult to differentiate from artifactual leak currents resulting from leaky patches on voltage-clamped cells, or punctures in the membrane. As such, attempts were made to validate NALCN-mediated leak currents in HEK-293 cells by applying compounds capable of blocking them, including impermeant cation $NMDG^+$, 10 μM gadolinium (Gd^{3+}), 1 mM Cd^{2+}, and 1 mM verapamil[120]. However in our hands, all of these compounds have non-specific effects on leak currents, regardless of the presence or absence of either human or *Lymnaea* NALCN (Chapter 2.4 supplementary figure 2A and B for currents blocked by $NMDG^+$; data not shown for other compounds). We therefore have some apprehension about the notion that NALCN conducts completely voltage-independent and non-selective cationic currents when heterologously expressed in mammalian cells[143].

Nevertheless, such a characterization for NALCN fits with the knockout data from vertebrates and invertebrates, where neurons lacking NALCN have hyperpolarized membrane potentials indicative of an absent depolarizing current[120,160,161]. Arguably, the punctate localization of NALCN along invertebrate axons[127], and the apparent association of NALCN with macromolecular lipid raft complexes[320,152], might indicate that very strict conditions are required to activate NALCN-mediated currents, and that these conditions are largely absent in HEK-293 cells. However, other explanations for membrane hyperpolarization in NALCN knockouts should be considered, including loss of a NALCN-mediated inhibition of some hyperpolarizing current (e.g. see Lear *et al*., 2005[121] and Bouhours *et al*., 2011[148]), compensatory changes in the expression or activity of other ion channels[321], or altered activity of pumps and/or exchangers that set resting membrane potential (i.e. the Na^+/K^+-ATPase). Finally, it is also possible that NALCN does not conduct at all, serving merely as a sensor for extracellular ions via the selectivity filter, and/or for changes in membrane potential similar to $Ca_v1.1$ in skeletal muscle[322].

3.2.4 Physiological roles for NALCN and NALCN pore variants

Variability in the selectivity filter of NALCN almost certainly alters the way in which extracellular cations interact with (and perhaps permeate) the pore. Based on homology with 4-domain channels, EEEE-containing variants of NALCN should have a high affinity for extracellular Ca^{2+}, while EEKE and EKEE should have less and thus be more permeable to Na^+. Notably in *Drosophila*, knockout of its invariable EEKE NALCN creates distinct phenotypes that cannot be fully compensated by reintroduction of a recombinant NALCN bearing an EEEE selectivity filter[121]. So, the EEKE configuration is required for normal functioning in insects, and furthermore, EEEE and EEKE/EKEE pores likely have non-overlapping properties. Recombinant rodent EEEE NALCN has been proposed to be non-conducting in HEK-293 cells[120]; however, considering the challenges with heterologous expression, as well as the existence of animals with only EEEE selectivity filters for NALCN (including extant relatives of ancestral primitive animals), this is debatable. As such, we propose that EEKE/EKEE and EEEE/EDEE channels are both physiologically 'functional', but have distinct roles that depend on differential interactions with extracellular cations within the selectivity filter.

Quantitative PCR in *Lymnaea*, using primers designed to selectively amplify either exon 15a (i.e. E**E**EE) or exon 15b (i.e. E**K**EE), indicates that both variants are abundantly expressed in the central nervous system (CNS), secretory albumen and prostate glands, and heart, with preferred expression of 15b/EKEE in the CNS and secretory glands, and 15a/EEEE in the heart (Chapter 2.4 figure 5E and

F). Unfortunately, without functional characterization of LNALCN, it is difficult to speculate on the functions of the two splice isoforms within the different *Lymnaea* organs/tissues. However, there is a sharp increase in expression of EKEE NALCN in secretory glands as sexual maturation ensues (Chapter 2.4 figure 5E1), consistent with a role in exocytosis as has been suggested for mammals[323], *Drosophila*[121], and *C. elegans*[128,127]. In the heart, there is a significant downregulation of NALCN channel expression from juvenile to adult (Chapter 2.4 figure 5F1), similar to but not as dramatic as LCa_v3 (Chapter 2.3 figure 4B), suggestive of a parallel diminishing contribution for both channels as the heart matures. It will be interesting to see if the two splice isoforms of LNALCN segregate to distinct neurons or cell types, and if their subcellular localization is different.

The physiological contributions of NALCN channels remain enigmatic. The most convincing data comes from knockout animals, where in rodents NALCN KO produces disrupted activity of respiratory neurons, apnea and perinatal lethality[120]. Interestingly, dsRNA/siRNA knockdown of *Lymnaea* NALCN also disrupts activity of respiratory neurons and respiratory rhythm[160], but unfortunately, the RNA-mediated knockdown strategy was designed against an incomplete cDNA sequence available on GenBank[238], and the authors unknowingly silenced both domain II pore isoforms of LNALCN via an invariable region of the mRNA[160]. As such, the specific contributions of the two pore variants were not delineated in these experiments. Furthermore, considering the highly divergent snail and mammalian nervous systems, this apparent conservation is likely restricted to a generalized role for NALCN in regulating excitability of rhythmically active neurons. Indeed, the general truisms about NALCN's physiological functions, elucidated by knockout animals, are that: 1) KO/knockdown of NALCN and/or its accessory subunits Unc-79 and Unc-80 leads to membrane hyperpolarization[120,160,161], so NALCN is involved in regulating membrane potential, 2) in *Drosophila* and *C.elegans*, KO leads to increased sensitivity to volatile anesthetics[129,126,122,125,123,152] attributed in part to hyperpolarized membrane potentials[161], 3) KO leads to defects in exocytosis[148,128,121,127], and 4) the most obvious phenotypes resulting from NALCN's absence involve disruptions in rhythmically active neurons[121,120,160,133,127]. As such, it is likely that NALCN's influence on membrane potential serves to regulate secretion in neurons that require fast or continuous vesicle turnover; however much more research is needed to elucidate the underlying cellular mechanisms responsible for these observations. Indeed, consolidating these truisms with the highly variable selectivity filter for NALCN presents some intriguing challenges for future researchers.

Chapter 4
Conclusions

Compared to HVA calcium channels and sodium channels, Ca_v3, and even more so NALCN channels, are poorly understood physiologically. Even less understood is the role that alternative splicing plays in the modulation of these two channels. We have shown that for Ca_v3 channels, alternative splicing can be highly analogous between very distant animals (i.e. exons 8b and 25c in mammalian and snail Ca_v3 channel homologues), starting with the gene sequences/structures that dictate intron splicing, to the temporal and spatial expression patterns for these splicing events, to the functional consequences of these structural alterations at the biophysical and cellular levels. Furthermore, the general expression patterns of LCa_v3 seem to mirror those of mammalian channels at the whole animal level and in homologous organs/tissues. Regardless of whether these conserved features arose out of convergent evolution, or are retained from a distant common ancestor, the functionality of Ca_v3 channels seems to be similarly adjusted in snails and mammals to fulfill different roles in different contexts. Although well documented, the physiological roles for alternative splicing of exons 8b and 25c in mammalian Ca_v3 channels are poorly understood. Changes in alternative splicing tend to occur on a large scale involving many different genes[185], and the function of a specific gene isoform can be difficult to determine within such a dynamic system, especially when there is overlapping expression of different splice isoforms of that same gene, or when there are closely related genes that create redundancy problems. The latter problem can be circumvented in *Lymnaea*, which only contains a single Ca_v3 channel gene and furthermore a much simpler nervous system, heart, and endocrine system. As such, the ground work established in this thesis might provide a useful framework for pursuing the physiological functions for 1) downregulating Ca_v3 channels during development, and 2) imposing differential alternative splicing schemes for exons 8b and 25c within distinct temporal and spatial contexts.

Working with *Lymnaea* Ca_v3 and NALCN channel homologues has also provided some unexpected insights into ion selectivity through 4-domain channels. For LCa_v3, we found that alternative splicing-induced alterations outside of the selectivity filter, ordained to be the primary determinant for ion selectivity, can nonetheless dramatically impact Ca^{2+} vs. Na^{+} selectivity. Remarkably, LCa_v3 containing deduced exon 12A, which resembles the ancestral Ca_v3 channel in domain II of the pore, has dramatically increased monovalent cation permeability when compared to

LCa_v3-12B and mammalian homologues[288]. Perhaps then Ca_v3 channels were at first non-selective, and calcium selectivity evolved later via duplication of exon 12A into exon 12B in protostome animals (e.g. *Lymnaea*), and by alternate means in deuterostome animals such as mammals. Our data thus supports the notion that sodium and calcium channels share an intertwined evolutionary history, and that Ca_v3 channels might be ancestors to 4-domain sodium channels[9]. It will be interesting to see what role LCa_v3-12A plays in heart function, and LCa_v3-12B in secretory glands, and indeed what both isoforms do in the CNS.

Finally, LNALCN was found to also undergo alternative splicing in the pore, but in this case converting the selectivity filter motif from a proposed non-selective configuration of EKEE (exon 15b) to a putatively calcium-selective EEEE (exon 15a). NALCN is extremely unconventional, in that it has independently evolved alternative splicing in the pore at least twice, in domain II as in *Lymnaea* and primitive bilaterian *Schmidtea mediterranea*, and in domain III in a subset of arthropod invertebrates. Furthermore, the ancestral state of NALCN was likely EEEE, which is inconsistent with sodium permeability and a proposed role for NALCN as being the major depolarizing current for setting resting membrane potential in neurons and other cell types[143].

Chapter 5
Materials and Methods

5.1 Molecular biology

5.1.1 Chemicals

Chemicals used for general molecular biology were mostly from Fisher Scientific (Fair Lawn, New Jersey), unless otherwise specified.

5.1.2 Lymnaea Genomic DNA extraction

For each preparation, one whole juvenile animal (1.0-1.5 cm shell length[292]) was flash-frozen in liquid nitrogen and ground with a mortar and pestle into a fine powder, which was then transferred to a 1.5 mL centrifuge tube. DNA extraction was performed according to van Moorsel *et al*., 2000[324], where briefly, 400 µL of homogenizing buffer (0.1 M NaCl, 0.2 M sucrose, 0.05 M EDTA, and 0.1 M Tris pH 8.0) was added to the tube and the ground tissue was gently mixed with the buffer with a hand held homogenizer. The tube was then centrifuged at 4^{o}C, 16000g for 10 minutes in a refrigerated Eppendorf 5415R centrifuge to pellet the snail tissue and the supernatant was removed. Cells were lysed with 320 µL of SDS buffer (1% SDS w/v, 0.01 M EDTA, and 0.02 M Tris pH 8.0) at 65^{o}C for 1 hour, and then cell debris was precipitated by adding 30 µL of 8 M potassium acetate, gently inverting the tube to mix, then incubating on ice for 1 hour. After centrifugation at 4^{o}C for 5 minutes at 16000g, the supernatant was transferred to a new tube containing 700 µL of pure ethanol, which was then mixed by inversion, and incubated at 4^{o}C for 1 hour. Nucleic acids were pelleted by centrifugation at 4^{o}C, 16000g for 12 minutes, the supernatant was decanted, and the pellet washed with 500 µL of 70% ethanol. The pellet was then air-dried and resuspended with 200 µL of water containing 20 µg/mL RNase A (BioShop Canada Inc., Burlington, ON) and the tube incubated at 37^{o}C for 45 minutes. To further purify DNA, 200 µL of 50:50 phenol/chloroform (Fisher Scientific) was added and the tube was placed on a tabletop rocking platform for 1 hour at a low speed, centrifuged at room temperature at 21000g for 6 minutes in an Eppendorf 5424 table-top centrifuge, and the supernatant was transferred to a new tube containing 20 µL of 3 M sodium acetate pH 5.2 and 440 µL of pure ethanol to precipitate DNA. After mixing by inversion, DNA was allowed to precipitate for 1 hour on ice, then centrifuged at 4^{o}C for 15 minutes at 16000g, the supernatant was removed with a micropipette, and the pellet washed twice with 500 µL of 70% ethanol. DNA was

resuspended with 50 μL of water, quantified by UV spectrophotometry (with a NanoDrop 1000 spectrophotometer; NanoDrop Technologies, Inc. Wilmington, DE), electrophoresed on a 1% w/v agarose gel in TAE buffer (20 mM acetate, 2 mM EDTA, 40 mM Tris pH 8.1), submerged in 0.1 μg/mL ethidium bromide in TAE buffer for ethidium bromide staining, and visualized under UV light with an AlphaImager HP (Alpha Innotech, Weltevreden Park, Johannesburg).

5.1.3 RNA extraction

RNA extraction for cDNA synthesis as well as for qPCR and semiquantitative RT-PCR was carried out using methods modified from Chomczynski and Sacchi 1987[325,326]. Briefly, dissected or ground tissues were placed in 1.5 mL centrifuge tubes and stored in either liquid nitrogen or at -80^{o}C until RNA extraction. For extraction, 1 mL of Tri-Regent (Sigma-Aldrich, St. Louis, MO) was added to the frozen tissues, and these were allowed to thaw at room temperature for 2 minutes and then thoroughly vortexed. A hand-held conical tissue grinder was used to further disrupt the tissue, then 200 μL of chloroform was added to each tube, and tubes were vortexed and centrifuged at room temperature at 10000g for 10 minutes; the supernatants were then transferred to new tubes and treated two additional times with 200 μL of chloroform. After the second treatment, the supernatants were individually combined with 500 μL of 2-propanol in 1.5 mL tubes to precipitate nucleic acids, where these were mixed by vortexing, incubated on ice for 1 hour, then centrifuged at 16000g at 4^{o}C for 20 minutes. The supernatants were decanted, and the resulting nucleic acid pellets were washed by adding 700 μL of 70% ethanol, vortexing, centrifuging at 16000g at 4^{o}C for 10 minutes, and decanting of the ethanol. Air-dried pellets were resuspended with 200 μL of diethylpyrocarbonate (DEPC)-treated water, then the RNA was selectively precipitated with 300 μL of 3 M LiCl, which was added to each tube and the tubes were vortexed and incubated on ice for 30 minutes. RNA was pelleted by centrifugation at 16000g at 4^{o}C for 30 minutes, LiCl was decanted, and the pellets were washed with 700 μL of 70% ethanol as before. Pellets were then each resuspended with 400 μL of DEPC water, and 35 μL of 2.5 M potassium acetate pH 5.5 (prepared in DEPC water) was added to each tube to precipitate polysaccharides (tubes were vortexed and centrifuged at 16000g at 4^{o}C for 20 minutes). Supernatants were then transferred to new 1.5 mL tubes, and RNA was precipitated with 800 μL of 100% ethanol, on ice for 30 minutes. RNA was then pelleted at 16000g at 4^{o}C, the supernatant was decanted, the pellets washed with 70% ethanol as before, and finally these were resuspended in 100 to 200 μL of DEPC water. RNA samples were quantified by UV spectrophotometry, and 1 μg of each was

typically electrophoresis through a 1% agarose gel and visualized by ethidium bromide staining in order to assess quality. RNA was stored at -80^{o}C until further use.

5.1.4 PCR

Polymerase chain reaction (PCR)[327], to amplify from complementary DNA (cDNA), genomic DNA, or plasmid DNA, was done in two ways, depending on the desired quality of the amplified products in terms of nucleotide error rates. Taq DNA polymerase (Fermentas-Thermo Scientific, Glen Burnie, MD), which lacks 3' to 5' exonuclease activity and proofreading ability and hence has lower fidelity, was used for amplification when DNA sequence integrity was not imperative, and when products were not larger than 2000 bases. Typical reactions were carried out in 0.2 mL flat top PCR tubes, with total volumes of 25 µL, containing 2.5 µL of 10x Taq buffer (with KCl; Fermentas), 1.5 µL of 25 mM $MgCl_2$ (Fermentas), 0.5 µL of 10 mM dNTP mix (10 mM each of dATP, dGTP, dCTP, and dTTP; Fermentas), 1.25 µL of primer 1 (at 10 µM), 1.25 µL of primer 2 (at 10 µM), 0.5 to 1 µL of template DNA, 0.25 µL of Taq DNA polymerase (if single tube, 0.125 µL if in a master mix), and water to 25 µL. Thermal cycling parameters were variable depending on the type of experiment and the length of the target DNA sequence. Typically, an initial DNA denaturation step at 95^{o}C for 2 minutes was carried out, then temperature cycling of 94^{o}C for 1 minute (denaturation), 56^{o}C for 45 seconds (primer annealing; in rare circumstances modified according to primer melting temperature), and 72^{o}C for between 45 seconds to 8 minutes (polymerase extension; roughly 1 minute per 1000 bases with a minimum of 45 seconds, and 4 to 8 minutes when product length was unknown), for a total of 32 cycles. After cycling, a 10 minute extension at 72^{o}C was carried out to maximize the number of full length PCR products.

For high-fidelity PCRs, PfuTurbo® DNA polymerase AD (Stratagene-Agilent Technologies Inc., Santa Clara, CA) was used. Typically, these reactions were carried out in 50 µL volumes, with 5 µL of 10x buffer (Stratagene), 1 µL of 10 mM dNTP mix (Fermentas), 1.5 µL of primer 1 (at 10 µM), 1.5 µL of primer 2 (at 10 µM), 0.5 to 1 µL of template DNA, 1 µL of PfuTurbo® DNA polymerase AD, and water to 50 µL. For PCR, an initial DNA denaturation step was done at 95^{o}C for 1 minute, then temperature cycling (typically 32 cycles) of 95^{o}C for 30 seconds (denaturation), then 56^{o}C for 45 seconds (primer annealing; also rarely modified), and then 68^{o}C for between 45 seconds to 8 minutes (extension; roughly 2 minutes per 1000 bases). Following cycling, an extension of 10 minutes at 68^{o}C was done.

Thermal cycling was done in a 96-well Mastercycler ep Gradient S apparatus (Eppendorf, Hamburg, Germany). All primers were ordered from either Sigma-Genosys (Sigma-Aldrich) or Eurofins MWG Operon (Huntsville, AL), diluted to 100 μM in water, and stored at -20°C. Successful amplification of target DNA was assessed by electrophoresis of 5 μL of each PCR through a 1% agarose gel products, which was then ethidium bromide stained and visualized under UV light (as above). Samples were either stored at -20°C for future use, or desired DNA fragments were purified by gel-extraction (see below).

5.1.5 Site directed mutagenesis

Site directed mutagenesis of plasmid DNA was done using the QuikChange protocol (Stratagene). For mutagenesis, reaction mixtures were prepared by adding 5 μL of 10x buffer (Stratagene), 1 μL of 10 mM dNTP mix (Fermentas), 125 ng of primer 1 (molarity converted to ng/μL using the specific molecular weight for each primer)), 125 ng of primer 2, 1 μL of template plasmid DNA (at 50 ng/μL), 1 μL of PfuTurbo® DNA polymerase AD, and water to 50 μL. Controls lacked PfuTurbo® polymerase enzyme and instead had one additional μL of water. For PCR, an initial denaturation step was done at 95°C for 1 minute, then temperature cycling of 95°C for 30 seconds, 56°C for 1 minute, and 68°C for variable times depending on plasmid length (roughly 2 minutes per 1000 bases), with 18 cycles using an Eppendorf Mastercycler ep Gradient S. Following PCR, 17 μL of 10x NEB buffer 4 (New England Biolabs, Ipswich, MA), 4 μL of *Dpn*I restriction endonuclease (NEB), and 130 μL of water were added to the PCR tubes and incubated at 37°C for 1 hour to degrade the methylated template DNA. Samples were then treated with 200 μL of 50:50 phenol/chloroform mixture (buffered at pH 8.0 with 1 M Tris), vortexed, centrifuged at room temperature at 21000g for 6 minutes, then the supernatants were transferred to new tubes. To precipitate DNA, 3 μL of glycogen (20 mg/mL; Fermentas), 20 μL of 3 M sodium acetate pH 5.2, and 440 μL of pure ethanol were added to each tube, and tubes were vortexed and incubated on ice for 20 minutes. Tubes were then centrifuged at 4°C for 16 minutes, and DNA/glycogen pellets were washed with 500 μL of 70% ethanol and resuspended with 10 μL of water. 2 μL of PCR synthesized plasmids were then transformed into heatshock-competent Stbl2™ bacteria as per manufacturer's instructions (Invitrogen) for plasmid isolation (see below).

5.1.6 Reverse transcription

Reverse transcription (RT), used to synthesize cDNA for cloning purposes or semi-quantitative RT-PCR (see below), was done using Superscript III RTase (Invitrogen, Carlsbad, CA). Primers used for

RT reactions were oligo(dT_{18}), random hexamers (Table M1), or gene specific; concentrations were varied depending on primer type. Reactions were done in 0.2 mL flat top PCR tubes, with an initial RNA denaturation step as follows: 1 to 4 µg of extracted RNA sample, 1 µL of primer (50 µg/µL oligo(dT_{18}), 50 nM random hexamer, or 2 µM gene-specific), 1 µL 10 mM dNTP (Fermentas), and nuclease free water (Fermentas) to a total volume of 13 µL were combined in a PCR tube on ice. Tubes were then transferred from ice to a water bath at 65°C for 5 minutes, and snap-cooled in ice water for 5 minutes. For cDNA synthesis, 4 µL of 5x First-Strand Buffer (Invitrogen), 1 µL of 0.1 M dithiothreitol (DTT; Invitrogen), 1 µL of RiboLock™ RNase inhibitor (Fermentas), and 1 µL of Superscript III RTase (Invitrogen) was added to each tube, then tubes were incubated at 54°C for 80 minutes (RTase reaction), then 75°C for 15 minutes (to heat-inactivate the RTase enzyme) using an Eppendorf Mastercycler ep Gradient S. Tubes were stored at -20°C until future use.

5.1.7 DNA Gel extraction

Linear DNA fragments of interest were purified from other DNA fragments and enzymatic reaction solutions by first separating the DNA on 1% TAE agarose gels by electrophoresis. Gels were stained with 0.1 µg/mL ethidium bromide in TAE buffer, and visualized under UV light. A scalpel was used to excises the desired DNA fragments, and these were transferred to pre-weighed 1.5 mL centrifuge tubes. The tubes were then reweighed to determine the mass of the gel, and the E.Z.N.A gel extraction kit (Omega Bio-Tek Inc., Norcross, GA) was used to isolate the DNA from the gel, as per manufacturer's instructions. DNA was typically eluted with 5 µL of elution buffer (Omega), and 55 µL of water pre-heated to ~50°C. Eluted DNA was quantified by UV spectrophotometry and stored at -20°C until future use.

5.2 qPCR

Quantitative PCR[328] was used to assess the relative transcript abundance of several *Lymnaea* genes and their splice variants. Some of this data is relevant to other projects not presented in the thesis; relevant qPCR data is presented in results chapters 2.2, 2.3, and 2.4

5.2.1 RNA extraction and DNase treatment

For whole animal experiments, RNA was extracted from *Lymnaea stagnalis* egg sacks containing embryos at 50-75% development and 100% near hatching (based on morphological embryonic development schedule put forward by Marois and Croll 1992[290] and Nagy and Elekes 2002[291]), and from entire juvenile and adult snails, where sexually immature juveniles have shell lengths of 1.0 to

1.5 cm, and reproduction-capable adults have shell lengths of 2.0 to 2.5 cm (according to McComb *et al*., 2005[292]). For isolation of specific *Lymnaea* organs, juvenile and adult animals were anesthetized with tank water chilled to ~10°C and containing 10% v/v Listerine (producing 2.69% ethanol and 0.0042% menthol), and dissected under a dissection microscope to remove the heart, central nervous system (CNS; a.k.a. central ring ganglia), the buccal musculature (buccal mass), the foot, and sexual secretory glands from the hermaphroditic snails (female albumen, male prostate). Upon dissection of each organ, they were immediately added to 1.5 mL tubes floating in liquid nitrogen. Like organs were isolated from 12 adults and 18 juvenile animals. RNA was then extracted, with Tri-Regent, as indicated above.

For DNase treatment, 10 μg of each RNA extract was micropipetted into separate 1.5 mL tubes and diluted to 100 ng/μL using DEPC-treated water (for a total volume of 100 μL). To each tube, 12 μL of 10x DNase buffer (Ambion® Life Technologies, Carlsbad, CA), 2 μL of RiboLock™ RNase inhibitor (Fermentas), and 2 μL of DNase I enzyme (Ambion) were added, and tubes were incubated at 37°C for 30 minutes. Samples were then phenol/chloroform treated (as above), and RNA was co-precipitated with 3 μL of glycogen (20 mg/mL RNA grade glycogen; Fermentas) by adding 300 μL of pure ethanol and incubating on ice for 10 minutes. Tubes were then centrifuged at 16000g at 4°C for 30 minutes, then supernatants were decanted and pellets washed with 500 μL of 70% ethanol in DEPC water. RNA pellets were resuspended with 50 μL of DEPC water, quantified by spectrophotometry, and 1 μg of each was run on a 1% agarose gel by electrophoresis. The gel was ethidium bromide-stained and visualized under UV light to asses RNA quality (Figure M1A).

5.2.2 cDNA synthesis

cDNAs were synthesized from the separate RNA extracts using an iScriptTM cDNA synthesis kit (Bio-Rad Laboratories, Hercules, CA). Briefly, each RNA extract was diluted to 80 ng/μL and 10 μL of each was added to separate 0.2 mL PCR tubes (kept chilled on ice as much as possible). A mastermix was prepared, containing a 2:3 ratio of 5x iScript RT supermix (Bio-Rad) and DEPC water, and 10 μL of this mixture was added to each 10 μL RNA sample. cDNA synthesis was carried out at 25°C for 5 minutes, 42°C for 30 minutes, and 85°C for 5 minutes in an Eppendorf Mastercycler ep Gradient S. 2.5 μL of each cDNAs were combined in a 0.2 mL PCR tube and 80 μL of DEPC water was added. This 1:5 dilution of pooled cDNA was then serially diluted by a factor of 5 (i.e. 1:25, 1:125; and 1:625) to be used for generating standard curves for each primer pair. For qPCR

experiments, 10 µL of each cDNA was separately diluted 20-fold by adding 190 µL of DEPC water, and all cDNA samples were stored at -80^{o}C.

5.2.3 qPCR

qPCR primers sets were designed to selectively amplify universal regions or specific splice variants of *Lymnaea* Ca_v3, NALCN, and $Ca_v\beta$ subunit cDNAs, and universal primer sets were designed for *Lymnaea* neuronal $\alpha_2\delta$, LCa_v1, and LCa_v2 (Table M2). For reference genes, primer sets were designed against *Lymnaea* actin, subunit A of the succinate dehydrogenase complex (SDHA), and hypoxanthine phosphoribosyltransferase 1 (HPRT1) (Table M2). Amplicons ranged from 102 to 145 bp. The specificity of PCR primers pairs was initially assessed by comparing the size of PCR products amplified from a pooled cDNA library (containing 1 µL of each cDNA from above), with those amplified from cloned cDNAs (Figure M1B). PCR primer efficiency for each primer set was then determined by generating relative standard curves using the 1:5 serial dilutions of pooled cDNA (1:5, 1:25, 1:125; and 1:625) as template for real time RT-PCR amplification. For each dilution, triplicate reactions were carried out in rigid 96-well PCR plates (Bio-Rad), with each well containing 0.5 µL of serially diluted cDNA, 5 µL of SsoFast^{TM} EvaGreen® Supermix (Bio-Rad), 0.5 µL of each 10 µM primer from a set, and 3 µL of water. PCR amplification, fluorescence reading, and melt curve analyses were done using a Bio-Rad C1000^{TM} Thermal Cycler equipped with a CFX96^{TM} Real-Time System and run by CFX Manager Software (Bio-Rad). Thermal parameters for PCR were 90^{o}C for 30 seconds followed by 40 cycles of 95^{o}C for 5 seconds and 56^{o}C for 5 seconds, with EvaGreen fluorescence readings taken between each cycle (SYBR setting on the CFX96^{TM} Real-Time System). For each primer set, triplicate cycle thresholds (CTs) corresponding to each of the cDNA dilutions, were plotted against the log of their corresponding cDNA concentrations, and the Bio-Rad CFX Manager Software was used to generate linear regressions through the dilution series providing goodness of fit (R^2) and slope values, the former of which measures the precision of the standard curve and the latter of which is used to determine the PCR amplification efficiency of each primer set (E values)[329]. All primers were found to have E values ranging between 86 to 110%, deeming them suitable for qPCR[329] (Table M2). Following qPCR, melt curve analysis was done by raising the temperature of each sample from 65 to 95^{o}C in 0.5^{o} increments, to gradually denature the PCR products and disrupt EvaGreen dye fluorescence, measured between temperature elevations. Plots of the first derivative for each melt curve (i.e. derivative of fluorescence intensity vs. holding

temperature) produced single peaks, indicative of single DNA product amplification for all primer sets[329] (not shown).

Quantitative PCR reactions were prepared as master mixes containing all ingredients except the template cDNA, and done in quadruplicate 10 µL reactions, each with a final volume of 5 µL of SsoFast™ EvaGreen® Supermix (Bio-Rad), 0.5 µL of each 10 µM primer from a set, 3 µL of water, and 1 µL of template cDNA (diluted 1/20 in DEPC water). For negative controls, 1 µL of corresponding DNase-treated RNA (diluted to 2 ng/µL) was used instead of cDNA, and for no template controls, 1 µL of DEPC water was used. To standardize between plates, triplicate qPCR reactions using HPRT1 primers and 1:5 diluted pooled cDNA as template were done on each plate. All CT values used for analysis were determined relative to the average CT of the HPRT1 controls from each plate. Thermal parameters for qPCR were 90°C for 30 seconds followed by 40 cycles of 95°C for 5 seconds and 56°C for 5 seconds, with fluorescence readings between cycles. Following PCR, a single peak was confirmed for all melt curves, indicative of single DNA product amplification. CT values determined using the CFX Manager Software were imported into Microsoft Excel for analysis.

5.2.4 Analysis

The CT values for the HPRT1 gene were found to produce the lowest stability value (i.e. 0.098) using NormFinder software[330], that quantifies the degree of fluctuation in CT values between the various qPCR samples (i.e. *Lymnaea* developmental stages and tissues), indicating its suitability as a reference gene. Conversely, actin and less so SDHA CT values varied considerably between tissues (stability values of 0.634 and 0.296, respectively), and thus were not used as reference genes. To quantify relative expression levels of genes/splice isoforms of interest relative to HPRT1, data was analyzed using the ratio[331]: $(E_{\text{target gene}})^{\Delta CT\text{target gene}}/(E_{HPRT1})^{\Delta CTHPRT1}$.

5.3 Semi-quantitative RT-PCR

Semi-quantitative RT-PCR was used to assess the transcript abundance in adult central nervous system RNA of several *Lymnaea* genes. The data is presented in chapter 2.1.

5.3.1 RNA extraction and DNase treatment

Total RNA was extracted from 6 adult central ring ganglia with Tri-Reagent (Sigma-Aldrich) and quantified (as indicated above). An aliquot of 14 µg was transferred into a 1.5 mL centrifuge tube and combined with 15 µL of 10x DNase buffer (Fermentas), 2 µL of RiboLock™ RNase inhibitor

(Fermentas), 10 μL of RNase-free DNase I (Fermentas), and DEPC water to 150 μL. The tube was incubated at 37°C for 30 minutes, and 10 μL of 25 mM EDTA (Fermentas) was added to stop the reaction. 50 μL of water was then added to the tube, and the sample was vortexed with 200 μL of phenol/chloroform, centrifuged at room temperature at 21000g for 6 minutes, and the supernatant RNA precipitated with 2 μL of RNA grade glycogen (Fermentas) and 400 μL of pure ethanol. The tube was incubated on ice for 10 minutes then centrifuged at 16000g for 35 minutes at 4°C to pellet the RNA/glycogen precipitate, which was then washed with 500 μL of 70% ethanol, briefly air-dried, resuspended with 25 μL of DEPC water, and quantified by spectrophotometry. 1 μg was electrophoresed and visualized on an ethidium bromide-stained 1% agarose gel under UV light to assess the quality of the extracted RNA (Figure M1C).

5.3.2 Semi quantitative RT-PCR and analysis

Complementary DNAs were synthesized from RNA using either oligo(dT_{18}) or random hexamer primers (Table M3) and Superscript III reverse transcriptase (Invitrogen), as indicated above. Negative controls were prepared for each RNA extract that were identical but reverse transcriptase was substituted with water. Primers used for PCR amplification of cDNA were designed to have similar melting temperatures, minimal secondary structure, and to amplify fragments between 500 to 600 bp. Primers spanned sequences from the following genes: *Lymnaea actin*, *LNALCN*, *LCa_v1*, *LCa_v2*, and *LCa_v3* (Table M3). PCR products were generated with Taq DNA polymerase (Fermentas) using typical reaction conditions (see above), but with an extension time of 8 minutes, and only 25 cycles rather than 32 to prevent consumption of limiting reagents. PCR samples were then electrophoresed on a 1% gel, which was ethidium bromide-stained and visualized under UV light. Densinometric analysis of DNA band intensity was performed using AlphaEase® FC software (Alpha Innotech).

5.4 General cloning methods

5.4.1 Restriction digests

Most enzymes used for restriction digest of DNA were obtained from New England Biolabs (NEB, Ipswich, MA). The volumes for digestions were varied depending on the amount of DNA. For cloning purposes, plasmid DNA or gel-purified DNA from a previous enzymatic reaction were digested in total volumes of 80 μL, with 8 μL of appropriate 10x NEB buffer, 8 μL of 10x bovine serum albumin (BSA; if required), 8 μL of total enzyme (the volume of each enzyme depended on the

number of enzymes used in the digest), the source DNA, and water to 80 µL. Reactions were carried out in 0.2 mL PCR tubes at 37^{o}C in an incubator for 3 to 4 hours.

5.4.2 Ligations

Ligation of linear DNA for generating recombinant plasmids was done using T4 DNA ligase (Fermentas). Typically, 100 ng of vector DNA was included in each ligation, and the amount of insert was varied at molecular ratios of 1:1, 1:3, 1:5, and 1:0, the latter being a no insert control for assessing the abundance of unwanted plasmid products (100 ng of vector x size of insert/size of vector = x ng of insert DNA). Preferably, reactions were carried out in 10 µL total volumes, unless the source cDNA was too dilute in which case the volume was scaled up to 25 µL. Regardless of volume, 1 µL of T4 DNA ligase was added per ligation reaction; therefore for 10 µL reactions, 1 µL of T4 DNA ligase, 1 µL of 10x T4 buffer, vector and insert DNA at given molecular ratios, and water to 10 µL were combined in separate PCR tubes on ice. Tubes were thoroughly pipetted and ligation was done using a ramp protocol (16^{o}C for 6.5 hours, then drop 1^{o}C every 30 minutes until 4^{o}C) in an Eppendorf Mastercycler up Gradient S. Before transformation into bacteria, ligations were typically diluted to 200 µL with water, vortexed with 200 µL of phenol/chloroform, centrifuged, and the ligated DNA was co-precipitated with 3 µL of glycogen (Fermentas) by adding 20 µL of 3 M sodium acetate pH 5.2 and 440 µL of pure ethanol. Tubes were vortexed, incubated on ice for 10 minutes, and centrifuged at 16000g for 12 minutes at 4^{o}C. Pellets were then washed with 500 µL of 70% ethanol, briefly air-dried, and resuspended with 10 µL of water.

5.4.3 Bacterial transformations

The four main types of *E. coli* derivative bacteria used for general cloning purposes were heat shock-competent DH5α (Invitrogen), heat shock-competent Stbl2 (Invitrogen), electrocompetent Stbl4 (Invitrogen), and electrocompetent CopyCutter^{TM} cells (Epicenter Biotechnologies, Madison, WI). For working with pIRES2 clones of LNALCN, LCa_v1, and LCa_v2, Stbl2 were the preferred cell type. For pIRES2 clones of LCa_v3, Stbl2 and Stbl4 were sometimes used, however CopyCutter^{TM} cells, which maintain a low copy number of transformed plasmids, were preferred due to the toxicity of the LCa_v3 insert. In fact, some splice isoforms of LCa_v3 in pIRES2-EGFP do not grow at all in Stbl2 or Stbl4, and in many cases, LCa_v3 plasmids tend to recombine regardless of cell type. Transformations were done according to manufacturer's instructions, with some modifications. For Stbl2 cells, 50 µL of cells were incubated with 2 to 3 µL of plasmid DNA on ice for 10 minutes. Cells were then heat

shocked for 30 seconds on an Eppendorf Mastercycler ep Gradient S set to 42°C, transferred to ice for 1 minute, then pipetted into a 1.5 mL centrifuge tube containing 1 mL of superbroth (SB; 3.2% tryptone w/v, 2% yeast extract w/v, and 0.5% NaCl w/v). Tubes were incubated at 30°C for 1.5 hours while gently rotating, centrifuged at 4000g at room temperature for 4 minutes, and most of the supernatant was removed with a micropipette leaving only ~100 µL of SB. The pelleted cells were then thoroughly resuspended with a micropipette in the remaining media and plated onto Luria-Bertani plates (LB; 1% tryptone w/v, 0.5% yeast extract w/v, 1% NaCl w/v, and 1.5% agar w/v) containing the appropriate antibiotic (typically 100 µg/mL ampicillin or 50 µg/mL kanamycin sulfate; EMD Millipore, Billerica, MA). Cells were incubated at 30°C until colonies appeared 1 to 3 days later, depending on the plasmid. Heat shock of DH5α cells was similar to Stbl2, with some minor differences. First, heat shock was performed for 1.5 minutes, second, the incubation in SB after heat shock was done at 37°C for 1 hour, and third, the LB plates were incubated at 37°C overnight.

For electroporation, 20 µL of electrocompetent cells were pipetted into 0.2 mL PCR tubes on ice, to which 1 to 2 µL of plasmid DNA was added using a cold micropipette tip. Cells were incubated on ice for 10 minutes, then transferred to pre-chilled (-20°C) 90 µL electroporation cuvettes (VWR, Radnor, PA) and quickly electroporated using an Eppendorf Electroporator 2510 set to 1200 volts. Electroporated cells were then quickly mixed with 1 mL of SB while still in the cuvette, and pipetted into 1.5 mL centrifuge tubes. Stbl4 cells were incubated and plated in a similar manner as indicated for Stbl2 above, while CopyCutter™ cells were incubated at 37°C for 1 hour after electroporation, and LB plates were incubated at 37°C for 1 to 2 nights until colonies appeared (depending on transformed plasmids).

5.4.4 Culturing bacteria and alkaline lysis plasmid isolation

For small-scale plasmid isolation, bacterial colonies were inoculated into 10 mL of SB containing the appropriate antibiotic. Stbl2 and Stbl4 cells were cultured at 30°C, and DH5α and CopyCutter™ cells at 37°C, in a bacterial incubator with shaking at ~300 RPM. Once cultures reached considerable growth densities (optical density > 3 at 600 nm), plasmids were isolated by alkaline lysis[332]. Briefly, 2 mL aliquots of each 10 mL culture were pipetted into separate 2 mL centrifuge tubes, and these were centrifuged at 4000g at 4°C for 3 minutes. The media was decanted and bacterial pelleting was repeated up to 4 more times to generate large bacterial pellets corresponding to each culture. Cells were then resuspended with 270 µL of solution I (50 mM dextrose, 10 mM EDTA, and 25 mM Tris pH 8.0), and 540 µL of solution II was added to lyse the cells (1% SDS w/v, 0.2 N NaOH), and tubes

were gently inverted to ensure complete lysis. 405 μL of cold solution III (-20°C; 3 M potassium acetate, 11.45% v/v glacial acetic acid) was then added to each tube, and these were gently inverted to ensure complete mixing, incubated on ice for 10 minutes, and centrifuged at 16000g for 10 min at 4°C to remove genomic DNA aggregated to precipitated SDS and other cellular debris. The supernatants were transferred to new 2 mL centrifuge tubes, to which 800 μL of 2-propanol was added to precipitate nucleic acids (i.e. plasmids and RNA). Tubes were incubated on ice for 10 minutes, then centrifuged at 16000g at 4°C for 12 minutes, then the supernatant was decanted and the nucleic acid pellets resuspended in 400 μL of water. To precipitate RNA, 400 μL of 5 M LiCl (at -20°C), was added to each tube, and tubes were incubated on ice for 10 minutes. RNA was removed by centrifugation at 16000g at 4°C for 10 minutes, then the supernatants were transferred to new 1.5 mL centrifuge tubes and combined with 500 μL of 2-propanol. Precipitated plasmids were isolated by centrifugation for 10 minutes at 4°C at 16000g, then the 2-propanol was decanted and pellets were washed with 500 μL of 70% ethanol. Plasmid pellets were then air-dried and resuspended in 400 μL of water. RNase A (BioShop) was then added to each tube at a final concentration of 20 μg/mL and tubes were incubated at 37°C for 30 minutes. Following RNase treatment, plasmid DNA was vortexed with 400 μL of phenol/chloroform, tubes were centrifuged at room temperature for 6 minutes at 21000g, then supernatants were micropipetted into new 1.5 mL tubes. The phenol/chloroform treatment was repeated until the no white precipitate was visible in the interface between the aqueous and organic phases, after which a pure chloroform treatment was done to remove phenol. The aqueous supernatants were then transferred to new 1.5 mL centrifuge tubes and plasmid DNA was precipitated by adding 21 μL of 10 M ammonium acetate and 840 μL of pure ethanol. Tubes were incubated on ice for >10 minutes, and centrifuged at 16000g at 4°C for 16 minutes. Plasmid DNA pellets were washed with 700 μL of 70% ethanol, air-dried, and resuspended with 100 to 200 μL of water. Plasmids were then quantified by UV spectrophotometry, and diagnostic restriction digests were typically carried out with 1 μg aliquots of plasmid DNA per digestion.

A similar methodology was done for large-scale plasmid preps, with some differences. Bacterial colonies were grown in 250 mL of SB in Erlenmeyer flasks, and after growth cells were centrifuged in 250 mL polypropylene wide mouth bottles (Beckman Coulter, Brea, CA) at 4000g at 4°C in an Allegra™ 25R centrifuge (Beckman Coulter) equipped with a TA-10-250 rotor. The media was decanted and the cells resuspended with 6 mL of solution I, lysed with 12 mL of solution II, and neutralized with 9 mL of cold solution III. Bottles were then centrifuged at 7000g at 4°C for 10 minutes, then the supernatants were decanted into 50 mL conical centrifuge tubes and combined with

17 mL of 2-propanol. Precipitated nucleic acids were pelleted by centrifugation using at TA-14-50 rotor at 4°C 7000g for 10 minutes, then propanol was decanted and nucleic acids resuspended with 3 mL of water and transferred to 15 mL glass centrifuge tubes (Kimble Chase, Vineland, NJ). RNA was then precipitated with 3 mL of cold 3 M LiCl, and tubes were incubated on ice for 10 minutes then centrifuged at 7000g in the TA-14-50 rotor containing rotor adaptors for 15 mL tubes. Supernatants were then transferred to new 15 mL tubes and plasmids precipitated by addition of 4 mL of 2-propanol, where tubes were incubated on ice for 10 minutes, centrifuged at 7000g at 4°C for 10 minutes. The supernatant was decanted, and plasmid pellets were each resuspended with 400 µL of water containing 20 µg/mL of RNase A (BioShop) and transferred to separate 1.5 mL centrifuge tubes. Tubes were incubated at 37°C for 30 minutes then plasmids were precipitated by adding 400 µL of 26% w/v polyethylene glycol in 1.6 M NaCl, and incubating tubes on ice for 20 minutes. Tubes were then centrifuged at 16000g 4°C for 30 minutes, then the supernatants were decanted and the DNA pellets washed with 500 µL of 70% ethanol. DNA was briefly air-dried and resuspended in 400 µL of water. The remaining steps of phenol/chloroform purification and ammonium acetate precipitation were the same as for the small scale isolation described above.

5.5 Sequencing and cloning of the LCa_v3 channel cDNA

The initial sequencing and cloning is presented in results section 2.1, and additional LCa_v3 constructs are presented in results sections 2.2 and 2.3.

5.5.1 Preliminary sequencing

A partial preliminary sequence for LCa_v3 (5991 base pairs), missing a large part of the N-terminal coding sequence, was previously determined and submitted to GenBank with accession number AF484084. The remaining coding sequence (2838 bp) was determined by PCR-screening of *Lymnaea stagnalis* central nervous system λZAP cDNA libraries[333] using Taq DNA polymerase (see above for general PCR conditions; 8 minute extensions). For the first round of PCR screening, λZAP vector-specific primer T77 was used along with LCa_v3 D2B primer (Table M1), which amplified a ~1000 base pair fragment. The amplified cDNA was cloned into the pGEM®-T Easy vector according to manufacturer's instructions (Promega, Madison, WI), and the plasmid was isolated by alkaline lysis and the insert sequenced with an 3130XL automated DNA sequencer (Applied Biosystems, Foster City, CA), providing 712 base pairs of novel N-terminal sequence. Nested primers were then designed using the novel sequence (LCa_v3 D1 Rev and LCa_v3 D1 Rev Nested; Table M1), and these were paired with nested primers complementary to one side of the λZAP cDNA vector (i.e. EV3 and

T33; Table M1) for further PCR screening of λZAP cDNA to complete the full length sequencing of LCa_v3. The primary PCR reactions therefore consisted of LCa_v3 D1 Rev with EV3 primer pairs, and the secondary PCR reactions consisted of LCa_v3 D1 Rev Nested with T33. The PCR produced a 2000 base pair fragment that was cloned into pGEM®-T Easy and sequenced. The novel sequence contained the putative translation initiation site for LCa_v3, which was confirmed based on homology with an expressed sequence tag from the Ca_v3 channel of marine snail *Aplysia californica* (GenBank accession number EB302921), containing a clear translation start site. The full length 9031-bp cDNA sequence of LCa_v3 was deposited to GenBank, replacing the previous accession AF484084.

5.5.2 Consensus sequencing

The consensus sequence of the full LCa_v3 open reading frame was determined by overlaying the sequence of a minimum of 3 independent DNA sequences spanning the entire coding sequence. For this, the LCa_v3 coding sequence was subdivided into 4 sections, and nested primers were designed to amplify these fragments with small overlaps between them (LCa_v3 R1 to R4; Table M1). Complementary DNA was then PCR-amplified from a combination of λZAP cDNA and freshly reverse-transcribed CNS RNA (see above). Amplified fragments were cloned into pGEM®-T Easy and sequenced, and sequences analyzed with Sequencher™ 4.10.1 software (Gene Codes Corporation, Ann Arbor, MI). Multiple alternative splicing isoforms were identified for LCa_v3 during consensus sequencing, including those presented in results chapters 2.2 and 2.3.

5.5.3 Cloning into pIRES2-EGFP

The four cloned fragments used for consensus sequencing above were used to assemble the full length LCa_v3 coding sequence into bicistronic mammalian expression vector pIRES2-EGFP (Clontech Laboratories, Mountain View, CA; Figure M2). Primers flanking the four regions were designed to contain either native or recombinant restriction endonuclease sites that would permit assembly into the pIRES2-EGFP vector by ligation. Briefly, the nested 5' primer, for the most N-terminal fragment of LCa_v3 (LCa_v3 R1 5' 2), contained a recombinant *Xho*I restriction enzyme site and a Kozak consensus sequence, followed by the LCa_v3 translation start site. The corresponding nested 3' primer for this fragment (LCa_v3 R1 3'2), contained a native *Spe*I site (Table M1). The nested 5' and 3' primers for the second fragment contained native *Spe*I and a *Sal*I sites, respectively (LCa_v3 R2 5'2, LCa_v3 R2 3'2; Table M1). The 5' primer for the third fragment contained a native *Sal*I site (LCa_v3 R3 5'2), and the 3' primer was designed to incorporate a recombinant *Mlu*I site that did not alter the amino acid coding sequence (LCa_v3 R3 3'2; Table M1). Finally, the 5' primer for the fourth fragment

incorporated the recombinant *Mlu*I site (LCa_v3 R4 5'2), and the 3' primer incorporated a recombinant *BamH*I site just downstream of the stop codon (LCa_v3 R4 3'2; Table M1). The four fragments (numbered by cDNA sequence positions along GenBank accession AF484084: *Xho*I-*Spe*I 209–2865; *Spe*I-*Sal*I 2812–4544; *Sal*I-*Mlu*I 4503–6874; and *Mlu*I-*BamH*I 6850–8869) were sequentially ligated into pIRES2-EGFP2. Before assembly, site directed mutagenesis using the QuikChange protocol (Stratagene, see above) was used to create silent mutations in a region of the third fragment of LCa_v3, thought to be toxic to bacteria due to instability of this particular pGEM® subclone in bacteria and frequent recombination at this locus (LCa_v3 R3 QC 5', LCa_v3 R3 QC 3'; Table M1). The final full length clone was diagnosed by restriction endonuclease digestion (Figure M3).

5.6 Cloning splice isoforms and HA-tagged versions of LCa_v3

The original clone of LCa_v3 in pIRES2-EGFP from above contained exon 8b in the I-II linker, exon 12B in the domain II P-loop, and lacked exon 25c in the III-IV linker (+8b/12B/-25c; summary figure). This clone was used to derive all splice variant clones.

5.6.1 Minus exon 8b and ΔAPRASPE variants

To create the minus exon 8b variant of LCa_v3, a *Bgl*II site present in the pIRES2-EGFP vector just upstream of the LCav3 coding sequence was first removed by linearizing the clone with *Nhe*I and *Xho*I restriction endonucleases, and inserting an annealed oligonucleotide adaptor with compatible *Nhe*I and *Xho*I restriction site overhangs but lacking the *Bgl*II site and incorporating a new *Age*I site (Table M4; Figure M4A). A *Bgl*II to *Sal*I fragment was then excised from the full length LCa_v3 clone (containing exon 8b) and inserted into a circularized pGEM®-T Easy vector (Promega) that had been modified by insertion of annealed oligonucleotides (Table M4; Figure M4B) into *Nco*I and *Mlu*I sites of the vector to introduce a *Bgl*II site. Removal of the exon 8b coding sequence was achieved by doing PCR (with high fidelity PfuTurbo® AD DNA polymerase; Stratagene), using the entire subclone as template and primers flanking exon 8b whose 3' ends were directed away from the optional exon such that PCR amplification would produce a linear plasmid lacking 8b (Table M4). 5' phosphate groups on the primers enabled blunt-end ligation and re-circularization of the PCR product, which was then transformed into Stbl2 bacteria (Invitrogen) for plasmid isolation. After confirmation of sequence, the -8b *Bgl*II to *Sal*I DNA fragment was re-inserted into the full-length LCa_v3 clone to produce the -8b/12B/-25c variant.

The ΔAPRASPE LCa_v3 clone was created in a similar manner as for -8b above, with primers containing 5' phosphates that removed the coding sequence for APRASPEQSD from the *Bgl*II to *Sal*I subclone by PCR (Table M4). The resulting mutant *Bgl*II-*Sal*I DNA was cloned back into the full-length LCa_v3 +8b/12B/-25c clone to create LCa_v3 +8b(ΔAPRASPE)/12B/-25c.

5.6.2 Exon 25c splice variants

To add the exon 25c sequence to the LCa_v3 clone, a *Sal*I to *Mlu*I fragment of the original full length clone was inserted into circularized pGEM®-T Easy (Promega). This subclone was used as template for two rounds of PCR, with 3' primers designed to introduce the exon 25c coding sequence followed by an *Apa*I restriction site present in LCa_v3 just downstream of the exon 25c splice site (i.e. first round with primers LCa_v3 +25c 5' and LCa_v3 +25c 3'1, second with LCa_v3 +25c 5' and LCa_v3 +25c 3'2; Table M4; Figure M5A). The PCR product, containing the additional exon 25c sequence, was then cloned back into the *Mlu*I-*Sal*I subclone via *Apa*I, present in both the pGEM® vector and the LCa_v3 coding sequence, and the resulting product was sequenced. This modified *Sal*I to *Mlu*I cDNA was then cloned back into the full-length LCa_v3 +8b/12B/-25c and -8b/12B/-25c pIRES2-EGFP clones, to create LCa_v3 +8b/12B/+25c and LCa_v3 -8b/12B/+25c in pIRES2-EGFP, respectively.

5.6.3 Exon 12 splice variants

Using the full length clone of LCa_v3 in pIRES2 (+8b/12B/-25c) as template, two separate high-fidelity PCR reactions were used to amplify a *Spe*I to *Sal*I region of the LCa_v3 coding sequence in two separate fragments, flanking exon 12B sequence. The first fragment was amplified with primers LCa_v3 R2 5'1 (Table M1) and several overlapping 3' primers designed to extend the 3' end of the LCa_v3 sequence to replace part of the exon 12B coding sequence with that of 12A (LCa_v3 12A F1 3'1, LCa_v3 12A F1 3'2, and LCa_v3 12A F1 3'3; Table M4). The second fragment was amplified with a 5' primer designed to overlap with the 3' end of the first PCR product, adding the remainder of the exon 12A coding sequence to the 5' end (LCa_v3 12A F2 5'; Table M4), and LCa_v3 R2 3'1 as the 3' primer (Table M1). The PCR reactions for both fragments were done using standard conditions with PfuTurbo® DNA polymerase AD (Stratagene), however, only 0.5 µL of primers LCa_v3 12A F1 3'1 and LCa_v3 12A F1 3'2 were added for amplification of first fragment, along with 1.5 µL of LCa_v3 R2 5'1 and LCa_v3 12A F1 3'3. The two PCR-amplified DNA products were then gel-purified, quantified by UV spectrophotometry, and 100 ng of each was used for an assembly PCR with primers LCa_v3 R2 5'2 and LCa_v3 R2 3'2, producing a single DNA product flanked by *Spe*I and *Sal*I restriction sites and

containing the exon 12A coding sequence (Figure M5B). This product was gel purified and cloned into the LCa_v3 *Bgl*II to *Sal*I subclone via *Spe*I and *Sal*I and the resulting subclone was sequenced. The modified *Bgl*II to *Sal*I fragment containing exon 25c was then cloned into the full length LCa_v3 clone (+8b/12B/-25c) producing LCa_v3 +8b/12A/-25c in pIRES2-EGFP.

5.6.4 HA-tagged channels

Hemagglutinin tag (HA) epitopes (YPYDVPDYA) were introduced into the domain I P-loop of LCa_v3, upstream of the selectivity filter, via a *Bgl*II site present in the LCav3 coding sequence. Briefly, full length LCa_v3 pIRES2-EGFP clones were linearized with *Bgl*II, and a double-stranded oligonucleotide adaptor, encoding the HA epitope and containing single stranded overhangs compatible with *Bgl*II (Table M4), was ligated into the full length clones to produce all four possible exon 8b and 25c HA-tagged variants (i.e. +8b/12B/-25c-HA, -8b/12B/-25c-HA, +8b/12B/+25c-HA, and -8b/12B/-25c-HA) (Figure M4C).

5.7 Southern blotting of LCa_v3

For Southern blotting[334] to determine the gene copy number of LCa_v3 (results chapter 2.1), 15 µg aliquots of extracted *Lymnaea* genomic DNA were digested with *EcoR*V, *Hind*III, *EcoR*I, and *Xho*I (NEB) and separated by electrophoresis through a 1% agarose gel. The gel was then submerged in 0.5 M NaOH with 1.5 M NaCl twice for 15 minutes to shear the large genomic DNA molecules, then the gel was rinsed with water and submerged for two 15 minute intervals in neutralization solution (3 M NaCl, 0.5 M Tris pH 7.5). DNA transfer onto positively charged nylon membranes (Roche Applied Science, Basel, Switzerland) was achieved by standard methods using 20 x SSC (3 M NaCl, 30 mM sodium citrate pH 7.0) as the transfer solution[335], and fixed by UV-crosslinking using a UVC 500 Ultraviolet Crosslinker (Hoefer, Holliston, MA).

A dNTP mixture containing 2 mM dATP, 2 mM dGTP, 2 mM dCTP, 1.7 mM dTTP (Fermentas) and 0.3 mM digoxigenin-11-2'-deoxy-uridine-5'-triphosphate (DIG-11-dUTP; Roche) was used to PCR amplify a 597 bp region of the LCa_v3 coding sequence using primers LCa_v3 probe 5' and LCa_v3 probe 3' (Table M5) with Taq DNA polymerase (Fermentas), and the resulting DIG-labeled probe was gel purified and added to 20 mL of EasyHyb solution (Roche), which was syringe-filtered through a 0.45 µM filter (Millipore, Billerica, MA). The nylon membrane containing the transferred digested genomic DNA was prehybridized in a hybridization tube containing 20 mL of EasyHyb solution at 32.5°C for 2 hours, then hybridization was carried out O/N at 32.5°C with the probe

solution. Following hybridization, the nylon membrane was washed twice for 5 minutes at 55°C with 20 mL of 2x wash solution (2x SSC, 0.1% w/v SDS), then two more times for 15 minutes at 56°C with 20 mL of 0.5x wash solution (0.5x SSC, 0.1% w/v SDS). The membrane was equilibrated with 20 mL of wash buffer (150 mM NaCl, 0.3% v/v TWEEN-20, 100 mM maleic acid pH 7.5) for 1 minute and blocked with 7.5 mL of blocking solution (150mM NaCl, 1% w/v blocking reagent (Roche), and 100 mM maleic acid pH 7.5) for 1 hour at room temperature. The blocking solution was decanted and 7.5 mL of blocking solution containing 1.5 µL of sheep anti-digoxigenin alkaline phosphatase conjugated antibody (Roche) was added to the tube at dilution of 1:5000, and the tube was incubated for 30 minutes at room temperature to allow the antibody to bind to the DIG-labeled probe. The membrane was then washed twice with 80 mL of wash buffer and subsequently equilibrated in 20 mL of detection buffer (0.1 M NaCl, 0.1 M Tris pH 9.5) for 2 minutes. The color substrate solution (10 mL detection buffer, 45 µL of NBT, and 35 µL of BCIP (Roche)) was applied to the membrane and colorimetric detection was carried out for 3 hours at room temperature in the dark. Once developed, the membranes were washed with water and scanned.

5.8 Sequencing the I-II linker and III-IV linker introns of the LCa_v3 gene

To assess whether the splicing of LCa_v3 transcripts in the I-II and III-IV linker coding sequences resembles that of mammalian $Ca_v3.1$ and $Ca_v3.2$ (results chapter 2.2), the genomic DNA sequences corresponding to these regions of the LCa_v3 gene were sequenced. Briefly, genomic DNA was isolated from adult animals ground in liquid nitrogen (see above), and this was used as template for nested PCRs with primers flanking respective intron splice sites (Table M5). PCR reactions were carried out using high fidelity PfuTurbo® DNA polymerase AD (Stratagene), and amplified DNA was electrophoresed, gel purified, and subject to direct sequencing.

Table M1. Primers used for cDNA synthesis and for sequencing and cloning of LCa_v3 +8b/12B/-25c into pIRES2-EGFP.

Application	Name	Sequence
cDNA synthesis		
	Oligo dT	TTTTTTTTTTTTTTTTT
	Random hexamer	NNNNNN
N-terminal sequencing		
	LCa_v3 D2B	GCTACATCAGCAATGGATTCAATGTG
	T77	GTAATACGACTCACTATAGGGCGA
	LCa_v3 D1 Rev	GGAATTGCTGGCTAATGTACTGC
	LCa_v3 D1 Rev Nested	GCTAATGTACTGCAAGACTGAAACC
	EV2	CGCCAGGGTTTTCCCAGTCACGAC
	EV3	AGCGGATAACAATTTCACACAGGA
	T33	AATTAACCCTCACTAAAGGGAAC
Consensus sequencing and cloning of LCa_v3 +8b/12B/-25c		
	LCa_v3 R1 5' 1	AGATACAATGCAACCTGGACGCTAAG
	LCa_v3 R1 5' 2	CACGTACTCGAGCCACCATGGCTGAAGAGTCTAG
	LCa_v3 R1 3' 1	CTTGATCTCATTGATACGCCAGACTC
	LCa_v3 R1 3' 2	ATTGATACGCCAGACTCATCTTTACTAGTC
	LCa_v3 R2 5' 1	GCTGGTGGCGACACTTTGGACTC
	LCa_v3 R2 5' 2	CGACACTTTGGACTCAGAATTAGAGACTAG
	LCa_v3 R2 3' 1	CCAAAGAATTTAAAGTACGATGGCTTGTAAAAG
	LCa_v3 R2 3' 2	GGCTTGTAAAAGAATTCTGTCGACTGAGC
	LCa_v3 R3 5' 1	CGGCAGTGGCAGGAGTATTTGCAAC
	LCa_v3 R3 5' 2	GCAACTCATTTGAGCTCAGTCGACAG
	LCa_v3 R3 3' 1	TATCCATTGAAGACCAAGAGGACCCCATG
	LCa_v3 R3 3' 2	TAGTGTCAATGACGCGTTCACAGGAG
	LCa_v3 R4 5' 1	GAGGATGCCACAGGTATGTCTCCTGTG
	LCa_v3 R4 5' 2	TCCTGTGAACGCGTCATTGACACTAG
	LCa_v3 R4 3' 1	AGATTGAAGCCCAACATGAGACAACTAAAC
	LCa_v3 R4 3' 2	GGGCGGGGATCCTCATAACTTGTCATCTGGATC
	LCa_v3 R3 QC 5'	CTCCGTCCTATTGGCAACATTGTACTCATCTGCTGCACATTCTTCATCATTTTTGGTATTC
	LCa_v3 R3 QC 3'	GAATACCAAAAATGATGAAGAATGTGCAGCAGATGAGTACAATGTTGCCAATAGGACGGAG

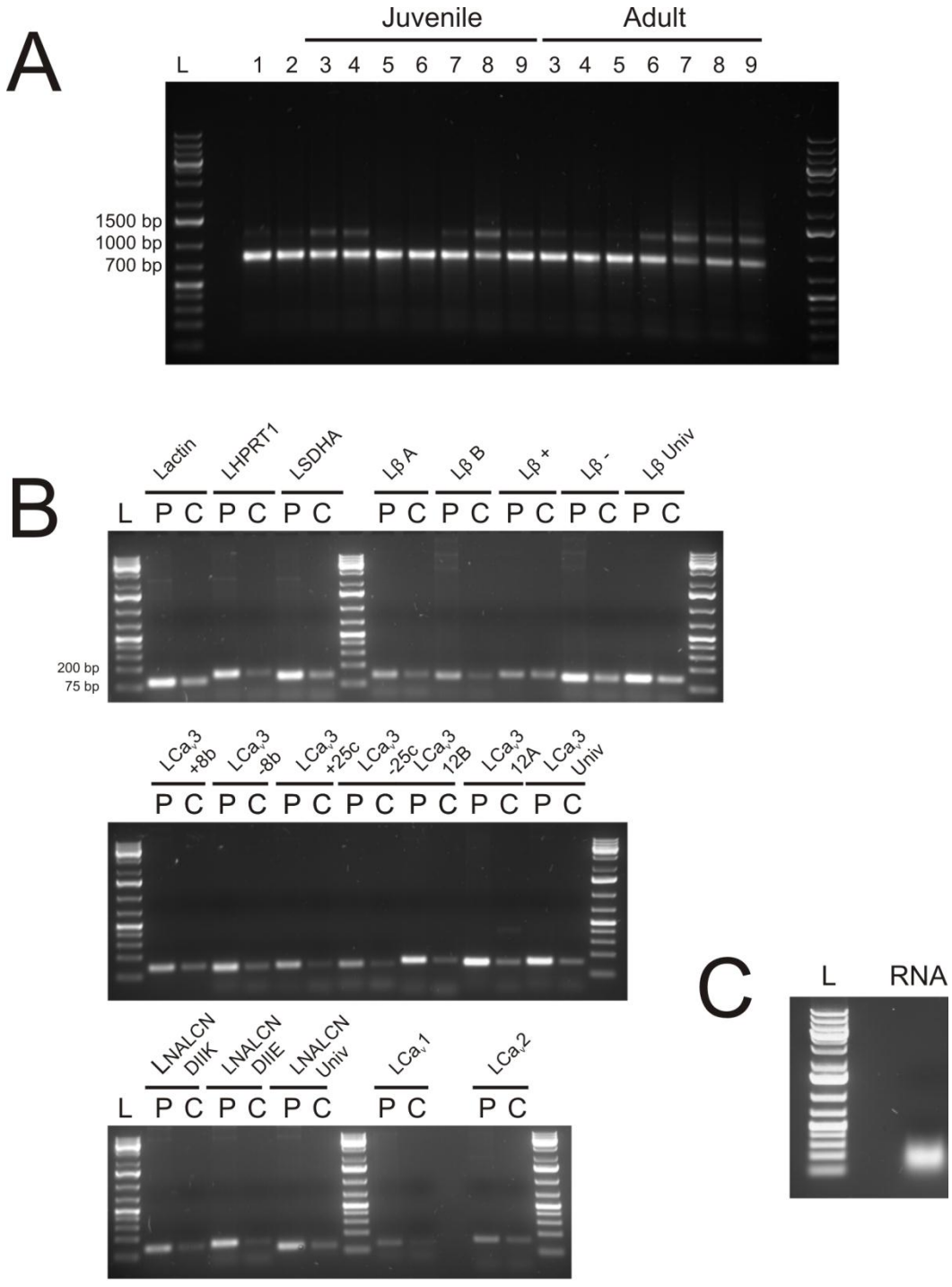

Figure M1. Images of ethidium bromide-stained agarose gels used for quantitative PCR experiments. A) 1 µg of each DNase-treated total RNA extract was electrophoresed through a 1% agarose gel to assess quality. L: Fermentas 1kb DNA ladder Plus; 1) 50-75% whole embryos, 2) 100% whole embryos, 3) juvenile whole animals, 4) adult whole animals, 5) central nervous system, 6) heart, 7) buccal mass, 8) foot, 9) prostate gland, and 10) albumen gland. **B)** PCR with Taq DNA polymerase, using either control cDNA cloned into plasmids (P) or pooled *Lymnaea* cDNA library (C) was used to assess whether primers amplified single DNA products from the cDNA library. **C)** 20 µg of DNase-treated total RNA extracted from adult central nervous system used for semi-quantitative RT-PCR (with Fermentas 1kb DNA ladder plus).

Table M2. Primers used for qPCR of several *Lymnaea* genes and gene splice isoforms.

Real time RT primers:		GenBank Accession	Ampl. Length	length	Tm (NN)	GC%	qPCR E	R2	Slope
Lymnaea actin 5'	CTCACCGACTACCTGATGAAGAT	DQ206431	102	23	55.16	48	92.9	0.998	-3.504
Lymnaea actin 3'	GTAGCAGAGCTTCTCCTTGATGTC			24	57.48	50			
Lymnaea HPRT1 5'	TGTAGAAGACATCATTGACACTGG	ES578163.1	145	24	53.86	42	90.4	0.985	-3.576
Lymnaea HPRT1 3'	GCCAATATAATCTGGTGCGTAAC			23	53.06	43			
Lymnaea SDHA 5'	GCTTCAAAGCTGCCTGTATAACTA	ES571571.1	122	24	55.74	42	93.9	0.997	-3.478
Lymnaea SDHA 3'	ATAGAAGTGGTACTGCCAGTGGT			23	55.07	48			
LCa_v1 5'	CCTCATCATCATTGGCTCATT	AF484079	119	21	51.41	43	99.1	0.990	-3.347
LCa_v1 3'	TCTCTCTCAGTTTCTGGAAGTCAC			24	55.56	46			
LCa_v2 5'	TCTCGATGAATATGTTAGGGTCTG	AF484082	142	24	54.1	42	107.9	0.982	-3.147
LCa_v2 3'	GTAGGCCAACTTGTAAGGACACTT			24	54.86	46			
$LCa_v\beta$ Univ 5'	AGGAACATGAATGTCCAGCTAGT	HM187675	123	23	54.45	43	102.4	0.996	-3.265
$LCa_v\beta$ Univ 3'	AAGAAACTCAGCTAAGTGCTCACA			24	56.73	42			
$LCa_v\beta$ (+) 5'	GGCAAGGCAAGCTCTATACAA	HM187675	131	21	53.89	48	85.4	0.995	-3.731
$LCa_v\beta$ (+) 3'	ACCTGGAGATACAAATTGAACACC			24	52.92	42			
$LCa_v\beta$ (-) 5'	GGCAAGGCAAGCTCTATACAA	HM187676	119	21	53.89	48	91.7	0.993	-3.538
$LCa_v\beta$ (-) 3'	CTCCTCTATACCTGGGGTTGG			21	53.11	57			
$LCa_v\beta$ A 5'	CTTTGCCTGCTGTTTCTCAG	AF484087	126	20	53.35	50	106.0	0.990	-3.187
$LCa_v\beta$ A 3'	TGTAGTTGGAATCCGCAGAA			20	51.45	45			
$LCa_v\beta$ B 5'	GGAGAGCAATCCCATAATGC	HM187675	119	20	50.95	50	110.0	0.996	-3.104
$LCa_v\beta$ B 3'	TGTAGTTGGAATCCGCAGAA			20	51.45	45			
LCa_v3 Univ 5'	CAGAGTGACACAGATGTGCTACAG	AF484084	139	24	57.34	50	104.7	0.986	-3.215
LCa_v3 Univ 3'	GGTTATAGGATAAAGTGCCATGCT			24	54.14	42			
LCa_v3 +8b 5'	AATCCTGAGAAATCTTTGTCCTTG	AF484084	123	24	53.09	38	92.5	0.954	-3.515
LCa_v3 +8b 3'	AGGAGGCTGATGAGATAATGAAAG			24	55.14	42			
LCa_v3 -8b 5'	AGGAAAAAGTCTAAAAAGAAAGGGCT	AF484084	114	26	55.36	35	98.6	0.995	-3.357
LCa_v3 -8b 3'	CTGTAGCACATCTGTGTCACTCTG			24	57.34	50			
LCa_v3 +25c 5'	GGGAGTCTCAAGAAATTGAGGAG	AF484084	122	23	54.2	48	95.8	0.986	-3.426
LCa_v3 +25c 3'	GTATGGAGGTTCTCTCATCTCAGAC			25	55.84	48			
LCa_v3 -25c 5'	GGTTGTAGTTGAAAACTTCCACAAATG	AF484084	121	27	54.59	37	91.5	0.982	-3.545
LCa_v3 -25c 3'	TGGAGGTTCTCTCATCTTCTTTCT			24	55.14	42			
LCa_v3 12B 5'	CGCACCATGGACAATGTAGCAAC	AF484084	145	23	57.05	52	90.4	0.984	-3.576
LCa_v3 12B 3'	CGTTAAGACGATCCTTGCAGGAG			23	57.82	52			
LCa_v3 12A 5'	CGCACCATGGACAATGTAGCAAC	NA	134	23	57.05	52	92.3	0.977	-3.523
LCa_v3 12A 3'	CGATCACATTTACGGAATCCACCATC			26	57.29	46			
LNALCN Univ 5'	GCTTTTACTGGTCCTAATTGATGC	GJQ806355	141	24	53.87	42	100.6	0.985	3.307
LNALCN Univ 3'	AACAGGGCTTCAAGAGAAAATAGA			24	54,19	38			
LNALCN DIIK 5'	CATGTTTCAAATCCTAACCCAGAAAG	GJQ806355	129	26	54.65	38	95.8	0.990	-3.426
LNALCN DIIK 3'	GGTGACAAACAAATGGTAGAAAATGAAA			28	54.39	32			
LNALCN DIIE 5'	CGTTTAAATCCATGTTCCAAATCATGTG	JQ806356	137	28	56.07	36	89.9	0.994	-3.592
LNALCN DIIE 3'	ATCACATTGACAAACAAATGGAAGATCA			28	55.68	32			
LAlpha2Delta 5'	AGACTTTAAGCTTGGTCTCAATGG	NA	141	24	54.99	42	107.9	0.990	-3.146
LAlpha2Delta 3'	TACTTTGGGCGAACTTTTAGTAGG			24	54.55	42			

Table M3.Primers used for semiquantitative RT-PCR of several *Lymnaea* ion channel genes.

Application	Name	Sequence	Accession
Semi-Q RT-PCR			
	Lymnaea actin 5'	CCAACAGGGAAAAGATGACACAGATCATG	DQ206431
	Lymnaea actin 3'	GCAATACCTGGGAACATGGTGGTGCC	
	LCa_v1 5'	CTGCAGCAACCAAGATGATTGGGATG	AF484079
	LCa_v1 3'	TCTGCCACCTGAGGATCCCTGTGAAC	
	LCa_v2 5'	ACACCATTGCAGACCAGGACAGACAG	AF484082
	LCa_v2 3'	TACCCAACCGTCCAGGTGGTGGTGC	
	LCa_v3 5'	AGATGTTCGCCTGCCGCCATGTTG	AF484084
	LCa_v3 3'	GAGACTGAATGTGGTGGGCTTGTGGAG	
	LNALCN 5'	TGGAGGTGGATCTAGAAAGGGACAGGC	AF484086
	LNALCN 3'	GTAGTGAAGGATGGAATCAAACAGGTCG	

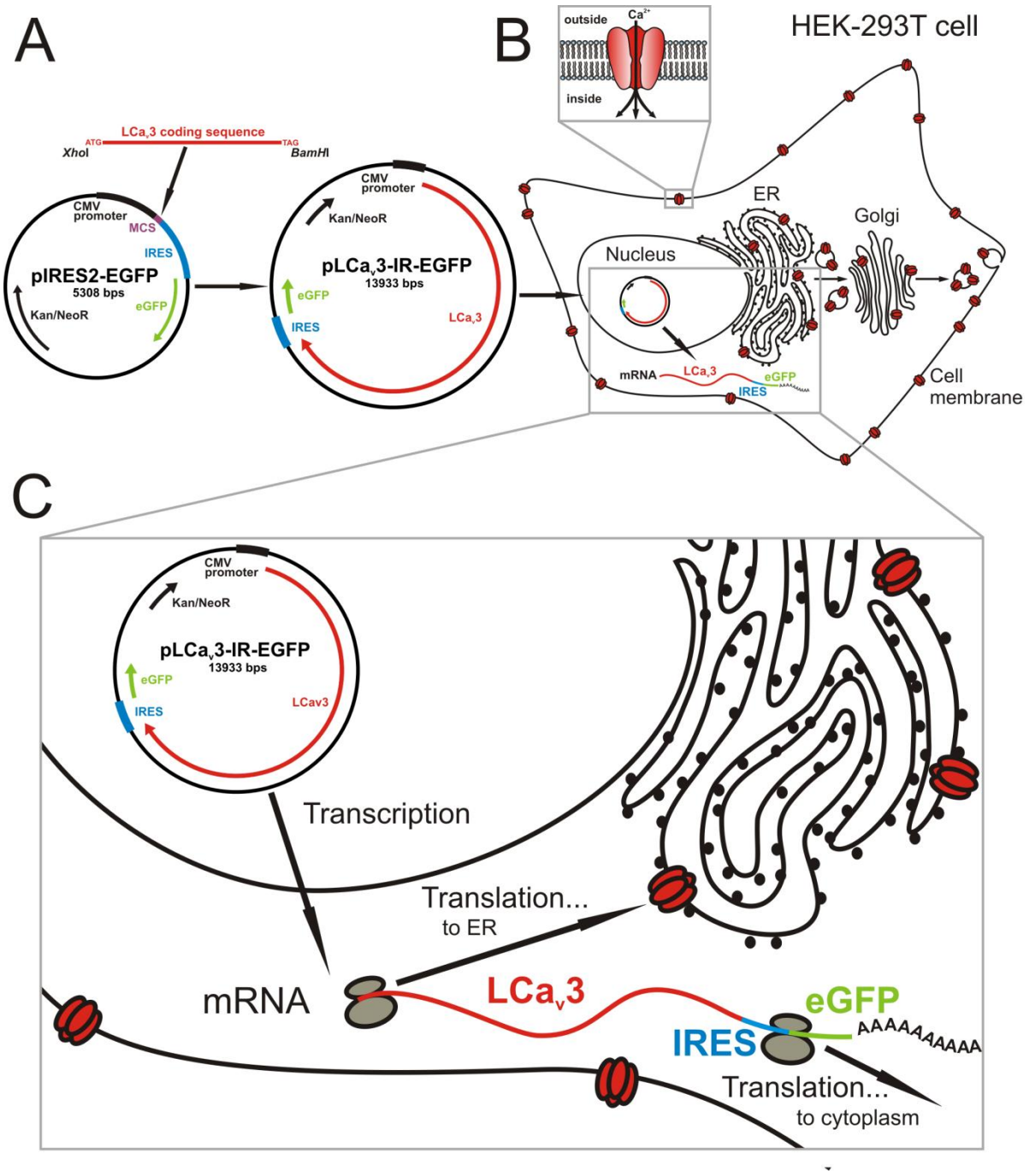

Figure M2. Expression of LCa$_v$3 channels in mammalian cells. A) The coding sequence of LCa$_v$3 was cloned into the mammalian expression vector pIRES2-EGFP via *Xho*I and *BamH*I restriction enzyme sites, which allows for amplification in bacteria via kanamycin resistance (Kan^R), as well as neomycin selection in mammalian cells. **B)** The pIRES2-EGFP vector contains a cytomegalovirus (CMV) promoter just upstream of the multiple cloning site (MCS), that when transfected into mammalian cells such as HEK-293T drives strong heterologous expression (i.e. transcription) of inserted gene sequences. Mammalian cells such as human embryonic kidney 293T (HEK-293T) are frequently used for heterologous expression of ion channels and electrophysiological recording of their ionic conductances. **C)** Messenger RNAs derived from pIRES2 constructs contain internal ribosome entry sites (IRES) that allow for independent translation of the inserted gene sequence (i.e. LCa$_v$3) and a downstream enhanced green fluorescent protein (eGFP) cDNA that permits for confirmation of successful transfection using fluorescence microscopy.

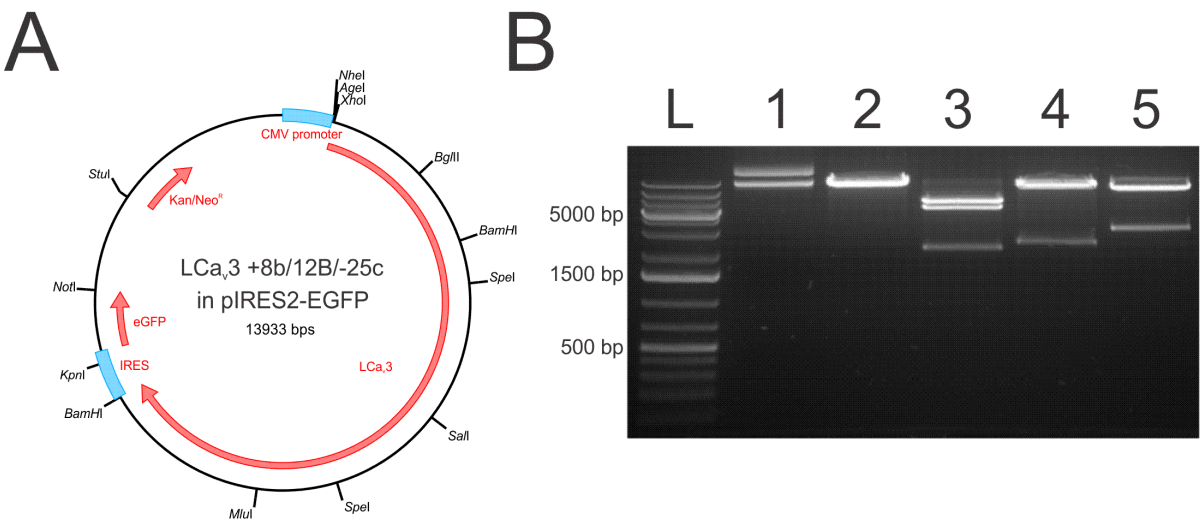

Figure M3. Cloning of LCa$_v$3 +8b/12B/-25c into the pIRES2-EGFP vector. A) Plasmid map showing some restriction enzyme sites used during cloning of LCa$_v$3 into mammalian expression vector pIRES2-EGFP. **B)** 1 µg aliquots of the LCa$_v$3 +8b/12B/-25c cDNA cloned into pIRES2-EGFP were restriction digested with various enzymes to assess proper cloning. The sizes of the digested DNA fragments are as predicted by the sequence. The DNA ladder (left lane) is Fermentas 1kb DNA Ladder Plus. Lane 1, uncut plasmid; lane 2, *Bgl*II digest produces a linearized plasmid with of 13933 base pairs; lane 3, *Xho*I/*BamH*I double digest produces three fragments of 6550, 5261, and 2122 base pairs; lane 4, *Sal*I/*Mlu*I digest produces two fragments of sizes 11596 and 2337; lane 5, *Spe*I digest produces two fragments of sizes 10870 and 3063.

Table M4. Primers used for cloning of several LCa_v3 splice variants and HA-tagged channels.

Application	Name	Sequence
Cloning LCa_v3 -8b/12B/-25		
	pIRES2 *Bgl*II removal 5'	CTAGCGCTACCGGTCTCTGATC
	pIRES2 *Bgl*II removal 3'	TCGAGATCAGAGACCGGTAGCG
	pGEM Adaptor 5'	CATGGCTCGAGATAGATCTATATGTCGACATCAAAA
	pGEM Adaptor 3'	CGCGTTTTGATGTCGACATATAGATCTATCTCGAGC
	LCa_v3 -8b +P 5'	[P]GCTTTTTGCTGACAATCTTCTTATGGAT
	LCa_v3 -8b +P 3'	[P]CCTTTCTTTTTAGACTTTTTCCTGCGC
Cloning LCa_v3 +8b/12B/-25c ΔAPRASPE		
	LCa_v3 ΔAPRASPE +P 5'	[P]CTGCGGGCTGCTAGACGGTCTCG
	LCa_v3 ΔAPRASPE +P 3'	[P]ATAGACTCCATGTCATCGCCACGACGACCC
Cloning LCa_v3 +8b/12B/+25c and -8b/12B/+25c		
	LCa_v3 +25c 5'	AATTGGGCCCGACGTCGCATG
	LCa_v3 +25c 3'1	CGGACGACGATGCTTTAGGTCCCTCACTCTTTCTTTTTTTATCCAGTTTCTC
	LCa_v3 +25c 3'2	TAGTGGGCCCAGTATGGAGGTTCTCTCATCTCGGACGACGATGCTTTAGGTCCCTCAC
Cloning HA-tagged LCa_v3 variant clones		
	LCa_v3 HA 5P 5'	P-GATCCCTACCCCTACGACGTGCCCGACTACGCCCCC
	LCa_v3 HA 5P 3'	P-GATCGGGGGCGTAGTCGGGCACGTCGTAGGGGTAGG
Cloning LCa_v3 +8b/12A/-25c		
	LCa_v3 R2 5' 1	GCTGGTGGCGACACTTTGGACTC
	LCa_v3 +25c F1 3'1	ACACGTACAGAATTTACAGCCAAATAAATTCATTCCAAGTATACTGAAT
	LCa_v3 +25c F1 3'2	GCGATCACATTTACGGAATCCACCATCTAGACACGTACAGAATTT
	LCa_v3 +25c F1 3'3	TAAAGCCCACAGCAGCGAATCAAAGTTCTTGCGATCACATTTAC
	LCa_v3 +25c F2 5'	CTGCTGTGGGCTTTAATCACTGTTTTCCAGGTACTGACAC
	LCa_v3 R2 3' 1	CCAAAGAATTTAAAGTACGATGGCTTGTAAAAG
	LCa_v3 R2 5' 2	CGACACTTTGGACTCAGAATTAGAGACTAG
	LCa_v3 R2 3' 2	GGCTTGTAAAAGAATTCTGTCGACTGAGC

Figure M4. Illustrations of adaptor sequences used to modify several plasmid vectors. A) An adaptor containing *Nde*I and *Xho*I restriction enzyme single-stranded overhangs was cloned into the LCa_v3 +8b/12B/-25c in pIRES2-EGFP vector to remove a *Bgl*II site and introduce an *Age*I site. **B)** An adaptor was inserted into a circularized and *Nco*I-*Mlu*I restriction-digested pGEM®-T Easy vector to remove a series of restriction enzyme sites and incorporate a *Bgl*II site. **C)** An adaptor was also used to insert the coding sequence for a hemagglutinin (HA) epitope tag (red amino acid sequence) into the domain I S5-S6 P-loop sequence of the four LCa_v3splice variants cloned in pIRES2-EGFP, using an endogenous *Bgl*II restriction site (i.e. LCa_v3 +8b/-25c HA, LCa_v3 -8b/-25c HA, LCa_v3 +8b/+25c HA, LCa_v3 -8b/+25c HA). Note that insertion of the adaptor resulted in loss of the *Bgl*II restriction site, and that the HA epitope was flanked by prolines (P).

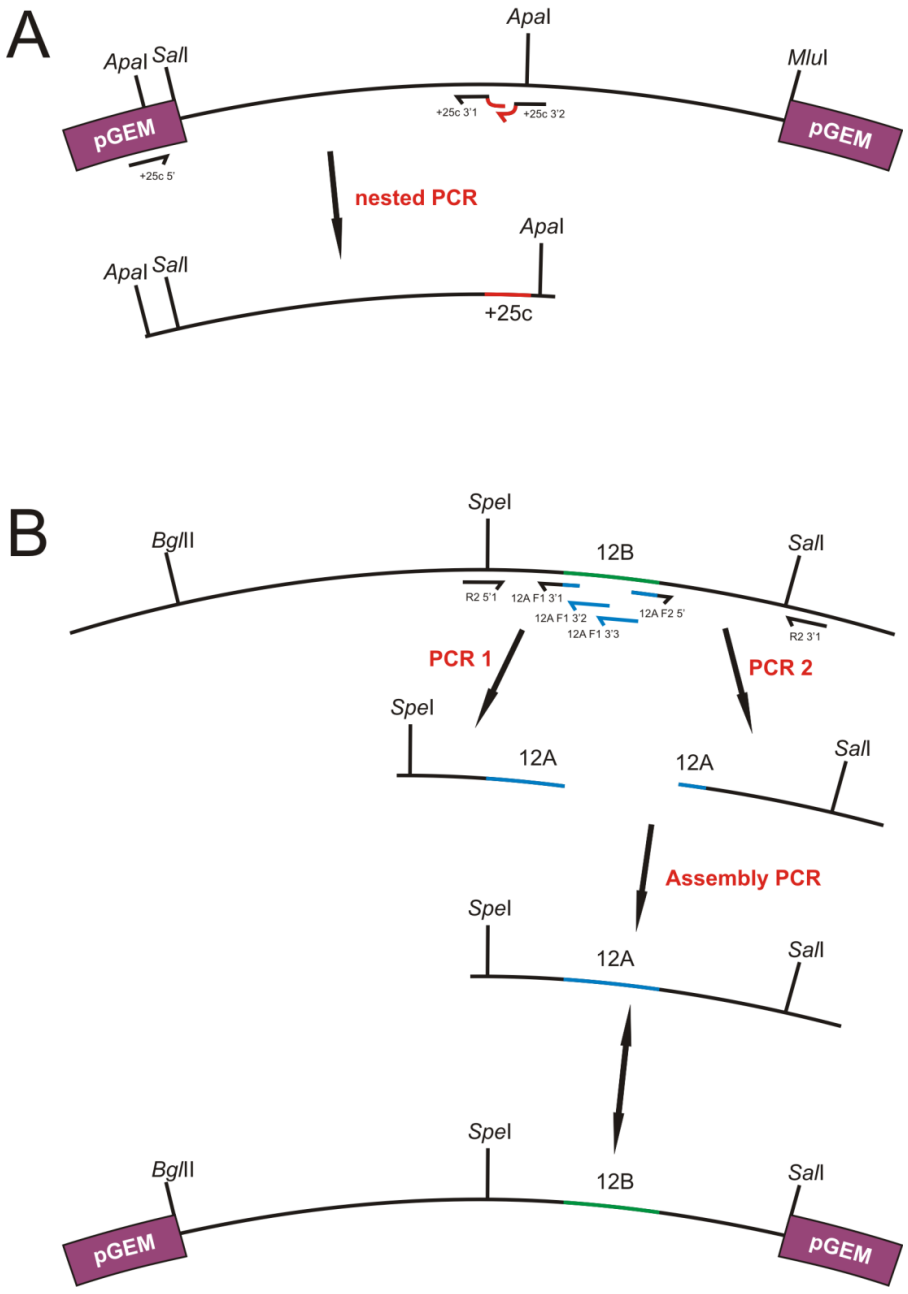

Figure M5. Illustration of cloning strategies used to produce exon 25 and exon 12 splice variants of LCa_v3. A) For cloning the exon 25c coding sequence into the +8b/12B/-25c clone, a SalI to MluI fragment of LCav3 was cloned into pGEM and used a s a template with primers designed to incorporate the exon 25c coding sequence into the PCR product. The resulting DNA fragment was then cloned back into the *Sal*I to *Mlu*I subclone, which was then used to replace the *Sal*I to *Mlu*I fragment of the LCa_v3 +8b/12B/-25c in pIRES2-EGFP, producing LCa_v3 +8b/12B/+25c sin pIRES2-EGFP. This same fragment was also cloned into the LCa_v3 -8b/12B/-25c clone to produce LCa_v3 -8b/12B/+25c in pIRES2-EGFP. **B)** Two separate PCR reactions were done to amplify an *Spe*I to *Sal*I fragment of LCa_v3 with the 12B sequence (green), however the primers were designed to replace the 12B sequence with that of 12A (blue). The two products served as templates for an assembly PCR reaction that joined them together to form a *Spe*I to *Sal*I fragment containing the 12A coding sequence. This PCR-amplified DNA was then cloned into a *Bgl*II to *Sal*I subclone of LCa_v3 in pGEM®-T Easy, and the resulting *Bgl*II to *Sal*I cDNA, containing the 12A coding sequence, was subsequently cloned into the LCa_v3 +8b/12B/-25c in pIRES2-EGFP construct to produce LCa_v3 +8b/12A/-25c in pIRES2-EGFP.

Table M5. Primers used for generating DIG-labeled probe targeted to the exon 8b sequence of LCa_v3 and primers used for sequencing of genomic DNA corresponding to portions of the LCa_v3 gene.

Application	Name	Sequence
Southern probe synthesis		
	LCa_v3 probe 5'	ACTAATAACCTAAGGTCCCAACAGCAG
	LCa_v3 probe 3'	GTCGGCTAACGATTGAGTTTTGCTAGG
LCa_v3 intron sequencing		
	I-IIL intron 5'1	CTGTGCTCGCAGCATCTAATATGCTG
	I-IIL intron 3'1	CTGAGTCTGGCCTGTGCCAAGCTGTA
	I-IIL intron 5'2	CTCAATGTGGATTATGAGCCTAGCAAAACTCA
	I-IIL intron 5'2	CATCTGTGTCACTCTGCATGGACAACTGTG
	III-IVL intron 5'1	CGGGAGTCTCAAGAAATTGAGGAG
	III-IVL intron 3'1	GCCAAATCAAAGTATTTGCTATTGATC
	III-IVL intron 5'2	GAGGAGCGGGCCAAGCGTGCTGCT
	III-IVL intron 3'2	TGTGTGAATGAGCAGACGGCTGTG

5.9 Sequencing and cloning of LNALCN and its splice isoforms

5.9.1 Determining the full length sequence of Lymnaea NALCN

Two preliminary non-overlapping sequences, spanning major portions of the NALCN channel coding sequence, had previously been deposited into GenBank (accession numbers AF484086 and AF484085). 5' *r*apid *a*mplification of *c*DNA *e*nds (RACE) was used to determine the missing N-terminal coding sequence, corresponding to the putative start codon, the intracellular N-terminus, and part of domain I of the predicted channel protein. Briefly, total RNA was extracted from isolated adult central ring ganglia (i.e. CNS) and whole animals using Tri-Reagent (Sigma), quantified, and quality assessed by visualization of 20 μg on an ethidium bromide-stained agarose gel (Figure M6A). Reverse transcription was carried out using 1 μg of each RNA extract diluted to 9 μL in water, to which the following reagents were added: 5 μL of 5x Moloney Murine Leukemia Virus (M-MLV) RTase buffer (Promega), 2 μL of 10 mM dNTP mix (Fermentas), 0.4 μL of 100 μM LNALCN NT primer (Table M6), 1 μL of RiboLock RNase inhibitor (Fermentas), 2.6 μL of water, and 1μL of M-MLV RTase enzyme. cDNA synthesis was done at 37^{o}C for 1 hour, products were then co-precipitated with 2 μL of 20 mg/mL glycogen (Fermentas) in ethanol, and pellets were washed with 70% ethanol and resuspended in 10 μL of water. 5' poly-A tailing of CNS and whole animal cDNAs was achieved by adding the following reagents (all from Fermentas) to the cDNA samples: 4 μL of 5x *t*erminal *d*eoxynucleotidyl *t*ransferase (TdT) buffer, 4 μL of 1 mM dATP, 1 μL of water, and 1 μL of TdT enzyme. Reactions were carried out at 37^{o}C for 15 minutes and then heat inactivated at 80^{o}C for 3 minutes. Nested PCR was used to amplify the NT coding sequence and 5' UTR of snail NALCN from the poly-A tailed CNS and whole animal cDNA, using nested primer pairs RACE-For1 plus LNALCN-Rev1, and RACE-For2 plus LNALCN-Rev2 (Table M6). For 1^{o}PCRs, used the following reagents (all from Fermentas): 2.5 μL of 10x High Fidelity PCR Buffer, 1.5 μL of 25 mM $MgCl_2$, 0.5 μL of 10 mM dNTP mix, 1.25 μL of each primer, 0.13 μL of High Fidelity PCR Enzyme Mix, 0.5 μL of tailed cDNA, and water to 25 μL. For 2^{o}PCRs the following volumes were used: 2.5 μL of 10x High Fidelity PCR Buffer, 1.5 or 3.0 μL of 25 mM $MgCl_2$, 0.5 μL of 10 mM dNTP mix, 1.25 μL of each primer, 0.13 μL of High Fidelity PCR Enzyme Mix, 0.5 or 2.5 μL of 1^{o}PCR, and water to 25 μL. 2^{o}PCR amplified ~650 base pair fragments, and these were separated on an agarose gel by electrophoresis, stained with ethidium bromide for visualization under UV light (Figure M6B), gel purified, and cloned into pGEM-T Easy (Promega). Two plasmids with 5' RACE inserts, representing

each of the two independent experiments (i.e. CNS and whole animal), were sequenced and found to contain the snail NALCN start codon and N-terminal sequence, as well as the 5'UTR.

To determine the unknown sequence located between the previously deposited AF484086 and AF484085 GenBank sequences, nested high-fidelity PCR spanning this region was carried out using *Lymnaea* λ-ZAP cDNA library as template, and primer pairs LNALCN gap 5'1 plus LNALCN gap 3'1 and LNALCN gap 5'2 plus LNALCN gap 3'2 (Table M6). DNA fragments from PCRs were gel-purified, cloned into pGEM-T Easy, and sequenced.

5.9.2 Consensus sequencing of Lymnaea NALCN

Primers were designed to PCR-amplify the snail NALCN coding sequence in 5 separate, overlapping regions, using the following nested primer pairs (listed in order from most N-terminal to most C-terminal along the cDNA sequence): LNALCN R1, LNALCN R2, LNALCN R3, LNALCN R4, and LNALCN R5 (Table M7). All PCR were carried out using Taq DNA polymerase AD (Fermentas), using as templates either the λ-ZAP cDNA library, CNS cDNA libraries prepared using a random hexamer primer (Table M1), or CNS cDNA libraries prepared using NALCN-specific primers LNALCN R1 3' 1, LNALCN R4 3' 1, or LNALCN R5 3' 1, (Table M7). All PCR products were cloned into pGEM-T Easy for sequencing, and a minimum of three independent PCR-amplified sequences, corresponding to each position along the *Lymnaea* NALCN transcript, were used to build consensus sequences. Sequencher^{TM} 4.10.1 software (Gene Codes Corporation) was used for sequence analysis, during which mutually exclusive alternative splicing was identified in the domain II P-loop of LNALCN, coding for alternate selectivity filter motifs in the channel protein (i.e. EKEE and EEEE). The full length sequences of both isoforms were submitted to GenBank (accession numbers GJQ806355 and JQ806356, for EKEE and EEEE respectively).

5.9.3 Cloning Lymnaea NALCN isoforms into pIRES2-EGFP, mRFP, and pEGFP-C1

Lymnaea NALCN domain II splice isoform variants (i.e. EKEE and EEEE selectivity filters) were each cloned into the bicistronic vector pIRES2-EGFP (Clontech) in three PCR-amplified fragments. Briefly, two cDNA fragments that were previously cloned into pGEM-T Easy for consensus sequencing (i.e. Regions 4 and 5; see above), were combined into a large 2925 bp fragment corresponding to the invariable C-terminal coding sequence of snail NALCN. These were joined by inserting a *Hind*III/*Sac*I-digested insert DNA fragment of the LNALCN R5 subclone into the same restriction enzyme sites of the LNALCN R4 subclone. This assembled DNA was then cloned into the

pIRES2-EGFP vector via *BamH*I sites flanking the insert. Large N-terminal portions of the two NALCN splice variants (~3500 base pairs) were then PCR-amplified using PfuTurbo DNA polymerase AD (Stratagene) from adult CNS cDNA made using a NALCN-specific primer (LNALCN R4 3' 1; Table M7). Nested PCR primer pairs (LNALCN S1 5' 1 and LNALCN S1 3' for 1^{o}PCR; LNALCN S1 5' 2 and LNALCN S1 3' for 2^{o}PCR; Table M7) allowed for high-fidelity PCR amplification of a large portion of the LNALCN N-terminus, and for direct cloning of this DNA into the pIRES2-EGFP vector harboring the C-terminal portion of the channel using *Xho*I and *Sal*I restriction enzyme sites. Clones were fully sequenced to confirm the absence of mutations and that both domain II splice variants were successfully cloned; these were transfected into HEK-293T cells to confirm expression of eGFP from the internal ribosome entry site located downstream of but on the same transcript as the NALCN insert cDNAs (Figure M2). To produce LNALCN vectors that would produce bicistronic expression of red fluorescent protein (RFP) rather and green fluorescent protein (GFP), the enhanced GFP (eGFP) coding sequence from the LNALCN pIRES2-EGFP clones was replaced with the coding sequence for monomeric RFP[336].

For vectors expressing the two pore isoforms of LNALCN containing N-terminal eGFP fusions, the full coding sequences (contained int the pIRES2-EGFP vectors from above) were excised and inserted into pEGFP-C1 (Clontech) via *Xho*I and *Apa*I restriction sites, producing in-frame fusions of the eGFP coding sequence with those of the ion channel isoforms.

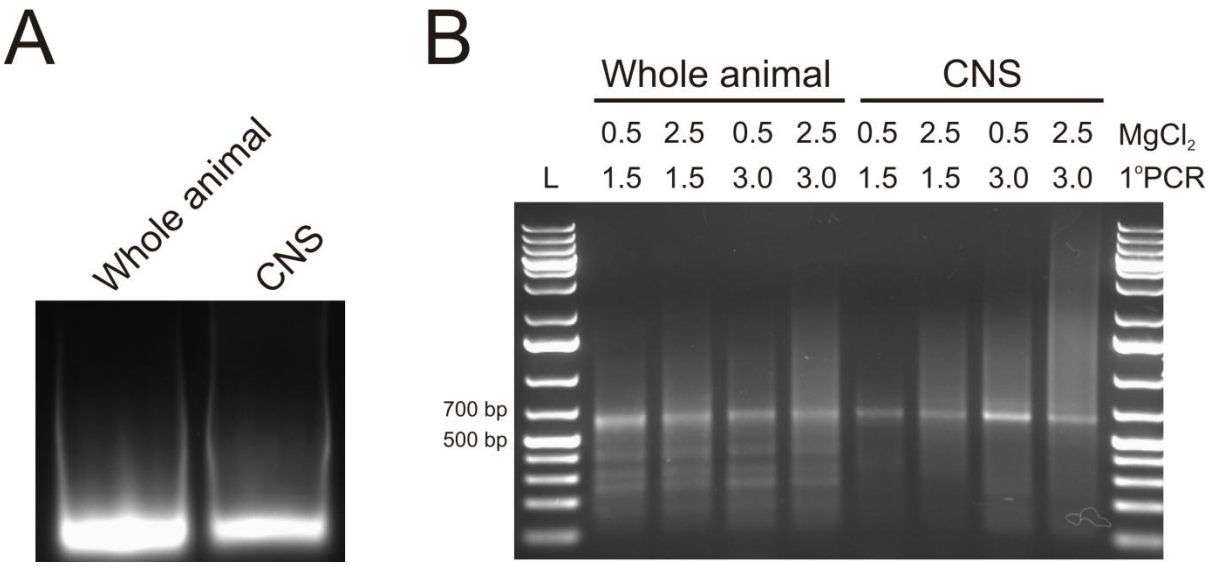

Figure M6. Ethidium bromide stained agarose gels from 5' RACE experiment to sequence the N-terminus of *Lymnaea* NALCN. A) 20 µg of extracted Lymnaea total RNA from whole animal and dissected central ring ganglia (central nervous system CNS), electrophoresed through a 1% agarose gel and stained with ethidium bromide for visualization under UV light. **B)** Results for 5' RACE from the two RNA sources, using various amounts of $MgCl_2$ and 1°PCR template (in µL) as listed above the gel image. The four bands for each experiment type (whole animal and CNS) were gel extracted, pooled, and cloned into pGEM®-T Easy for sequencing.

Table M6. Primers used to complete the preliminary sequencing of *Lymnaea* NALCN. 5'RACE was done to determine the N-terminal sequence, and the gap primers were used to sequence a gap between two LNALCN sequences previously deposited to GenBank (accession numbers AF484086 and AF484085).

Application	Name	Sequence
5' RACE		
	LNALCN NT	GAGATCGAATGATCCTGATGGTAGC
	RACE-For1	CGATCTCGACTCGAGTCTTTTTTTTTTTTTTTT
	LNALCN-Rev1	GAGTTGATGCTGGGTTCAGCTCC
	RACE-For2	CGATCTCGACTCGAGTC
	LNALCN-Rev2	TACAGATCCCCAAAGGCATAAGACC
Gap sequencing		
	LNALCN gap 5' 1	CCGGACACATTCTGCTCCCCTGACC
	LNALCN gap 3' 1	GATTTGAAACATGGACATGAAGGCCTGC
	LNALCN gap 5' 2	GCTCCCCTGACCCAGAACCAGACTC
	LNALCN gap 3' 2	ACTTGTCAAACCCTTCAATGAAGCAG

Table M7. Primers used for consensus sequencing and cloning of *Lymnaea* NALCN.

Application	Name	Sequence
Consensus sequencing and cloning		
	LNALCN R1 5' 1	GGACTGCACCAGAAACTTGACTTATGC
	LNALCN R1 3' 1	CCCAACCTTCCTGAGAGGCCGCC
	LNALCN R1 5' 2	CACGTACTCGAGCCACCATGTTAGTGAATCGTAAAACC
	LNALCN R1 3' 2	CGGGACTCATGGTCAATTCCAAGCATACC
	LNALCN R2 5' 1	CCGGACACATTCTGCTCCCCTGACC
	LNALCN R2 3' 1	GATTTGAAACATGGACATGAAGGCCTGC
	LNALCN R2 5' 2	GCTCCCCTGACCCAGAACCAGACTC
	LNALCN R2 3' 2	ACTTGTCAAACCCTTCAATGAAGCAG
	LNALCN R3 5' 1	GCTTGGCAGCTTAATCCTGTTCAC
	LNALCN R3 3' 1	TCATGGCTGGGTGGGCTTTTAGC
	LNALCN R3 5' 2	ATCATCGCATCAAGCATCAGCCTG
	LNALCN R3 3' 2	CTTCAAACTTGTCGGCCGGGATCC
	LNALCN R4 5' 1	ACATCAGCATCAGATTCGTATGGAACG
	LNALCN R4 3' 1	ATTTCGCTCAGGTCTTGGTGGAATGTGC
	LNALCN R4 5' 2	GTATGGAACGAAGTCGTAGCACAAGGG
	LNALCN R4 3' 2	GGAATGTGCAATGGCCGAGCAAGC
	LNALCN R5 5' 1	AGGAGATGGCTTGACCTTAAGGGC
	LNALCN R5 3' 1	ACCCCCATAATTGCTGTATCCACATTGTTC
	LNALCN R5 5' 2	AGAATAAAGCTTGCTCGGCCATTGC
	LNALCN R5 3' 2	TATTAGGGATCCTCACGTATCCATCACAACCC
Cloning		
	LNALCN S1 5' 1	GGACTGCACCAGAAACTTGACTTATGC
	LNALCN S1 3'	GGAATGTGCAATGGCCGAGCAAGC
	LNALCN S1 5' 2	TTTTGCTAGCGCTACCGGACTCAGATCTCGAGCCACCATGTTAGTGAATCGTAAAACCAG

5.10 Cell culture and electrophysiology

For a detailed description of techniques and equipment used for the culture of mammalian cells (i.e. HEK-293T; Invitrogen), calcium phosphate transfection, as well as techniques and equipment used for whole-cell patch clamp electrophysiological recording, see Senatore *et al*., 2011[297].

5.11 Electrophysiological recording solutions

5.11.1 LCa$_v$3

The initial characterization of LCa$_v$3 (results chapter 2.1) was done using solutions used by Scheglovitov *et al*., 2008[195] for electrophysiological recording of mammalian Ca$_v$3.1 channel in HEK-293T cells. The external solution contained in mM: 5 $CaCl_2$, 166 tetraethylammonium (TEA)-Cl, and 10 HEPES (pH 7.4 with TEA-OH), and the internal: 125 CsCl, 10 EGTA, 2 $CaCl_2$, 1 $MgCl_2$, 4 Mg-ATP, 0.3 Tris-GTP, and 10 HEPES (pH 7.2 with CsOH; all chemicals from Sigma). For comparing Ca^{2+} and Ba^{2+} permeabilities, a Valvelink8.2® gravity flow Teflon perfusion system (AutoMate Scientific, Berkeley CA) was used to toggle between 5 mM Ca^{2+} and 5 mM Ba^{2+} external solutions during electrophysiological recording. Perfusion of 5 mM Ca^{2+} externals with different concentrations of solubilized Ni^{2+} (Sigma) or mibefradil (Sigma) was used for pharmacological studies.

The solutions used for electrophysiological characterization of the various LCa$_v$3 alternative splice isoforms, presented in chapters 2.2 and 2.3, were prepared according to Chemin *et al*., 2002[275], with an external solution containing (in mM): 2 $CaCl_2$, 160 TEA-Cl and 10 HEPES (pH 7.4 with TEA-OH), and an internal solution containing: 110 CsCl, 10 EGTA, 3 Mg-ATP, 0.6 Li-GTP, and 10 HEPES (pH 7.2 with CsOH). For replacement of internal cesium with large impermeant monovalent N-Methyl-D-Glucamine$^+$ ($NMDG^+$; results chapter 2.30, 110 mM CsCl was replaced with 110 mM NMDG and the pH was adjusted to 7.2 with HCl. To determine the effect of adding sodium to the external solution for LCa$_v$3 exon 12 variants (results chapter 2.3), gravity flow perfusion was used to toggle between the 2 mM Ca^{2+} external and a modified external containing 2 $CaCl_2$, 25 TEA-Cl and 10 HEPES (pH 7.4 with TEA-OH). Perfusion was also used to toggle between the 2 mM Ca^{2+} external and one containing 300 μM $NiCl_2$.

5.11.2 LNALCN

For whole-cell patch clamp recording of *Lymnaea* NALCN clones expressed in tsA201 cells, solutions were made according to Lu *et al*., 2010[134]. The internal contained (in mM): 120 Cs-methanesulfonate, 10 NaCl, 10 EGTA, 4 $CaCl_2$, 0.3 Na_2GTP, 2 Mg-ATP, and 10 HEPES (pH 7.4

with CsOH; ~300 mOsm/L), and the external: 150 NaCl, 3.5 KCl, 1 $MgCl_2$, 1.2 $CaCl_2$, 20 glucose, and 10 HEPES (pH 7.4 with NaOH; ~320 mOsm/L). Osmolarity was measured with a Löser Micro-digital Osmometer (Löser Messtechnik, Inh., Berlin, Germany).

5.12 Western blotting

5.12.1 SDS-PAGE

Acrylamide gels used for *s*odium *d*odecyl *s*ulfate-*p*oly*a*crylamide *g*el *e*lectrophoresis (SDS-PAGE)[337], were prepared with different concentrations of acrylamide depending on the size of target proteins according to Table M8 (5 to 7.5% acrylamide for large proteins, 12 to 14% for small proteins). 1 mm thick gels were prepared using a Mini-PROTEAN® Tetra System (Bio-Rad), with resolving buffer containing 0.4% w/v SDS 1.5 M Tris pH 8.8 and stacking (well) buffer containing 0.4% w/v SDS 0.5 M Tris pH 6.8. Prior to loading on gels, protein samples were combined equal volumes of 2x sample buffer (100 mM DTT, 2% w/v SDS, 15% glycerol, 0.006% Bromophenol blue, and 80 mM Tris pH 6.8) and heated to 95^{o}C for 5 minutes. Electrophoresis was carried out using a Laemmli Tris-glycine buffer (192 mM glycine, 0.1% w/v SDS, 25 mM Tris pH8.8) for 1 to 3 hours at 100 volts using a Mini-PROTEAN II Electrophoresis Cell (Bio-Rad), then gels were either Coomassie-stained or transferred to nitrocellulose membrane for immunoblotting.

5.12.2 Coomassie staining of acrylamide gels

Staining of acrylamide gels with Coomassie Blue R-250[338] was performed by submerging gels in a solution containing 0.1% w/v Coomassie Blue R-250, 50% v/v methanol, and 10% v/v acetic acid over night at room temperature. Gels were de-stained by submersion in de-staining solution (8% v/v acetic acid, 12% v/v ethanol) for about 4 to 8 hours at room temperature on a shaker. Stained gels were then either scanned or imaged using a gel documentation system (Alpha Innotech).

5.12.3 Western transfer

Western transfer[339] onto 0.45 µm PROTRAN® nitrocellulose membranes (Whatman International, Maidstone, UK) was typically achieved as follows: acrylamide gel and nitrocellulose membranes were equilibrated in wet transfer buffer (39 mM glycine, 1.3 mM SDS, 20% v/v methanol, 48 mM Tris pH 8.3) for 15 minutes at RT. A sponge, two pieces of 8.5 x 6.0 cm Whatman filter paper, the gel, a 8.5 x 6.0 cm piece of nitrocellulose membrane, two more pieces of filter paper, and another sponge were then sequentially placed into a gel holder cassette, which was clamped shut and placed into a Mini Trans-Blot Electrophoretic Transfer Cell (Bio-Rad) filled with transfer buffer (with the

membrane situated between the gel and the cathode). The assembly was placed in the fridge and transferred at 25 Volts overnight.

5.12.4 Immunoblotting

After transfer, membranes were placed in blocking solution containing TBS with 0.1% v/v Tween-20 (TTBS) and 5% w/v skim milk powder, and either for 2 hours at room temperature or overnight at 4^{o}C. Typically, membranes were then incubated with 1^{o} antibody diluted in TTBS 5% skim milk at various dilutions (1:500 to 1:2000), at 4^{o}C overnight. All 2^{o} antibodies used for western blotting were conjugated to HRP by the manufacturer, and were applied at dilutions from 1:1500 to 1:2000 in TTBS with 5% skim milk at room temperature for 2 to 3 hours. Membranes were washed three times with TTBS both prior and after incubation with 2^{o} antibody. For HRP-activated chemiluminescence, two 20 mL solutions were prepared in separate 50 mL conical centrifuge tubes, one containing 2 mL of 1 M Tris (pH 8.5), 200 µL of 250 mM luminol dissolved in dimethyl sulfoxide (DMSO), 88 µL of 90 mM p-coumaric acid in DMSO, and 17.7 mL of water, and the other containing 2 mL of 1 M Tris (pH 8.5), 12 µL of 30% v/v hydrogen peroxide, and 18 mL of water. Just prior to chemiluminescence detection, the two tubes were combined the membranes were incubated in this mixture for 2 minutes. Luminescence was detected in a dark room by exposing the membrane to BioMax Light Film (Kodak, Rochester, NY) for various times (5 seconds to 10 minutes). The developed film and the Coomassie-stained gel were imaged either by scanning or with an AlphaImager HP acquisition system and the AlphaEase® FC software (Alpha Innotec).

5.13 Expression of LCa_v3 peptides and antibody production

5.13.1 Design and cloning of protein expression vectors

In order to be able to study both endogenous LCa_v3 proteins and recombinant versions expressed in heterologous systems, rabbit polyclonal antibodies targeted against the I-II linker of LCa_v3 were generated. At first, expression in bacteria of various portions of the I-II linker peptide sequence was unsuccessful (data not shown). Critical for expression of proteins in bacteria is that they do not contain highly hydrophobic regions in the N-terminus[340]. Also, proteins with interrupted secondary and tertiary structures tend to be quickly degraded (personal communication from Dr. Joseph Lam, University of Guelph). Therefore, secondary structures for putative I-II linker peptides were predicted to select regions that do not interrupt alpha helix or beta strand structures

(http://bioinf.cs.ucl.ac.uk/psipred/) to ensure that the expressed proteins were not rapidly degraded in the bacterial cytoplasm.

Two LCa_v3 peptides, one corresponding to optional exon 8b, and the other to the I-II linker region flanking but not including exon 8b (see summary figure; Figure M7), were expressed in bacteria for generating polyclonal antibodies. Primers were designed for PCR amplification of the desired LCa_v3 cDNA sequences (Table M9), which incorporated *Nde*I and *Xho*I restriction sites for cloning into bacterial protein expression vector pET-22b(+) (Novagen EMD Biosciences, Madison, WI). pIRES2 vectors LCa_v3 +8b/-25 (for 8b peptide) and LCa_v3 -8b/-25c (for I-II linker peptide lacking 8b) were used as templates for separate PCRs using Taq DNA polymerase, and products were gel purified and directly cloned into pET-22b(+) via *Nde*I and *Xho*I (Figure M7 A and B). Both clones were sequenced to confirm the sequence of the two inserts, and the in-frame fusion with C-terminal 6x histidine stretches upstream of the stop codon, required for nickel affinity purification (Novagen; Figure M7C). The predicted sizes for the expressed LCa_v3 peptides with C-terminal 6x histidine tags were 23.011 kDa and 17. 609 kDa for the exon 8b peptide and the I-II linker peptide lacking 8b, respectively (predicted using ExPASy ProtParam: http://web.expasy.org/protparam/).

5.13.2 Protein expression

Protein expression from the two LCa_v3 pET-22b(+) constructs was initially performed and optimized by small-scale experiments in *E. coli* Rosetta™ (DE3) cells (Novagen). Subsequently, the optimized conditions were scaled up for large scale expression. The constructs were heatshock transformed into competent Rosetta™ (DE3) cells, and these were plated onto LB ampicillin plates and incubated over night at 37°C. The following day, two cultures were prepared by transferring a single colony of each clone type into separate culture tubes each containing 10 mL of LB broth supplemented with 100 µg/mL ampicillin. Tubes were incubated overnight at 37°C with shaking, and 250 µL aliquots of each culture were used to inoculate 250 mL of LB ampicillin broth. Cultures were incubated on a shaker at 37°C until the bacteria reached an optical density of 0.35 at 600 nm (measured with a NanoDrop). A 1 mL aliquot was removed from each culture for the visualization of protein expression prior to induction (see below), then 1 M isopropyl β-D-1-thiogalactopyranoside (IPTG) was added to a final concentration of 1 mM for induction of protein expression. Induction was carried out for 3 hours at 37°C with shaking, then cells were pelleted by centrifugation for 10 minutes at 4000g 4°C and resuspended in 20 mL of binding buffer (0.5 M NaCl, 5 mM imidazole, 20 mM Tris pH 7.9). Cells were then lysed by 3 freeze-thaw cycles using liquid nitrogen and boiling water, and by sonication

using a Misonix XL2000 sonicator (Misonix Inc., Farmingdale, NY) at a power setting of 6.5, with six pulses for 45 seconds per pulse. The insoluble fraction was removed by centrifugation at 9000g for 30 minutes at 4^{o}C, then the supernatant was run through glass columns (Bio-Rad) containing 2.5 mL bed volumes of nickel-charged His•Bind® resin (Novagen). Beads were subsequently washed with 25 mL of binding buffer, then 15 mL of wash buffer (0.5 M NaCl, 60 mM imidazole, 20 mM Tris pH 7.9), and proteins were eluted with 5 mL of elution buffer (0.5 M NaCl, 1 M imidazole, 20 mM Tris pH 7.9). To confirm successful expression and isolation of the two LCa_v3 peptides, protein samples from uninduced cells, the insoluble fractions, the soluble unpurified fractions, the flowthrough of the soluble fractions after going through the columns, and finally the eluted affinity-purified proteins were electrophoresed through a 12% PAGE acrylamide gel, which was then Coomassie-stained and scanned (Figure M8A). The protein solutions were then placed into clipped SnakeSkin dialysis tubing (7 kDa MW cutoff; Fisher) and proteins were dialyzed in 500 mL of 0.85% saline over night at 4^{o}C, then quantified using the Bio-Rad Bradford assay kit (Bio-Rad) and determined to be 140.9 μg/μL for the LCa_v3 exon 8b linker peptide, and 126.6 μg/μL for the LCa_v3 I-II linker peptide lacking the exon 8b sequence.

5.13.3 Production of polyclonal antibodies in rabbits

Rabbits were each injected three times with 500 μL of designated recombinant proteins emulsified with 500 μL of Freunds complete adjuvant (Sigma) for the first injection, and 500 μL of Freunds incomplete adjuvant (Sigma) for three subsequent injections. A small amount of serum was extracted before the first antigen injection (pre-immune bleed), and serum was extracted after the third and fourth injections; red blood cells were removed by incubating the extracted blood at 37^{o}C for 1 hour, and tubes were centrifuged at 500g for 10 minutes; supernatants were then aliquoted into 500 μL cryovials and these were stored at -80^{o}C until future use. IgG rabbit antiserum was tested for immune-reactivity with the antigen by western blotting. Briefly, the dialyzed proteins were electrophoresed through four 12% SDS-PAGE gels, and these were transferred onto nitrocellulose membranes. Immunoblotting was then carried out on all four membranes, with 1:2000 goat α-rabbit horseradish peroxidase (HRP; Jackson ImmunoResearch Laboratories Inc., West Grove, PA) as 2^{o} antibody (diluted in TTBS with 5% w/v skim milk powder). For primary antibodies (all at 1:1000 dilution), gel 1 was probed with 1:1000 αLCa_v3 exon 8b preimmune serum; gel 2 was probed with 1:1000 αLCa_v3 exon 8b antibody; gel 3 was probed with 1:1000 αLCa_v3 I-II linker -8b preimmune serum; and gel 4

was probed with 1:1000 αLCa$_v$3 I-II linker -8b antibody. Chemiluminescent detection of western blots was carried out as indicated above and photographic films were scanned (Figure M8B).

5.14 Immunolabeling

Antibodies raised exclusively against exon 8b of LCa$_v$3 were used for immunolabeling of HEK-293T cells expressing LCa$_v$3 +8b/12B/-25c as presented in results chapter 2.1, and the antibodies raised against the invariable portion of the I-II linker, lacking exon 8b, were used for immunolabeling of similar cells in results chapter 2.2. Briefly, HEK-293T cells were calcium-phosphate transfected with either 8 μg of LCa$_v$3 +8b/-25c in pIRES2-EGFP or with 3.2 μg of LCa$_v$1 in pIRES2-EGFP[214] plus 2.4 μg of rat β1 subunit in pMT2 and 2.4 μg of rat $\alpha_2\delta$ in pMT2. Cells were plated onto glass coverslips after incubation at 28^{o}C for 7 days and left at 37^{o}C for 6 hours to allow for adhesion to the glass substrate. Cells were then fixed with 1% paraformaldehyde in PBS overnight at 4^{o}C, washed twice with PBS, then permeabilized using PBS containing 0.2% TWEEN-20 (PBST) for 10 minutes at room temperature. Cells were then blocked with PBST containing 3% BSA at room temperature for 2 hours then incubated over night at 4^{o}C with PBST containing 3% BSA and either 1:500 1^o LCa$_v$3 antibody or no antibody. The next day, the cells were washed 3 times for 20 minutes each with PBST 3% BSA, then blocked again with PBST containing 5% BSA for 45 minutes at room temperature. AlexaFluor® 594 goat anti-rabbit 2^o antibody (Invitrogen) was diluted 1:1000 in PBST containing 3% BSA, added to the cells, and cells were incubated for 1 hour at room temperature. Cells were then washed with PBST four times for 15 minutes each then directly imaged at 40x magnifications using a Zeiss motorized AxioObserver Z1 inverted epifluorescent microscope using eGFP and rhodamine excitation filters to detect the eGFP and AlexaFluor 594 antibody fluorescence. Images were captured using Zeiss AxioVision software and brightness/contrast modifications were made using Adobe Photoshop.

5.15 Experiments to compare surface expression of LCa$_v$3 channel variants in HEK-293T cells

This research is presented in results chapter 2.2.

5.15.1 Biotinylation

Measurement of total and surface-expressed LCa$_v$3 channel variants, as presented in results chapter 2.2, was achieved using the Pierce® Cell Surface Protein Isolation Kit (Pierce, Rockford, IL). Briefly, a fully confluent monolayer of HEK-293T cells, adhered to a vented 6 mL tissue culture flask

(Greiner Bio-One, Frickenhausen, Germany), was detached with 1 mL of 37°C warm trypsin (Sigma) and cells were split 1:6 into 4 new flasks. After cellular adhesion (5 hours at 37°C), the media was changed to one lacking antibiotic, and flasks were incubated over night at 37°C. The following day, equimolar aliquots of the four splice variants of LCa_v3 cDNAs in pIRES2-EGFP were prepared: ~6 µl of 1 µg/µl +8b/+25c vector (quantified by UV spectrophotometry) was used as a reference amount, and the amount for the other three variants (i.e. -8b/-25c, +8b/+25c, and -8b/+25c) was scaled up or down from 6µg based on agarose gel quantification (Figure M9). The four aliquoted LCa_v3 vectors were then each transfected into the HEK-293T cells using Lipofectamine™ LTX (Invitrogen). Briefly, each LCa_v3 plasmid aliquot was diluted with 1.5 mL of Opti-MEM® (Invitrogen), 18.7 µL of Lipofectamine LTX was added to each tube, and tubes were incubated at room temperature for 20 minutes then the reagents were micropipetted dropwise into the separate 6 mL flasks. Transfections were incubated at 37°C for 6 hours then the media replaced with 6 mL of media lacking antibiotics. The next day, cells were transferred to 28°C for overnight and subsequently washed once with 5 mL of warm (37°C) phosphate-buffered saline (PBS; 137 mM NaCl, 2.7 mM KCl, 10 mM phosphate pH of 7.4) and once with 5 mL of ice cold PBS. 3.5 mL of ice-cold Sulfo-NHS-SS-Biotin (Pierce) was then added to each flask and these were incubated on a rocking platform at 4°C for 30 minutes. 175 µL of Quenching Solution (Pierce) was added to each flask and the cells were gently resuspended and transferred to separate 5 mL conical tubes; remaining cells were obtained using 830 µL of Tris-buffered saline (TBS; 150 mM NaCl, 2 mM KCl, 25 mM Tris pH 7.4) to rinse out the flasks using a micropipette. Tubes were then centrifuged in a Hettich Rotofix 32 centrifuge equipped with a swinging bucket rotor (Hettich Instruments, Beverly, MA) at 500g for 3 minutes, and the supernatant was discarded. Cell lysis was achieved by adding 130 µL of the provided Lysis Buffer (Pierce), supplemented with 1/10th volume of Calbiochem Protease Inhibitor Cocktail III (EMD Millipore) in 1.5 mL centrifuge tubes, and Misonix XL2000 sonicator (Misonix Inc.) at low power (e.g. 3.5) on ice using 5-second bursts over the course of 45 minutes. Lysates were centrifuged at 10000g for 2 minutes at 4°C, and supernatants transferred to new tubes. 100 µL of each supernatant was removed for isolating biotinylated proteins and another 50 µL for total protein evaluation, the latter of which was combined with 50 µL of 2 x sample buffer (15% glycerol (v/v), 100 mM DTT, 2% SDS (w/v), 0.006% Bromophenol blue (w/v), and 80 mM Tris pH 6.8) and heated to 95°C for 5 minutes. The membrane-localized biotinylated protein fractions were isolated from each 100 µL aliquot on columns loaded with 200 µL of 50% slurry of NeurAvidin® Agarose (Pierce). After a 2 hour incubation at 4°C, unbound proteins were eluted by centrifugation and columns washed 3 times with

Wash Buffer (Pierce) supplemented with protease inhibitor (EMD Millipore). Biotinylated proteins were then eluted using 200 µL of SDS-polyacrylamide gel electrophoresis (PAGE) sample buffer (10% v/v glycerol, 1% SDS, 50 mM DTT and 62.5 mM Tris pH 6.8) and centrifugation. 15 µL aliquots from each protein sample were separated on two identical 7.5% SDS-PAGE gels; one gel was Coomassie-stained and the other transferred to 0.45 µm PROTRAN® nitrocellulose membrane (Whatman International). After blocking in TBS with 0.1% v/v Tween-20 (TTBS) containing 5% w/v skim milk powder, the membrane was incubated with α-LCa_v3 universal antibody (1:500 in TTBS with 5% milk) overnight a 4°C, washed the next day 2 x 15 minutes with TTBS, then incubated with 1:1500 goat α-rabbit conjugated to HRP (Jackson ImmunoResearch Laboratories Inc.) at room temperature for 3 hours. The membrane was subsequently washed 3 x 15 min with TTBS, HRP-activated chemiluminescence was detected by exposing the membrane to BioMax Light Film (Kodak), and both the developed film and the Coomassie-stained gel were imaged and densinometric analysis carried out using an AlphaImager HP acquisition system and the AlphaEase® FC software (Alpha Innotec).

5.15.2 Current density recordings

Equal amounts of all four LCa_v3 splice variant constructs (+8b/12B/-25c, -8b/12B/-25c, +8b/12B/+25c, -8b/12B/+25c) and one containing a deletion of the APRASPEQSD peptide sequence within exon 8b (LCa_v3 +8b/12B/-25c ΔAPRASPE) were calcium phosphate-transfected into HEK-293T cells cultured 6 mL vented flasks[297]. The following day, cells were washed with warm 37°C media and incubated at 28°C overnight, after which they were detached with trypsin (Sigma), plated at ~10% confluency onto glass coverslips, and incubated at 37°C for 1 hour to permit cellular adhesion to the glass. For measurement of peak current, whole-cell patch clamp was used voltage-clamp transfected cells in 2 mM calcium external solution (see above) with 250 ms voltage steps from -110 mV to -42.5 mV. The peak current and cell capacitance was recorded for each cell, and current density was determined by dividing the peak calcium current of each cell by its cell capacitance (pA/pF).

5.15.3 Luminometry

As indicated above, HA tags were introduced into the domain I S5-S6 extracellular loops of the four full-length LCa_v3 variant pIRES2-EGFP constructs, upstream of the domain I pore helices, using an annealed oligonucleotide adaptor (Figure M5C). As for biotinylation experiment, agarose gel

electrophoresis and ethidium bromide-based quantification of the four HA-tagged LCa_v3 constructs was used to ensure transfection of equimolar amounts plasmid (~8 µg depending on size of constructs; not shown) into HEK-293T using Lipofectamine LTX reagent (Invitrogen). For controls, mock-transfected cells and cells transfected with untagged LCa_v3 (+8b/12B/+25c) were included in the experiment. After transfection, cells were incubated at 28°C for 2 days, then each split into 4 wells of poly-L-lysine-coated (Sigma) 24-well plates (Black Visiplate™, PerkinElmer, Waltham, MA), incubated at 37°C for 3 hours, washed twice with warm PBS (37°C), then fixed with warm PBS containing 4% paraformaldehyde for 5 minutes. Cells were then washed 2 x 5 minutes with PBS, and ½ of wells were permeabilized with PBS containing 0.1% v/v Triton X-100 for 5 minutes and all wells washed 3 x 5 minutes with PBS. All cells were blocked for 50 min at room temperature (1% fetal bovine serum/FBS and 0.05% TWEEN-20 in PBS), incubated with rat α-HA monoclonal antibody (Roche; 1:1000 in PBS with 1% v/v FBS and 0.05% TWEEN-20), washed 4 x 10 minutes with PBS, then incubated with goat α-rat HRP-conjugated secondary antibody (Jackson ImmunoResearch Laboratories; 1:1000 in PBS with 1% v/v FBS and 0.05% TWEEN-20) for 30 minutes. After washing 3 x 10 minutes with PBS, 400 µL of SuperSignal® ELISA Femto Maximum Sensitivity Substrate (Thermo Scientific) and plates were detected using a FilterMax F5 Multi-Mode Microplate Reader (Molecular Devices) using the luminometer setting of SoftMax Pro 6.1 software (Molecular Devices) for data acquisition and analysis.

Table M8. Reagents and volumes used to prepare SDS-polyacrylamide gels for protein electrophoresis (SDS-PAGE).

1mm spacer	5.0%		7.5%		10.0%		12.0%		14.0%		16.0%	
	2 Gels	4 Gels	2 Gels	4 Gels	2 Gels	4 Gels	2 Gels	4 Gels	2 Gels	4 Gels	2 Gels	4 Gels
mL Acrylamide Stock	2.50	5.00	3.75	7.50	5.00	10.00	6.00	12.00	7.00	14.00	8.00	16.00
mL Resolving Buffer	3.80	7.60	3.80	7.60	3.80	7.60	3.80	7.60	3.80	7.60	3.80	7.60
mL ddH2O	8.58	17.16	7.33	14.66	6.08	12.16	5.08	10.16	4.08	8.16	3.08	6.16
mL 10% APS	0.115	0.230	0.115	0.230	0.115	0.230	0.115	0.230	0.115	0.230	0.115	0.230
uL TEMED	7.50	15.00	7.50	15.00	7.50	15.00	7.50	15.00	7.50	15.00	7.50	15.00
Total Volume (mL)	15.00	30.00	15.00	30.00	15.00	30.00	15.00	30.00	15.00	30.00	15.00	30.00

1mm spacer Stacking Gel	2 Gels	4 Gels
mL Acrylamide Stock	0.85	1.70
mL Stacking Buffer	1.25	2.50
mL ddH2O	2.85	5.69
mL 10% APS	0.05	0.10
uL TEMED	5.00	10.00
Total Volume (mL)	10	20

Resolving Buffer:
1.5 M Tris pH 8.8
0.4% SDS

Stacking Buffer:
0.5 M Tris pH 6.8
0.4% SDS

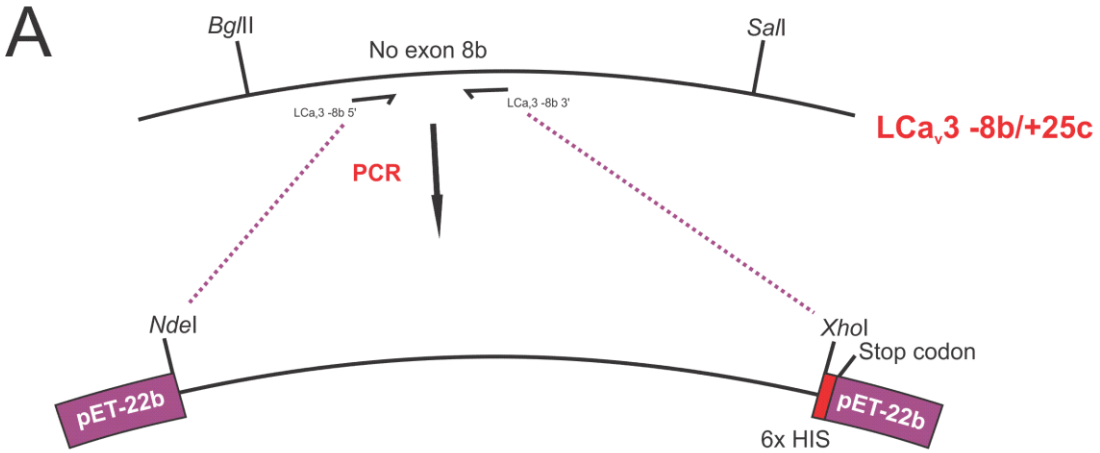

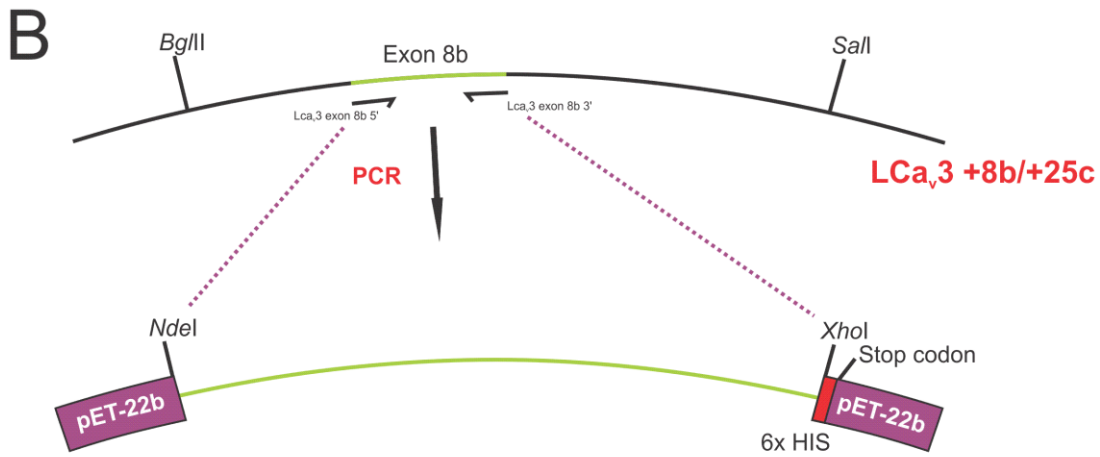

C

LCa$_v$3 I-II linker -8b:

MGTNNLRSQQQYPSVVRQLSLSHQPPVHHHQHQHLLPLPSPLPPQHLHHINLVTPDIRYQSPPRPSSSPQAPRA
SPEQSDIDSMSSPRRPNYLVLPSSNYSLNPSSESLAMSHLSMDPFTPVLFKSQQNSPNHLTTNFGFAFPLLLSR
ASSFNSGACGPGKIMPSLPEVLAAQGAKNAVLAASNMLLNVDYEPSKTQSLADLE**HHHHHH**

LCa$_v$3 exon 8b:

MSETKKRETERMMQERKRFQSCSTLASNSEPGGYYSELLKLVAQVYRRVKRKVIKTRGLQKINPEKSLSLRRKK
SKKKGLFADNLLMDIVGDKQLTTQLSMQSDTDVLQLGTGQTQADQEASSCGGGGVIGAGDKELAGEHGTLSYNP
TALE**HHHHHH**

Figure M7. Cloning of LCa$_v$3 I-II linker cDNA isoforms into IPTG-inducible protein expression vector pET-22b(+). A) For cloning the exon 8b cDNA into pET-22b(+), primers were designed to PCR amplify this exon from a cDNA template containing exon 8b (LCa$_v$3 +8b/-25c in pIRES2-EGFP). The PCR product was cloned into pET-22b(+) using *Nde*I and *Xho*I restriction sites incorporated by the 5' and 3' primers, respectively. **B)** A similar strategy was used to clone a large portion of the LCa$_v$3 I-II linker, lacking the exon 8b cDNA sequence, into pET-22b(+) (using LCa$_v$3 -8b/-25c in pIRES2-EGFP as template). In both cases, primers were designed to place the LCa$_v$3 cDNA sequences in frame with N-terminal ribosome binding sites and C-terminal 6x histidine coding sequences, followed by stop codons, all contained within pET-22(+). **C)** Predicted protein sequences for peptides expressed in bacteria using the LCa$_v$3 I-II linker pET-22b(+) constructs. The predicted molecular weights are 23.011 and 17.609 kDa for the I-II linker peptide lacking 8b and exon 8b peptide, respectively (predicted using ExPASy ProtParam: http://web.expasy.org/protparam/).

Table M9. Primers used for cloning of LCa_v3 I-II linkers cDNA sequences into bacterial protein expression vector pET-22b(+).

Application	Name	Sequence
Peptide expression		
	LCa_v3 -8b 5'	AAATGTCATATGTCTGAAACAAAGAAGAGAGAGACAGAG
	LCa_v3 -8b 3'	GAATCTCTCGAGGGCAGTAGGGTTATAGGATAAAGTGC
	LCa_v3 exon 8b 5'	AAAACATATGGGTACTAATAACCTAAGG
	LCa_v3 exon 8b 3'	AAAACTCGAGGTCGGCTAACGATTGAGT

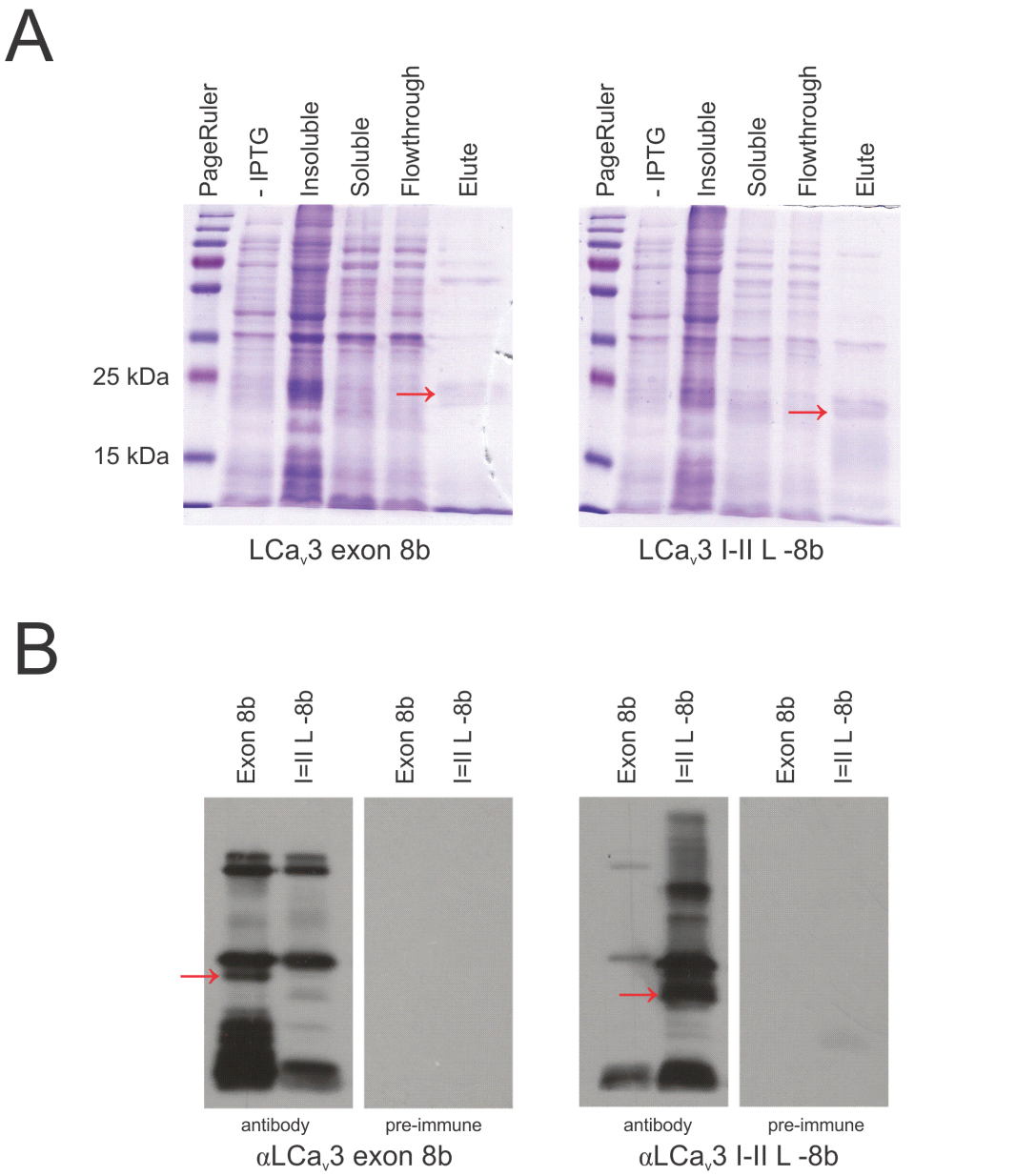

Figure M8. Expression and affinity-purification of LCa_v3 I-II linker peptides for polyclonal antibody production, and testing of antibodies using the expressed proteins. A) Image of a Coomassie-stained SDS-polyacrylamide gels containing various electrophoresed protein fractions (30 µL of each) obtained during expression and affinity purification of LCa_v3 I-II linker peptides. Lanes (left to right): 1) PageRuler™ Plus Prestained Protein Ladder (Fermentas), 2) 1 mL of each culture was removed just prior to IPTG induction, cells were centrifuged at 4000g, resuspended with 100 µL of PBS, then lysed and proteins solubilized with 100 µL of 2x sample buffer, 3) insoluble pellets were each resuspended with 20 mL of PBS, and 80 µL aliquots were each combined with 120 µL of PBS and 200 µL of 2x sample buffer, 3) 80 µL of soluble supernatants were combined with 120 µL of PBS and 200 µL of 2x sample buffer, 4) 80 µL of each column flowthrough was collected and combined with 120 µL of PBS and 200 µL of 2x sample buffer, and 5) 50 µL of Ni^{2+} affinity-purified elutes were combined with 50 µL of 2x sample buffer. The red arrows point to the purified proteins, corresponding to histidine-tagged I-II linker peptides of LCa_v3 (left = exon 8b at ~21 kDa; right = I-II linker lacking 8b at ~17.6 kDa). **B)** Testing of LCa_v3 I-II linker polyclonal antibodies, raised in rabbits using dialyzed peptides from above, by western blotting. Four SDS-PAGE gels, each containing 15µL aliquots of the two expressed, affinity-purified, and dialyzed LCa_v3 peptides (exon 8b on left and I-II linker lacking 8b on right for each set) were transferred onto nitrocellulose and blotted with either pre-immune serum (right panel of each set) or αLCa_v3 I-II linker antibody (left panel of each set). Both the exon 8b and I-II linker lacking 8b antibodies detect their corresponding peptides on western blots (red arrows).

A

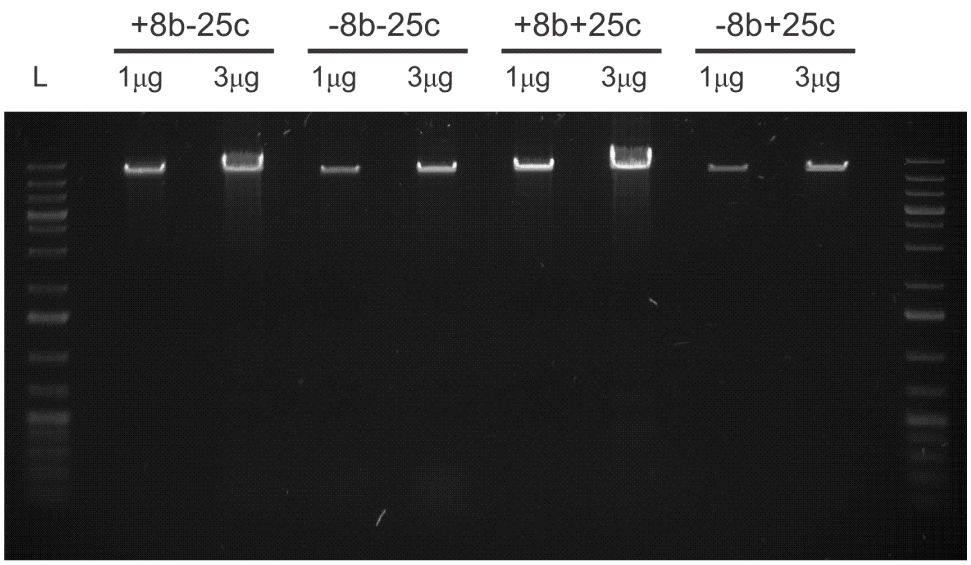

B

Plasmid	µg DNA	Source	IDVs	Signal	Rel. amt.	Vol. (µL)
+8b-25c	1	DNA	43223898	22621271	71.48%	8.4
		Bkgrnd	20602627			
	3	DNA	62924750	36559810		
		Bkgrnd	26364940			
-8b-25c	1	DNA	33038049	11966851	37.82%	15.9
		Bkgrnd	21071198			
	3	DNA	46473948	23699100		
		Bkgrnd	22774848			
+8b+25c	1	DNA	56094682	31645086	100.00%	6.0
		Bkgrnd	24449596			
	3	DNA	77942423	49240768		
		Bkgrnd	28701655			
-8b+25c	1	DNA	28219491	8404959	26.56%	22.6
		Bkgrnd	19814532			
	3	DNA	38835067	19018456		
		Bkgrnd	19816611			

Figure M9. Agarose gel electrophoresis-based quantification of LCa$_v$3 pIRES2-EGFP constructs. A) Image of ethidium bromide stained agarose gel containing 1 and 3 µg (based on UV spectrophotometric quantification) of *Xho*I restriction-digested LCa$_v$3 splice isoform constructs in pIRES2-EGFP. B) For quantification, densinometric measurements were made from the gel image using an AlphaImager HP acquisition system with AlphaEase® FC software (Alpha Innotec). **B)** Rectangular boxes of equal sizes were used to sample the integrated density value (IDVs) of each DNA fragment and a corresponding background reading just below each band. Signals were determined by subtracting the background IDV from each DNA fragment IDV, and the 1 µg value for LCa$_v$3 +8b/+25c (yellow) was used as a reference to upscale the volumes of the other plasmids, based on their 1 µg signal values (right column).

Appendix A
Additional materials for Chapter 2.1

Materials and Methods

Cloning and Sequencing of LCa_v3

The complete open reading frame for *LCa_v3* was determined from at least three independent, overlapping DNA fragments from the PCR screening of *L. stagnalis* central nervous system λZAP cDNA libraries to generate a consensus gene. The full-length 9031-bp cDNA transcript is available in DDBJ/EMBL/GenBank™ databases under accession no. AF484084 and replaced a previous partial coding sequence entry of 5991 bp. The final clone was assembled from four overlapping PCR with sticky ends (numbered by cDNA transcript positions), *Xho*I-*Spe*I (209–2865), *Spe*I-*Sal*I (2812–4544), *Sal*I-*Mlu*I (4503–6874), and *Mlu*I-*BamH*I (6850–8869). Silent mutations were created in a Kozak consensus sequence upstream of the start codon (209–211), an *Mlu*I site (6858–6863), and several hairpin structures thought to interfere with the site-directed mutagenesis reaction (5225–5285). The full-length *LCa_v3* coding sequence was assembled between *Xho*I and *BamH*I sites in bicistronic vector pIRES2-EGFP (Clontech). Low frequency of positive recombinants during cloning and the slow rate of growth of the full-length plasmid in bacteria (five full days before a colony appears on a bacterial plate after transformation) suggest that the plasmid insert is toxic to bacteria.

Transfections

HEK-293T cells (M. Calos, Stanford University) were cultured in Dulbecco's modified Eagle's medium (Sigma) with 10% fetal bovine serum (Sigma) and supplemented with 0.5% (v/v) penicillin-streptomycin solution (Sigma). For electrophysiology, 6 μg of the *LCa_v3* pIRES2-EGFP construct was transfected into cells at 40–50% confluency using the standard Ca^{2+} phosphate transfection method. After overnight transfection, the cells were washed twice with culture media and incubated at 28°C in a humidified, 5% CO_2 chamber for 3 days. After incubation, cells were detached using a trypsin-EDTA solution (Sigma), plated at 10% confluency onto glass coverslips, and incubated at 37 °C for 4 h because adhesion to the glass substrate requires warmer temperatures[341].

Whole Cell Patch Clamp Recordings

Whole-cell recordings were carried out at 23°C using either a 5 mm external Ca^{2+} solution (5 mm $CaCl_2$, 166 mm tetraethylammonium chloride, 10 mm HEPES, pH 7.4) or 5 mm external Ba^{2+}

solution (5 mm $BaCl_2$, 166 mm tetraethylammonium chloride, 10 mm HEPES pH 7.4) and an internal solution consisting of 125 mm CsCl, 10 mm EGTA, 2 mm $CaCl_2$, 1 mm $MgCl_2$, 4 mm MgATP, 0.3 mm Tris-GTP, and 10 mm HEPES, pH 7.2. Recordings were obtained using an Axopatch 200B amplifier, sampled to a PC through a Digidata 1440a A/D converter. Data were filtered at 2 kHz and digitized at 5 kHz and acquired using pCLAMP 10.1 software (Molecular Devices). The pipette resistance was maintained between 3 and 5 megaohms, and the typical access resistance was between 4 and 5 megaohms. Only recordings with minimal leak (<10%) and small current sizes (<2 nA) were used for analysis, and offline leak subtraction was carried out using the Clampfit 10.1 software (Molecular Devices). Series resistance was compensated to 70% (prediction and correction; 10-μs lag). A gravity flow system was used to perfuse 5 mm Ca^{2+}- or Ba^{2+}-containing extracellular solution or 5 mm Ca^{2+} external solution containing solubilized Ni^{2+} (Sigma) or mibefradil (Sigma).

Data Analysis

Ca^{2+} current activation curves were constructed by converting the peak current values from each current-voltage relationship data set to conductance using the equation gCa = $I_{peak}/(V_{command} - E_{Ca})$, where I_{peak} is the peak current, $V_{command}$ is the command pulse potential, gCa is the calcium conductance, and E_{Ca} is the Ca^{2+} reversal potential as determined by linear extrapolation of the current values in the ascending portion of the current-voltage relationships. Conductance values were then normalized and individually fitted with the Boltzmann equation, $g/g_{max} = (1 + (\exp(-V_{command} - V½)/K)) - 1$, where g is the peak conductance, g_{max} is the maximal peak Ca^{2+} conductance, $V_{command}$ is the conditioning potential, $V½$ is the half-maximal activation, and k is the activation slope factor. The steady-state inactivation curves were constructed by plotting normalized current (peak test pulse current/peak prepulse current) as a function of the inactivating potential. The data were fitted with a Boltzmann equation, $I/I_{max} = (1 + \exp((V_{inact} - V½/k)) - 1$, where I is the peak test pulse current, I_{max} is the peak test pulse current when the conditioning pulse was −110 mV, V_{inact} and V½ are the conditioning potential and the half-maximal inactivation, respectively, and k is the inactivation slope factor. Kinetics of activation, inactivation, and deactivation were determined by fitting monoexponential functions over the growing or decaying phases of each current trace using the software Clampfit 10.1.

Antibody Production

LCa_v3 I-II linker coding sequence (1976–2575 bp) was PCR-amplified and cloned into the bacterial protein expression vector pET-22b(+) (Novagen) via *Nde*I and *Xho*I restriction sites. Peptide

expression was induced by 1 mm isopropyl 1-thio-β-d-galactopyranoside in Rosetta™ (DE3) cells (Novagen) transformed with the pET22b(+) plasmid-containing construct. Supernatant of lysed bacterial cells containing His_6 *LCa_v3* I-II linker expression was run and washed through a column containing Ni^{2+}-charged His·Bind® resin (Novagen), then eluted off of the beads, dialyzed, and quantified using the Bradford assay. A rabbit was injected three times with recombinant proteins emulsified with Freund's complete adjuvant for the first injection and Freund's incomplete adjuvant (Sigma) for the subsequent injections. IgG rabbit antiserum was tested for immune reactivity with the antigen by Western blotting.

Immunolabeling of Recombinant LCa_v3 in HEK-293T Cells

HEK-293T cells were transfected with either 8 μg of *LCa_v3* in pIRES2-EGFP alone or with 3.2 μg of *LCa_v1* α1 subunit in pIRES2-EGFP[214] plus 2.4 μg of the rat β1 subunit in pMT2 and 2.4 μg of rat $\alpha_2\delta$ in pMT2. Cells were washed after transfection and incubated at 28°C for 1 week before trypsinization and plating onto glass coverslips. Cells were then fixed with 1% paraformaldehyde in PBS overnight at 4°C, washed twice with PBS, then permeabilized using phosphate-buffered saline containing 0.2% Tween 20 (PBST) for 10 min at room temperature. 1:500 primary antibody or preimmune serum was applied to preblocked cells overnight in PBST containing 3% bovine serum albumin. 3×-washed cells were incubated with 1:1000 diluted AlexaFluor 594 goat anti-rabbit secondary antibody in PBST containing 3% bovine serum albumin for 1 h at 23 °C, washed 4×, and imaged at 40× magnification with a Zeiss AxioObserver Z1 inverted epifluorescent microscope to detect AlexaFluor 594 antibody and EGFP. Images were captured using Zeiss AxioVision software, and brightness/contrast was adjusted using Adobe Photoshop.

Southern Blot

15-μg aliquots of genomic DNA isolated from *Lymnaea* tissue were digested with *Eco*RV, *Hind*III, *Eco*RI, and *Xho*I, and DNA fragments were separated through a 1% agarose gel. Digested DNA was transferred onto a positively charged nylon membrane (Roche Applied Science), and a standard hybridization procedure was carried out using manufacturer's instructions (EasyHyb, Roche Applied Science). Membranes were probed with a gel-purified 597-bp PCR product of the *LCa_v3* gene (1979–2575 bp) incorporated with DIG-11-dUTP (Roche Applied Science). The probe was localized on the membrane using anti-digoxigenin alkaline phosphatase-conjugated antibody (Roche Applied Science; 1:5000 dilution) and color substrate solution nitro blue tetrazolium/5-bromo-4-chloro-3-indolyl phosphate (Roche Applied Science).

Semiquantitative RT-PCR

RNA was extracted from the central nervous system of *L. stagnalis* using Tri Reagent (Sigma) and optimized from standard methods[325]. RNA was treated with DNase (Fermentas) to remove contaminant DNA for RT-PCR analysis. RNA was quantified by spectrophotometry and visualized by gel electrophoresis to confirm the lack of degradation. First-strand cDNA were synthesized from RNA at 54°C for 80 min and 70°C for 15 min using either oligo-dT or random hexamer primers and Superscript III reverse transcriptase (Invitrogen) and controls were prepared that lacked reverse transcriptase. Primers used for cDNA amplification were designed to have similar melting temperatures, minimal secondary structure, and amplified fragments of similar sizes (500–600 bp). PCR primers spanned sequences from the following genes (GenBank™ accession nos.: cDNA transcript positions): *Lactin* (DQ206431: 38–628), *LNALCN* (AF484086, 3149–3761), *LCa_v1* (AF484079: 5421–6103), *LCa_v2* (AF484082: 5427–6095), *LCa_v3* (AF484084: 7816–8546). PCR products generated after 25 cycles in the thermocycler were imaged in ethidium bromide-stained gels using a gel documentation system (Alpha Innotech) under UV light. Densinometric analysis of DNA band intensity was performed using AlphaEase® FC software (Alpha Innotech).

Appendix B
Additional materials for Chapter 2.2

Materials and Methods

Source of animals

Giant pond snails, *Lymnaea stagnalis* were raised in-house in a snail vivarium and breeding facility in B1-177, Department of Biology, University of Waterloo.

Identification of splice variants

During the initial sequencing and cloning of LCa_v3[1], multiple variable sequences were identified, including conserved optional exons 8b in the I-II linker and 25c in the III-IV linker. PCR-screening attempts with *Lymnaea* cDNAs did not reveal exon 26, found in the III-IV linkers of mammalian $Ca_v3.1$ and $Ca_v3.2$ channel genes (Fig. S5). Genomic sequence surrounding optional exons 8b and exon 25c were obtained by PCR and compared to other available snail and mammalian sequences (Figs. S1, S2, S3; Table S1). PCR was also used to generate the APRASPEQSD sequence deletion, HA-tagged channels and -/+ exon 8b and -/+ exon 25c splice variants (Table S1).

RNA extraction and PCR

mRNA for cDNA analyses was extracted[325] from 50-75% and 100% embryos grouped according to morphological features of egg capsules[290] and the shell length of juvenile and adult snails[292]. *Lymnaea* transcripts were amplified by quantitative RT-PCR (qPCR) with primers designed against LCa_v1[214], LCa_v2[213], LCa_v3 and -/+ exons 8b and 25c splice isoforms of LCa_v3 (Table S2). qPCR transcripts were normalized against standards, actin, SDHA and HPRT1. Cycle threshold (CT) values for the HPRT1 gene were found to produce the lowest stability value (i.e. 0.098) using NormFinder software[330], indicating its suitability as a reference gene. Expression levels of genes/isoforms were normalized relative to HPRT1[331] where ratio = $(E_{\text{target gene}})^{\Delta CT\text{target gene}}/(E_{HPRT1})^{\Delta CTHPRT1}$. Amplicons ranged from 119 to 145 bp, producing single products, with PCR efficiencies (E) ranging from 86 to 110%, with templates generated with 1:5 serial dilutions of pooled cDNA as templates (Table S2). qPCR reactions were carried out in quadruplicate, and standardized between 96 well plate samples with primers against HPRT1.

Cloning, transfection and electrophysiological recording

Previously, the full-length coding sequence of LCa_v3 +8b -25c was cloned into the pIRES2-EGFP vector for heterologous expression in HEK-293T cells with bicistronic expression of eGFP (BD Biosciences Clontech)[1]. The other three splice variant combinations, -8b -25c, -8b +25c and +8b +25c as well as +8b (ΔAPRASPE) -25c were created by PCR cassette mutagenesis and reinserted into pIRES2-EGFP vector (Table S1).

We use an optimized cell culture and $CaPO_4$ transfection strategy for heterologous expression and patch clamp recording of ion channel cDNAs in HEK-293T cells, previously outlined in video protocol format http://www.jove.com/video/2314[297]. Whole cell patches were sealed with pipette resistances of 2-5 MΩ, and with typical access resistance maintained after breakthrough between 4 and 6 MΩ[297,1]. Series resistance was compensated to 70% (prediction and correction; 10-μs time lag). Only recordings with minimal leak (<10% of peak) and small current sizes (<500 pA) were used for generating peak current-voltage relationship curves due to loss of voltage clamp above 500 pA; all other recordings were typically maintained below 1.5 nA. Offline leak subtraction was carried out using the Clampfit 10.1 software (Molecular Devices). Voltage-command protocols and the curve fitting of data are described previously[297,1].

Measurement of membrane expression

Current densities (pA/pF) were measured from transfections of 6 μg of plasmid of the LCa_v3 splice variants[297], quantified to equal amounts by plasmid linearization, electrophoresis and densinometric analysis.

Luminometry

Single hemagglutinin (HA) epitope tags were introduced into the Domain I s1-s2 extracellular loops of the four full-length LCa_v3 variant constructs. Equimolar amounts of mock, epitope-tagged and un-tagged LCa_v3 were transfected into HEK-293T cells, and after incubation cells were labeled with rat α-HA monoclonal antibody under membrane permeabilized and non-permeabilized conditions, and luminometry quantified using a FilterMax F5 Multi-Mode Microplate Reader (Molecular Devices) with a chemiluminescence reaction catalyzed with a goat α-rat HRP-conjugated secondary antibody.

Biotinylation

Surface-expressed channels were measured by biotinylation and identified in Western blots with snail Ca_v3 channel-specific polyclonal antibodies raised in rabbits using as antigen a large portion of the LCa_v3 I-II linker peptide lacking exon 8b expressed and purified from bacteria using a pET-22b(+) protein expression vector (Table S1). Antibodies were pre-tested for immune reactivity in Western blotting and immunolabeling, as reported previously for antibodies produced strictly against the exon 8b peptide sequence[1]. HEK-293T cell were transfected with equimolar amounts of LCa_v3 channel variants and biotinylated with Sulfo-NHS-SS-Biotin (Pierce). Surface-labeled, biotinylated fractions were isolated using NeurAvidin® Agarose columns, with the Ca_v3 channel surface and total protein pools quantified on Western blots using HRP-activated chemiluminescence from a goat α-rabbit secondary antibody.

Supplementary Materials and Methods

Identification of LCa$_v$3 channel splice variants

During the initial sequencing and cloning of LCa$_v$3[1], multiple sites containing splice variability were identified, including conserved optional exons 8b in the I-II linker and 25c in the III-IV linker. Exon 26, found in the III-IV linkers of mammalian Ca$_v$3.1 and Ca$_v$3.2 channel genes was not detected in these preliminary studies, prompting us to do a comprehensive search for an equivalent exon in LCa$_v$3. Briefly, *Lymnaea* adult CNS and embryonic whole animal cDNAs were PCR-screened using two nested primer pairs flanking the variable site of the III-IV linker coding sequence (Table S1). Only two DNA bands were visible in ethidium bromide-stained agarose gels after electrophoresis (Fig. S5 *A*), whose intensity suggested an enrichment of the ΔΔ variant in the embryo. Since exon 25c and 26 PCR products could be of similar size, secondary PCRs were repeated and further analyzed using an Experion^{TM} automated DNA 1K electrophoresis system (BioRad), which provides both high resolution of separated DNA molecules and quantitative output of their relative abundance. Only two sizes were detectable, and the corresponding peak signal amplitudes demonstrate that the ΔΔ variant is enriched in the embryo (Fig. S5 *B*). These same DNA products were gel-purified and ligated into pGEM-T Easy Vector (Promega), the ligations were transformed into *E. coli* DH5α, and the resulting white colonies were used for plasmid isolation via the alkaline lysis method (modified from Birnboim and Doly 1979[332]. Plasmids were then restriction digested with *EcoR*I (NEB), which flanks the multiple cloning site of the pGEM-T Easy, and the sizes of cloned PCR amplified inserts were evaluated using agarose gel electrophoresis. Again only two sizes were visible (Fig. S5 *C*), and sequencing of several clones of either size failed to identify an exon 26.

To assess whether the splicing of LCa$_v$3 transcripts in the I-II and III-IV linker coding sequences resembles that of Ca$_v$3.1 and Ca$_v$3.2, we sequenced the genomic DNA corresponding to these regions along the gene. Genomic DNA was isolated from adult animals ground in liquid nitrogen[342], and this was used as template for nested PCRs with primers flanking respective intron splice sites (Table S1). PCR reactions were carried out using high fidelity DNA polymerase PfuTurbo AD (Agilent Technologies Inc.), and amplified DNA was electrophoresed, gel purified, and subject to multiple rounds of sequencing to obtain the complete sequence (Figs. S1, S2).

Measuring mRNA expression levels of LCav3 channel splice variants

Tissue isolation and RNA extraction: The embryonic development schedule was adopted from Marois and Croll, 1992[290] and Nagy and Elekes, 2002[291] and spans between a range of 1 to 100% development based on morphological and histological criteria. The juvenile to adult development

schedule was adopted from McComb, Varshney and Luckowiak, 2005[292] and is based on shell length. Embryonic development was assessed by observation of egg capsules under a light microscope, and sacs were grouped into two groups of 50-75% and 100% developed. Juveniles were selected and grouped based on shell lengths of 1.0 to 1.5 cm while adults contained shells 2.0 to 2.5 cm in length; this criteria was previously shown to separate non-sexually mature juvenile animals from sexually mature adults. For whole animal RNA extracts, egg capsules or entire animals were ground in liquid nitrogen and stored in 1.5 mL centrifuge tubes at -80^{o}C until RNA extraction. Juvenile and adult organs were dissected from anesthetized animals (10% v/v Listerine 5 to 10 min) and placed directly into 1.5 mL tubes in liquid nitrogen. RNA was extracted with Tri-Reagent[325], quantified using UV spectrophotometry and quality assessed by agarose gel electrophoresis and visualization of ethidium bromide-stained gels under UV light. For DNase treatment, 10 µg of each RNA extract was diluted to 100 ng/µL in a volume of 100 µL in separate 1.5 mL tubes and to each added 12 µL of 10x DNase buffer (Ambion), 2 µL of RiboLockTM RNase inhibitor (Fermentas) and 2 µL of DNase I enzyme (Ambion) and tubes were incubated at 37^{o}C for 30 minutes. Samples were then treated with an equal volume of 50:50 v/v phenol/chloroform, precipitated with ethanol, and resuspended with 50 µL DEPC-treated water.

Reverse transcription and qPCR: Reverse transcription was carried out using a iScript^{TM} Reverse Transcriptase Supermix (BioRad) with each reaction containing 800 ng of RNA, 5 µL of iScript RT supermix, and DEPC water for a total of 20 µL. Temperature cycling for the reactions was 25^{o}C for 5 min, 42^{o}C for 30 min, then 85^{o}C for 5 min. qPCR primers were designed to selectively amplify a universal region and specific splice variants of *Lymnaea* LCa_v3 transcripts, and universal primers were designed for LCa_v3 as well as *Lymnaea* neuronal $\alpha_2\delta$, LCa_v1, and LCa_v2 (Table S2). The specificity of PCR primers for particular splice isoforms was assessed by comparing the size of PCR products amplified from a pooled qPCR cDNA library with those amplified from cloned cDNAs, as well as by analyzing the melting curves of PCR products after all qPCR experiments. Amplicons ranged from 119 to 145 bp, and PCR primer efficiency was determined using relative standard curves generated with 1:5 serial dilutions of pooled cDNA as templates. All primers were found to have PCR efficiencies (E) ranging from 86 to 110%. qPCR reactions were done in quadruplicate 10 µL reactions using, each containing 5 µL of SsoFastTM EvaGreen® Supermix, 0.5 µL of each primer at an initial concentration of 10 µM, 3 µL of water, and 1 µL of template cDNA. For negative controls, used 1 µL of DNase-treated RNA at 40 ng/µL instead of cDNA, and 1 µL of DEPC water for no the template controls. To standardize between plates, each contained triplicate qPCR reactions using primers

against HPRT1 (see below) and 1:5 diluted pooled qPCR cDNA as template. All cycle thresholds (CT) used for analysis were determined relative to the average CT of the HPRT1 controls in each plate. PCR amplification and fluorescence reading was done in a Bio-Rad C1000^{TM} Thermal Cycler equipped with a CFX96^{TM} Real-Time System, with cycling parameters of 90^{o}C for 30 seconds followed by 40 cycles of 95^{o}C for 5 seconds and 56^{o}C for 5 seconds.

qPCR data analysis: Primers were designed against *Lymnaea* actin (GenBank accession number DQ206431), subunit A of the succinate dehydrogenase complex (SDHA; GenBank accession number ES578163.1), and hypoxanthine phosphoribosyltransferase 1 (HPRT1; GenBank accession number ES571571.1) for use as reference genes (Table S2). CT values for the HPRT1 gene were found to produce the lowest stability value (i.e. 0.098) using NormFinder software[330], indicating its suitability as a reference gene. Conversely, actin and less so SDHA CT values varied considerably between tissues (stability values of 0.634 and 0.296, respectively). To quantify relative expression levels of genes/splice isoforms of interest relative to HPRT1, data was analyzed using methods published by Pfaffl 2001[331], where ratio = $(E_{\text{target gene}})^{\Delta CT\text{target gene}}/(E_{HPRT1})^{\Delta CTHPRT1}$.

Cloning of LCa$_v$3 channel splice variants for expression in HEK-293T cells

Previously, the full-length coding sequence of LCa$_v$3 +8c -25c was cloned into the pIRES2-EGFP vector for heterologous expression in HEK-293T cells with bicistronic expression of eGFP[1] (BD Biosciences Clontech). To create the -8b sub-clone, a *Bgl*II to *Sal*I fragment was excised from the full length clone (containing exon 8b) and inserted into a circularized pGEM-T Easy vector (Promega) that had been modified by insertion of annealed oligonucleotides (Table S1) into *Nco*I of the vector to introduce a *Bgl*II site. Removal of the exon 8b coding sequence was achieved by doing PCR (with high fidelity PfuTurbo AD DNA polymerase), using the entire subclone as template and primers flanking exon 8b whose 3' ends were directed away from the optional exon such that PCR amplification would produce a linear plasmid lacking 8b. 5' phosphate groups on the primers enabled blunt-end ligation and re-circularization of the PCR product, which was then transformed into Stbl2 bacteria (Invitrogen) for plasmid isolation. After confirmation of sequence, the -8b *Bgl*II to *Sal*I DNA fragment was re-inserted into the full-length LCa$_v$3 clone to create a full-length -8b -25c variant. To create the +25c sub-clone, a *Sal*I to *Mlu*I fragment of the original full-length LCa$_v$3 clone was inserted into circularized pGEM-T Easy. Two rounds of Assembly PCR were used with the -25c sub-clone as template with 3' primers designed to introduce the exon 25c coding sequence followed by an *Apa*I restriction site present in LCa$_v$3 just downstream of 25c (Table S1). The PCR product containing the additional 25c sequence was then cloned back into the *Mlu*I-*Sal*I sub-clone via *Apa*I, present in

both the vector and the LCa_v3 coding sequence, and confirmed by sequencing. The modified *Sal*I to *Mlu*I cDNA was then cloned back into the full-length LCa_v3 +8b -25c and -8b -25c pIRES2-EGFP clones to create LCa_v3 +8b +25c and LCa_v3 -8b +25c in pIRES2-EGFP, respectively. The ΔAPRASPE sub-clone was created in a similar manner as -8b, with primers that removed the coding sequence for APRASPEQSD (Table S1). The mutant *Bgl*II-*Sal*I DNA was cloned back into the full-length LCa_v3 +8b -25c to create LCa_v3 +8b(ΔAPRASPE) -25c in pIRES2-EGFP.

Transfection and electrophysiological recording

Previously, we reported an optimized cell culture and $CaPO_4$ transfection strategy for heterologous expression of ion channel cDNAs in HEK-293T cells for electrophysiological recording[297]. This methodology was used for all transfections of LCa_v3 splice variant vectors for electrophysiological recording, using 6 µg of vector DNA per transfection. Whole-cell patch clamp technique was done as previously reported[297,1] using a 2 mM external calcium solution (2 mM $CaCl_2$, 160 mM TEA-Cl, 10 mM HEPES pH 7.4 with TEA-OH) and an internal solution containing 110 mM CsCl, 10 mM EGTA, 3 mM Mg-ATP, 0.6 mM Na-GTP, and 10 mM HEPES pH 7.2 with CsOH (11). All chemicals were from SIGMA. Recordings were done at room temperature; the pipette resistance was maintained between 2 and 5 megaohms, and the typical access resistance between 4 and 6 megaohms. Series resistance was compensated to 70% (prediction and correction; 10-µs time lag). Only recordings with minimal leak (<10% of peak) and small current sizes (<500 pA) were used for generating peak current-voltage relationship curves due to the loss of voltage clamp above 500 pA; all other recordings were typically maintained below 1.5 nA with the exception of current density analysis (see below). Offline leak subtraction was carried out using the Clampfit 10.1 software (Molecular Devices).

Data Analysis of electrophysiological data

Summary of electrophysiology data is provided in Table 1. For the calcium current activation plots corresponding to cloned LCa_v3 channel variants, the peak current values from each current-voltage relationship data set were converted to conductance values using the equation $gCa = I_{peak}/(V_{command} - E_{Ca})$, where gCa is the calcium conductance, I_{peak} is the peak calcium current, $V_{command}$ is the command potential, and E_{Ca} is the Ca^{2+} reversal potential extrapolated from the linear ascending portion of the averaged current-voltage relationship curve for each variant. Conductance values were then normalized and individually fitted with the Boltzmann equation, $g/g_{max} = (1 + (\exp(-V_{command} - V_{½})/K)) - 1$, where g is the peak Ca^{2+} conductance, g_{max} is the maximal peak conductance, $V_{command}$ is the conditioning potential, $V_{½}$ is the half-maximal activation, and k is the activation slope factor.

Steady-state inactivation curves were constructed by plotting normalized peak currents (peak test pulse current/peak pre-pulse current) as a function of various inactivating potentials. The data were fitted with a Boltzmann equation, $I/I_{max} = (1 + \exp((V_{inact} - V_{½}/k)) - 1$, where I is the peak test pulse current, I_{max} is the peak test pulse current from a conditioning potential of -110 mV, V_{inact} and $V_{½}$ are the conditioning potential and the half-maximal inactivation, respectively, and k is the inactivation slope factor. Kinetics of activation, inactivation, and deactivation were determined by fitting monoexponential functions over the growing or decaying phases of each current trace using the software Clampfit 10.1. Recovery from inactivation of peak Ca^{2+} currents, elicited by stepping to -35 mV, were assessed for each channel variant using a two pulse protocol, with a 1 second pre-pulse to inactivate channels paired to subsequent test pulses occurring at increasing time intervals from the inactivating pre-pulse to measure recovery. Plots of the standardized recovery (test pulse peak current/pre-pulse peak current) as a function of the time between pre- and test pulses were fitted with monoexponential curve functions.

Measurement of membrane expression of LCa_v3 channel splice variants in HEK-293T cells

Current density analysis

Equal amounts of all four LCa_v3 splice variant and ΔAPRASPE pIRES2 constructs (6 µg: quantified by plasmid linearization, electrophoresis and densinometric analysis on ethidium bromide-stained agarose gels) were transfected into HEK-293T cells as previously reported[297,1]. The next day cells were washed and left over night at 28°C in a humidified, 5% CO_2 chamber. After incubation, cells were detached using a trypsin-EDTA solution (Sigma), plated at ~10% confluency onto glass coverslips, and incubated at 37 °C for 1 h to permit adhesion to the glass substrate[297,1]. For peak current, 250 ms steps from -110 mV to -42.5 mV were taken, and the cell capacitance was recorded. Current densities (pA/pF) were determined by dividing the peak current by the cell capacitance of each cell.

Luminometry

Briefly, the coding sequence for the hemagglutinin (HA) epitope was introduced into the domain I s1-s2 extracellular loops of the four full-length LCa_v3 variant constructs using an annealed oligonucleotide adaptor bearing 5' phosphates and single-stranded overhangs complementary to a *Bgl*II site in LCa_v3 (Table S1). Agarose gel electrophoresis and ethidium bromide-based quantification of the four HA-tagged LCa_v3 channel constructs was used to ensure transfection of equimolar amounts plasmid (~8 µg depending on size of constructs) into ~80% confluent HEK-293T cells in 6 mL flasks, each transfection having 18.7 µL of Lipofectamine LTX reagent (Invitrogen) and

a total volume of 1.5 mL with OptiMEM (Sigma). For controls, mock-transfected cells and cells transfected with untagged LCa_v3 (+8b +25c) were included in the experiment. After transfection the cells were incubated at 28°C for 2 days, following which cells were split each into 4 wells of poly-L-lysine-coated (Sigma) 24-well plates (Black Visiplate™, PerkinElmer), incubated at 37°C for 3 hours, washed twice with warm PBS (37°C), then fixed with warm PBS containing 4% PFA for 5 minutes. Cells were then washed 2 x 5 minutes with PBS, and ½ of wells were permeabilized with 0.1% Triton X-100 in PBS for 5 minutes and all wells washed 3 x 5 minutes with PBS. All cells were blocked for 50 min at room temperature (1% FBS, 0.05% TWEEN-20 in PBS), incubated with rat α-HA monoclonal antibody (Roche), washed 4 x 10 minutes (1:1000 in PBS with 1% FBS, 0.05% TWEEN-20), and incubated with goat α-rat HRP-conjugated secondary antibody (1:1000 in PBS + 0.05% TWEEN-20) for 30 minutes. After washing 3 x 10 minutes with PBS, 400 µL of SuperSignal® ELISA Femto Maximum Sensitivity Substrate (Thermo SCIENTIFIC) and plates were detected using a FilterMax F5 Multi-Mode Microplate Reader (Molecular Devices) using the luminometer setting of SoftMax Pro 6.1 software (Molecular Devices) for data acquisition and analysis.

Biotinylation

Polyclonal antibodies were produced in rabbits using as antigen a large portion of the LCa_v3 I-II linker peptide lacking exon 8b. The desired coding sequence was PCR-amplified (for primers see Table S1) and cloned into pET-22b(+) bacterial protein expression vector (Novagen) via *Nde*I and *Xho*I restriction sites, and the 17.6 kDa protein was expressed, purified, dialyzed, and injected into rabbits as previously reported[1]. Notably, during dialysis prior to injection, some of the protein precipitated, however a substantial amount remained in solution. It is expected that the precipitated component might actually have enhanced antigenicity due to more stability of precipitated proteins in the interstitial fluid. IgG rabbit antiserum was tested for immune reactivity with the purified antigen by Western blotting (not shown), and further tested in LCa_v3-transfected HEK-293T cells, where we performed immunolabeling experiments with cells transfected with either 8 µg of LCa_v3 +8b -25c in pIRES2-EGFP or with 3.2 µg of LCa_v1 α1 subunit in pIRES2-EGFP^{214} plus 2.4 µg of the rat β1 subunit in pMT2 and 2.4 µg of rat $\alpha_2\delta$ in pMT2 as previously reported[1]. AlexaFluor® 594 goat anti-rabbit IgG was used as the secondary antibody (Invitrogen), and cells were imaged at 40 × magnification using a Zeiss AxioObserver Z1 inverted epifluorescent microscope to detect the AlexaFluor® 594 antibody and eGFP. Images were captured using Zeiss AxioVision software, and brightness/contrast was adjusted using Adobe Photoshop.

For biotinylation of surface expressed channels we used the Pierce® Cell Surface Protein Isolation Kit. Briefly, a fully confluent 6 mL flask of HEK-293T cells was split 1:6 into 5 new flasks. After 5 hours at 37^{o}C, media was changed to no antibiotic and flasks left over night at 37^{o}C. The following day, equimolar amounts of the four LCa_v3 channel variants were transfected into the cells (~ 6 µg; quantified and transfected as indicated in the current density section of the materials and methods above), and cells were incubated at 37^{o}C for 6 hours then media replaced with 6 mL of media lacking antibiotics. The next day, cells were transferred to 28^{o}C for overnight and subsequently washed once with 5 mL of warm (37^{o}C) PBS and once with 5 mL of ice cold PBS. 3.5 mL of ice-cold Sulfo-NHS-SS-Biotin (Pierce) was then added to each flask and these were incubated on a rocking platform at 4^{o}C for 30 minutes. 175 µL of Quenching Solution was added to each flask and the cells were gently resuspended and transferred to separate 5 mL conical tubes; remaining cells were obtained using 830 µL of TBS to rinse out the flasks using a micropipette. Tubes were then centrifuged in a swinging bucket rotor at 500 x g for 3 minutes, and the supernatant was discarded. Cell lysis was achieved using 130 µL of the provided Lysis Buffer, supplemented with 1/10th volume of CALBIOCHEM Protease Inhibitor Cocktail III in 1.5 mL centrifuge tubes, and sonication at low power (e.g. 3.5) on ice using 5-second bursts over the course of 45 minutes. Lysates were centrifuged at 10 000 x g for 2 minutes at 4^{o}C, and supernatants transferred to new tubes. 100 µL of each supernatant was removed for isolating biotinylated proteins and another 50 µL for total protein evaluation, the latter of which were combined with 50 µL of 2 x sample buffer (15% glycerol (v/v), 100 mM DTT, 2% SDS (w/v), 0.006% Bromophenol blue (w/v), and 80 mM Tris pH 6.8) and heated to 95^{o}C for 5 minutes. The membrane-localized biotinylated protein fractions were isolated from each 100 µL aliquot on columns loaded with 200 µL of 50% slurry of NeurAvidin® Agarose. After a 2 hour incubation at 4^{o}C, unbound proteins were eluted by centrifugation and columns washed 3 times with Wash Buffer supplemented with protease inhibitor. Biotinylated proteins were then eluted using 200 µL of SDS-PAGE sample buffer (10% glycerol (v/v), 1% SDS, 50 mM DTT and 62.5 mM Tris pH 6.8) and centrifugation. 15 µL aliquots of each protein sample were separated on two identical 7.5% SDS-PAGE gels; one gel was Coomassie-stained while the other transferred to 0.45 µm PROTRAN® nitrocellulose membrane (Whatman®). After blocking in Tween-20 Tris-buffered saline (TTBS) containing 5% skim milk powder (w/v), the membrane was incubated with α-LCa_v3 antibody (1:500 in TTBS with 5% milk) overnight a 4^{o}C, washed the next day 2 x 15 minutes with TTBS, then incubated with 1:1500 goat α-rabbit HRP (Jackson ImmunoResearch Laboratories, Inc.) at room temperature for 3 hours. Membrane was subsequently washed 3 x 15 min with TTBS, HRP-activated

chemiluminescence was detected by exposing the membrane to BioMax Light Film (Kodak), and both the developed film and the Coomassie-stained gel were imaged and densinometric analysis carried out using an AlphaImager HP acquisition system and the AlphaEase® FC software (Alpha Innotec).

Appendix C

Additional materials for Chapter 2.3

Annotated splicing of Ca_v3 channel genes from various species of animals in the regions corresponding to exons 11, 12A/12B and 13

Nematostella vectensis Ca_v3 (JGI scaffold 154:248090-279585)

```
ATACGGTTTTCACACGATTTTATTGAGGGTAATACAAAAGTTCTCTTCCTTGTTTCTCAAGCGTTGTTGAGCTGTTCGGTGATGACGAC
                                                          V  V  E  L  F  G  D  D  D
AGTGGAATATCTGTACTCCGCTCATTCCGTCTCCTGCGCGTGTTCAAGCTCGTCCGGTTCCTCCCCGCGCTTCGTCGTCAACTCCTGGT
 S  G  I  S  V  L  R  S  F  R  L  L  R  V  F  K  L  V  R  F  L  P  A  L  R  R  Q  L  L  V
GATGATACACACCATGGATAACGTCATGACCTTCTTGGCCCTACTCGTCATCTTCATGTTCACCGCCAGTATTCTGGGTATGAACCTGT
  M  I  H  T  M  D  N  V  M  T  F  L  A  L  L  V  I  F  M  F  T  A  S  I  L  G  M  N  L
TTGGCGGGAAATACCGGTTTCCTAACGACGAGGGAGTCATGGAGACGTCAAGAGCTAACTTTGATGATTTATTCTGGGCGATTGTCACC
F  G  G  K  Y  R  F  P  N  D  E  G  V  M  E  T  S  R  A  N  F  D  D  L  F  W  A  I  V  T
GTGTTCCAGGTAAGTAACATTCTGTATTCTACGTGTAGTCAATCTACGATAGTTCTAGGCCACAGGGTGTGATGGAAGTCGTACTGAAA
 V  F  Q
AGTTCATTCGATGTGAACATCCAAAAAACAAGCATGAAGCAATTTCCTTTAGTCAATCTTCTTGGAATTTATAATTTAATGACGCTAGC
GCACTTTTGGTAGTCTCGGCCACCTTGATTTCGGCCTGAAAAGAGAGATCAAAATCACTATTTTCAGAGGAAAGGATGTACATAATTGG
AGATTTAAATAAGCAATAACAAAATAAAATTTTAATCGCTAGATTTAGAGATTTCAATATGATGTTTACTAGATAAGCTATTACTCGTC
CGTCATCCAGTAAGAAGAATTCCACCATTTTTACTCAAACTTGACTGGACTGACTGGATGAAGGTGTGATTGTTTTGCGTGCGTCAGTA
CTCGAAATCATACAGATGCTGTCACATGTCGGGACAAGTCAAGTTGTTGTGTGAATAGAGTATACCCTGACCCTAGAGTTTCAGAATAT
TAGTCCCCAAAAGACTCGTCTGATTCATGTTTACCAGCGACGTGAAAGGAATGAGCCAGACTGCAAAACGATCACTAGTTATTGACTTT
GTAACCTCGCCTCAGGTGCTGACCCAGGAAGACTGGAACATCGTGATGTATGATGGGATGCGTGCGACAAGCAAGTGGGCGGGGCTATA
                  V  L  T  Q  E  D  W  N  I  V  M  Y  D  G  M  R  A  T  S  K  W  A  G  L  Y
CTTTATCCTTCTCATGACGATTGGGAACTACATCTTGTTTAACCTGCTCGTCGCTATCTTAGTCGAGGGATTCGCATCAGCACCGGTAT
  F  I  L  L  M  T  I  G  N  Y  I  L  F  N  L  L  V  A  I  L  V  E  G  F  A  S  A  P
```

Acropora digitifera Ca_v3 (GenBank accession BACK01025054)

```
GTTGATATCTTTACTTTTCCAGTATCGTCGAACTCTTTGGCGAAGGTGACAGCAGCATTTCTGTCCTGCGGTCTTTCCGGTTACTACGC
                        I  V  E  L  F  G  E  G  D  S  S  I  S  V  L  R  S  F  R  L  L  R
ATATTCAAACTGGTGCGTTTCTTACCAGCGTTGCGTCGTCAGCTGCTTGTGATGATCCACACTATGGACAACGTGGTGACATTTCTGGC
 I  F  K  L  V  R  F  L  P  A  L  R  R  Q  L  L  V  M  I  H  T  M  D  N  V  V  T  F  L  A
TTTGCTCGCTCTGTTCATTTTCACCGCCAGTGTACTGGGAATGAACTTGTTCGGGGGCAAGTATACATTCGAGGATGAGGATGGGGGAA
  L  L  A  L  F  I  F  T  A  S  V  L  G  M  N  L  F  G  G  K  Y  T  F  E  D  E  D  G  G
AAGTTACGGCGCGAGCAAATTTTGACGACTTGTTCTGGGCCTTAGTCACTGTGTTCCAGGTAAGGGTACATTAGAAATCGAGGCCGCTT
K  V  T  A  R  A  N  F  D  D  L  F  W  A  L  V  T  V  F  Q
CAGTAGAGCGGCTCTATTCAAGATGCAAGGCGCAATAGGCACAAAGAGAATATGAAGATCTTTTGTAGTTTTCTTTCATACTTAACACA
AGATTCAACGTTAACGTTGATTGCTGAATTATCCTTTGACCAGCAATTGATTAGTAGGAAATTAAATCAAAGCGATGACTTTTCAAGTG
GTATTCTCATTAATCTAGTGTAGTGCAAAAGATTTTACTTCTGGTTTCTGTGCTATTGGTTTCCAAAACTCTTGTTCCAAGGATGAGGA
AAGTTTCAATAGAAGAAAGTCTTATTCCTCAAGCCAACCAAGGGAAATAAACTGACCAGAAATAAAGAAGTTATGCATTGCGTCGGACG
ACGTTTGTAGCGATAAATAAATACCATATCATTAAGGGAGTACGAGGCATTTTCTTGTAGTACTGCGTCAGAGAGTAACACGAAAAATC
TGGTAATGTAGATAAAGGTCAAATTAGCACCGTAGGAAGATAATAAAACTGACTTTTCGAGTTTAAGCCCTTTCAGATCGAGAGACAGA
GAGAATAATACATGGGCGCGAGGAAATATGGAATTTCACTTCGATTGTTCAACTCGATATCTCAAGAGTCAGCGCAGCATGTTTATTAT
ATAAATACCTTACTTTATTCTCGTTTCAAAAGGAGAACGCGTGAAATTTATTCCATATCTCTAAGCAACTGTGTATTAATCTATTTATT
ATATAAACATCTTAATAACAAGAAGAACCTGACTTAATTCACCTTTCAAAAAGACAACAAGTTGCCATTCTTTTATGGCGCTAAATAGA
GCGGGTGACATGCCAGCAGCTGATTGGCTATCTCAAACACGTTAAAAATTACGGCAATTTTTCACTTCTGGTGATAGGATTTTTCTCAG
CGGTGGAAATCCCTTTAAAGCATTCCAGTTTATATAATAAAAGGATAAACTATCGAAACGTCAAGTTCGTAATCTTCTTACTGTTGTAA
TTAAACCATTATCAACTTTTTTGATACAGAGTTCTCATTTTCTGTACGGTTAAGTTATGGTATGCAAGAGTGGTCGCCCATAGAAAGAG
CAATAGTTCATTTTTTTGGTATCATAAGTACGAGGAAGTCATGAATCGCTCTTATGTAGGTTTTGACCCAAGAGGACTGGAACACAGTG
                                                          V  L  T  Q  E  D  W  N  T  V
ATGTACGATGGAATGAGAGCTACCACCAAGTGGGCGGCGCTGTACTTCATCTTACTCATGACCATTGGAAATTACATTCTCTTCAACTT
 M  Y  D  G  M  R  A  T  T  K  W  A  A  L  Y  F  I  L  L  M  T  I  G  N  Y  I  L  F  N  L
ACTGGTCGCCATCTTGGTGGAAGGATTTGCCAATCAACCGGTAAAAAAGAAATTGTGTTAAATTGTGCCCGGCAAGTAACGGAGGACGC
  L  V  A  I  L  V  E  G  F  A  N  Q  P
```

Hydra magnipapillata Ca_v3 (GenBank accession NW_002182072.1)

```
TGTTGTAAAAACTTTTTTGTCTTTAATTTTTCTTTTTAAAGAAACTTTTTTTATTTTAGTCTTGTTGAATTTATTGGGGCAAGCAAAGG
                                                          L  V  E  F  I  G  A  S  K  G
TGGCGGAGTTTCTGTTTTGAGAACATTTCGTTTAATGAGAATTTTCAAGTTAATACGCTTTATGCCAATGCTTCAAAAACAAGTTAAAG
  G  G  V  S  V  L  R  T  F  F  R  L  M  R  I  F  K  L  I  R  F  M  P  M  L  Q  K  Q  V  K
TTATGTTAGCAACTCTTGATAGTGTCATGACTTTCCTTGGCTTACTTTCTATTTTTATATTTACATGTTCAATTCTTGGAATGCATTTA
V  M  L  A  T  L  D  S  V  M  T  F  L  G  L  L  S  I  F  I  F  T  C  S  I  L  G  M  H  L
```

```
TTTGGTGCAAAAATGATATTTGAGGAAGGTTCTGTTCGGCATAACTTTGATAACCTAATGTGGTCGCTAATAACTGTGTTTCAGGTGAT
 F  G  A  K  M  I  F  E  E  G  S  V  R  H  N  F  D  N  L  M  W  S  L  I  T  V  F  Q
AAAAGAATTGAAAGGTTTTTGAAAAAAATTTTAACATATTTATAATTTATATATTTATACTTTTTACATATTATTATTTATTTTTATGA
TTTATATTATGATATATTTTTTAAAATACCATTATATGTCTTCCCCTATTATTATGACTGAGGTGTCAGTATAATGAACGCTACTATTAT
CATGACTAGGTAATGAACATCACTATTATTATGACTAGGGTGTCAGTAAAATAAACACTACTATTTTGTGTTGTTTGAGGAAACATAGT
TATGATAAATAATAATGATAATATTTATTTTTCATAATCTTGTTTTTATTATATAATTATTACTGTTATTTTTTTGTACGACTAATATT
TGATTAATTTGACTTGGAGTCAAGTTAATCAAATTGATATAAGGCCTTAATGAATATTATCAATTAATGATTATCAATTTTTTTTATCA
TTAATTGCCAGAACTTTTGCACTATTGTCACCCAAAACACTTTTTTCTTATTAATTTTAATCTTTGTAGTTTCTATTTTTTTTAACTTT
TTTAACAAACTTTTTTTCTTCTTTAAAACAACTTTTTTCAACTATTCTTTCTCATTTTCTTTTTCCTTTTTTATAAAAGTTTTATTTTC
ATTAAGTTTTGAACAAAGAAGCTTTGTAGTACCAATATTAAAATTTATTACTTTTTTTAAAAAGATTTTTTTTTTTTTTTTTTNNNNN
NNNNNNNNNNNNNNNGAGAAAGAGAAGCAACATTACGACGATGTGACAAAGGTTGGAGATTGGCTGCCAGAGCAGGTCCAACTATGTTT
ACAATTCGTTTTTGCACCTTGTCTAAAAGAGAAAGAGCATCATTAGAAGATCCGCCCCAGATGTGGCAACAGTATTCCATACAGGGACG
GATTTGAGATTTATAGAGATAGAGAATAGAATCTGGAGTAAGAAAGTGTCGAGCTCGATAAAGAGATGCAACCTTAGCAGATGCTAATT
TTGCAATGGATTTGATATACGGTTTAAAAGAAAGATCAGAAGTAAGAGTTAATCCTAGAAGATGAATGGTAGATGACTCATCTAGTACA
TTACCATTCATAAATATAGGAAGATCTAAATTATTACGATAACGATTGGCCGAATAAAATTGAGTTTTATCTGAATTAAAGTTCACCAG
CCACTGTGAGCCCCATGCTGTAGCAGAAGTGAGATCCTTTTCAAGCTCAGATACCCCCTCCAAGCAATCAGAGAGTGTAGGCTTCTTAT
CATGACAAGAGTAAATGGTAGTGTCGTCAGCGAATAATGCCACCTTAGATGTGAGAATATCTGGAAGATCGTTAATGTAAATTAAAAAG
AGTATAGGGCCAAGGATTGAACCTTGAGGAACCCCTGAAGTTACAGGATGTGAAGAAGAGTGTTGTCCATCGAGGACAACTTTTATACT
ACGATTGGAAAGAAAGGACTCAATAATCTTAAAGACGTTACCAGCTACACCATAAGAAGAAAGCTTATGGAGAAGACCAGCATGCCAAA
CTTTATCAAAAGCTTTAGAAATGTCAAGTGCAATAGCCTTAACCTCTCCACCTCTATCTAATGCACGGTAAAACCTATCGGTTATTACT
GTTAGTACATCAGAGTTTTTAAAGCAATTTAAACAAAAAGTTTTAATTTTAATTTTTTTGTAAATTATTTTATTTTGATTTTGTATTTG
TATCTTTTTTTAAATTAAATAATAAATAAATTGGTTTTTTACAAAAAGTTTGTTAAAATTTATAAAGTATTGAAAATATTGAGTTTAAA
TAAAAACTTTGAAAAATTTGTTTACTTTTCTTTTATATTCTTTTTTAAAGGTTTTGACGCAAGAAGATTGGAATGCAGTACTTTATGAT
                                                  V  L  T  Q  E  D  W  N  A  V  L  Y  D
GCTGTTCGAGGAACTACTAAATGGGCATCAATTTATTTTATTTTTATTATGGTTCTTGGAAACTACATTCTATTTAATCTTCTAGTTGC
 A  V  R  G  T  T  K  W  A  S  I  Y  F  I  F  I  M  V  L  G  N  Y  I  L  F  N  L  L  V  A
CATTCTTGTTGAAGGTTTCTCTACAGAAACAGTAATTAATAATTTTTTTTTTCTAATTTAAATAATGAACTTGTGGACCCAAGCTAATA
  I  L  V  E  G  F  S  T  E  T
```

Trichoplax adhaerens Ca_v3 (JGI scaffold 2:6781672-6793175)

```
TTACTTTTATTTCCTGGCTCTCTAACTGGACCATAAAGATTAATATTTTTGTATTTGTGTCGTTTTAATCTTTGTTAGCCTTGTTGAAA
                                                                              L  V  E
TTGCTACTGATGGCAAGGGATTATCTGTTCTACGATCTTTCCGATTATTGAGAATCTTTAAGATTGTTCGCTTTCTGCCAACACTACAA
I  A  T  D  G  K  G  L  S  V  L  R  S  F  R  L  L  R  I  F  K  I  V  R  F  L  P  T  L  Q
CGTCAAATGATGGTCATGGCGCAAACATTCGATAATGTTGTCATCTTTCTTGGATTACTATTCCTATTTATGTTCACTTTCAGCATATT
 R  Q  M  M  V  M  A  Q  T  F  D  N  V  V  I  F  L  G  L  L  F  L  F  M  F  T  F  S  I  L
AGGAATGCATCTTTTCGGTAATCGATTCTGCTTAGCACGCGTAAAGGATGGCCCAGTCGTTTGTTCGCGTAAAAATTTCGATAGTTTAC
  G  M  H  L  F  G  N  R  F  C  L  A  R  V  K  D  G  P  V  V  C  S  R  K  N  F  D  S  L
TATGGGCATTTGTAACGGTCTTTCAGGTAGCAATCTACACTATTAGTACATTAAATCGTAGTAATTTTATCTCGTAATTAATTATTAA
L  W  A  F  V  T  V  F  Q
ATAAAAAGCTTTTTTTCTTCAAACTATGCATATTACTTGCATATATAAAATTAGATTTTAACACAAGAAGATTGGAACGTCGTCATGTA
                                                      I  L  T  Q  E  D  W  N  V  V  M  Y
TGATGGGATGTTAGCTCGTGGTAAATGGGCTGCAATTTACTTCCTAGCTTTGGTCACATTAGGCAATTATGTGCTACTTAATCTATTGG
  D  G  M  L  A  R  G  K  W  A  A  I  Y  F  L  A  L  V  T  L  G  N  Y  V  L  L  N  L  L
TTGCTATATTAGTTAACGGTTTCCAAGAGCAGGAGAAGGTATAATACATATATCAATATTTCTGGTTATA
V  A  I  L  V  N  G  F  Q  E  Q  E  K
```

Schmidtea mediterranea Ca_v3 (The Genome Center contig 13897)

```
TTATTTACTTAAATATAATAATATTAAGTGTGATCGAGCTTTGCCAGCAAGGAGGGACCTCAGGTTTATCAATTTTAAGGACGTTCAGG
                           V  I  E  L  C  Q  Q  G  G  T  S  G  L  S  I  L  R  T  F  R
TTACTAAGAATTTTAAAATTGGTAAGATTTATGCCTGCTCTTCGACAACAATTATTCGTAATGATTCGAACAATCGACAATGTCGCTAC
 L  L  R  I  L  K  L  V  R  F  M  P  A  L  R  Q  Q  L  F  V  M  I  R  T  I  D  N  V  A  T
ATTTTTTGCTCTTTTAATATTATTTATTTTCATCTTCAGGTAAGATTTTGTAACGATTTCATGAAAAAATATAACTCATAAAACATTAG
  F  F  A  L  L  I  L  F  I  F  I  F  S
TATTTTAGGAATGAGCCTATTTGGTTGTAAATTTTGTACGATAGAAAACAATAAACGAACTTGCGATAGAAAAAATTTTGATTCATTGC
  I  L  G  M  S  L  F  G  C  K  F  C  T  I  E  N  N  K  R  T  C  D  R  K  N  F  D  S  L
TTTGGTCAATTGTAACTGTTTTTCAAGTATATACTGTTTTTAATTAATTTATTTTTTATTACTGATTAGGTTTTACAAAATATTTAGTT
L  W  S  I  V  T  V  F  Q
TTACCTCATTACTTTGTTTTGTCAAATTGATTTAAACTCTAAAATGAATCAAATAACAAATAATTTTAAGATATAGTTGCTAGAATTTT
```

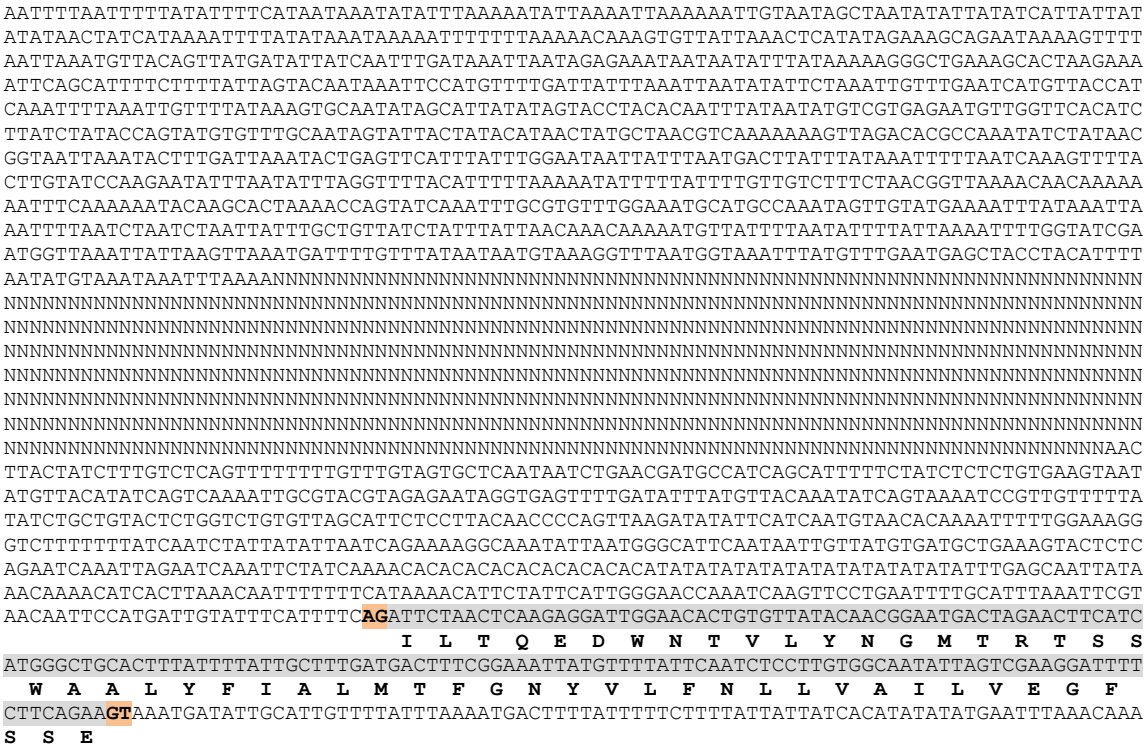

Ciona intestinalis Ca_v3 (JGI chr_06q:1934655-1959987)

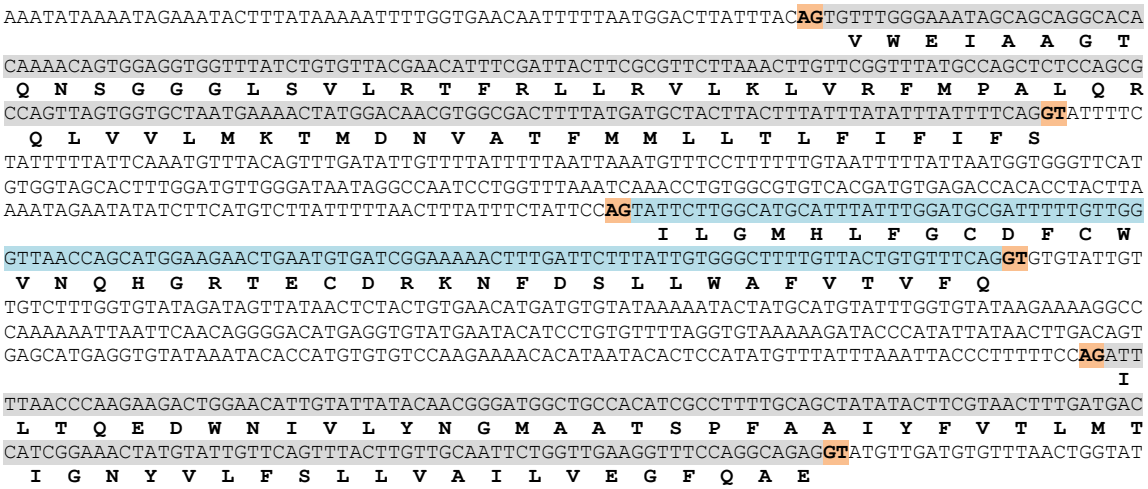

Branchiostoma floridae Ca_v3 (JGI scaffold 437:150934-189990)

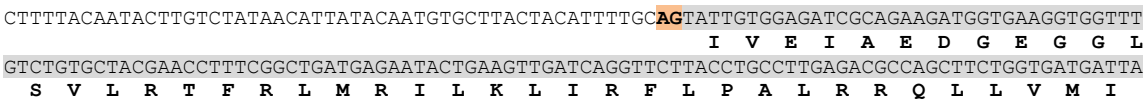

AGACGATGGACAATGTGGCAACCTTCTTTGCCCTCCTTATCCTGTTCATCTTCATCTTCAGGTACGTCTTGTAAAAAAGTGTTGAACAA
K T M D N V A T F F A L L I L F I F I F S
TAATATTTACTGGGATTATGAACATGTCATGAGATTGCACAGAGTAAATTATGAACATCTCATGAGATTGCACCGAGCAAATTAGTATA
AAGAAACTGTAACAGTTGTACTGTTGAATCCTTTAAAGTTACGTTTTACTGATGTTATGGATTCATTTATCATGTTTGACACATTAAAT
GGTAGCAGGCAATGAATATCTACTATCTTGAACAACTTCATTTCTCATGATNTATGACTTTCATTGCAGTGTGATTCATAAAAGAGAGA
TATGGATATCAATTTCAGTTTATCATAAGTATTTATCATTTACTTATTTGATGCAGATTATTAACTTAGTAGTTATGAATCAAGCCACA
TTATCTTACAGGTTTGTAGTTAAGCTGTATTTTCAGACTAAATGAATACGAATGTTGATTTTCAGTATTCTGGGCATGCATCTGTTTGG
I L G M H L F G
CAACAAGTTTTGTGAGCCTGATCCAGTACACAACAAGAAAGTGACCTGTGATCGGAAGAACTTTGATACCCTGCTGTGGGCCCTTGTGA
N K F C E P D P V H N K K V T C D R K N F D T L L W A L V
CAGTGTTCCAGGTGAGATAACCTTACATAATGGTTTTACTTCCTCCTTACAATTGTGTTGACATTACCTGCACACTGCAACTAATCCTT
T V F Q
CATTATAACTTTTCTTCAGTTTCACAGCTACATTTGAATGCCATCTATCAATAATAACTGTTGAGACACTCATAGGATACTGTTGTCGA
AGATCAAGTCCTCAGGCAGATACCTGACCAACTTTCCTTATCAAGATGCTTGGTAATGTAATACAACCTGTACTGTATAATGCACCGCA
CCTCCATTCATACTTAGTCACATTAAAACAGTTCCAACTTTTATCCCACCCAGTCTTGAGCAACCACCTGTCCTCAGCAACTCCCTTGA
GTGGTTGCTAAATCCATATTTTATTGTATGTAAAGTGTTCTTATTCATTTATATATATAATCTTTTGTCACTAACAGATCCTGACACAG
I L T Q
GAAGACTGGAACCTGGTTCTCTACAACGGCATGAAGAACACGTCTCCGTGGGCGGCTCTATATTTCATTGCTCTCATGACCTTCGGGAA
E D W N L V L Y N G M K N T S P W A A L Y F I A L M T F G N
CTACGTCCTGTTCAACCTGCTGGTGGCCATCTTAGTGGAGGGCTTTTCTGCTGAGGTGAGGCTTCAGATGTGCTCTGTGATGCTGTCAT
Y V L F N L L V A I L V E G F S A E

Strongylocentrotus purpuratus Ca_v3 (HGSC Baylor CM lcl|AAGJ04068834.1 Contig68853)

ACCTGTCTCTCTATGCCCTACGTACTTCATACAGTGTGGTAGAGGTTCTTCAAGATGGCAGTGGAGGTCTCTCTGTTTTGAGGACCTTC
V V E V L Q D G S G G L S V L R T F
CGTCTTCTTCGTATCCTCAAGTTGGTCCGCTTCATGCCCGCCCTCAGGAGGCAGCTTTTGGTCATGCTGCGCACCATGGATAACGTGGC
R L L R I L K L V R F M P A L R R Q L L V M L R T M D N V A
TACCTTCTTCTCCCTTCTAGCTCTCTTCATCTTTATTTTCAGGTAAGAATACATTGACCTAAGACATGAAAAATATCAGGTAGCTTTCT
T F F S L L A L F I F I F S
GGCTTTTTTTTGTGTGTGGTAGATATTTGTATTGGTATCAAGAAGCATGAAATCAACTCAAATATCTGTCAAATCAACTGTATACACTA
TAAACTCAATTAACCCCATATTGACTATAATTTACTGCCAATAATTGATTGATAATAAAATGACTTAAAACCTACTACTACTACCGCTT
GAAAAGTAATTATAAATTGCCAATTTTTGTTCATGTGGAAATATTATAGCATAAATAGTCATACAAAACAACTTTGGAAATGCTATCCA
GGATATTGTTTGCCTGATAAATTGCATAGACAAAAAACAAGAAAAAAAGAAAGAATTGTATGAGTTTTATCAAATGGGAGATATGTGTT
TTTCAGCAACAAATTTCCTCCTAGCTTACCTCCCTGATTGTCTCATATGCTATCTATATCTTACCGCATTGCCATATATCTCGCAGCAA
AGATATATATTTCTGCGAACATGATATGGTTTCTATCTCTCTAGACATTAGCTAACCACAAGATAGATGCTGTTAGCGAGATAGGGATA
CAATGTGACGTTGTTGATAATACCTTTACATCATGGCGTAAGTGTTTCCTCCTGGCAACCATTTCATCAGCACAATGTCTCTCTGTATT
AGGGAGCTTTGTATCCTTTCCTGATGAGGGGGCATTAATACTCAGAATATTGCTCAAAATGGGTTGATTTTTTCCTTCCAAAAGAATAG
AAGTTTAATGACATGGAATTTTCCATTTTTATGCGTGTAGAGTCAGGCATAAGAAGGTTATTTATGTGGTAATCTAGAATAAAGACCCC
CATAAAGTAAGATTTTCAAAGACTATGAAGAGTAAGAATTGCTGAGGATAAACTAGATAAGCATTATCGAGGGCACTGGAGTCATTGGC
ATTTGGACAGGAAGTGGGTTAAATGAGGCAAACCTTAGGCAAACAATCACATGACCCGATAATAGGGTTTCTCCCCATCAAGCACCTCA
TTGATAATATTCCCAGCATCTTCTCAAACTCATATATTCCCAGCGTTTTTTAGCAGTGAAGACGACTTGGAATCATGCTGTAGCAAGGA
TATTGTTTCAGTAACTGAAATAACATTACTTAAATTGCATACTCCAATAGGCCTTTTAAGTTGTATGAATTTTGACGTTATATGAAAAT
GCTCTGGCCCAAGAAATAGAAAATGGGTTAGTCAATTTGTTGTCGGTTATCGTGGAACCTTTTTGCATCAACATGAATTCAGAAAAATG
GCTGTTGTAAGAAAACTTGTATCAAAAAAATATCTTTGTGATGTACATTTGAAAACCTGTGCCTCTGTAAAGGCCCGGTCACACAGGGA
GGACGCATGGGGAACGCACGGCCAGCGCATTGGAAATTTGCAATTTGGGCCAGTGCGTTGTCGTTCGCTAGGCGTGCGTCATCATTCGT
TACTCGTTCGTCGAGCGCGCTGGACCAACGCTGGACCAGCGCTATGCATGCGTCGTCATTCGCTGTGTGCGTCGGGATTTTTTGAGCAT
GCTCAAAAACGTGCGCCGAGCTCGACGCATGAATATACACGCCAAAGGCACGCCAGACATGCGTGGAGCGCGCTAGACCAGTAATAATA
TTTGTTTGATTAAGTAATTGAAGCGATCTCTCTCTCTCTCTCTCTCTATCTTTCAGTCTCTCCATTTACATCTTTTCATTTCCTTTTTA
GATCTAATATTTCACTATTTTTGTATGCTCGATACCAATCCCTCTCACTCCTAGATCCTTCGTATGTACGATGGTTGGCTATGAACTTC
TAACCCTTCTCGTTAGTGTACTGATGGATGATCTAACATTGGTCATCGACGCATGAATTAACGATCCCTTGTTGGGAGGAAGATATTGA
TTAGTATAATTAGATTATCTAACGAGCTGAACGAGTGCTAAACCTGACACTGATCATACCCTTGTGAATGGTCTACGTTCTATTTTCTC
TCCATCCATCCATCCATCATTTTTTGTTGACACAGGTGATGTGAAACACTCTTTAAAAAAAAAAAAAAAAACAACACCCACTCCCACACC
CACAAACATGTATAAGACATCTTCATATAATTGCTAGAAGGATGTTAACTCTGTATCAGAGTGATATGAGTTTAATAACACCCTTCTAG
CTCTCACGCAATGATATCTCCATACCTGCTTGAACCATATACTGCCCTCAATTATGCTTTCACATTTGCTATCGGGAGAGATCCCTGAT
CTATCAATTATTCAAAACATGCAGGAACTAGTACATGCATTAGTTATGTTCACTTATGTTTCTGTGCATGCATGGGAAATTGGAGTGAG
GTAGAACATGTAGTGAATCTCAGCACCCAAAGCTGTTCAATTATCCTTGCTATTTATAGGCTTCCAGAGAGAGTTTTCTGAATAATGTG
CTTTATCCAAGGGTGTGCAAATGTTAAGTGCTTGCCTTTTTTTTTCTTCAAACAAACAGTCATCTGACCAAACAACATTATGATAATAA
CTTTCTCAAATTTACATTAAAAAACTTTCCACTAGATATTATTGTATGTTTTGTATTGTTTTGTAATCCCTCTATTTCTCTTGTGTTTA
TAATTGTTTGACATTTTGTTCATCTTGCCCTTTTCATGAATTTTCTGTCTTTCTTGCTATATCTTTTTGCTTTGTTTTACTTTCCCTTT
TTTCTGAATGTTTCTTACTTAATTGGTCTCATCCTTTTTCTTTTTGTCTTAATTCTCTCCCCCTTTCTCTTTATGTTTCACCTTTCATA
TTCAGTATTTTTCTTTCTTTCTTTCCCTCCCTAGAACTAGCTAACCCCCCTCTCTCTCTCTCTCTCTCTGTCTCTGTCTCTCTTTCT
GTCTCTCTCTCTATCTCTCTCTCTATCTCTTTCTCTTTCTTTCTCTCTCTCTCTCTCTCACTCTTTCTGTCTCTGCTTACCTATCTCTA
GTTTATGCATTCTACTTTCCCTTATGTGATGTAATAAAAAGGAACATGCAGCTAGGGCCTCTACATGCATCACACACCCAATTACCTCA

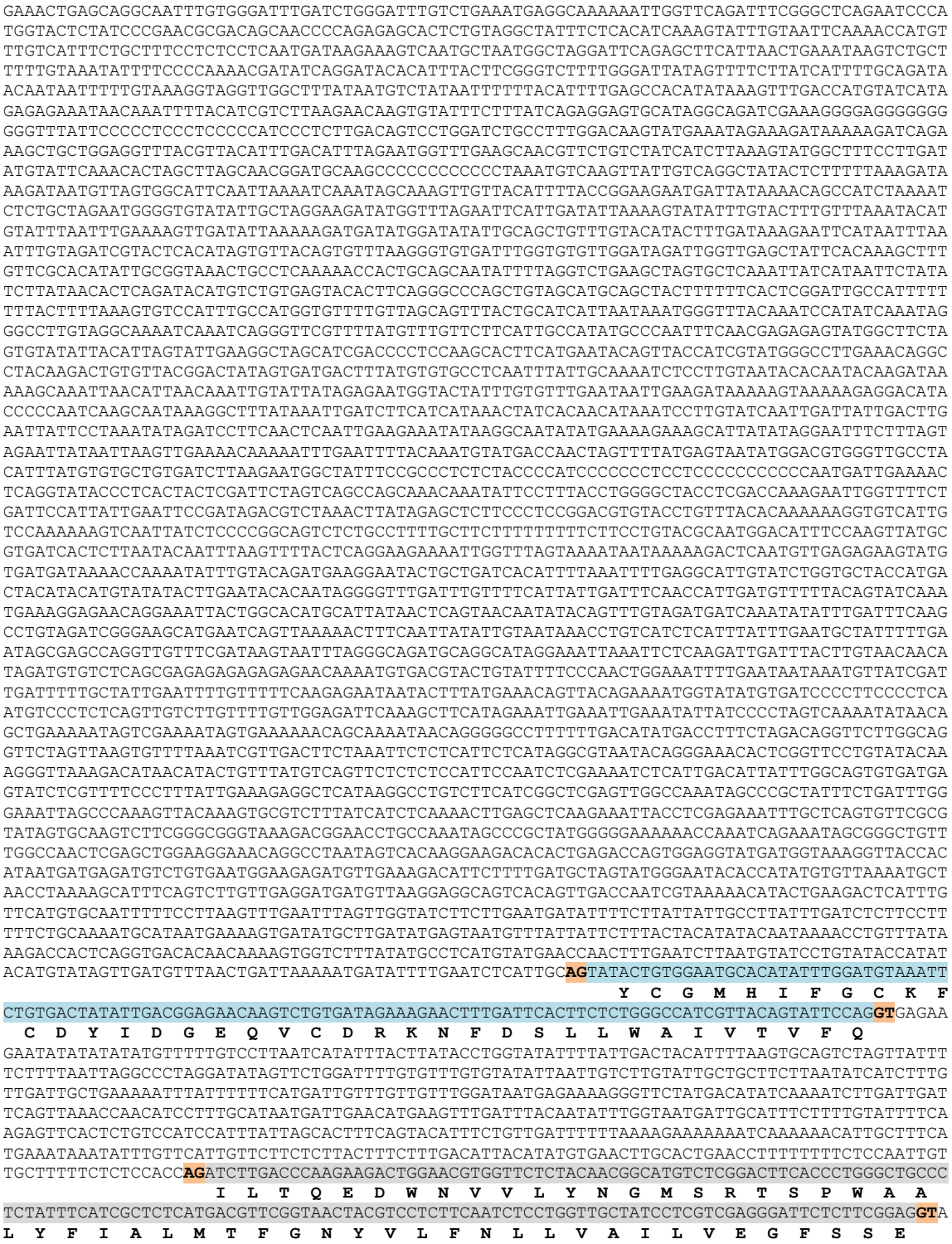

Xenopus tropicalis $Ca_v3.1$ (JGI scaffold 504:370750-417802)

```
ATGGAAGTGACTCATTGTGTTCCCTGCAGCGTCTGGGAGATCATTGGCCAACAAGGAGGAGGTCTCTCCGTTCTGAGAACGTTCCGGCT
                                  V  W  E  I  I  G  Q  Q  G  G  G  L  S  V  L  R  T  F  R  L
AATGAGGGTTCTCAAACTGGTACGGTTCATGCCTGCTCTGCAGCGCCAGCTGGTGGTCCTAATGAAAACCATGGACAATGTGGCCACTT
  M  R  V  L  K  L  V  R  F  M  P  A  L  Q  R  Q  L  V  V  L  M  K  T  M  D  N  V  A  T
TCTGCATGTTGCTGATGCTCTTCATCTTCATATTTAGGTGAGCTCACAGGATAGGAAGCATAAGCAGCTCCTCTTCTGTTATTCCTCAT
F  C  M  L  L  M  L  F  I  F  I  F  S
GTAGGGGAGTTTGGGTTGGTCTGTGTGGTCTTGATTTCTACTGCCGTGCAAAGTTTGGTGGAGCAGAAGCTCCCTCTAGTGACCACAGT
AACAGGCGCAATACAAGCAAAAAGCATGGCAGCTTTGGGTTTCCTTGAGAGAACTAAGCAGGTAAGTACTGAACTAGAGAGAGAACTGT
CACATTCTTCAGGAGAATGATCAAGTGGTTGAGGTGAGAAGAGCAGCAACAGTCTCTTCCATCTACAAATCTGTTATCTTTTCCATAAC
ACTCTTGCTTTGTGTTCCACCATACACTCAGAGCCAAAATGTCTTTCAGTATCCTAGGGATGCATCTGTTCGGCTGCAAATTTGCCTCC
                                                  I  L  G  M  H  L  F  G  C  K  F  A  S
GAGAAAGATGGCGACACTCTACCCGACAGGAAGAATTTTGACTCTCTGCTGTGGGCTACGGTCACGGTGTTCCAGGTACTCTGCACTCT
 E  K  D  G  D  T  L  P  D  R  K  N  F  D  S  L  L  W  A  T  V  T  V  F  Q
CTTGTCTAAAAAGGACTGGATTCCATTAGAGAGTTTCCCTCTGTAACTCTTGTGTCTTAACGTAGATCCTAACCCAAGAGGACTGGAAC
                                                        I  L  T  Q  E  D  W  N
AAGGTTCTGTACAACGGCATGGCTTCAACGTCTTCTTGGGCTGCCCTCTACTTCATCGCGCTGATGACGTTTGGAAATTACGTTCTCTT
 K  V  L  Y  N  G  M  A  S  T  S  S  W  A  A  L  Y  F  I  A  L  M  T  F  G  N  Y  V  L  F
CAACCTGTTGGTGGCCATCCTTGTAGAGGGGTTTCAGACTGAAGTAAGAGCCCTCCACATATGGAAAGTAATACTTGCCCTTTTCTGTT
  N  L  L  V  A  I  L  V  E  G  F  Q  T  E
```

Xenopus tropicalis $Ca_v3.2$ (JGI scaffold 27:3974572-4090184)

```
TTGTGACATTGGTCTTTCCCATGCATGCAGTGCCTTTATCCAATCAATGATCTCTATATTGCAGTGTGTGGGAAATCATCGGTCAGTCG
                                                        V  W  E  I  I  G  Q  S
GACGGAGGTCTGTCTGTGCTTAGAACATTTCGCCTCCTTCGTGTGCTGAAGCTGGTACGATTTATGCCAGCACTGCGGCGTCAGCTGGT
 D  G  G  L  S  V  L  R  T  F  R  L  L  R  V  L  K  L  V  R  F  M  P  A  L  R  R  Q  L  V
GGTCCTGGTGAAGACGATGGACAACGTTGCCACCTTTTGCATGCTTCTTATGCTCTTCATCTTTATATTCAGGTACTACATCATTTTTT
  V  L  V  K  T  M  D  N  V  A  T  F  C  M  L  L  M  L  F  I  F  I  F  S
AAACACAGTAGAGTAGTCAAAACCAATTTTAAAGTTCTAGTAAATTATTTAGAGAATTCTGAAATGGAAATAGCATCCTTAGGGGTGGA
ATCTAATTGCAAGCCTTATAACAAGGAGTACCAGTGTCATATTTTTGCTGATATCACGGTTTTGTTGCCCTGTCTTCTGTGAACTTTTA
AAAAACATCAGTTTTATATCAGTTGTGTTGTGATTGATGGTTTGCCAACTTGTATTTTCTTTCTTGGGTATCTGGTTTATGCAGCATCC
                                                                                  I
TTGGCATGCATCTGTTTGGGTGTAAGTTTACTTGGACTGCAGACACCGGAGAGACAGTCAAAGACAGAAAGAACTTTGATTCTTTGCTT
L  G  M  H  L  F  G  C  K  F  T  W  T  A  D  T  G  E  T  V  K  D  R  K  N  F  D  S  L  L
TGGGCGATTGTCACCGTCTTCCAGGTAAGGGCATTGCATTCTTTTACATATCAGTACTGGATATAAATATTTATATGTGCTCTCTGTCC
 W  A  I  V  T  V  F  Q
AATTGGCCCAAGGGCTGAATCAACAGAAAGCTTACAAGGAGCTACACACAGTATGGTTACTTTCCTAGCCTTGCTAAGAGCACTAACCA
ACCTTATTATCACAGGGGGTCAGTTGGTTGTTGAGAACAGTCTTCCAGGCTTCCTTTTTAACAGACCCAATTTCAGTAATATAGCTACT
GACGCATGGGTCACTTAGGAGGAAATTTACAAGAGACATGAACATGTAAAAGTAAACAACGGCCTGGGACCGGATGGGATTCATCCAAG
GGTATTAAATGACCTTAGCGCTGTGATTGCCAAACCTATGTACTTAATTTTTTTAGGATTCATTGAGGTCTGACATGGTGCATAAATAT
CCAAGGCTATTTTAATACTAAAATCTACAGATATGGTGGTGGAATATAAAGTTTATTTAAGTAAATGCCTAGATAGGTTGGTATGGACC
TGTGTGTGCTGGGGTTTGCTTTGGTCTTTTTCCAACACAACTTACCTATGTAACTAGTTGCTGTCAGCTCTCCATGCACCATGATGTGC
CCGACATTGTTAGTTAGCAAATTACATTTTCAAACCTGCCCTGCCAACTGATATGTGTAGAATGTGGATAGGAGTTAGCACAGTTTTAT
TCAAGTTTTTGCATAAGATGTTGTTGGTACGTAGGGTTGCCACCTCTGCCGGCTTTCTTAGTCAGGTAGGGGGCGGGGGGGATGTCACG
GGGGGCAGAGGTGGGGCTGTGACTTTGTGGGGCGGGGAAAAGGTGGTGTTTTGACGTCACGGGCAGGACTATAACACGATCAGTGAGTC
CTGCCCAGTTTTCCTAATTTGGGAAACCGGGCAGGAGGTTTTGACCCAGACAGTCCTTCCGAAACTGGGCTGTCCTGGTCCAAACCAGA
CAGGTGGCAACCCTATTGGTATGTGTATGGCCAGCTATAGTGTGGGAGATTGACCGATTCAAAATGGCAAAGCATTCCAGAGGCATGCA
GCAATCAGGGAGAATGGTTTTATTTGTAAATCAGCTCTTGTGGGCAGATCTATAGAGAGGAACGAAGAAGGAACCAGGAAGGAGTGTAA
CCTTAATGGCAGTATGATTCTGGGAGAGCTCTGTTTCTTAGTGTTTTAGGGTAGATTTGTAAGAGTGGGTGTTAAGAAGGTCACAAGAA
ATGAGAAGGTCACCAAAGGGAAGAGTGGGAATCTGAGTTAAGGTCCCCATACACTATAAGATCCGCTTGCTTGGTGATGTCGCCAAGCG
AGCGGATCTTCACCCGATATCCCCACCTACGGCTGGGGCCAAACGATCGGATCACATTTGTGGTTATGGGGTAGTCGGTTCGGGGACCG
CATCAACGAGCCGATGCGGTCCCCGATCCGACTGGATTTTCTAACCTGGCCGATCGAGATCTGCCCAATTTCAGGCCAGATATCGGTCG
GCCAGGCCGCTCTGTTCTGCCCATACACGGGCCGATTAGCTGCCGATTTGGTCCAAGGGACTGATATCGGCAGCTATAGTCGGCCCGTG
TATGGGGACCTTAAGATTGGGAGGGGCAGGTGAGGGAAATGGCACAACAAAGGGGAAGAATATCTTGGGCAAATTATAAATGTGGCAGT
GACGAGGGTTTAGAGAGAAATCCTTTGTAAAAACAGTAGGGACGGAGAGGAGATGAGCATGTGTAGTATAAAAATCTATTTCATTTGTA
TAGAATAACTGGAATAAATATAATGACTTCCTTGAGGACTGAACTGGTTGAGGCACTTAAGGATGACAGTAAGATGGGCCAAGCTAGCT
CTTATCTGCCAACAAATTACATTACTCTACGGCTTCCGGAATTACAGGCATTTTATGAAATTTGACCGTACTCCTTCACATTAGCATTT
TTTTTTCATTATCTTTGTCAAACACAACTGGGGAGTGGGAGCATTGGGATAAATTGAGTTCAGGGTTCAGATTTGAAAGCCAAAGATTG
GTTTTCTGAGTTTTAGGCCTGGGATATAGAGTTAAAAAGGAAAGCCCTGTTTTTCTGTTTCTCCTCAGACTGGTGTATTTCACTGGGAA
CATATTTCCAATCACAAATCTAAATCTATTTGAAGTCACTTTAAACTAAACTCTCATCCGAAATGCAGCCTCCTTTCTGGCCTGACCTC
TAAAAGTCTCATTAGAAAATGTTATTCCAAAGTATTTCAAATGCGTTTCGCTTATCTGACGCCGCCGTCCGGAGCTGAAATGTGAAAAT
TTTAAAAGCAGCCGTACCCTTCCCTTTGAGGTCCGACAGAAATGATGTCCTCAGTAAAAAAAAAATATTTGGATTGAATAAGGAGAATT
```

GTATTCGTTATTAGGAGTTATTTATATAGTTTTATTCAACTTGTGATAAATGTATGTTTATTATCTTACCTCTTCTCTTATTGGCTGAT
TCCAACATGAGTTAGGGTGCCCATACACGTGAAGATCTGCTCGCTTAGAGAGGTCACCAAGCAAGTGGATCTTCTCCCGATGCATAGAG
GCTGCCTAATAGCCAATCGACCCGTGTATGGCCACCTTTAGCAATATGCATAGAGGCTGCCTAATAGCCAATCACCCGTGTATGGCCAC
CTTTAGCAATATGCATAGAGGCTGCCTAATAGCCAATCAGCCCGTGTATGGCCACCTTTAGCAATATGCATAGAGGCTGCCTAATAGCC
AATCGGCCCGTGTATGGCCACCTTTAGCAATATGCATAAAGGCTGCCTAATAGCCAATCGGCCCGTGTATGGCCACCTTTAGCAATATG
CATAGAGGCTGCCTAATAGCCAATCGACCCGTGTATGGCCACCTTTAGTAATATGCATAAAGGCTGCCTAATAGCCAATCGGCCCGTGT
ATGGCCACCTTTAGCAATATGCATAGAGGCTGCCTAATAGCCAATCGGCCCGTGTATGGCCACCTTTAGCAATATGCATAGAGGCTGCC
TAATAGCCAATCGGCCCGTGTATGGCCACCTTTAGCAATATGCATAGAGGCTGCCTCATAGCCAATCGGCCCGTGTATGGCCACCTTTA
GCAATATGCATAGAGGCTGCCTAATAGCCAATCGGCCCGTGTATGGCCACCTTTAGCAATATGCATAGAGGCTGCCTCATAGCCAATCG
GCCCGTGTATGGCCACCTTTAGCGATATGCATAGAGGCTGCCTAATAGCCAATCTTAGCCCTTATTTGGCTCCTCCATGAACTTTTATG
GTGCTTGTGTTGCTCCCCAAGTATTTTTACATTTGAGTAAGAAAGGTTGGGGGACCCCAGTTTTAGAATAAACATTAAATGATCTCCAA
CTGATGTTGGACTATGACTCATTATTCTTTTAGAGTGGGGCGTCTGTTTCTTGTCTGTTTCTGTAATCTTTTTTTTTTTTCTCCCAAGA
TTCTCACCCAAGAAGACTGGAACATGGTCCTATACAATGGCATGGCTTCCACCTCCTCCTGGGCAGCTCTCTACTTTGTGGCCCTGATG
I L T Q E D W N M V L Y N G M A S T S S W A A L Y F V A L M
ACATTTGGAAATTACGTGCTTTTCAACTTGTTAGTAGCCATCTTAGTCGAAGGCTTCCAAGCAGAGGTAAAGTGATGAGAGCTTCAAAA
T F G N Y V L F N L L V A I L V E G F Q A E

Xenopus tropicalis $Ca_v3.3$ (JGI scaffold 69:134011-190844)

AAAATTATCAGTCTACAGGTAATTATATTATATTTACTACTCATTTGATTGTGATCTTGTCTCCAGTGTCTGGGAGATAATTGGGCAGA
V W E I I G Q
ATGATGGAGGGCTGTCTGTACTGAGAACTTTCCGACTTCTGCGAGTACTGAAGCTGGTCCGGTTTATGCCTGCCTTAAGGCGTCAGTTG
N D G G L S V L R T F R L L R V L K L V R F M P A L R R Q L
GTGGTTCTGATGAAGACTATGGACAACGTGGCCACATTCTGCATGCTTCTGATGCTCTTCATCTTCATTTTCAGGTGCAGAATATTAGT
V V L M K T M D N V A T F C M L L M L F I F I F S
TCTTGAAAAGCAAGTGAAAATCATGTACAGTTTATACATCAGGAAACAAACTGGGTCCCTGTGCCATTTAGATTGGGTCTTTGTCATCA
CCAAATAATGTAATGATTCTGCAACATAAGTTCCCTGTTATTAGGTTTATAATATATTACATAGGAACATATCACCTTAGTGTGTGTGC
CTATTGCAATCACTTTTTAGTGGGCAGAGATAAGGACCTAACTTTTCAGAGCATTAGAACGTTTTCATGCAAACACCTTCCTGTAGCCA
CCACTTTTTATAAAATATTCAAAGTTTGCACATTTATAGTCAGACTCCATCTCTAATATGATCAGCCACATAATTAGTGATGTAAATTT
TTTACTGGAAAGTTTGGAAAGTTTAGAAATCCAAATGTAGATTTTTTTTCATGCACAACAAGGGTTTTTTTTCTCTCAATGTAGTATCC
I
TTGGGATGCATATCTTTGGATGTAAATTCAGTTTAAGAACTGATTCTGGAGACACTGTTCCAGATAGGAAAAACTTTGATTCGCTACTG
L G M H I F G C K F S L R T D S G D T V P D R K N F D S L L
TGGGCCATTGTCACGGTTTTCCAGGTGGTGCATAATGCTTATTCATATTTCATGTTACAAAATGTGTGCTTTAAGCTACTGCCATTAT
W A I V T V F Q
ACATTCCTTCTTGTGCAGGTTTAAATATTTATATAGGAGCCATAGTGGAAGCACTATTTGCTAGTGTTTTGCACCACTTTTTTGTTTTG
AACCAATCCTGATCAATTTTGTTATTAAACATATTTACACTGAAATGTAGATGTATCCTTTCTTGGTTGCCTTCAGGGCCGGAACTAGG
GGTAGGCAGAAGAGGCAGCTGCCTAGGGCGCAACGATTGGGGGGCGCCAGGCTGGAACCTCTCCTGCCTACCCCTAGTACACGATCAGT
TTTGCGGCGCGCCCGCGCCCCCCCTGTGCTCGAACTGCGCATGCTCGTGGGGTGCACGATGTAGGTGCAGGGGCGAGGTAGCAGACCGGG
TTGCCTAGGGCGCCCGGTCGGCTCGGCCCGCCCCTGGTTGCCTTTGCCACCAACAGGCAGTTGACTTTTCAATTAACATAGTAATTATT
TAAGGTTAAAAAAGTCATATTCTAAGCAAATTCCATGTTCTAATCATAAAGAGATATTATAGGTGTCATTTACAAAATGCAGGGTGCCT
TTCCCATGAATACAGTGAAGCCTGCATTCAGCTTTATCCTTTTAATTGCATTTTGTGACTATTGATATTTCAGTAGTGCGAGTAATAGT
GATGAGTGAATCTGTCCTGCGAAAATGACACATGCTTCATTTTTTTTTGAGGCGTTATGTTTTTGATAATTTTGCCGTAGCAAATTTTT
GCAAAAAAATCTGCCAATGGCAAAACACAGAATTTGCTGCAAATCCATGTCTGGCAAAACATTTTGCCCAATTTTTTTACCAACCTATC
AGCAGTAAGCTACAGTTGTAGTTCAGGAAAGGGAAGCTGCACATCCAGCAAACATTAAAATGTAATTTTATTATAGTCCATTTATAAAC
ATTTAAGTACAAGTCAGGATTGGTATTGCCTGGAGCATTTTGAAGTTTTTTTCTGAAACTTACTTACGTAATTTAGCATTCAGTATTTC
TGAAAAATTTGAATAGCAAAAATTGTTTTTTCAATTCGCAAAAAAATCTCATTTACCAAGAACATCATATTATTCCATTTATCTTCCCC
AGTTCCAATGTTTAAAAACTTTGAGAAAGAAAAAGCTTGCATGTTGAAAATATACCTCTCAGGGAATAGAGATACAAACCCTCGACAGG
TTTCTGCTAGTGAATGTTTTCATTCAAAAGTTTTGGTTTTTTTTCGATAAATCTTTCAAATTGATGTCACTGCCAATCGCAACACATGC
AGAAATATACATAGCAATATATTACTCGTGTTTGTATTGCTGGTTGGTACATTTTCTATCCATTATACAAATACTTAGGGTGAAAATGT
TCCCTGTGCAGTCCATGATCTTCCCTTGTTTAGAATCAGCCTATACAGTACAATTGCCCTAGTATCCAAGTATTGTTTTGATCATTCTA
ACAATCCTAGACCAGCATTTTGCCCATGTTGCTTTGTACCCAACAATTGTTTTAAATGATTTGATATTCAGCTGAAGTCTTTCTTCCAT
TTGTACTTGAGTTAAATCAGGCAGAAAATATATCCGCATGTCTATAGAAAGCGGGGCTCAGGTGTGCAATCAAATCGACTCCTTCTCTT
CAGTCGTGATCATTTTTCTGTAGAATACTGAGATATCCTTTCCAGTGCAGAGTAGTCAGTGCTGTAGATACTGTGTTATTGGATCAGCT
TCTATGATTTCTTCTAGAACACTGTCTTCAAGGTCATAGAAGTGGTCTTTAAGGGAATCTACCAATAATGGTAGATAAATGTTATATGT
TAATATAGCAAAACTATTTATATAAAGTTAATTACAGGTATAGGGCCTGTTATCCATAATGATCGGAACCTGCGGCTTTCCATATAAGG
GTTCTTTCTGTAATTTGGATCTCAATAACTTATATCCACTAAAATCATTCAATTACAGGTATGGGATCCCTTATCTGGAAACCCGTTAT
CCAGAAAGCTCCGAATTACGGAAAGCCTGTCTCCCATAGGCTCCATTTTAATCAAATAATTTAGAATTTTAAAACTGATTTCATTTTTC
TCTGTAATAACAAAACAGTACCTTGTAATTGATCCCAACCAAGATAAAAATAATCCTTATTGGATGCAAAACAATCCTATTGTGTTTTA
TTAATGTTTTATTGATTTTTTAGTAGACTTAAGGTATGGAGATCCAAATTACGGAAAGACCCCTTATACGGAATACCTTTGGTCCCGAG
CATTCTGGATAACGGGTCCTATACCTGTATTAATTTAATTATTTGATTAAAGTGCAGTCTATGGGAGATAACCTTCCCATAATTTGGGA
GTTTTCTGGATAATGAGTTTCTGGATAATAGGTCCGATACCTGTACAATGAATATCTATCCTTTACCAAGGGAGTGTATTACTGGTTTA
TCAAGGGAATGTCTAAATTATTTCACCGAAACAAAACAAGAGCCCTGCAGTATATTATACAGGTATAGGACCCGTTATCCAGAATGCTT
GGGACCAAGGATTTTCCAGATAACGGGTCTTCCGTAATTTAGATCTTCATACCTTAAGTCTACTAAAAAATCAATAAAACACTAATTAA

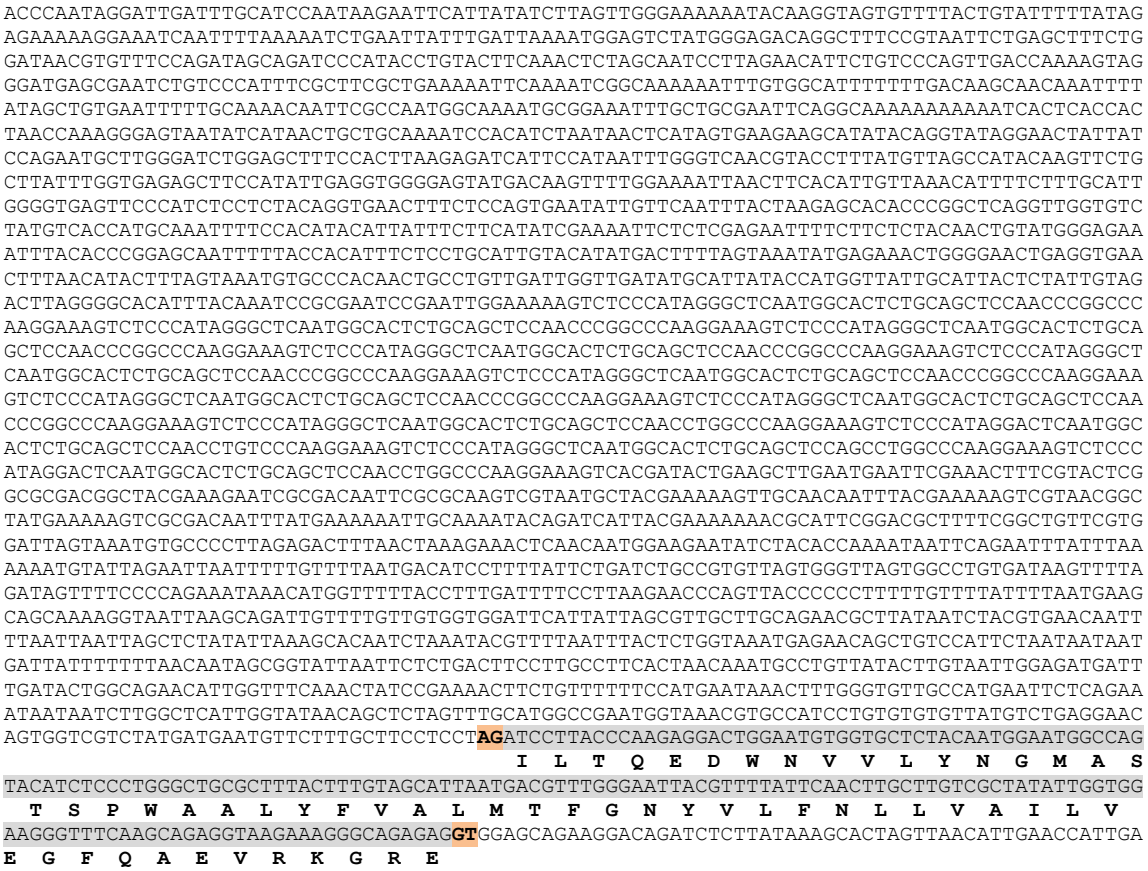

Homo sapiens $Ca_v3.1$ (GenBank accession number NG 032024)

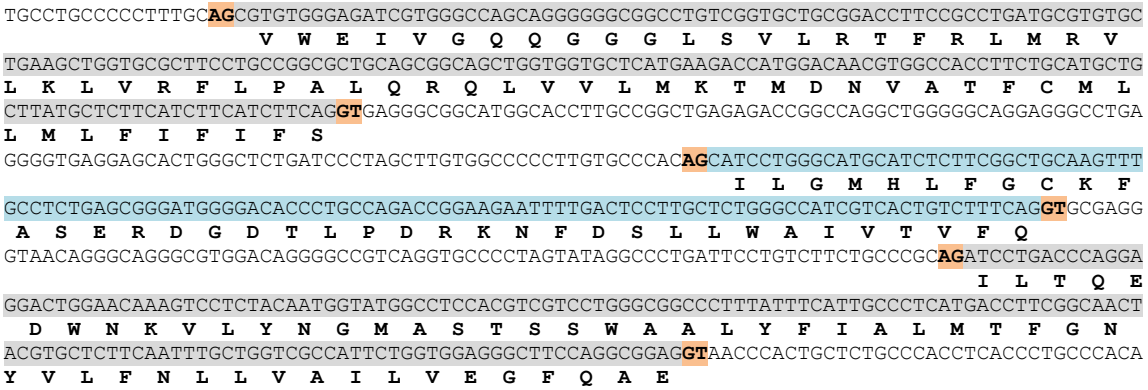

Homo sapiens $Ca_v3.2$ (GenBank accession number NG 012647)

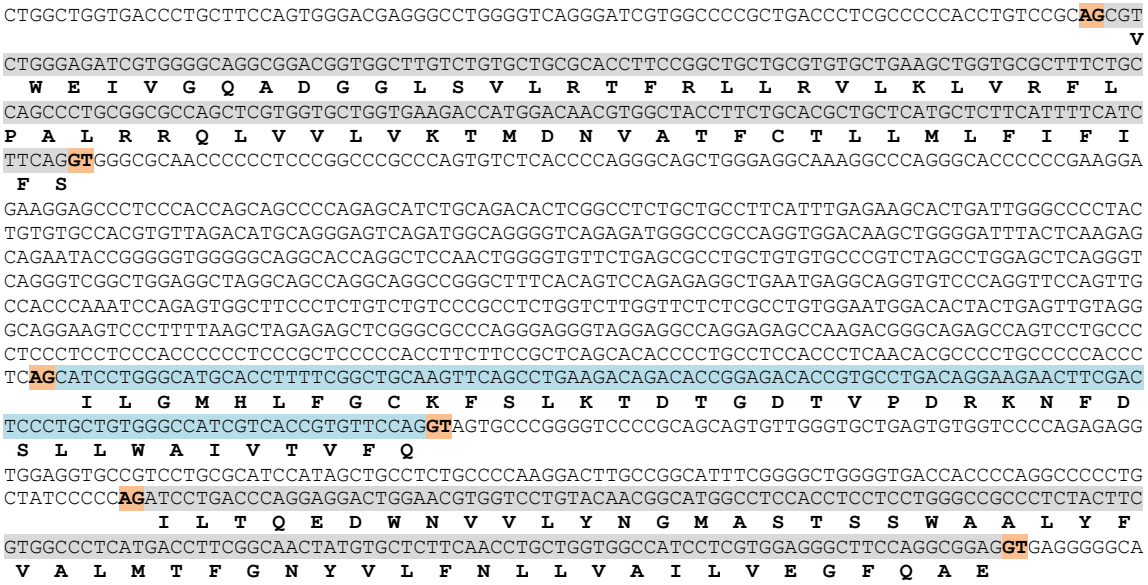

Homo sapiens $Ca_v3.3$ (GenBank accession number NC 000022 region: 39966758..40085740)

Saccoglossus kowalevskii Ca_v3 (GenBank accession number NW_003105613.1)

ATGCCTATGCCCATCACTGGGTGTGTCTCTAGCAACCATGCCTATGCTCATCACTGGGTGCGTCTCTAGCAACCATGCCTATGCTCATC
ACTGGGTGCGTCTCTAGTAACCATGCCTATGTCCATCACTAGGTGTGTCTCTAGTAACCATGCCTTTGTCCATCACTGGGTGTGTCTCT
AGTAACCATGCCTATGTCCATCACTGGGTGTGTCTCTAGCAACCATGCCTATGTCCATCACTTAGTGTGTCTCTGGCAACCATGCCTAT
GTCCATCACTTAGTGTGTCTCTGGCAACCATGCCTATGTCCATCACTGGGTGTGTCTCTAGCAACCATGCCTATGTCCATCACTGGGTG
TGTCTCTAGCAACCATGCCTATGTCCATCACTGGGTGTGTCTCTAGTAACCATGCCTATATCCCATCACTGGGTGTGTCTCTAGAAACC
ATGCCTATGTCCATCACTGGGTGTGTCTCTAGCAACCATGCCTATGTCCATCACTGGATGTGTCTCTAGCAACCATGTCTATGTCCATC
ACTGGGTGTGTCTCTAGCAACCATGCCTATGTCCATCACTGGGCGTGTCTCTAGCAACCATGCCTATGTCCATCACTGGGCGTGTCTCT
AGCAATCATGCCTATATCCCATCACTGGGTGTGTCTCTAGCAACCATGCCTATGTCCATCACTGGATGTGTCTCTAGCAATCATGCCTA
TGTCCATCACTGGGTGTGTCTCTGGCAACCATGCCTATGTCCATCACTGGATGTGTCTCTAGCAACCATGCCTATGTCCATCACTGGGC
GTGTCTCTAGCAACCATGCCTATGTCCATCACTGGGCGTGTCTCTAGCAATCATGCCTATATCCCATCACTGGGTGTGTCTCTAGCAAC
CATGCCTATGTCCATCACTGGATGTGACTCTGGCAACCATGCCTATGTCCATCACTGGGTGTGTCTCTAGTAACCATGCCTATGTCCAT
CACTGGGTGTGTCTCTAGCAACCATGCCTATGTCCATCACTGGGTGTGTCTCTAGTAACCATGCCTATGTCCATCACTGGGTGTGTCTC
TAGTAACCATGCCTATGTCCATCACTGGGTGTGTCTCTAGTAACCATGCCTATGTCCATCACTGGGTGTGTCTCTAGCAACCATGCCTA
TGTCCATCACTGGGTGTGTACAGGGAAAATGTCTGTTGTCATTGTTAATTCTAGAGAGTTTAAGATTTGCGTACCTAACAGGAACATAA
CATGTTGTTCTAATTTTGTTTGCGTTACGTTCTTGGGTGTCAAAACAATGACGTACAAACGTAACTGAAACAAAACCATGTCAATTCGT
CTCTCATTGAGCAACCATGATAAAACTATCCAATAAAATCTGTTATGTCATTTCACGTCCAGAATCTGAATTAGTAGTTAGTTCCCAGG
CATTTGACAGAGCTCTTGCATCCACTCTGCTGAGGTCCCAGGCCTGTTTGCCGAATCCTCTTTCAGCAGATCAATGTCATGCGTTTTCA
GTGGATATAAATATCAGCTAAAATACATCCAATATTTCTTATTTCAGCATGAATATACAAAATCACTCTAATATAAAGCGTTTTATCAA
TGTCAGTGAGTAAAAATTAATCAAAATTGACAGCGAGAAAAGCTCTCAGGAAATCAACTACGAGTCAGTCATCTTGATCACGTTCAAAA
CGACTGCCGTACGACCAGGCAATCGATGACATCATTGGTTTGCGTGGAGGTCATGCACAAAGCAGTGACATACCCGTTCTTGTTCCGTT
CTCGTATGTGCATCTTAAAGTCTCTAATTGTTAATGTGTACAAGATAAATAAGTTACTGTTTTTCACACTGTATCGAACTTGCTTATGT
TGCAGCTCACATTCAGAGATATGTATAACATACAAGTATTATCAATTTGTCATTTGTCATGTTACTCAAGGTGTGATATTGTGATGAAC
AGTTCCTTGTGACAATGGATGGCTTCCCTCCATTAGCTGTAGCATAGCTATATAACTGAAGTGACATTAGTGCAAGTCTGTGTCATTAG
TTTAATTTTTATGCATTTTGCCAATTTTTTCGAGTTAGGTCTCTCATCTACTACCAAATACCCTCACTTGTTTATAAATTTTAATTGTA
AATATCTTCTTCTTTTCCTCTTTAGCATTCTTGGCATGCATTTATTTGGCTGTAAATTTTGTGAATATTTACATGATGGTACCAGAATA
I L G M H L F G C K F C E Y L H D G T R I
TGTGACAGGAAAAACTTTGACTCCTTACTCTGGGCAATTGTTACTGTGTTTCAAGTAAGTAAGAAATAATGCGTTTTACTTGTATTTCA
C D R K N F D S L L W A I V T V F Q
GGTATGTACGACCTAGAAAAAGTGCCATATGCGAGTACCAAGTTGCGAGTCGCAAGTAGCAAAATATGCCATATGCTAGTGGTAAAAAC
GGCATATGTGAGTGGTAAAATGTATCATTTGCTAGTAGCAAAAAAGCCCTATGCGAGGAGTAATACAAAGGCCAGGAAAACCGGTGTAT
GCGAGGGGTGGAGTCATTTGCCATTTTGCTCAATGGCTGGATTCGTTTGCTTATAATATAATATAATATAATATAATATAATATAATAT
AATATAATATAATATAATATAATATAATGTAATGTAATGTAATGTAATGTAATGTAATGTAATGTAATGTAATGTAATGTAATGTAATG
TAATGTAATGTAATGTAATTACACGCAACCCGGATCAAATTTGAATTGAAACAAAGAAGCATCTGCCGTTGCTTGATCGTGATAGAGAG
ACAATTTTTACGGGTAAATGCTAGTAGAAGACTTAGCCTCAATGCCCTAAACACTTCGACCTAGCCACTTCACTTGTACAAGTAGAAAC
AGTTTTATGTTTCGTTAAAATATGAATGGACATGTTAGCGTTGAAATAATCATAGAATTACAGTTATCATCAGTACAAGTAGACTCGCT
GAACAGGAATTCACACGCCAGCTAGTTTCAAAGTAATTTTGTCCCAGACAACGTTATGTTCATTTCATGGTATTTCAACAGTTTTGTAA
TGAAGTAAATCCTATACACTATTGATTCTGTCGACCAATGGGAACCAGACTACTTGGACCTAGAACGTGTGCGGTGATTGGACTTAAGC
ACGACTTGTGTCTATGAATGTTGATGTAAATGCGTTTACAGCCAAAACAAAGTCAGCTTGGTCATTCAGTTGTTAGAAATGAAAAAATA
AACGGTGCCAGCGATACATTTCGAAAATAAAGGAACAAAATAAACACAATCAAATTATTATGACACGATCGATAGACATTCCAAACAAA
TGAAATTATTAACGAAAGACAAGATTTTTCTAGATATTTACGAACATACTGTCATACCAAATATATACAAAATTGACAAATACACAAAG
AAGTGTAATATTAGGTTTTATTTTGCCTTAATATTTTCTTTCACTCAATTCATGCGTGGGACTTCTATTTAGCTTCATGGTCATTCGGC
TTGTCTTCTCCTTCAGGGAAAAACAACAGTAATCATACAAATCGTAAACACATTGCAAAGACTCACTCAGGAAAGAAAACCCAGACAAC
CATATTGTACTTATATTGAAATACATTTCAAAATATTGTTTAAAAAAAATATTCAATCCCAGCCAAATCCTAGGTCAAAGGGTCAGATT
GCGTGCATATAATTATAGATAGTTAAAACAAAAAGGATTTGAACTTTTGACGGTTGTTTAACAACCAGAAAATGTTTAGTAGTCCGAAT
TTTAAATGCAAGCGAGCGGATGGTGATATTTTCGGGTTTGCACGTCGAAAATAAAGTGGAAATTGTCTGGTCAAATTCAACAAGTGGTC
GCAAAAGCTTGGGTTGTGGCATATCTATATATCTATTCAATAGATGCATATGCCTTGAAAAATATGTTTTGTGATCTGATCTTATTATA
AATTTTGCATGGTTTTGTTCAGAATCTGTACAATGATTCTACATACTGAATTGTGGTTGCTCATTACATTGTTTAGTGATTCAATGCTC
AGCTCATTACATTGTTTAGTGATTCAATGCTCAGCTCATTACATTGTTTAGTGATTCAATGCTCAGCTCATTACATTGGTTTCTGATTC
AATGCTCAGCTTATTACATTGGTTTCTGATTCAATGCTCAGCTTATTACAGTGTTTTGTGATTCAATGCTCAGCTTATTACATTGTTTT
GTGATTCAATGCTCAGCTCATTACATTGTTTTGTGATTCAATGCTCAGCTTATTACAGTGTTTTGTGATTCAATGCTCAGCTCATTACA
TTGTTTTGTGATTCAATGCTCAGCTCATTACATTGTTTTGTGATTCAATGCTCAGCTCATTACATTGTTTTGTGATTCAATGCTCAGCT
CATTACAGTGTTTTGTGATTCAATGCTCAGCTTATTACATTTTTTTGTGATTCAATGCTCAGCTCATTACATTGTTTTGTTTTGTGATT
CAATGCTCAGCTCATTACATTGTTGTGTGATTCAATGCTCAGCTCATTACATTGTTGTGTGATTCAATGCTCAGCTCATTACATTGTTT
TGTGATTCAATGCTCAGCTCATTACATTGTTTTGTGATTCAATGCTCAGCTCATTAGTGTTTTGTGATTCAATGCTCAGCTCATTACGT
TGTTTTGTGATTCAATGCTCAGCTCATTACAGTGTTTTGTGATTCAATGCTCAGCTCATTACATTGTTTTGTGATTCAATGCTCAGCTC
ATTACAGTGTTTTGTGATTCAATGCTCAGCTCATTACATTGTTTTGTGATTCAATGCTCAGCTCATTACAGTGTTTTGTGATTCAATGC
TCAGCTCATTACATTGTTTTGTGATTCAATGCTCAGCTCATTACAGTGTTTTGTGATTCAATGCTCAGCTCATTACAGTGTTTTGTGAT
TCAATGCTCAGCTCATTACATTGTTTTGTGATTCAATGCTCAGCTCATTACAGTGTTTTGTGATTCAATGCTCAGCTCATTACATTGTT
TTGTGATTCAATGTTCAGCTCATTGAAGTGAATTGCNNNNNNNNNNNNNNNNNNNNNNNNNNNNNN **10331** NNNNNNNNNNNNNNNNNN
NNNNNNNNNNNNNNNNNNNNNNNNNNNNNNNNNNNNNNNNNNTGCATTGCACATCATGTCACTGCAGGACAAGAGAAAGCAATGCTGTATTG
CACATCATAACACTGCAGGACAAGAGAAAGCAATGCTGTATTCCACATCATAACACTGCAGGACAAGAGAAAGCAATGCTGTATTCCAC
ATCATGTCACTGCAGTGCAAGAGAAAGCAAAGCTGCATTGCACATCATGTCACTGCAGGACAAGAGAAAGCAATGCTGTATTGCACATC
ATGTCACTGCAGGACAAGAGAAAGCAATGCTGTATTGCACATCATGTAACTGCAGGACAAGAGAAAGCAGGTTCTTCACTCGCACATAC
AGCAAAATACAATAAAAAACATATACATTTGAAATATCTGAATTTATCTTTAAATAATTAACTGATGTACCTTAGATTTAAAACGGCTC
AAATTACTTAAAATATCAAGTCCTGAACCATTCTGCAATAAACTGTTGAAACTAGTTATGCATCTCACAAGTGGAGAATATTTAAAAAT
ATCATTACGACAGTGCGCTAGACAAAACAGAGGGGTAAAACGTAAACTATGATTTGGGACATAAAAATTTCACGCTGATAAACCACTTG
ATGAGTTGTATAAGCTGTTAAGACATTTGTATAAAAATAATATATCTATGAATAAACCACGCTGACTGAAAGTTAAAAACCCAAAATAG

GCACACAAAGCTGAGTATTGCACATTCGGTCACCTGTTTACTGTAAAATTCGATTGGTACATGTAGTTTATCTTATATGTTCACGACTT
GTTTATTTTCTTTTATAGATTTTAACACAAGAAGACTGGAATGTTGTGTTGTACAATGGAATGTCAAAGAACTCGCCTTGGGCTGCTCT
I L T Q E D W N V V L Y N G M S K N S P W A A L
TTACTTCATAGCATTGATGACATTTGGAAATTATGTTTTGTTCAATCTACTCGTAGCAATCTTAGTTGAGGGATTCTCTGCTGAGGTAA
Y F I A L M T F G N Y V L F N L L V A I L V E G F S A E

Drosophila melanogaster Ca_v3 (GenBank accession number AE014298.4)

AGTGCCATTGAGATCTGTCAGACGTTCATGGGCAACGGAACGGGTGGTGGTGGCTCCGGACTGTCCGTGTTGCGGACATTCCGGTTGCT
A I E I C Q T F M G N G T G G G G S G L S V L R T F R L L
GCGAATCCTCAAATTGGTCCGGTTTATGCCCAATCTGCGACGCCAGCTATTCGTGATGCTGCGCACAATGGACAACGTGGCCGTGTTCT
R I L K L V R F M P N L R R Q L F V M L R T M D N V A V F
TCTCCCTTCTCGTTTTATTCATCTTTATATTCAGGTGAGTTGGATTGCCGACTGTTCACAATAACTCACAAACACACACGGCCACAAAA
F S L L V L F I F I F S
CACACCAAACACACACACAGAAAGACTCACATGCACAAGAAAAGAAGACACCAACACGAACACATAAGACACACGAGAAGAAAGCGGAG
ATAACAAAAGTAATGATGAAAAAGAAAGAAAATTCAATATAATCAACAAACGATAGCCAATCAGTTATCGACCGCGACCCCACAAACAT
GAAATTGATGTATTGAAAAAGAGTGATTAACACAAAGAACCCGAGCCACAAAAACAGAAACAGTTCAATTTCGTTAACCCATAGCAGTC
GTCTTATGCCTAACAGTTCCTAGCGCCTTCCTAGCTGCCTACTGCATAGATAAGAGTCCTTCATCTAACCCATCGAGTCAATAACTTCT
TCATTAAAAAACACCCTTCCCTCCTGAAGAATGTTGTCCATTATACGGCAGTTTTTTTTTAATTTTTTTTGGTGATAGAAGAAGCGTTT
AAAAAGTCTAAGGATTTTAAAAACAATTCCCTAAAACATAGCGGCAAAACAAATCTTAAGAACTTAACAAATAATGAGCTCCTATGTTT
AGACTTTCTGAATTCAAACCCATTTATATTGGAGTTAGTAATTGAAGTTTGAGTACATTTGCAATTTTCCTGATTACCCACAACTGCTA
TAGGTACCTTTGACCATTTGATATATGTATCACTTTCTGCCTCCGTCACCCATTAGTATCCCAGTTCTCGGGATCTCATAGACCTTTAC
CTTTTTCCAACCCATGATCATACAAAAACTTACACGTATCTCTTGAACCCCTGACTCTCCGAACTCCCAACCTCATTTAAGTGCTTCTG
CGATACGATCCTTTCTACTGTGTACTACTTGAGCATTGCCTATATAAGTAAAGATTTGCCTTAACGTCTCTTCAAGTGATCTCTTTACG
ACTTCTCTCTTCTCTCTCTCTCTCTCACCGCTTATCCTTAAGTTCTAACTCTTGGTATTTTTCTCACTTACTGTGTCTGAGTAACATTT
GAAAATTCTGGAAGATTCGTAGTTAGATGACGTTACAAGTTGTGTAACTTTTAAAGCAATCGATCTTGTATCCGTACCAGCAAGAAATG
TACCCGTATCACTTGATATATATATATATATATCTCTTTCTATCTTGCTATATATTTCCCCAAATCTCTTAACCCCCATTTACGTCATT
TTATCCAACCCCCAAAGTGCCGTTAGTTGTCGTATACTTTGACTCCTCGTTCGTTCACTTTGCTTTACACTTACACTTTTTACACTTTC
TAACACCTCACTAAGACGAAAAATATTTTTCCTTCCATCTCTCTCTAATATCTCTCTAATATCTGAATTTCTCTGTATCTCTCACTCTT
TCGCTCGGTTCACTATCGATTTGAGTTCGATTTCAAGCACCGACCACGTCGCTGCCTTTTAAATCATTTTTTATGGTATATATTCTTTC
TACTCAAAACCTTAGAACATTACTTTCCAACACATCATGTTCACCGTCTCCCTTTGAAACACTATCACTGTTTTTTTGCTTTCCTTCTC
TCTGTACAACATCCAATCATGTGAAGCTCTTTTGGTTAAACACACTACAACTACAGCAATAACAGCCACAGAAACAATTAGTTAGCTTA
GTTAGTTAGCCAAAAACGCTTTATTCCATTTCAAATTAAATAAGTGTGTATCCTAGCTTCTTTTAGCGTTAACCGACACTGCAACACAC
ACTTATACTCGTACACACTACCAAACACTAAAGGCTCGGCTTGGCTTGATGCATTGTCCAAAGGACCTGATAATGCGGCCTTTAAAGCT
TTCCTGCTCGGAGCTTGTCACACGGACACGGCACACGCACACTCACGCTCAAATATATACCTGACACAAAGTACTTGAAAAATTGAAAC
TAAAAAAAAATCGTACGCTTACTTATTGTGTAGTTGCAGTCGCTGCAGTTTGATACATACCTATATATACTCGTACTCTCTCTCTCTATC
TCTATATATACCTATCTATGGTTACTCGTAATTGATATTATTGTATAACTATGAATATCAAGTAAACACACAGAACTTCAACAGTGAAA
ACAACAATAAGAACACGCATAATAGCTAGACTAGTTGCTAAAGTAAATGTAATCGAGTTTGTGTAGTTAGAATAGAAAAGACACAACAG
CCACACGAAACATCCGACCAGACTCTATATAACTTTACATTCTATGTATTAACAAGCGAATAATGAAACGAACGAACTGTTAATGGAGC
TGCAAGGAAGCCAGCATCGCTAACGATAAATCAACTCAATAAATGCCCCGAATAAACTCAAAACAGAAAACTAAAATAAAGCTGAAACT
GAAAACAGACTATCAAAAGCCAGACCAAAAATAAACCAAATCCAAGGGCCGATTTTACCTCATTAAACGCAAGGCTTTAGCTTCTTAGT
TCCTTTGGAGCGAACTGTACCTTTGTTTCATTTCCATTTTATTCCGTGGTCCGATCTGAGTCGCGGAAGTGGTCCTCTAAAAGGGTATT
TACGAGTATCACCGTTCCCCTTTTTCCAAATGCTTTCATTTGCTAGCTTTCGTTTGCCGCTCACTTCACTGACAAGAACACTTACTAGC
TCAAGCCCTTTCTCCCTTGCTCTCTCTCTCTTTTAGTCTCTGTAAATCAATCACCCACACTCTGTCTCTTTCTTTCTTTACTGTCTCTC
TCTCTTTCTCTCTATAAATATATTTTTGTATCTCTCTCTCTTTCTCTCTTTGTCACACTCCACACAATTTAAAAAATATACTAAAAACA
ATCCAATAATAATAAAATAAATTGAAAACCGAAAATTAAAATAAATCTAAACAACTGTATGCTAAACACAACCCAAAAAAATACCCCCA
AAAACCAAAAACACAAAAAATATATAAGAATATATATTTAAATAAAATTAATCGAAAACGAAAAACCAAACAACAACCAAAAAATATAT
ATATATATATCATATTATATATCAACAAAACCAAACCATCACTTTAGTATACTCGGCATGAATCTGTTCGGATGTAAATTCTGCGAGAA
I L G M N L F G C K F C E K
AGTTAACGGAGAGATGATTTGCGATCGTAAGAATTTCGACAGCCTGCTCTGGGCGCTCGTCACAGTGTTCCAGGTAGACCCATTGCTAT
V N G E M I C D R K N F D S L L W A L V T V F Q
CAGTCTTTTACCATACGTAAACCTATATATGTATATATCTATACTACTACTACTACTACTACTACTTCTAATGTTACGCCATAATCTGC
TAACGATATGATTACGATAACCTACTGTTCATAAAACCGAAAAAGAAAAAAAAAACAAGATGAAAGCCCAAACCCATTACGAATCCCCA
GTGAAATACGTTTTGATACGTTGAGCATTTAGCTTTCTTTCGTTTTCACTTTTTTCTATTTCGATTTTAATGGTGTTTCTGTTCTAATT
TCCGTTTCCGTACCGATTCGATTAACCGTTTGTTTTCTGCTTAAATCGATAACTGTTGTGACGTCCTATCGCCATCTTACCCTCGCTCT
GAGCCTTTGTCTCTGTCTGTCTGTCTAACCATTAAATATTTGAGTGCGTGCGAGTGATTTTGAGATCTACAAACCGTCATAATCGCCCG
CACACACATAACATAATTTTTTATGTTTTTTTTTTTTATATTGCTTTTCGATTGCCAGACATCGAGATCGACTAGATAGCTAGCCATCT
TGCTCGCTCTCACTAATTTGTGGTGTGCCCTTGATTTAGTGTGGTATTAAGTTGAAGATTTGATTTCATCTTTAGTTTCTTAGATTTCG
ATACCGATTACGATTCTTGGTTTGGCATGCATGCGTTGACCGTTGCGATTACCGTTACCTAACCGTTAGCGTTAGTGATAGCATTACCG
TTACGAGTTCCATAGCAAGCAGCGCGCATCCGCATGTCGTTCGGAGTGTTCGTATATGGGAATGTCCATAAGCCATAGATGTTCTTAAG
ATCGTTGTATATGTGTATGTATTTGTGTGATGTACATTGATGCACCAGGTAAGCATTTCGGTTCGAGTTTCTTGAGCTTCCAGCATGCA
AAATAATGTACATAATTGTATATACATATAACCGAGTGGAACTCTGTTTGCATCTAGCATCTCGAACACTTTGAATACACTCCTCGAAA
CACATACGCATTTTTTGTACACCTCTCACTCTTCTTATTCGCTCTTTCTCTCTGTCTCGCTCGTGCTCTTATTTATGTAATATATATAT
ACATATATATGCCTCGATTTTGTCATCCACTTTGCTCAATGTCTTATGTTTAAGTATATACTTTTCTTTAGTCCATATGCTATTCTAGA

Drosophila mojavensis Ca_v3 (UCSC Genome Bioinformatics droMoj2_dna range=scaffold_6328:1703916-1714239)

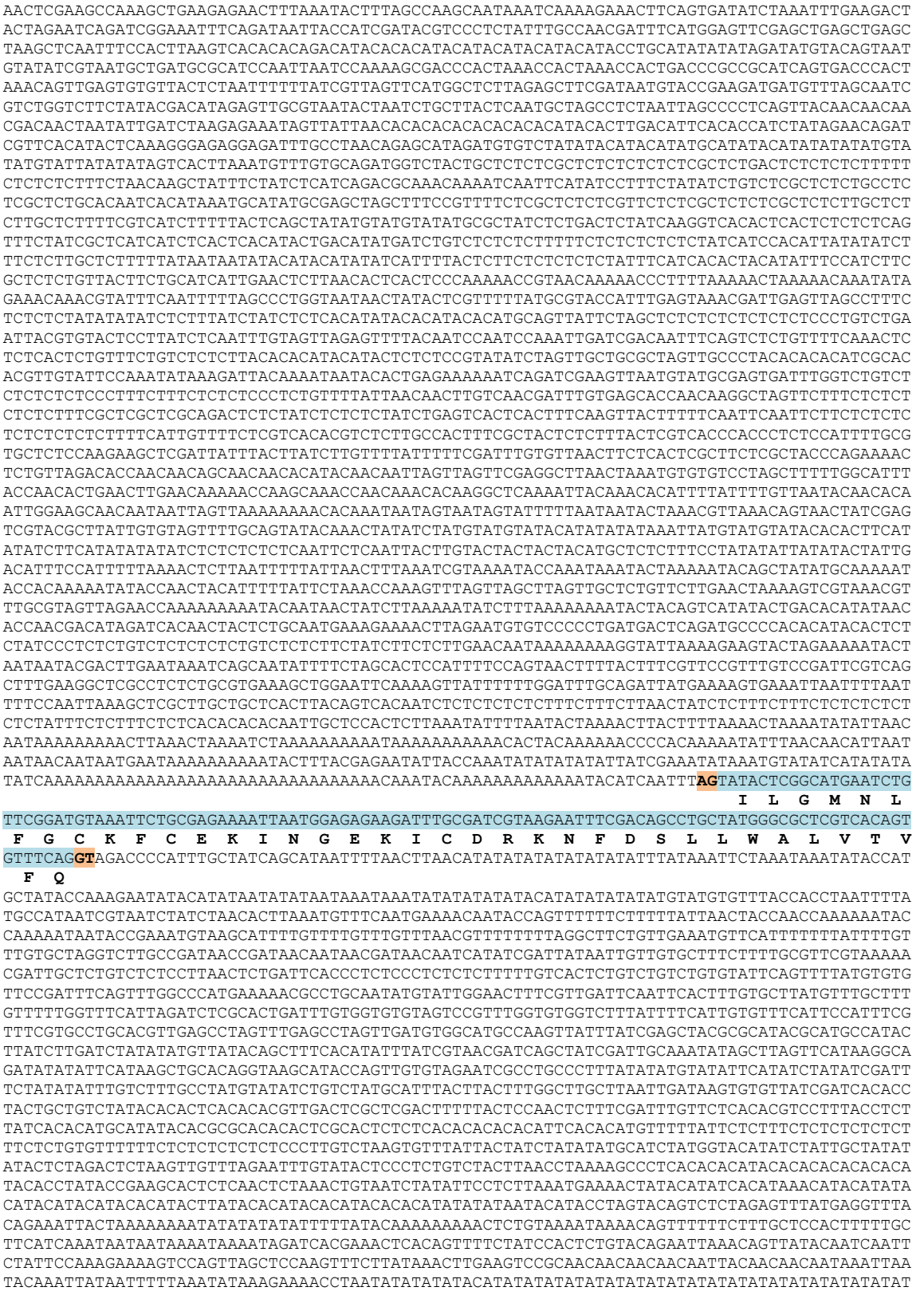

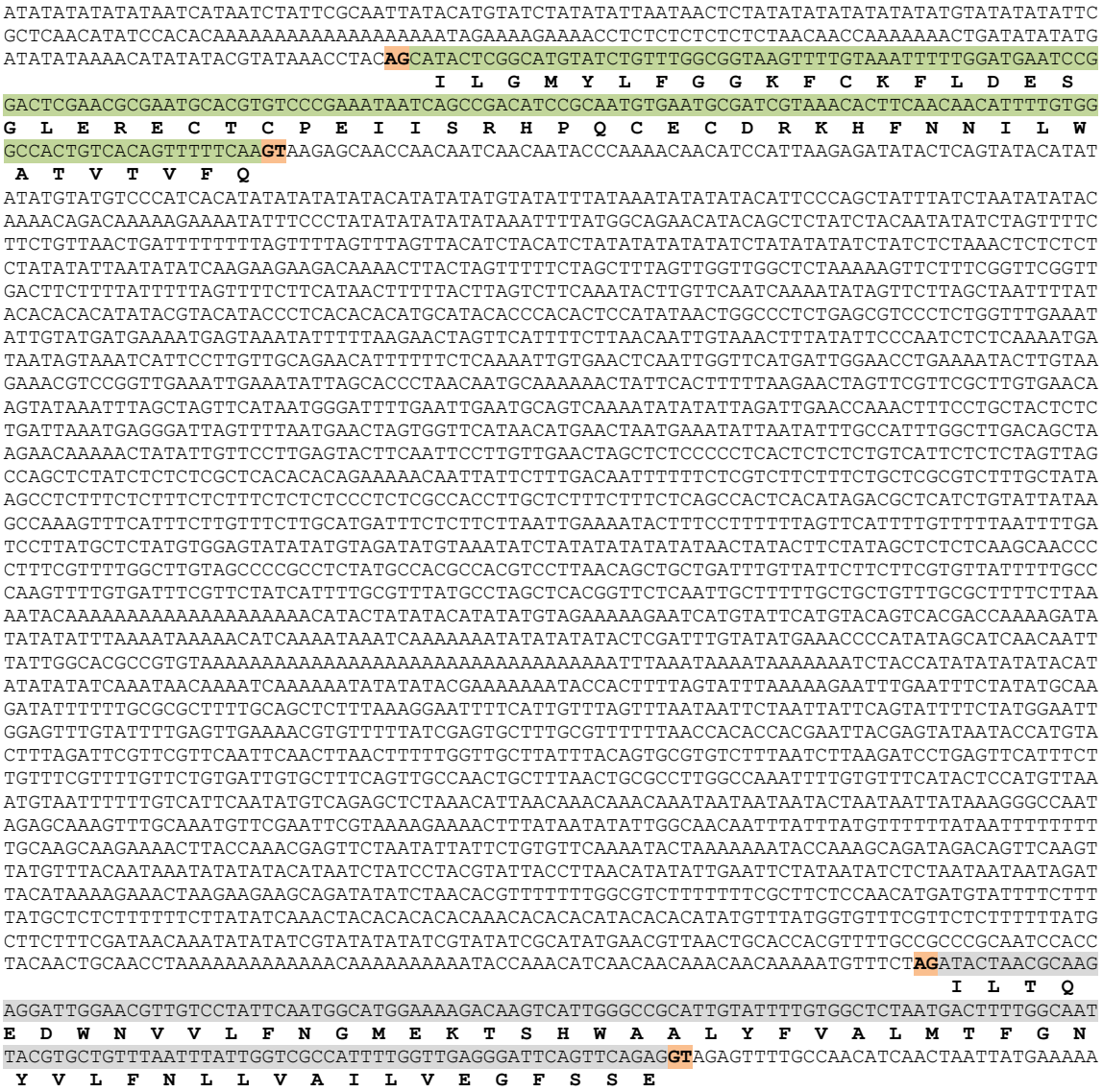

Apis mellifera Ca_v3 (GenBank accession number NC_007080)

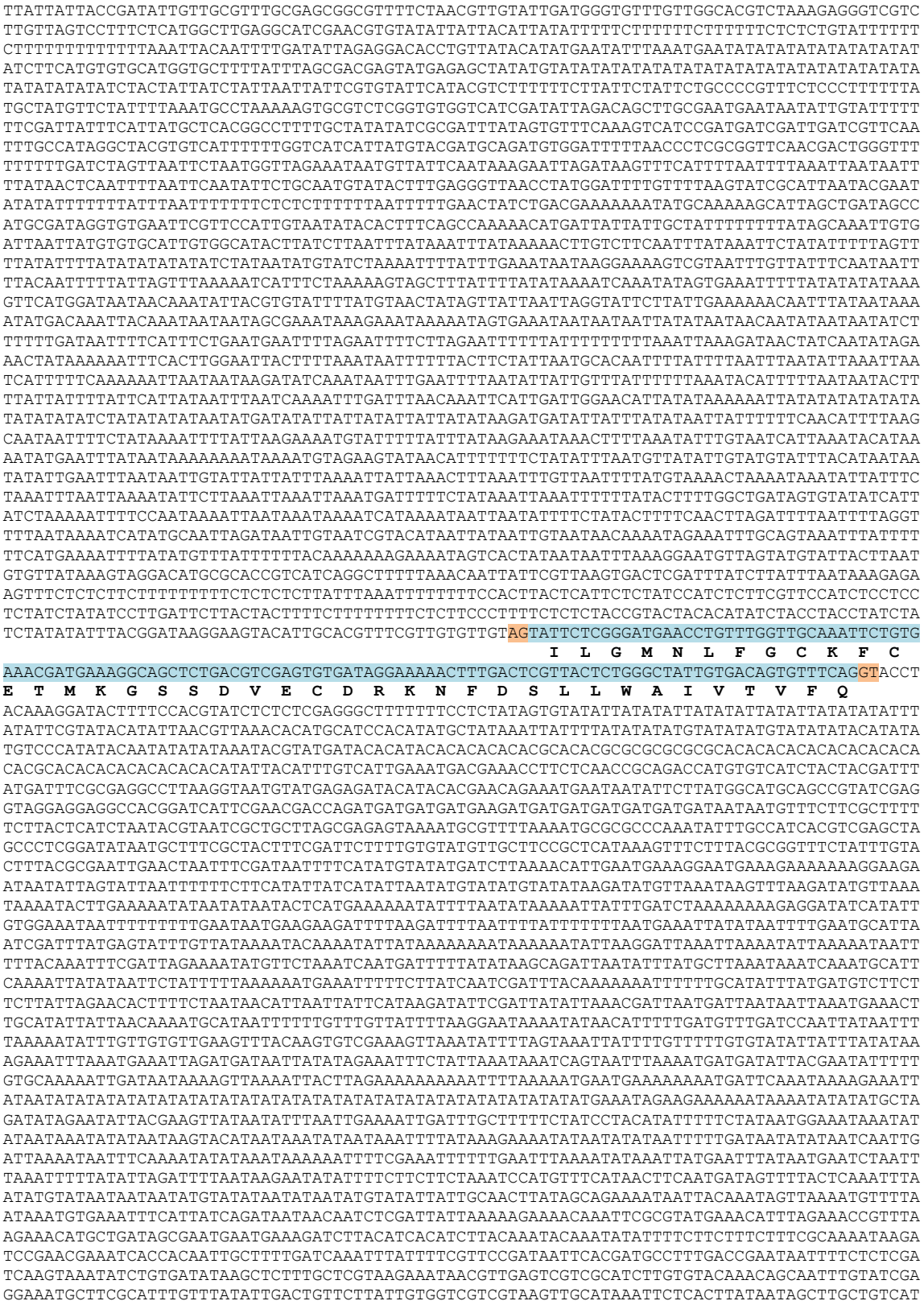

245

GATTTTTCCCTACAATTTCTTCTCTGACATGAAATGAAGTGATAAGCGACTGATATTTCTATATTTTCTTTTTAGCATTCTAGGTAGAA
GGTTGAAGAATTTTCTCCGTAAATAACCGGAGATATTGTTTTGAATTGTCGCATCAACATAGATGGAAAATACCAATCATTTTTTTTCT
ATTTTTCTTTCTTTCTTTCTTTCTTTTTTCGTATCAGCGTTTTTTCAAGCTTTGATCGCTTTTATTTCGATTGATCGTACGCTCGTGTC
GTGCATGTTAATTATTATCGTTCACATTCTATATACGCTTTGCATGCTGATATGTTTCTCTAAAGTAATCGTGTTATTGTTGCTGCTTC
TCATCGCTATTAGCCCTGACAGTGTTTCAATACGCACACATTTCCTTACAATATCTACATTCGATCATAGGACATTCCGTTACACTGTA
AAAAACGGCAATCTGAATTATAAATATGATACAATACATATATTTGGCCGATTGACGCAGGGATCTCTAACTTTTGTGATGGTATTTTT
CACCGGTGAATTTTGAAATTCGTATTTTTATTCCAATAAAATATAATAAAATATAATAAATATAATAAAATTAAAGAATTGAAGTATTC
ATTGAGGTAAAAAATATTTGATTTAAAATTTATTTTTTGAGTAGTTTAATTTCTATAACTTAATTTTAATAGATTGAATTAATATTGAA
TTAATAACATTAGATAAAATTTATAAGATTACAATTTGAAATCGATTTGTCTTGAAATAAAATATAATTTGTTATTTGTATGAGTTGAT
TTGTCTTGAAATAAAATATAATTTATTATTTGTATGAGTTATATGAACGATTATAATAATTTAGATTAGATTTCAGAATTTAAATGAAT
TTATGTTAAAACATAATTTCATATTTTCGTGCTATTCAATACTGAATTCATATCTATTAATCATAAATAATAACAAGTTTAATTAGAGA
TTTTATATATTATATATTTATATATTTATATATTAGATTTATATATGAGATTTATATATTATATATTTAAATATTATGATTTAAAATCA
ATGTCTTGCAATAAAGTATAGTTTTATATTATAAGTAATTTAATTATGAACTTAGTATTGTTAGACATTATTATTAGAAATTAAAAAAT
TTTTTATGTAGATTATGATTTAACTAAAATATTTTAAAATTATATACATATATTTCTATATCAAATATTCAAATATATCATATTCTATA
TCATTATTGTAAATATATAATATATCATAATATATCATAATATATTTTTTAATATAAATTATTTATAATATTAGAAAATGAACTATATT
TTGCATAACATATTAAATATTCACACATCTCAACATTTTGTATAAAAAAAAAAAAGAATTAAACTATATATATACGTTGAAATACTATT
AGTTTCAGAAATATTTTATATTTAATTTTGTAAAATATATTGTATGAAAGACAAGAAAGACATAAAAAGAATTTTGTGTTTCTTGTCTT
TTATATCATAAGATTTACAAAATTAATATTAAAAATTTAATATAAAAATATAAAAATAAAATAAAATTAAAATTAAAATATTTCTTAAA
TTAATACTTTTTCGATGTAAATAAATTAATAATTTTTTTATAAAGAATCAACATGCATAAAAAAAAAATGNNNNNNNNNNNNNNNNNNN
NNNNNNNNNNNNNNNNNNNNNNNNNNNNNNNAAATTAATAATTTTTTTATAAAGAATCAACATGCATAAAAAAAAATGATTCCATTTAAA
AAAATAAAAGTAACTTCAAAATTGAAACTTTTAATTATTGTTTTAATTAAAACTTACTAGTTATAAAAAAAAAACTATCATATAGTCCT
GTTTATATTTTTTTTGTTCATAAAATTTCAATAATTTTTGTTCATAAAATTTTATTTATAAAATTTTGATTTTATTATATGTACATTTT
ATTATGGTAATTGAAATATATTATTTATTTTTTTATAAATATATTACATTATATTTATTGACAAATAAATAAAATATAAAGACGAATAA
ATCAAACTGATTAAATCTTCTAATAAGAAGACAATGTATTAAATATCTATATAAACTTTATTTTGTAGAAAATATATTGACTTTAGAAT
TTATGAAATATTTTTTATCCATTTTGATGAATTTTAAAATTCTTGAATTCTTTGTAATAAAATAATTTAATAATATGAAAAGTTAAGAA
ATTCAAAAATTTAGAAAATTATAAAATTTTATATACGTATAAATTAAATAAATTAATTTAATTTATTCATAACAAAGAATTTTTTTGTC
TCTAATGCATTTTTAAAAAAATTAAATTATTGCTTATTATATTTTTATTTTTTATAGTATTTTTTTAAAACTAATCATAAAATTAATTT
TCAAAGAAATTACGCTTTCCAAACTATTCTTATTCTATTTTTAAAAAAATTAAATTTTTTTACTTCGTTATTTATTGTTTATTTAATAT
GAAGATTCATGGTTTTGATAAATATCTATTATAATTATGATAATAAATTTCATAATTTTATAATTATCATTTAAACTTCATTAAGATTT
AATAACTATGATTATGATAAATAATATATGAAGTGTAATTTATTTAAAAATTTATATTATTTATATCATTTTTTTATATTGATAATGAT
ATGATTAAAAAAAACGTATATAAAATAAAATATATAAAATAAATATTTAAAAAACTTTTATTCTTAAAAATAATTTTTTTTAATTTAAA
TTTAATTAAATTAAATATATTAGATTAATTAATTTGGTATATAATCTTTGAATCTAATTTTTAAAAATCTCATAATATGTGTAAAAAAA
TTATCATTATCATTGTCATTGTCATTGTCATTATTATCATCATTGTCATTATCATTATTAATCTCTATCTTTATCTTGTTTATATCTTT
ATTACATTAACTGTATAATGTAAATATATGAAAATAATATAGATAAATAAATTATTATATGATATGAAGTTTATTTATGCAATTGGGAC
AAAATTGATTTTTTTCTTATATTGTGTTATTATCAATATTAAGAAATGATATATTTCTTNNNNNNNNNNNNNNNNNNNNNNNNNNNNN
NNNNNNNNNNNNNNNNNNNAATAAATTATTATATGATATGAAGTTTATCTATGCAATTAAGACAAAATTGATTTTTTTCTTATATTGT
GTTATTATCAATATTAAGAAATGATATATTTCTTAATATATTTTCTATTAAAACGCGTTTTTGAGGATAAACATATTAAAATGATTATT
TATAGATCTGTTTATTTCAATTCGTCGTTTATGATTACAATTTCATATTATAAAAAATTATTAACAACTTACTTGAAATTATTAATTAT
ACTTGACGAGAAGATTAATTTACTTAAAAAATTATTTTTTTAATGGGTCATGTTATATATCATTATTTATTTTTGTTATAATTCTTATT
TTTAATAAATTTATTTTTGTTATGATTATTTTTTTTATTTTCGTTGTAATTAGGTATTTCTATTACAAATATTCTTTTTATAATTATTT
TTTTACGATTATATCTAATATTTCTGTTACATTCATATTGTTCATGAATATTCACAACAATTATTATTATAATTTCTGCGATATTGCAA
ATTTACATAAATATCCGCATGTATATATATGTATATCGTCATGTGTACATATTCTCATATTTTGTTATATATCTCACTGTTATCAAATA
GTTTATTTGCAGTAATTATTAATTCTAGATTTCCATATCAAATCAAAAATTATAATTATAATTATAATATTATTAATTTTATTTTCATG
GAAACAAATAGAATTAGAGAGTTATATCCAAACTTCATTTGTCAGTAAAATGTGTGACATCCATTCTACCATATGGCTCTGTTTAAAGA
AAAATATAGAAGTGATGGAAAAGGTAGAAAAAAAGAGGAAAGCACTATTACATCTTCTGATTTTTTTCTGAATTTTTCTATAATGATTA
TATATAAAGACCAATAAACCTATGTATATAATAAAAGATTTCATTCATTCCATAAATGGAACGATTGTCTTTTGATAATAAAAATATAT
AGAGTTATAAATCTTAAAAAAAAATTTAAAAATATAAATTTTAAATCTATCGTTTTCCGGATATTTAATCTTTAATTATTTCTGTTTTA
TGAATCGATTCTTTTGTTGTGAAAAATAATGTAACAATTGGAAATGTATTTTTCTTTATACAGTAATATTCAATCAATCATCAAAACGT
TTGAACATTTTAAAATCTAAATTAAAACGAATATTAACCAGTTATAAGAACTAAATATGTACGTCTTCAGATTTTTTGTTTTTAAAATA
TTTAATTTTCTATAGCAGTATGTAATATTTTTATGATCTTCATATAGTTAACTATAACTTTTAATCATAAATATATAGTTGACATTAAA
ACTTAATAATCTAATAAAAAAAAAAGTTTATATAAGTAAATTTTAGTACAAATTTTTAATATTATTATATATAACATAATATTTATTAT
ATTATTTTATTTATTATATATATATATATAAATTACAAAATAAAATGTGAAATTATATGTAGTATTATATAATAAATGTATATAATATTTA
TAACATTTTATATATACATTTTTTACAAAATATTTAATTATTACAAAATATGTAAAAATATAATATGTAAAAATATAAATATAAATGTG
AAAAATTTAATAAACTTATTAAATGTTAAATGTTTAAAATCTATTACACATAATGCAATTAATAATTTATTATTATTACAAAAAGTTAG
AAAAATAATTATTTTATATATATTTTATAATTATTGAGAACATATAAGAAAATAAATATTTTCTAAGTAATAATTTCATTCCAGTTATA
AAAGGATTAAAAGGGCATTAAGGGTTATTGATTTATATGAAATAGATTTAAAATGATGTATATATTATATTTTTTATTTTTATTATTGT
CTACAATTATGTAAAATAATTTATTTATTTTAAAATTTTATATTTTTATTAAATAATTTGAATTATATTTTTATATTTTCTAAATTTGA
CTTTTCATGAAAAATATTTTATAAATTTCGAAATGATTTTATTTTAAAATTATAAAAATAGGAATATTTAAATATTATAAATTTTAATA
ATTTTAGTTGTATCATAAAGAATTTTGAAATAAAAGATTTGATAAAAAGATAAAATATTTGTAAATAATATGTATCTATATTTATACTC
CACGTTCCTTTTTTTTTTTATTAAAGTTCATATTTCCATTTGAAAGAATATTTTTGAATGTAAACTATTATTAATTTAGAACAAAGTTT
TCTTTTTTAAATATTCAAAAGGAAAACTTTTTGTTTGTTTTGCAATTAGTTTTTTTAAAAATAGAAATAGAAAGTGGAAATGGAAATCT
ATTAAAATCCTATTTAACAAATGCTTTTTAATTGATCTATACTATATCTACAATTAAAAATATTATAATTAAATTGTTTCTTATTTTTA
TCTTAAATATAAATATAAATTGATTTTTATAAATTATTTCAAATTCTATTATTCAATTATTCCTTACATGTGATTGTTCATTTTGTAAT
ATTCAAATTTCTGAAATATTTCTTGAAATATTAGCATTTATTATTAAAGATGGTTGAATTTATTATTCAAGCTAGTATTTAACCAGATA
ATTAGAGAGATGATATATCTTTTTTTATTCTATCTATTAGAAATTTAAGTATATACTCACAATTGTGCTGTAATAGTTTTTCTCGACTG
TTTCCGTTACAGCTAGAGGGTTAAACCTTCTTTGCTTGTATACTTTGTGTACAAATGCGAATATGTAACATTTCTCTATGAAAAAAATA
TATAATACGCAGATGAATTTTATCTTTTTGTCCAATATATTACAATATATTTTTTGCCATGTAATATAATATAATATAATAAAATAATA

TAATATATTGTTTTTGGATAAATAATAACAAAAATATATCATGATTAATTTTGGAATATAATATACTAATAATAAATTAAAAAAATTAA
CAATAATAAAAATAGTAATAATAAATTTTTTGAAAAAATAATTTATATTTTTTTTTATATCGGTAATTCCTTTTATGTTTAGAATGTGA
GTAAATCATTATAAATTATTATAACGGTATAATATGCAATGCTATCTTAGTAATTCCTTTTATGTTTAGAATGTGAGTAAATCATTGTA
AATTATTATAATATGCAATGCTATCTTCATTTACAATAAAATTATTATTATTATACTATTATTATTATTATTATTATACTACATTCGTT
GAAATCATAAATTATAAATTTTTCTAATATTAAATTTTTCTAATAATTCTAATTTCTCATAATTTTTCTATTATTTGAAATTAATACCA
AAAATTAGTTTTCAGGTAAGCTAATTTAATGAATTAGTCCGTATATTTTTCTTCAGTGGAATGTATATATCTACAAAATATATCAAAGA
ATATTGAACAAGTATTTTTCATGATTAACATATTATAAAAAAATGTCATTTAAATGTTTATTTAATTGGAAATTTTACATAATATTAAA
TTGATGCATATCAAATTTTTTTTTTAAATAATATCAACTATGTAATTAGTTCATAAAAATCATTGAAGTTGCATTCAATTTTATTTCTA
TAGATTTTTAATTTTTAAAAAAATTGGTATTTGTTAAAAAATTATTTAGAAAATTATAATTATGTTTTCGTATATAATAATTGTTACAA
TTATTACAAATTATAATTATTAAAGTTTAATTATTAAAATTTTATGTTATTTAAAAATGTTATTTAAAATTTTATGTTACTTAAAAAAA
TTATTTTTTATTTTTATTGCATTTTGTATTCCATTAATTCAATATACATGTATTTGTTTTAATTGTATTTATTTTAAAATGTATTTATT
TTAAAATGTAAGAAGTAATAGTAAATAAATAAATATTATAAATAATCTGGAACAATTATTCTATTCTATATATTTTATATGTTTATTTT
TATCAATTTTTTTAATATTTTTAACTTATTGTCTTAAATATCTTTAATCGTCTTAAAAATATTTATTAATAGAAATTTTAAATATTCAA
TATAAATAATAAATATAAGTTTTTATTAAAACTAATGATATATTTTAAAGATGGATCATTTTATTTATTTCTCATTCTCTATCTATTTC
TCTTAATTTTAATGATTAACTTTTATTTCTCTTGTTTATTGCTTAACTCATATGGAATCCATTTGTCTATTTTCTTTAGCTTCTCCATT
TGAATTAAATACACAAATAATAGCTTGCTCTCTTTTGAAATATTATTTATCTTGTTCATGGATTAGTTTCAATAATATTTCTTAAAACA
TTATTATTGATGGTATATCCCAATTTTTTTTTCAATTCATGTAATGAAAAATCATTTAACTTAAATATTAAATTATCGTTGAAAGTTTT
TAACAAAAATTTTATTTAAATTTTAAATTTATTAATATTTATGCTATACACATTAATATTATTAAATTTAAAATTATATACAAAAATCA
TATAAGAATAATTTTTTATGACAATATAGTTCTAAAATTTTTAAACAATTAATATTATAAATCAATTAATATTAATGTATTTTATATAC
ATATAACAAATTTTTTTTAATAATTTTTTAATAACAGATATATAAATTATATTTAAAATAAAATAAAAATTTTGAAATATATCTTTTAT
TATATTTTTTATATTTTTAAATAATAATTATTAGATAATTAAAAATTATAATTAAATATAAAATTAAATTTATTCTAATTTCTAAGAAT
GCAGAAGTATCAATATGTTTTGCAAATATAAATTATTCATTTTCGAAAACATCAAAGCAATAAATCAAAATCTCTACCTTAACATAAAA
TACATTTTTGTAATCCAAAGTTATGTTACTCAATTGAATCAATTTTTCTTTATTCTCTCAAGAATAAGGAATTCAAATTCATACCCGTA
AACAATCAAACATGACACAATTCTAACTATAATGTTGAGAAAGATGTTCATTCAATAATAAATTCTAATTTCACCGGAAACTAGCCATA
AATTAAGAAATCACAACACGTGAGATCGTTTGAAGTCAATTTTGATAGTTAAAGCTTCCTGCGCTATGCCGCTAAAAAATAATGTAGCA
TGAACTATAAATAACGGAACGGATTAAAATTATTTCAACAATAAAACAATTTCTTATAATCATGGAACAGTACACAGAAACAGGATACA
ATAACGCGTATTGGCCATTACGCCATGAATTTTTAACAGTGTAGCACATTTTGAACCTATCATACCATTTTTTTTCTCAGATAGTTACA
TTTGGTGTCATTTATGTTCCATATCTGTACATGTTTGTTTATTATACAAATTCGAATTTTTAAGTTTCATAATTATAAGGAAAGTAATT
CAAATTTTAAATTTTAAATTAATTCTAAAAATTGGAAGAAAAACTCTTTAACTATTAATAATTGAAATAAATTTGTAATGTTTATAATT
TTCTTTCTTGTTCCAAGTTTTTTATTTTTTAAATTTATTTAAAAAATGAATCATTTCTTTTTATAATCGATTATGCTATCATTTGAACG
TCATTTTTTTGATCGATGTAAAATCCTTGAACGAATATTGCTCATTTAATTTAGGAAATAGAATGATATTATTTCCATTAGTCATTATT
TTCTTAAAACTTATATAAAATTTGGATAATTTTCCTTTTTAGTATCTCTAATTCATTCGATATTTTCACACTATTTCTATCATTTTTAC
TTTATTTATATTCTCAATCTCTCTATCTCTCTTTATTCGATTCTTCACTTTCTATTCCAACATGTCCGCGCACGAATATTCGATAAATA
AAATGATATGTCGCGATGATATAATGATATAAATGATAAATGATATAAATGCGTACAGGAGTCTCAATATTCCGGATTGAAAAAATCGA
TGCGTGATACGTCCGTTGAACTAAAGAAAAGTAAAAGTAAATTATTTGAAACGAAAAAAAGAAAAAAAATAAAAATGATGAATCCATAA
AAAAAACAAAACAGAAAAGAGAGTAAGAAGGAAAAACAAAAATAAAAAGTACAACCGTTTCCCATTGTGTACGATTTACGTTACTATTA
ATATCTCTCCGTTTAGCTGCTGTAGATAGACACCTTTATTATCCAATACCCAAATATCCATGCTATTCAAATTCCAAGTAGACTGTATT
CTAGAGACATATATATATATGAAATATATAACAACAATATTACAAATACTGCTAATACCGATAGCTAGTGTGTAATTGTGCAACCAACC
GCTGAAAGTTCGTTTTAAGATTTTTAACCTTACTTATTATATTTAGAGAAATTATACATTATATTATATTATATATACATATTTATGCT
TTGCCGTTACTTGTTTTTTTTTATTTTTTATTTTTATTGTTTATGTTCTTTTATTCTCTCCTAGTTTCTTTTTATTCGAATAAATGTCAA
CTGTGGCATTCTGCAACGACAGGTACTATATGACTTCTCCGCGACTGCGCTAACATTAATTTTTATTAAATTAATAATAAAATTGATAT
AATTGAAATTTTAAAATTGTATTTATTTTTTGGATTAGATATAAATCAACATGAGCAATATGATAATGCGAGATGATTTTGTACAATAG
ATTTATATTTCTAACATAACATAGATATAATAACAAAATGATATATTTTCTTCCGAATAATTAATGAGAATGTTAAAATAGTTTGCTTT
CTATTCTCAAAATAACTAAGAAGAAGAATTTTATAAAATGGATCTTAGAATATTACAACTAATTATATATAGATATATATGTGATTTTA
AAAGCAGATTAATTGTTTAGAATTTTAATACTTTAATACTTTAATATTAAACTTTTAAATCTATTTATGTTGGAGATGTGAGAACATTT
ATCAAAGATTTAGTGTAGTAAAAATATATTTTACCATAACTTTAATGTTAAATATCTTGAATTAATTATTTGATCTAAAAATAAAATAC
TATTTTCTTTAAAATCTATTATTGTGTAAAATTTTACTAAAAAGATTAATATTCAAATATTCTCTTAAGATAGAAAATAAGAAACTTTA
GATTTAAAATATTTATATTTTTAATTAAGCAATATATATTTAGAATATGAGGTATGTGTATAATTGGAGAAGGAATGTGTATCATTCTA
AATAATGGTCATTCTAAATATCGATTATATAATTTAGTAAAGAAGTGATTCTACATATAAAAATAAGTCAGAAATAAAAAATAACATTT
TTTTGAGACTTCATTTTTCATCAAGAAAATTAAATTTGAAATTAGGCTAATTTTTGATTAAATATGTAATATTATTTTTACATAAATGA
TAAATATAGAAAAATTTTTTATTTCAAGTTGAATACTTAATTGCTTACTTATGTTTAATTTTAATTTTCTTGAAAATGAAAATTTAAAT
AAAATAATTTTTTTTTTATATTTTTTGTTTATTTTCGTCTATAGAATCATTTTTTTTATCAATAATTCATTTGTATTTAGTTCTAATGGA
AATTCAGTTTTTAATTCAATTTTCTCGAAAATGGATATCCAATATAAAAATATTATTATAATTAATTAAATATTTTCTTATGATTTATT
TTCGATTTATGTAGAGGAACATTCTATTCATTGGTTATATCATTTTGTATATAAAAATATAACGAATTGTACAAAATCATTGATTACAA
AGATATTGCTCGTTGCAAAATGATATTTTGAACAACGGATACTGGTTGATATTATTTATACACGGAGTATAGGAAGATTGGACAAAAAT
TTATGTTTAATTTTTATCTGTAAAAATACAAATATTATAATATATATGAAAATACAAATGTTATAAAATGAAATACATTTAAATAATTT
AACTTATTATTAGTTAGATAAGTAATTTAATACAGTTAGTTTATTATTTTCTTCAAATTTTTGTAATATTCTTTAAAAAAACTACATAT
ATATCATACATCGTTTATTCTTAAATTATAATTAAATTAAAATTGATATATTTTTTATAATTACTTCATAAATTTATTCATAATATTTG
TAATCATTTATTTATAACACTCATTAATTTTTTAAGAATTGGATTATATTATTAAATATTGTTTATTAATAATTATTTATAATTATTTT
TTTTCTAATTAAATTTCTAATTAAATTTTAATTACTTTCTTTATAGTTAAATGAAAGATTCAGAGGAAGAAGAATACATATATATATAA
CAAAATTTTTTACTTGAAAAAATTAATAAAAATTAATTTTTATTTGAATAAAATTAAATTTAAACAAATTTTGTACTTTCAAATATTTT
ACTTCATTTATTAAAGAGATTTTTATTAGAAGTTAAATTGATAAAATTTTCTAATTAAATATAAATCTTGTTCACTGTTTTTTATACTT
ATTTTATTTCTAAAAAAAAGATTATTTATATATTTTTATAAATTCCTGTAATGTAATGTAATAAATGTAATTTTAATATTATATAATAA
ATTTTATTATTACTAAGTACCTATATTCTGTTTATAGAGAATTAATATGTATCTTTTATTTGTTTCTATATATTTGTCTGAAATTTGTA
GCAAAATATTATAAATATATAATAAAAGAATATAAAAAAATATAAAAGAATATGCATAAAAGAATCTCATTAAATATCTATATTTAAAA
CTATAATTTTTTAAATTTTTTAAATTTTGAATTTATTATTTTAATATCTTTGTTAAAATTTATTGACAAATATTACTTTATTAATATAT
AAATTTTTTTTTCTTATTCTGAGATATATAACTATTATAAAATTTTGTTCAATCTTTTCGATATATTCTGTTTTAACCAATAACGTCGAT

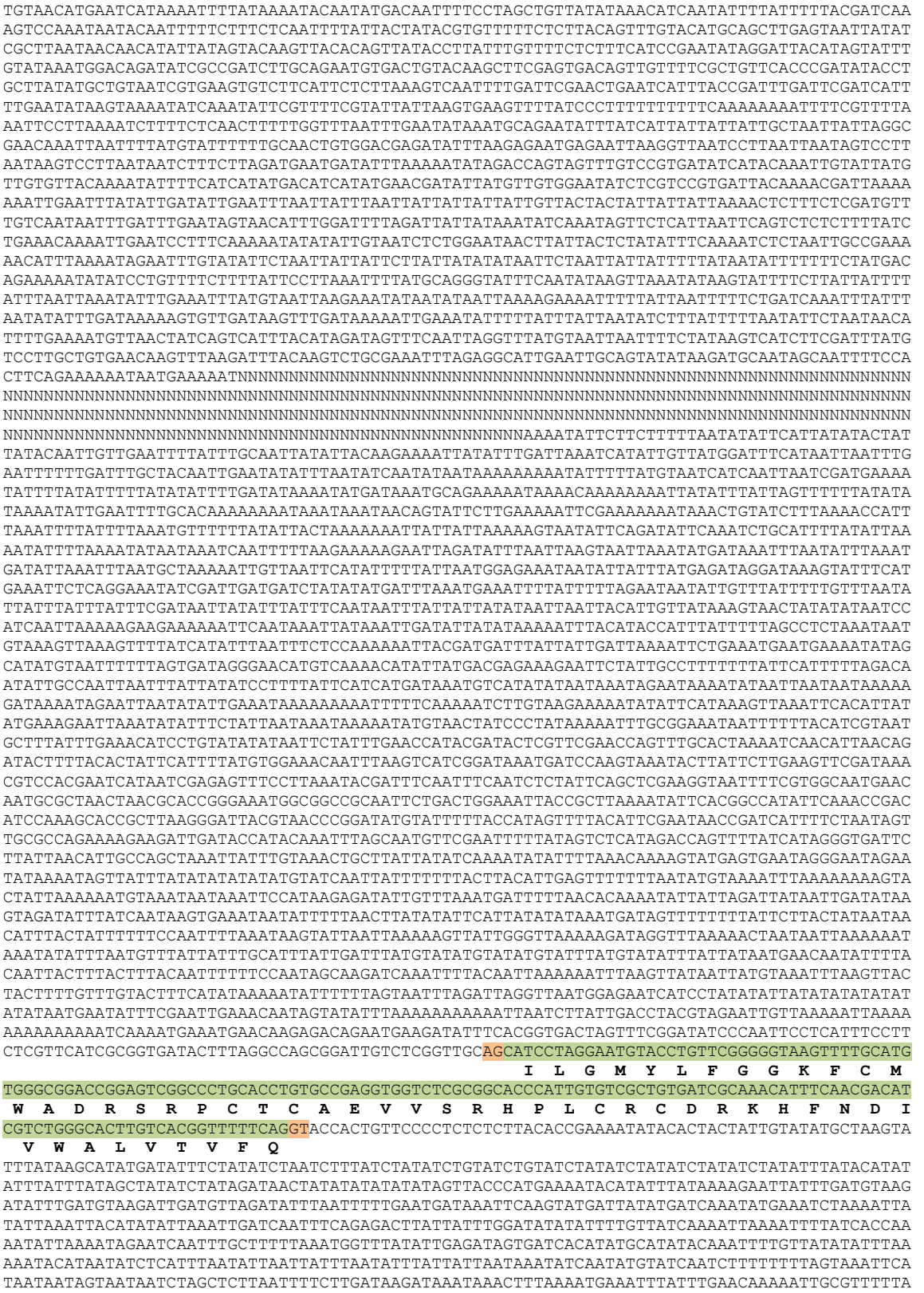

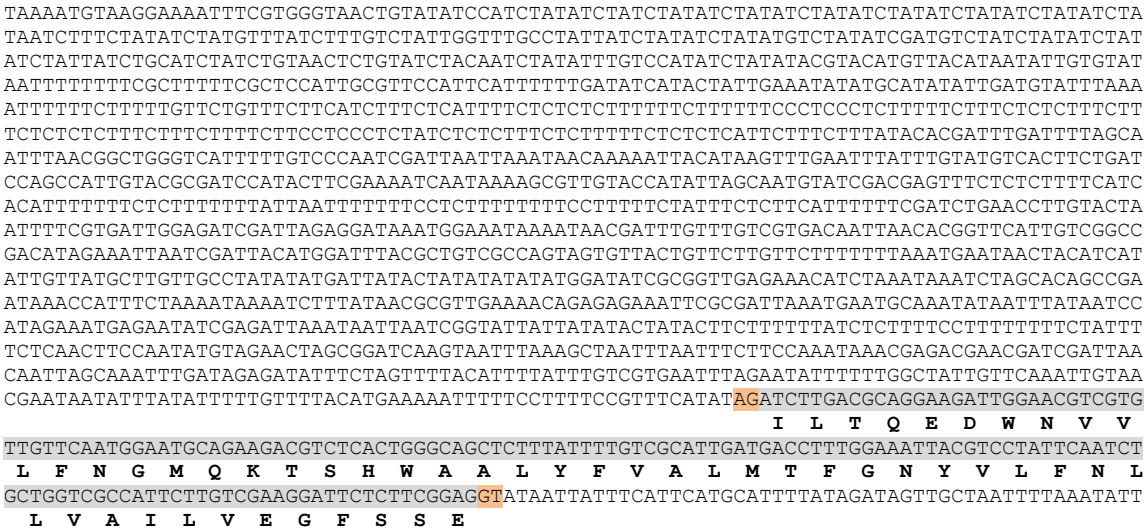

Anopheles gambiae Ca_v3 (UCSC Genome Bioinformatics anoGam1_dna range=chr2R:22075315-22082523)

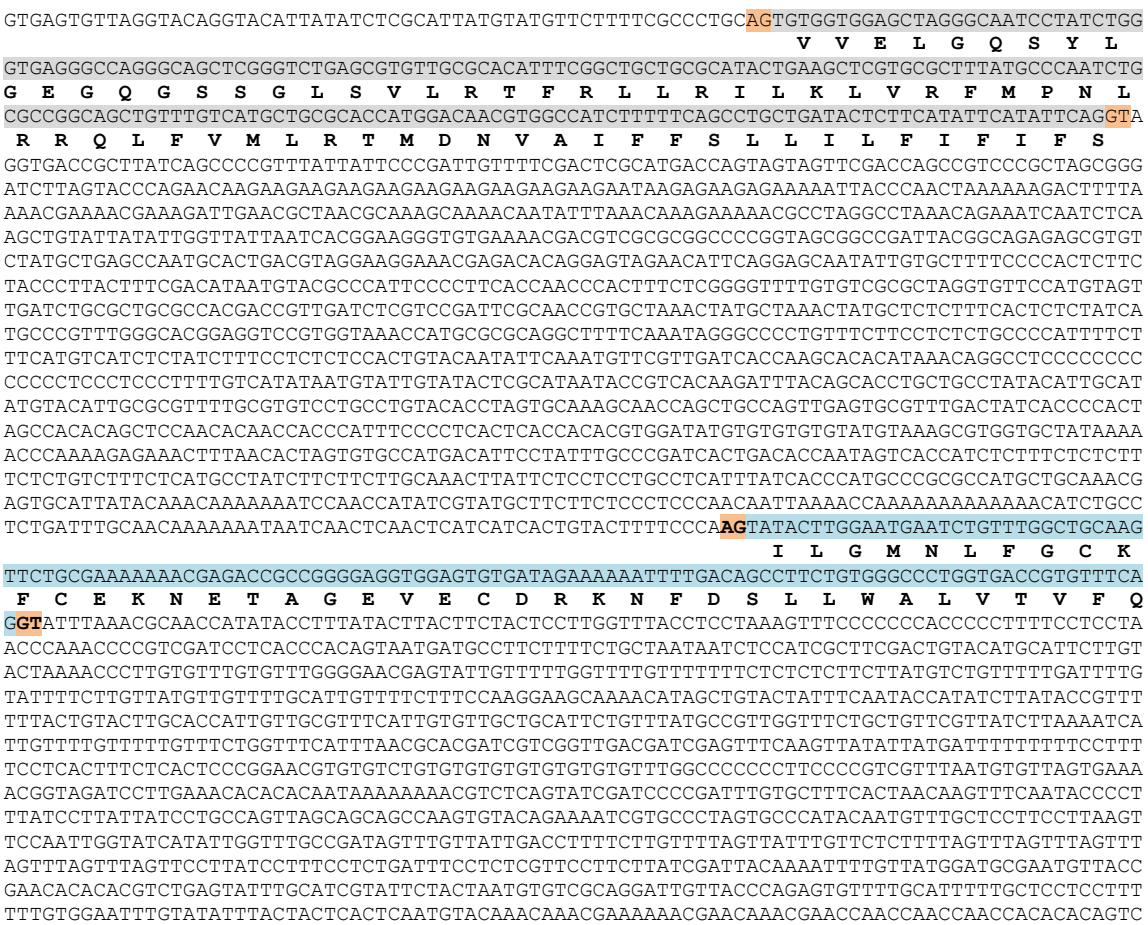

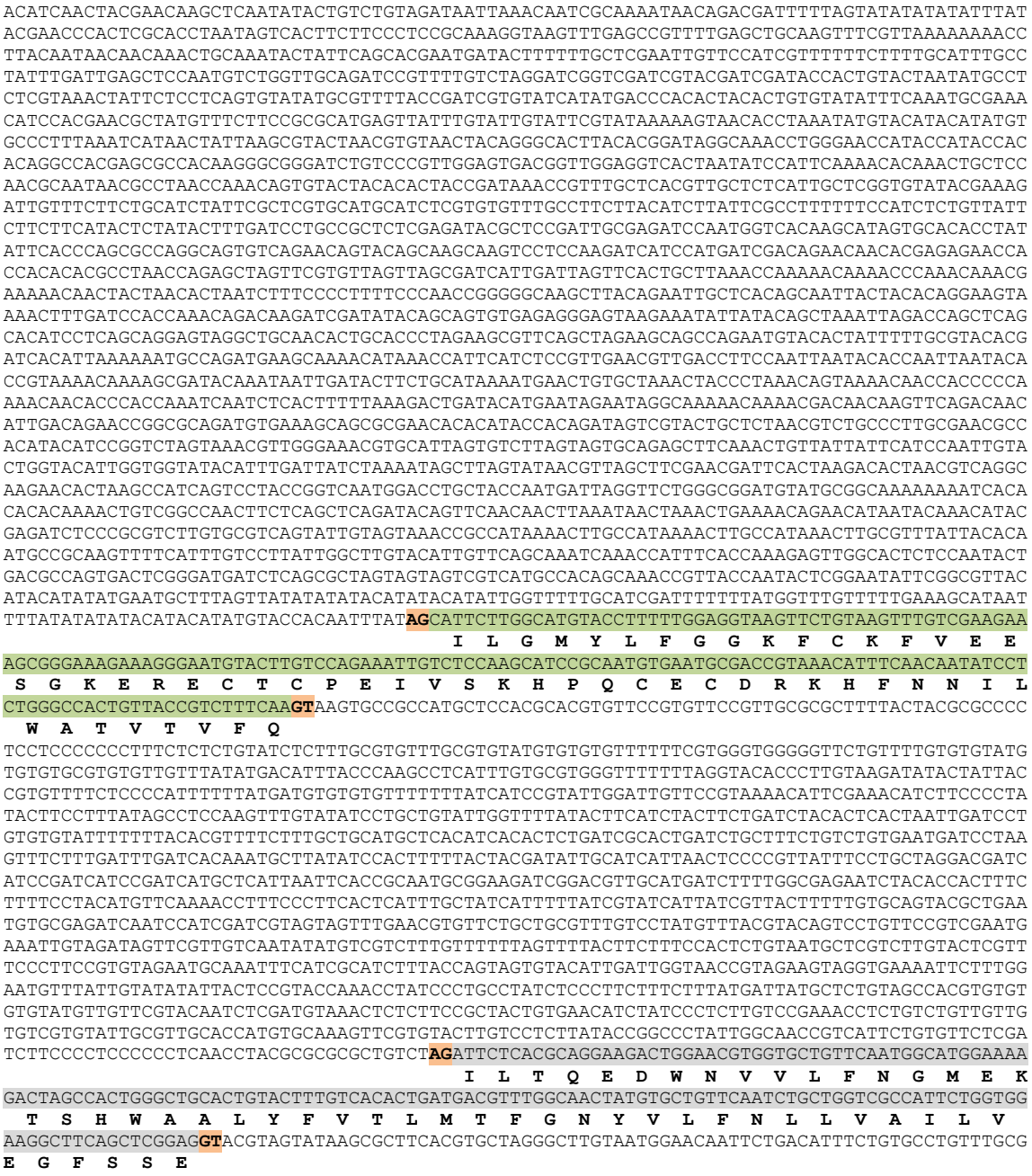

Ixodes scapularis Ca_v3 (GenBank accession DS930826.1)

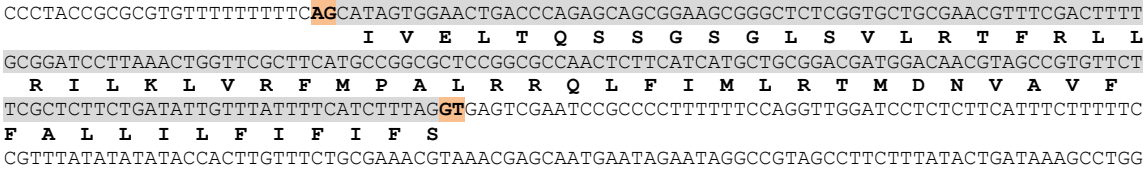

CAGATCTCCACAAGACGCGGCCGCCGAAAGTGAAAAGATTGAGCGGCAGACAACGAATGAAAGGCGAGGCGTGTAACGGGCGCCCCGCT
GCGGCGAGACGCCGAAACACAGTTCTTCCGAGCGATGGAATGTCCGCTCGTGCTCCTCGCGTTCTTCGCGCTACCGCTTCTTTTCTCCT
CGTGTTTGAAAACCACGTTTCGGGTCCTCGCTGTCGCGGAAGCTGTGCGCTGAATACCAGAAATGCTCTGTGCTACCAGATTCTCGTGC
TCCAAATTTGCGACCGGGCACTGTATGGCTCCGTCGTCGAACTGCCAGGCTTTGTGAGTAAAGAGGAGCCTATGATTAGCCTTTCCTAT
CCTTACACAAATCGTTGAGGCGCTACTGATGCCCCATCAGATAAAACGCGTCGTCCAGCATTGGGTAGTAAATGGGGTAAACCTAAGGC
AGTAGTGTATTCTTAGTATCGCGTTTTACTTAAGCAATAACGGTAGCTTCTTTTCGGCGAATAAAGTGTTACTACTTTACTTACCCTTG
CAGAACTTTATTTTGTGCCATTTTGTTAGCGGACCAATCTTCGAGTGGCTTTTCACTCGTTAAATCACTTTGCTTGAATATGTATACTG
TGAGTACTACAATTAGTCGTTATTTTATTTTTTCATGTCATTGCCATTTTTTTTCCTAACGTCAATTCCAGTAAATTGCTCCCTACCAT
GCAGCTGCAAGGGCGGGTGTCGCTATGCATTAAGTTATTTCTGTGTAGAAATGTTAGCATTGTACAAGTGACCCTGAGTGACGCCGGCT
GTAATATGTCATTAAAATTGTTCAAGTTGATTGTGCGATAAACGAAACATATAGGTTCTATTGTACCTTCAATTCAAAGATTCTCTGTT
AGATTGACGAAAAAAATGGTTCCTTTGATTTTAAGGTACTGTGTTTTTATGTATTTTTTATTACTTCTTAAAAATGTGTTTATTAGAGG
AGATAAAATGTCCCATCTTATGCCTTACCTTTGTTAATCTAGATGTCCAAGCTATATATATTACCACAGTTGCAATATGGTTGCCAGTC
AGTAATAGTGAATGTTCTAACATTTACGCGTCAGTTGTTAAAAAAGGTTTTTTTAGTGTGTCATTGTTTAGCTAAAACTAAGAAACAGA
CCACAACGCCCGCCTCGTCACCTGCACAGACTTCGGACCGGGAGCCTCAATGCTAATTTTTTTTAACGTTTTAAGTCCAATGTTTTTAA
TTAGTTTTATTATCTTTACAGTTCCTAGTGGAAGAGAAAAACAATTCTCCTCTAACTTGTACCGACGTCCCTACGAAGCCCCCTCACTA
CTCGCACAAATGAAAAACTTTAGCTCATTGGGTTGAGAAAACATTGCATCTCAAATGACATCTTATGTCATATGTCGAATATTAGGCTT
TCGGTGTTATTAATATAAATTGCCTGTGGCCATCGCTATTGGGCCAAGAGGGAACATGTCGCTCAGCCTTGTTTTTCTTTTCCAGTAGG
GACGTACCCTATTCTTTCCCCCTGCCGGCTGCTGTCTCCCTCCACTAAACACGTGCCGGAAGTGCGCACACGACGCCGTAGGCCCCCAC
GTATTCTGCACGTGCGTGTGTTACCCGCCTCCGCCTGGCCCCCGTGTTCCTTGCTTGGGCCTTTTTCGCTCCGAAGTCACGCTGTGCCC
GGTCTTCATCACCAGCCACCATTACTGTCCCCCCGACGCCAAGCCCCTGCGCTGATGGCGACGTTTTTTATAAATATTTTCCACAGGAG
TGCCGCCATCTTGAATTGTCGTCACTTCCAGTATCGGCGACAAAATAGTAAAACGTTTCAACCTGTAACTAGTTAAAAAATAGAGGGGA
GCCAAAACGAGAATGTGTGACGCTTATATCCTAAATGTCTTCCGTTGGCGTGGTGACGGCAAAGTAATGTTTTCGCTCATACTGGAAGT
GACGACAACTCAAGATGGCGGCGCCCTTGTGGAAAGGTCTATAGGTCGAGTCGTAGCCTGGTTTGAGAACCGCGTAGACGCAGCAAAAC
TAGAGCAATAGCTCGCGCTACTCCGCCGGATGCCGACGCTAATTCAATCCTTTATGTACATGTCCCGTTTGAGCAAGAATAGTAAACAA
CCAACAAAGACCAACTTCTGCACGCGAAGACGTCTTCCGCAAGCTCGCAATATCTCGAAGCCTACCTTCGCTTTCATGCTGCACGTCAT
GAGCTTGGTCGGCGTCGGTTGTTGCTGTTTGTCACTCTTGTAGGACTTGAGCTTTATCGCCCTGGGAGCTTTCGGTGCTTACAGCTTCC
TGAAATTAAAGAGCGCAAAGGACAGGCAAGGACATGAAGTAGACAAATTGTTGTGTGCGTGTTTATACAACCGGAAGTTAGTCTGCCTC
GGTGGACGTCTGGTGTCTCAGCTGTAGATGAGCCTTTTAGCCAGTGCAGTACAACCGCCAGCCTGGAGTCTTTAATGTGCACCACGCAG
TAGGGATACACGACCGCACGCCGGTACGATGCTCATCCAGATCGAAACGGGAGAAAGTAGACAGGACAGCGCTATACTCAGAACTGGCG
TTTTACTAGAAAACTAAGGAAAAGGAGGCAGAAGTGATAGAAGTTATACGGAAGATAAAAAAACGGAAATAAAAGACACAACCATCATA
GCAACTGTAGAGTCACATGCATATGCGTAAAAGTAGTGCAAATAAAAACAGTATTTTATTATTAAAAACAATGTATAAAATATAACTTT
AAAAAATGATTGCAAGATGACTTTCAAGGATGAAGTTTGAGATGATCACCCACCTAACAATAAGATACCTGACACCTTATGTAGCGTGG
TGGTGGTACAATAGTTCTTTGTCTGACAGAGACACAAAAGGCGCGCTGACACAGACGTCACCACAACCCTTGATGGTCTGTGCCTCGCA
AAGTTCTTTTGACATTTTTTTCACGGTACTGCCACAAAACACTGTTTTTTTTTTCTTTTTTTTAAAGATCGGCGTGCAGTGGCAGTCAC
GTGCGTGTATTGCGAGATGTCCTGCGGTGAGGAGTTGAGAGATATTGCATTTTCCCGGAGTCTTGTATTTACACTCCGGTCAGATCGTT
CCACATAAACTTTCCAGCAGGTGATTGACTGTTTGTTTACTATAGCGTTGCGGCATGGTATATATCTATGCTTGTGCTTCGCTTTCCAA
TCATTCTGATGGTTTTACGGAGAATTGATCTGAGGGCACAGCCTCTTCAGCTTGTCCGGTGCAGAAAATACTGAGAAATATAAAATCTA
GATGCAACCGTTTTGATGTTATGGAATATGTATGGCATAATTGGTAGGCGTCAATTCCTGCTCTCGCTTTTTTATTTCTGTTGTTTTGA
GCTAATCATATTTTCGACAACGTCAAGATATCCAGGCGTCTTGAGTTTTTCCACTTGTGTTTCAAGGCTCTGTCTCGCCTTATGGACAC
ATGATTTCTTGAGAGCAGCGCAGATTCAGGTATTCACATTCGCTCTTTTTCTGAGTTTGGAATGCACACTCAAACTCTTATGTCTACCT
CGTGTCCTCGTCTGTACTGGCGTTTTATAGTTTCAGTTTGTTGAACCAACTAGCCAACCTTAATATTATGGTGCGGACAGCTTCCTCGA
AAGGCCTTTGCAGCGGTGTTTACGCTCCCTTGACCAGGGTTATTGGTATCGGGGTGCTTGTTTAGCGCCGCCTCACTACCAGTTGGCAT
CCGCCTACAAGGGCATGGCTTCCGATAGAGCAGGAGCGCAGTGCTGGCTTATATTCAGAGCATTGGAGAAGCACAGTACGGGCATTCAG
TCAGAGGCCTTGAGAAGTATTGCGCTGGCATACGGTAAAAGCTTGTGTGGAACCGCGCTTCACGTAAGCAAGCGGGTTCTGATTATGCC
CGGCCGGTGGCCGGGGGTAGCAGAGCCACGGCTCTTTGCTAAAAATCCCATCATAGCCCGTCAATGCACTTCGGCTAGCGCCGCGAGGC
AGCTGCGTACCAGTTAAGTACCGTCCATGCGGAAACCCGTGCCACCGTTCTTTGGCGTGCATAACCGTACCAGTGCGCGACGTCGTTTT
TAATTTAGCTGCCTCAGATTTGGGAACTTATCTCTTTCTCAGCCCTAGTACGTCGTCCGCGGGTCGCCTTGGAAAGTTTTAGTTGGCGT
TATAAGAGGCACAAGAGCCAGAACACAAGTCGGCGGAACGCTTTGATGGCACGAATAAATGTTTATTATAACCACCCTCTGAGCCAGCG
TTCCCGTGTCTCTGTCTCTCAATGCCTCTAGCAACCCACAAATTCGCTGCAACAGTTGCTAAAAAAATACCTATTTGGTCGGATTTCGG
CTCTGTTTCTCAGACCGGAGATAGGAAAGCATTTTCAAGACAGCCTTGTTCATGATTTGAGAAACATTCCCGCAGACTCGGACAAACGT
GTCGCTTCGGATTAATTTTGAGTTTGAGCTAGCGAGACTTGAAGTTTCCGTCCTGTTAATGATAATTCATGCCTATCAAATGATCAATC
AAGGTCTGCTTCATCTTTTTTTTTTTTTTTGTGGTGCGGCGTGCTCTTATGTTTATCAAACTATCCCCATTTATCTAAAAAAAAAAAAAA
ACATCAGTGACTGTCATTGTTTAAACCTGTGTTTTTCTATAACTGACCTGGACAACCCGAGGTTTTCATCATAGACACCACTGAATTGA
CTGAAAGTCATCGCGCCTATTCAATGAAATGTAATGTAACCTTATTTACCATCGTGGTGCCTAGATCATGTACCCGAATGGTGTGTTTA
CCGCGTCTTCAATATGGTCCCTCCCTCGATTTCTACCTGATGACTTCATAGAAGTCCAATGCCCTTGACTGCCGCGATTCTGGCAGCGG
CGGCCCAGCAGCACCGGTGGATGCGGTGGACGCCTGTTATGCTGTTGGTCGCTCTGCATCCTGACAGTCAATGGGAACCTTAAGCAAAC
GCAAAATGGGATGCCGTGACGACAGCGAGCCACGCGTCACACTCGCCTTTTCCGCCAAAATATCTACGTCCAACCTCCAGGATTCTGAC
ATCCTACAGCATGTCACACTGCTCTTGCGACGCAATGTGTTGCCACTTTGGGACCGTCTTCGATGAATGTGTGGGATAGAATGGTAAAC
ACCAGTCTCAAGACGCGTTCGAGTCAACGTACTACCAGTCACGTGCTAAAACTGACGGATTTAGTGGCAATATAGGACATTTCAGTAAA
GACTTCGGTAACAAAATAATATTATTTAGGCAAAAGCCTGATATGTCTCATCGTTCAGTCGACCTTCAAACTCCTTGAGCAAAAACACG
TCGGCGACACGAGAGGTACCAAAGCGTTCACGTTTTGGTACCTTTGCCTTTAAATCGCCTTTCGTGTTACTCAGGCGAATTAGAGGCAA
TGAAAATAAGGATGACAAAGGCGAACTAAAAGGAAACCTAAAAGGAAAGGGACCTAAAAGGAAAGGAAAGGAAGGTAAATTCCTAGACT
TCGTCTTTTAGGCTTCGTTCTCAAGGTCGTCCTAGGCGTCGCCCTTGAGGTCGTCCTAGAAATCGTCCTAGAAGTCGTCTTACACGTCG
TCCTAGAAGTCATCCTAGACGTCGTTCTTGACGTCGTCCCAGACGTCGCTCTTGACGTCGTCCTAGAGGTCGTCCTAGACGTCCTCTAG
ACGTCGCCCTAGACGTCGTTCTTAAAATCGTCCTAGAAGTCGTCCTAGGCGTCATCTTTGACTGGCTTTTGATTTCCTACACGTAAGCA
GTCTTAAGTGTACTCGTGAATTTTTTAATACAATATTCCAGCAGTACACGTCCAAAATATATTTGAACGTATCATTCGTAACATCATGG
TGACCGGAAGGTGTCTCCGGCCCGTGTGCTTAACATCATATCCCCTCTATAGACCGAAAGTGGTCACGAACTGGCAACGTATGACGCCA

CGAAATCCGGAGTGCCAAGATTTCGAACTTCGCGACCCTGGCGGTTGATCGTGCAAATGGTGCGGAAAAGCACCAGCGAACACGAGTGT
CGCTGTTGTCGCGGTGTCCCAACTTCAGACTTCCGAAAGTTCCGTAGACCGTCAAGCTGGAAGGCGACCTACGGTGTTAACAGACGCCT
ACCCCATGCACCAACTCCACTGCTGTCACATCGCCAGGATCGCTGCCAGCGACATGCTAATTTTATGACATCGTCAGGCGGAAATCGAG
GAACCATTTTTTGTGGCTCACTAAAACGCGTTCCAGGCACCATAGTAACGTCATGCCTTTCTTTTCACCCAACGCAACCTTCGACTGTC
CAAAACAAAACCTCACTCATTTACATTTTTAGCGAATCTTTGGAGACACTAAAACCTCTTTCACATAAGATATAAGGAAAGGAAGCAGT
ATATCTCACTCAGTAAAGAAAGTTAAGAAATTTAAAGGTACGTCGTGTGCTTCAAATATGCTAACTTCACTGCTCCTGAACAAGATGTA
AGAACCCCCTACCCCCGCTCCCTTTTCTAAAACTCCCACTACGTGATTTTCGAGACTTTCATTGCAAAAAATGGCTCGCCTCCTTTGAA
CATACGCAACGCAGATACTGCTATGTTTAACTAAATTATAGTGTATACTCACTCCAACCCTCTGCGCTTCGCAGGACTTAGTCAAACTT
TTTAATTTGCCTGGCCATAGCATTTAGACTTCACAGAGATGGTAGACAATACCGTTATCTTTTGTAATGACAGAGCAAAGCGCATCTGC
ATTGTCATAGCCAAGGTTATAAAATGTTTCATTTTCACCTTACAAAAGTCAATGCAATACGACTTCGTCAGATTGTAGGCCCCTCTTGA
AATTTTCAAATCGGATAGATGGAAGTGCGCAGGCTGACGCCTCACTTTGGAGCCACGAGGCCCTTTTAACCCTTCTTTTCAGTTTTCAG
CCCAGGACTTAAAGGTGCAATTAAATTTTATGAGTGTCCTGGAATGTCATAGTTTGGGCAAGGTAGTAGAGATTAGTGTACCAAACTAG
CCTCTTCGTGATGAAGCGACAATGCTACGTTTGGTTAACTTTATGGCGCAACTTAAAATAATAGGGAAATCGGTTAGCACTTTAGATTC
ATCTAGGGTACACTCTCAACGGGCTAGAATTTAAGGCAACAACAAAAACGTTTAGCCATGTGATATTGCAGGAATTCGCTAATCTTGAG
AACTTCCAGTATGAGATATAAAGATTTTTGCGATGGGGATATGGGGCATAGAAGATGTGGCTTTCTGTGATGCTATTGGGCCGGATCCT
TGTTTGGTTTATTCTGTTGTGATATTAATGACATCAGAGAAGCACGTTGCAATAGAAACTTATACAAAGTCATCGGTGATTGATAAACT
AGACAAAATATCAAAGCAGTGCTCCGCCGAAGCGACAATCGTACATTATTGGTAAGAGAAAAAAAAAGTATGATTGAGAATCGCCCTCT
TCCGTGATCATTACTGTCTTCATCGGAAATGGCCGTCGCTGGCGCTTTCATGAAATTCCCGCACTCCATAACCGCTTCTTGTCCTTGTA
TTTGTTATGTATGTCTGGCTATTAACCCGCTGATCCACTAACATTGTTCCTCCTAACCATACTTCCTTTATTACGTCAAATAACTGATA
GCAGGCCGTACCAAAAAAATAAAAAGGATGAAGCGGCGGGCGGGCCTCCATGCGACCTCTTAGTTCAGCGTCGAAATTTCAGGCTTCTT
AAACAGGATATATTTGAGAGCCTGGCAGCCATATTGAACTGCGGTTTAACCCGACTAATGACACGCCTTTTGCATTCCAGTCTTTATGA
ATGCTCCAACACGCGCGATCTCGACGTCCTACTGCTCTGAGTCGTGCGTGCGGACTCCGAAGAGACCTTTGACCTGTGGCGCTTTTCTT
TTTGTCTCTCTTCCACGTACGGCGGCGCTCGAAAACGTTATTTCGC**AG**CGTTCTGGGCATGAACCTTTTCGGCTGCAAATTCTGTGTCA
V L G M N L F G C K F C V
AGGAACCCGATGGGACCGTGCAGTGTGATCGCAAGAACTTTGACTCCCTCCTCTGGGCGCTAGTTACCGTGTTTCAG**GT**ACCGTGTTCC
K E P D G T V Q C D R K N F D S L L W A L V T V F Q
ACGCCGCCTGCTAAGCCTCTGCGGAGGTCCTATCAGAACTATCAGAAAACGGTGCCCCCTCCATGTCCACGCCGTGCTCGGGGGTTCGT
TTAACGCCTCGTAAAAGAGCCATACTAAATGGTGCAGACTGAAGCCAGACCAAATTTATGTTATTAGTTTTCTTTGATCCAGCTTTAAA
AGAATCAATTTCCTTCTGTTCGATGAATCACCGGACGGAATACCAGAAGTCATTCCGTTGTAATACAAATGTTAGCCTAAGAGCAAAAT
TTAAGAAAAAAAATCTCCCCTCTGAAACTATTGCGAGTCATGTTCAAATAAACGTGCGAGACACATGCTTAATACCAAGGCATAGGATT
GATTCTTTTAAGGGTAAACTAGTTAGACGGACTGATTTTACAGTTTTCTTGAGGTGTTATTGACCACCGATTAAAAAGCGGCGCCAGCC
AGGGGCGCACCGTTTTCAGCTTAATTTTTACAATGATGGTTCACAAAGGGGAGACAAAGCGATCTAGAGTAGCCTGTGGACAATTCTGT
AAGCACGCGCCTATACGTATACTTCCCAAATCTAAGAAACTAAGGTTATGCGACACAGAGCGGAGGGCCGGGACCTTTCCAACACCTTT
CCAATTCATCTGCTTCACTTGTCTTACCCGGTAGATGAGCGGTTCTGGTAACTCTGCGATTGCTCCGAAGGATGCCATCGCTTTTGCTT
CTGTGTAGCCTCGCTTCAAACTGCACACCAATTGGGGATGAAAATATTCCAAAATAAGGCCATGCGTTGCATTTGGAAAACGTGATTTC
TGCCACTTTACTAGGTGGTAATCTGAAAAAAATTATGGTGTTGTTTTTGTTTCTTTTTTGTGGCTGGGGCACCACTTAAAGTCAATAAG
CTTCCAGCGGTGATAGATATTGAGCACCGAGTATTTCGTTTCTACTTAAGCTGTGCAGCCGCATTCGCGAGCGAGTTCCCCAAATGAGA
GCTGATGGAAGCAATCGCAGAAGGGCCAGAACCGTCTTAATGGAGTTGTGACCGCCTGCCCTGTCAAGACCCGCATCGGTGTTGTCAAT
CTGCACACCGTAGACGAAAGATCACCCCGTGCGTACGTCATTGGTTTGTATCCTTCCCGTAGCCACAAAAAAACGAGAGAAAAAAGACA
CCCCTCATACTTGGTCGGCCCTTCGGCCCGGACTGGCGAGTTCCTGTCCATAAACCAAATGCAAGCCCCTTGCAGCTCCGAGTGCATTC
ATGGCTTGTGGCATTTCGAGATTCGTACGTGTGTGTGCGTGTGTGTTTCAACTGGCTGTTTGGCTGCTTTGATGTCCTCCATCTTTGTT
TGTGTGTGTATGTGTTACGAGACACGAGTGTTCGACACGTCTTTGCTTTTTTCTCTCGAGAATAATATTTATACGAGAGTCATTCCTTG
CTTATGGTATTTTCGATTATCTTGTAAAGGTTAATTGAAAATATCTGTAGAATTCGGGTTAAGCACATATACAGAAATTCTCACATAAA
AGTTACCCATATCTATCTGTACACCTTAGTTAACTCGGGCATTTGCCCTGTGCACCTTTGGCCCTAGCTTCTTTGTTGTGCGCTTTTAT
TTTTAATGATTTGTTGATGATCAGCGAACTAGCCCCAATTTATTTTACCTTATATCGGGAAAAGAATTTTGTGAGCAAATAGAAATCCC
CCCATCCTACGTCACGCTATCATAAAGTTTCATCTAGTCAGGTTTGTTTTTTTTTAATTAGTGCGTTGGCATGCCGACCCCTGGTTATC
CAACTCGCTAGAAAACCGAACTTAGTGTGAATTTCTCAGACTGACAATCGGAAAAACGTCATAAAATTTCATATAATGTTTTTTTCGAA
AAGATCAGCTAGATATCTAAGTTAAGATGGAAGCTTGGGCGAGTTTGCAATTCATCACAGCAGCAACTGCGCAAAAAGACAGCGACAAA
AAGAGGCGAGAGCCATAACTAACAAGGGACATGCGGGTATTGCGCACTTATGATCGCTGAATAATAGGAAATGTAAATTTCTTTAGGCT
CCGTTCTAGATATCTAGCTCAAGTGTGTATGCTTGTGTTTTTCTTTTGACTGCGTCTGCTCAATGTTGTGTGTTCCCCGCCAGACCTGA
CATGGCTTTTGTTTGTGGACCGGTGTCTGTATGTTCCATATATGTTCCTCAGGCAACGTGCAAGCTTGGCTTTAGGTGTGCTCCAAAAC
CCGCTCGCTCTCCGATCCGTGCCTGCGTCTGGCCTTTTGCTTTTTCTTTTGCCCTTGTCTTCTGAGCTTCTTTCGATGTCACTTGAGGC
ACTCTCGTGACAGTCTGGTTTCTTTTTTTATTTTACCGGAGACGCCGAACGGAAATGACGAGGCATATTGGTCCTTTTCGATAAAGTGA
TCGTAACGTGGTTGGTGATGTTTTTTGGAAACCATTTCTCGATCAACTCTGCGTTTATAGCAGTTAGTGTAGTGACTGTGGCTAACACG
TGAGAAAGATAATGTGCTATTACGCTCAAGGTAGCGCATACAAACGTCAAAATGATCCGCTGTAACCTGCTAGATTGTTGCTAAAGACG
CTAGTTTATTGTAATGATATGTTCTCTATACAACAGTAGCGTTTGATCCAAACCTCACTAGAGATAAGCCTACAAAGCTTCAGCTTTCA
GTATTATGAATAGTTTCAGATGCAAACTGCAGTTCTTGACTTTATCTCGAGCTGTGTGAAGTACCTGAAGCTGTATGTCGCGTACTGAT
ATCTGTAAAGTGTAGCCTTTCTGGTTTTGCTTTCTGGATGCAGTTGAAGCATCATTAGATATTCCATACCGTATTCATCTAGATTATAA
TTGCCATCATCTGAAGGCAATTATAATTGCCTTCATCAGGTTAAAATTGCAAATGCAAATGGTGTCTCCAAGCATCAATATTTAAACTT
TTGTAAAAAAAAAGGCTTACGAAGATGCAATAGTGCGAAAGAAATCGTTCTACATATGTGAGATATTTAATCTTCAACTTCACATTAAC
TTTCAGTCACCTGTTATGTACACAAATGTGAATTATGCGTAACTTCCTTACAGTTTTATGTAGATCACATAAAAGTAAACAAAACAGGT
GACTGGTTACTGTGTGGGTTGCTTGCTTGGCCGAAATTAATGCATTGTAAAGTAGGAGCGAAACAGCCAACTTCATATACTAACCGATT
CGAGCTAATGACTAAGCTCCACAGAGCTAGAACTGGCAGCGTGAATACTGCATCGCGATGCACACTGAACACAAATCACCAATGCCCAT
TTCGTGACACAAGGCTGTACAAACGTTGGGTGGTGCCAGGCCCCATCTCTAGGGCAGCGCCAGCGGCAAAATGTGTGGATTCCCTTCTT
TCGTTGTAACTGCGCCAGCGTCTTAGCGTAGTTGAGCTCGTCCTTCTCACTGGTTACGCTGATAAAAAAAAATAAGTAGTAATTGGCAT
TTAGAAAGCATCGCGGAGCAGAGTTTATGAAAATATTTCTATGAGGTAGCGCAGAAAGGGTGCTCTTTCACGGCCCCTCAGATGTCGGA
GTTGATCGGGAAAGCCTGCACGTTGCAGCGGTGACCGGCGTTCTCTTGGAGGCCGAGGCATCAGTGGTCGTCCCGTGTCTGTGCTGGGT

CTCGTGACGTCTGTCCGCTTGTGGTCTTTTGTTTAGGCCGCACGCGAGGTCCATGTCTTGTGCGTACGTTCGAGGAGGGCACACTGCCC
GTGGCACGCGTTACCACGAAGGCGCCACGGTTTTCGCGACCACGCAGTTGCCGTGAGCGTAGCGACATTTATGCACCAGAAACCATCTG
CGTTTGTTGAAAACAAGATGAATGGTAAAATTACGAAACCAGACTTTCAGAGGCTAGTTGTATGATAATGGGAAGTTTTTCCGCCTACA
CATACACACAAAAAAAAAGAAAAACAACGTAGGCGTTGTGCTTGATAGCACTAGAGTGTATAAGTAGCAGTTTGTCCAGAAGCTCTTTT
CTCTGAAGTGTGCTGATCTATCTCCAATAGTCAAGTGGAATATTACGATATGGCATATCAAACACGAAAACCGAGTTTCCGAACCCTCC
AGATACCTTCACAATTTCTTAACTCTCTCACTTGTTCGCGTCAGATCAGTGTTACAAATTCCAGATCCCTCGATCTGGCAATCGAACTT
CAATTTCCTTTGCCGTGTATCATGTACTCCTTGAACAGGGACGCAGAAAACCGTGGCGACCTCGCAGTGCAGACGAATTGAGAGTTAAG
AAAAAGCTCGCCCTAGGGCTTTTACTGAACATATGAGACATCTTGACACTGGGGGATCTGGTTGTCAGTGAAGAGGACCCTGGGGGAGT
CTGCACTGCCGTGGAGCGGGTCAGTGACCCTGTATGTACTCGC**AG**CTGCTTGGGGATGCATTTGTTCGGCGGTAAGTTTTGCGTCCGGA
C L G M H L F G G K F C V R
CCGACGGGACGACGCTTTGCACGTGTGCCGACCTGTACAACCCGGCCCTCAAGTGCCTCTGCGACCGCAAGCATTTCAACACCTTCCTC
T D G T T L C T C A D L Y N P A L K C L C D R K H F N T F L
TGGGCCACGGTCACCGTGTTTCAG**GT**GAGGACAGTGGGTAGAGGCCATACCACCTACAAGACAAGGCCTGTGCATGACGTCATCGTTAG
W A T V T V F Q
TGGACCCAAGCGGCAAATACGCCGAAGCTACACGAGGTCCACCGCAAAGCGTCCGTCTTTGCGTCGCCGCGTGCTGACGTCACGCTCGT
TGTAAGATTCTCTAAAAGGCGGTGTGGACGATGCTGACGTAAGCTTTGCGACTCCGCGTGAATCCACTTGTGATGACGTTTGGGGGGTG
AGGGGTGGGGGGGGGGAGGGGGCTTTGTCGTTTAAATTATGTTGGAAAAGGCCAGACGTGGTACCGGCCTGTGTCGGGTGCTACTACAA
GGTACTTGGCACCCAAAGGATGACTGCTTCTCATATCGCACTTTGGAGCAGAGATCTCGGCAACAATGATAAAAGATAACGCATAACTC
TGCAGAAGCATGCATACAAGTGGCACAATGAATCAGAAACATTAGCCCGTAACAAGTCCTTAGAATTGATTAAAGACAATGACTTGTAG
TCTCTTTTACTTACCGGGCAAGATAAATGCTGCAAGTGAGGACGGGAAGTAGCTCGATTGCGTTCCAACAAAATTTTACCTCAAGTTTT
CTGCCTATTAGTGCGGGTCATCACTTGAGAAATGTATATGAAAACCTTTGTCTCCTCTTTATAACAGGTATATTTTTCTTCCCCACTAT
TTACTAATTGAAGAGTCTATTTTAATGTAACTTTGTCGTGACAAATGACTTCTTAACTGCTTGATTACGTGAAACGTTCATTTGTGTTG
CTTCCGTGAAAGATGCTGGCGTCCACGGATTTTGAGATGAGCGCAGTTTAAACATGTTACTCAGAGACGCGAAAGGTTAGCGAACACCT
TCCGCATGTCAGTGTATGAAAGGACGCTAAACTACCCCGGCTTGCAATAAGAAAACAGTTTTGTTATGCCGGACTCGTCGTAAAACTTT
TAACAAGAAAACATTGATTTTTTAATAGAGTAGCTGGGCCCGCCAGAATATTTATTCAAATTTAACATTCATTGTACCATTAAACAGAA
GAACTGTCAATTTTAAATTGCACTTACCATCACTGCTTCACACACAAAATATGAACATTCCTTCAACAGCTGAAAAATAACACCGTAGC
CTCCAATCACTTCTATATCGTGAATTATTTAATTTTAAGCCATCAATGAATTGTTTCCAATATATTCCTTAGAATGAAAATAACTTTCT
TCGACTTAATCATTCCCAAACCCGGCAATATGTTTTTTTTTGTTTTGTTTTGTTTCTTTTTTTGTGCCAGAAATTACAAAAATATTTAT
TGAATCCCGAGCCAAATCAAAGCGTGGAATATATAAGAATTTTGAGGTTCTATCAGTACAAGGATATTTTGTAGATTATGTCGAAAATT
GTCGTCTTGTTGTTACAAAAAAATTATTTATGTGGCTGAGCTTTAGTAGTTAGTTTTTCTGTGTGAACTTCTAAGACGTTACTTGGCTC
CCAGGATAAATGAGCACACAACAAAAAGTTTTACGGCATACGCTCACATGCCGATTGCCACATTGGGCCCAGGGCCACATATCGTGTAT
CGTGTGAGATGTGACAACACCAATGTTTTTTTCATATCAACAGCAAAGGGATCTTTAACACACATATTGTACAAACCAGTGCCGAGTCA
GCTGTAGGCCAGCACAAGCGCGTTTGACCTTATGTATTTTATTCACGTTTTTTTACTTCACCGTAAAAGTTTAATTTTAAACGAAAGTC
AATTTACATAGACAATATTCAATCGCATTGCCCGATGCCATCACAACATTTCCCAGTAGCAACAAGTGGCGCCACCTCTCTATATGAGC
ATCCGATCTCCCTTTCGGTCAGACTCGGTCATCTGAGTCAAGGTTCGACTTAATAATATTTATATATTTTATTATTAGTTCTAGTTTTT
AATAGGAATATACCTACGTCTTCATATTTCTCACTCTATAACCGGCCATTAAAGTGCACCTTTAAATCAATTTTCATCCCTCTCCAAGC
AGACTTTAGAGCGTATTCTGAACCGTGTAAGCAAACATCGCATGCATTTTTTTTATCTCTATGCATTTCACACTTCTATGTTCTGCGGA
TATACGCCAACACACACTTTGAGGTGTTGTTATGAGACAGTCCCAATAAAACCAACGATTAAGGTAGGAAATTGGCCAAAACAAACTTG
GAAACCACACCTTTCACGTCATTTTAGTTCCCAGTTAGCCCACAAGCTTTGAAATTAGGCACTCTGGAGCGATATTTGTACTCGTTTTT
GTTATACAGCAAGCTTGTCGAAGCTTACGTTGTAAAGATAGGCACGGTAGCTTACGCTAAGATGTTTTAATCGAAGGTGTTAATGATTT
TATAAGCATTATATTATAAACAGTTGCTTAGCAAGTGCAATAGGTAAAATAATAGCAACATATTTGGAAATATGTCAATGCCAACGACA
TTTTTGTATATAAAATTACAAGAAAAAAAATAGATTTTTCAAAAGCGCGCTTAAGCAAGAATCGTGTTTCAAGTTTGCAAGAATCGTGT
TTCAAAAGCTAGTCTGGCCACGGGGGTGGAAAACGCTTTTTTGGGGCACCAATCTGGTAATTGTGTTTGCGCCTTAGCAAGGCTTGACT
ACGAGGTGTAACAATTTAATTCCCTCAATTGCCTCACGAAAACAACGTTTGCTTACCTGTGCACTAGAGGCATAAAGCTATCTTTAAAG
TGCTTCCCTGGTAAAGCAATGCACGTGGTGAGACAGAGGCGTCATTACCGAATAAATTCTTAAATTTTGTTTTCAGGAATACCTTGAAG
TAGCCTTGTCGCGTCAATATTTCTTCTGGGAACTTTTTTTTTAATTTGAAACACACTAATGATGGTTGTGGCTAAGACAGCGAAACAGT
GTGGGCAGTTATTTCTGTAGGGTATTTCTTAGCCAGGAACTCGCGGAACTTTAAAGGAATTCGCGCAGTGGCATTATCATGATGGATAA
TCCACGCAAAATTCGAGGCACCTTTTTTGCAGGAATTCTTTTTGTTTCCAAAATCTCGGTTAGAAATTTTCACACTGCCTCCCTGTACA
CATTCCACTTTTCTGCTGTCAGTCGGATACCTAATATTTGATCTGAGAGCACCAGGGTTTACTCTCTGCCCACATTTGGGTCAGCCCTT
TTTGTTTTTGGCTGTCCTCCTCTTGGGACATGGGGCACTTCTTCTCGACCTTGCTTGAACTGTCTCTGCAAACATACACAAATCAATTT
CTTTGTAGCATGGTCACCACAACCATCGTTAACAGGGCTATTGCTTCACTGGCACATTTACCAAACATCGCACGAAACTTGACGTTAGT
CAGCTCCTCCAGATTTCTGACACTCTTTCCCCCGCAACAGTGTAATATGAATGCGTACAGATTCATCTCCTGGTCAAAAGCAAATTCAT
AAAAAGGCCAAAGTCTCTCAAAAGCGCAAGTAGGAACATGTCCGGACCTGCTCTGGTAGAAATCTCTGTCTGGTTTGCCGCCCCAGTGT
CACGCTTCTGGCGTTCTGGGAATTGAATTGTCACACCTCGTAACACGATCTGCACACACCAGAAACAAGATGGCGGCACCCAGATGCCG
TAGTTGCAAACTTGTATAGGGTGACATAAATAGTGAGGTTGGTTATAAAATAAGCCGGAAAATGTCGGCGCCTGCATGTTCGGAGCTCA
AATTCTTATCAATTGTGTCTTTTCATGGTGCATGACACCTTGTAAAAATTTCAAAGCTCAGGTCCTATAAGAAATGAGAAAAACCTTCT
TGGGAGTTTCAACCCGGGCGCTGACGTGGGCCGCAAAGTCCCACCTAGAGTTACCTTTGAAGCTGCTACCGAAACGCGGCGCCGAACGT
CGCGTTTGTATAAAAATACCTTAAAGTTAAAAAATAAGGAAAGTAGAAGTAATTAACGTGTATTCTGGCGCACAAATAAGCCCCAGGCA
AGGTGAACGATACCGGAAGCGTGCAGCTATACGCGAGCAAGGCAAGAAGATTCACCACCAAAACCAGAGTAGGGGGGAGTCCGGAAGGA
GGAGGTTCGTAGACAAATGCTAGCCGCTGTCCTACCGCAAGAGCCATGCCCGATGCCGCCCCACTTTAGCAGGTGGGAGCTAGCGAACC
GCAGAAGGATGCAAAGCAAAGCTGCCATAACATTCAATTACAGACGATGTTTTACAAATTGACTACGCCGGACTACAGCGAATCGGATC
CGCAAAGGAACACATGCCAAGTCCCGCGCACATGCATGCGCTTTGCGTGGAAATACGACGAGATGAAGACGCAAAGAATCTAAGGCCTT
GAACAAATTCCGCGAGAAACAAGCCCAAAGTCCTACGCAAAATGGAAAAACTCGTCCACCGAGAATTCGCGCCGCAAGAAAGTCCTTGA
CTCCCTGTTAAGCTACGTGTGTTTAACGGGCAACCTCTCCCTTCATTTAACCAATGTCCCCAACCGCTCAACGCACCCTGAATTTACCT
CCACTACCAGGAACAAATCGATGATGGTTAACAAGAACCGAAATCTCAGTCATAAAATGAGTGTTAATACTACTATCCCGGTCATATAG
GAAAAGGAAGGTTGTGCATTGAAATACATAAGAATACGCTATGACGGTAGCGGTCGTAATGGTCGATTGAAGTTCATCATCGTGCCATC
TAACATCCATCTAAAATTAATGATTCTAGATGATGCTAACACCGAAATTCCAGGTTACTAAATAATTCAGTAGGAAAACTAAGATAGGA

GTCTGCTTTGACGAACTAACTCCAACTGGTCATTCAGAGCCGAGCTAGATGCCATTGCAGCGCCACCCTTTCCGCCGCAGCGGGCCCTC
CCGGAACTGTATATTGCGAAACAGAAAATATAGTGCAGTCGCACCATGCGGCGACTTCCTCGCGAACTTCCCCATCCAGAGAAGGCAAA
GCAGAAATAAAAAAATATATATACTTTATACCGAAACGGAAAATATATTGCAGTCGCGTCATGCTGTAACGTCCTCGCGAACTTCCCAA
ACAAAACAAAAACCAAAAAACACAACGCAGAAAAAAAACATATGCTAGTATACTTTTGCCGGTTAGGTGAGCTTTTGCTGACTCCCCCT
GTCTCAAATCGTATTACCTACCGCTAACTCATCGAAGCACTACCACCAAACTGACGGGATGTGTTTGCCGCGAAAAAGCGGCGCTGTAA
TCAAACCTCGCTAGCAGTGGCTCGGTTCCGGTGGATATGAGGAATCCGCGTTTCAAGGAGGAGTTTCCCAACTTCGCTTCTTTATGAGC
TTTGCCGAAACTTACAAAAATAAACGCAAACTTGATTATGCAAACCCGCAGCAAATGCGTCGCTCAGTTCTGTCGTCTGCTGTTGCGTT
ATCATGTTGCGTCACTTCTCTGTAGCAGCCCCGAATACGACACTCGAGTAGCGCTAACTCGCTCGCCTGTGTCGGCGCCCTGTCTTTGA
AACATTTCAAAGAAATCCTCATTTTTCGCAGGTAGGAACGGCGCTTTAAAATTTCACAAGTTATCGTGCACCCCTAAAACGCACCTTTG
ATGAAAAACTTGAGCTCTCTAAATGCATGAAGTGATTTTTCCGGCTCAACTTAGTCTTCGGCTTCAAATTTAACGCCATCTTAAAGTAT
GAGGCTGCAATCCCGAAAATAGCCCTTAGGTAGTAAAAGATTTCTCAATGCTGATGCAGCTTGGCATGGAATTGTAAGTGAACATATTG
CAGAGGATTTACTTAGCTCGAAAGTGATTGATATGTTCTAAACAAAAACTGTCGTTATGCCGGTAGATATACTTTCAAGACTGTTAGAG
ATATCTCGCGGGTTGTGTAGTCTGGCCAGTCGAAACTATCAACTGGGCTCTATCACAAAAACAAAAGTATTCAACGAAACCGAGAATTT
TCGAAAGATAAATTGAAAACATCGCGGACGCATGCCTAGCAGTGGAGCACTAAAAGGCGGATGATTTGCGGGATTTGAAACGTGTTTCT
TTCTTTCC**AG**ATCCTCACACAGGAGGACTGGAACGTCGTGCTCTTCAACGGCATGGAGAAGACCTCTCCGTGGGCGGCCCTCTACTTCG
I L T Q E D W N V V L F N G M E K T S P W A A L Y F
TGGCGCTCATGACATTCGGAAACTATGTCCTTTTCAATCTTCTCGTTGCCATCCTGGTCGAGGGATTCTCAGCTGAG**GT**GCGCACGTCC
V A L M T F G N Y V L F N L L V A I L V E G F S A E

Strigamia maritime Ca_v3 (Baylor College of Medicine ID lcl|ctg7180001233225)

TTCATTCTTTTTCTTTACTTTTAAATTTTTTTTTTTTTTTTTTGTATTGC**AG**TGTAGTGGAATTATTACAAGACAGCGAGGGCAGTGCC
V V E L L Q D S E G S A
CTTTCCGTTCTCCGGACTTTCCGCCTTCTGCGTATCCTCAAATTGGTCCGCTTTATGCCTGCGCTTCGACGCCAATTGTTCGTCATGAT
L S V L R T F R L L R I L K L V R F M P A L R R Q L F V M I
TCGCACGATGGACAATGTGGCTGTCTTCTTCGCTCTTCTCATACTGTTTATATTCATATTCAG**GT**AAGATTTTTATTCAAAAGCTCAAT
R T M D N V A V F F A L L I L F I F I F S
ATGCTTTTATGAGTGAACAAATTGAAGATGTAAAACTTTGTCTCATTAAAAACCTTCAGATATCGAAGGATTTTTAATCCCATTGGTTT
AACATGGGAGTTCTGCACTCACAAATGACACTTTAAATGCTTTTTTGATTTATTTTGTGGGTATGTTGACTTTTAAAAAATTGAGTTAG
TTCAAACGGAAGTTCAATTGGCGCCGTTAATAATAATCGAAAAATGCACTTTTTGTTGAGTGAAACTGGAAATCTCATTTGGCCAAATG
CATTTACGCCTATCGGTATCGATAGTGTCTACATTTGAATAGAGTAAGTGCTTTCCAACACACTCGTGTTAAATTGGAAACCACTTTAT
TTAAATGTGTACGCTTTTAAGCATGAATAATATGCATTTTAGACGTGAGACAAGTTTTTATTTCTTTAGAATTTTTTTAGAGCAAATGC
TATATGCTGTTATAAGATAGTTCTAAACCTAATGTAAAGAACAATTCATAAAATTAATGGGCAAAATTGAAAATGTAGTTTTTTAGTAA
AAAAACATCATCTGTCTTGTGAAATTACCATTAAATTCTCACATTATGTCATTAAAAATTTAAAAACATTAAACTAAGGAAATTTGACT
GCTGCAAAGTGCAAACTCATCATTTCAAAAGCAGAATGAAAAAAAAATTGAAGGATCATTTAATTTTGACTGACATTTTTTAGGGGTAC
AAACGTTAAATAGAAGGAGCAAGATTGATGAAACATTAGTTGGTAGTGATAAGCTATCAGCAAATGGACTTTCATGCTATTAGTTTGTC
AATGTCAGTGTCAAAGTGGACGAATATGACAGGGATGGCTGATATACTGCAACTTTTAAACTTATTGGTTGATGGGGCAAAGGGGATAC
TAAAATAAAAAGGAAAGGCTTCAACTACCCTGGAATCAAGGACTTCTTTGTACATATGGGTTCTTGCTTGTATGGTAGTTTTTATTCAC
GGCATAGCACACAATGCACTTCCTTTTGCATGAATTTCTAATGCAATTCTAATGAACTGCAAATGCCATTCAATTTTCCCACTGGCCTT
TCCTTTTCTCTTCTGCTCTTGTCATATTCTGCTACTGGCACTCTTTTTCACTTCTTTTCTTTTACTTTTTTTCTTTATTTAATATATAT
ATTTTTTTATAATTTTTTTTTTGTCGAATGTACAGTGAAAATCTTCAAGAACTGGGCATAAGACGGCCCTGATTTTATTCAATTTTGGA
ATTTAAGTGATTTTTTTATATAAATTTCTATTATTGATTTTTTTTTTTTGGATTTTTGGAAATTTTGGCTTTTTTGGATCTTTTTTGAA
TTTTAATTAAATGATGTTTATCAACGTGCCGTAATGACAATGTACATTTATGTGTCGAATTTTGCTTCCATCATTCACTTCAATATTTT
TTTCACTTCAATTTTTTGTTTTTGGTCATTAGAATATTTAATCATTTTGTTTCTTTAT**AG**CATTCTCGGGATGAATCTTTTCGGCTGTA
I L G M N L F G C
AATTCTGCGTCAAAATAGATGACGTCTTAACTTGCGATCGCAAGAATTTTGATTCTCTTCTATGGGCCATTGTAACAGTTTTTCAG**GT**A
K F C V K I D D V L T C D R K N F D S L L W A I V T V F Q
GCACAAACAAACCAAATCTTCACTATATATATTTTTTCTCTATAAATATATGTGTATATTTATATATCTACATTTTTTTTTAAAGAAAA
ATTTCCTTATTATTTTTCTCTGATTTAGTTTTGACAAATCTCTACTGTATATTTCTTTCTGGAGATATTGACTGTAGCCCAGACCACAC
TGTCGTCTCTATTCTTGCATGTGCTTAACGCATTTTACATTTATTTTATCCACACAAAAGTAGCATAAAGTCTTTTCCTCAAGTTGCAA
TTGCAAGTGCACTCTTTTTAATTGCCAACAGTAATGACAAAACGCAACAACCAGCGCATGCTAAATCTAAATCCTCTAAACAACGTTGC
AATTGCGACAAACTAAAGAGTATTCAGATTCTGTTTTCACATTTCAATTTCAATATACCGTTACATTTTTAAGGTTGATGATTGCACAC
TCGTAATCTCGCTACTGGGAAAGGTATTTGGTCTCTTATTGGTTCATCTTGAAAAACCTTTTAACATTTGGCTACTTAAATTACCGCCC
CAATTTCACTTTGAATGACTCTAAAATGTGCACTTAGTCACTCTTGATGATTCCATTGACACAAAGATGTTTAGTGTAAAGTTATAAAC
CTAATAAAAAGTTCTTTTAAACGCCAATGAGTATAAGGAAATACGTAACCACAAATAACAAATACGTTCACTAATTCTGGAATGATTTT
TAAAGGAAAAGTGAGCTTGGATTCTTAAAATTTCACTAAAAAGTGCAATTTTTCATTGGTTTAGTCACAAAATAAACTAACAAATTTGT
AAATAAATTTGTTTTAATGAGTAACGAGTAACAAATTGCAACTTCAAAAAGGCGATTATTTACTTGTCTTATATTGATGCACAATGCAC
ACATTCTAACAAAAAAAAGAAGGAAAATAGAATTGTGTCTGAATGACATATTTGGTATTTTTAGTCGTCCCTGTCAGATGCAGCCACAC
TTCAGTTAATGGCTGTTAATCATCTGCCATACATTAATTTTTTTCTTTTTGCTTTGTGTACGGTACGTACCTTAATTGCTTGCATTCGA
AATGAAATGCAGATGTTTTCATCATTTTTAGTAATTGCTTCTTCATCTCACAGCATTTGCATTTGCTGCTAATGCACATATAATTCACG
ACATAATCAATTTGACAAAGAAATTTAATTTAAAGGGTAATGAGTTAACAAATATTAGTTTTTGTTTTTTGTTTTTTCCTTTTGTTTTCT
TTATTTGTTTTC**AG**CTGCTTGGGTATGTATTTGTTTGGGGGTAAATTTTGCATGCGTGCTGATGGTTCAGACGTTTGCACGTGTGAAGA
C L G M Y L F G G K F C M R A D G S D V C T C E D
CCTCGAAAATCCTTCGTTAGACTGTGCGTGTGAACGAAAACATTTCGACAATTTCCTCTGGGCTACAGTTACTGTTTTTCAG**GT**ATGAT

```
  L  E  N  P  S  L  D  C  A  C  E  R  K  H  F  D  N  F  L  W  A  T  V  T  V  F  Q
TTTTAATCACGTTTGCGCATTAATCAAGCAGAGAAAATAATAATCAAATATAAACATTGCTATTCTAATTAATTCAAATTCAAATTTGA
TGTGTTGTTGTCAAATGCTAATAGCTGCGTTTTATATATATATATATATATATATATATATATATATATATATATATTTATTCCTTC
TTTAAATAGTACCAAAAGCGCATTGTAAAAAAAAAGTTGAGTACCTAAAACCAGGAAAAAAAACCAAAGAACATAAATAGTTATCATTT
TTGTCTATTGGTGTAGTGGCTCTGCCATATGGCAAACTAGGCAACTGACTTTTATTTCATTCTTTGTACGACTTTCGCCCAGGGACTCG
TTAGCTTCTCAGAGCTGTTCCCGAAAATGTTATGTCACGTCTTTTAAGATCTTTATCGTGTAACATCATAATAATACAAAAACTGCAAA
AACATTAAATCATACAGCATCAGTATGTCACTTACCCAAGTACTGGCTAAATCCAATACTGCTTAAATTGTGTTCTGATGGGAACAAGT
GTTCAGCTTGACGAGTCATTCCTGCCCCACATTGTACTATTGGGGTTAAACGTTGCCATTTACGCGGCGTTATAACCGAGATAGGCATC
TGCCTTTGGGGTTTTTTGTTGAGCAATCGGCGTTTTGCATCTATTTTTATGCATAATAACTATACTATTCTTAAAATTGTATCGTAAAG
GTTAAAAAATACTTCCACGGAGCAATTTTTGATGGAAATGATAACTATTTATTAATTTAACATGTTCCGCATTGGTTATTAGGCATTTT
GTGTTTATTCGTTATGATTATTGCTAATGTTATTTATATATGAAGATATTGACTCAAGAAGATTGGAATATCGTTTTGTTCAATGGCAT
                                                I  L  T  Q  E  D  W  N  I  V  L  F  N  G  M
GGAGAGAACTTCGCATTGGGCAGCTCTGTATTTCGTTGCTCTTATGACCTTTGGCAATTATGTTCTGTTCAACCTGCTGGTCGCCATCT
  E  R  T  S  H  W  A  A  L  Y  F  V  A  L  M  T  F  G  N  Y  V  L  F  N  L  L  V  A  I
TAGTTGAAGGTTTTTCTGCTGAAGTAAGTGTTTGTTTTGTTTTTATTCTTCTTTATTCTGCTTTCATTTTATTTTTTCAAATTACAAAG
L  V  E  G  F  S  A  E
```

Aplysia californica Ca_v3 (UCSC Genome Bioinformatics aplCal1_dna range=scaffold_1525:56054-67089)

```
TTCCCCTCCCCTCCCCTCCCCTCCCTCCTAGCATTGTGGAGCTGGCCCAAGGTGGGGCGAGCGGCCTCTCTGTACTTCGTACATTCCGT
                                I  V  E  L  A  Q  G  G  A  S  G  L  S  V  L  R  T  F  R
CTCCTGAGAATCCTCAAACTGGTTCGTTTCATGCCCGCCCTGCGACGGCAGCTGGTGGTGATGTTGCGCACCATGGATAATGTGGCGAC
 L  L  R  I  L  K  L  V  R  F  M  P  A  L  R  R  Q  L  V  V  M  L  R  T  M  D  N  V  A  T
CTTCTTCGCTCTTTTAGTTTTGTTCATGTTCATATTCAGGTAAGCACTGTACTGTACGATGCATTTGTTTAATTATTATAAATCTTCAT
  L  L  V  L  F  F  A  F  M  F  I  F  S
TAATTAAGTGCAGGTATTGAAAATGTTTATTATCATTATTTTTGTTATGGATAAATGTCAGTTAGAATTGTTAGGGAGTGAGAAGAGAC
TTTTCAAATTTTGCCCTTTCATCTATTTCGTCTTTTGTTCGGGCGGGAAAAGTAGCGGGCAGGTTTGGTTAAACTGTTTAATGAAGTGT
TTGGTTCCATTTTACTTCAAGGTTAAGGAATTTTTTTTGTGTGTATTTGGTATTACGCTTACATAAATGCCAAAGTTGGGATTTTCTGG
GTTTGTTTTGCTCTATTTTTGGGAGGGGGGGGGTGTAACAAAAAAACAAAACTTTTAGGTAGTAATACATCAGTCTTTTAAGATGTCCA
CTTATTTGAAATTGCTGAATTGTTCTATGAGCGAATAACAACATACTTTGTGAGTTGAAAAGTTTGTTTTGTTTTTGTTTTGTACACTC
TGACTCAGCCACAACCCCCAGTTATATACATATGTTTCTCAATGCTGACTGAAGTACTTGTTTCGACAACCCTGATTTCCTTATCTCAG
AAACAAATATAAAACAAGATATTTACACGCATTCTTCAAGATATTTTATGCCCTCTAGCTCCCATGTTCAGTGTGAGGTTCTAAATCCT
GAAATACATACGTGTATTCAAAGAGGATATAAACTTGCAGTGTGTGAAATTACTTTATAATACCTTGACTTCCCTACTCTAGAATCTAG
CAAATAATCTGTATTTCCTTTTGGCTTCTTCCTTTCCCCTTCTCCCCACTTGACATGTGTTCAGCATTCTGGGAATGAATTTGTTTGGC
                                                        I  L  G  M  N  L  F  G
TGTAAATTCTGTAAGAAGCTGGACGACGGCAGTCGTAAATGTGATCGCAAGAACTTTGATTCCCTTCTGTGGGCAATAATCACTGTCTT
 C  K  F  C  K  K  L  D  D  G  S  R  K  C  D  R  K  N  F  D  S  L  L  W  A  I  I  T  V  F
TCAGGTATTTGCTTTGCCCCCGGTTATGCTAGATGCATTATTCCTAAACGCCGGGTGCAGCGTGTCGTGGGTACGCGTGGAGCACCCCG
  Q
TGCGTCCATCAGTGTGTTAGTAGTGGACGGCTTTCGTGTTCACCTTGGCCTGCCCTCAAACCTCTTTCTCCTGTAGTCAGCTGGTTTTA
TTTTCCCCCGCCCACCTACCTAACCCCCTAACCCCTGACCCCTGACCCTGACCCCTCGAATTCTCTGACCTCTTGACCCGTATAACCTC
CACCTCTGTCCTTGACCGCATGCTGTAGGCTGTTCTCCTTTCACTGTGTGCTATGTGACTGACTCTCAATCGAAAGTGTACAGCGGTCA
GCTGAGATGTTTCACTCTGGTTGTTAGCTTACGTCCGCCATGTTTTAGACAGGGAAGAAATCTTCCACGGTTTATGGAGAACTTATGTC
TGCTTTCACCGTCATAGTAAGCTAAAGACACGTTCGTTGGTCCTCTTGATATTTAACAAATGGCAATGTGTACTGAAGGATGAGCAGGC
TATGTGTTGTAGATGTTGTGACAAAATTTGATAAAGACATATATTTGCATACCCACACAAGTCAAGCTTGGTATGCATGCATAAGTTCC
AAATCGGGTCTCTCACCGACATGCTTATTTAGATTGTAACGGTAAAATGAGGCCTATCTTGCAGAGAAGTCTAATTTCTTTTACAAGAG
CAGACTGTTAAGCTAACTCTAAAAGTGATACGCATTATAAAATGCACGAACTGCTGCAGAGAACGGGTTGGAATATCATACTAACAAAA
ATCAGAAGGCATGTCTCTAATGAAACAGTTTATTTCTTTTAATGTAGATCTAGTGAATTTCTCCTCCTATTGTTCCTTTGAGTTTCTAC
AGCAAAACATAATATGTGTGCAGTTAGTAATATAGAAGTCTTTCTCTTTCTTTTTTTTTTTAGAGTAGAGTCATCAGTTTTGTTTATAC
GTATAACCAGATCGAGCTAGAGACAATTCGTATTTGTTCTTTCTTTCCTGTCTATATGTGTTAGATAACTGACTTGAGGTCGATAGTCC
TTAATAGACATTTAACAAGTTGGTTCTTTTCCCTACTCCATTTTTCTTGTCCGAACCTCACATGCCCTACACCTGGCCCCTTTTCCGAC
CAAAACGCGTATCCATAGATAACCCCCCCCCCCCCCCCTTTCTGCACCTGCACCCCCAAACCCAACATGCCCGAAGTAATTGAAACCTG
GCAATGTTTGTTTATAAATTTCTAATAGCGGCATAATAAATTTCTAAAATAATCAAAGTGCTAGAAAGTATACTATTTTATTTGGGTAA
ATGATTCAAAGCCCCAATTAGTAAAACGTTAAATAACTAGAAGATACAAGTGTATTCCGTTTGTTTTGGCTGACTAAAAGGCATCGGTG
CAATGTTCAGAACATAGTGCAATAGTACTAATTAAGATTGGAGTAGTTCAAAGAATATATTATATTATGTCATACTATTATTATCAT
CAAGACATCCTAATCTTACCGTTTCAAGGCTAATGTATAGCATAATAATGAGAAGCAGTATTGTGATAACTCAAGCTTTCTAATCTAGT
CTGTAAATTGGCAAGTCAATAACAACCAAATCTTTTTTTAAACGACATTCCCTCCTCTCTTCTCCTTCCCCCCTCCCTCTCCATCACCT
TTTCATCCATCCCCTTTACACCCCCTCTTCCAGCCGTTTCTTGGCTTCCCACTTTTGCGAGCAACAGCGCACACTTGCGACCATAATAT
CTTTCAGATGAGCGAAAATTAGAACTAAGCTAAGTCTTTTTCCAAGCTCAATTTTTGTTCAGTTTTGAGGTTTTAAGAAAATTAAAGGA
TAAAAAGAGAACACAAATCAGAACTATGACTCGGACACTTGTTATATTTCGATTTCAAAACTAAGAAAGGACTAAGGAAACGGAAATTG
TAATAAATATTCTAGTAGATCCATTTATATTTGTTATTCAAATAACAGCTTTAAATGGAAACTCTAGGATATTGATTTTGATCATTGTT
AAACGATGCTGGCGGAAAGCAAGCCTTTGCTACTTAGACAAATACATAACCCAATCCCAAAGGACGTTTAATGTCAAGCGGAAATCTGT
CCCCTTGCTATAACTTTCTAAATAGATACTAGGGCAACTCTGTTCGCAGCTTGTGTTCGTACAGAAGTGTCGATAGTGGTAACTGGACA
```

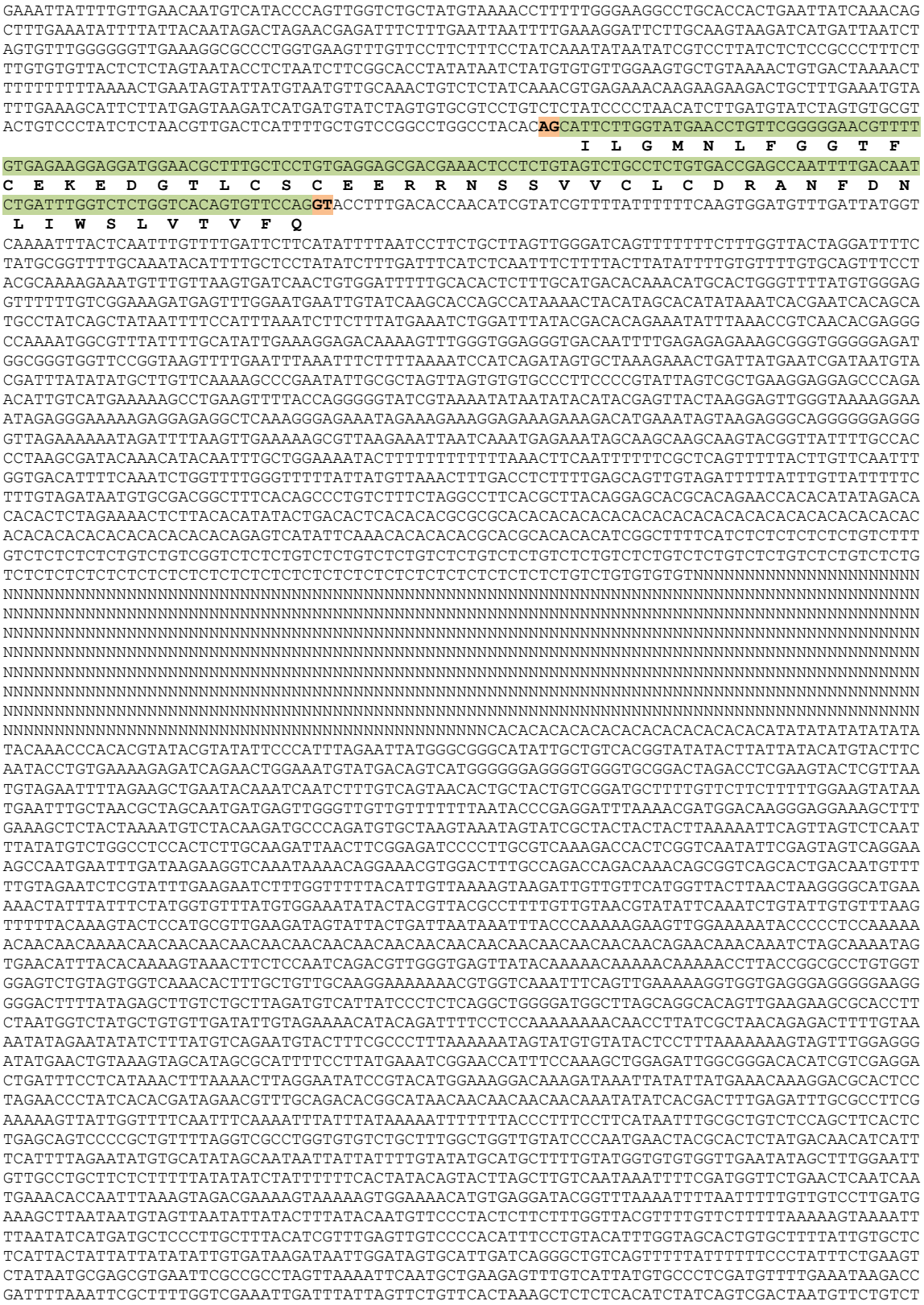
I L G M N L F G G T F
C E K E D G T L C S C E E R R N S S V V C L C D R A N F D N
L I W S L V T V F Q

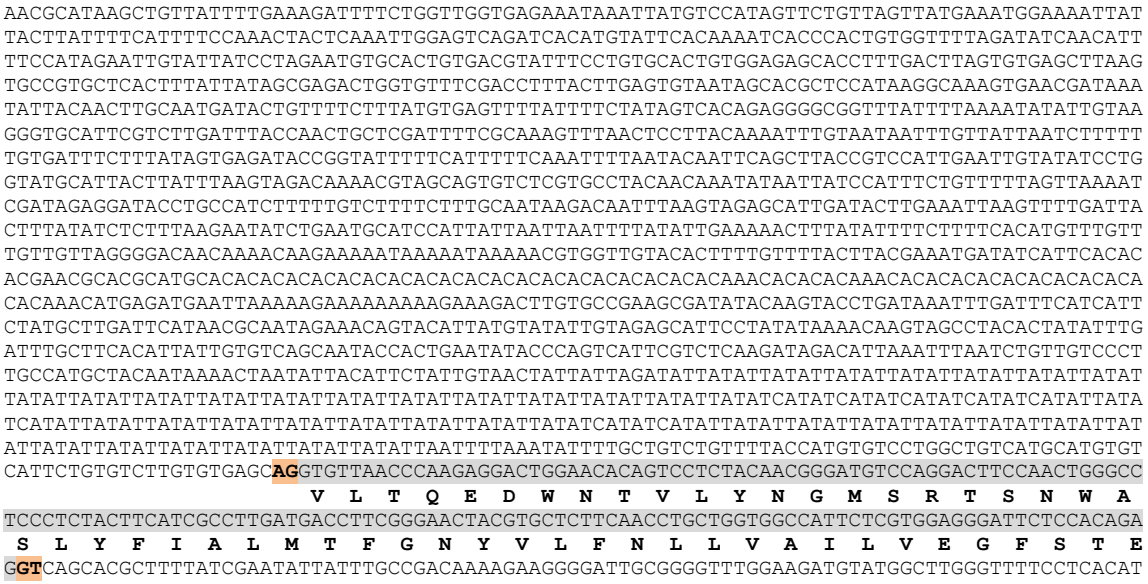

Lottia gigantea Ca_v3 (JGI scaffold 59:70243-103522)

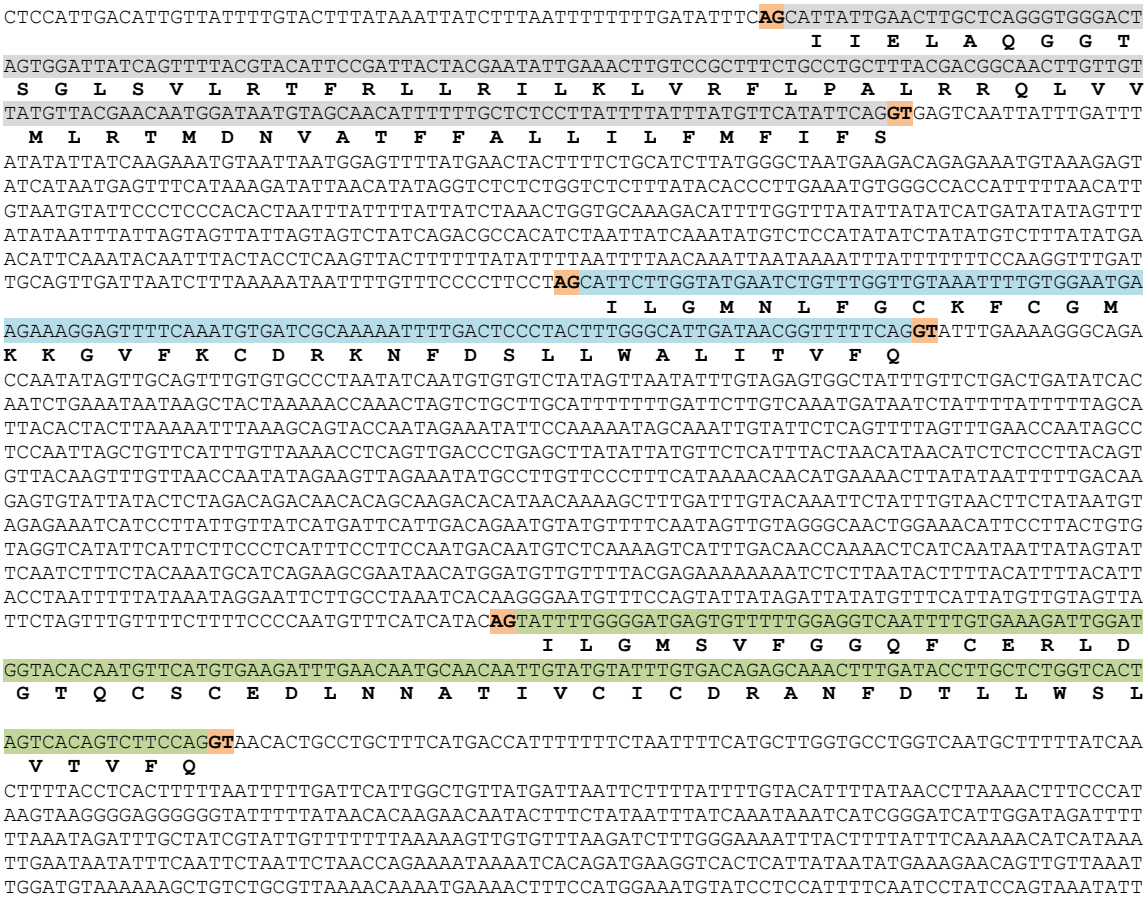

```
TTCTAATTTTTCACCTGTTGACAAATCTCAGAACCAAATAAAATCCATTCCTTCATTGTTGCTCCTCCTGCAGCTTTCATTATACCTGC
ACTGTTTTGTACCTATGACCTTGTAAAATTTGTTGTAAATTTTAATCTGTGTGTCCTGTAATGTCTTTGTCTTATTCAAAATGATCTTT
TTATTTTCAATTTTCAATTTATTTTTTCACAATTTCACTTTTTACCCACCATCACTTATATTTTGAAAAAATATTCTTAAATTTTCTAC
CTTTATCGAATTCAACTTTAAATGTTTTAAATGTTCAAAGTAATGACTATAATCAAATTTAATATTAGATAACATTGTTACAGTCTGAA
ATATAAAATATTGTTTATTTTCTGTAGGTATTAACCCAAGAAGATTGGAATACTGTGTTGTATAATGGTATGTCTAAAACATCTCCCTG
                         V  L  T  Q  E  D  W  N  T  V  L  Y  N  G  M  S  K  T  S  P  W
GGCATCTCTGTATTTTATTGCATTGATGACATTTGGAAACTATGTCCTCTTCAATCTACTGGTTGCTATCCTGGTTGAAGGATTTGCTA
   A  S  L  Y  F  I  A  L  M  T  F  G  N  Y  V  L  F  N  L  L  V  A  I  L  V  E  G  F  A
CTGATGTGAGTATATAATTTCATAGTGAAAATGAATAGATTAAAAATGGTTTCAATGAATGGTTGGATTAGAAGTGGCAAACAAATCTA
T  D
```

Biomphalaria glabrata Ca_v3 (NCBI Contig188.27)

```
CATTACAGTATTGTTGAATTGGCCCAGCCAGGTGAGAATGGGGCCAGTGGTCTATCTGTACTTCGAACATTCCGTCTTTTGAGAATTCT
          I  V  E  L  A  Q  P  G  E  N  G  A  S  G  L  S  V  L  R  T  F  R  L  L  R  I  L
AAAATTGGTACGCTTTATGCCCGCCTTAAGGAGACAGCTGGTGGTCATGCTACGCACCATGGACAATGTAGCAACATTTTTTGCTCTGT
  K  L  V  R  F  M  P  A  L  R  R  Q  L  V  V  M  L  R  T  M  D  N  V  A  T  F  F  A  L
TAGTTTTATTTATGTTTATATTCAGGTTGGTATCTATATATATACATTTATGTTTATTTAAGGAAATAATTTAATCATGTATGATTTGT
L  V  L  F  M  F  I  F  S
TCTTTTTTTGGAAAGATGCATTTTTAATGTTTAGCTTAGGTTAAAAGGTCATATAGAGATGTACAGAGAAGCTATTATTAGCAATGACT
AGATCAGAAAATGAAATGTTGTTTCCCTTAATCTTCTCTCCTTCTCCTTCTTGAAAACCTTCCAGCATTCTTGGAATGAATTTATTTGG
                                                          I  L  G  M  N  L  F  G
CTGTAAATTCTGTAGAAGACTAGAAGATGGAAGTCGTAAATGTGATCGCAAGAACTTTGATTCGCTGCTGTGGGCAATTATCACTGTCT
  C  K  F  C  R  R  L  E  D  G  S  R  K  C  D  R  K  N  F  D  S  L  L  W  A  I  I  T  V
TTCAGGTATCCCAGTGGCAGGTTCTGGCCACTTAGGTCCCTTGCCTTTTATCTGGCTGTAGCCTGGCGTGTCCAATATGTAGTCTAGTG
F  Q
GATCTCATCCGTCCCAAATAGTGGTTTAACCTTTATTGTGCTCTCATACCGAAGAATACTTTGTACAATGCTGGCTGCATGTCATCAAC
ATCGTTTGCTGTGATGGTTATAGTTTCATTTTGAACAAAAAAAATAAGGATATTTCACTTTTTATGTTGTTTTTAGGATACAATACGTA
TCAATATAAAAAAAAAGAATAAAATTAGCTATAACACTTGCAGCCTATAGTATCTTGTTCTTTTGAATAAACAGATTAATGTCAATAAT
TGTATACAACGTGTCTCAGTGTGTAATCGTTAAATTTCTACTGCAATATTGCTTCCTAAGCTGAATGTCAATTTTCAATGTAGTATCTT
GTTTTCACTGGATCAGAATAACTGAAATAACTTTAATTCTTAGTTCTTAAGTCAGAAAATAATTAACTACAATTTTTTTTAACATATAC
ATAGAATGAGCAATATTATACTTTCAAACCATCACTAGATTAAAAAAATAATAGTTAGCTTTTTTTTTATAACATTTTGTTCAACTTT
GTCCTGTAGCTCTTGTGTAAACCAAGCAAAATAGTGCTACTATGTTTCTTTATTTATTCTTTTTTTTTCCTAAGTTTTCTTAGTGAATT
TCTCTGGCTCTTTTTTTTTAATTATAGAATTATCATTTAGTACTTTAATAGACCTTTAGCTAAGTGAAATTCTGTTAAAGTACTTAAAG
ATATCTTATTATCACCCTGGCATTATCCTTGATCACCCAGTACTAATCCACAGAGATTAACCTTTACTACTTATAAATGCTCAACCTTC
AGTCCAACTAAATTATTCTATATGACCTCAAAAGCTTTAGTGCATCTCTGATGAAGTACTTGTATGTCAATGCTTTCATCTCAATTTGT
CCATGTACAGTAGACAAAAAATGACATGTTCACTCTCATCATTTCATTTAATTTGGGCCAGGTTCATCTGCAATCTTCAATGCAATCTA
TTTAGCAATCAAATTTGGGCAGATGTGGAACAAAAAAAAACTCTTTAATTTCAAGTCTGCTGAATCAGCCATGCATATGAATTTGGTCC
TTGATAATCAAGTTTCATGTGAAATTTAGATATTTTTTTCGAATGTCTCACTTTATCACAATCAACTTTAAAAAAAAGACATGCACATA
CAAAACAAATCCATATTTTCTTGTCATTTACTTGGAATATGCTGAACTTGAATGTCAGCCATTCTCAACCAGCCCAATGTTCTTAGGCT
CAGACATGTACAAAACCAAAGAAGTGCATGATTTATTTATATACAATCTTAAAATATGAGCACCACCAATAGTTAGCCCTGTGTGAATA
AAACATTTTTTCCACTTGAAATAATAACGTTTCACATCTTCTTTGTAATGAGTAAAGAATTTCAAGCTAGTTATTGTATGGGCTTATGT
TCTGAATGACAATATCAACTTCCATAACCATAGACATAAATGTAGGTTTGTTTTTGATTGGACTGTACAGTCAGGTGTGCTGGGCTCCC
AAGATTAATTGTATTTCCAAATTTTATTAAATTAATGCAGCCTGGATTGCTGCTAAACATGTTTGTGAATAATGTCTATATTCACAATT
TTTCAACTGCTTAATTTGATTTGAATTCAACACTGTTTGATTCATATTCATATTTTTTTTCAATATTCGCAAAGGGCTACATTAATGAA
AAAAAAACATACATATCATCTGTATGAATATTCCTAACAAATCACACTCACAACAGTACATGTATTTCAACATGAACATCACATGAAAA
TTATCTACCTTTAACTACTTCTGTTGATGACCCACTTTGCATGCAGTATTCTGGGAATGAACCTATTTGGGGGCTCATTCTGTGAGATG
                                                  I  L  G  M  N  L  F  G  G  S  F  C  E  M
GAAGATGGGACCGCTTGCTCCTGCAAGGAGCGTTGTAATGCTTCATTATGCAAGTGTGACCGTGCCAATTTTGACAATCTCTTATGGTC
 E  D  G  T  A  C  S  C  K  E  R  C  N  A  S  L  C  K  C  D  R  A  N  F  D  N  L  L  W  S
ATTGGTAACTGTATTTCAGGTATTTAAAGTTTATCCAAAAATGTCCTTTTCCTCATTCCTATAGCATTTGTATCATATCCATTTTTTTT
  L  V  T  V  F  Q
TCAAATGTTGCAAATCAAATTCAGTTGCAGTGAATAAAAACAAAGTTTTGCTTCTTACTTTACAACTATAGCTGACAATGTCAAAGGTT
AAAGCCCAAAGCTAGCAGTAAATGAATAAATATTTGCTTTTTCTTTTTGTTAAAAATGTTATGCCTTTAAAACAATAATTTTAAGTCAT
TTGTTTGATTTGTTGGTCTTTGAAAATGAAAACTAATGCGAAATTGACCACAACAAAAGTAATTTACTAAATTAAATAAAGATATTTGT
AATATGGAGATTTTTTGAGTCAAAAGACATTGGATAAATCACTTGACAAGTTTGTTTTTGAAAGTAGCAGAAGATGAAAACACTATTTT
GCTTCACATTTCTAAACACCCTTTGGTTTGATTTTTTTGTCATGTTTTTCTCATTTTTTCTGTGATTTTTCACCTGAACACCATCCATA
CGCTTGCTTTCATTTTAGTCAAAACTGTTTTACTTTGTGAATTCAAGTTATCCCTTTTTTTTATTTTTCATTTTTCTTAAGTAGATCTA
GTTGCAGACAAAAAAAATATTCACATCAATTCTTATACTATATTCCAAATACATATATATTGTACATTATACATCTAAATGTATACATA
TATTATTAAAATTACAATTAACATTTCTTCTCTCATAATTCATCAAATTTAAGTTCATAATTAGTCAATATGATAAATTACATTATGTA
AGACTAATCTAAATACACTGGAGTTATCACAACAAATTTTGTTTTTCATTTTGTGACCTATTATGTCTAAATCTAAGGGTTTTATTTTT
TGTGTAGAATTCTTTTCAAAGGGTGAATTGAACATTGGCCATTTTACTAGTAATGTTTGAGAGACTGTAAATTATTATTTGCGTGTACA
TTTTGTTATAAAAAAGTAACAGCAATTAATGTGCTAAATTAATTAACTAAAATGGATTAGACAATTATCTCCTTACCTATGTACACCTG
CTTTCACTTAATCACACCTAGCATCTTGAAATGCAAGCCAACATTCTAGCACTGATGTCTTTTGTTTTCTAAACTGATGGTTTTCTACC
```

Caenorhabditis elegans Ca_v3 (WormBase Locus C54D2.5)

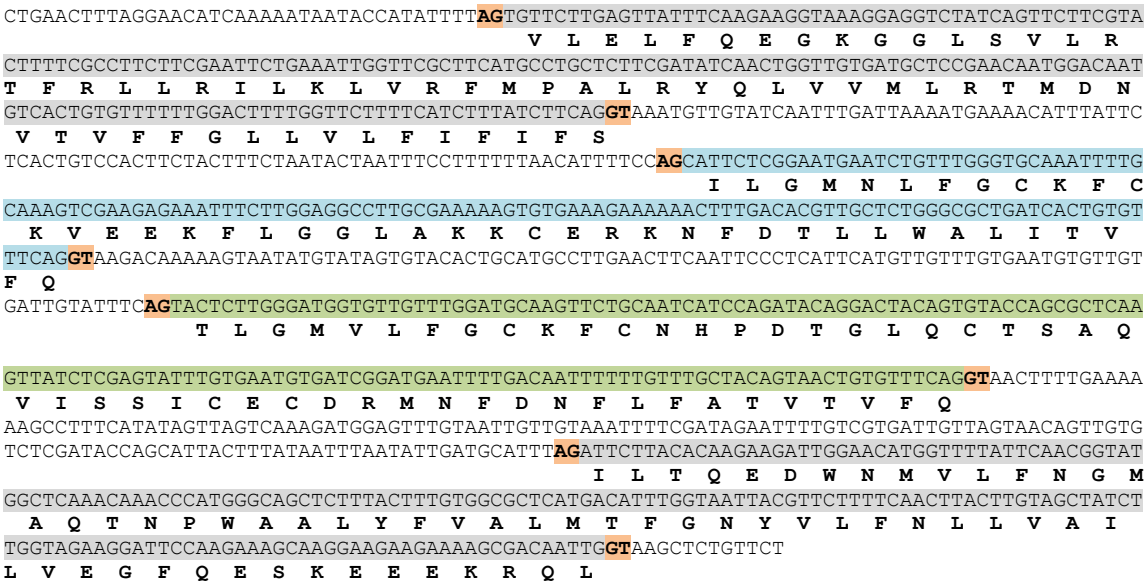

Caenorhabditis briggsae Ca_v3 (UCSC Genome Bioinformatics cb3_dna range=chrX:13547850-13548838)

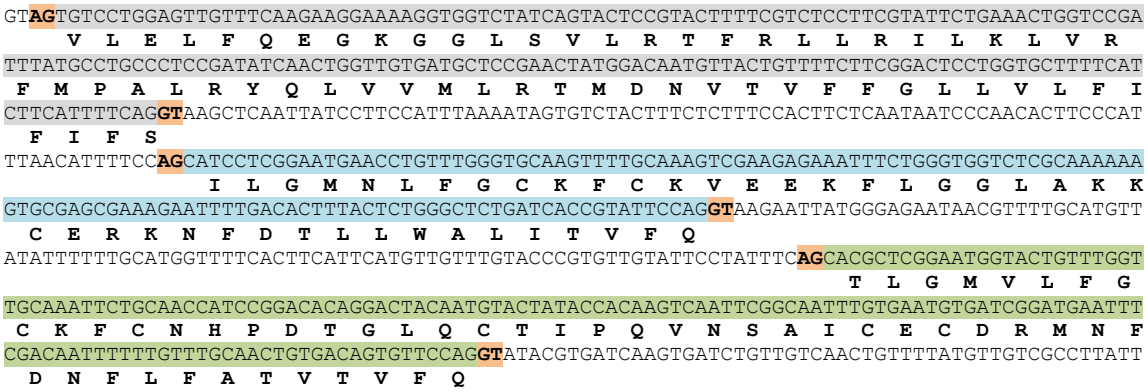

```
TGTTGTGCACTTCTCAAAAATATTTTCCAGATTCTGACTCAAGAAGACTGGAACATGGTCTTATTCAACGGAATGGCTCAAACCAATCC
                                I  L  T  Q  E  D  W  N  M  V  L  F  N  G  M  A  Q  T  N  P
ATGGGCTGCACTCTATTTCGTTGCTCTCATGACATTTGGAAACTATGTTCTCTTTAATCTACTCGTTGCTATCTTGGTTGAAGGATTCC
  W  A  A  L  Y  F  V  A  L  M  T  F  G  N  Y  V  L  F  N  L  L  V  A  I  L  V  E  G  F
AAGAAAGTAAAGAGGAGGAGAAACGTCAGTTGGTAAGTTGGAAGACTTCTTCTCTTTTCTCTTTTTCATTTTACGATCCCCCGAAGTTT
Q  E  S  K  E  E  E  K  R  Q  L
```

Capitella telata Ca_v3 (JGI scaffold 351:145937-179675)

```
CAGTCTTGTGGAGCTGGTTCAGGGTGGCGCCGGTGGCCTGTCTGTGTTACGAACATTCAGACTGCTGCGAATCTTAAAGCTGGTTCGCT
     L  V  E  L  V  Q  G  G  A  G  G  L  S  V  L  R  T  F  R  L   L  R  I  L  K  L  V  R
TCATGCCCGCTTTACGCTACCAACTGGTCATCATGCTGAGGACAATGGACAACGTAGCGACGTTCTTCGCCCTGCTCGTACTTTTCATC
F  M  P  A  L  R  Y  Q  L  V  I  M  L  R  T  M  D  N  V  A  T  F  F  A  L  L  V  L  F  I
TTCATCTTCAGGTTTGTGCTGAGAGAGAAAGGATAAGTGCCTCCGCGACCTGCGTCAAGGTCGAATTCCTTCTCCAATCGTTCTCGCGT
 F  I  F  S
CCCGTTTGCGTGCCGCCGGAAAATGAATAGCGAAATGAACGAATTGACGTAATTGAGCGTGCGGCGCTGTGAGTGCTTCCTGCTGTTGG
CTACATTCAGATGCTTCATTCAGCGTTGATTTCAGACAGCCGAGTGTAATGGCAGGTCGAAGCTGCCATACGTATTCCAGCGTTCATGG
AAGCAACCATAAACGAGAAGCACGGAGTAAATAGCAGGAACCACCCATGATATATATACTAGTTATTATAGTCAACAATGGGAACTATT
ACATGTACAAGTCCGCTAAGCCAATGATATGGATGCTTTCACAAGGCAATGTCCGATGTGGGGTTGCGGCCAATATTAGAGGCTTTGTG
CTTGGAGATGAACGGTATAAACGCTGACCGCAGCTACATCGTTCGGGCAGATATAAAACTGTCAATTGAAATCTGATTTCTCTCGTGGC
TATTCGATGTCGTCCTTGTCAATGAGGCCTGTTTCCATTCAGCTGCGATGAGCCGGTTGCCCATTAGGCGTTTCGACGCATGGACGGCG
CCTTTGTGCGGTGTAATGAACGCCCCCTGCCGCCCCATCACGTCATGCCTCCCGCGGCACAGGGCGACATGGACATGCATCACTGCCAA
TGCAGCGGCCCCCGCTTCGCCGTGACCGAAACTGACGCGGTGAATATTTCAAGAAGCTAAAGTGAATTACGCTTTGTCATAATGACGAT
CGCTCTCCCATTTCTGTATTGCTCAAAGTAATGGCTGTATAGCCTTTGTTAATGTCAGTGCATGTTGATAATGCTCCTTCTTCTTATTC
TGTGTACCAGTGTACTAGGAATGCATTTATTCGGAGGCAAGTTCTGCACTCATCCGGTCACAGGACGCCAGTGCACCTGCGCTGAGATC
            V  L  G  M  H  L  F  G  G  K  F  C  T  H  P  V  T  G  R  Q  C  T  C  A  E  I
ACAAGCGTTCCGTGCAAGTGCGAGCGGAAGAACTTCGACACCCTGTTGTGGTCGCTGGTTACTGTGTTTCAGGTGAGGAGATCAAACCC
 T  S  V  P  C  K  C  E  R  K  N  F  D  T  L  L  W  S  L  V  T  V  F  Q
ACCTTCGGTTCATGCAGCAGCTCTATGCAGCCACAGAGCACACTATTTAGTGGTGCAGACACATGCGATGCATTACGGACTTCACATTG
TTCCGTTCCGGCATTCGCGGCCCGGCAACCGAGCGCAACCCCTTTTTATTGCGCACTCGGGCAGCTTTATGCCCGCTCAGCCCTCGGCA
CGATGACTTCCTTGTGCTCGAGGGAGGCCCGGACTGCAGCAAGACCATGCCCTGTCTACTGCGCCCATTCATAATACACGCGATTAAAC
ATATCAACAAGCCACTAGTACTGACCTTGAATCCCAACTTTATGACTTTGGTGAAGATCAGTCACGTCCTTCTGGCAGGGAGCATCCAT
TTACTGATCTGATTCACGAACCTTCACAAGTGCGAACCAATAAATGTCTCTCTTATGAATCTGAGCTGTGCTTGTTCGTGCCCATGTCA
CCGCGGTGAGCATTGACAGCGCTGCTCTGGGATTGGTTCGCCGTTATGATGTATACCTGTTGAGCGAAGGTAGCCAAAACCCTCAGAGT
AAGCATCAGTAAAAGATATAAAACCTGTCTTGGATATCTCTGTTATATCCTGACGAAATATATAGCCTTCGTCTGGTGCAATGAAGGCT
GCACACCTGGCCAACGTTCACCTGTGTCTGGCAATGATTACCTCTCTTTGACACTTGCAAGCTTTGATCATTGCAAGGCATATCAGAAC
GCCATCTCTGCCTGCCAGCCTTTGTTCTGCATGGGCTGTCCATTACGCCCTTGGTGATCGCGATCTTCATTAGACGAACTTGACGATGC
TTATTAACGAAATTAACTATGCATATATCTCGTCAGATTCTCACCCAGGAGGATTGGAACGAAGTTCTGTACAATGGCATGTCGATGAC
                                I  L  T  Q  E  D  W  N  E  V  L  Y  N  G  M  S  M  T
ATCGGCTTGGGCAGCGCTCTACTTCATTGCACTGATGACGTTCGGGAACTACGTCCTGTTCAACCTCCTGGTCGCCATCTTGGTGGAAG
  S  A  W  A  A  L  Y  F  I  A  L  M  T  F  G  N  Y  V  L  F  N  L  L  V  A  I  L  V  E
GCTTCTCCACAGAGGTGAGTTCAAATGCATTGTGGCGGATTCCGCAGATAACTCACTTTTTGTGATATGTTTATATCTCCGAATCGAGC
G  F  S  T  E
```

Lumbricus rubellus Ca_v3 (Lumbricus rubellus Genome Project contig_47399)

```
TGATATGTTTTGGTGATATGTTTTGTGATAGTCTGGTGGAACTGATGCAAGGTGGAGCTGCAGGGTTGTCAGTCCTTCGAACGTTCCGT
                                L  V  E  L  M  Q  G  G  A  A  G  L  S  V  L  R  T  F  R
CTCCTTCGGATTCTTAAACTCGTGCGATTTCTGCCAGCGCTGCGCTATCAGCTGGTCGTCATGCTTCGCACGATGGACAACGTTGCAAT
 L  L  R  I  L  K  L  V  R  F  L  P  A  L  R  Y  Q  L  V  V  M  L  R  T  M  D  N  V  A  M
GTTCTTTGCGCTTCTTGTGCTCTTCATATTCATATTCAGGTCTGTAAAAAACTCATTTCTGAGCTCATTTGGCATGTATGTAGTTGAAT
  F  F  A  L  L  V  L  F  I  F  I  F  S
TTAGTATATATTTTGTAGTTTACTGTTATTCTTCTTATAATGTCTGAGCCTTATTTCTATTTCCTCAAAATATGATTACTAGCGTGCAC

ATTGAAATTGTAAAAAATCAATCATCAATCTAAAGAGAATATCGGTTAATATAAATCTATGTTGATAATTTGATTGTTGCAGCATCCTT
                                                                                I  L
GGAATGAATCTTTTTGGATGCAAGTTTTGTGATGTGATGGCTAATGGAACTAAACGTGGCTGCAAAAGGAAAAACTTTGATAGTCTGCT
 G  M  N  L  F  G  C  K  F  C  D  V  M  A  N  G  T  K  R  G  C  K  R  K  N  F  D  S  L  L
TTGGGCGATAATAACCGTCTTTCAGGTAAATATTCTCGTGCGTTGATCAAAATGTTTTTGTTAATTCGACCAATCCAAATGTTGACAGG
  W  A  I  I  T  V  F  Q
TTTATTGCAGTTTTGATATTAAATATATTGATGTAGTGAATGCCACAAGTTAATTCCTAATAGACGTGATGTGGAAGCCTTTGGGACGT
```

```
TCCCACTGAAGCCAGAATACTTGAGTATAGAAAACTTGGCAGCTGACTTTTCTTAAGGGATTTCAGTCTTCATTCTCTTTGTAGAGAAG
CCTTTGAACAGCCTGCTATCTGACTCATTCCATCATGTTTTGCATTTATATTGCATTTATTTAGGGAATTATTTCATATCATGTATTTT
CGGTTTTTATTAAGGTATGGTAATTATAATCATGTGTCATTTCATTTTTTATTTACCTCTTTTCCGCAGACTTATTAGCTATCTAGGTT
AAGTCTCTATGTTAATAATCAAGATGTGCAATGTGATGTAAATGTGCAGATACTGACGCAAGAGGATTGGCACGAAGTTCTTTACATTG
                                                 I  L  T  Q  E  D  W  H  E  V  L  Y  I
GAATGTCAAAGACGACGCCGTGGGCGTCTCTCTACTTCATTGCGTTGATGACTTTTGGCAACTACGTCCTATTTAATCTCTTGGTCGCA
G  M  S  K  T  T  P  W  A  S  L  Y  F  I  A  L  M  T  F  G  N  Y  V  L  F  N  L  L  V  A
ATCCTGGTCGAAGGATTCTCTGCAGAAGCTGAGGTCAGTTTGATCAGACGTAAAAGATAATTGCTTTTAATGACCACGATGGTGATGCT
 I  L  V  E  G  F  S  A  E  A  E
```

Helobdella robusta Ca_v3 (JGI scaffold_1:8257825-8258517)

```
ATACATAAATCAGTGTGATGGAATTATTTTATCGGACCGAAACTGCGGGCTTGTCAGTTTTGAGGACGTTCAGACTGCTTCGAATACTT
               V  M  E  L  F  Y  R  T  E  T  A  G  L  S  V  L  R  T  F  R  L  L  R  I  L
AAACTGGTGCGCTTCCTGCCGGCTCTCCGATACCAACTTCTGATTATGTTGAAAACCATGGACAACGTCGCTACTTTCTTTGCTCTACT
 K  L  V  R  F  L  P  A  L  R  Y  Q  L  L  I  M  L  K  T  M  D  N  V  A  T  F  F  A  L  L
CTGCCTTTTCATTTTCATTTTCAGGTTTTAAAGATTATTTTGTTACATTTCATCAAAATTAAATTGCTAAATTATTTTTTTTATTAATTG
  C  L  F  I  F  I  F  S
GCATTTGATCGTTCAGCATATTAGGTATGAATATTTTTGGATGTAAGTTGTGCTCAGAAAAATCAATACGAATATCGAAACATAGCTGT
                  I  L  G  M  N  I  F  G  C  K  L  C  S  E  K  S  I  R  I  S  K  H  S  C
GGAAGAAAAAATTTTGACAGTCTTCTCTGGGCAGTTGTTACTGTTTTTCAGGTTTCTTAGTTTTTGCATTAAAATATCTATTAAGGTA
 G  R  K  N  F  D  S  L  L  W  A  V  V  T  V  F  Q
CTTTTGAAAATTTTTCAAAAAATGCGATTGGTAACTGTCGCATCCAATTAGATTCTAACGCAAGAGGACTGGAACGAAGTGCTGTACAC
                                                    I  L  T  Q  E  D  W  N  E  V  L  Y  T
AGGGATGTCGATGACGTCAGCCTGGGCCTCCCTCTACTTCATCGCCCTCATGACGTTTGGCAACTACGTCCTCTTCAATCTCCTGGTGG
  G  M  S  M  T  S  A  W  A  S  L  Y  F  I  A  L  M  T  F  G  N  Y  V  L  F  N  L  L  V
CCATTTTGGTCGAAGGCTTCTCGGCGGAGGTTATTAAATGTTGTCAAGAGTTGTTCAAAATTGAATATTTTCACATCACTTACTTCCGT
A  I  L  V  E  G  F  S  A  E
```

Appendix D
Additional materials for Chapter 2.4

Materials and Methods

Source of animals

Giant pond snails, *Lymnaea stagnalis* were raised in-house in a snail vivarium and breeding facility in B1-177, Department of Biology, University of Waterloo.

Cloning of full-length snail LNALCN

A major portion of snail NALCN was previously sequenced[238]. The full length sequence was determined and confirmed by three independent PCR products amplified from brain cDNA; the only major variation outside of minor single nucleotide polymorphisms, was in the alternative splicing of exons 15a and 15b, coding for alternate domain II P-loops. We have updated files of the full-length NALCN sequences for LNALCN–EKEE (GenBank: GJQ806355) and LNALCN-EEEE (GenBank: JQ806356). Full length NALCN variants were cloned by the concatenation of five PCR-amplified fragments using nested primer pairs using cDNA template generated from snail mRNA (see suppl. Materials and Methods). We have illustrated our method of propagating human cell lines (e.g. HEK-293T), transfections of ion channels, and their recording in a published JoVE video[297], (and see Suppl. Materials and Methods).

qPCR of NALCN

Measurement of the expression of mRNA transcripts of snails at different stages of development has been described previously[289]. Briefly, mRNA for qPCR analyses was extracted from animals age determined by shell length of juvenile (1-1.5 cm) and adult snails (2-2.5 cm)[289]. *Lymnaea* transcripts were amplified by quantitative RT-PCR (qPCR) with primers designed against an invariable portion of the LNALCN cDNA as well as primers specific for LNALCN-EEEE and LNALCN-EKEE (see Suppl. Materials and Methods).

Phylogenetic analyses of NALCN

NALCN orthologs were gathered by BLAST data-mining of available genomic databases NCBI (Bethesda, MD), Joint Genome Institute, Department of Energy and University of California (DOE-JGI), Washington University in St. Louis (Genome Institute at WUSTL), Baylor College (HGSC),

Broad Institute of MIT and Harvard. Sequences were aligned using MUSCLE and evolutionary trees were inferred by maximum parsimony (PAUP 4.0, Swofford) and maximum likelihood (PAML4, Yang).

Reverse Northern blotting

Soma-ablated axons adhered to culture dishes were rinsed three times in sterile saline before cultured axons were bathed and lifted from the adhesive substrate by trituration in Trizol reagent (Invitrogen). Subsequent to Trizol extraction, total RNA (200 ng) was amplified by SMART cDNA synthesis (Clonetech). 32P-labeled/PCR-amplified cDNA inserts were served as probes on blots spotted with DNA plasmids (200 ng) on a Hybond-N nylon membrane (Amersham Biosciences) coding for DNA fragments of *Lymnaea* calcium channel and NALCN clones (GenBank accession number, corresponding to the amino acid sequences, LCa_v1 (AF484079 [GenBank], 373-670)[215,238,214], LCa_v2 (AF484082 [GenBank] , 302-621)[343,213] 39,40, LCa_v3 (AF484084 [GenBank], 848-1111)[289,1], LNALCN (JQ806355 [GenBank], 4525-5285)[238] and subsequently imaged via a PhosphorImager (Bio-Rad).

Supplementary Materials and Methods

Source of animals

Giant pond snails, *Lymnaea stagnalis* were raised in-house in a snail vivarium and breeding facility in B1-177, Department of Biology, University of Waterloo.

Determining the full length sequence of snail NALCN

Two preliminary non-overlapping sequences, spanning major portions of the NALCN channel coding sequence, had previously been deposited into GenBank (Accession numbers AF484086 and AF484085)[238]. 5' RACE was used to determine the missing N-terminal coding sequence, corresponding to the putative start codon, the intracellular N-terminus, and part of domain I of the predicted channel protein. Briefly, total RNA was extracted from isolated central ring ganglia (i.e. CNS) and whole animals using Tri-reagent (Sigma)[325], and quality was assessed as described previously[289]. Reverse transcription was carried out using 1 µg of each RNA extract diluted to 9 µL in water, to which the following reagents were added: 5 µL of 5x Moloney Murine Leukemia Virus (M-MLV) reverse transcriptase (RTase) buffer (Promega), 2 µL of 10 mM dNTP mix (Fermentas), 0.4 µL of 100 µM LNALCN NT primer (Sigma-Genosys; see Table I), 1 µL of RiboLock RNase inhibitor (Fermentas), 2.6 µL of water, and 1µL of M-MLV RTase enzyme. cDNA synthesis was done at 37^{o}C for 1 hour, products were then co-precipitated with 2 µL of 20 mg/mL glycogen (Fermentas) in ethanol, and pellets were washed with 70% ethanol and resuspended in 10 µL of water. 5' poly-A tailing of the CNS and whole animal cDNAs was achieved by adding the following reagents (all from Fermentas) to the cDNA samples: 4 µL of 5x Terminal Deoxynucleotidyl Transferase (TdT) buffer, 4 µL of 1 mM dATP, 1 µL of water, and 1 µL of TdT enzyme. Reactions were carried out at 37^{o}C for 15 minutes and then heat inactivated at 80^{o}C for 3 minutes. Nested PCR was performed to amplify the NT coding sequence and UTR of snail NALCN from poly-A tailed CNS and whole animal cDNA, using nested primer pairs RACE-For1 plus LNALCN-Rev1, and RACE-For2 plus LNALCN-Rev2 (Sigma-Genosys; see Table I). For PCRs, used the following reagents (all from Fermentas): 2.5 µL of 10x High Fidelity PCR Buffer, 1.5 µL of 25 mM $MgCl_2$, 0.5 µL of 10 mM dNTP mix, 1.25 µL of each primer, 17.38 µL of water, 0.13 µL of High Fidelity PCR Enzyme Mix, and 0.5 µL of tailed cDNA (for 1^{o}PCR reaction) or 1^{o}PCR (for 2^{o}PCR). PCR samples were separated on an agarose gel by electrophoresis, stained with ethidium bromide for visualization under UV light, and DNA fragments were gel purified using the QIAGEN gel extraction kit. Products were then cloned into pGEM-T Easy (Promega) as per manufacturer's instructions, and blue/white

selection allowed for identification of positive clones for alkaline lysis plasmid isolation. Two plasmids representing each of the two independent RACE experiments (i.e. CNS and whole animal) were sequenced and both found to contain the snail NALCN start codon and N-terminal sequence, as well as the 5'UTR for LNALCN–EKEE (GenBank: GJQ806355) and LNALCN-EEEE (GenBank: JQ806356). To determine the unknown sequence located between the previously deposited AF484086 and AF484085 GenBank sequences, nested PCR spanning this region was carried out using *Lymnaea* λ-ZAP cDNA libraries made from CNS as template, and primer pairs LNALCN gap 5'1 plus LNALCN gap 3'1 and LNALCN gap 5'2 plus LNALCN gap 3'2 (see Table I) as previously described[1]. DNA fragments from PCRs were gel-purified, cloned into pGEM-T Easy, and sequenced as indicated above.

Table I. Primers used for qPCR, PCR cloning, and sequencing.

***Lymnaea* NALCN**		
qPCR	LNALCN control2 5'	GCTTTTACTGGTCCTAATTGATGC
	LNALCN control2 3'	AACAGGGCTTCAAGAGAAAATAGA
	LNALCN DIIK 5'	CATGTTTCAAATCCTAACCCAGAAAG
	LNALCN DIIK 3'	GGTGACAAACAAATGGTAGAAAATGAAA
	LNALCN DIIE 5'	CGTTTAAATCCATGTTCCAAATCATGTG
	LNALCN DIIE 3'	ATCACATTGACAAACAAATGGAAGATCA
	Lymnaea actin 5'	CTCACCGACTACCTGATGAAGAT
	Lymnaea actin 3'	GTAGCAGAGCTTCTCCTTGATGTC
	Lymnaea HPRT1 5'	TGTAGAAGACATCATTGACACTGG
	Lymnaea HPRT1 3'	GCCAATATAATCTGGTGCGTAAC
	Lymnaea SDHA 5'	GCTTCAAAGCTGCCTGTATAACTA
	Lymnaea SDHA 3'	ATAGAAGTGGTACTGCCAGTGGT
5' RACE	LNALCN NT	GAGATCGAATGATCCTGATGGTAGC
	RACE-For1	CGATCTCGACTCGAGTCTTTTTTTTTTTTTTT
	LNALCN-Rev1	GAGTTGATGCTGGGTTCAGCTCC
	RACE-For2	CGATCTCGACTCGAGTC
	LNALCN-Rev2	TACAGATCCCCAAAGGCATAAGACC
Preliminary sequencing	LNALCN gap 5' 1	CCGGACACATTCTGCTCCCCTGACC
	LNALCN gap 3' 1	GATTTGAAACATGGACATGAAGGCCTGC
	LNALCN gap 5' 2	GCTCCCCTGACCCAGAACCAGACTC
	LNALCN gap 3' 2	ACTTGTCAAACCCTTCAATGAAGCAG
Consensus sequencing	LNALCN R1 5' 1	GGACTGCACCAGAAACTTGACTTATGC
	LNALCN R1 3' 1	CCCAACCTTCCTGAGAGGCCGCC
	LNALCN R1 5' 2	CACGTACTCGAGCCACCATGTTAGTGAATCGTAAAACC
	LNALCN R1 3' 2	CGGGACTCATGGTCAATTCCAAGCATACC
	LNALCN R2 5' 1	CCGGACACATTCTGCTCCCCTGACC
	LNALCN R2 3' 1	GATTTGAAACATGGACATGAAGGCCTGC
	LNALCN R2 5' 2	GCTCCCCTGACCCAGAACCAGACTC
	LNALCN R2 3' 2	ACTTGTCAAACCCTTCAATGAAGCAG
	LNALCN R3 5' 1	GCTTGGCAGCTTAATCCTGTTCAC
	LNALCN R3 3' 1	TCATGGCTGGGTGGGCTTTTAGC
	LNALCN R3 5' 2	ATCATCGCATCAAGCATCAGCCTG
	LNALCN R3 3' 2	CTTCAAACTTGTCGGCCGGGATCC
	LNALCN R4 5' 1	ACATCAGCATCAGATTCGTATGGAACG
	LNALCN R4 3' 1	ATTTCGCTCAGGTCTTGGTGGAATGTGC
	LNALCN R4 5' 2	GTATGGAACGAAGTCGTAGCACAAGGG
	LNALCN R4 3' 2	GGAATGTGCAATGGCCGAGCAAGC
	LNALCN R5 5' 1	AGGAGATGGCTTGACCTTAAGGGC
	LNALCN R5 3' 1	ACCCCCATAATTGCTGTATCCACATTGTTC
	LNALCN R5 5' 2	AGAATAAAGCTTGCTCGGCCATTGC
	LNALCN R5 3' 2	TATTAGGGATCCTCACGTATCCATCACAACCC
Cloning	LNALCN-RT 3'	ATTTCGCTCAGGTCTTGGTGGAATGTGC
	LNALCN S1 5' 1	GGACTGCACCAGAAACTTGACTTATGC
	LNALCN S1 3'	GGAATGTGCAATGGCCGAGCAAGC
	LNALCN S1 5' 2	TTTTGCTAGCGCTACCGGACTCAGATCTCGAGCCACCATGTTAGTGAATCGTAAAACCAG
Human Unc-80		
Cloning	PCR-H1 sense	AGGAGGGGATGAGAGTTGGGA
	PCR-H1 antisense	TGCCTGCAGGCTTAGATTCCT
	PCR-H2 sense	AGATGAGCAGGTGTGACCAA
	PCR-H2 antisense	ACCTGCAGAGCTTACAAGAT
	PCR-H3 sense	AGCAATAGACAAGATGAGTT
	PCR-H3 antisense	GCAAATATTCAGTAAGGACT
	PCR-H4 sense	GCTGCGCTTCAACCACACAT
	PCR-H4 antisense	TGACCTCCGGAAAGGATAAA

Determining the consensus sequence of snail NALCN

Primers were designed to PCR-amplify the snail NALCN coding sequence in 5 separate, overlapping fragments, using the following nested primer pairs (listed in order from most N-terminal to most C-terminal along the cDNA sequence): LNALCN R1, LNALCN R2, LNALCN R3, LNALCN R4, and LNALCN R5 (see Table I). All PCR were carried out as indicated above for the screening of λ-ZAP cDNA libraries, using as templates either the λ-ZAP cDNA library fractions, a CNS cDNA library prepared using a random hexamer primer (see Table I), or cDNA libraries generated with NALCN-specific primers. All PCR products were cloned into pGEM-T Easy as indicated above for sequencing, and a minimum of three independent sequences for each position along the transcript were used to build the consensus for both domain II pore isoforms of snail NALCN for LNALCN–EKEE (GenBank: GJQ806355) and LNALCN-EEEE (GenBank: JQ806356). Sequencing of snail NALCN cDNAs confirmed the existence of two mutually exclusive splice variants with variable coding sequences for domain II pore regions of the putative channels.

Cloning snail NALCN isoform cDNAs for expression in mammalian cells

Lymnaea NALCN splice isoform variants (i.e. domain II K and domain II E) were each cloned into the bicistronic vector pIRES2-EGFP (Clontech) in three PCR-amplified fragments. Briefly, two cDNA fragments that were previously cloned into pGEM-T Easy for consensus sequencing of snail NALCN (see above), were combined into a large 2925 bp fragment corresponding to the invariable C-terminal coding sequence of snail NALCN. These were joined by inserting a *Hind*III-*Sac*I-digested insert DNA fragment of the LNALCN R5 subclone into the same restriction enzyme sites in the LNALCN R4 subclone. This assembled DNA was then cloned into the pIRES2-EGFP vector via *BamH*I sites flanking the insert. Large N-terminal portions of the two NALCN splice variants (~3500 bp) were then PCR-amplified from adult CNS made using a NALCN-specific primer (LNALCN-RT 3'; see Table I). Nested PCR pairs (LNALCN S1 5' 1 plus LNALCN S1 3', and LNALCN S1 5' 2 plus LNALCN S1 3'; see Table I) allowed for direct cloning of the PCR product into the pIRES2-EGFP harbouring the C-terminal portion of the channel via *Xho*I and *Sal*I restriction enzyme sites. Clones were fully sequenced to confirm the presence of both domain II splice variants and lack of mutations, and these were transfected into HEK-293T cells to confirm expression of eGFP from the internal ribosome entry site located downstream of but on the same transcript as the NALCN insert cDNAs (Promega). For electrophysiological recording, the eGFP coding sequences from the NALCN mammalian expression vectors were replaced with the coding sequence for monomeric red

fluorescent protein[336]. For N-terminal fusions with EGFP, cloned LNALCN cDNAs were excised from the corresponding pIRES2 vectors and inserted into the pEGFP-C1 vector (Clontech) via *Xho*I and *Apa*I.

Cloning of human Unc-80

Primers pairs were designed to amplify the entire coding region of the human Unc-80 cDNA in 4 partial fragments designated PCR-H1 to PCR-H4 (see Table I). Reverse transcription was performed using 5 μg of total RNA from human brain (Clontech) with Superscript III reverse transcriptase (Invitrogen) and 50 pmoles of random hexamers (Invitrogen), according to the manufacturer. PCR was performed using a mix of 2.5 Units of Taq DNA Polymerase (Invitrogen) and 2.5 Units of Pfu Turbo DNA Polymerase (Stratagene) with 50 pmoles of each primer, 2 μL of the reverse transcription product, 0.2 mM of equimolar dNTP mix, buffer (20mM Tris-HCl pH 8.4, 50mM KCl), in a final volume of 50 μL. The PCR fragments were cloned in the cloning vector pCR2.1 using the TA cloning kit (Invitrogen) and several clones were sequenced on both strands. The Unc-80 cDNA was constructed using unique restriction sites and subsequently subcloned into the mammalian expression vector pIRES2-EGFP (Clontech).

Transfections and electrophysiological recordings of snail NALCN

Mammalian cells (HEK-293T) were cultured as previously described[297]. For transfection of snail NALCN, fully confluent cells in a 6 mL vented flask were detached using warm Trypsin (Sigma-Aldrich) and split 1:4 into 35 mm culture dishes containing Dulbecco's Modified Eagle's Medium (DMEM) supplemented with 10% fetal bovine serum (FBS; Sigma) and 100 μM sodium pyruvate (Sigma-Aldrich). After over-night incubation at 37^{o}C to permit cell adhesion and recovery, transfections were prepared by combining 10 μL of Lipofectamine 2000 (Invitrogen), 1 μg of either SNAIL NALCN in pIRES2-mRFP or pIRES2-DsRed2 as control (Promega), 1 μg of human Unc-80 in pIRES2-EGFP, and 1 μg of constitutively active SRC kinase SRC Y529F in a pUSEamp vector (kindly provided by Dr. Dejian Ren) in 1.5 mL of OptiMEM (Sigma-Aldrich). Reagents were then incubated for 20 minutes, applied to the cells dropwise, and cells were incubated at 37^{o}C for 4-6 hours, washed 1x with warm supplemented DMEM lacking antibiotics, and incubated overnight at 37^{o}C in the same media used for the wash. The next day, the media was replaced with the same but also containing penicillin/ streptomycin (Sigma-Aldrich; as per manufacturer), and cells were transferred to 28^{o}C. After 1-2 days, transfected cells were detached by trypsinization (as above) and plated onto 2 mL round culture dishes containing 2 mL of supplemented DMEM and incubated at

37°C for 1-3 hours to allow cells to attach to the substrate and recover prior to electrophysiological recording.

Whole-cell patch clamp technique was performed as reported previously[343,215,297,289,1] using as external bath solution (in mM; all chemicals from Sigma): 150 NaCl, 3.5 KCl, 1 $MgCl_2$, 1.2 $CaCl_2$, 20 glucose, and 10 HEPES (pH 7.4 with NaOH) with a measured osmolarity of ~320 mOsm/L. For replacement of external sodium, 150 mM NaCl was replaced with 150 mM NMDG, where the pH was adjusted with HCl and the osmolarity was also measured at ~320 mOsm/L. The internal solution contained (in mM): 150 Cs, 120 MES, 10 NaCl, 10 EGTA, 4 $CaCl_2$, 0.3 Na_2GTP, 2 Mg-ATP, and 10 HEPES pH 7.4 with CsOH (~300 mOsm/L). Recordings were done at room temperature, with patch pipettes bearing resistances between 2 to 5 megaohms, and patches had typical access resistances between 4 to 6 MΩ. Series resistance was compensated to 70% (prediction and correction; 10-μs time lag).

Western Blotting

EGFP-LNALCN and pEGFP-C1 transfected HEK-293T cells were directly lysed in 2x sample buffer (10% glycerol (v/v), 1% SDS, 50 mM DTT and 62.5 mM Tris pH 6.8), and 25 μL aliquots of each protein sample were separated on 7.5% SDS-PAGE gels. Proteins were transferred to a 0.45 μm PROTRAN® nitrocellulose membrane (Whatman®) and blocked in Tween-20 Tris-buffered saline (TTBS) containing 5% skim milk powder (w/v). The membrane was then incubated with α-GFP antibody (Amsbio; 1:2000 in TTBS with 5% milk) overnight a 4°C, washed the next day 2 x 15 minutes with TTBS, then incubated with 1:1500 goat α-rabbit HRP (Jackson ImmunoResearch Laboratories, Inc.) at room temperature for 3 hours. Membrane was subsequently washed 3 x 15 min with TTBS, HRP-activated chemiluminescence was detected using the Super Signal West Pico Chemiluminescent system (Pierce Chemical).

Immunocytochemistry of sections of Lymnaea brain

The snail NALCN polyclonal antibody was generated using 15mer SYRSVDIRKSLQLEE C-terminal peptide sequence of NALCN coupled to KLH, and raised in rabbits. Central nervous systems from snails were dissected and fixed in 1% paraformaldehyde and 1% acetic acid, and embedded in paraffin. Seven μm sections were immunocytochemically stained with LNALCN antiserum with a procedure described previously[344].

qPCR of Lymnaea tissues

Developmental schedules of *Lymnaea*, as well as the methods used for both qPCR and semi-quantitative RT-PCR have been described previously in detail[289,1]. Briefly, mRNA for qPCR analyses was extracted from 50-75% and 100% embryos, grouped according to morphological features of embryonic animals within egg capsules[290], and shell length of juvenile vs. adult snails (1-1.5 cm and 2-2.5 cm respectively)[292]. *Lymnaea* transcripts were amplified by quantitative RT-PCR (qPCR) with primers designed against an invariable portion of the snail NALCN cDNA (i.e. LNALCN qPCR UNV 5' and LNALCN qPCR UNV 3'; see Table I), as well as primers specific for each of the domain II splice isoform (LNALCN DIIK 5' plus LNALCN DIIK 3', and LNALCN DIIE 5' plus LNALCN DIIE 3'; see Table I). qPCR transcripts were normalized against standards, actin, SDHA and HPRT1 (see Table I). Cycle threshold (CT) values for the HPRT1 gene produced the lowest stability value (i.e. 0.098) using NormFinder software[330], indicating its suitability as a reference gene. Expression levels of genes/isoforms were normalized relative to HPRT1 using the ratio[331]: $(E_{\text{target gene}})^{\Delta CT\text{target gene}}/(E_{HPRT1})^{\Delta CTHPRT1}$. Amplicons ranged from 102 to 145 bp, producing single products (as determined by melting curve analysis and visualization of electrophoresed qPCR products on ethidium bromide-stained agarose gels), with PCR efficiencies (E) ranging from 89.9 to 100.6 % (see Table I), using 1:5 serial dilutions of pooled cDNA from all RNA extracts as template. qPCR reactions were carried out in quadruplicate, and standardized between 96 well plate samples with primers against HPRT1.

Reverse Northern blotting

For reverse Northern blot analyses, soma-ablated axons adhered to culture dishes were rinsed three times in sterile saline before cultured axons were bathed and lifted from the adhesive substrate by trituration in Trizol reagent (Invitrogen). Subsequent to Trizol extraction, total RNA (200 ng) was amplified by SMART cDNA synthesis (Clontech). 32P-labeled/PCR-amplified cDNA inserts were served as probes on blots spotted with DNA plasmids (200 ng) on a Hybond-N nylon membrane (Amersham Biosciences) coding for DNA fragments of *Lymnaea* calcium channel and NALCN clones (GenBank accession number, corresponding to the amino acid sequences, LCa_v1 (AF484079 [GenBank], 373-670)[215,238,214], LCa_v2 (AF484082 [GenBank] , 302-621)[343,213] 39,40, LCa_v3 (AF484084 [GenBank], 848-1111)[289,1], LNALCN (JQ806355 [GenBank], 4525-5285)[238] and subsequently imaged via a PhosphorImager (Bio-Rad).

References

1. Senatore A and Spafford JD. (2010) Transient and Big Are Key Features of an Invertebrate T-type Channel (LCa_v3) from the Central Nervous System of *Lymnaea stagnalis*. *J Biol Chem.* 285:7447-7458.

2. Srivastava M, Begovic E, Chapman J, Putnam NH, Hellsten U, Kawashima T, Kuo A, Mitros T, Salamov A, Carpenter ML, et al. (2008) The Trichoplax genome and the nature of placozoans. *Nature* 454:955-960.

3. King N, Westbrook MJ, Young SL, Kuo A, Abedin M, Chapman J, Fairclough S, Hellsten U, Isogai Y, Letunic I, et al. (2008) The genome of the choanoflagellate Monosiga brevicollis and the origin of metazoans. *Nature* 451:783-788.

4. Mobasheri A, Avila J, Cozar-Castellano I, Brownleader MD, Trevan M, Francis MJ, Lamb JF, Martin-Vasallo P. (2000) Na+, K+-ATPase isozyme diversity; comparative biochemistry and physiological implications of novel functional interactions. *Biosci.Rep.* 20:51-91.

5. Peroutka SJ and Howell TA. (1994) The molecular evolution of G protein-coupled receptors: focus on 5-hydroxytryptamine receptors. *Neuropharmacology* 33:319-324.

6. Hulpiau P and van RF. (2009) Molecular evolution of the cadherin superfamily. *Int.J Biochem Cell Biol* 41:349-369.

7. Hulpiau P and van RF. (2011) New insights into the evolution of metazoan cadherins. *Mol Biol Evol.* 28:647-657.

8. Yu FH and Catterall WA. (2004) The VGL-chanome: a protein superfamily specialized for electrical signaling and ionic homeostasis. *Sci STKE.* 2004:re15-

9. Hille B. (2001) Ion Channels of Excitable Membranes. (Sunderland, MA: Sinauer Associates, Inc.).

10. HODGKIN AL and HUXLEY AF. (1952) Currents carried by sodium and potassium ions through the membrane of the giant axon of Loligo. *J Physiol* 116:449-472.

11. HODGKIN AL and HUXLEY AF. (1952) A quantitative description of membrane current and its application to conduction and excitation in nerve. *J Physiol* 117:500-544.

12. Clapham DE. (2007) Calcium signaling. *Cell* 131:1047-1058.

13. Case RM, Eisner D, Gurney A, Jones O, Muallem S, Verkhratsky A. (2007) Evolution of calcium homeostasis: From birth of the first cell to an omnipresent signalling system. *Cell calcium* 42:345-350.

14. Finkbeiner S and Greenberg ME. (1998) Ca^{2+} channel-regulated neuronal gene expression. *J Neurobiol.* 37:171-189.

15. Ma H, Groth RD, Wheeler DG, Barrett CF, Tsien RW. (2011) Excitation-transcription coupling in sympathetic neurons and the molecular mechanism of its initiation. *Neurosci Res* 70:2-8.

16. Dolmetsch R. (2003) Excitation-transcription coupling: signaling by ion channels to the nucleus. *Sci STKE*. 2003:E4-

17. Senatore A and Spafford JD. (2007) Calcium channels: Regulation of gene expression. Binder, M. D., Hirokawa, N., Windhorst, U., and Hirsch, M. C. Springer Verlag GmbH, Heidelberg.

18. Berridge MJ. (2006) Calcium microdomains: organization and function. *Cell calcium* 40:405-412.

19. Ikeda SR. (2001) Signal transduction. Calcium channels--link locally, act globally. *Science* 294:318-319.

20. Jiang Y, Lee A, Chen J, Cadene M, Chait BT, MacKinnon R. (2002) Crystal structure and mechanism of a calcium-gated potassium channel. *Nature* 417:515-522.

21. Clayton GM, Altieri S, Heginbotham L, Unger VM, Morais-Cabral JH. (2008) Structure of the transmembrane regions of a bacterial cyclic nucleotide-regulated channel. *Proc Natl Acad Sci U S A* 105:1511-1515.

22. Nimigean CM, Shane T, Miller C. (2004) A cyclic nucleotide modulated prokaryotic K+ channel. *J Gen Physiol* 124:203-210.

23. Lee JH, Cribbs LL, Perez-Reyes E. (1999) Cloning of a novel four repeat protein related to voltage-gated sodium and calcium channels. *FEBS Lett.* 445:231-236.

24. Zhou W, Chung I, Liu Z, Goldin AL, Dong K. (2004) A voltage-gated calcium-selective channel encoded by a sodium channel-like gene. *Neuron* 42:101-112.

25. Charalambous K and Wallace BA. (2011) NaChBac: the long lost sodium channel ancestor. *Biochemistry* 50:6742-6752.

26. Yu FH, Yarov-Yarovoy V, Gutman GA, Catterall WA. (2005) Overview of molecular relationships in the voltage-gated ion channel superfamily. *Pharmacol Rev.* 57:387-395.

27. Swartz KJ. (2004) Towards a structural view of gating in potassium channels. *Nat.Rev.Neurosci* 5:905-916.

28. Anderson PA and Greenberg RM. (2001) Phylogeny of ion channels: clues to structure and function. *Comp Biochem Physiol B Biochem Mol Biol* 129:17-28.

29. Strong M, Chandy KG, Gutman GA. (1993) Molecular evolution of voltage-sensitive ion channel genes: on the origins of electrical excitability. *Mol Biol Evol.* 10:221-242.

30. Hedrich R and Marten I. (2011) TPC1-SV channels gain shape. *Mol Plant* 4:428-441.

31. Jammes F, Hu HC, Villiers F, Bouten R, Kwak JM. (2011) Calcium-permeable channels in plant cells. *FEBS J* 278:4262-4276.

32. Clapham DE and Garbers DL. (2005) International Union of Pharmacology. L. Nomenclature and structure-function relationships of CatSper and two-pore channels. *Pharmacol Rev.* 57:451-454.

33. Paidhungat M and Garrett S. (1997) A homolog of mammalian, voltage-gated calcium channels mediates yeast pheromone-stimulated Ca2+ uptake and exacerbates the cdc1(Ts) growth defect. *Mol Cell Biol* 17:6339-6347.

34. Fujiu K, Nakayama Y, Yanagisawa A, Sokabe M, Yoshimura K. (2009) Chlamydomonas CAV2 encodes a voltage- dependent calcium channel required for the flagellar waveform conversion. *Curr Biol* 19:133-139.

35. Merchant SS, Prochnik SE, Vallon O, Harris EH, Karpowicz SJ, Witman GB, Terry A, Salamov A, Fritz-Laylin LK, Marechal-Drouard L, et al. (2007) The Chlamydomonas genome reveals the evolution of key animal and plant functions. *Science* 318:245-250.

36. Martinac B, Saimi Y, Kung C. (2008) Ion channels in microbes. *Physiol Rev.* 88:1449-1490.

37. Wang DY, Kumar S, Hedges SB. (1999) Divergence time estimates for the early history of animal phyla and the origin of plants, animals and fungi. *Proc Biol Sci* 266:163-171.

38. Zhorov BS and Tikhonov DB. (2004) Potassium, sodium, calcium and glutamate-gated channels: pore architecture and ligand action. *J Neurochem.* 88:782-799.

39. MacKinnon R. (2004) Potassium channels and the atomic basis of selective ion conduction (Nobel Lecture). *Angew.Chem Int.Ed Engl.* 43:4265-4277.

40. Bichet D, Haass FA, Jan LY. (2003) Merging functional studies with structures of inward-rectifier K(+) channels. *Nat.Rev.Neurosci.* 4:957-967.

41. Choe S. (2002) Potassium channel structures. *Nat.Rev.Neurosci* 3:115-121.

42. Tikhonov DB and Zhorov BS. (2005) Modeling P-loops domain of sodium channel: homology with potassium channels and interaction with ligands. *Biophys J* 88:184-197.

43. Cheng RC, Tikhonov DB, Zhorov BS. (2010) Structural modeling of calcium binding in the selectivity filter of the L-type calcium channel. *Eur Biophys J* 39:839-853.

44. Tikhonov DB and Zhorov BS. (2011) Possible roles of exceptionally conserved residues around the selectivity filters of sodium and calcium channels. *J Biol Chem* 286:2998-3006.

45. Doyle DA, Morais CJ, Pfuetzner RA, Kuo A, Gulbis JM, Cohen SL, Chait BT, MacKinnon R. (1998) The structure of the potassium channel: molecular basis of K+ conduction and selectivity. *Science* 280:69-77.

46. Jiang Y, Lee A, Chen J, Ruta V, Cadene M, Chait BT, MacKinnon R. (2003) X-ray structure of a voltage-dependent K+ channel. *Nature* 423:33-41.

47. Long SB, Tao X, Campbell EB, MacKinnon R. (2007) Atomic structure of a voltage-dependent K^+ channel in a lipid membrane-like environment. *Nature* 450:382-382.

48. Ren D, Navarro B, Xu H, Yue L, Shi Q, Clapham DE. (2001) A prokaryotic voltage-gated sodium channel. *Science* 294:2372-2375.

49. Koishi R, Xu H, Ren D, Navarro B, Spiller BW, Shi Q, Clapham DE. (2004) A superfamily of voltage-gated sodium channels in bacteria. *J Biol Chem* 279:9532-9538.

50. Shafrir Y, Durell SR, Guy HR. (2008) Models of the structure and gating mechanisms of the pore domain of the NaChBac ion channel. *Biophys J* 95:3650-3662.

51. Yue L, Navarro B, Ren D, Ramos A, Clapham DE. (2002) The cation selectivity filter of the bacterial sodium channel, NaChBac. *J Gen Physiol* 120:845-853.

52. Payandeh J, Scheuer T, Zheng N, Catterall WA. (2011) The crystal structure of a voltage-gated sodium channel. *Nature* 475:353-358.

53. Rosati B and McKinnon D. (2009) Structural and regulatory evolution of cellular electrophysiological systems. *Evol.Dev.* 11:610-618.

54. Durell SR and Guy HR. (2001) A putative prokaryote voltage-gated Ca(2+) channel with only one 6TM motif per subunit. *Biochem Biophys Res Commun.* 281:741-746.

55. Tang S, Mikala G, Bahinski A, Yatani A, Varadi G, Schwartz A. (1993) Molecular localization of ion selectivity sites within the pore of a human L-type cardiac calcium channel. *J Biol Chem* 268:13026-13029.

56. Heinemann SH, Terlau H, Stuhmer W, Imoto K, Numa S. (1992) Calcium channel characteristics conferred on the sodium channel by single mutations. *Nature* 356:441-443.

57. Talavera K and Nilius B. (2006) Biophysics and structure-function relationship of T-type Ca^{2+} channels. *Cell calcium* 40:97-114.

58. Spafford JD, Spencer AN, Gallin WJ. (1999) Genomic organization of a voltage-gated Na+ channel in a hydrozoan jellyfish: insights into the evolution of voltage-gated Na+ channel genes. *Receptors.Channels* 6:493-506.

59. Liebeskind BJ, Hillis DM, Zakon HH. (2011) Evolution of sodium channels predates the origin of nervous systems in animals. *Proceedings of the National Academy of Sciences* 108:9154-9159.

60. Gillespie D. (2008) Energetics of divalent selectivity in a calcium channel: the ryanodine receptor case study. *Biophys J* 94:1169-1184.

61. Corry B and Thomas M. (2012) Mechanism of ion permeation and selectivity in a voltage gated sodium channel. *J Am Chem Soc.* 134:1840-1846.

62. Catterall WA. (2010) Ion channel voltage sensors: structure, function, and pathophysiology. *Neuron* 67:915-928.

63. Nilius B, Talavera K, Owsianik G, Prenen J, Droogmans G, Voets T. (2005) Gating of TRP channels: a voltage connection? *J Physiol* 567:35-44.

64. Senatore A, Zhorov BS, Spafford JD. (2012) Ca_V3 T-type calcium channels. *WIREs Membrane Transport and Signalling* doi: 10.1002/wmts.41:

65. Lee JH, Daud AN, Cribbs LL, Lacerda AE, Pereverzev A, Klockner U, Schneider T, Perez-Reyes E. (1999) Cloning and expression of a novel member of the low voltage-activated T-type calcium channel family. *J Neurosci* 19:1912-1921.

66. Cribbs LL, Lee JH, Yang J, Satin J, Zhang Y, Daud A, Barclay J, Williamson MP, Fox M, Rees M, et al. (1998) Cloning and characterization of alpha1H from human heart, a member of the T-type Ca2+ channel gene family. *Circ Res* 83:103-109.

67. Perez-Reyes E, Cribbs LL, Daud A, Lacerda AE, Barclay J, Williamson MP, Fox M, Rees M, Lee JH. (1998) Molecular characterization of a neuronal low-voltage-activated T-type calcium channel. *Nature* 391:896-900.

68. Ertel EA, Campbell KP, Harpold MM, Hofmann F, Mori Y, Perez-Reyes E, Schwartz A, Snutch TP, Tanabe T, Birnbaumer L, et al. (2000) Nomenclature of voltage-gated calcium channels. *Neuron* 25:533-535.

69. McCleskey EW, Fox AP, Feldman D, Tsien RW. (1986) Different types of calcium channels. *J Exp Biol* 124:177-190.

70. Putnam NH, Srivastava M, Hellsten U, Dirks B, Chapman J, Salamov A, Terry A, Shapiro H, Lindquist E, Kapitonov VV, et al. (2007) Sea Anemone Genome Reveals Ancestral Eumetazoan Gene Repertoire and Genomic Organization. *Science* 317:86-94.

71. Jegla TJ, Zmasek CM, Batalov S, Nayak SK. (2009) Evolution of the human ion channel set. *Comb.Chem High Throughput.Screen.* 12:2-23.

72. Piontkivska H and Hughes AL. (2003) Evolution of vertebrate voltage-gated ion channel alpha chains by sequential gene duplication. *J Mol Evol.* 56:277-285.

73. Hamid J, Peloquin JB, Monteil A, Zamponi GW. (2006) Determinants of the differential gating properties of Cav3.1 and Cav3.3 T-type channels: a role of domain IV? *Neuroscience* 143:717-728.

74. Li J, Stevens L, Klugbauer N, Wray D. (2004) Roles of molecular regions in determining differences between voltage dependence of activation of CaV3.1 and CaV1.2 calcium channels. *J Biol Chem* 279:26858-26867.

75. Arikkath J and Campbell KP. (2003) Auxiliary subunits: essential components of the voltage-gated calcium channel complex. *Curr Opin Neurobiol.* 13:298-307.

76. Buraei Z and Yang J. (2010) The ß subunit of voltage-gated Ca2+ channels. *Physiol Rev.* 90:1461-1506.

77. Catterall WA. (2000) Structure and regulation of voltage-gated Ca^{2+} channels. *Annu.Rev.Cell Dev.Biol.* 16:521-555.

78. Altier C, Garcia-Caballero A, Simms B, You H, Chen L, Walcher J, Tedford HW, Hermosilla T, Zamponi GW. (2011) The Cavbeta subunit prevents RFP2-mediated ubiquitination and proteasomal degradation of L-type channels. *Nat.Neurosci* 14:173-180.

79. Dubel SJ, Altier C, Chaumont S, Lory P, Bourinet E, Nargeot J. (2004) Plasma membrane expression of T-type calcium channel $alpha_1$ subunits is modulated by high voltage-activated auxiliary subunits. *J.Biol.Chem.* 279:29263-29269.

80. Lin Z, Witschas K, Garcia T, Chen RS, Hansen JP, Sellers ZM, Kuzmenkina E, Herzig S, Best PM. (2008) A critical GxxxA motif in the gamma6 calcium channel subunit mediates its inhibitory effect on $Ca_v3.1$ calcium current. *J Physiol* 586:5349-5366.

81. Thompson WR, Majid AS, Czymmek KJ, Ruff AL, Garcia J, Duncan RL, Farach-Carson MC. (2011) Association of the $alpha_2delta_1$ subunit with $Ca_v3.2$ enhances membrane expression and regulates mechanically induced ATP release in MLO-Y4 osteocytes. *J Bone Miner Res* 26:2125-2139.

82. Perez-Reyes E. (2010) Characterization of the gating brake in the I-II loop of Ca_V3 T-type calcium channels. *Channels* 4:453-458.

83. Karmazinova M, Baumgart JP, Perez-Reyes E, Lacinova L. (2011) The voltage dependence of gating currents of the neuronal CA(v)3.3 channel is determined by the gating brake in the I-II loop. *Pflugers Arch* 461:461-468.

84. Shcheglovitov A, Kostyuk P, Shuba Y. (2007) Selectivity signatures of three isoforms of recombinant T-type Ca2+ channels. *Biochim.Biophys Acta* 1768:1406-1419.

85. Lux HD, Carbone E, Zucker H. (1990) Na+ currents through low-voltage-activated Ca2+ channels of chick sensory neurones: block by external Ca2+ and Mg2+. *J Physiol* 430:159-188.

86. Fukushima Y and Hagiwara S. (1985) Currents carried by monovalent cations through calcium channels in mouse neoplastic B lymphocytes. *J Physiol* 358:255-284.

87. Talavera K, Janssens A, Klugbauer N, Droogmans G, Nilius B. (2003) Pore structure influences gating properties of the T-type Ca2+ channel alpha1G. *J Gen Physiol* 121:529-540.

88. Talavera K, Staes M, Janssens A, Klugbauer N, Droogmans G, Hofmann F, Nilius B. (2001) Aspartate residues of the Glu-Glu-Asp-Asp (EEDD) pore locus control selectivity and permeation of the T-type Ca^{2+} channel $alpha_{1G}$. *J Biol Chem* 276:45628-45635.

89. McKay BE, McRory JE, Molineux ML, Hamid J, Snutch TP, Zamponi GW, Turner RW. (2006) Ca_V3 T-type calcium channel isoforms differentially distribute to somatic and dendritic compartments in rat central neurons. *Eur.J.Neurosci.* 24:2581-2594.

90. Westenbroek RE, Hoskins L, Catterall WA. (1998) Localization of Ca^{2+} channel subtypes on rat spinal motor neurons, interneurons, and nerve terminals. *J Neurosci* 18:6319-6330.

91. Lipscombe D, Helton TD, Xu W. (2004) L-type calcium channels: the low down. *J Neurophysiol* 92:2633-2641.

92. Dreyfus FM, Tscherter A, Errington AC, Renger JJ, Shin HS, Uebele VN, Crunelli V, Lambert RC, Leresche N. (2010) Selective T-Type Calcium Channel Block in Thalamic Neurons Reveals Channel Redundancy and Physiological Impact of $I_{Twindow}$. *The Journal of Neuroscience* 30:99-109.

93. Shipe WD, Barrow JC, Yang ZQ, Lindsley CW, Yang FV, Schlegel KA, Shu Y, Rittle KE, Bock MG, Hartman GD, et al. (2008) Design, synthesis, and evaluation of a novel 4-aminomethyl-4-fluoropiperidine as a T-type Ca^{2+} channel antagonist. *J Med Chem.* 51:3692-3695.

94. Perez-Reyes E. (2003) Molecular physiology of low-voltage-activated T-type calcium channels. *Physiol.Rev.* 83:117-161.

95. Anderson MP, Mochizuki T, Xie J, Fischler W, Manger JP, Talley EM, Scammell TE, Tonegawa S. (2005) Thalamic $Ca_v3.1$ T-type Ca^{2+} channel plays a crucial role in stabilizing sleep. *Proc.Natl.Acad.Sci.U.S.A.* 102:1743-1748.

96. Lee J and Shin HS. (2007) T-type calcium channels and thalamocortical rhythms in sleep: a perspective from studies of T-type calcium channel knockout mice. *CNS Neurol Disord Drug Targets* 6:63-69.

97. Lee J, Kim D, Shin HS. (2004) Lack of delta waves and sleep disturbances during non-rapid eye movement sleep in mice lacking A_{1G}-subunit of T-type calcium channels. *Proc.Natl.Acad.Sci.U.S.A.* 101:18195-18199.

98. Cheong E, Lee S, Choi BJ, Sun M, Lee CJ, Shin HS. (2008) Tuning Thalamic Firing Modes via Simultaneous Modulation of T- and L-Type Ca^{2+} Channels Controls Pain Sensory Gating in the Thalamus. *The Journal of Neuroscience* 28:13331-13340.

99. Peloquin JB, Khosravani H, Barr W, Bladen C, Evans R, Mezeyova J, Parker D, Snutch TP, McRory JE, Zamponi GW. (2006) Functional Analysis of $Ca_v3.2$ T-type Calcium Channel Mutations Linked to Childhood Absence Epilepsy. *Epilepsia* 47:658-658.

100. Vitko I, Chen Y, Arias JM, Shen Y, Wu XR, Perez-Reyes E. (2005) Functional characterization and neuronal modeling of the effects of childhood absence epilepsy variants of *CACNA1H*, a T-type calcium channel. *J.Neurosci.* 25:4844-4855.

101. Vitko I, Bidaud I, Arias JM, Mezghrani A, Lory P, Perez-Reyes E. (2007) The I-II loop controls plasma membrane expression and gating of $Ca_v3.2$ T-type Ca^{2+} channels: a paradigm for childhood absence epilepsy mutations. *J.Neurosci.* 27:322-330.

102. Chen Y, Lu J, Pan H, Zhang Y, Wu H, Xu K, Liu X, Jiang Y, Bao X, Yao Z, et al. (2003) Association between genetic variation of *CACNA1H* and childhood absence epilepsy. *Annals of Neurology* 54:243-243.

103. Liang J, Zhang Y, Wang J, Pan H, Wu H, Xu K, Liu X, Jiang Y, Shen Y, Wu X. (2006) New variants in the *CACNA1H* gene identified in childhood absence epilepsy. *Neurosci.Lett.* 406:27-32.

104. Swayne L and Bourinet E. (2008) Voltage-gated calcium channels in chronic pain: emerging role of alternative splicing. *Pflugers Arch.* 456:459-466.

105. Todorovic SM and Jevtovic-Todorovic V. (2007) Regulation of T-Type Calcium Channels in the Peripheral Pain Pathway. *Channels* 1:238-245.

106. Zamponi GW, Lewis RJ, Todorovic SM, Arneric SP, Snutch TP. (2009) Role of voltage-gated calcium channels in ascending pain pathways. *Brain Res.Rev.* 60:84-89.

107. Vassort G, Talavera K, Alvarez JL. (2006) Role of T-type Ca2+ channels in the heart. *Cell calcium* 40:205-220.

108. Ono K and Iijima T. (2010) Cardiac T-type Ca^{2+} channels in the heart. *J Mol Cell Cardiol.* 48:65-70.

109. Ono K and Iijima T. (2005) Pathophysiological significance of T-type Ca2+ channels: properties and functional roles of T-type Ca2+ channels in cardiac pacemaking. *J Pharmacol Sci* 99:197-204.

110. Lin YC SA. (2001) Calcium currents from jellyfish striated muscle cells: preservation of phenotype, characterisation of currents and channel localisation. *J Exp Biol.* 204:3717-3726.

111. Yeoman MS, Brezden BL, Benjamin PR. (1999) LVA and HVA Ca^{2+} Currents in Ventricular Muscle Cells of the *Lymnaea* Heart. *J.Neurophysiol.* 82:2428-2440.

112. Liu P, Ge Q, Chen B, Salkoff L, Kotlikoff MI, Wang ZW. (2011) Genetic dissection of ion currents underlying all-or-none action potentials in *C. elegans* body-wall muscle cells. *J Physiol* 589:101-117.

113. Shtonda B. (2005) CCA-1, EGL-19 and EXP-2 currents shape action potentials in the Caenorhabditis elegans pharynx. *J Exp Biol.* 208:2177-2190.

114. Bean BP. (2007) The action potential in mammalian central neurons. *Nat.Rev.Neurosci* 8:451-465.

115. Miller HM. (1934) Sex-linked mutant characters induced by X-ray dosage of 5000 r-u. *Drosophila Information Service* 2:9-

116. Nash HA, Scott RL, Lear BC, Allada R. (2002) An unusual cation channel mediates photic control of locomotion in Drosophila. *Curr Biol* 12:2152-2158.

117. Lee JH, Cribbs LL, Perez-Reyes E. (1999) Cloning of a novel four repeat protein related to voltage-gated sodium and calcium channels. *FEBS Lett.* 445:231-236.

118. Swayne LA, Mezghrani A, Varrault A, Chemin J, Bertrand G, Dalle S, Bourinet E, Lory P, Miller RJ, Nargeot J, et al. (2009) The NALCN ion channel is activated by M3 muscarinic receptors in a pancreatic beta-cell line. *EMBO Rep.* 10:873-880.

119. Snutch TP and Monteil A. (2007) The sodium "leak" has finally been plugged. *Neuron* 54:505-507.

120. Lu B, Su Y, Das S, Liu J, Xia J, Ren D. (2007) The neuronal channel NALCN contributes resting sodium permeability and is required for normal respiratory rhythm. *Cell* 129:371-383.

121. Lear BC, Lin JM, Keath JR, McGill JJ, Raman IM, Allada R. (2005) The ion channel narrow abdomen is critical for neural output of the Drosophila circadian pacemaker. *Neuron* 48:965-976.

122. Krishnan KS and Nash HA. (1990) A genetic study of the anesthetic response: mutants of Drosophila melanogaster altered in sensitivity to halothane. *Proc Natl Acad Sci U S A* 87:8632-8636.

123. Morgan PG, Sedensky M, Meneely PM. (1990) Multiple sites of action of volatile anesthetics in Caenorhabditis elegans. *Proc Natl Acad Sci U S A* 87:2965-2969.

124. Sedensky MM and Meneely PM. (1987) Genetic analysis of halothane sensitivity in Caenorhabditis elegans. *Science* 236:952-954.

125. Morgan PG, Sedensky MM, Meneely PM, Cascorbi HF. (1988) The effect of two genes on anesthetic response in the nematode Caenorhabditis elegans. *Anesthesiology* 69:246-251.

126. Humphrey JA, Hamming KS, Thacker CM, Scott RL, Sedensky MM, Snutch TP, Morgan PG, Nash HA. (2007) A putative cation channel and its novel regulator: cross-species conservation of effects on general anesthesia. *Curr Biol* 17:624-629.

127. Yeh E, Ng S, Zhang M, Bouhours M, Wang Y, Wang M, Hung W, Aoyagi K, Melnik-Martinez K, Li M, et al. (2008) A putative cation channel, NCA-1, and a novel protein, UNC-80, transmit neuronal activity in C. elegans. *PLoS Biol* 6:e55-

128. Jospin M, Watanabe S, Joshi D, Young S, Hamming K, Thacker C, Snutch TP, Jorgensen EM, Schuske K. (2007) UNC-80 and the NCA ion channels contribute to endocytosis defects in synaptojanin mutants. *Curr Biol* 17:1595-1600.

129. Campbell DB and Nash HA. (1994) Use of Drosophila mutants to distinguish among volatile general anesthetics. *Proc Natl Acad Sci U S A* 91:2135-2139.

130. Speca DJ, Chihara D, Ashique AM, Bowers MS, Pierce-Shimomura JT, Lee J, Rabbee N, Speed TP, Gularte RJ, Chitwood J, et al. (2010) Conserved role of unc-79 in ethanol responses in lightweight mutant mice. *PLoS Genet.* 6:

131. Wang H and Ren D. (2009) UNC80 functions as a scaffold for Src kinases in NALCN channel function. *Channels* 3:161-163.

132. Lu B, Su Y, Das S, Wang H, Wang Y, Liu J, Ren D. (2009) Peptide neurotransmitters activate a cation channel complex of NALCN and UNC-80. *Nature* 457:741-744.

133. Pierce-Shimomura JT, Chen BL, Mun JJ, Ho R, Sarkis R, McIntire SL. (2008) Genetic analysis of crawling and swimming locomotory patterns in C. elegans. *Proc Natl Acad Sci U S A* 105:20982-20987.

134. Lu B, Zhang Q, Wang H, Wang Y, Nakayama M, Ren D. (2010) Extracellular calcium controls background current and neuronal excitability via an UNC79-UNC80-NALCN cation channel complex. *Neuron* 68:488-499.

135. Lee JH, Cribbs LL, Perez-Reyes E. (1999) Cloning of a novel four repeat protein related to voltage-gated sodium and calcium channels. *FEBS Lett.* 445:231-236.

136. Snutch TP and Monteil A. (2007) The sodium "leak" has finally been plugged. *Neuron* 54:505-507.

137. Lu B, Su Y, Das S, Liu J, Xia J, Ren D. (2007) The neuronal channel NALCN contributes resting sodium permeability and is required for normal respiratory rhythm. *Cell* 129:371-383.

138. Starace DM and Bezanilla F. (2004) A proton pore in a potassium channel voltage sensor reveals a focused electric field. *Nature* 427:548-553.

139. Cannon SC. (2010) Voltage-sensor mutations in channelopathies of skeletal muscle. *J Physiol* 588:1887-1895.

140. Tombola F, Pathak MM, Isacoff EY. (2005) Voltage-sensing arginines in a potassium channel permeate and occlude cation-selective pores. *Neuron* 45:379-388.

141. Tombola F, Pathak MM, Gorostiza P, Isacoff EY. (2007) The twisted ion-permeation pathway of a resting voltage-sensing domain. *Nature* 445:546-549.

142. Sokolov S, Scheuer T, Catterall WA. (2007) Gating pore current in an inherited ion channelopathy. *Nature* 446:76-78.

143. Ren D. (2011) Sodium leak channels in neuronal excitability and rhythmic behaviors. *Neuron* 72:899-911.

144. Parent L and Gopalakrishnan M. (1995) Glutamate substitution in repeat IV alters divalent and monovalent cation permeation in the heart Ca2+ channel. *Biophys J* 69:1801-1813.

145. Zhao Y, Scheuer T, Catterall WA. (2004) Reversed voltage-dependent gating of a bacterial sodium channel with proline substitutions in the S6 transmembrane segment. *Proc Natl Acad Sci U S A* 101:17873-17878.

146. Zhao Y, Yarov-Yarovoy V, Scheuer T, Catterall WA. (2004) A gating hinge in Na+ channels; a molecular switch for electrical signaling. *Neuron* 41:859-865.

147. Irie K, Kitagawa K, Nagura H, Imai T, Shimomura T, Fujiyoshi Y. (2010) Comparative study of the gating motif and C-type inactivation in prokaryotic voltage-gated sodium channels. *J Biol Chem* 285:3685-3694.

148. Bouhours M, Po MD, Gao S, Hung W, Li H, Georgiou J, Roder JC, Zhen M. (2011) A co-operative regulation of neuronal excitability by UNC-7 innexin and NCA/NALCN leak channel. *Mol Brain* 4:16-

149. Harris TW, Hartwieg E, Horvitz HR, Jorgensen EM. (2000) Mutations in synaptojanin disrupt synaptic vesicle recycling. *J Cell Biol* 150:589-600.

150. Yeh E, Kawano T, Weimer RM, Bessereau JL, Zhen M. (2005) Identification of genes involved in synaptogenesis using a fluorescent active zone marker in Caenorhabditis elegans. *J Neurosci* 25:3833-3841.

151. Rizzoli SO and Betz WJ. (2005) Synaptic vesicle pools. *Nat.Rev.Neurosci* 6:57-69.

152. Morgan PG, Kayser EB, Sedensky MM. (2007) C. elegans and volatile anesthetics. *WormBook.* 1-11.

153. Hawasli AH, Saifee O, Liu C, Nonet ML, Crowder CM. (2004) Resistance to volatile anesthetics by mutations enhancing excitatory neurotransmitter release in Caenorhabditis elegans. *Genetics* 168:831-843.

154. Maclver MB, Mikulec AA, Amagasu SM, Monroe FA. (1996) Volatile anesthetics depress glutamate transmission via presynaptic actions. *Anesthesiology* 85:823-834.

155. Perouansky M, Baranov D, Salman M, Yaari Y. (1995) Effects of halothane on glutamate receptor-mediated excitatory postsynaptic currents. A patch-clamp study in adult mouse hippocampal slices. *Anesthesiology* 83:109-119.

156. Nishikawa K and Kidokoro Y. (1999) Halothane presynaptically depresses synaptic transmission in wild-type Drosophila larvae but not in halothane-resistant (har) mutants. *Anesthesiology* 90:1691-1697.

157. Nakayama M, Iida M, Koseki H, Ohara O. (2006) A gene-targeting approach for functional characterization of KIAA genes encoding extremely large proteins. *FASEB J* 20:1718-1720.

158. Morgan PG and Sedensky MM. (1995) Mutations affecting sensitivity to ethanol in the nematode, Caenorhabditis elegans. *Alcohol Clin.Exp Res* 19:1423-1429.

159. Kayser EB, Suthammarak W, Morgan PG, Sedensky MM. (2011) Isoflurane selectively inhibits distal mitochondrial complex I in Caenorhabditis elegans. *Anesth.Analg.* 112:1321-1329.

160. Lu TZ and Feng ZP. (2011) A sodium leak current regulates pacemaker activity of adult central pattern generator neurons in Lymnaea stagnalis. *PloS one* 6:e18745-

161. Singaram VK, Somerlot BH, Falk SA, Falk MJ, Sedensky MM, Morgan PG. (2011) Optical reversal of halothane-induced immobility in C. elegans. *Curr Biol* 21:2070-2076.

162. Stewart GW and Turner EJ. (1999) The hereditary stomatocytoses and allied disorders: congenital disorders of erythrocyte membrane permeability to Na and K. *Baillieres Best.Pract.Res Clin.Haematol.* 12:707-727.

163. International Human Genome Sequencing Consortium. (2004) Finishing the euchromatic sequence of the human genome. *Nature* 431:931-945.

164. Hahn MW and Wray GA. (2002) The g-value paradox. *Evol.Dev.* 4:73-75.

165. Gregory TR. (2005) Synergy between sequence and size in large-scale genomics. *Nat.Rev.Genet.* 6:699-708.

166. Gerstein MB, Lu ZJ, Van Nostrand EL, Cheng C, Arshinoff BI, Liu T, Yip KY, Robilotto R, Rechtsteiner A, Ikegami K, et al. (2010) Integrative analysis of the Caenorhabditis elegans genome by the modENCODE project. *Science* 330:1775-1787.

167. Ramani AK, Calarco JA, Pan Q, Mavandadi S, Wang Y, Nelson AC, Lee LJ, Morris Q, Blencowe BJ, Zhen M, et al. (2011) Genome-wide analysis of alternative splicing in Caenorhabditis elegans. *Genome Res* 21:342-348.

168. Pan Q, Shai O, Lee LJ, Frey BJ, Blencowe BJ. (2008) Deep surveying of alternative splicing complexity in the human transcriptome by high-throughput sequencing. *Nat.Genet.* 40:1413-1415.

169. Graveley BR, Brooks AN, Carlson JW, Duff MO, Landolin JM, Yang L, Artieri CG, van Baren MJ, Boley N, Booth BW, et al. (2011) The developmental transcriptome of Drosophila melanogaster. *Nature* 471:473-479.

170. Wang ET, Sandberg R, Luo S, Khrebtukova I, Zhang L, Mayr C, Kingsmore SF, Schroth GP, Burge CB. (2008) Alternative isoform regulation in human tissue transcriptomes. *Nature* 456:470-476.

171. Sterck L, Rombauts S, Vandepoele K, Rouze P, Van de Peer Y. (2007) How many genes are there in plants (... and why are they there)? *Curr Opin Plant Biol* 10:199-203.

172. Kim E, Goren A, Ast G. (2008) Alternative splicing: current perspectives. *Bioessays* 30:38-47.

173. Artamonova II and Gelfand MS. (2007) Comparative genomics and evolution of alternative splicing: the pessimists' science. *Chem Rev.* 107:3407-3430.

174. Allen SE, Darnell RB, Lipscombe D. (2010) The neuronal splicing factor Nova controls alternative splicing in N-type and P-type CaV2 calcium channels. *Channels* 4:483-489.

175. Schulz DJ, Temporal S, Barry DM, Garcia ML. (2008) Mechanisms of voltage-gated ion channel regulation: from gene expression to localization. *Cell Mol Life Sci* 65:2215-2231.

176. Liao P, Zhang HY, Soong TW. (2009) Alternative splicing of voltage-gated calcium channels: from molecular biology to disease. *Pflugers Arch* 458:481-487.

177. Fodor AA and Aldrich RW. (2009) Convergent evolution of alternative splices at domain boundaries of the BK channel. *Annu.Rev.Physiol* 71:19-36.

178. Schroeter A, Walzik S, Blechschmidt S, Haufe V, Benndorf K, Zimmer T. (2010) Structure and function of splice variants of the cardiac voltage-gated sodium channel Na(v)1.5. *J Mol Cell Cardiol.* 49:16-24.

179. Vazquez E and Valverde MA. (2006) A review of TRP channels splicing. *Semin.Cell Dev.Biol* 17:607-617.

180. Kalsotra A and Cooper TA. (2011) Functional consequences of developmentally regulated alternative splicing. *Nat.Rev.Genet.* 12:715-729.

181. Andreassi C and Riccio A. (2009) To localize or not to localize: mRNA fate is in 3'UTR ends. *Trends Cell Biol* 19:465-474.

182. Hughes TA. (2006) Regulation of gene expression by alternative untranslated regions. *Trends Genet.* 22:119-122.

183. Keren H, Lev-Maor G, Ast G. (2010) Alternative splicing and evolution: diversification, exon definition and function. *Nat.Rev.Genet.* 11:345-355.

184. Bland CS, Wang ET, Vu A, David MP, Castle JC, Johnson JM, Burge CB, Cooper TA. (2010) Global regulation of alternative splicing during myogenic differentiation. *Nucleic Acids Res* 38:7651-7664.

185. Kalsotra A, Xiao X, Ward AJ, Castle JC, Johnson JM, Burge CB, Cooper TA. (2008) A postnatal switch of CELF and MBNL proteins reprograms alternative splicing in the developing heart. *Proc Natl Acad Sci U S A* 105:20333-20338.

186. Will CL and Lührmann R. (2011) Spliceosome structure and function. *Cold Spring Harb.Perspect.Biol* 3:

187. Chen M and Manley JL. (2009) Mechanisms of alternative splicing regulation: insights from molecular and genomics approaches. *Nat.Rev.Mol Cell Biol* 10:741-754.

188. Gabut M, Chaudhry S, Blencowe BJ. (2008) SnapShot: The splicing regulatory machinery. *Cell* 133:192-

189. Bertolesi GE, Jollimore CA, Shi C, Elbaum L, Denovan-Wright EM, Barnes S, Kelly ME. (2003) Regulation of alpha1G T-type calcium channel gene (CACNA1G) expression during neuronal differentiation. *Eur J Neurosci* 17:1802-1810.

190. Emerick MC, Stein R, Kunze R, McNulty MM, Regan MR, Hanck DA, Agnew WS. (2006) Profiling the array of $Ca_v3.1$ variants from the human T-type calcium channel gene CACNA1G: alternative structures, developmental expression, and biophysical variations. *Proteins* 64:320-342.

191. Mittman S, Guo J, Agnew WS. (1999) Structure and alternative splicing of the gene encoding alpha1G, a human brain T calcium channel alpha1 subunit. *Neurosci Lett.* 274:143-146.

192. Chemin J, Monteil A, Bourinet E, Nargeot J, Lory P. (2001) Alternatively spliced $alpha_{1G}$ ($Ca_V3.1$) intracellular loops promote specific T-type Ca^{2+} channel gating properties. *Biophys.J.* 80:1238-1250.

193. Monteil A, Chemin J, Bourinet E, Mennessier G, Lory P, Nargeot J. (2000) Molecular and functional properties of the human $alpha_{1G}$ subunit that forms T-type calcium channels. *J.Biol.Chem.* 275:6090-6100.

194. Ernst WL and Noebels JL. (2009) Expanded alternative splice isoform profiling of the mouse Cav3.1/alpha1G T-type calcium channel. *BMC Mol Biol* 10:53-

195. Shcheglovitov A, Vitko I, Bidaud I, Baumgart JP, Navarro-Gonzalez MF, Grayson TH, Lory P, Hill CE, Perez-Reyes E. (2008) Alternative splicing within the I-II loop controls surface expression of T-type $Ca_v3.1$ calcium channels. *FEBS Lett.* 582:3765-3770.

196. Baumgart JP, Vitko I, Bidaud I, Kondratskyi A, Lory P, Perez-Reyes E. (2008) I-II loop structural determinants in the gating and surface expression of low voltage-activated calcium channels. *PloS one* 3:e2976-

197. Vitko I, Bidaud I, Arias JM, Mezghrani A, Lory P, Perez-Reyes E. (2007) The I-II loop controls plasma membrane expression and gating of Ca(v)3.2 T-type Ca2+ channels: a paradigm for childhood absence epilepsy mutations. *J Neurosci* 27:322-330.

198. Mittman S, Guo J, Emerick MC, Agnew WS. (1999) Structure and alternative splicing of the gene encoding alpha1I, a human brain T calcium channel alpha1 subunit. *Neurosci Lett.* 269:121-124.

199. Murbartian J, Arias JM, Perez-Reyes E. (2004) Functional impact of alternative splicing of human T-type Cav3.3 calcium channels. *J Neurophysiol* 92:3399-3407.

200. Zhong X. (2006) A profile of alternative RNA splicing and transcript variation of CACNA1H, a human T-channel gene candidate for idiopathic generalized epilepsies. *Hum.Mol.Genet.* 15:1497-1512.

201. Jagannathan S, Punt EL, Gu Y, Arnoult C, Sakkas D, Barratt CL, Publicover SJ. (2002) Identification and localization of T-type voltage-operated calcium channel subunits in human male germ cells. Expression of multiple isoforms. *J Biol Chem* 277:8449-8456.

202. Murbartian J, Arias JM, Perez-Reyes E. (2004) Functional impact of alternative splicing of human T-type Cav3.3 calcium channels. *J Neurophysiol* 92:3399-3407.

203. Murbartian J, Arias JM, Lee JH, Gomora JC, Perez-Reyes E. (2002) Alternative splicing of the rat Ca(v)3.3 T-type calcium channel gene produces variants with distinct functional properties(1). *FEBS Lett.* 528:272-278.

204. McRory JE, Santi CM, Hamming KS, Mezeyova J, Sutton KG, Baillie DL, Stea A, Snutch TP. (2001) Molecular and functional characterization of a family of rat brain T-type calcium channels. *J.Biol.Chem.* 276:3999-4011.

205. Gomora JC, Murbartian J, Arias JM, Lee JH, Perez-Reyes E. (2002) Cloning and expression of the human T-type channel $Ca_v3.3$: insights into prepulse facilitation. *Biophys J* 83:229-241.

206. Klockner U, Lee JH, Cribbs LL, Daud A, Hescheler J, Pereverzev A, Perez-Reyes E, Schneider T. (1999) Comparison of the Ca2 + currents induced by expression of three cloned alpha1 subunits, alpha1G, alpha1H and alpha1I, of low-voltage-activated T-type Ca2 + channels. *Eur J Neurosci* 11:4171-4178.

207. Monteil A, Chemin J, Leuranguer V, Altier C, Mennessier G, Bourinet E, Lory P, Nargeot J. (2000) Specific properties of T-type calcium channels generated by the human alpha 1I subunit. *J Biol Chem* 275:16530-16535.

208. Mezghrani A, Monteil A, Watschinger K, Sinnegger-Brauns MJ, Barrere C, Bourinet E, Nargeot J, Striessnig J, Lory P. (2008) A destructive interaction mechanism accounts for dominant-negative effects of misfolded mutants of voltage-gated calcium channels. *J Neurosci* 28:4501-4511.

209. Benjamin PR. (2008) Lymnaea. *Scholarpedia* 3:4124-

210. Feng ZP, Zhang Z, van Kesteren RE, Straub VA, van Nierop P, Jin K, Nejatbakhsh N, Goldberg JI, Spencer GE, Yeoman MS, et al. (2009) Transcriptome analysis of the central nervous system of the mollusc Lymnaea stagnalis. *BMC genomics* 10:451-

211. Moroz LL, Edwards JR, Puthanveettil SV, Kohn AB, Ha T, Heyland A, Knudsen B, Sahni A, Yu F, Liu L, et al. (2006) Neuronal transcriptome of Aplysia: neuronal compartments and circuitry. *Cell* 127:1453-1467.

212. Kaang BK, Pfaffinger PJ, Grant SG, Kandel ER, Furukawa Y. (1992) Overexpression of an Aplysia shaker K+ channel gene modifies the electrical properties and synaptic efficacy of identified Aplysia neurons. *Proc Natl Acad Sci U S A* 89:1133-1137.

213. Spafford JD, Chen L, Feng ZP, Smit AB, Zamponi GW. (2003) Expression and modulation of an invertebrate presynaptic calcium channel alpha1 subunit homolog. *J.Biol.Chem.* 278:21178-21187.

214. Spafford JD, Dunn T, Smit AB, Syed NI, Zamponi GW. (2006) *In vitro* characterization of L-type calcium channels and their contribution to firing behavior in invertebrate respiratory neurons. *J.Neurophysiol.* 95:42-52.

215. Senatore A. (2011) Mapping of dihydropyridine binding residues in a less sensitive invertebrate L-type calcium channel (LCa v 1). *Channels* 5:173-187.

216. Syed NI, Bulloch AG, Lukowiak K. (1990) In vitro reconstruction of the respiratory central pattern generator of the mollusk Lymnaea. *Science* 250:282-285.

217. Kemenes G, Staras K, Benjamin PR. (1997) In vitro appetitive classical conditioning of the feeding response in the pond snail Lymnaea stagnalis. *J Neurophysiol* 78:2351-2362.

218. Taylor BE and Lukowiak K. (2000) The respiratory central pattern generator of Lymnaea: a model, measured and malleable. *Respir.Physiol* 122:197-207.

219. Jones NG, Kemenes I, Kemenes G, Benjamin PR. (2003) A persistent cellular change in a single modulatory neuron contributes to associative long-term memory. *Curr Biol* 13:1064-1069.

220. Grant AO. (2009) Cardiac ion channels. *Circ Arrhythm.Electrophysiol.* 2:185-194.

221. Yeoman MS and Benjamin PR. (1999) Two Types of Voltage-Gated K+ Currents in Dissociated Heart Ventricular Muscle Cells of the Snail Lymnaea stagnalis. *J.Neurophysiol.* 82:2415-2427.

222. McAllister-Williams RH and Kelly JS. (1995) The temperature dependence of high-threshold calcium channel currents recorded from adult rat dorsal raphe neurones. *Neuropharmacology* 34:1479-1490.

223. Chemin J, Mezghrani A, Bidaud I, Dupasquier S, Marger F, Barrere C, Nargeot J, Lory P. (2007) Temperature-dependent modulation of CaV3 T-type calcium channels by protein kinases C and A in mammalian cells. *J Biol Chem* 282:32710-32718.

224. Rosen AD. (1996) Temperature modulation of calcium channel function in GH3 cells. *Am J Physiol* 271:C863-C868.

225. Iftinca M, McKay BE, Snutch TP, McRory JE, Turner RW, Zamponi GW. (2006) Temperature dependence of T-type calcium channel gating. *Neuroscience* 142:1031-1042.

226. Peloquin JB, Doering CJ, Rehak R, McRory JE. (2008) Temperature dependence of Cav1.4 calcium channel gating. *Neuroscience* 151:1066-1083.

227. Allen TJ. (1996) Temperature dependence of macroscopic L-type calcium channel currents in single guinea pig ventricular myocytes. *J Cardiovasc.Electrophysiol.* 7:307-321.

228. Allen TJ and Mikala G. (1998) Effects of temperature on human L-type cardiac Ca2+ channels expressed in Xenopus oocytes. *Pflugers Arch* 436:238-247.

229. Nobile M, Carbone E, Lux HD, Zucker H. (1990) Temperature sensitivity of Ca currents in chick sensory neurones. *Pflugers Arch* 415:658-663.

230. Hedges SB. (2002) The origin and evolution of model organisms. *Nat.Rev.Genet.* 3:838-849.

231. Ono K and Iijima T. (2010) Cardiac T-type Ca2+ channels in the heart. *J Mol Cell Cardiol.* 48:65-70.

232. Kim D, Song I, Keum S, Lee T, Jeong MJ, Kim SS, McEnery MW, Shin HS. (2001) Lack of the Burst Firing of Thalamocortical Relay Neurons and Resistance to Absence Seizures in Mice Lacking A_{1G} T-Type Ca^{2+} Channels. *Neuron* 31:35-45.

233. Chemin J, Monteil A, Briquaire C, Richard S, Perez-Reyes E, Nargeot J, Lory P. (2000) Overexpression of T-type calcium channels in HEK-293 cells increases intracellular calcium without affecting cellular proliferation. *FEBS Lett.* 478:166-172.

234. Lory P, Bidaud I, Chemin J. (2006) T-type calcium channels in differentiation and proliferation. *Cell calcium* 40:135-146.

235. Shin HS, Cheong EJ, Choi S, Lee J, Na HS. (2008) T-type Ca^{2+} channels as therapeutic targets in the nervous system. *Curr Opin Pharmacol* 8:33-41.

236. Hagiwara S, Ozawa S, Sand O. (1975) Voltage clamp analysis of two inward current mechanisms in the egg cell membrane of a starfish. *J Gen Physiol.* 65:617-644.

237. Nowycky MC, Fox AP, Tsien RW. (1985) Three types of neuronal calcium channel with different calcium agonist sensitivity. *Nature* 316:440-443.

238. Spafford JD, Munno DW, van NP, Feng ZP, Jarvis SE, Gallin WJ, Smit AB, Zamponi GW, Syed NI. (2003) Calcium channel structural determinants of synaptic transmission between identified invertebrate neurons. *J Biol Chem* 278:4258-4267.

239. Bittner KC and Hanck DA. (2008) The relationship between single-channel and whole-cell conductance in the T-type Ca^{2+} channel $Ca_V3.1$. *Biophys J* 95:931-941.

240. Lee JH, Gomora JC, Cribbs LL, Perez-Reyes E. (1999) Nickel block of three cloned T-type calcium channels: low concentrations selectively block alpha1H. *Biophys.J.* 77:3034-3042.

241. Kang HW, Park JY, Jeong SW, Kim JA, Moon HJ, Perez-Reyes E, Lee JH. (2006) A Molecular Determinant of Nickel Inhibition in $Ca_v3.2$ T-type Calcium Channels. *J Biol Chem.* 281:4823-4830.

242. Milescu M, Bosmans F, Lee S, Alabi AA, Kim JI, Swartz KJ. (2009) Interactions between lipids and voltage sensor paddles detected with tarantula toxins. *Nat.Struct Mol Biol* 16:1080-1085.

243. Ertel SI and Clozel JP. (1997) Mibefradil (Ro 40-5967): the first selective T-type Ca^{2+} channel blocker. *Expert Opin Investig.Drugs* 6:569-582.

244. Martin RL, Lee JH, Cribbs LL, Perez-Reyes E, Hanck DA. (2000) Mibefradil block of cloned T-type calcium channels. *J.Pharmacol.Exp.Ther.* 295:302-308.

245. Arias-Olguin II, Vitko I, Fortuna M, Baumgart JP, Sokolova S, Shumilin IA, Van Deusen A, Soriano-Garcia M, Gomora JC, Perez-Reyes E. (2008) Characterization of the gating brake in the I-II loop of Ca(v)3.2 T-type Ca(2+) channels. *J.Biol.Chem.* 283:8136-8144.

246. Serrano JR, Perez-Reyes E, Jones SW. (1999) State-dependent inactivation of the $alpha_{1G}$ T-type calcium channel. *J Gen Physiol* 114:185-201.

247. Richards MW, Butcher AJ, Dolphin AC. (2004) Ca^{2+} channel beta-subunits: structural insights AID our understanding. *Trends Pharmacol Sci* 25:626-632.

248. Di B, V and Franzini-Armstrong C. (2005) Evolution of skeletal type e-c coupling: a novel means of controlling calcium delivery. *J Cell Biol* 171:695-704.

249. Atwood HL. (2006) Neuroscience. Gatekeeper at the synapse. *Science* 312:1008-1009.

250. Iftinca MC ZG. (2009) Regulation of neuronal T-type calcium channels. *Trends Pharmacol Sci.* 30:32-40.

251. Spafford JD and Zamponi GW. (2003) Functional interactions between presynaptic calcium channels and the neurotransmitter release machinery. *Curr Opin Neurobiol.* 13:308-314.

252. Molineux ML, McRory JE, McKay BE, Hamid J, Mehaffey WH, Rehak R, Snutch TP, Zamponi GW, Turner RW. (2006) Specific T-type calcium channel isoforms are associated with distinct burst phenotypes in deep cerebellar nuclear neurons. *Proceedings of the National Academy of Sciences* 103:5555-5560.

253. Carbone E, Giancippoli A, Marcantoni A, Guido D, Carabelli V. (2006) A new role for T-type channels in fast "low-threshold" exocytosis. *Cell calcium* 40:147-154.

254. Steger KA, Shtonda BB, Thacker C, Snutch TP, Avery L. (2005) The *C. elegans* T-type calcium channel CCA-1 boosts neuromuscular transmission. *J Exp Biol.* 208:2191-2203.

255. Mackie GO and Meech RW. (1985) Separate sodium and calcium spikes in the same axon. *Nature* 313:791-793.

256. Perchenet L, Benardeau A, Ertel EA. (2000) Pharmacological properties of $Ca_V3.2$, a low voltage-activated Ca^{2+} channel cloned from human heart. *Naunyn Schmiedebergs Arch Pharmacol* 361:590-599.

257. Ferron L, Capuano V, Ruchon Y, Deroubaix E, Coulombe A, Renaud JF. (2003) Angiotensin II signaling pathways mediate expression of cardiac T-type calcium channels. *Circ Res* 93:1241-1248.

258. Lalevee N, Rebsamen MC, Barrere-Lemaire S, Perrier E, Nargeot J, Benitah JP, Rossier MF. (2005) Aldosterone increases T-type calcium channel expression and in vitro beating frequency in neonatal rat cardiomyocytes. *Cardiovasc.Res* 67:216-224.

259. Obejero-Paz CA, Gray IP, Jones SW. (2008) Ni^{2+} block of $Ca_V3.1$ ($alpha_{1G}$) T-type calcium channels. *J Gen Physiol.* 132:239-250.

260. Bosmans F, Martin-Eauclaire MF, Swartz KJ. (2008) Deconstructing voltage sensor function and pharmacology in sodium channels. *Nature* 456:202-208.

261. Kang HW, Vitko I, Lee SS, Perez-Reyes E, Lee JH. (2010) Structural Determinants of the High Affinity Extracellular Zinc Binding Site on $Ca_v3.2$ T-type Calcium Channels. *J Biol Chem.* 285:3271-3281.

262. Lee TS, Kaku T, Takebayashi S, Uchino T, Miyamoto S, Hadama T, Perez-Reyes E, Ono K. (2006) Actions of mibefradil, efonidipine and nifedipine block of recombinant T- and L-type Ca channels with distinct inhibitory mechanisms. *Pharmacology* 78:11-20.

263. Wu S, Zhang M, Vest PA, Bhattacharjee A, Liu L, Li M. (2000) A mibefradil metabolite is a potent intracellular blocker of L-type Ca^{2+} currents in pancreatic beta-cells. *J Pharmacol Exp Ther* 292:939-943.

264. Gray LS and Macdonald TL. (2006) The pharmacology and regulation of T type calcium channels: new opportunities for unique therapeutics for cancer. *Cell calcium* 40:115-120.

265. Latour I, Louw DF, Beedle AM, Hamid J, Sutherland GR, Zamponi GW. (2004) Expression of T-type calcium channel splice variants in human glioma. *Glia* 48:112-119.

266. David LS, Garcia E, Cain SM, Thau E, Tyson JR, Snutch TP. (2010) Splice-variant changes of the $Ca_V3.2$ T-type calcium channel mediate voltage-dependent facilitation and associate with cardiac hypertrophy and development. *Channels* 4:389-389.

267. Ohkubo T. (2005) Identification and electrophysiological characteristics of isoforms of T-type calcium channel $Ca_v3.2$ expressed in pregnant human uterus. *Cell Physiol Biochem.* 16:245-254.

268. Kim T, Kim S, Yun HM, Chung KC, Han YS, Shin HS, Rhim H. (2009) Modulation of $Ca_v3.1$ T-type Ca^{2+} channels by the ran binding protein RanBPM. *Biochem.Biophys.Res.Commun.* 378:15-20.

269. Liu JH, Konig S, Michel M, Arnaudeau S, Fischer-Lougheed J, Bader CR, Bernheim L. (2003) Acceleration of human myoblast fusion by depolarization: graded Ca^{2+} signals involved. *Development* 130:3437-3446.

270. Taylor JT, Zeng XB, Pottle JE, Lee K, Wang AR, Yi SG, Scruggs JA, Sikka SS, Li M. (2008) Calcium signaling and T-type calcium channels in cancer cell cycling. *World J Gastroenterol.* 14:4984-4991.

271. Eaholtz G, Scheuer T, Catterall WA. (1994) Restoration of inactivation and block of open sodium channels by an inactivation gate peptide. *Neuron* 12:1041-1048.

272. Hertel KJ. (2008) Combinatorial control of exon recognition. *J Biol Chem* 283:1211-1215.

273. Broicher T, Kanyshkova T, Landgraf P, Rankovic V, Meuth P, Meuth SG, Pape HC, Budde T. (2007) Specific expression of low-voltage-activated calcium channel isoforms and splice variants in thalamic local circuit interneurons. *Mol Cell Neurosci* 36:132-145.

274. Tscherter A, David F, Ivanova T, Deleuze C, Renger JJ, Uebele VN, Shin HS, Bal T, Leresche N, Lambert RC. (2011) Minimal alterations in T-type calcium channel gating markedly modify physiological firing dynamics. *Journal of Physiology-London* 589:1707-1724.

275. Chemin J, Monteil A, Perez-Reyes E, Bourinet E, Nargeot J, Lory P. (2002) Specific contribution of human T-type calcium channel isotypes (A_{1G}, A_{1H} and A_{1I}) to neuronal excitability. *J.Physiol.* 540:3-14.

276. Astori S, Wimmer RD, Prosser HM, Corti C, Corsi M, Liaudet N, Volterra A, Franken P, Adelman JP, Luthi A. (2011) The $Ca_V3.3$ calcium channel is the major sleep spindle pacemaker in thalamus. *Proc Natl Acad Sci U S A* 108:13823-13828.

277. Crandall SR, Govindaiah G, Cox CL. (2010) Low-Threshold Ca^{2+} Current Amplifies Distal Dendritic Signaling in Thalamic Reticular Neurons. *J Neurosci.* 30:15419-15429.

278. Kang HW, Park JY, Lee JH. (2008) Distinct contributions of different structural regions to the current kinetics of the $Ca_v3.3$ T-type Ca^{2+} channel. *Biochim.Biophys Acta* 1778:2740-2748.

279. Groome JR, Dice MC, Fujimoto E, Ruben PC. (2007) Charge immobilization of skeletal muscle Na^+ channels: role of residues in the inactivation linker. *Biophys J* 93:1519-1533.

280. Perez-Reyes E. (2010) G Protein-Mediated Inhibition of $Ca_v3.2$ T-Type Channels Revisited. *Mol.Pharmacol.* 77:136-138.

281. Hildebrand ME, Isope P, Miyazaki T, Nakaya T, Garcia E, Feltz A, Schneider T, Hescheler J, Kano M, Sakimura K, et al. (2009) Functional Coupling between mGluR1 and $Ca_v3.1$ T-Type

Calcium Channels Contributes to Parallel Fiber-Induced Fast Calcium Signaling within Purkinje Cell Dendritic Spines. *The Journal of Neuroscience* 29:9668-9682.

282. Anderson D, Mehaffey WH, Iftinca M, Rehak R, Engbers JDT, Hameed S, Zamponi GW, Turner RW. (2010) Regulation of neuronal activity by Ca_v3-K_v4 channel signaling complexes. *Nat.Neurosci.* 13:337-337.

283. Yang J, Ellinor PT, Sather WA, Zhang JF, Tsien RW. (1993) Molecular determinants of Ca2+ selectivity and ion permeation in L-type Ca2+ channels. *Nature* 366:158-161.

284. Kim MS, Morii T, Sun LX, Imoto K, Mori Y. (1993) Structural determinants of ion selectivity in brain calcium channel. *FEBS Lett.* 318:145-148.

285. Payandeh J, Scheuer T, Zheng N, Catterall WA. (2011) The crystal structure of a voltage-gated sodium channel. *Nature* 475:358-358.

286. Catterall WA. (2012) Voltage-Gated Sodium Channels at 60:Structure, Function, and Pathophysiology. *J Physiol*

287. Talavera K, Staes M, Janssens A, Klugbauer N, Droogmans G, Hofmann F, Nilius B. (2001) Aspartate residues of the Glu-Glu-Asp-Asp (EEDD) pore locus control selectivity and permeation of the T-type Ca(2+) channel alpha(1G). *J Biol Chem* 276:45628-45635.

288. Shcheglovitov A, Kostyuk P, Shuba Y. (2007) Selectivity signatures of three isoforms of recombinant T-type Ca2+ channels. *Biochim.Biophys Acta* 1768:1406-1419.

289. Senatore A and Spafford JD. (2012) Gene Transcription and Splicing of T-Type Channels are Evolutionarily-Conserved Strategies for Regulating Channel Expression and Gating. *PloS one* 7:e37409-

290. Marois R and Croll RP. (1992) Development of serotoninlike immunoreactivity in the embryonic nervous system of the snail *Lymnaea stagnalis*. *J Comp Neurol.* 322:255-265.

291. Nagy T and Elekes K. (2002) Ultrastructure of neuromuscular contacts in the embryonic pond snail *Lymnaea stagnalis* L. *Acta Biologica Hungarica* 53:125-139.

292. McComb C, Varshney N, Lukowiak K. (2005) Juvenile *Lymnaea* ventilate, learn and remember differently than do adult *Lymnaea*. *J Exp Biol* 208:1459-1467.

293. Ono K and Iijima T. (2010) Cardiac T-type Ca(2+) channels in the heart. *J Mol Cell Cardiol.* 48:65-70.

294. Nagle GT, de Jong-Brink M, Painter SD, Li KW. (2001) Structure, localization and potential role of a novel molluscan trypsin inhibitor in Lymnaea. *Eur J Biochem* 268:1213-1221.

295. Kumar A, Bhandari A, Sinha R, Goyal P, Grapputo A. (2011) Spliceosomal intron insertions in genome compacted ray-finned fishes as evident from phylogeny of MC receptors, also supported by a few other GPCRs. *PloS one* 6:e22046-

296. Thompson JD, Higgins DG, Gibson TJ. (1994) CLUSTAL W: improving the sensitivity of progressive multiple sequence alignment through sequence weighting, position-specific gap penalties and weight matrix choice. *Nucleic Acids Res* 22:4673-4680.

297. Senatore A. (2011) Optimized transfection strategy for expression and electrophysiological recording of recombinant voltage-gated ion channels in HEK-293T cells. *J Vis Exp.*

298. Holland LZ. (2000) Body-plan evolution in the Bilateria: early antero-posterior patterning and the deuterostome-protostome dichotomy. *Curr Opin Genet.Dev.* 10:434-442.

299. Letunic I, Copley RR, Bork P. (2002) Common exon duplication in animals and its role in alternative splicing. *Hum Mol Genet.* 11:1561-1567.

300. Talavera K, Janssens A, Klugbauer N, Droogmans G, Nilius B. (2003) Extracellular Ca2+ modulates the effects of protons on gating and conduction properties of the T-type Ca2+ channel alpha1G (CaV3.1). *J Gen Physiol* 121:511-528.

301. Hess P, Lansman JB, Tsien RW. (1986) Calcium channel selectivity for divalent and monovalent cations. Voltage and concentration dependence of single channel current in ventricular heart cells. *J Gen Physiol* 88:293-319.

302. Brezden BL and Gardner DR. (1992) A review of the electrophysiological, pharmacological and single channel properties of heart ventricle muscle cells in the snail Lymnaea stagnalis. *Experientia* 48:841-852.

303. Sinke AP, Caputo C, Tsaih SW, Yuan R, Ren D, Deen PM, Korstanje R. (2011) Genetic analysis of mouse strains with variable serum sodium concentrations identifies the Nalcn sodium channel as a novel player in osmoregulation. *Physiol Genomics* 43:265-270.

304. Lipkind GM and Fozzard HA. (2008) Voltage-gated Na channel selectivity: the role of the conserved domain III lysine residue. *J Gen Physiol* 131:523-529.

305. Spafford JD, Spencer AN, Gallin WJ. (1998) A putative voltage-gated sodium channel alpha subunit (PpSCN1) from the hydrozoan jellyfish, *Polyorchis penicillatus*: structural comparisons and evolutionary considerations. *Biochem Biophys Res Commun.* 244:772-780.

306. Schlief T, Schonherr R, Imoto K, Heinemann SH. (1996) Pore properties of rat brain II sodium channels mutated in the selectivity filter domain. *Eur Biophys J* 25:75-91.

307. Locke EG, Bonilla M, Liang L, Takita Y, Cunningham KW. (2000) A homolog of voltage-gated Ca^{2+} channels stimulated by depletion of secretory Ca^{2+} in yeast. *Mol Cell Biol* 20:6686-6694.

308. Anderson PA, Holman MA, Greenberg RM. (1993) Deduced amino acid sequence of a putative sodium channel from the scyphozoan jellyfish *Cyanea capillata*. *Proc Natl Acad Sci U S A* 90:7419-7423.

309. Catterall WA. (2010) Signaling complexes of voltage-gated sodium and calcium channels. *Neurosci Lett.* 486:107-116.

310. Ramsey IS, Delling M, Clapham DE. (2006) An introduction to TRP channels. *Annu.Rev.Physiol* 68:619-647.

311. Enyedi P and Czirjak G. (2010) Molecular background of leak K^+ currents: two-pore domain potassium channels. *Physiol Rev.* 90:559-605.

312. Cai X. (2008) Unicellular Ca^{2+} signaling 'toolkit' at the origin of metazoa. *Mol Biol Evol.* 25:1357-1361.

313. Bannister RA, Papadopoulos S, Haarmann CS, Beam KG. (2009) Effects of inserting fluorescent proteins into the alpha1S II-III loop: insights into excitation-contraction coupling. *J Gen Physiol* 134:35-51.

314. Hiyama TY, Watanabe E, Okado H, Noda M. (2004) The subfornical organ is the primary locus of sodium-level sensing by Na_x sodium channels for the control of salt-intake behavior. *J Neurosci* 24:9276-9281.

315. Wicher D, Messutat S, Lavialle C, Lapied B. (2004) A new regulation of non-capacitative calcium entry in insect pacemaker neurosecretory neurons. Involvement of arachidonic acid, no-guanylyl cyclase/cGMP, and cAMP. *J Biol Chem* 279:50410-50419.

316. Kawabe H and Brose N. (2011) The role of ubiquitylation in nerve cell development. *Nat.Rev.Neurosci* 12:251-268.

317. Acconcia F, Sigismund S, Polo S. (2009) Ubiquitin in trafficking: the network at work. *Exp Cell Res* 315:1610-1618.

318. Page KM, Heblich F, Davies A, Butcher AJ, Leroy J, Bertaso F, Pratt WS, Dolphin AC. (2004) Dominant-negative calcium channel suppression by truncated constructs involves a kinase implicated in the unfolded protein response. *J Neurosci* 24:5400-5409.

319. Kornblihtt AR, de la Mata M, Fededa JP, Munoz MJ, Nogues G. (2004) Multiple links between transcription and splicing. *RNA.* 10:1489-1498.

320. Morgan PG, Humphrey JA, Sedensky MM. (2007) Physical Interaction of Proteins Which Control Volatile Anesthetic Sensitivity in *C. elegans* (Abstract). *Anesthesiology* 107: A10:

321. Marder E and Goaillard JM. (2006) Variability, compensation and homeostasis in neuron and network function. 7:574-574.

322. Proenza C, O'Brien J, Nakai J, Mukherjee S, Allen PD, Beam KG. (2002) Identification of a region of RyR1 that participates in allosteric coupling with the alpha(1S) (Ca(V)1.1) II-III loop. *J Biol Chem* 277:6530-6535.

323. Swayne LA, Mezghrani A, Lory P, Nargeot J, Monteil A. (2010) The NALCN ion channel is a new actor in pancreatic beta-cell physiology. *Islets.* 2:54-56.

324. van Moorsel CHM, van Nes WJ, Megens HJ. (2000) A quick, simple, and inexpensive DNA extraction protocol for PCR-based techniques. *Malacologia* 42:203-206.

325. Chomczynski P and Sacchi N. (1987) Single-step method of RNA isolation by acid guanidinium thiocyanate-phenol-chloroform extraction. *Anal Biochem* 162:156-159.

326. Chomczynski P and Sacchi N. (2006) The single-step method of RNA isolation by acid guanidinium thiocyanate-phenol-chloroform extraction: twenty-something years on. *Nat.Protoc.* 1:581-585.

327. Saiki RK, Scharf S, Faloona F, Mullis KB, Horn GT, Erlich HA, Arnheim N. (1985) Enzymatic amplification of beta-globin genomic sequences and restriction site analysis for diagnosis of sickle cell anemia. *Science* 230:1350-1354.

328. Heid CA, Stevens J, Livak KJ, Williams PM. (1996) Real time quantitative PCR. *Genome Res* 6:986-994.

329. Kubista M, Andrade JM, Bengtsson M, Forootan A, Jonak J, Lind K, Sindelka R, Sjoback R, Sjogreen B, Strombom L, et al. (2006) The real-time polymerase chain reaction. *Mol Aspects Med* 27:95-125.

330. Andersen CL, Jensen JL, Orntoft TF. (2004) Normalization of Real-Time Quantitative Reverse Transcription-PCR Data: A Model-Based Variance Estimation Approach to Identify Genes Suited for Normalization, Applied to Bladder and Colon Cancer Data Sets. *Cancer research* 64:5245-5250.

331. Pfaffl MW. (2001) A new mathematical model for relative quantification in real-time RT-PCR. *Nucleic acids research* 29:e45-e45.

332. Bimboim HC and Doly J. (1979) A rapid alkaline extraction procedure for screening recombinant plasmid DNA. *Nucleic acids research* 7:1513-1523.

333. Smit AB, Spijker S, van MJ, Burke JF, De WF, Van ER, Geraerts WP. (1996) Expression and characterization of molluscan insulin-related peptide VII from the mollusc Lymnaea stagnalis. *Neuroscience* 70:589-596.

334. Southern EM. (1975) Detection of specific sequences among DNA fragments separated by gel electrophoresis. *J Mol Biol* 98:503-517.

335. Sambrook J and Russell DW. (2006) Southern blotting: capillary transfer of DNA to membranes. *CSH.Protoc.* 2006:

336. Campbell RE, Tour O, Palmer AE, Steinbach PA, Baird GS, Zacharias DA, Tsien RY. (2002) A monomeric red fluorescent protein. *Proc Natl Acad Sci U S A* 99:7877-7882.

337. Laemmli UK. (1970) Cleavage of structural proteins during the assembly of the head of bacteriophage T4. *Nature* 227:680-685.

338. Fazekas de St GS, Webster RG, Datyner A. (1963) Two new staining procedures for quantitative estimation of proteins on electrophoretic strips. *Biochim.Biophys Acta* 71:377-391.

339. Towbin H, Staehelin T, Gordon J. (1979) Electrophoretic transfer of proteins from polyacrylamide gels to nitrocellulose sheets: procedure and some applications. *Proc Natl Acad Sci U S A* 76:4350-4354.

340. Vernet T, Tessier DC, Laliberte F, Dignard D, Thomas DY. (1989) The expression in Escherichia coli of a synthetic gene coding for the precursor of papain is prevented by its own putative signal sequence. *Gene* 77:229-236.

341. Thomas P and Smart TG. (2005) HEK293 cell line: A vehicle for the expression of recombinant proteins. *J.Pharmacol.Toxicol.Methods* 51:187-200.

342. van Moorsel CHM, van Nes WJ, Megens H-J. (2000) A quick, simple, and inexpensive DNA extraction protocol for Gastropods. *Malacologia* 42:203-206.

343. Huang X, Senatore A, Dawson TF, Quan Q, Spafford JD. (2010) G-proteins modulate invertebrate synaptic calcium channel (LCa_v2) differently from the classical voltage-dependent regulation of mammalian $Ca_v2.1$ and $Ca_v2.2$ channels. *J Exp Biol.* 213:2094-2103.

344. De Lange RP, van Golen FA, van Minnen J. (1997) Diversity in cell specific co-expression of four neuropeptide genes involved in control of male copulation behaviour in *Lymnaea stagnalis*. *Neuroscience* 78:289-299.